



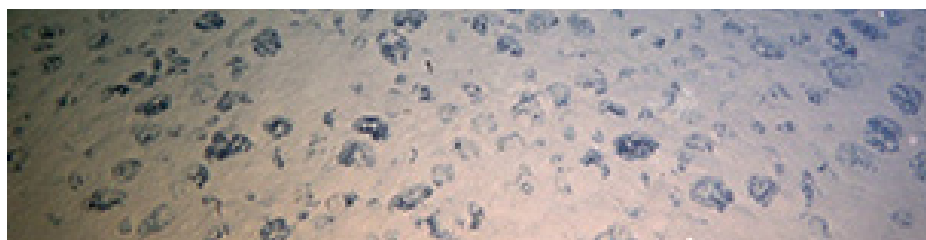
GSR

Global Sea Mineral Resources

Member of the DEME Group

Environmental Impact Statement

Small-scale testing of nodule collector components on the seafloor of the Clarion-Clipperton Fracture Zone and its environmental impact



DEME: creating land for the future

Executive summary

Global Sea Mineral Resources (GSR) is developing a pre-prototype collector vehicle equipped with a launch and recovery system planned to be deployed and trialled in the GSR Contract Area in the Clarion-Clipperton Fracture Zone (NE Pacific Ocean) in April 2019. The present Environmental Impact Statement was built up in the framework of two distinct projects: (1) the ProCat#2 project; and (2) the JPI-OII MiningImpact 2 program. The former focusses on the technical validation of the design of a pre-prototype vehicle (PPV, provisionally named Patania II) with a nodule collector component in its actual intended environment in the Clarion-Clipperton Fracture Zone (CCFZ), whereas the latter aims to evaluate environmental impacts that a future nodule collection activity may generate. During the trial, nodules will be collected from a small area of seafloor (approximately 0.1 km²) at a water depth of ~4400 m over a time period of maximal 4 days.

From a technological point of view, the component validation of GSR's 4-m-wide Patania II, equipped with hydraulic collector head components, focusses on validating its manoeuvrability, reliability and nodule pick-up efficiency as part of an eventual future overall mining system, as well as analysing potential environmental impacts in order to inform and assess the environmental performance of the component system design.

From a scientific point of view, the GSR PPV trial offers a unique opportunity to realistically assess for the first time potential environmental impacts that may arise from a potential future nodule mining operation on the seafloor. This assessment is planned to take place in the framework of the European “Joint Programming Initiative – Oceans” project “MiningImpact 2”, which has been positively evaluated and is set to start on 1 August 2018 for 3.5 years. The consortium, with 31 partner institutions from science and industry, spread out through 9 European countries, aims to deliver new scientific information on future deep-sea nodule mining by (1) developing, standardising and testing monitoring concepts and strategies, (2) investigating the short- and medium-term potential environmental impacts of nodule collection, that in turn feed into the (3) proposal of potential mitigation measures and (4) the development of spatial management plans, and (5) developing sound methodologies to assess risks, benefits and uncertainties that can be implemented in future regulations and guidelines. These goals and this activity, together with the small spatial and temporal scope of the latter, which is being conducted under an exploration contract with the International Seabed Authority (ISA), are consistent with the aforesaid exploration contract and are subject to a “prior Environmental Impact Assessment (EIA),” i.e., an EIA that is conducted within the context of an exploration contract and pursuant to the relevant ISA requirements for such an EIA. The EIA process culminates in an Environmental Impact Statement (EIS) and this is the context in which this EIS is presented. It is important to note that the results of the proposed activity presented here are likely to be the primary inputs to EIAs for later mining tests and eventual commercial-scale mining.

The JPI-O MiningImpact 2 consortium will set up and evaluate a comprehensive monitoring programme that, amongst others, focusses on three major research topics associated with eventual future nodule mining: (1) the potential large-scale environmental impact caused by a suspended sediment plume, (2) the regional connectivity of species and the biodiversity of biological assemblages and their resilience to impacts, and (3) the integrated effects of disturbance on ecosystems and their functions, such as the benthic food web and biogeochemical processes.

Due to the small spatial and temporal scale of the trial activity, no serious harm will be caused to the marine environment at any depth within the water column. Small-scale impacts on faunal communities may occur due to (1) habitat/nodule removal, (2) sediment disturbance and plume formation/deposition, (3) biogeochemical alteration of the sediment (i.e., change of habitat integrity), (4) potential release of possibly toxic sediments and/or substances into the lower water column, and (5) potential noise and light pollution.

Using an integrated 3D hydrodynamic and sediment transport model developed by International Marine & Dredging Consultants (IMDC), the distance that the suspended plume in the water column is likely to have spread after 4 days of testing is predicted to vary between 1 and 3 km (cut-off concentration value respectively 10 mg/L and 1 mg/L) and 5-12 km (cut-off value 0.1 mg/L), depending on the current conditions at the seafloor. For the intended disturbance experiment, the sediment deposition from the plume is expected to reach approximately 500-750 m (cut-off value of 1 mm deposition) and roughly 5 km (cut-off value of 0.1 mm deposition) from the source. For the determination of geographical scale / sampling scale of the monitoring survey and the definition of impact zones in the Environment Monitoring Plan, these modelled results have been used for initial orientation, but may be adapted and/or refined prior to testing if necessary (e.g., due to refinement of models and/or collection of new baseline data shortly before the test takes place). Dedicated monitoring surveys will take place in the area of direct impact (nodule removal), the area of plume deposition surrounding the impact area (transects up to non detectable impact), and in an ecologically similar non-impact reference site. The plume monitoring results will be further used to validate the sediment transport numerical model to inform future EIAs.

The JPI-O MiningImpact 2 scientific consortium will be analysing and monitoring the impacts created by the Patania II. The collaboration with the JPI-O MiningImpact 2 project offers a transparent approach to assess the environmental performance of GSR's future mining technology. This should promote a greater understanding and comprehensive assessment of the potential environmental effects of GSR's future mining activities, the design of fit-for-purpose monitoring programmes, and environmentally and commercially responsible standard development. The JPI-O MiningImpact 2 project is committed to organising, facilitating and effectively managing the archival of generated environmental data and samples in databases with established structures and capabilities, such as PANGAEA and European museum collections, based on established protocols and best practices for research expeditions, the specific code of conduct for marine sciences, and the ISA's and the EU's principles of data- and knowledge-sharing. GSR will follow the ISA's reporting requirements.

Author Global Sea Mineral Resources NV

Date April 1st 2018

Ref. Doc ISA_EIA_2018_GSRNOD2019

Contents

Executive summary	1
Contents	4
Figures.....	8
Tables	17
1 Introduction	19
1.1 Background and rationale.....	19
1.2 The technical project – ProCat#2	19
1.3 The environmental project - JPI-O MiningImpact 2.....	20
1.4 This report.....	21
2 Policy, legal and administrative context.....	23
2.1 Applicable mining and environmental legislation, agreements and policies	23
3 Project description.....	23
3.1 Purpose of the proposed project.....	23
3.2 Locations	23
3.3 Mineral Resource estimation	27
3.3.1 Geochemical analyses.....	35
3.4 Patania II - description and design.....	37
3.4.1 Background – Patania.....	37
3.4.2 Patania II and nodule collection methodology	40
3.5 Project duration	46
3.5.1 In field collector test plan.....	46
3.5.2 Project scale	48
3.6 Support equipment.....	52
3.6.1 Vessel.....	52
3.6.2 AUV and ROV.....	52
4 Description of the existing environment	52
4.1 The physico-chemical environment.....	52
4.1.1 Climatology	52
4.1.2 Geomorphological settings.....	54
4.1.3 Physical oceanographic setting.....	68
4.1.4 Chemical oceanographic setting	87
4.1.5 Seabed substrate characteristics	89
4.1.6 Natural hazards	111
4.1.7 Noise and light.....	112
4.2 The biological environment.....	113
4.2.1 Key messages	114
4.2.2 Biological communities	115
5 Assessment of impacts and proposed mitigation	129
5.1 On the physico-chemical environment.....	130

5.1.1	Description of potential impact categories.....	130
5.1.2	Emissions to air	130
5.1.3	Geological setting	131
5.1.4	Natural hazards	147
5.2	On the biological environment	147
5.2.1	Description of potential impact categories.....	147
5.2.2	Surface	147
5.2.3	Midwater	148
5.2.4	Seafloor	148
5.2.5	Cumulative impacts.....	157
6	Accidental events and natural hazards	158
6.1	Extreme weather and natural hazards.....	158
6.2	Potential accidental events.....	160
6.2.1	Vessel failures	160
6.2.2	Patania II – System failures	160
6.2.3	Patania II – Emergency Recovery.....	161
7	Environmental management, monitoring and reporting	164
7.1	Organisational structure and responsibilities	164
7.1.1	Organisation on board on board of GSR vessel.....	164
7.1.2	Organisation within JPI-O MiningImpact 2 consortium	167
7.1.3	Coordination between GSR and JPI-O MiningImpact 2 consortium	167
7.2	Environmental Management and Monitoring Plan (EMMP)	167
7.2.1	Technical mitigation	170
7.2.2	Choice of impact reference zone and reference zone	171
7.2.3	Environmental monitoring plan.....	177
7.3	Reporting	194
7.3.1	Monitoring.....	194
7.3.2	Exploration and trials reporting	198
7.3.3	Incident reporting	199
8	Abbreviations	200
9	Study team.....	202
9.1	EIA specialist sub-consultants.....	202
9.2	JPI-O MiningImpact 2 Applicants	202
10	Expert review.....	203
11	References.....	204
11.1	Scientific literature	204
11.2	Online resources	215
12	Appendices.....	217
12.1	Technology development	217
12.1.1	Background : theory approach of the hydraulic collector	217

12.1.2	Choice of pick-up system.....	218
12.1.3	Pre-design study : Optimized collector design.....	221
12.1.4	Laboratory tests with the hydraulic collector.....	230
12.2	Pre- and Post-Dive Check-up list.....	234
12.3	Panolin oil Safety data sheet	235
12.4	Sediment plume results	236
12.4.1	Scenario 1 results	236
12.4.2	Scenario 2 results	236
12.4.3	Scenario 3 results	236
12.4.4	Scenario 4 results	236
12.5	Risk Assessment Table.....	334

Figures

Figure 1: Structure of the JPI-O MiningImpact 2 project.....	21
Figure 2: Location of the GSR contract area in the CCFZ. The shapes of the three domains B2, B3 and B6 are coloured in dark green (source: International Seabed Authority, 2018., consulted on March 21, 2018).....	24
Figure 3: Close-up on the three domains of the GSR contract area and high resolution stations showed in red	25
Figure 4: B4S03 sub-zone and sampling locations during expeditions of 2014, 2015 and 2017 and location of MiningImpact 2 Program area	26
Figure 5 : Qualitative nodule coverage classification in the sub-zone B4S03 and its vicinity	33
Figure 6: Quantitative nodule coverage map of polymetallic nodules in area B4S03 and its vicinity	34
Figure 7: Launching of TSTD (20/01/2017) (left) and mud trials in Belgium (February 2017) (right)	38
Figure 8: TSTD Patania on the seabed (GSRNOD17)	39
Figure 9: Conceptual sketch of the PPV	41
Figure 10: Nodule collector head	42
Figure 11: Collector head height control.....	42
Figure 12: Collector pump lay-out	43
Figure 13: Nodule separation system.....	44
Figure 14: High level planning GSRNOD19	47
Figure 15 : Example of the pattern of the JPI-O MiningImpact 2 area. Red dots represent the piles of nodules collected	49
Figure 16: Turning procedure.....	49
Figure 17: Scenario mining overview	51
Figure 18: Average wind speed over a period of one year at station 51307 (8°N 125°W) of the MeteOCean database	53
Figure 19: Contour Map of area B4S03 (and surrounding features in grey) generated with the EM120 multibeam data	56
Figure 20: Benthic Terrain Model (BTM) of the main geological structures in area B4S03	57
Figure 21: Slope map of area B4S03 based on the bathymetry measured during the 2014 offshore campaign	59
Figure 22: Bathymetric Map of area B4S03 generated with the EM120 multibeam data and superimposed with the topographical lines (crest and valley lines).....	60
Figure 23: Mounds observed in area B4S03	61
Figure 24: Inner walls of a sub-circular depression located in the B4S03 area, showing layered consolidated sediment exposed in a vertical escarpment of metric scale (AUV dive 11, photo 7633). Coordinates: Lat.: 14.083N, Long.: -125.897W	62

Figure 25: AUV side-scan sonar (SSS) data collected in the area B4S03 superimposed with the geological interpretation	63
Figure 26: Sedimentary and geological features observed in area B4S03.....	65
Figure 27: AUV high-resolution multibeam data superimposed with sample locations collected during the 2015 offshore campaign in area B4S03 (surrounding features are displayed in grey).....	66
Figure 28: Temperature, Salinity and density profiles measured at CTD011 location (14° 02.61' N, 125° 55.17' W) on 28 May 2017 during the GSRNOD17 campaign over the entire water column (upper panel) and over the upper layer (lower panel).....	69
Figure 29: Current representation 24 m above seabed at MOR001 location (in the MiningImpact 2 Program area). Time series of the current speed (top) and direction (lower panel) along with the rose diagram (left) and the scatter plot (right) averaged over the deployment period	70
Figure 30: Current representation 2 m above seabed at MOR002 location (in the Reference Area). Time series of the current speed (top) and direction (bottom) along with the rose diagram (left) and the scatter plot (right) averaged over the deployment period	72
Figure 31: Outline of model domain and bathymetry	74
Figure 32: Mesh size in the model for the different zones	75
Figure 33: Velocity variability at the surface (z=0), defined as the RMS (root mean square) difference between the instantaneous velocity and the 90-day running average from HYCOM expt. _19.1), calculated over period 1995-2012	77
Figure 34: Location of three moorings for short-term model validation. The GEBCO bathymetry is used as background, and the boundaries of B4, B6 and B4S03 are superimposed	78
Figure 35: Measured time series 35 m above bottom of total velocity magnitude at locations MOR001 (top), MOR002 (middle) and MOR005 (bottom).	79
Figure 36: Vertical velocity profiles at the MOR001(top), MOR002 (middle) and MOR005 locations (model and measurements)	80
Figure 37: Current direction time series 35 m above bottom at MOR001 location of measurements (top for the deployment period between 26 May 2017 and 3 June 2017) and model (bottom for the 3 time series of 21 days in March, April and May 2009).....	81
Figure 38: Current direction time series 35 m above bottom at MOR002 location of measurements (top for the deployed period between 28 May 2017 and 6 June 2017) and model (bottom for the 3 time series of 21 days in March, April and May 2009).	82
Figure 39: Current direction time series 35 m above bottom at MOR005 location of measurements (top for the deployed period between 7 June 2017 and 24 June 2017) and model (bottom for the 3 time series of 21 days in March, April and May 2009).	83
Figure 40: Current velocity [m/s] rose 35 m above bottom for MOR001 location. Top left: Average measurements over the deployed period (26 May 2017 to 3 June 2017). Top right: 21-day average model results (March 2009). Bottom left: 21-day average model results (April 2009). Bottom right: 21-day average model results (May 2009).	84
Figure 41: Current velocity [m/s] rose 35 m above bottom for MOR002 location. Top left: Averaged measurements over the deployed period (28 May 2017 to 6 June 2017). Top right: 21-	

day average model results (March 2009). Bottom left: 21-day average model results (April 2009). Bottom right: 21-day average model results (May 2009)	85
Figure 42: Current velocity [m/s] rose 35 m above bottom for MOR005 location. Top left: Averaged measurements over the deployed period between 7 June 2017 and 24 June 2017. Top right: 21-day average model results (March 2009). Bottom left: 21-day average model results (April 2009). Bottom right: 21-days averaged model results (May 2009).	86
Figure 43: Time series of the background turbidity measured by the turbidity sensors located at 3.5 (blue) and 12.5 m (black, dashed) above seabed on MOOR001 (top panel) and located at 3.4 (blue) and 9.6 m (black, dashed) above seabed on MOR002 (bottom panel) during the GSRNOD17 campaign. Unfortunately, due to a failure of the CTD sensor, only 3 days of data were recorded for MOROO1. It must be noted that x-axis are not aligned, and that the turbidity event of June 06 th 2017 for MOR002 could not be explained.	87
Figure 44: Burrows piercing the geological cores BC017 (left), BC020 (middle) and BC022 (right) in Area B4S03. The crack planes in BC017 and BC020 are visible (horizontal and vertical). Only few micronodules are present (red).	90
Figure 45: Diagram of the different facies characterizing the sediment cores recovered in the GSR Contract Area, based on colour and burrowing.....	91
Figure 46: Box-core and multicore sediment samples recovered in area B4S03 and its vicinity during Y1, Y2 and Y4 (see Figure 48 for location). The samples recovered from the same sub-zone have been grouped within a box with dashed borders. The red dashed lines indicate the depth every 10 cm	93
Figure 47: Diagram interpreting the box-core and multicore sediment samples recovered in area B4S03 and its vicinity during Y1, Y2 and Y4 (see Figure 48 for location)	94
Figure 48: Distribution of the various vertical sediment patterns in area B4S03 and its vicinity ..	95
Figure 49: Average composition of the sediment recovered in campaigns GSRNOD14A and GSRNOD15A in the GSR Contract Area, according to estimations using smear slides.....	96
Figure 50 : Clay mineralogy distribution in area B4S03.....	99
Figure 51: Summary of the moisture content determination during GSRNOD15A Campaign...	100
Figure 52: Average values of granulometric variables in function of sediment depth in the nodule-free and nodule-rich sediments sampled at site B4S03 in the GSR contract area. The left-hand panels show only samples collected in flat areas (n=3 for both nodule-free and nodule-rich sediments), and the right-hand panels include the samples collected on the slope areas (n=4 for both nodule-free and nodule-rich sediments). Error bars denote standard deviations. MGS: median grain size, SC: sediment-sorting coefficient.	104
Figure 53: Average sedimentary total organic matter (TOM) content in function of sediment depth in the nodule-rich and nodule-free sediments sampled at site B4S03 in the GSR contract area. Plot A shows only samples collected in flat areas (n=3 for both nodule-free and nodule-rich sediments), and plot B also includes the samples collected in the slope areas (n=4 for both nodule-free and nodule-rich sediments). Error bars denote standard deviations	104
Figure 54: Average values of (A) TOC (total organic carbon content), (B) TN (total nitrogen content) and (C) TOC/TN (molar sediment total organic carbon-to-total nitrogen ratio) in function	

of sediment depth in the nodule-free and nodule-rich sediments sampled at site B4S03 in the GSR contract area. The left-hand panels show only samples collected in flat areas (n=3 for both nodule-free and nodule-rich sediments), and the right-hand panels include the samples collected on the slope areas (n=4 for both nodule-free and nodule-rich sediments). Error bars denote standard deviations.....	105
Figure 55: Bottom-water and pore-water concentration of (A) ammonium, (B) nitrite, (C) nitrate, (D) silicate, and (E) phosphate in function of sediment depth in the nodule-free and nodule-rich sediments sampled at site B4S03 in the GSR contract area. The sediment-water interface is demarcated by the black horizontal line. Values plotted above this line represent bottom-water concentrations	106
Figure 56: Average concentration of (A) ammonium (TON), (B) nitrite, (C) nitrate, (D) silicate and (E) phosphate in function of sediment depth as measured during GSRNOD15A (September-October 2015) and GSRNOD17 (May-June 2017) at site B4S03 sub-zone. Error bars denote standard deviations. The sediment-water interface is demarcated by the black horizontal line. Values plotted above this line represent bottom-water concentrations	107
Figure 57: Summary of the bulk density determination during GSRNOD15A campaign.....	108
Figure 58: Undrained shear strength measurements in box core BC028 during GSRNOD15A	108
Figure 59: Sub-zone B4S03 (left) and high resolution box within B4S03; proposed GraviProbe-trajectory for testing (middle) and in-situ penetration points within area B4S03 (right).....	109
Figure 60: Unprocessed GraviProbe data at location GP022_03	110
Figure 61: Processed GraviProbe profiles at location GP022.....	110
Figure 62: Undrained shear strength (kPa) vs depth below seabed (Source: Torvane and penetrometer measurements collected in box-core BC021).....	111
Figure 63: Shipping routes across the Pacific Ocean.	113
Figure 64 : Detailed map of the deployments done at site B4S03 with an indication of the nodule-free and nodule-rich areas sampled, and the area sampled for temporal comparison (GSRNOD17 vs. GSRNOD15A).	114
Figure 65: Monthly-averaged NPP at all sites sampled during GSRNOD17 in the GSR contract area for the period October 2014 - June 2017. The dashed vertical lines denote the timing of the previous expeditions during which these sites were sampled. Only B4S03 and B6S02 were sampled during GSRNOD15A, and only B6S02 was sampled during SO239 (JPI-O 1 campaign). For each site, NPP data were obtained 7 months prior to the first sampling expedition undertaken at that particular site.....	116
Figure 66: Bacterial biomass in function of sediment depth for all MUC samples in B4S03 during the GSRNOD15A. Note that the 5-6 and 6-7 cm samples were pooled to get a value for 5-7 cm sediment depth, and the 7-8, 8-9 and 9-10 cm samples were pooled to obtain a measurement for 7-10 cm sediment depth.....	117
Figure 67: Temporal comparison between the different expeditions (GSRNOD15A: September-October 2015, GSRNOD17: May-June 2017) within sites B4S03, From left to right : Average values of total meiofaunal abundances. Error bars denote standard deviations (right); Average values for calculated diversity: taxon richness (T), Shannon-Wiener diversity (H'), Pielou's	

evenness (J') and the expected taxon richness for a sample of 51 individuals (ET(51)). Error bars denote standard deviations (centre). Relative abundances of higher meiofaunal taxa per MUC sample (right) “Other taxa” are higher meiofauna taxa that comprised < 1 % of total meiofauna abundance.....	119
Figure 68: Average values of total macrofaunal abundances for the different expeditions (GSRNOD15A: September-October 2015, GSRNOD17: May-June 2017) within sites B4S03. Error bars denote standard deviations (left) and Relative abundances of higher macrofaunal taxa excluding typical meiofaunal groups per boxcore sample for the different expeditions (GSRNOD15A: September-October 2015, GSRNOD17: May-June 2017) within site B4S03. “Other taxa” include Acari, Brachiopoda, Chaetognatha, Gastropoda, Oligochaeta, Scaphopoda and unknown individuals (right).....	120
Figure 69: Examples of identified and measured megafauna taxa. A , radius from body centre to end of arm of Echinodermata, Asteroidea - Brisingida morphotype. B , body length (without spines) of Echinodermata, Echinoidea – Aspidodiadematidae morphotype. C , diameter of the central chamber of Porifera, Hexactinellida - Hyalonematidae morphotype. D , length of Arthropoda, Decapoda – Aristeidae morphotype. E , body length (excluding velum) of Echinodermata, Holothuroidea - Elpidiidae (Peniagone “tulip” morphotype?). F , radius from body centre to end of arm of Echinodermata, Ophiuroidea.....	121
Figure 70: Relative abundance of nematode (left) families and (right) genera in nodule surface and crevice samples (all nodules combined) in B4S03 during GSRNOD15A expedition. Other families and genera comprise those that accounted for <5 % of total (over all nodule samples of all stations) nematode abundance	122
Figure 71: Vertical profiles of nematode families (left) and genus (right) diversity in B4S03 station during GSRNOD15A. Bars denote average (SD). From top to bottom, (A) values of families richness F and genus richness G ; (B) Pielou’s evenness J' ; (C) Shannon-Wiener Diversity H' ; (D) expected Families richness for 8 individuals $EF(8)$ and expected genus richness for 6 individuals $EG(6)$	123
Figure 72: Visualization of isotopic carbon and nitrogen ratios of different macrofaunal taxa from GSRNOD17 samples. Carbon and nitrogen stable isotope ratios are noted in the delta notation (data provided to ISA by GSR in its 2017 AR, file numbers ISA-GSR_AR2018).....	124
Figure 73: Principal component analysis (PCA) of sedimentary environmental variables comparing the different macrohabitats , i.e. the nodule-free (light blue) and nodule-rich (dark blue) areas, at site B4S03 in the GSR contract area. MGS = median grain size, TOC = total organic carbon content, TN = total nitrogen content, TOC/TN = molar sediment total organic carbon-to-total nitrogen ratio, TOM = total organic matter content, SC = sediment-sorting coefficient. Eigenvectors (black lines) are superimposed	125
Figure 74: Average values of total macrofaunal abundances in the nodule-free and nodule-rich area (flat+slope) within site B4S03 in the GSR contract area sampled during GSRNOD17. Error bars denote standard deviations	125
Figure 75: Left : Average values for calculated macrofaunal diversity indices in the nodule-free and nodule-rich area (flat+slope) within site B4S03 in the GSR contract area sampled during	

GSRNOD17: taxon richness (T), Shannon-Wiener diversity (H'), Pielou's evenness (J') and the expected taxon richness for a sample of 11 individuals (ET(11)). Error bars denote standard deviations.	
Right : Relative abundances of higher macrofaunal taxa excluding typical meiofaunal groups (namely Ostracoda, Nematoda and Copepoda) per boxcore in the nodule-free and nodule-rich area (flat+slope) within site B4S03 in the GSR contract area. "Other taxa" include Acari, Brachiopoda, Chaetognatha, Gastropoda, Oligochaeta, Scaphopoda and unknown individuals.	126
Figure 76: Average values of total meiofaunal abundances in nodule-free and nodule-rich areas (flat+slope) within site B4S03 in the GSR contract area during the GSRNOD2017 campaign. Error bars denote standard deviations	126
Figure 77: Average values for the calculated diversity indices in the nodule-free and nodule-rich area (flat+slope): taxon richness (T), Shannon-Wiener diversity (H'), Pielou's evenness (J') and the expected taxon richness for a sample of 15 individuals (ET(15)) (left) and Relative abundances of higher meiofaunal taxa per MUC sample in the nodule-free and nodule-rich area (flat+slope) (right) within site B4S03 in the GSR contract area sampled during GSRNOD17. "Other taxa" are higher meiofaunal taxa that comprised < 1 % of total meiofaunal abundance. Error bars denote standard deviations.	127
Figure 78: Condensed neighbour-joining phylogenetic tree using the p-distance method of polychaete COI sequences for different contract areas in the CCFZ (indicated by the different colours). Bootstrap values (n = 500; values lower than 50 % are not displayed) are shown on the branches of the trees. Subtrees were made of the clades indicated in red ("Subtree 1") and blue ("Subtree 2"). The analysis involved 604 nucleotide sequences. All ambiguous positions were removed for each sequence pair. All sequences without taxon name were identified as "Polychaeta sp". GSR = Global Sea Mineral Resources n.v., BGR = Bundesanstalt für Geowissenschaften und Rohstoffe, IFREMER = Institut Français de Recherche pour l'Exploitation de la MER, UKSR = UK Seabed Resources, OMS = Ocean Minerals Singapore	129
Figure 79: Distribution of d10, d50 and d90 from 50 sediment samples taken from the top 0.50 m of the seafloor	133
Figure 80: surface mesh at the walls of the collector, front	134
Figure 81: Contours of sediment concentration (mg/l) along the central symmetry plane (Y=0 m), and along lateral planes (X=25, 50, 100 and 150 m)	136
Figure 82: Integrated and normalised sediment flux, as function of vertical height above the bed. Blue dashed line is same as full blue line but without flow guidance	137
Figure 83: Program area location within B4S03	138
Figure 84: Map detail of Patania II track during scenario 3 and 4	139
Figure 85: Simulated time series of the near-bed current velocity at the MiningImpact 2 program area	140
Figure 86: Location of cross section for vertical sediment contour figures	141
Figure 87: Zoom of sediment deposition [mm] map for Scenario 3 – April 2009 (see appendices for full figure and location reference area) 18 days after the initiation of MiningImpact 2	142

Figure 88: Suspended sediment concentration contours at 1 m above seabed at the end the 4 days of activity of the Patania II for scenario 1 - March 2009	143
Figure 89: Vertical cross-sectional sediment concentration contours at the end the 4 days of activity of the Patania II for scenario 1 - March 2009. Location of cross-section line is shown in Figure 86	144
Figure 90: Changes in effects of mining activities over time on faunal density and diversity (from Jones et al., 2017). Changes shown for megafaunal density (top left), macrofaunal density (top right) and meiofaunal density (bottom left) and diversity (including evenness) of megafauna and meiofauna (bottom right). If totals were not available, the value for the most abundant taxon was plotted and indicated in the legend. Values represent standardised mean differences (SMD) between faunal densities or diversities at impact sites and control sites and 95% confidence intervals. Diversity was reported as Shannon-Wiener diversity and evenness was Pielou evenness index in the studies used.....	152
Figure 91: Oxygen penetration depth and diffusive oxygen flux in sediments from the DISCOL experimental area (Peru Basin) 26 years after the disturbance and in a 5-week-old EBS track. a) Depth at which oxygen reaches concentrations below 5 μM for the different microhabitats of the disturbance, b) Diffusive oxygen flux from the bottom water into the surface sediment (Figure from Vonnahme, 2016).	154
Figure 92: A) Meiofaunal densities per core expressed in ind. 10 cm^{-2} . The line and error bars indicate mean and standard error, all data points are shown. B) Proportion of nematodes, copepods and nauplii that migrated into the added substrate. NS = no sediment addition, UnC = addition of uncontaminated sediment, C1-C4 = addition of sediment spiked with 1, 5, 10 and 20 ppm Cu.	155
Figure 93: Generic outline for cumulative effect assessment of potential future mining-related activities that may generate pressures on different ecosystem components. The conceptual scheme visualizes potential relationships between impact intensity and sensitivity that need to be assessed (modified after Tamis et al., 2017).....	157
Figure 94: Simplified Graph showing the average cyclone repartition between 1966 and 1996 and their intensity.....	159
Figure 95: Storms recorded by the NOAA Hurricane center between 1951 and 2015 for the months February, March, April and May. The red square represents GSR Contract Area. Hurricane wind categories are as follows: H5 (> 135 knots), H4 (114–135 knots), H3 (96–113 knots), H2 (83–95 knots), H1 (64–82 knots), TS (tropical or subtropical storm; 34–63 knots), TD (tropical depression; < 34 knots), and ET (extra-tropical storm, varies). Source : NOAA, Coastal Zone Management. 2017, Consulted on March 21, 2018).....	159
Figure 96: Organigram of the GSRNOD19 campaign in the CCFZ	166
Figure 97: Outline of the JPI-O MiningImpact 2 project structure.	167
Figure 98: Schematic presentation of the spatial and temporal coverage of pre- and post-impact assessment, and the restoration/recovery experiment	169

Figure 99: Map of site B4S03 showing the biological deployments, i.e. box corer (BC), multicorer (MUC) and CTD-carousel water sampler (CTD) collected during expedition GSRNOD17. Red boxes indicate the renamed stations B4S03A and B4S03B that are referred to in this section.	172
Figure 100: Average values of variables associated with the sediment granulometry in function of sediment depth in samples collected during the GSRNOD17 expedition at sampling stations B4S03A and B4S03B. Error bars denote standard deviations.	173
Figure 101: Average values of total organic matter (TOM), total organic carbon (TOC), total nitrogen (TN) and the molar sediment total organic carbon- to- nitrogen ratio (TOC/TN) in function of sediment depth in samples collected during the GSRNOD17 expedition at sampling stations B4S03A and B4S03B. Error bars denote standard deviations.	174
Figure 102: Average values of pore water nutrient concentrations (Ammonium, Nitrite, Nitrate, Silicate, Phosphate) in function of sediment depth in samples collected during the GSRNOD17 expedition at sampling stations B4S03A and B4S03B. Error bars denote standard deviations.	175
Figure 103: Principal component analysis (PCA) of samples from stations B4S03A (red) and B4S03B (blue) collected during expedition GSRNOD17 according to their sedimentary environmental variables across all depth layers (0-10 cm).	176
Figure 104: A) Total meiofaunal abundance and B) relative abundances of meiofaunal taxa in samples collected during GSRNOD17 at site B4S03A and B4S03. In A): Lines indicate mean values and error bars denote standard deviations.	176
Figure 105: A) Total macrofaunal abundance and B) relative abundances of macrofaunal taxa in samples collected during GSRNOD17 at site B4S03A and B4S03. In A): Lines indicate mean values and error bars denote standard deviations.	177
Figure 106: Examples of mechanical collectors Fenestrated ramp (cutter blade scraper) (left) and Rotating drum (right)	218
Figure 107: Hydraulic lift concept	221
Figure 108: Example of 3D scan of characteristic nodules : Side view of Nodule 3 (left); side view of Nodule 2 (centre) and Top view of Nodule 3 (right)	222
Figure 109: Flow over a nodule.	222
Figure 110: Forces on nodule in water flow	223
Figure 111: Pick-up force	223
Figure 112: "Ventouse" deployed by IFREMER during Nixonaut - 1998 (Michel Hoffert)	224
Figure 113: Analogy with cutter heads allowing geometrical variations depending on the soil : Sand cutter head on CSD Ambiorix– open design (left) and Rock cutter head on CSD Ambiorix – robust and “closed” design (right)	226
Figure 114: Different collector defining parameters (status: initial with differentiation for V_{PU} and V_{TR})	227
Figure 115: Geometrical configurations (CFD Part 1) : (1) Circular configuration (left), (2) Ellipsoid configuration (centre) and (3) Rectangular configuration (right)	228
Figure 116: Optimized nozzle shape : (1) Semi-circular (left), (2) Semi-ellipsoidal (centre) or (3) Rectangular (right)	228

Figure 117: Overview results rectangular configuration : 2D streamlines by cross section (Rectangular) (left); 3D streamlines (Rectangular) (upper right) and Jet path - Velocity magnitude (Rectangular) (lower right)	229
Figure 118: Example of Initial 2D variations for the design of the duct : Water only (left) and water with nodules (right).....	229
Figure 119: Example of CFD analysis using nodules, sediment and water in 2D (left) or in 3D for a validation simulation (left).....	230
Figure 120: Laboratory test set-up.	231
Figure 121: Lava stones handling : Lava stones being separated into different sizes (left) and 1 m ² of nodule traveling carriage (right).....	231
Figure 122: Artificial sediment: Testbed (left) and Loam pit (North-East Belgium) (right).....	232
Figure 123: Test runs with clear water	233

Tables

Table 1: Percentage of potentially minable area in B4S03	27
Table 2: Overview of the input data used during the model development.....	28
Table 3: Criteria based on intervals for the ship-based geophysical parameters in sub-zones B4S03 linked the D/I class or the Bare class from the AUV pictures. The grey colour is used for criteria that are not linked to a specific class. The column “DI/(B+DI) #Pics” indicate the strength of the criteria related to one of both classes (empirical factor). The 95% percentile for the slope will be used as upper limit intervals for the results in the highest Level of Confidence.....	29
Table 4: Results of the first model in the B4S03 sampling sub-zone	30
Table 5: Average abundance per identified interval of ship-based geophysical parameters in sub-zone B4S03 for the three Levels of Confidence. This information will be applied to “extend” the quantitative resource estimation from the AUV tracks to the southern part of zone B4. Measured Backscatter values are rounded to the nearest integer.....	31
Table 6: Surface area assessments and estimated tonnage in sub-zone B4S03. All groups are combined per LoC. The corresponding maps are presented below. The Area in term of percentage [%] is related to the area considered minable. The described tonnage remains an estimation.	32
Table 7: Averaged Results of the geochemical analyses conducted on several nodule samples from each box-core collected in B4SO3 for the MiningImpact 2 Program area (BC018, BC019, BC021 during GSRNOD15A and BC050,BC052 during GSRNOD17) and for the PRZ (BC025 during GSRNOD2015A and BC042, BC043, BC045 during GSRNOD17).....	35
Table 8: Executive overview TSTD Patania operations. HPU stands for Hydraulic Power Units. ECM stands for Earth Continuity Monitoring.....	39
Table 9: Result overview TSTD Patania.....	39
Table 10: PPV general characteristics	40
Table 11: Time required for turning process.....	50
Table 12: Monthly distribution of wind speed (m/s) for model output point 16°00’N, 125°00’W in wave model. (Data from 1992 to 2012, results based on 61368 model records) (Source: BMTARGOSS, October 2013)	53
Table 13: Side scan sonar facies classification for area B4S03. Based on the work by Lee and Kim (2004)	64
Table 14: Current statistics along the vertical profile at MOR001 location (in the MiningImpact 2 Program Area) over the deployment period (May 26, 2017 to June 03, 2017). All speeds are expressed in cm/s	71
Table 15: Current statistics along the vertical profile at MOR002 location (in the Reference Area) over the deployment period (May 28, 2017 to June 06, 2017). All speeds are expressed in cm/s	73
Table 16: Overview of short term mooring locations and terms (Metadata). UTC stands for Coordinated Universal Time.....	78

Table 17: Nutrient concentrations of the water samples collected during GSRNOD17 in the B4S03 sub-zone. Except for the deepest water samples collected at 200 m above the seabed, for which exact depths are given, water depths provided are approximated to allow for comparisons between CTD-carousel water sampler casts	88
Table 18: Particulate nitrogen (PN) and carbon (PC) data of water column samples taken during GSRNOD17 in B4S03. Except for the deepest water samples collected at 200 m above the seabed, for which exact depths are given, water depths provided are approximated to allow for comparisons between CTD casts. Because of a shortage of pre-weighed and muffled GF/F filters, no data are available for the 3-4 shallowest depths (i.e. 4, 64 and 84 m) sampled by CTD013.	89
Table 19: Percentage of the major elements analysed with ICP-AES (LOI = Loss on ignition)...	96
Table 20: Content of trace elements (in ppm) analysed with ICP-AES	97
Table 21: Estimated clay content at the top of the sediment cores (2 cm deep) based on the analysis of the oriented and glycolysed diffractograms for samples recovered in GSRNOD17A cruise. hSm/hI – Height of smectite divided by height of illite peaks. Colors used in the table correspond to the colours of Figure 50.....	98
Table 22: Pore water analysis (cations) from the BC during the GSRNOD2017 campaign. For dilution factor of 1, units are in ppm, and for dilution factors of 5, , 50 or 100, units are in ppb. Al content has been tested with a dilution factor of 5 (¹) and 50 (²) while Co content has been tested with a dilution factor of 100 (³) and 5 (⁴).....	102
Table 23: Pore water analysis (anions) from the BC during the GSRNOD2017 campaign. Depth are expressed from the surface of the sediment.....	102
Table 24: Summarized table of the geotechnical laboratory tests performed in BC samples of the area B4 during the various GSRNOD expeditions.....	109
Table 25 :Multiple sediment fractions in the sediment plume emission.....	133
Table 26: List of scenarios executed for CFD modelling of the near-field dispersion	135
Table 27: Overview of the 21-days model simulation period	137
Table 28: Overview of model scenarios	140
Table 29: Area of sediment deposition zone	142
Table 30: Storms recorded by the NOAA Hurricane center in the North Eastern Pacific Ocean in February, March, April and May between 1951 and 2015. Chronological order is applied.....	159
Table 31: Collection principle trade-off	220
Table 32: Characteristic nodule sizes.....	221
Table 33: Drag and lift characteristics	222
Table 34: Pick-up force for 3 characteristic nodules	223
Table 35: Initial variable parameters	224
Table 36: Results laboratory tests.....	233

1 Introduction

1.1 Background and rationale

This introduction is important to create the correct framework for the Legal and Technical Commission (LTC) to assess the study proposed. This includes the overall projects setup. The Environmental Impact Assessment was built up in the framework of two distinct projects:

- (1) the ProCat#2 project focusses on the technical validation of the design of a pre-prototype vehicle (PPV, provisionally named Patania II) with a nodule collector component in its actual intended environment in the Clarion-Clipperton Fracture Zone (CCFZ),
- (2) The JPI-OII MiningImpact 2 project, aims to evaluate the environmental impacts of the PPV tests and the results will inform engineering design and environmental management for future full-scale mining operations. An environmentally acceptable, socially responsible and economically viable, integrated mining plan is a priority for GSR. The first part of the JPI-O II MiningImpact 2 program will be conducted within the GSR contract area.

Additionally, a second part of the JPI-O II program will involve similar work being conducted in the CCFZ contract area of BGR, however, this part of the program is covered by a separate EIA/EIS, to be submitted to the ISA by BGR and is not further subject of this study. We note however that planned disturbance experiments and related monitoring programs are similar. After consultation with the ISA, a separate EIA/EIS was requested per Contract Area.

In the sections below we further describe the background and study objectives of the above projects.

1.2 The technical project – ProCat#2

GSR is currently working on a pre-prototype of a seabed nodule collector. The program, called ProCat, started in 2016 and will finish at the end of 2019. ProCat can be split up in 2 phases:

- ProCat#1 [2016 – 2017]: separate parallel testing of the collection mechanism and driving mechanism (Tracked Soil Testing Device (TSTD) Patania). The manoeuvrability (trafficability) test needs to be done in-situ; the collection mechanism is tested in a laboratory. Phase 1 was completed successfully in September 2017.
- ProCat#2 [2017 – end of 2019]: the knowledge acquired during the first phase will be used in this 2nd phase. Both collection mechanism and driving mechanism have to be integrated into the design of a pre-prototype seabed nodule collector. This pre-prototype will be used for in situ tests in early 2019 in the GSR contract area.

The extreme environmental conditions in the salt water environment of the deep sea, with pressures of ca. 500 bar and temperatures of ca. 2°C, necessitate the development of an extremely robust technology for the future mining of manganese nodules. The aim is to develop a system that is both economically viable and that exerts as small an impact as possible on the environment (Best Available Technology). From a technological point of view, the small-scale trial of the pre-prototype collector vehicle equipped with hydraulic collector head components ahead of any larger test activity focusses on validating its manoeuvrability, reliability and nodule

pick-up efficiency as part of an overall mining system, as well as analyzing environmental impacts, in order to environmentally validate our engineering design.

The main objective of the ProCat research program, and especially the 2nd phase, is to integrate the hydraulic collector with the tracked chassis and **develop an operating vehicle causing minimal environmental impact, hereby validating the requirements for a full-scale polymetallic nodule collecting vehicle in the actual operational environment of the CCFZ.** The in-situ trial program with the ProCat#2 vehicle concludes GSR's current development program on the mining vehicle: it focusses on the development of a collector head with an appropriate production capacity with minimal environmental impact, optimal nodule pick-up efficiency and minimal downtime. The purpose of in-situ trials with this pre-prototype is to validate the working principle of the hydraulic collector in the CCFZ, and to obtain an insight into environmental impact induced and the monitoring approach to measure this impact.

1.3 The environmental project - JPI-O MiningImpact 2

The main goal of the JPI-O MiningImpact 2 project is to reduce existing knowledge gaps and uncertainties about environmental impacts of deep-sea polymetallic nodule mining. For GSR, the aim, as part of the JPI-O program, is to gather data on operational impacts and to develop a precautionary approach for a future potential mining plan. GSR provides the opportunity to the scientific community to follow the deep sea trials, but is not part of the scientific consortium on the research vessel Sonne analyzing and monitoring the environmental impacts created by the PPV. Therefore, the project offers a transparent, objective, collaborative, adaptive and effective approach to the development and testing of mining technology. This should promote a greater understanding and comprehensive assessment of environmental effects of future mining activities, the design of fit-for-purpose monitoring programs, and industry-led standard development. The overall aims of the project are reflected in the project structure involving three work packages (WPs) (see Figure 1): WP1: address the biodiversity, connectivity and resilience of biological assemblages, WP2: the impact and behaviour of the sediment plume, WP3: benthic ecosystem functions and processes; WP4 facilitates data exchange and archival storage for the project.

Furthermore, three cross-cutting themes (CCTs) aim to ensure integration of the different aspects into a coherent work flow at sea to accomplish effective monitoring of the pre-prototype collector trial (CCT1), to synthesize scientific results into a comprehensive assessment of environmental impacts (CCT2), and to develop joint policy recommendations on risks and best practices of deep-sea mining operations (CCT3). WP5 will coordinate the project activities and communicate and disseminate project results. The complete monitoring program to be implemented is described in section 7 of the present document, Environmental management, monitoring and reporting, pp 164.

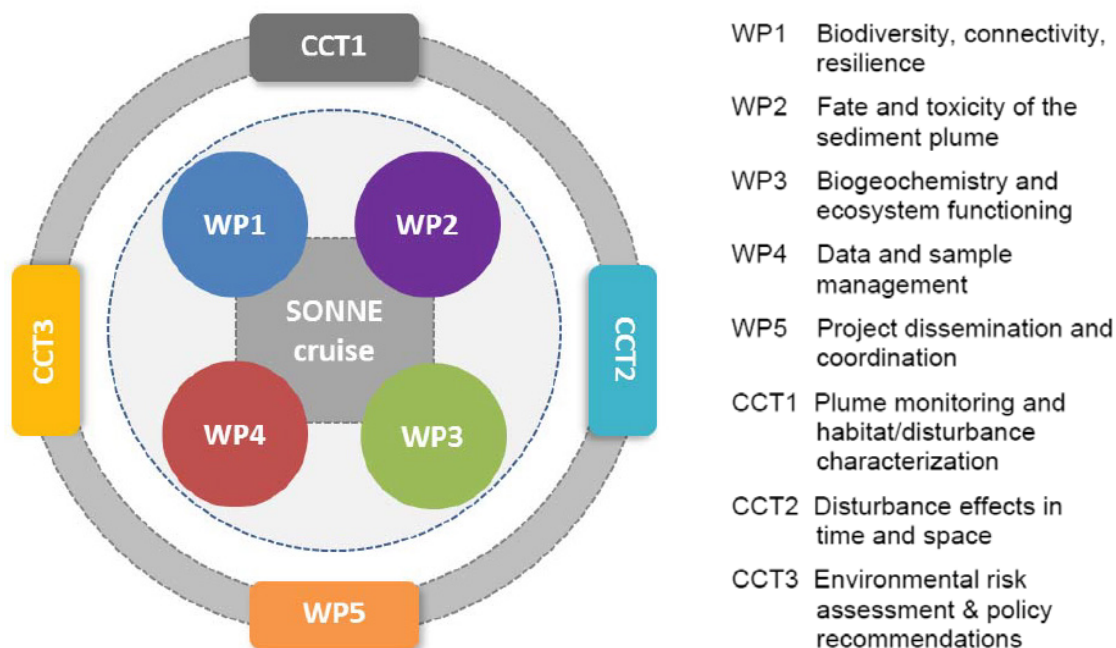


Figure 1: Structure of the JPI-O MiningImpact 2 project

1.4 This report

Aligned with the ISBA/19/LTC/8 “Recommendations for the guidance of contractors for the assessment of the possible environmental impacts arising from exploration for marine minerals in the Area,” to realise the above program an EIA is recommended to be provided. The most important elements of the EIA presented here are the description of the technology, the Patania II trial in the framework of a scientific project (JPI-O MiningImpact 2) that in itself aims at delivering new and relevant scientific information and knowledge on future deep-sea polymetallic nodule mining by (1) developing, standardizing and testing monitoring concepts and strategies, (2) investigating the short- and medium-term environmental impacts of nodule collection that in turn feed into the proposal of potential mitigation measures and the development of spatial management plans, and (3) developing sound methodologies to assess risks, benefits and uncertainties. These goals, together with the small temporal and spatial scales of the activity involved, which are spatially and temporally comparable to those of the benthic impact experiments (BIEs) carried out in the CCFZ in the eighties and nineties (JET-BIE, IOM-BIE, NOAA-BIE), show that the framework of the EIA presented here is conceptually different from that of a full-scale, long-term industrial mining activity. It is important to note that the results of the proposed activity presented here are likely to be the key inputs to the EIA for mining tests and commercial-scale mining at a later stage, which will be subject to consultation in accordance with future exploitation regulations.

There are no distinct ISA regulations and guidelines for the development of an EIA during the exploration phase. According to the Recommendations for the guidance of contractors for the assessment of the possible environmental impacts arising from exploration for marine minerals in the Area (ISBA/19/LTC/8), a contractor is recommended to submit an Environmental Impact Assessment (EIA) to the ISA when activities such as those listed in Section IV B of the above-mentioned document are undertaken. Such activities include (1) the use of systems to create artificial disturbances on the seafloor (paragraph 19(b)), and (2) if any one sampling activity by

epibenthic sled, dredge or trawl, or a similar technique, exceeds 10,000 m² (paragraph 31). The planned activities of testing a pre-prototype vehicle on an area between 0.022 km² and 100,000m² (depending on actual nodule abundance and in-situ nodule pickup and discharge efficiency) of seafloor in the GSR contract area above meet both of these recommendations for the submission of an EIA to the Secretary-General of the ISA. Under JPI-O MiningImpact 2 project the intention is to repeat this disturbance experiment in the German Contract Area. As per similar recommendation, a submission of EIA for the German Contract area will be submitted to the ISA by the Federal Institute for Geosciences and Natural Resources (BGR, in Hannover, Germany). There is no obligation for public consultation at this stage of the process. No guidelines or templates are available that go beyond Section IV C of ISBA/19/LTC/8 (information to be provided by the contractor) to guide contractors in developing EIAs during the exploration phase. This means that specific requirements regarding the environmental data to be provided and common standards for impact-related environmental surveys and monitoring plans are not available at the time of writing. In the absence of specific requirements, GSR has taken the approach to follow the best practices of other industries, such as the offshore dredging industry, where applicable.

The structure and content of this EIA report is generally based on the template for an Environmental Impact Statement as laid out in Annex V of the Draft Regulations on Exploitation of Mineral Resources in the Area of August 2017 (ISBA/23/LTC/CRP.3*) and draws on other ISA-related EIA documents (ISA Technical Study 10, 16; Clark et al., 2017), but it has some essential differences. Because environmental impacts of the pre-prototype vehicle test will be limited to the vicinity of the direct impact area of seafloor (between 0.022 and 0.1 km²) for a very short period of time (4 to 5 days per test area), socio-economic considerations are not included here. The scale of the environmental impact disturbance is limited and controlled. Also, as nodules will not be transported to the sea surface or to land, there is no commercial or industrial developmental context to this EIA (e.g., no transport or materials handling, on-site processing). Furthermore, as pre-prototype vehicle testing will cease in the test area after 4 to 5 days of activity, a relatively simple Environmental Impact Monitoring Plan is presented. In this context, it is premature to present long-term conservation goals. In the JPI-O MiningImpact 2 project the benefit for the contractor, sponsoring State (Belgium), and the wider stakeholder community consists of advances in deep sea science and contributions to environmental management knowledge related to potential future polymetallic nodule mining in the CCFZ. The Procat#2 project focusses on the technical and environmental validation of the proposed pre-prototype collection technique at the seafloor.

2 Policy, legal and administrative context

2.1 Applicable mining and environmental legislation, agreements and policies

The activity that is the subject of the present Environmental Impact Assessment (EIA) is being conducted in "the Area" as defined by the 1982 UN Convention on the Law of the Sea (LOS), i.e., on the seabed and ocean floor and subsoil thereof beyond the limits of national jurisdiction (LOS Article 1 (1.) (1)).

This is an activity of exploration for manganese nodules, and hence falls within the LOS definition of "activities in the Area" (LOS Article 1 (1.) (3)) and of "resources of the Area" (LOS Article 133(a)).

This activity is therefore governed by the LOS, its 1994 Implementing Agreement (IA) and the rules, regulations and procedures issued by the International Seabed Authority (ISA), which "is the organization through which States Parties shall, in accordance with this Part [XI of the LOS], organize and control activities in the Area, particularly with a view to administering the resources of the Area." (LOS Article 157.) Relevant appropriate national requirements by the Sponsoring States, Belgium and Germany, must also be observed.

The Environmental Impact Assessment for this activity has been carried out in accordance with the requirements set out in the legal instruments listed immediately above.

3 Project description

3.1 Purpose of the proposed project

The proposed project in the CCFZ aims to (1) test and validate in-situ the pre-prototype design and (2) evaluate environmental impacts and develop a strong, efficient environmental management and monitoring plan.

The vehicle to be deployed in 2019 is a pre-prototype. A prototype is considered as an early example, a "first of its kind". However, the 2019 vehicle is not a first of its kind: it is significantly smaller than the envisaged commercial vehicle. It is neither a scaled version of the commercial-size vehicle, as it is not possible to scale the collector head. A pre-prototype is therefore the appropriate characterization of this vehicle.

3.2 Locations

The area designated in the exploration contract signed between ISA and GSR in 2013 (the Contract) is located in the eastern part of the CCFZ. The exploration area of 76,728 km² is divided into three domains (B2, B4 and B6) located between 122 and 128° W and between 13 and 15° N (Figure 2 and Figure 3).

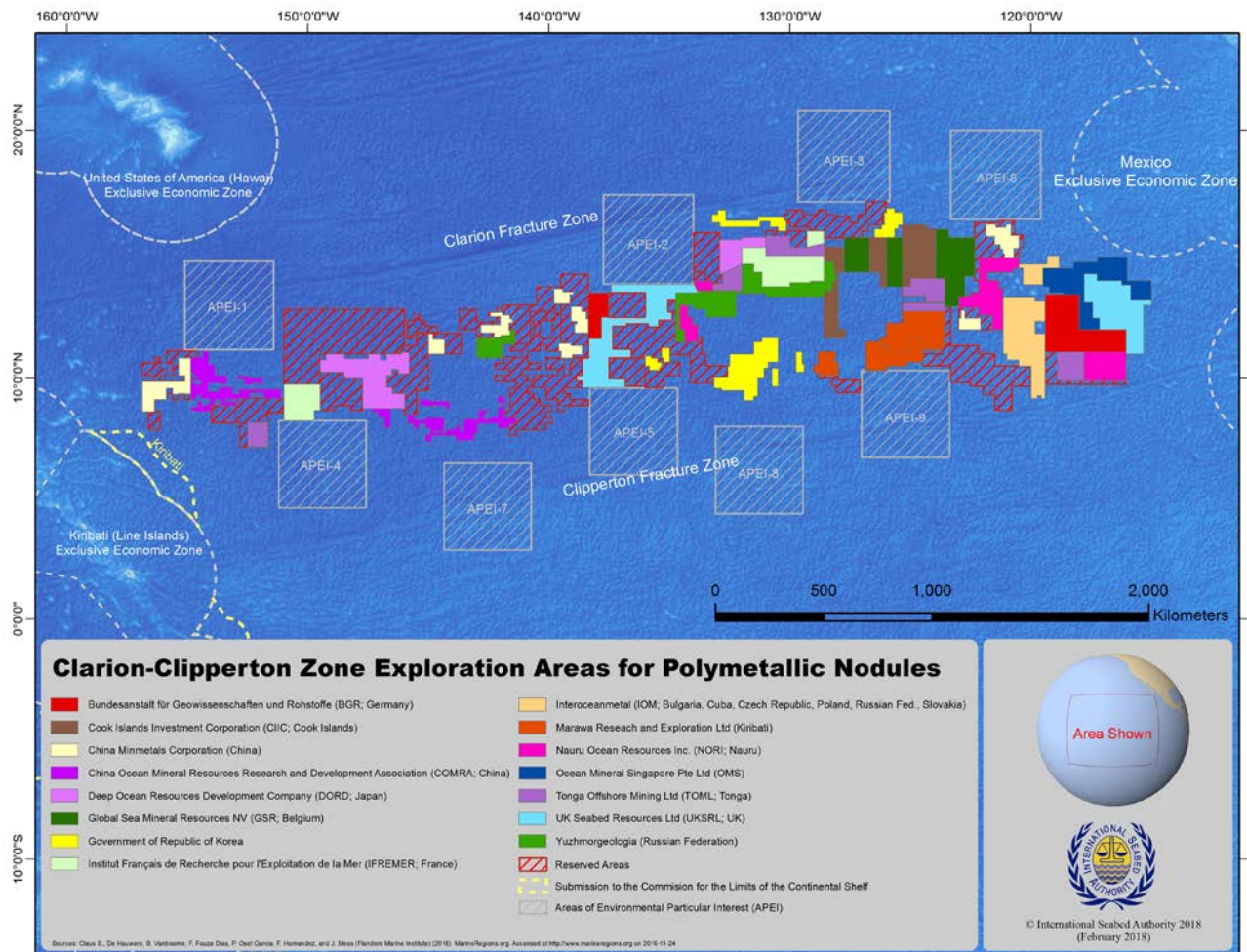


Figure 2: Location of the GSR contract area in the CCFZ. The shapes of the three domains from West to East) B2, B4 and B6 are coloured in dark green (source: International Seabed Authority, 2018., consulted on March 21, 2018)

The extent of impact is expected to be restricted based on the geographical (0.022 km² to 0.1 km²) and temporal (4 to 5 days) scales of trials of the present project. Therefore, this document focuses on only one of the subdomains, the B4 domain. This latter was chosen because the environmental baseline there is more complete and more suitable for potential future mining projects.

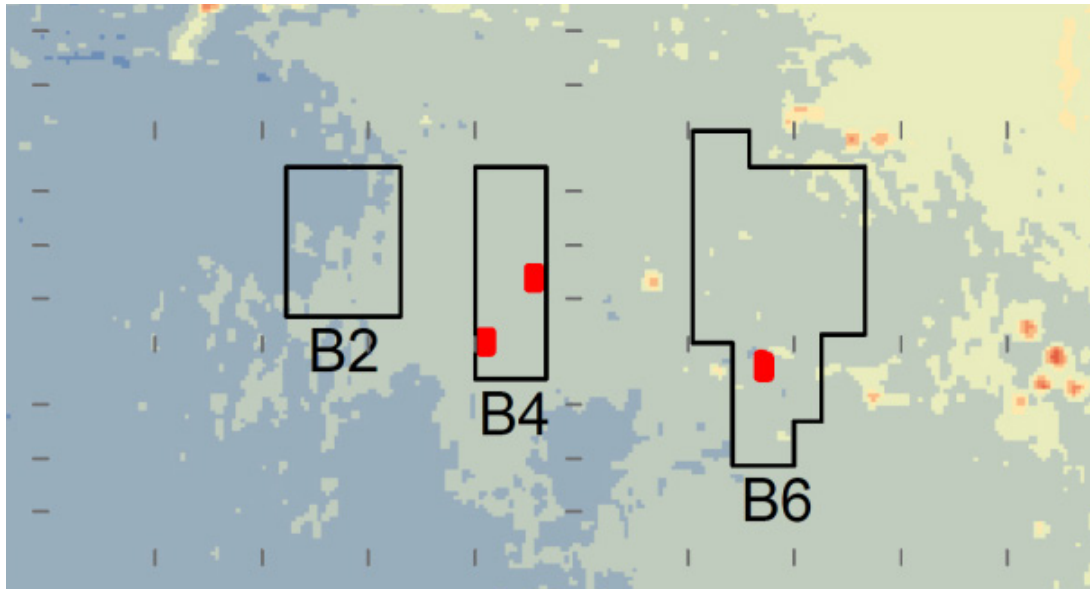


Figure 3: Close-up on the three domains of the GSR contract area and high resolution stations showed in red

In the South-West of the B4 domain, a station was established, B4S03 (Figure 3), considered as a relatively flat and nodule-rich area (high reflectivity on the backscatter data) and for which high-resolution AUV data (Remus 6000) were acquired during the GSRNOD15A campaign (data provided to ISA by GSR in its 2015, 2016 AR, file numbers ISA-GSR_AR2014, ISA-GDR2016 respectively). More biological, geological and oceanographic samples are available for this station. In the framework of the current project, this station was selected to further compare results with the 2015 seabed images (Figure 4). This high-resolution area covers 200 km² (bounded between 125.94 and 125.84 °W, 14.00 and 14.18 °N).

The potential area covered by the activity is expected to form a rectangle of ~0.022 to 0.1 km², depending on the technical choices and limitations (speed of the PPV, technical downtime) and the nodule coverage of the area. This area will be called MiningImpact 2 Program Area or Impact Reference Zone (IRZ) here after. The Impact Reference Zone (IRZ) of the PPV trial can be defined as the area that is directly affected by the trial (i.e. in which the nodules are removed). The total Impact Zone, however, is expected to cover a larger area than that directly affected by the trial, due to the development and spreading of an operational particulate plume; it theoretically extends to a distance where the impact of the plume can no longer be detected. We refer to this area as the Plume Impact Reference Zone (PIRZ).

An additional area, designated as a Control Reference Zone (RZ), is included for further critical scientific data comparison. This area has geophysical, biological and chemical features comparable to the affected area and is displayed on the next chart (ISBA/19/LTC/8, Para. 26(d)). This RZ has been located far enough (~11 km) from the activity location to avoid it being affected by operations, based on initial plume modeling work that has so far been undertaken. Again, this distance, including a safety margin over the worst case scenario, was determined through the hydrodynamic model (see 5.1.3.2.2, Sediment transport modelling, pp 133), current measurements from the GSRNOD17 campaign and other available current data for the area.

As explained in the introduction of this document, the environmental consequences of the PPV tests will be evaluated in two areas: the GSR contract area (as presented above) and the BGR contract area. For the latter, please refer to the EIA submitted by BGR to the ISA.

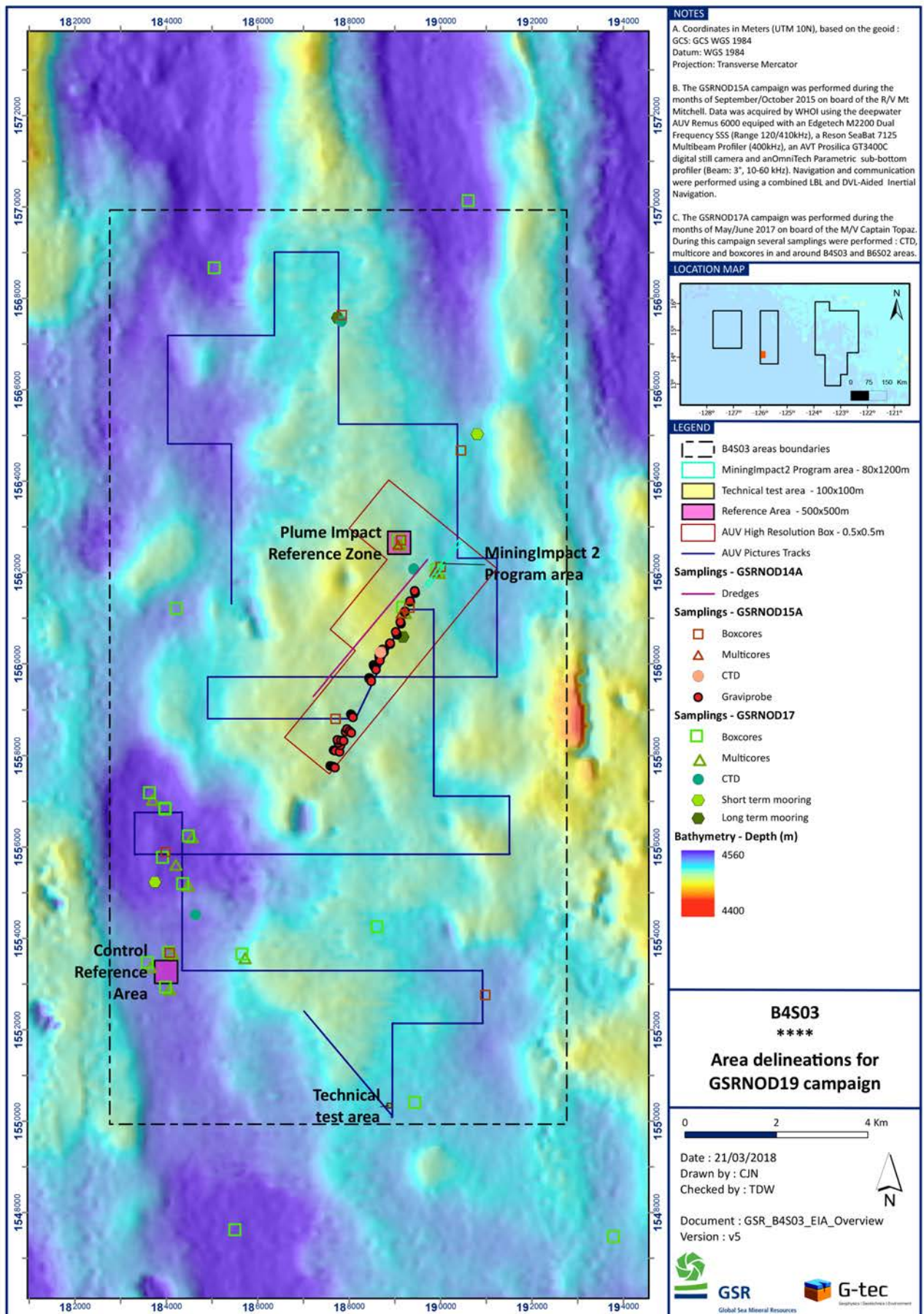


Figure 4: B4S03 sub-zone and sampling locations during expeditions of 2014, 2015 and 2017 and location of MiningImpact 2 Program area

3.3 Mineral Resource estimation

To obtain an insight into the nodule abundance in the B4 block, a model was developed by the Belgian company G-Tec, to build up a resource estimation using seafloor photogrammetry. The model is based on geophysical data acquired from the vessel (large scale / low resolution), integrated with the Automated Underwater Vehicle (AUV) pictures acquired at a limited height above the seabed (small scale / high resolution). The detailed information from the AUV track-lines was extrapolated to the above-mentioned sub-zones (B4S03, B4N01 and B6S02) and then to the full GSR contract area in order to make a resource estimation for areas lacking AUV pictures. The quality and extension of this extrapolation depended strongly on the variation in quality and resolution of the AUV pictures data set.

It must be noted that after the first in-situ trials in the GSR contract area with the Tracked Soil Testing Device (TSTD) "Patania" (as mentioned in the section Key conclusions of the in-situ trial of Patania in the CCFZ (GSRNOD17), pp37)), it was concluded that one of the main limitations of the collector from a mining point of view is the slope. Therefore, areas with a slope higher than 15% are considered in this report as technically not minable. They are marked separately on the maps (diagonal hatching) and are excluded from the area assessments.

Table 1: Percentage of potentially minable area in B4S03

	B4S03	
	Km ²	%
Potentially minable area	195.23	99.32
Considered not minable area	1.33	0.68
Total area	196.56	100

The resource estimation method was constructed gradually, through two phases/types of models. First, a qualitative nodule coverage classification model was developed (areas with many nodules vs areas with no or few nodules). Second, the nodule deposits in terms of abundances (kg/m²) were quantified, based on the results from the first classification model. Both model types were developed per zone (i.e., either B2, B4 or B6). Nodule coverage was modelled by correlating picture analysis results and indirect variables (i.e. slope, backscatter and Benthic Terrain Model (BTM)). Third, data retrieved from box-core sampling during the two GSR campaigns and the historical free-fall grabs taken during the NIXO campaigns by Centre National pour l'Exploitation des Océans (Cnexo, precursor of the Institut Français de Recherche pour l'Exploitation de la MER (IFREMER)) were used to validate the models.

To describe a complete model, different Levels of Confidence (LoC) will be used in this section, depending on the availability of data used to validate the extrapolation. Three LoC and their definition are given below:

- **LoC 3 = Highest Level of Confidence [70-100%]** with 100% inside a sub-zone and 70% on the point in the zone the furthest away from a sub-zone;
- **LoC 2 = Middle Level of Confidence [30-60%]** with 60% inside a sub-zone and 30% on the point in the zone the furthest away from a sub-zone;
- **LoC 1 = Lowest Level of Confidence [0-10%]** with 10% inside a sub-zone and 0% on the point in the zone the furthest away from a sub-zone.

Furthermore, to facilitate readability in the present section, resource estimations are summarized in tables and maps following a specific colour code.

Initially, an ordinary least-squares model (referred to in the B4 global model) was developed based on the detailed zones B4S03 and B4N01. This approach explained 50% of the variation. Nevertheless, extrapolation of this model to the entire GSR contract area proved to be an inadequate fit. As elevation range in B4N01/B4S03 ($\pm 4,400$ to $4,600$ m below surface) is smaller than in the complete GSR contract area ($\pm 3,300$ to $5,000$ m below surface), it became obvious that the absolute elevation had a significant impact on the model behaviour, resulting in an inadequate fit on the higher and lower regions of the GSR contract area.

However, this first approach enabled highlighting the important factors for nodule coverage classification. For example, **bathymetry** has proved to be very important for nodule coverage classification. Based on this first approach, a **statistical approach for nodule coverage classification** has been developed. **Histogram analysis** was used to define **general qualitative groups** (bare/intermediate/dense) and the corresponding intervals of **bathymetry** and **backscatter**. Later, the Dense/Intermediate (D/I) group was split up based on histogram analysis of the nodule coverage to obtain a quantitative classification.

An overview of the data used for the estimations in this chapter is given in Table 2.

Table 2: Overview of the input data used during the model development

Zones	B4S03		X
	B4N01		X
	B6S02		X
AUV Picture	AUV Height	5m	X
		7m	X
		10m	X
	Picture Processing - Phase 1	D/I	X
		Bare	X
	Picture Processing - Phase 2	Nodule Coverage	X
Geophysical data	Slope		X
	Backscatter		X
	Bathymetry		X
	BTM-class		X

offers a visualization of the criteria created for the various combinations of large-scale geophysical data (BTM, slope, bathymetry and backscatter) and the number of AUV pictures corresponding to each of those criteria.

Table 3: Criteria based on intervals for the ship-based geophysical parameters in sub-zones B4S03 linked the D/I class or the Bare class from the AUV pictures. The grey colour is used for criteria that are not linked to a specific class. The column “DI/(B+DI) #Pics” indicate the strength of the criteria related to one of both classes (empirical factor). The 95% percentile for the slope will be used as upper limit intervals for the results in the highest Level of Confidence

	Ship-based Geophysical data				AUV pictures						
	BTM	Slope	Bathymetry	Backscatter (3)	BARE		D/I		DI/ (B+DI) #Pics [%]	DI/ (B+DI) %Pics [%]	Per. 95% Slope
	[-]	[%]	[m]	[dB]	# Pics	%	# Pics	%			
1a(1)	[9;10]	[0;10%]	[4450;4520[[-25;-21[-	-	-	-	-	-	-
1b				[-21;-10[0	0	21241	88.9	100	100	5.7
2a			[4520;4550[[-21;-15[171	10.9	1279	5.4	88.2	32.9	5
2b			[4520;4560[[-15;-10[20	1.3	732	3.1	97.3	70.5	5.2
3a(1)		[0;5%]	[4520;4560[[-∞;-21[-	-	-	-	-	-	
3b(2)		[0;10%]			127	8.1	0	0	0	0	5.7
4		[0;10%]	[4560;4580[[-18;-10[12	0.8	0	0	0	0	-
5a		[0;5%]	[4560;4580[[-∞;-18[695	44.4	6	0	0.9	0.1	4.2
5b]5;10%]			28	1.8	0	0	0	0	5.2
6a(2)		[0;10%]	[4580;4600[[-∞;-16[377	24.1	0	0	0	0	3.6
6b(1)			[-20;-14[-	-	-	-	-	-	-	
Total # AUV Pictures after pre-filtering which apply to one of criteria 1-7					1430	91.4	23258	97.3			
Total # AUV Pictures after pre-filtering					1564	100	23897	100			
(1) These criteria will only be applied to zone B4N01 and not to zone B4S03 or the complete GSR concession area. (2) These criteria will only be applied to zone B4S03 and not to zone B4N01 or the complete GSR concession area. (3) Backscatter values have been rounded to the nearest integer for all AUV pictures in order to determine if falling in the interval											

The table below depicts the results of the first model (Table 4). The surface estimated to be abundantly covered by nodules, with the highest level of confidence, reaches 143.38 km² in B4S03, i.e., 73 % of the minable area.

Table 4: Results of the first model in the B4S03 sampling sub-zone

Classification	Level of confidence	Sub-zone B4S03	
		Area	% of minable area
		[km ²]	
Dense/Intermediate	3	143.38	73.4
Dense/Intermediate	2	25.57	13.1
Dense/Intermediate	1	8.21	4.2
Bare	3	6	3.1
Bare	2	1.4	0.7
Bare	1	1.83	0.9
Unidentified	-	8.84	4.5
Minaable area	-	195.23	100
Not minable area	-	1.33	-
Total classified area	-	196.56	-

Based on the formula of Piper (M. Hoffert, personal communication), a quantitative abundance value [kg/m²] can be estimated from the AUV pictures (once nodule presence is described from the pictures). The equation relates abundance to **nodule coverage** and **average nodule diameter**. M. Hoffert adapted this formula to compensate for the fact that the nodules in situ are partly buried or covered with sediment. The **burial ratio (BR)** is introduced and is calculated by comparing the in situ box-core pictures with the nodule measurements on deck from these same box-cores in the GSR contract area.

$$Abundance = \frac{2}{3} \times f \times \rho \times BR \times nodcov \times \emptyset_{avg}$$

- Where -
- f represents nodule flatness (considered as constant, 0.63)
 - ρ represents the nodule density (considered as constant, 1.99 g/cm³)
 - BR represents the burial ratio (estimated at 1.24 in B4 area)
 - $nodcov$ represents the nodule coverage per picture (measured from AUV pictures)
 - \emptyset_{avg} represents the average nodule diameter (measured from AUV pictures)

The quantitative results of the second model are presented in Table 5. The estimated nodule abundance is indeed variable in the sampling area (visible on Figure 5 and Figure 6), ranging between 12 and 24 kg/m² (Table 5). Taking into account the areas already presented as abundantly covered by nodules, the expected tonnage was calculated for the B4S03 sub-zone (Table 6).

Table 5: Average abundance per identified interval of ship-based geophysical parameters in sub-zone B4S03 for the three Levels of Confidence. This information will be applied to “extend” the quantitative resource estimation from the AUV tracks to the southern part of zone B4. Measured Backscatter values are rounded to the nearest integer.

Group	SHIP-BASED GEOPHYSICAL DATA				AUV PICTURES
					Average Abundance
	Slope	BTM	Bathymetry	Backscatter	[kg/m ²]
	[%]	[-]	[m]	[dB]	
B4S03-LoC3-G1	[0;5]	[9;10]	[4450;4480[[-16;-9[24.0
B4S03-LoC2-G1]5;15]	[1;10] U]12;13]			23.7
B4S03-LoC3-G2	[0;5]	[9;10]	[4480;4500[[-19;-9[23.8
B4S03-LoC2-G2]5;15]	[1;10] U]12;13]			22.9
B4S03-LoC3-G3	[0;5]	[9;10]	[4500;4515[[-17;-9[20.4
B4S03-LoC2-G3]5;15]	[1;10] U]12;13]			19.9
B4S03-LoC3-G4	[0;5]	[9;10]	[4518;4523[[-18;-13[U [-12;-10[16.7
B4S03-LoC2-G4]5;15]	[1;10] U]12;13]			N/A
B4S03-LoC3-G5	[0;5]	[9;10]	[4532;4550[[-20;-13[12.5
B4S03-LoC2-G5]5;15]	[1;10] U]12;13]			N/A
B4S03-LoC3-G6	[0;5]	[9;10]	[4500;4515[[-20;-17[19.3
			[4515;4518[[-18;-13[U [-12;-10[
B4S03-LoC2-G6]5;15]	[1;10] U]12;13]	[4523;4532[[-18;-11[18.5
B4S03-LoC1-G1	[0;15]	[1;10] U]12;13]	< 4515	≥ (-16) OR Areas qualitatively classified as D/I but not quantified in B4S03-LoC3 or B4S03-LoC2	19.0
B4S03-LoC1-G2			[4515;4532]		16.0
B4S03-LoC1-G3			> 4532		12.0

Table 6: Surface area assessments and estimated tonnage in sub-zone B4S03. All groups are combined per LoC. The corresponding maps are presented below. The Area in term of percentage [%] is related to the area considered minable. The described tonnage remains an estimation.

	Level of Confidence	Sub-zone B4S03		
		Area [km²]	Area [%]	Tonnage [mT]
Quantitative	LoC3	119.92	61.42	2,469,542
	LoC2	24.03	12.31	502.775
	LoC1	33.35	17.08	480.42
	LoC3 + LoC2 + LoC1	177.30	90.82	3,452,737
	D/I area (Qualitative)	177.20	90.76	N/A
Qualitative	LoC3 (Bare)	6.00	3.1	N/A
	LoC2 (Bare)	1.40	0.7	N/A
	LoC1 (Bare)	1.83	0.9	N/A
	Bare area	9.23	4.7	N/A
Potentially minable area		195.23	100.00	

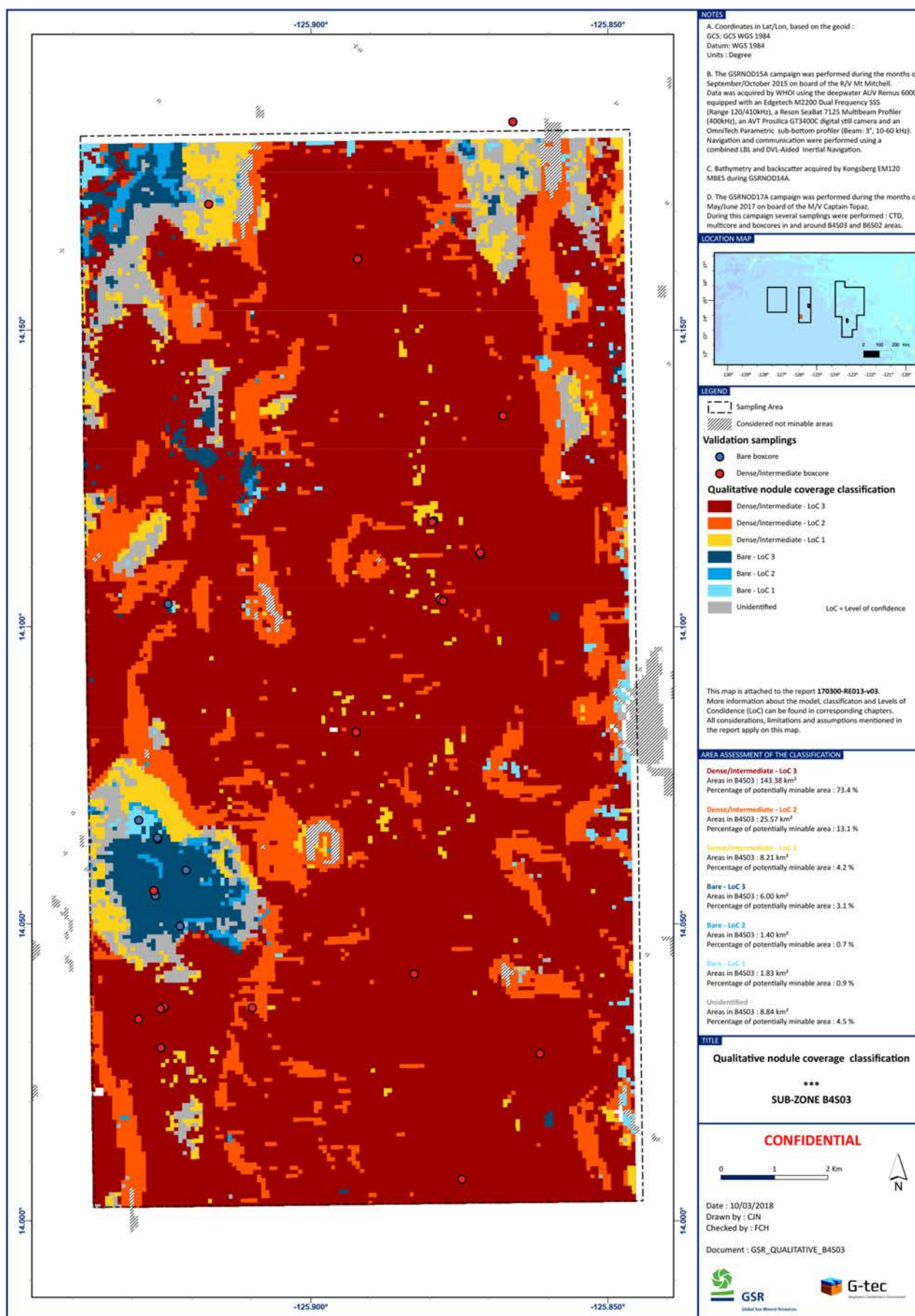


Figure 5 : Qualitative nodule coverage classification in the sub-zone B4S03 and its vicinity

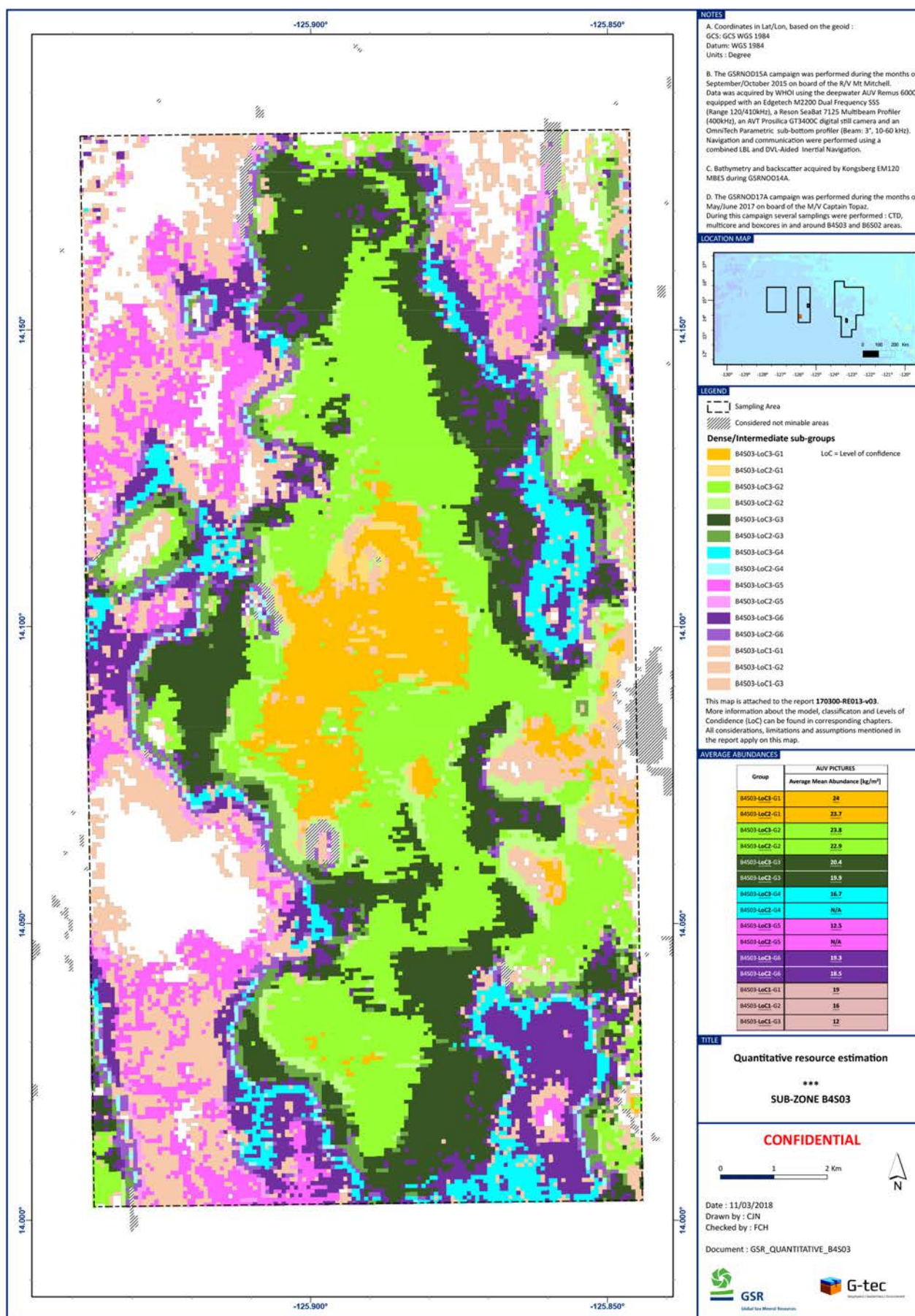


Figure 6: Quantitative nodule coverage map of polymetallic nodules in area B4S03 and its vicinity

3.3.1 Geochemical analyses

Preliminary results of the geochemical analysis conducted on nodules from the MiningImpact 2 Program Area and from the Control Reference Area (PRZ) during GSRNOD2015A and GSRNOD2017 expeditions are displayed on Table 7 below. The major elements found in nodules (Mn, Fe, Ni, Cu, Co) are present, at nearly constant concentrations between boxcore samples. Nodules of the B4S03 sub-zone are mainly of the diagenetic type (Mn/Fe ratio > 5) following the classification of Halbach et al. (1988). As a comparison, the statistical average of elemental analysis for all the nodules samples collected in the sub-zone B4S03 is also presented.

Table 7: Averaged Results of the geochemical analyses conducted on several nodule samples from each box-core collected in B4S03 for the MiningImpact 2 Program area (BC018, BC019, BC021 during GSRNOD15A and BC050, BC052 during GSRNOD17) and for the PRZ (BC025 during GSRNOD2015A and BC042, BC043, BC045 during GSRNOD17)

		BC-018 (15)	BC-019 (15)	BC-021 (15)	BC-025 (15)	BC-042 (17)	BC-043 (17)	BC-045 (17)	BC-050 (17)	BC-052 (17)	Average B4-S03
Major element (%)	Mn	29.2	29.6	30.4	30	30.3	29	29.9	29.6	30.2	29.7
	Fe	5.5	5.3	5.2	5	4.9	5.4	5.8	5.6	5.7	5.4
	Ni	1.45	1.47	1.5	1.48	1.33	1.29	1.3	1.46	1.19	1.39
	Cu	1.15	1.13	1.16	1.2	1.17	1.17	1.23	1.16	1.09	1.15
	Co	0.22	0.22	0.21	0.21	0.21	0.23	0.25	0.24	0.25	0.23
	Mn/Fe	5.4	5.6	5.9	6	6.2	5.3	5.2	5.3	5.3	5.5
	Ni + Cu + Co	2.82	2.82	2.87	2.89	2.71	2.69	2.78	2.86	2.53	2.76
	Si	7.3	7	6.7	7.3	/	/	/	/	/	7.2
	Al	2.6	2.5	2.4	2.8	2.8	2.8	2.7	2.8	2.5	2.7
	Na	2.2	2.2	2.1	2.2	2.2	2.3	2.3	2.3	2.2	2.2
	Mg	1.8	1.8	1.8	1.9	1.8	1.8	1.8	1.8	1.7	1.8
	Ca	1.5	1.5	1.4	1.4	1.4	1.6	1.5	1.5	1.4	1.5
	K	1.1	1	1	1.1	1.2	1.2	1.1	1.1	1.1	1.1
	Ba	0.3	0.3	0.2	0.3	0.3	0.3	0.3	0.3	0.3	0.3
	Ti	0.3	0.3	0.3	0.3	0.3	0.3	0.3	0.3	0.3	0.3
	P	0.14	0.14	0.14	0.13	0.13	0.14	0.14	0.14	0.14	0.14
	Zn	0.14	0.15	0.16	0.15	0.14	0.14	0.15	0.16	0.14	0.15
	S	0.09	0.1	0.08	0.08	0.1	0.11	0.1	0.09	0.1	0.1
	Mo	0.05	0.05	0.05	0.05	0.05	0.06	0.06	0.05	0.06	0.06
	Sr	0.06	0.07	0.06	0.06	0.06	0.06	0.06	0.06	0.06	0.06
	Pb	0.04	0.04	0.04	0.04	0.04	0.04	0.04	0.05	0.04	0.04
	V	0.05	0.05	0.05	0.04	0.04	0.04	0.05	0.04	0.05	0.04
	Zr	0.03	0.03	0.03	0.03	0.03	0.03	0.03	0.03	0.03	0.03
	Si/Al	2.8	2.8	2.8	2.6	/	/	/	/	/	2.8
Rare-earth element (ppm)	Y	84	88	82	74	74	76	77	79	80	80
	La	110	115	108	100	94	94	92	98	96	102
	Ce	350	358	327	326	311	314	292	322	324	329
	Pr	38	39	37	32	31	30	29	31	29	32
	Nd	167	173	161	140	128	123	120	126	121	139
	Sm	42	44	41	36	32	31	29	32	32	35
	Eu	9	10	9	8	7	7	7	7	7	8
	Gd	34	36	34	29	28	27	27	28	28	30
	Tb	5	6	5	5	4	4	4	4	4	5
	Dy	29	30	28	24	24	23	23	24	24	25
	Ho	5	6	5	4	5	5	4	5	5	5
	Er	14	15	14	12	12	12	12	12	12	13
	Tm	2	2	2	2	2	2	2	2	2	2
	Yb	15	15	14	12	11	11	11	12	12	13
	Lu	2	2	2	2	2	2	2	2	2	2
	total TR	906	937	868	804	764	761	731	783	777	819

		BC-018 (15)	BC-019 (15)	BC-021 (15)	BC-025 (15)	BC-042 (17)	BC-043 (17)	BC-045 (17)	BC-050 (17)	BC-052 (17)	Average B4-SO3
Traces (ppm)	Ag	0.03	0.03	0.02	0.03	0.01	0.01	0.01	0.01	0.01	0.02
	As	70	72	67	65	36	70	72	73	74	69
	Au	0.004	0.001	0.002	0.001	0.005	0.004	0.001	0.004	0.005	0.003
	Be	2	2	2	2	2	2	2	2	2	2
	Bi	5	5	5	5	5	6	5	6	5	5
	Cd	19	21	20	21	21	22	22	20	23	21
	Cr	20	20	20	15	25	25	19	19	19	20
	Cs	2	2	2	2	2	2	2	2	2	2
	Ga	37	37	35	36	52	50	49	51	48	44
	Ge	0.4	0.4	0.4	0.5	0.4	0.4	0.4	0.4	0.4	0.4
	Hf	4	4	4	4	4	4	4	4	4	4
	In	0.1	0.1	0.1	0.1	0.1	0.1	0.1	0.1	0.1	0.1
	Li	115	166	172	147	157	135	136	135	152	142
	Nb	22	23	21	20	19	20	19	21	19	20
	Pd	0.004	0.003	0.004	0.005	0.007	0.007	0.008	0.009	0.008	0.006
	Pt	0.1	0.1	0.1	0.1	0.1	0.1	0.1	0.1	0.1	0.1
	Rb	31	30	27	31	31	30	28	28	28	29
	Re	< 0,002	< 0,002	< 0,002	< 0,002	0.002	< 0,002	< 0,002	0.002	< 0,002	0.002
	Sb	54	56	54	55	49	52	51	53	52	53
	Sc	11	10	9	11	10	11	10	11	10	11
	Se	7	5	5	6	1	1	1	1	1	3
	Sn	2	2	2	1	2	2	2	2	2	2
	Ta	0.4	0.3	0.3	0.3	0.4	0.4	0.4	0.3	0.3	0.3
	Te	4	4	3	4	3	4	3	4	4	4
	Th	21	22	20	20	20	20	18	20	20	20
	Tl	182	220	219	228	178	179	171	200	122	185
	U	4	4	4	4	4	4	4	4	4	4
	W	57	58	56	54	55	55	59	54	53	56

3.4 Patania II - description and design

This chapter includes information recommended according to ISBA/19/LTC/8 (Section C, 26, *Information to be provided by the contractor*) and describes the technical development and equipment design of the pre-prototype vehicle (PPV) Patania II.

3.4.1 Background – Patania

The current design of the PPV is based on the results and the lessons learned during the first phase of the ProCat program. During this stage, the Tracked Soil Testing Device (TSTD) Patania was developed and successfully tested in-situ on GSR ground. The Patania was an experimental ‘Soil Testing Device’: it did not collect any nodules or soil samples. The main objective of the TSTD Patania was to acquire in-situ terramechanical parameters that would enable GSR to develop an optimized design of the pre-prototype Patania II.

3.4.1.1 Key conclusions of the in-situ trial of Patania in the CCFZ (GSRNOD17)

The construction of the Patania started in October 2016. By the end of February 2017, the Factory Acceptance Test (FAT) tests and subsequent mud and wet trials were completed. In June 2017, during the GSRNOD17 campaign in the CCFZ, in-situ experiments were conducted.

The tests with the TSTD Patania had the following objectives:

1. Evaluation of the overall performance of a tracked vehicle on the seabed of the CCFZ.
2. Speed variances and effect on traction and slippage
3. In-situ pressure-sinkage relationship (terramechanical test)
4. Ex-situ shear stress - shear displacement relationships (terramechanical test)
5. In-situ thrust – slip relationship (terramechanical test)
6. Quantitative and qualitative measurements of sediment dispersion generated by the tracks (environmental)
7. Qualitative measurements of sediment dispersion generated by a horizontal water flow parallel to the seabed (environmental)



Figure 7: Launching of TSTD (20/01/2017) (top) and mud trials in Belgium (February 2017) (bottom)

3.4.1.1.1 Dive results

It took some effort to reach to the seabed. Dive PAT08 was an equipment check after heading back to port because of the faulty fibre-optic connector on the ePOD of the Patania. PAT09 was the first successful dive on the seabed.

An executive overview of the different dives is given in the table below (Table 8):

Table 8: Executive overview TSTD Patania operations. HPU stands for Hydraulic Power Units. ECM stands for Earth Continuity Monitoring

Dive	Date	Area	Comments (on failure)	Max depth
PAT01	5/25/2017	B4S03	Not compensated hydraulic valve & water ingress Bevameter 1	146 m
PAT02	5/28/2017	B4S03	Shuttering counterbalance valves on winch & shifting winch drum	650 m
PAT03	5/30/2017	B4S03	Wire length payout error resulting in damaged umbilical during pick-up	650 m
PAT04	5/31/2017	B4S03	Compensator failure shutdown HPU; not able to restart ECM trip	2833 m
PAT05	6/4/2017	B4S03	Compensator failure	97 m
PAT06	6/5/2017	B4S03	ECM trip of the POD (4078m) – shut down HPU Communication failure	4423 m
PAT07	6/8/2017	B6	Communication failure: fiber optic connection failure Transit to San Diego	1729 m
PAT08	6/17/2017	N/A	Equipment check outside EEZ US on transit back to B6 – no touchdown	4050 m
PAT09	6/19/2017	B6	Successful dive – Focus on trafficability (speed and traction)	4115 m
PAT10	6/21/2017	B6S02	Successful dive – Focus on terramechanics (Pressure sinkage) & slope (15%)	4552 m
PAT11	6/23/2017	B6S02	Successful dive – Focus on terramechanics & water pump test	4563 m
PAT12	6/24/2017	B6S02	Successful dive – Focus on turbidity (plume test) & terramechanics	4571 m
PAT13	6/26/2017	B6S02	Promotional dive Patania with covers	15 m

3.4.1.1.2 Main results

An overview of the most important results is given in the table below (Table 9):

Table 9: Result overview TSTD Patania

Parameter	Measured Value	Unit
Maximum speed driven on seabed	0.65	[m/s]
Total distance travelled on the seabed	14.5	[km]
Total time on the seabed	>30	[hours]
Maximum slope [PAT10]	>15	[%]
Number of in-situ plate measurements (sets)	23	[-]
Shear strength – shear displacement measurements (ex-situ samples)	42	[-]

Two video snapshots recorded by the cameras of the TSTD Patania are shown below (Figure 8).



Figure 8: TSTD Patania on the seabed (GSRNOD17)

3.4.2 Patania II and nodule collection methodology

ProCat2 will deliver the PPV, Patania II, and continues the development of Patania I by adding a collector suction head for testing the pickup collection methodology.

The hydraulic lift concept, although tested in the 1970s by the Ocean Management Inc. (OMI) consortium, has fundamental engineering uncertainties:

- (1) How great is the pick-up efficiency and how much energy (and thus water) is required to reach that efficiency?
- (2) How is the seabed affected by the hydraulic lift collector; what is the expected depth of penetration?

In order to answer these questions, GSR conducted an extensive series of laboratory tests in collaboration with the Flanders Hydraulic Research Laboratory in Antwerp. The design of the tested collector head was based on a pre-design study using Computational Fluid Dynamics (CFD). The set-up of the trials and the results are set out in the Appendices to the present document (see 12.1.3, Pre-design study : Optimized collector design, pp. 221). Those results were used as a baseline for the design of the equipment presented below. The pre-prototype vehicle Patania II is an active pick-up system which is broken down into four major subsystems:

- (1) **Nodule collection system:** the nodule collection system consists of the collector head, the jet water pumps and all sensors to monitor the suction process. The design of the collector head is based on the results obtained from the laboratory tests.
- (2) **Propulsion system:** a two-track system will be used for the propulsion system. The terramechanical values measured in-situ with the TSTD Patania were used for the design of the propulsion system.
- (3) **Nodule separation and discharge system:** there will not be a riser to pump the collected nodules to the surface vessel. Hence, a dumping system is incorporated into the design of the vehicle.
- (4) **Vehicle systems:** this part comprises all components for the proper functioning of the vehicle. This includes hydraulic power units (HPUs), telemetry, buoyancy, etc.

These 4 different subcomponents are described in more detail below. The general characteristics are provided in Table 10 below and a conceptual sketch of the PPV with all its major components is shown on Figure 9.

Table 10: PPV general characteristics. O.a. stands for over all.

Description	Nominal value	Unit	Comment
Vehicle physical properties			
Vehicle length o.a.	12	[m]	Including "selfie sticks"
Vehicle width o.a.	4.7	[m]	
Vehicle height o.a.	4.5	[m]	
Vehicle Weight in air	35	[mT]	
Vehicle weight submerged	15	[mT]	
Vehicle operational properties			
Vehicle nominal speed	0.5	[m/s]	
Vehicle maximum speed	1	[m/s]	

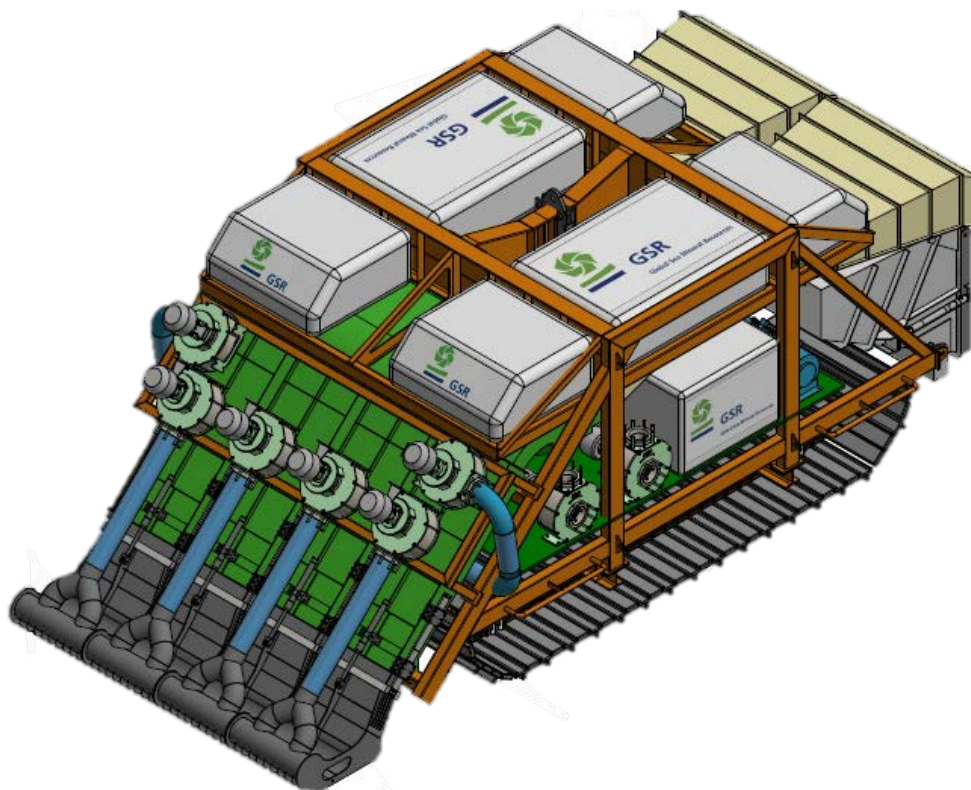


Figure 9: Conceptual sketch of the PPV

3.4.2.1 Nodule collection methodology

Results from laboratory tests show four main control parameters as determining the collection process: (1) the pick-up jet velocity (v_{PU}); (2) the transport jet velocity (v_{TR}); (3) the height of the collector above the seabed (H_{jet}) and (4) the collector's forward speed (v). Patania II was designed so that these parameters can vary during the in-situ collection process.

Figure 10 shows the most important parts of the nodule collector head. A commercial-scale collector system is envisaged to comprise several of these units. For in-situ tests in 2019, the Pre-prototype vehicle Patania II will be equipped with four of these modules. Every module is 1m wide, and sets the total width of the PPV (4 m).

The nodule collection system is based on the results of the laboratory tests as described in the appendix (see 12.1.4, Laboratory tests with the hydraulic collector, pp. 230). One of the main conclusions of the laboratory tests is the importance of the height of the collector above the seabed. Therefore an important control parameter to be taken into account is H_{jet} .

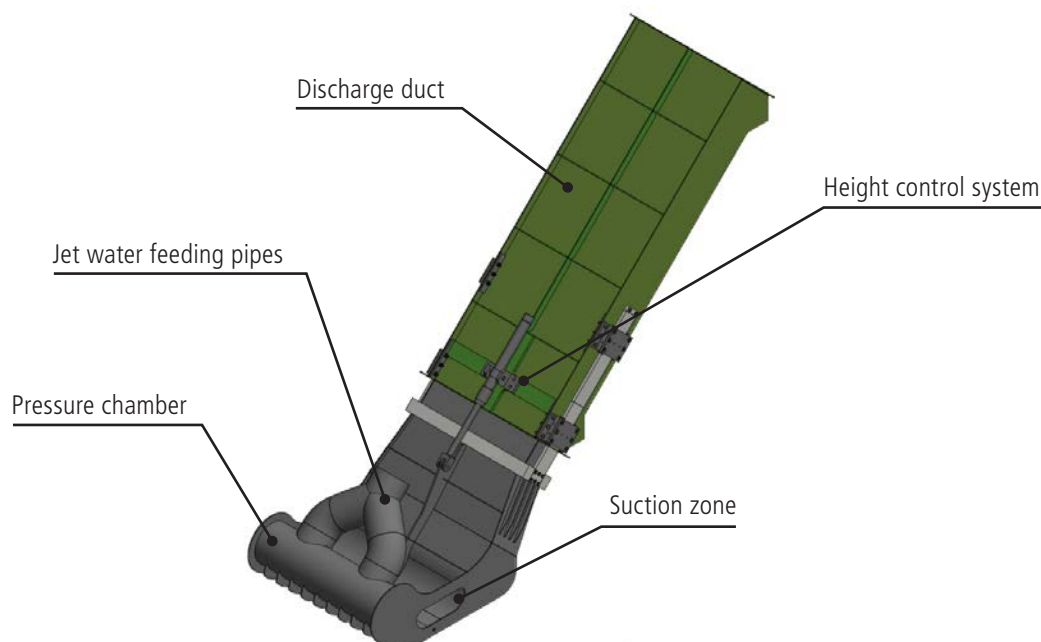


Figure 10: Nodule collector head

3.4.2.1.1 Collector Height control and penetration depth

Two different height-reading systems will be placed in front of the collector head. The primary height measurement will use altimeters. Because turbidity might affect the readings, an additional mechanical back-up system will be installed as well.

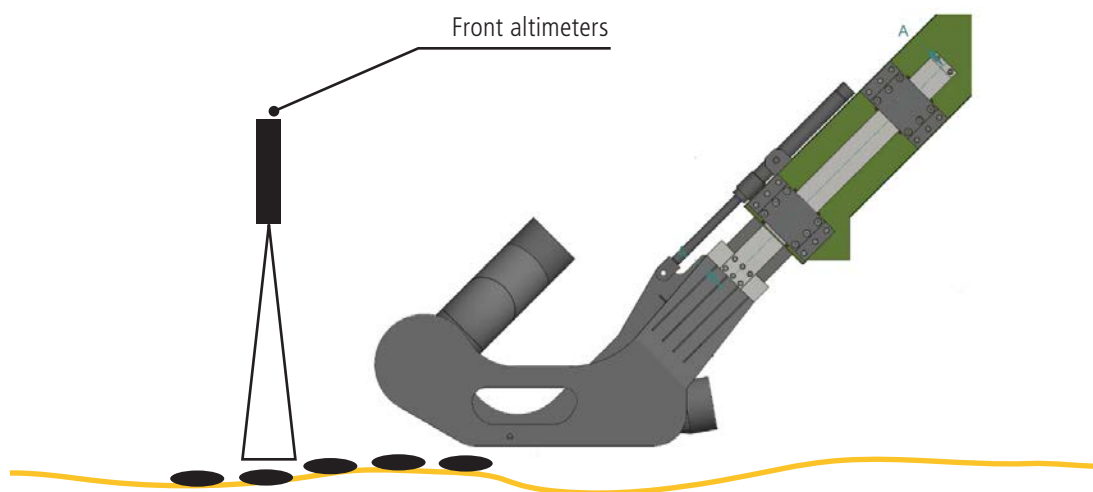


Figure 11: Collector head height control

Every head is equipped with its own altimeter, returning the distance to the highest point within its measurement beam. The system processes these measurements and translates them to a certain stroke of the hydraulic piston on top of the discharge duct. Only the forward part is translated up and down. This procedure is automated.

The in-situ penetration depth into the seabed, i.e., the depth of influence, is difficult to predict. As mentioned in the previous section, the laboratory tests with the hydraulic collector were not

designed to validate a figure. At the time of writing, an assumption is made that the depth of influence of the water jets varies between $50 \text{ mm} < \text{depth of influence} < 150 \text{ mm}$. The maximum depth depends mainly on the thickness of the unconsolidated top layer of the seabed.

3.4.2.1.2 Flow velocities

Six identical jet water pumps are mounted on the collector: four pumps are used for the pick-up jet and two for the transport jet. A single-line diagram of the pump lay-out is shown in Figure 12. Alternatively, the velocities of the pick-up and transport jets will be controlled by the revolution per minute of the jet water pumps: by varying the rotation per minute (rpm) of the pump, the flow will vary accordingly and as the cross-section remains the same, the jet velocity will change. The nominal working point of the pumps is $600 \text{ m}^3/\text{h}$ at a height of 10 m .

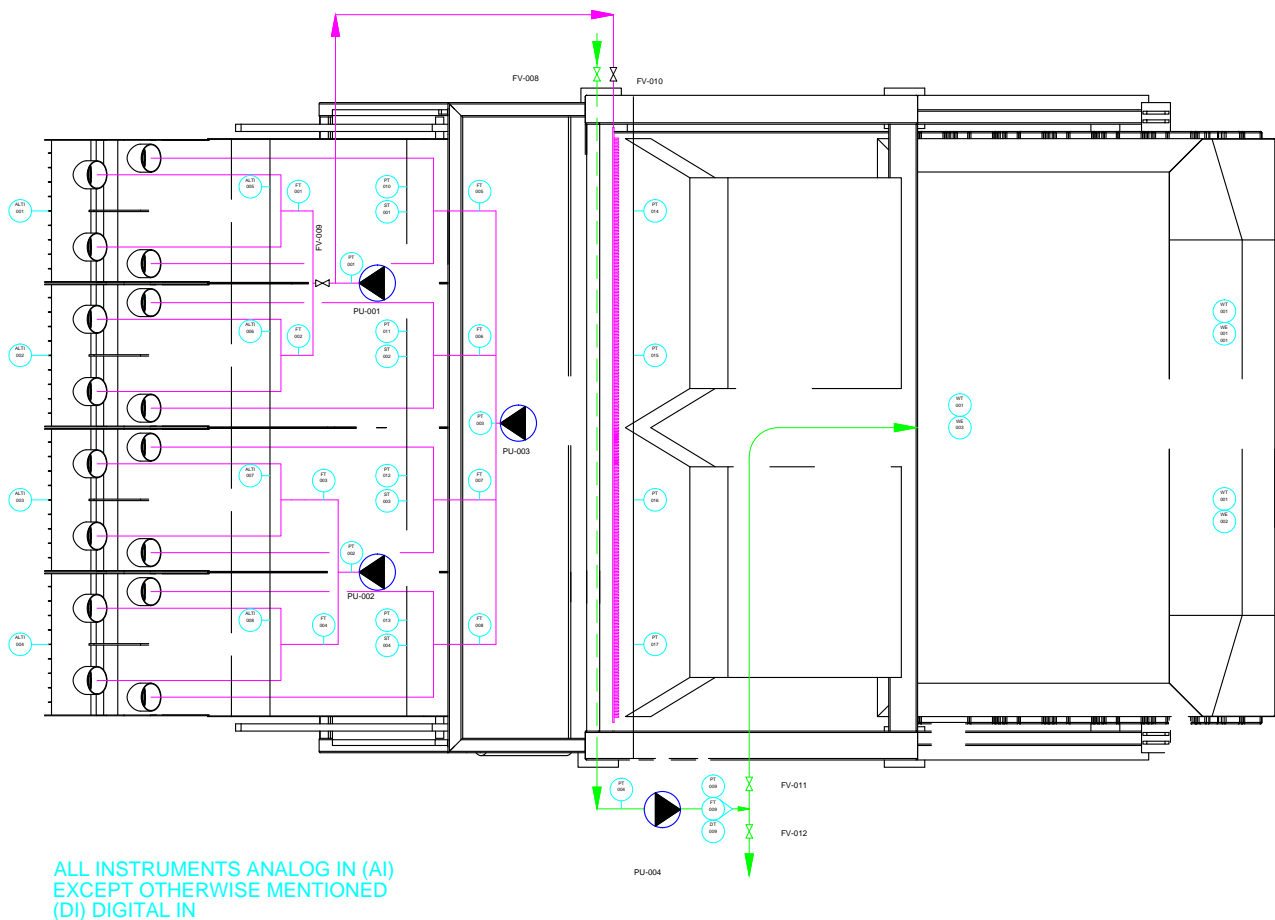


Figure 12: Collector pump lay-out

3.4.2.1.3 Nodule separation and discharge system

After being collected, the nodules move up the discharge duct and are deposited in a hopper at the end of the duct. Gravity is used to **separate the nodules from the water/sediment mixture**. The heavier nodules inside the mixture fall by gravity into the hopper. At the opposite side from the duct inlet in the hopper is a grate. The majority of the water flow used to transport the nodules up the duct passes through the grate towards the diffuser-exhaust. The grate prevents the smaller and fragmented nodules entrained by the inlet flow from going to the diffuser-exhaust. The nodules are subsequently collected at a centralized discharge pipe that pumps the nodules towards the nodule container at the back of the vehicle.

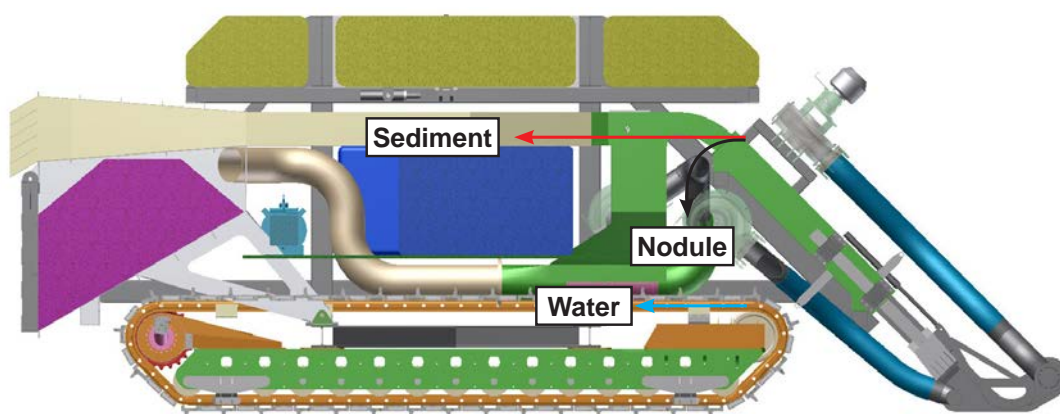


Figure 13: Nodule separation system

Clogging or blockage remains a significant risk for the hydraulic transport process. Two flushing valves are installed to bring water into the system, if needed. A hopper dump valve is installed to deal with any clogging of the hopper if it occurs. Although the design is as open as possible, obstruction of nodules inside the hopper can always happen. In this case, the collector head is lifted from the seabed and a large volume of flushing water is pumped into the system.

Ambient water is brought into the process at the central discharge point of the hopper. Flow and density measurement systems, together with a discharge valve (gate valve) are installed in the discharge pipe of the hopper towards the nodule container. Approx. 3 mT of nodules (submerged weight, including a bulking factor of 60%) can be stored inside the container. The nodule payload inside the bucket is shown in purple in Figure 13). The discharge or dump hatch is the back vertical plate of the container and is controlled hydraulically. A part of the back plate consists of a fine meshed grate that enables water and remaining sediment to exit the container. If operations do not require nodule collection (operational mode (1)), the dump hatch remains open and nodules that are being collected are discharged back on the seabed while driving.

Subsequently, no method will be used to **process or crush the nodules at the seabed**. There is no connection between the PPV and the surface vessel for **continuous vertical transportation** of nodules to the vessel. All the collected material will remain on the seabed during the in-situ trials, except for any nodules remaining in the bucket during retrieval of the PPV to the surface. Therefore, no **separation process between sediment and resource** or **return discharge water characterization** is applicable for the campaign in 2019.

3.4.2.1.4 Power and electronics

An umbilical will power the vehicle. Two types of power conductors are available: 4.2kV conductors for the electrical motors driving the (HPUs and 1kV conductors (transformed to lower voltages on the PPV) for telemetry, etc. Data (video, controls, etc.) will be transmitted via fibre-optic cables incorporated into the umbilical.

Several ePODs must be installed on the vehicle to accommodate the electronics that cannot withstand the ambient pressure of 450 bar. The ePODs will be decentralized according to their functionality: (1) nodule collector system, (2) telemetry system and (3) all auxiliary systems.

3.4.2.1.5 Hydraulic system and track drive

Two (or possibly three) hydraulic power units will be installed on the vehicle to operate all hydraulic systems. These HPUs will be installed underneath the discharge diffuser-exhaust.

One of the major consumers of the hydraulic system are the track drives. Two hydraulic motors each drive a track chain. The track pads are mounted on these track chains.

Additionally, hydraulic cylinders are needed for different functional objectives. In total 16 hydraulic cylinders are installed on the vehicle:

- 4 units for height control of the collector head (1 cylinder per module)
- 2 units for rotating the separation grate inside the hopper if needed
- 2 units for discharge from the hopper
- 1 unit for gate valve to discharge line towards nodule container
- 2 units for the dump hatch of the nodule container
- 4 units for a height measurement mechanical back-up system
- 1 unit for an active air relief system on top of the discharge diffuser-exhaust duct.

3.4.2.1.6 Additional elements related to the Recommendations ISBA/19/LTC/8, section C

Following validation of in-situ trials with the TSTD, Patania II has been equipped with two caterpillars made of a type of Nylon (Ertalon 6PLA Tracks, commonly used for trenching, (supplier: Quadrant, 2018. Consulted on March 21, 2018)). The tracks are 1.5 m wide with a thickness of 12 cm. Furthermore, caterpillars are equipped with alternating grousers. The total length of each caterpillar is 6 m. According to previous in-situ tests of the Patania I in the CCFZ, DEME-GSR expects that the Patania II caterpillars will penetrate up to 5 cm into the sediment. This will be confirmed during the 2019 trial. The depth of influence of the water jets at the collector head will be investigated in-situ for the first time in 2019. Based on the laboratory experiments, DEME-GSR assumes that the depth of influence will be between 5 and 15 cm, depending on the thickness of the unconsolidated top layer of the seabed.

3.4.2.1.7 Telemetry

The PPV will be equipped with several sensors, divided according to the following categories:

- **Positioning:** as on the TSTD Patania, a combination of Doppler Velocity Log (DVL) and Inertial Navigation System (INS) will be mounted at the front of the PPV. The DVL measures the Speed Over Ground (SOG) and the INS system returns the absolute position, trim and list.

- **Vehicle systems:** Sensors measuring hydraulic pressures, hydraulic volumes, pump rotation per minute (rpm) (such as the track drive motors), etc., will monitor the status of the PPV in operation.
- **Dredging and nodule collection:** flow and density of the nodule mixture will be measured in the hopper discharge pipe towards the nodule container. The nodule container is mounted on 3 load cells providing a mass indication of the content of the container. Additionally, the container will be equipped with proximity switches to provide a back-up measurement of the content of the nodule container.
- **Environmental sensors:** a Conductivity, Temperature and Depth (CTD) measuring probe with turbidity sensor and an Acoustic Doppler Current Profiler (ADCP) will be mounted to obtain a better understanding of the sediment plume. Water samplers will be installed to capture the plume sediment/water mixture for later analysis.
- **Other:** in order to measure the load at the end of the umbilical, a load cell will be mounted on the suspension point of the PPV to the umbilical.

3.5 Project duration

3.5.1 In field collector test plan

The seagoing campaign to the CCFZ, GSR's 4th offshore campaign GSRNOD19, will focus on the deployment of the pre-prototype mining vehicle. The campaign will consist of two distinct legs (Deep Sea Functionality Testing in CCFZ and GSRNOD19 impact experiment and component validation), as shown in the high-level planning in Figure 14 below.

The first leg, the functionality testing, is foreseen to mitigate any technical issues before the actual operations within the framework of the JPI-Oceans MiningImpact 2 program. Despite a full technical testing program prior to vehicle deployment (FAT testing, land and wet trials, hyperbaric testing), it is not guaranteed that all systems will perform as expected in the deep sea. The conditions are extremely harsh and per not always reproducible on land. Additionally, certain components cannot be tested prior to deep sea deployment. For example, verification of the functioning of the umbilical winch (spooling and fleeting system) when the umbilical is fully deployed and an integrated hyperbaric test of the entire vehicle must occur in situ. Moreover, several consecutive deployments are necessary because the system oil must be allowed to creep up the umbilical because of the increase in pressure while the vehicle is gradually deployed.

During the GSRNOD17 trials with the TSTD Patania, nine different dives spread over 14 days were required before the Patania touched seabed. Therefore the GSR functionality period is foreseen to guarantee operational continuity during the second leg of the campaign.

Additionally, a buffer period of 21 days is foreseen to rectify any technical issues that may be identified during the functionality period.

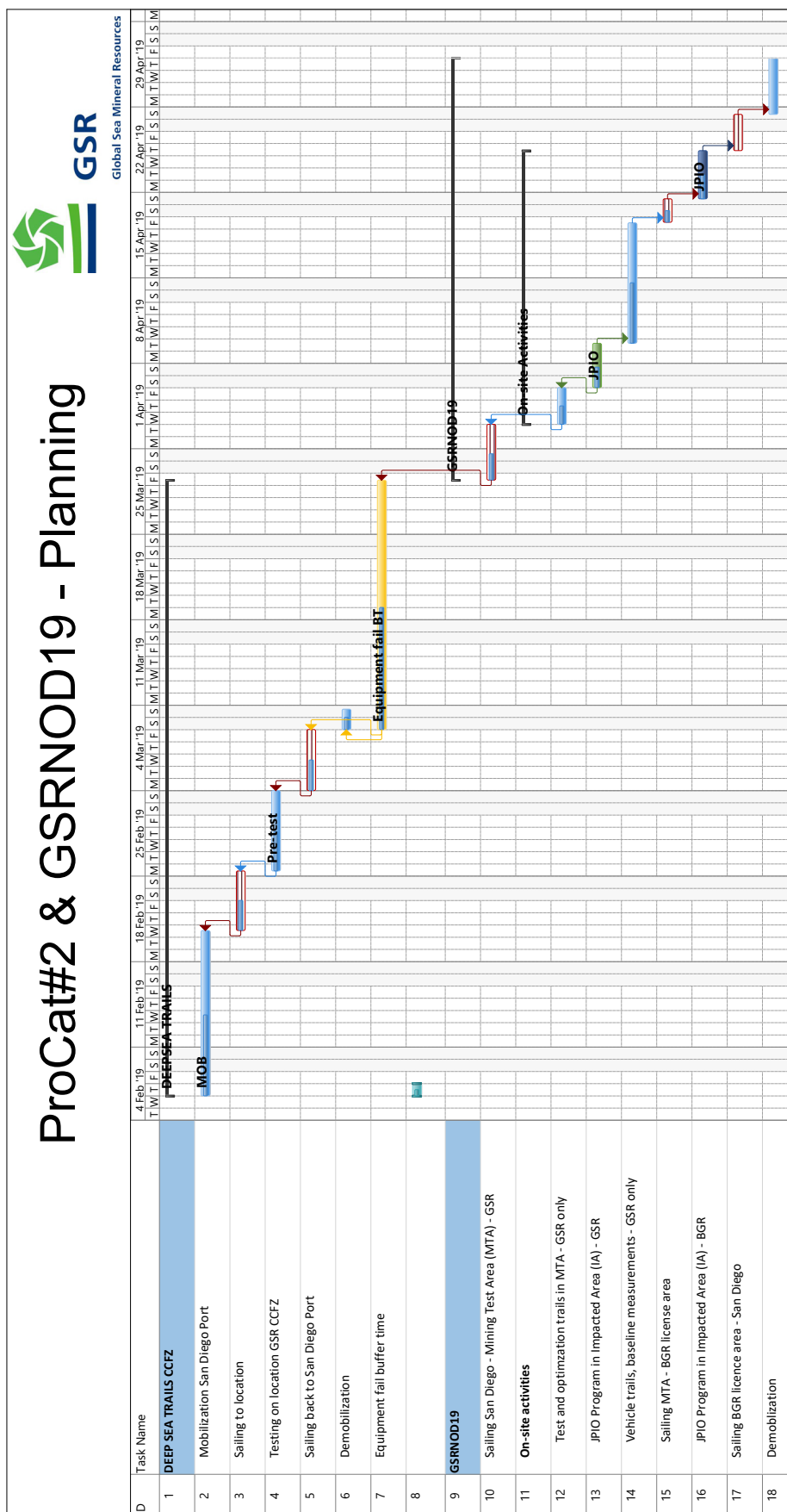


Figure 14: High level planning GSRNOD19

Subsequently, the GSRNOD19 campaign will have 2 major operational modes:

- (1) First operational mode: In-situ validation and optimization of the nodule collection system as tested in the laboratory (GSR technical department). The focus is on the optimization of the collection process. For the validation of the collector principle in-situ and further optimization nodule storage is not necessary. Hence, operations can be performed while the dumping valve remains open and collected nodules are being reintroduced into the environment directly after pick up “on-the-go” (same principle as side-casts). The main research topic is operational efficiency of the nodule collector head. The findings from the test runs in the hydraulic laboratory must be validated in-situ. These mainly consist of the following two subtopics:
 - Height of the collector head above the seabed and the impact on the collection process;
 - Speed variability and the impact on the collection process.

The sediment/nodule concentration during the collection process is an important parameter required to design the operational steering system of the collector and the vertical transport system.

- (2) Second operational mode (green for GSR contract area and dark blue for BGR contract area on Figure 14 above): Environmental impact experiment in the context of the **JPI-O MiningImpact 2** collaboration. The objective of the experiment is to assess the impact of the sediment plume generated by the PPV and to assess the short (scale of days)- and long (scale of months or year)-term impact on the ecosystem. This second scope will be explained in detail in the second part of the present report, i.e., assessment and monitoring of the anthropogenic impact.

3.5.2 Project scale

For the environmental impact experiment in the context of the JPI-O MiningImpact 2 collaboration, a continuous area must be cleared of nodules. As no riser system connects the PPV and the vessel for the test, nodules will be collected in a container on the back of the Patania II and must be dumped outside the Direct Impact Area. Several possibilities for dumping have been investigated: a nodule container at the back of the vehicle is the preferred option. The container (cross-section shown on Figure 13 above) has a dumping valve at the back. When closed, approximately 3 mT of nodules can be stored inside the container. Depending on the nodule abundance on the seabed, a distance between 50 m and 150 m can be driven before the container must be emptied. Consequently, piles of nodules will be gathered on the longitudinal sides of the test area. Figure 15 illustrates an example of a possible path of the PPV on the seabed.

The longitudinal distance (in Figure 15 indicated 340 m) can be changed depending on the progress of the test and the available operational time. The red dots at the extremities of the traverses indicate the dumping locations. The width of a single lane is equal to the total width of the PPV, which is assumed to be 4 m. The longitudinal distance will therefore be a multiple of 4 m, depending on the number of lanes. The example in Figure 15 shows 85 lanes resulting in a longitudinal length of 340 m.

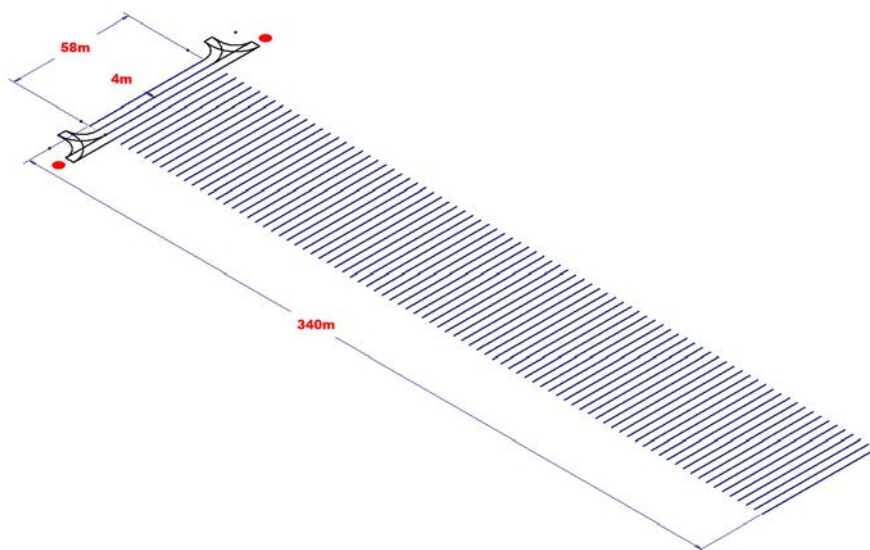


Figure 15 : Example of the pattern of the JPI-O MiningImpact 2 area. Red dots represent the piles of nodules collected

At the end of every lane, a 180° turning procedure as shown on Figure 16 below will be performed. Several phases are distinguished (refer to Figure 16 below):

1. The length of the lanes is dictated by the average nodule abundance (15kg/m^2 - 30 kg/m^2) and the available volume in the nodule container on the PPV. At the end of every lane, the nodule container is fully loaded and the collection process is stopped. To prevent clogging of the system it is not possible to abruptly stop the flow of the water pumps. Water is required to flush the system. Hence, at the end of every lane, the nodule collection heads are retracted so only water is pumped through the system.
2. Subsequently, a 90° turn to port is executed. At this moment, all pumps are stopped.
3. In order to finalize the 180° turn, the pre-prototype performs a 90° back turn to starboard with a lateral offset equal to the width of the collector. Thus the front of the nodule collector is facing the target area again. In this position, the nodule container is unloaded by opening the hatch. By starting the water pumps, the nodule container can be flushed and cleaned of any remaining nodules and chunks of sediment. The nodule collector heads are subsequently lowered while the pre prototype vehicle is slowly picking up speed in the forward direction. The collection process can now be restarted.

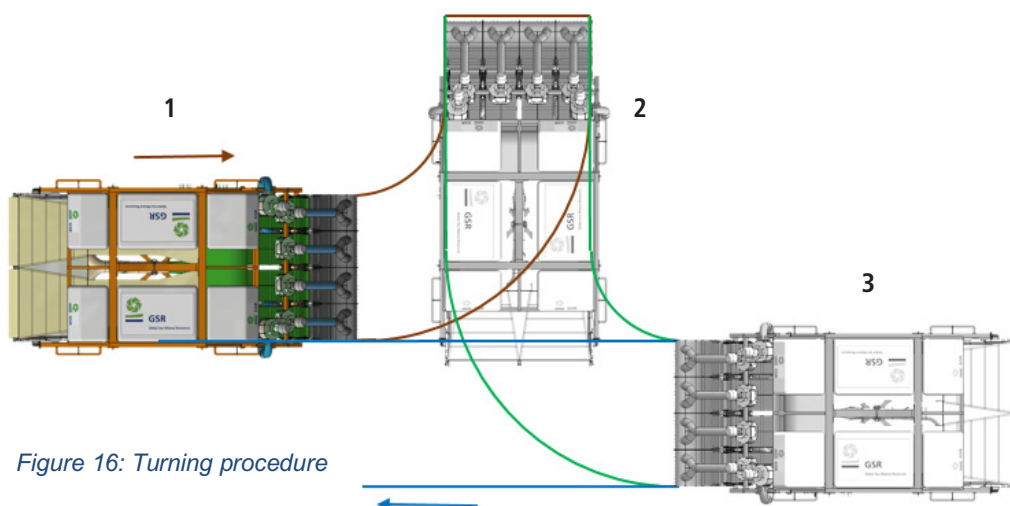


Figure 16: Turning procedure

Table 11 below gives an indication of the expected times required for the turning process.

Table 11: Time required for turning process

Action	Maximum [min]	Minimum [min]
Flushing after lane	5	2
Settling time and retraction of collector heads	3	0
90° turning to port	3	1
90° back turning to starboard with offset	5	2
Dumping of nodules	2	1
Start-up pump system and flushing of nodule container	5	2
Total time required for turning	23	8
Average time require for turning	15 min	

In order to develop a plan, several building blocks have been defined. They are distinguished according to the flowing categories:

Part 1: Start-up: every time the vehicle is deployed on to the seabed, several functional checks must be performed. These mainly cover all hydraulic and electrical systems. Subsequently, the water pumps must be started.

Part 2: Mowing 1 lane: This part gives an estimate of the time required for covering 1 lane. Again, this depends mainly on the nodule abundance and the net available volume inside the nodule container. The breakdown of turning and all associated activities that are required at the end of every lane are described in Table 11.

Part 3: Technical downtime (assumed simple error): Part 3 and Part 4 cover technical downtime. Part 3 assumes a technical issue that can be resolved but for which the vehicle must be recovered. As an example in the overview below, 3 hours on deck are allowed for fault finding and rectification.

Part 4: Technical downtime: Part 4 assumes a technical issue that can be resolved in-situ. Full recovery of the vehicle is not required.

Combining the building blocks above and other operational restrictions, several possible realistic scenarios can be predicted. As an example, two cases are presented in the overview below. These yield an operational area of 0.022 km² and 0.1 km².

JPIO Test Program - Detailed planning breakdown				Case 1	Case 2
Geometrical design assumptions					
Nominal forward speed		0,30	0,50	[m/s]	
Max. design forward speed		1,2	1,2	[m/s]	
Envisaged collector width		4	4	[m]	
Physical properties					
Seawater density		1 048	1 048	[kg/m ³]	
Nominal nodule abundance		15	15	[kg/m ²]	
Nodule wet density		2 000	2 000	[kg/m ³]	
Nodule bulking factor		60%	60%	[%]	
Nodule basket - Nodule payload					
Geometric volume of basket		3	3	[m ³]	
Bruto volume of nodules in basket		3	3	[m ³]	
Mass of wet nodules in basket (incl. bulking factor)		3	3	[ton]	
Mass of submerged nodules in basket		1,43	1,43	[ton]	
Corresponding collecting distance		50	50	[m]	
JPIO Test Program - building blocks					
Time required for turning		5	5	[min]	
Time required for pile dumping (incl. manoeuvring and flushing of basket)		15	5	[min]	
<u>Part 1: Start up</u>					
Vehicle system check after touch down		45	30	[min]	
Start-up		10	5	[min]	
Total time - Part 1: Start-up		55	35	[min]	
<u>Part 2: Mowing 1 lane</u>					
Time required for 1 lane until nodule basket is full		2,78	1,67	[min]	
Time required for pile dumping		15	8	[min]	
Time required for turning		5		[min]	
Start-up		3		[min]	
Total time - Part 2: Mowing 1 lane		25,78	9,67	[min]	
<u>Part 3: Technical downtime (assumed simple error)</u>					
Vehicle recovery		240	240	[min]	
Vehicle - Fault finding		60	60	[min]	
Vehicle - Fault technical solution (simple)		180	180	[min]	
Vehicle re-deployment		240	240	[min]	
Total time - Part 3: Technical downtime (assumed simple error)		720	720	[min]	
<u>Part 4: In-situ technical downtime</u>					
Fault finding		30	30	[min]	
Fault rectification		60	60	[min]	
Total time - Part 4: In-situ technical downtime		90	90	[min]	
JPIO Test Program - Example					
Part 1: Start up		3	1	[units]	

Figure 17: Scenario mining overview

3.6 Support equipment

3.6.1 Vessel

At the time of writing the vessel has not been contracted. The vessel will be inspected and approved by a GSR surveyor prior to mobilization to site. The vessel will be required to meet all appropriate international standards regarding, e.g., waste discharge, oil spill mitigation measures, safe operation protocols and emergency response procedures.

3.6.2 AUV and ROV

Regarding the environmental assessment and the monitoring, the JPI-O MiningImpact 2 Consortium will deploy AUV and Remote Operated Vehicle (ROV) in the water for pre- and post-impact study. One AUV is the REMUS 6000, from Kongsberg (Kongsberg, 2018. Consulted on March 21, 2018), and the ROV is the ROV Kiel 6000 of Geomar (Geomar, 2018. Consulted on March 21, 2018) manufactured by Schilling Robotics, Davis, California.

4 Description of the existing environment

So far, three GSR sampling expeditions have been undertaken in the GSR Contract Area in the CCFZ, namely GSRNOD14A (August-September 2014), GSRNOD15A (September-October 2015) and GSRNOD17 (May-June 2017). In addition, this area was sampled during the JPI Oceans “Ecoresponse” expedition SO239 in March-April 2015 in the context of the project on “Ecological impacts of deep-sea mining”. The sampling strategy of each GSR expedition was set up with the biological and environmental data generated from previous expeditions in mind, which enabled us to address certain questions that remained unanswered after the preceding expedition while developing the baseline in an area of interest.

4.1 The physico-chemical environment

The GSR contract area lies in the area of influence of the ~decadal El Niño-Southern Oscillation (ENSO) (Lavín et al., 2006). Therefore, a certain variability can be expected regarding the characteristics presented. The Eastern Tropical Pacific Ocean is also characterized by considerable spatial and temporal variability in oceanographic characteristics, such as temperature, oxygen concentration, surface nutrient concentrations and salinity (Fiedler and Talley, 2006). The spatial variability within the GSR contract area and the area of interest B4S03 for the experiment itself is considered limited.

4.1.1 Climatology

Based on the European Centre for Medium-Range Weather Forecast Re-Analysis (ECMWF) (Dee et al., 2011), the climatology of the area of interest is typical of tropical climates.

4.1.1.1 Precipitation

For precipitation, seasonality is less marked than for the wind. Two different regimes are observed: one long dry season and one relatively shorter wet season. The GSR contract area is located between 13 and 15 °N, above the Intertropical Convergence Zone (ITCZ). The latitude of the ITCZ fluctuates between 5 and 10 °N and is characterized by substantial precipitation. During the July-September period, this ITCZ moves northwards, inducing wet weather in the south of

GSR contract area, including B4S03. The season-averaged total precipitation rises to ~5 mm/day in summer, and it is close to 0-2 mm/day during the rest of the year.

4.1.1.2 Wind

At ten meters above the ocean surface, the wind blows mainly from the North-East sector over the GSR contract area. The most windy season appears to be the winter, with monthly-averaged velocities reaching 8 m/s (i.e., nearly 30 km/h). The wind intensity diminishes during the spring to a minimum in summer (~2-4 m/s, i.e., ~10 km/h) and subsequently rises again during autumn. Topographic influences from the American continent are observed on the Eastern Pacific Ocean. Three "jets" are forcing this seasonality : the Tehuntepec jet, the Papagayo jet and the Isthmus jet or the Panama jet.

Figure 18 below presents average *wind* speed measured at station 51307 QM006a, for 12 months between March 2012 and March 2013. The average wind speed varies between 2 and 8 m/s (3.5 to 15.5 knots) with a yearly average of 5 m/s (9.5 knots). The stronger winds appear from January to April, the calmer period occurs between May and July.



Figure 18: Average wind speed over a period of one year at station 51307 (8°N 125°W) of the MeteOcean database

The average wind speeds resulting from the model on the Wave and Climate website (BMT ARGOS BV, 2018, consulted on March 21, 2018) for the selected area vary between 6 and 8 m/s (11.5 to 15.5 knots) with a prevailing wind direction of 230° North for most of the selected area and 190° North for the Northeastern part of the area (Table 12).

Table 12: Monthly distribution of wind speed (m/s) for model output point 16°00'N, 125°00'W in wave model. (Data from 1992 to 2012, results based on 61368 model records) (Source: BMTARGOSS, October 2013)

lower	upper	Jan	Feb	Mar	Apr	May	Jun	Jul	Aug	Sep	Oct	Nov	Dec
0	1	0.1	0	0	0	0	0.1	0.4	0.4	0.7	0.3	0	0
1	2	0.2	0.3	0.1	0	0.1	0.4	1.6	2.2	1.7	1	0.3	0.2
2	3	0.7	0.9	0.3	0.4	0.5	1.5	3.5	6.2	5.3	2.9	0.5	0.5
3	4	1.5	1.9	1.2	1.2	1.8	4.8	7.2	8.9	11.6	5.6	1.7	1.1
4	5	3.4	3.6	3.1	3.3	7.1	12.9	13	15.9	17.4	16.7	3.8	1.9
5	6	6.2	7.2	7.2	8.8	16.3	20.4	17.9	16.5	19.6	14.6	7.5	5.2
6	7	12.8	14.8	15.4	16.6	24.6	26.5	21	16.2	18.5	19	13.5	11
7	8	20	21.5	24	24.9	25.4	21	19.3	16.3	12.9	20	19.6	15.7
8	9	23.2	21.3	26.3	24.2	17	9.1	11.4	10	7.4	14.3	23.5	22.5
9	10	18	17	14.1	14.7	6.5	2	2.8	4.1	3.1	7.5	17.5	21.1
10	11	9.5	8.1	6.3	5.2	0.6	0.8	0.8	1.8	0.9	2.8	8.6	13
11	12	3.3	2.9	1.8	0.6	0.1	0.1	0.5	0.6	0.4	1.2	2.7	6.1
12	13	1	0.5	0.2	0	0	0.1	0.2	0.3	0.1	0.2	0.8	1.5
13	14	0.3	0	0	0	0	0	0.2	0.3	0.2	0	0	0.1
14	15	0	0	0	0	0	0	0	0.1	0.1	0	0	0
15	16	0	0	0	0	0	0	0.1	0.1	0	0	0	0
16	17	0	0	0	0	0	0.1	0	0	0	0	0	0
17	18	0	0	0	0	0	0	0.1	0	0	0	0	0

18	19	0	0	0	0	0	0	0	0	0	0	0	0
19	20	0	0	0	0	0	0	0.1	0	0	0	0	0
20	21	0	0	0	0	0	0	0	0	0	0	0	0
21	22	0	0	0	0	0	0	0	0	0	0	0	0
22	23	0	0	0	0	0	0	0	0	0	0	0	0
23	24	0	0	0	0	0	0	0	0	0	0	0	0
24	25	0	0	0	0	0	0	0	0	0	0	0	0
25	26	0	0	0	0	0	0	0	0	0	0	0	0
26	27	0	0	0	0	0	0	0	0	0	0	0	0
27	28	0	0	0	0	0	0	0	0	0	0	0	0
28	29	0	0	0	0	0	0	0	0	0	0	0	0
29	30	0	0	0	0	0	0	0	0	0	0	0	0
30	31	0	0	0	0	0	0	0	0	0	0	0	0
total		100	100	100	100	100	100	100	100	100	100	100	100

4.1.1.3 *El Niño-Southern Oscillation (ENSO)*

The CCFZ is located in the zone of El Niño influence. The El Niño-Southern Oscillation (ENSO) consists of a set of interannual variations in regional climate patterns caused by fluctuating winds and ocean temperatures. Initially, *El Niño* refers to a weaker warmer ocean current (due to a weakening of the Trade winds eastwards) flowing along the coast of Peru and Ecuador until in direction of the Cape Horn end of December. Now, it refers to the negative phase of the ENSO, inducing an increase of Sea Surface Temperature (SST) in either the central and eastern tropical Pacific Ocean. This warming causes a modification of the atmospheric circulation (rainfall and tropical cyclones formation enhanced in the tropical Pacific Ocean). By contrast, the cooling phase is called *La Niña* oscillation.

4.1.2 *Geomorphological settings*

The following section, but also the seabed substrate characterization below) is mainly based on the research carried by the Renard Centre of Marine Geology group from the University of Ghent, coordinated by Dr. Carmen Juan Valenzuela, under the supervision of Prof. David Van Rooij. This research is described in GSR's annual reports to the ISA from 2014, 2015, 2016 and 2017 (2014, 1015, 2016 and 2017 AR, file numbers ISA-GSR_AR2014, ISA-GDR2016, ISA-GSR_AR2016, ISA-GSR_AR2018).

Large morphological features of the B4S03 sub-zone correspond to a structure commonly observed in the CCFZ, i.e., an irregular succession of crests and valleys aligned along the N-S axis with a vertical amplitude of a few tens of meters for a horizontal range of one kilometre. This dominant morphology is complicated by local tectonic mechanisms (faults) and by the variable thickness of the sediment layer due to sediment transport phenomena. Therefore, major (visible on topographic maps) and minor (local) morphological features must be distinguished.

4.1.2.1 *Major morphological features*

The area of interest presents depths between 4425 and 4589 m, with an irregular seafloor (4512.09 m below sea surface on average, with a standard deviation of 26.7 m). The morphology of the area B4S03 is characterized by a central irregular plateau (with depressions, small valleys and small crests), and three large valleys to the west, NE and SE, each with a basin along their path (Figure 19). Most of the irregularities are distributed along a NW-SE belt in the central part of the area, which corresponds to other NW-SE-trending features.

The Benthic Terrain Model (BTM) map of area B4S03 (Figure 20), reveals a variety of environments. The circular depressions and broad valleys crop up as areas in lighter blue hues completely surrounded by orange, yellow and red colours. The main basins are represented by vast dark blue areas. The plains and plateaus are crossed by orange lineations which represent the convex border of gullies and the crests of sediment undulations.

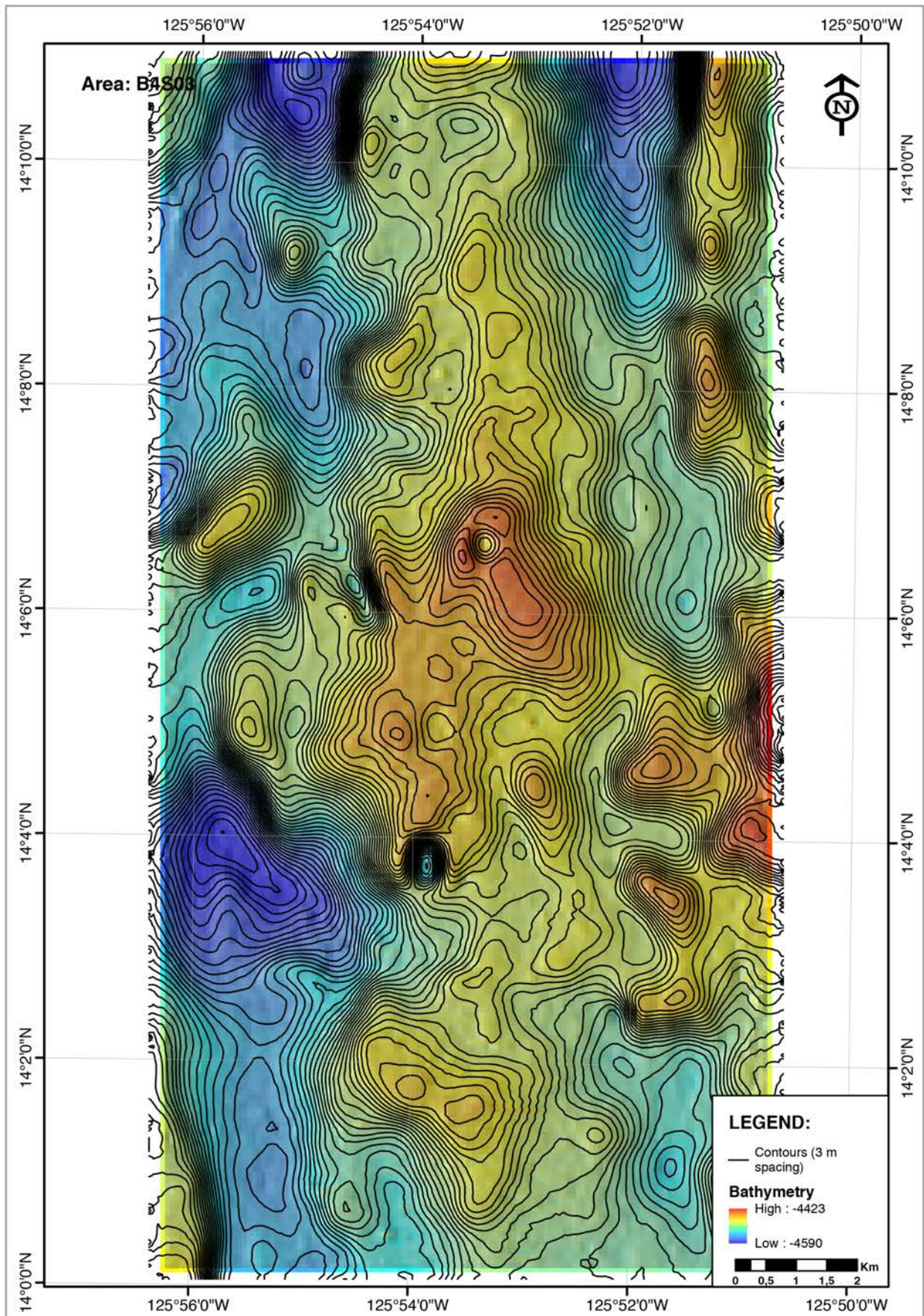


Figure 19: Contour Map of area B4S03 (and surrounding features in grey) generated with the EM120 multibeam data

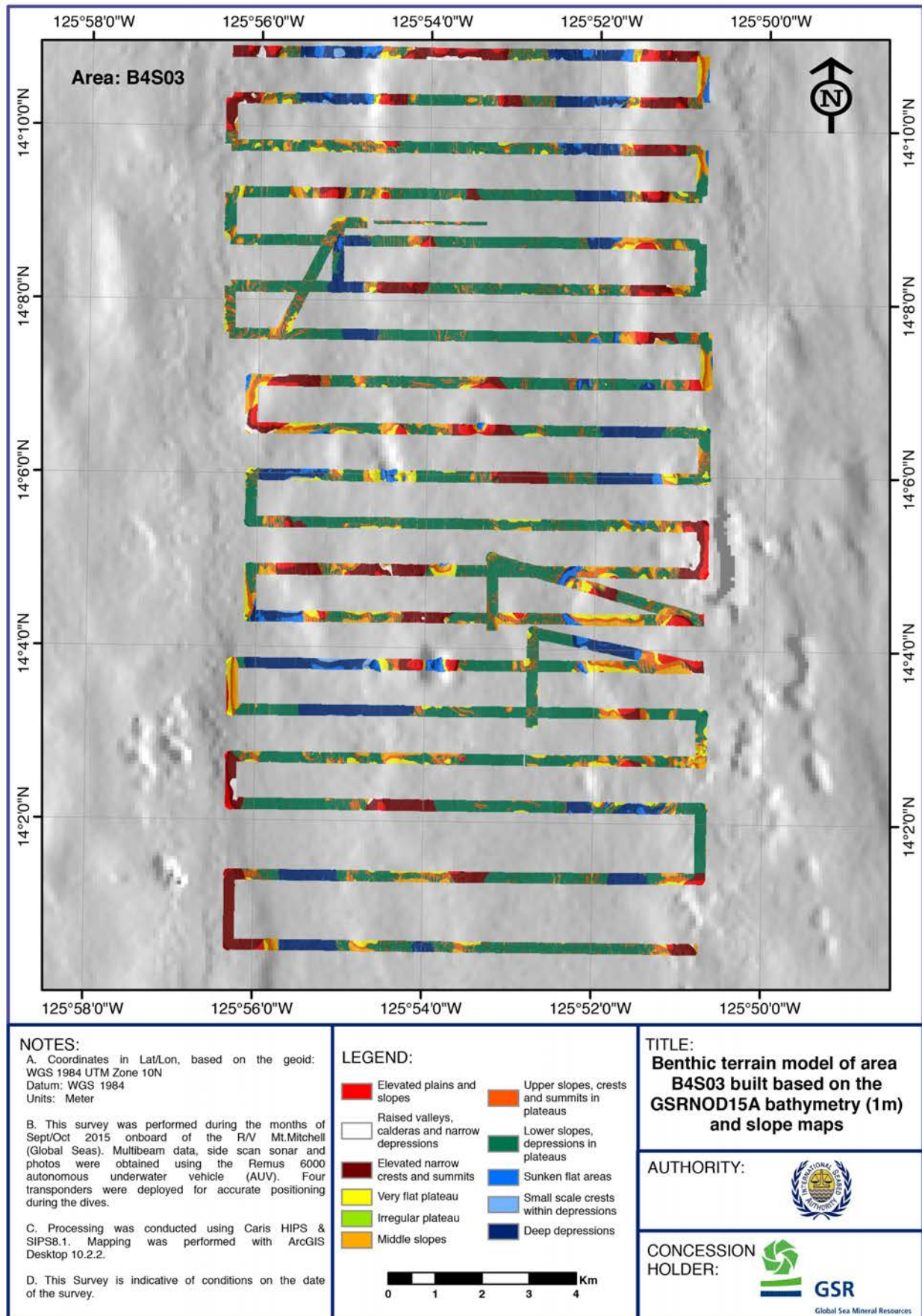


Figure 20: Benthic Terrain Model (BTM) of the main geological structures in area B4S03

4.1.2.2 Slope distribution

Most of the irregularities are distributed in a NW-SE belt in the central part of the area. The maximum slope is 12.63° (22.42%), but the average slope is around $2.03 \pm 1.43^{\circ}$ (3.55 %) (Figure 21). In general terms, the seafloor is slightly irregular. The central plateau has a North-South fusiform shape, and the largest depressions are located NE, NW and SW (Figure 22).

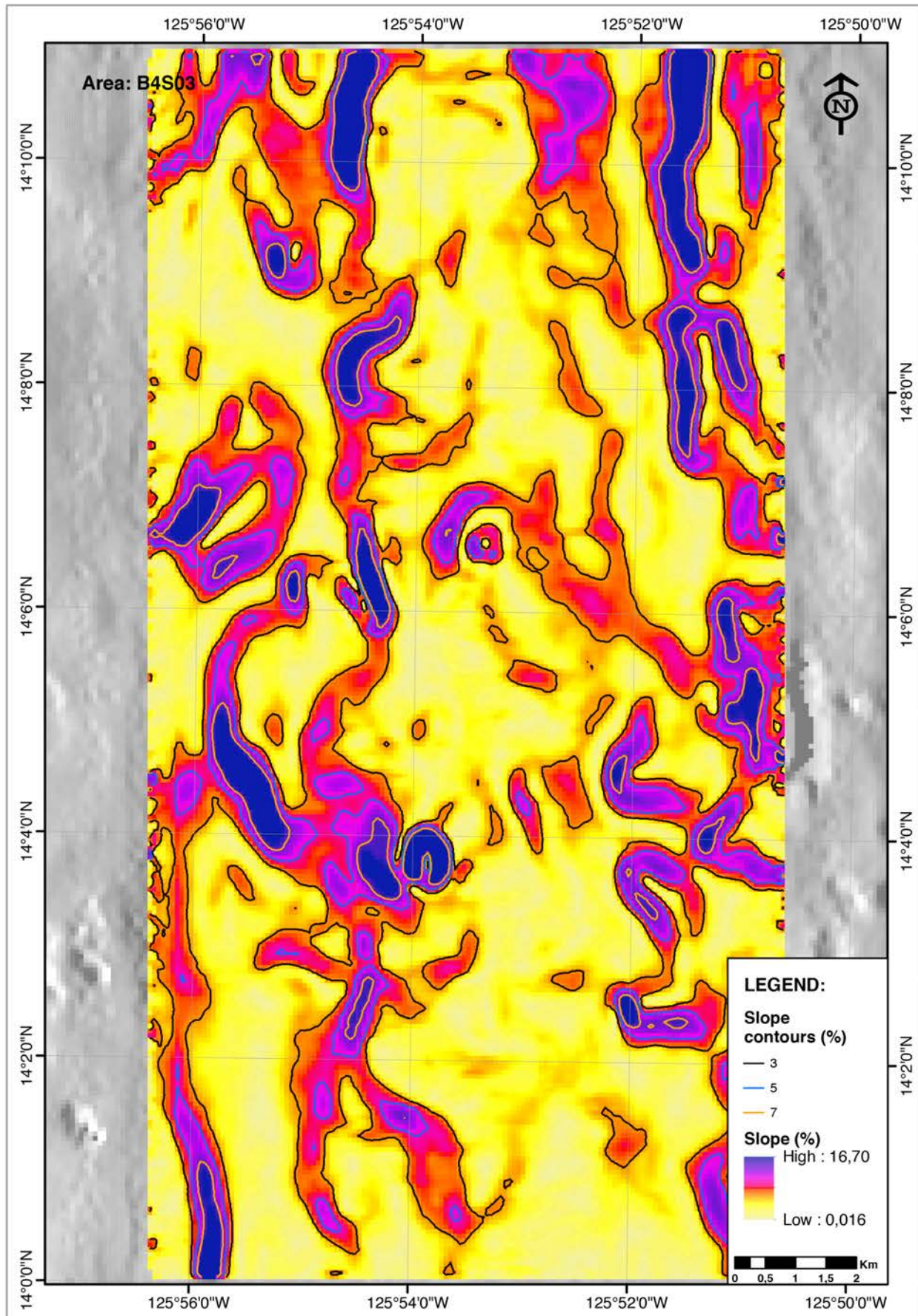


Figure 21: Slope map of area B4S03 based on the bathymetry measured during the 2014 offshore campaign

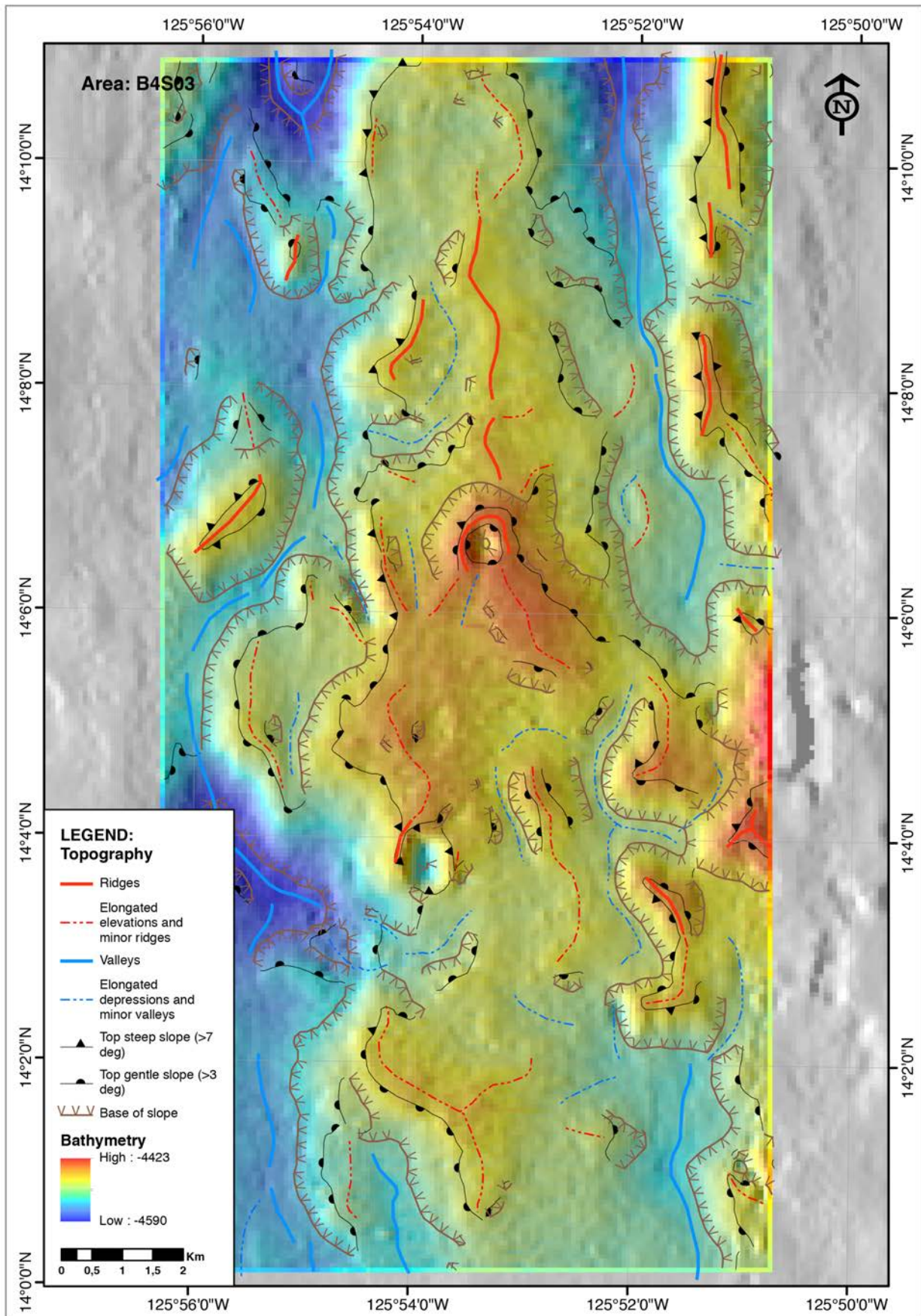


Figure 22: Bathymetric Map of area B4S03 generated with the EM120 multibeam data and superimposed with the topographical lines (crest and valley lines)

4.1.2.3 Detailed morphology

The features observed in the bathymetric data, Side-scan sonar (SSS) and AUV pictures were simultaneously compared with the different SSS and bathymetry datasets. The largest features (rocky outcrops, mounds) were better observed in the SSS and bathymetry datasets; some medium-sized features could be observed in all datasets (i.e. furrows and downslope channels), and the smallest features were only visible in the AUV pictures (i.e., small furrows, local escarpments, etc.)

The mapped area features comprise mounds, rocky outcrops, circular depressions, patches of sediment not covered with ferromanganese nodules (hereby named as bare sediment) and areas characterized by sediment with variable reflectivity in a patchy pattern (Figure 25). Mounds were only present in area B4S03, and consist of a cluster of conical rocky outcrops ranging from 20 to 160 m in diameter, and surrounded by metric to decametric circular depressions and moats on a slope at 4478 m deep (Figure 23 and Figure 24).

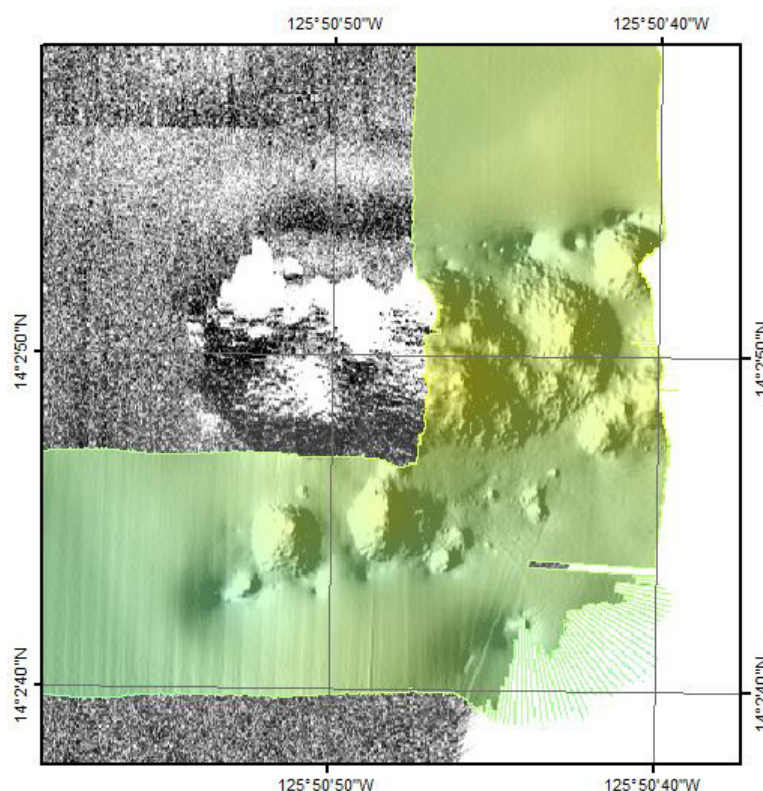


Figure 23: Mounds observed in area B4S03

Rocky outcrops were observed and mapped based on SSS and bathymetry data, with a good level of detail. Rocky outcrops are frequent in the inner walls of local circular depressions (Area B4S03, Figure 24). However, when areas characterized by rocky outcrops according to SSS and bathymetry are directly observed in seabed imagery, the outcrops frequently appear to be covered by a thin layer of sediment, nodules and debris, and thus are difficult to observe.



Figure 24: Inner walls of a sub-circular depression located in the B4S03 area, showing layered consolidated sediment exposed in a vertical escarpment of meter scale (AUV dive 11, photo 7633). Coordinates: Lat.: 14.083N, Long.: -125.897W

Patches of sediment, with very scarce or no nodules, typically cover small areas within valleys, as well as wider areas in the deepest basins. Additionally, areas with very low backscatter that correlate with very low concentrations of nodules (confirmed by the AUV photos) typically appear in the deep basins.

The mapped linear features have been interpreted, based on their combined observation with AUV photography, as lineations (e.g., escarpments, outcrops), furrows and low-relief slide scars. The lineations include escarpments with up to 15 m offset found in outcropping indurated sediments, sharp changes in reflectivity most likely caused by a change in nodule facies, the walls of downslope channels (abundant in area B4S03, Table 13 and Figure 26), and sedimentary undulations.

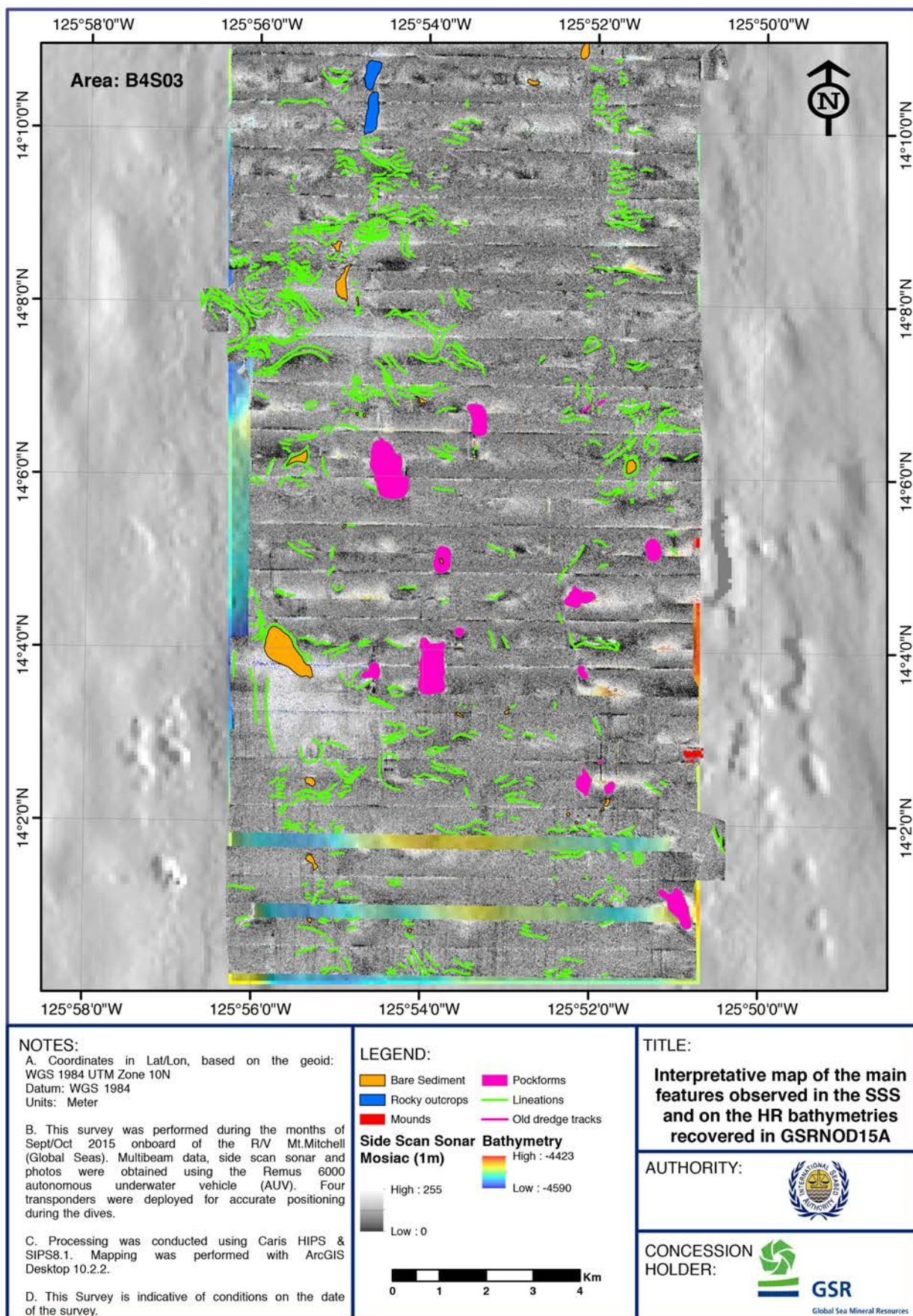


Figure 25: AUV side-scan sonar (SSS) data collected in the area B4S03 superimposed with the geological interpretation

Table 13: Side scan sonar facies classification for area B4S03. Based on the work by Lee and Kim (2004)

Class	Sonar facies	Description	Occurrence	Interpretation for areas B6S02, B4S03 and B4N01
I	I-1	Strong back-scattering intensity; circular shape; a few hundreds of meters to several tens of kilometers in diameter	Abyssal hills, seamounts, circular depressions	Volcanic outcrops, circular depressions
	I-2	High back-scattering intensity; linear geometry; either straight or slightly curved geometry in plan view	Steep slopes, flat areas at the base of abyssal hills	Carbonate-rich outcrops, escarpments, axis of gullies and furrows, high nodule coverage
	I-3	Strong back-scattering intensity; irregular shape; diffuse borders	Lower slopes and relatively flat areas	Large patches of sediment with variable reflectivity, high nodule coverage
II	II-1	Medium back-scattering intensity; linear shape; generally alternated with facies I-2 and III-1	Steep slopes bounding abyssal hills; crests of abyssal hills	Rocky outcrops (bounding faults of abyssal hills; crests of abyssal hills)
	II-2	Medium back-scattering intensity; semicircular or lobate geometry	Lower slopes of abyssal hills and seamounts	Mass-flow deposits
	II-3	Medium back-scattering intensity; irregular shape; either rough or smooth surface texture	Relatively flat areas	Medium nodule coverage
III	III-1	Low back-scattering intensity; linear geometry; generally alternated with facies I-2 and II-1	Troughs between abyssal hills; walls of channels and furrows.	Shadow of linear features, muddy undulations, low to very low nodule coverage
	III-2	Low back-scattering intensity; irregular shape; laterally associated with facies II-1 and II-3	Relatively flat areas	Very low or no nodule coverage

The facies I-2 can be associated to outcrops in areas where the current is strong enough to prevent deposition of sediments (Table 13). The facies I-3, which appear to be scattered into large patches of sediment with variable reflectivity, as well as all the intermediate facies (class II) show diffuse borders with lateral variations in backscatter intensity. The facies III-1 can also be associated with facies I-2.

Additionally, most facies III-1 (low backscatter intensity and linear geometry) in the database corresponds to the slope of channels with low or absent nodule coverage and to the shadow of low-relief morphologies (i.e., slide scars, escarpments, muddy undulations).

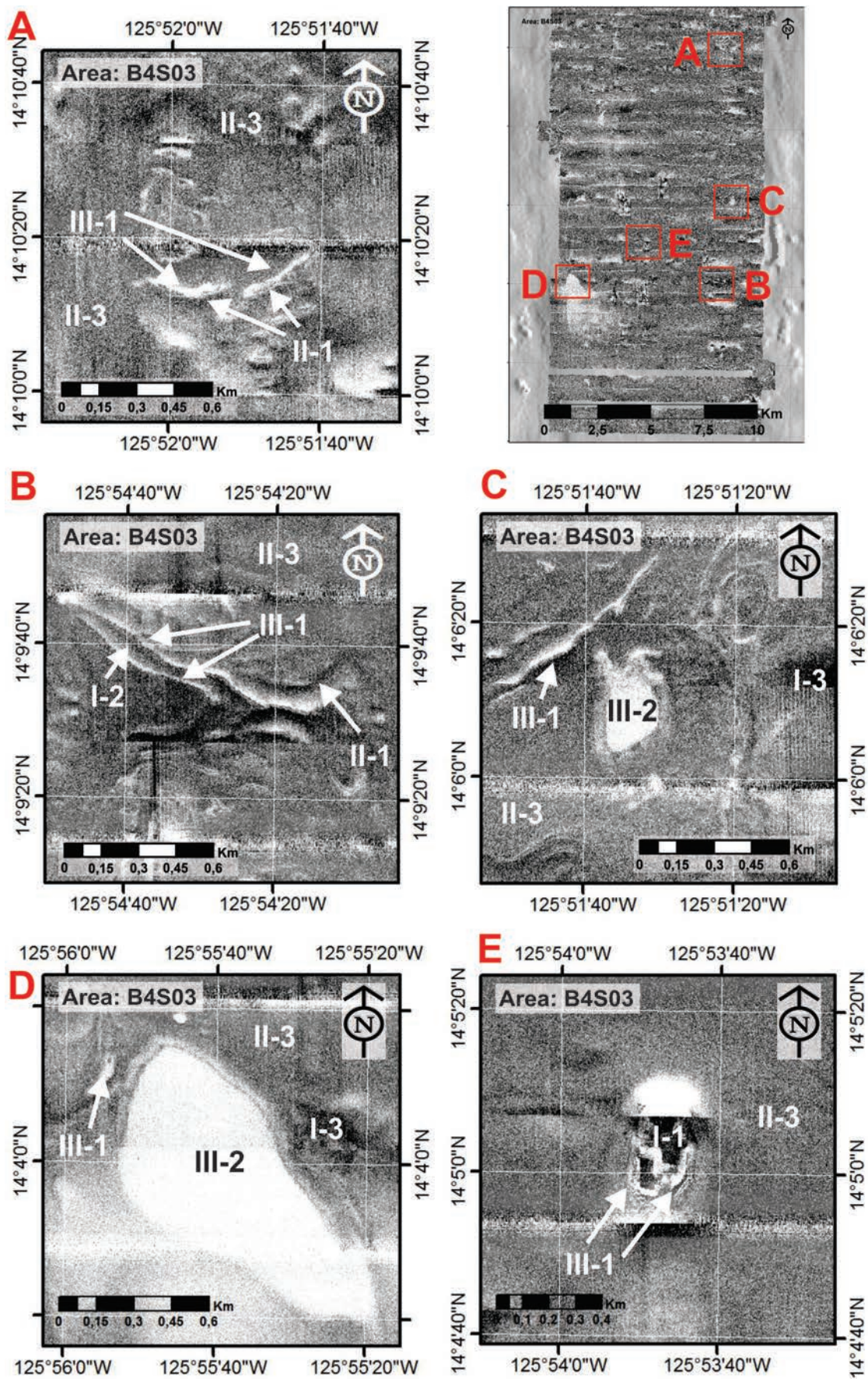


Figure 26: Sedimentary and geological features observed in area B4S03

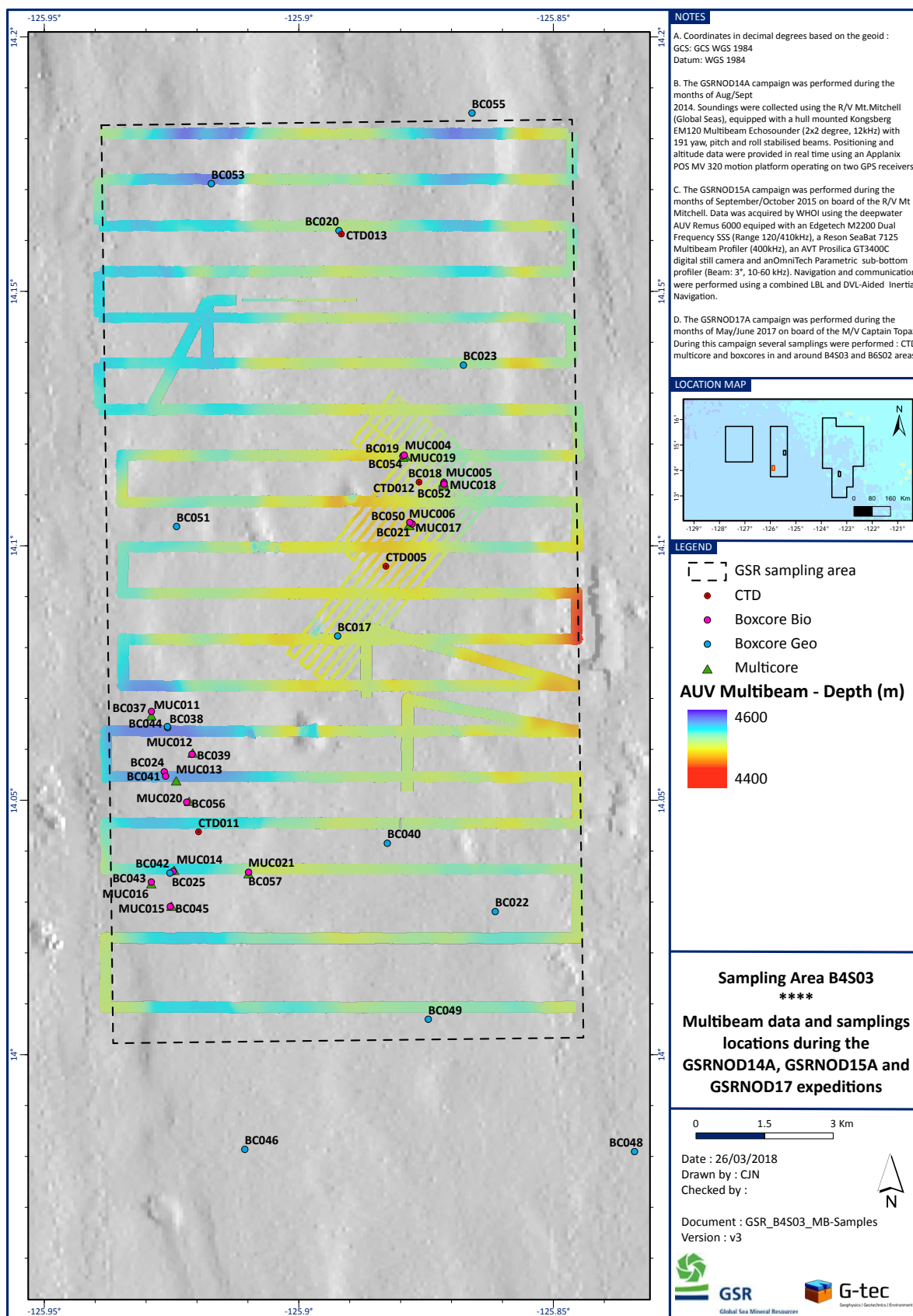


Figure 27: AUV high-resolution multibeam data superimposed with sample locations collected during the 2015 offshore campaign in area B4S03 (surrounding features are displayed in grey)

4.1.2.4 AUV image analyses for sediment features and morphology

Few geological features could be recognized in the seabed imagery; these mostly comprise changes in the nodule facies, and the presence of downslope channels and furrows.

- a. **Changes in the nodule coverage, burial degree and facies** - The AUV photo analysis has shown that the ferromanganese nodules appear in almost every single environment, and show a high variety in concentration and size (the smallest nodules are associated to higher-energy environments, such as gullies, furrows, base of slopes and topographic highs, etc.). Small patches with sparse or no nodule coverage (tens to hundreds of metres long and wide) appear in the deep valleys and basins, but in most cases nodules are present in various concentrations.
- b. **Gullies and furrows** – The gullies are abundant in area B4S03 and can be distinguished by their dominant downslope trend, with along-slope trends; they are frequently related to obstacles. When observed in seabed images, both features share similar characteristics, with smaller nodule size and a denser nodule coverage in the axis of the gully or furrow (where the energy is higher), very sparsely distributed nodules on the flanks of the cleft, frequently flipped over or partly covered with sediment, and large nodules out of the channel, in high contrast with those of the axis. Furrows can also appear as sharp changes in SSS reflectivity nodule facies with cleft at the base of slopes and ridge escarpments.

The biogenic features that can be observed in the seabed photos comprise megafauna trails and tumuli (COPANO, 1984; Du Castel, 1985; Hoffert, 2008). These biogenic features are not the subject of this study, but their frequent presence is noteworthy.

- c. **Megafauna trails** - Some non-sessile benthic creatures, like *Holothuroidea*, can create tracks that cause lineation of ferromanganese nodules and can look similar to current ripples in areas with no nodule coverage, but no current characteristics can be deduced from them. These megafauna trails are abundant in certain areas, and absent in other areas with the same nodule facies, suggesting a possible ecological zonation of the various species causing them, that may be dependent on a deep current-sustained nutrient input, energy of the environment, availability of shelter, distance below surface, etc. These megafauna trails can have a metric to decametric scale in length, but typically do not surpass 0.5 m in width. Megafauna trails are extremely abundant in areas with bare (i.e., nodule-free) sediment, suggesting that the erosive and homogenizing action of the currents do not reach these patches.
- d. **Tumuli** (COPANO, 1984; Du Castel, 1985; Hoffert, 2008) – These features consist of accumulations of sediment with no nodule coverage and typically showing signs of recent biological activity; these are the strongest evidence of biological activity on the seafloor in the area of interest. The tumuli were not mapped due to their abundance in areas with good nodule coverage (~25 large tumuli in a 30x30 m area); they were absent in areas with bare (nodule-free) sediment. The tumuli were not only visible in the seabed photos, but also in the very high-resolution SSS, appearing as scattered light dots on the otherwise grey hues characterizing the nodule fields.

4.1.3 Physical oceanographic setting

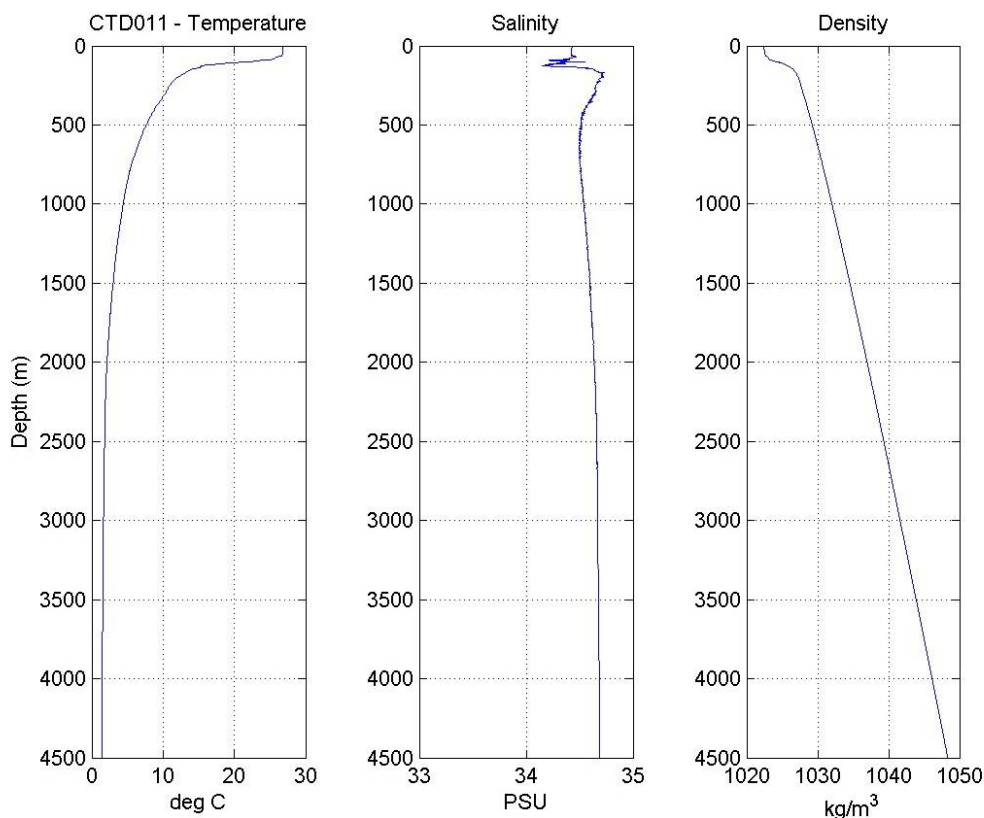
4.1.3.1 Water column characterization

Subtropical regional waters often present a strong pycnocline preventing vertical mixing. In the GSR contract area, and more particularly at the B4S03 sub-zone, vertical profiling during GSRNOD15A and GSRNOD17 confirms this paradigm.

Regarding temperature (example on Figure 28, left-hand graphs), the shallow thermocline is situated between 75 and 150 m below the sea surface, presenting a decrease in temperature from more than 25 °C (shallower than 75 m) to 13 °C (at 150 m). Below that depth, the temperature decreases gradually to 2 °C at the seabed.

Vertical gradients of salinity profiles are not as marked as for temperature. The halocline is smoother, separating less saline water (at the surface, 33-34 PSU) and more saline water (34.7 PSU) from about 150 m down to the seabed (example on Figure 28, central graph).

Based on these vertical profiles of temperature and salinity, the density rises from around 1022 kg/m³ at the surface to around 1048 kg/m³ at the seabed (data provided to ISA by GSR in its 2015, 2016 and 2017 and 2018 AR, file numbers ISA-GSR_AR2014, ISA-GDR2016, ISA-GSR_AR2016 and ISA-GSR_AR2018 respectively).



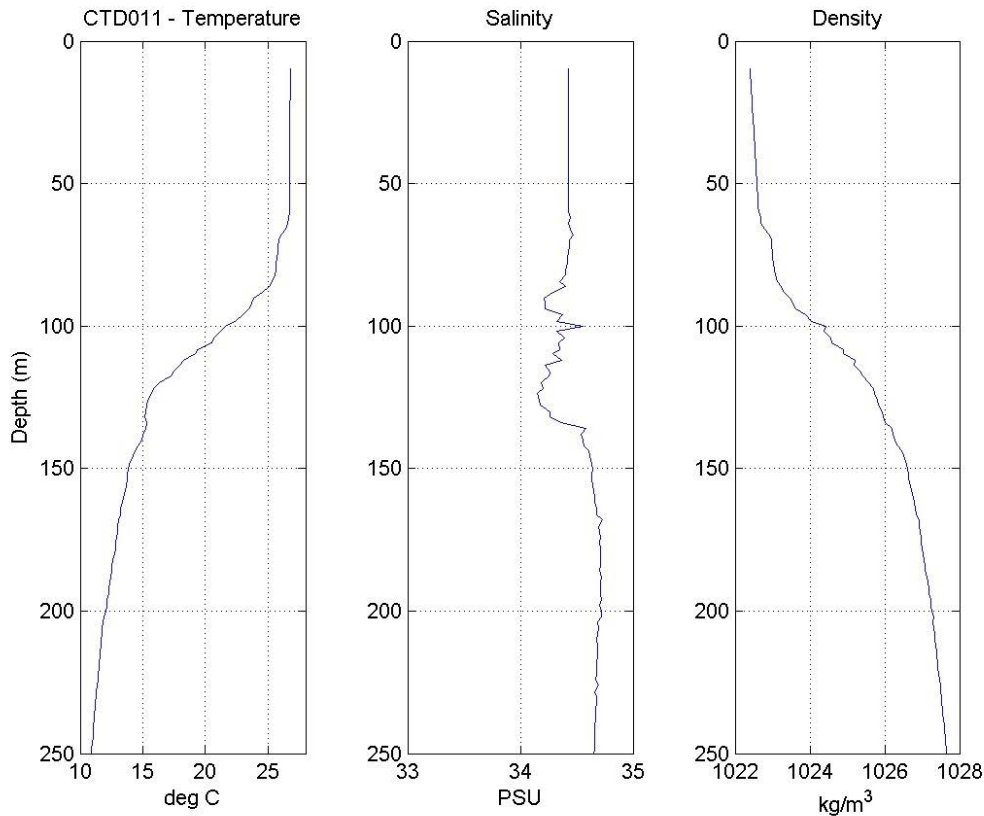


Figure 28: Temperature, Salinity and density profiles measured at CTD011 location (14° 02.61' N, 125° 55.17' W) on 28 May 2017 during the GSRNOD17 campaign over the entire water column (upper panel) and over the upper layer (lower panel)

4.1.3.2 Current

The combination of historical review, model results and collected field data offers an insight into the circulation pattern prevalent in the area. At a larger scale, the Eastern Pacific Ocean is dominated by wind-driven surface currents subject to topographical forcing by the American continent. The current direction depends on latitude. At the surface, a westward surface current, the North Equatorial Current (NEC), is observed at the latitude and longitude of the GSR contract area. The NEC is the lower branch of the North Pacific Tropical Gyre. This current has speeds around 0.2 m/s on average. Additionally, influences of the California Current (east of the GSR contract area, above 20°N, flowing southward along the western coast of the continental US) and of the North Equatorial Countercurrent (8° N, eastward) are also noted (Kessler et al., 2006). Moreover, the important jets presented in the previous section induce the creation of eddies able to propagate into the Belgian contract area (Amador et al., 2006).

Below the surface, the averaged velocity of the currents is less well marked. Between the NEC and 150 m, a second current flows southward, at a speed higher than 0.1 m/s. Below 150 m depth, current speed is low: around few cm/s. Neither direction nor seasonality is marked.

The mesoscale (10s to 100s of km wide) activity is strong in the area; eddies are present on short time scales (~days). These eddies are due to the presence of various currents, and the consequent induced shearing forces. Variability regarding their velocities or their occurrences, increases with proximity to the equator. Those eddies can also elicit deep sea eddies (at the seafloor) that might influence sediment dynamics (proven in BGR area not in the GSR area).

During the GSRNOD17 campaign, current data was collected at sub-zone B4S03 (where the present operation will take place), preliminary results suggest a weak bottom flow, on the order of

cm/s. It varies between 2 to 15 cm/s. An important velocity shear is detected for the last 10 m of the water column above the seabed, reducing the flow even further. Tidal energy was also observed: M2 lunar semi-diurnal tide and S2 solar semi-diurnal tide, associated with systematic direction change of the current from north-westward (weaker) to southward (stronger relatively to the northwestward current) as visible on Figure 29 here below. Unfortunately, at the MiningImpact 2 Program area, no data was collected below 24 m above seabed. It is worth noting that three mooring are currently in the water, and two years of data will be available at the initiation of the project.

Figure 29 and Table 14 offer a view of the current during GSRNOD17 in the area of the Belgian Contract Area where the deep sea trials of Patania II and its environmental impact will be conducted.

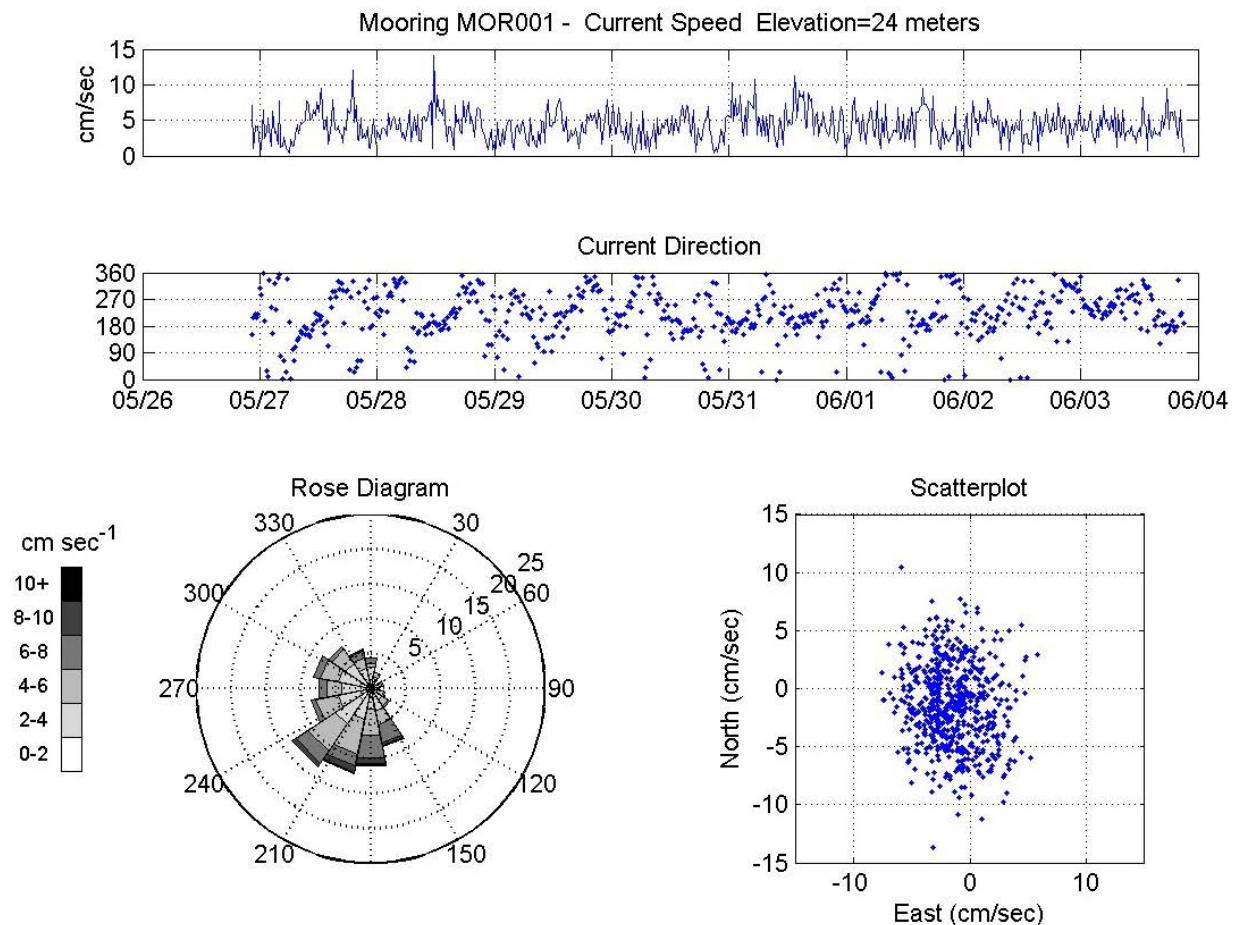


Figure 29: Current representation 24 m above seabed at MOR001 location (in the MiningImpact 2 Program area). Time series of the current speed (top) and direction (lower panel) along with the rose diagram (left) and the scatter plot (right) averaged over the deployment period

Table 14: Current statistics along the vertical profile at MOR001 location (in the MiningImpact 2 Program Area) over the deployment period (May 26, 2017 to June 03, 2017). All speeds are expressed in cm/s

Elevation above seabed (m)	Average Speed	Maximum Speed	Direction of Max speed	Vector-Average Speed	Vector-Averaged Direction	Variance	2% exceedance	5% exceedance	10% exceedance
99	3.86	10.31	150	2.63	211.4	12.08	8.9	7.5	6.5
95	3.12	8.10	160	2.16	216.0	7.74	6.8	5.9	5.4
91	3.08	8.93	184	2.10	220.3	7.70	6.6	6.0	5.5
87	3.19	9.85	193	2.18	219.3	8.29	7.0	6.2	5.6
83	3.34	9.44	193	2.22	222.0	8.99	7.3	6.6	5.8
79	3.38	8.91	192	2.03	219.6	10.47	7.5	6.6	5.9
75	3.84	10.82	184	2.37	224.3	12.89	8.5	7.2	6.6
32	3.20	10.30	191	1.82	224.8	9.62	6.9	6.2	5.5
30	3.41	9.51	183	2.13	225.3	9.83	7.3	6.3	5.6
28	3.41	9.91	182	2.05	226.2	10.77	7.4	6.5	5.9
26	3.72	10.92	168	2.04	227.4	13.23	8.1	7.2	6.3
24	4.26	14.07	193	1.97	226.5	18.68	9.0	7.8	7.0

Table 15 offers a view of the current during GSRNOD17 in the area of the Belgian Contract Area assigned as Control Reference Area for the coming trials. As expected, deep sea currents are comparable to the proposed test site, even if at the time of writing, the data available are limited.

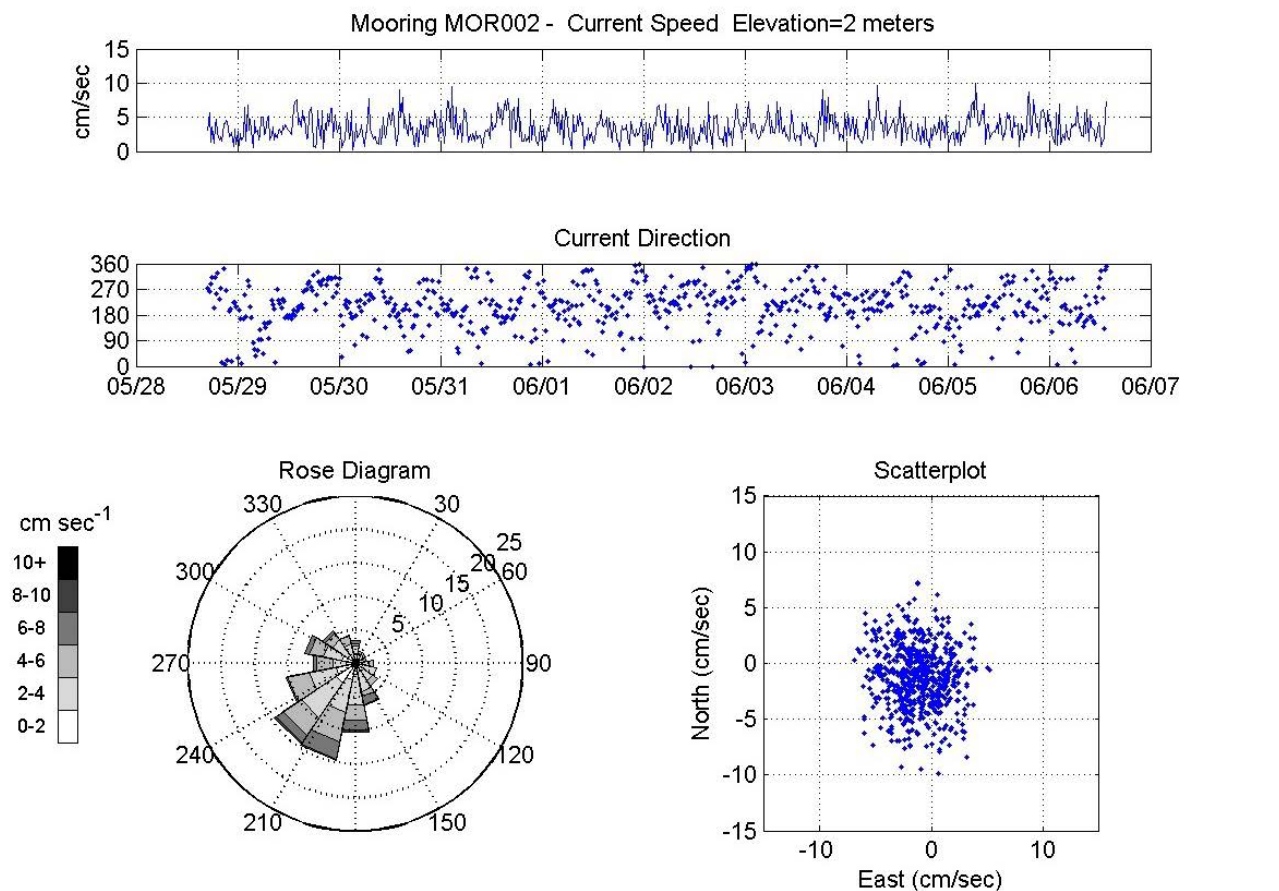


Figure 30: Current representation 2 m above seabed at MOR002 location (in the Reference Area). Time series of the current speed (top) and direction (bottom) along with the rose diagram (left) and the scatter plot (right) averaged over the deployment period

Table 15: Current statistics along the vertical profile at MOR002 location (in the Reference Area) over the deployment period (May 28, 2017 to June 06, 2017). All speeds are expressed in cm/s

Elevation above seabed (m)	Average Speed	Maximum Speed	Direction of Max speed	Vector-Average Speed	Vector-Averaged Direction	Variance	2% exceedance	5% exceedance	10% exceedance
74	4.44	15.24	252	0.93	277.0	24.76	10.3	9.4	7.7
70	4.05	11.40	138	0.75	173.9	20.64	9.3	8.1	7.0
66	4.54	14.48	214	0.91	274.1	25.52	10.4	9.1	7.8
62	3.99	12.71	18	0.90	304.3	20.46	9.2	8.6	7.5
58	4.10	11.91	193	1.00	232.4	20.48	10.0	8.1	7.0
54	4.42	13.78	174	0.91	197.9	24.19	9.9	8.4	7.6
50	4.81	12.71	35	1.05	336.3	29.14	10.5	9.7	8.8
46	4.59	11.90	115	0.21	159.7	26.41	9.9	9.0	8.0
42	4.86	12.95	5	0.88	37.3	29.85	10.6	9.8	8.5
38	5.51	15.77	191	0.55	314.3	39.35	13.2	11.0	9.5
34	5.10	14.48	6	0.57	98.8	33.17	12.4	9.8	8.6
30	4.01	12.35	175	0.44	238.0	20.73	9.3	8.0	7.0
8.5	2.76	7.99	304	1.68	294.1	6.73	6.2	5.2	4.7
8	2.80	7.06	218	1.49	250.2	7.57	5.9	5.2	4.6
7.5	3.07	9.80	216	1.89	224.0	8.19	6.5	5.8	5.2
7	3.13	7.90	181	1.87	227.2	8.78	6.6	6.0	5.2
6.5	3.11	8.42	223	1.90	229.0	8.29	6.6	5.6	5.0
6	3.10	7.98	168	1.92	227.5	8.26	6.4	5.9	5.2
5.5	3.17	7.69	196	1.98	231.9	8.62	6.7	6.0	5.3
2.5	3.32	9.14	175	1.64	230.3	11.37	7.3	6.7	5.7
2	3.46	9.92	177	1.71	222.7	12.34	7.6	6.9	6.0

4.1.3.3 Hydrodynamic model development

The numerical model used in the present section has had a limited calibration for hydrodynamics. Therefore, the findings presented in this report are preliminary results. Nevertheless, it will be improved with the available in-field data as soon as available (April 2018 for 8 months of data).

4.1.3.3.1 Model set-up

The model simulations were performed using TELEMAC-3D (Hervouet, 2007), an open source finite-element model that solves the three-dimensional shallow water equations. Vertical turbulent quantities are calculated using the GOTM turbulence model (Burchard *et al.*, 1999) that was coupled to TELEMAC.

The model domain consists of a rectangular area of size 6.78°x6.64° (756 km x 763 km) bound between 127.9200°W to 121.1200° W and between 11.2800°N to 17.9200° N (Figure 31).

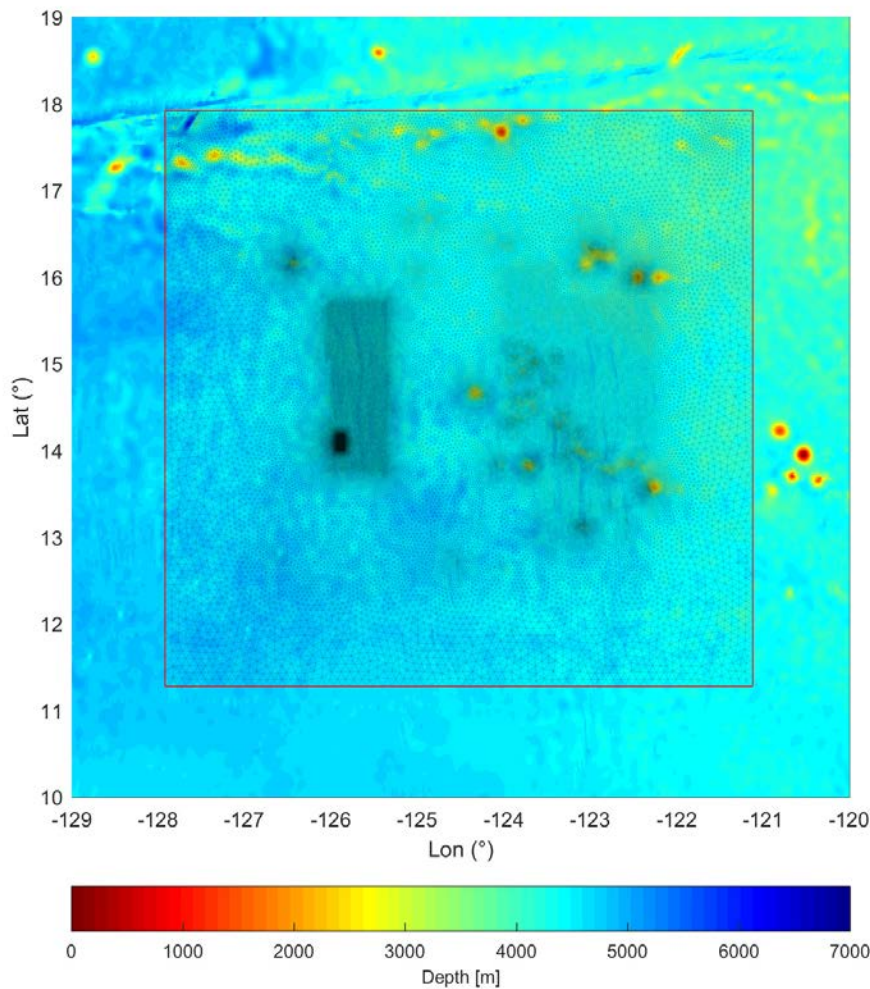


Figure 31: Outline of model domain and bathymetry

The following target element sizes were used for the horizontal mesh generation (Figure 32) :

- 10000 m in a nudging zone (similar to the resolution of HYCOM that is used to obtain the nudging data);
- 1000 m in zone concession zone B4;
- 200 m in the area B4S03, the zone of interest;
- 2500 m in concession zone B6;
- 5000 m elsewhere in the central domain (outside of the nudging zone).

Local refinements were also made near several seamounts, especially those in areas where the (background) grid density is coarse. These refinements are imposed to avoid spurious artefacts due to hydrostatic inconsistencies. The resulting horizontal mesh contains 67,141 nodes and 133,899 elements.

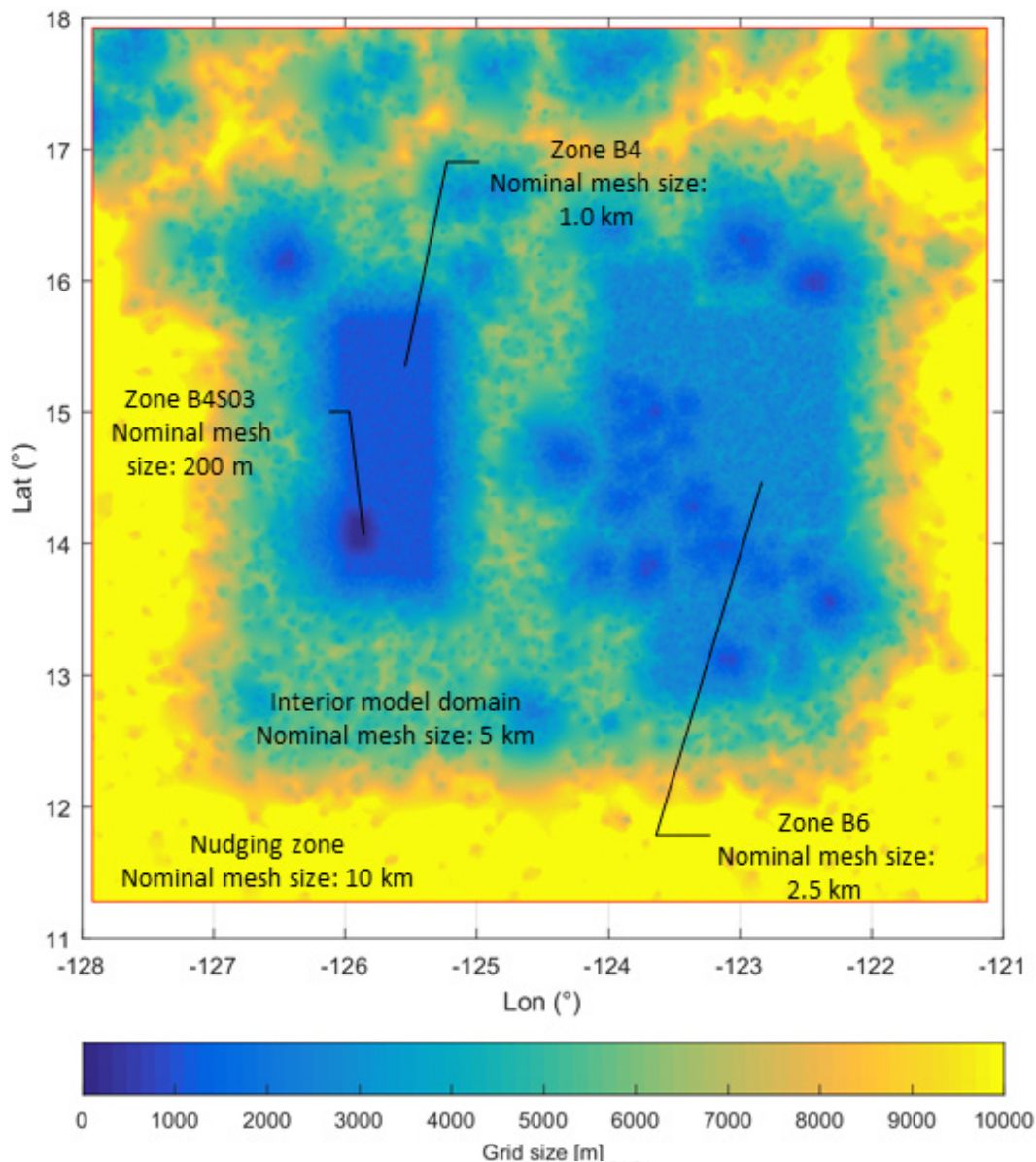


Figure 32: Mesh size in the model for the different zones

The GEBCO_2014 bathymetric dataset was used to provide bathymetric data, which has a 30 arcsecond resolution (roughly 0.9 km) in combination with high-resolution data (resolution <1m) from several local surveys in concession zones B4 and B6 as well as on the seamount between these two concession zones. These survey data have a resolution of 75 m. The resulting mesh and bathymetry are shown in Figure 32.

Vertically, 66 layers are used, consisting of 20 z-layers in the upper kilometre (with a mesh spacing Δz gradually increasing from 2 m near the surface to 100 m at a depth of 1000 m) and 46 sigma layers below 1 km, with a highest resolution of $\Delta z/H = 2.5 \cdot 10^{-3}$ for the 7 layers near the bed (which roughly corresponds to a mesh spacing 1 m), where H is the water depth.

4.1.3.3.2 Initial and boundary conditions and surface forcing

The boundary conditions for surface elevations are taken from HYCOM expt_19.1 (Chassignet *et al.*, 2007). The tidal elevations from OSU/TPXO (Egbert and Erofeeva, 2002) are superimposed to the HYCOM forcing, in order to take the effect of the tide into account. Horizontal velocities

and temperature and salinity values were nudged to the HYCOM data in a nudging band that extends 1.2° from the model boundary, using a nudging time scale that decreases from 1.12 days to 0 within this band. A sponge layer with an increased eddy viscosity of $500 \text{ m}^2/\text{s}$ is also used over the entire water column in the nudging band (same horizontal extent of 1.2°). The initial conditions for surface elevation, velocity, temperature and salinity were derived from the same HYCOM experiment, superimposed with the OSU/TPXO tidal elevations at the start of the simulation.

Surfacing atmospheric forcing data were obtained from the Climate Forecasting System Reanalysis (CFSR), executed by the National Centers for Environmental Prediction (NOAA NCEP). This dataset is available on a T382 Gaussian grid (576×1152 , resolution in the B4 zone approximately 0.312°).

4.1.3.3.3 Model settings

The hydrodynamic model (TELEMAC-3D) takes the following physical processes into account: (1) barotropic forces, (2) wind stresses and atmospheric pressure gradients, (3) bed friction, (4) Coriolis force, (5) horizontal and vertical turbulent diffusion, (6) baroclinic forces due to salinity and temperature gradients and (7) tidal body forces.

The following parametrisations were used:

- **Equation of state:** the 25-term equation of Jackett *et al.* (2006) was used as the equation of state.
- **Surface heat exchange:** heat exchange at the ocean surface is calculated from the net long-wave radiation according to Swinbank (1963) in combination with the sensible and latent heat fluxes according to Salençon and Thebault (1997) and Lalot *et al.* (2015) and these taken into account in the temperature surface boundary condition. Short wave radiation is introduced in the model using a Lambert-Beer law inside the water column.
- **Horizontal turbulence:** horizontal momentum diffusivity is parameterized using the Smagorinsky turbulence model (Smagorinsky, 1963), in combination with a background viscosity of $50 \text{ m}^2/\text{s}$. For scalar transport, the horizontal diffusivity is switched off due the limited horizontal gradients in the temperature and salinity fields.
- **Vertical turbulence:** this is calculated using the KPP turbulence model (Large *et al.*, 1994) as implemented in Global Ocean Turbulence Model (GOTM) including parametrizations for surface layer mixing, bottom boundary layer mixing, non-local transport of salinity and temperature, and internal waves. A bulk Richardson number of 0.3 was used to delimit the boundary layers. For the other parameters, the default parameters of GOTM were used.
- **Bottom friction:** this is calculated from Nikuradse's equation (Nikuradse, 1933) using a bottom roughness of 0.035 m.
- **Numerical scheme:** For the advection of momentum, the characteristic method is used (Hervouet, 2007), whereas the advection of scalars is calculated using the NERDS scheme (N-Edge-based Residual Distribution Scheme, J.-M. Hervouet *et al.*, 2015; Pavan, 2016).

The two main sources of mesoscale eddies in the eastern Tropical Pacific are Tropical Instability Vortices (Contreras, 2002; Marchesiello *et al.*, 2011) and eddies generated by isthmic wind jets through three large gaps in the Central-American mountain ranges (Aleynik *et al.*, 2017). Tropical Instability Vortices are mostly confined to the region south of 10° N , whereas isthmic jet-

generated ocean eddies generally do not propagate further westward than 125° W. Since the MiningImpact 2 program area lies at 14° N, 126° W, strong mesoscale eddies are not expected in the program area (Figure 33).

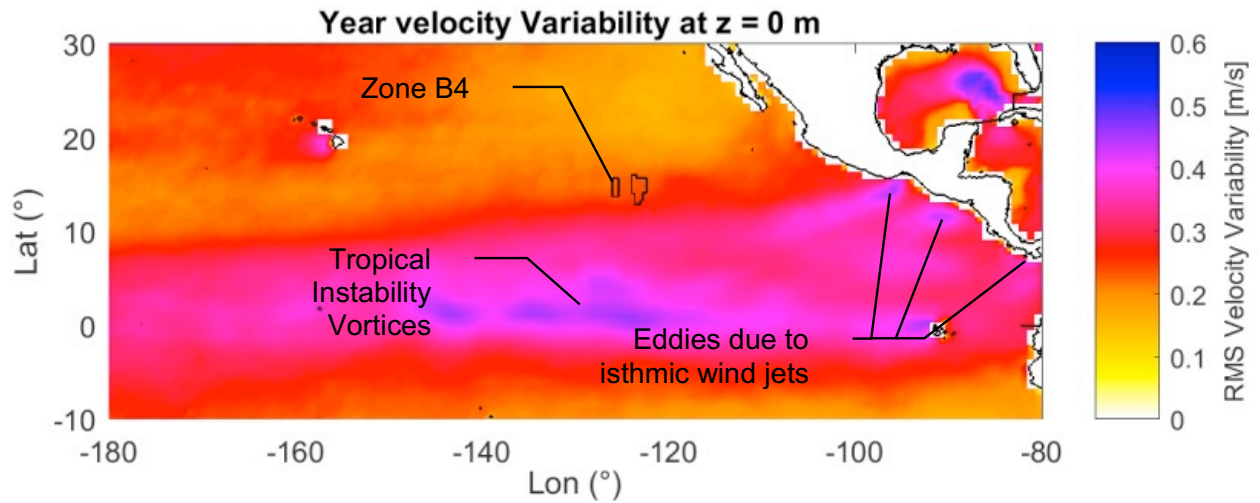


Figure 33: Velocity variability at the surface ($z=0$), defined as the RMS (root mean square) difference between the instantaneous velocity and the 90-day running average from HYCOM expt. _19.1), calculated over period 1995-2012

4.1.3.3.4 Preliminary comparison between hydrodynamic output and short-term field data

A preliminary comparison of the hydrodynamic model was performed based on available mooring data. The model will be further validated as more in-situ measurement data becomes available: by the time of execution of the MiningImpact 2 program, 2 years of mooring data will become available.

Measurements from three near-bottom ADCP moorings are available for a preliminary validation of the model hydrodynamics. Two moorings (MOR001 and MOR002) are located in zone B4S03; the third mooring is located in zone B6S02 (Figure 34). For the current stage of model validation, short-term mooring data is available with a duration of 8-17 days per mooring (Table 16).

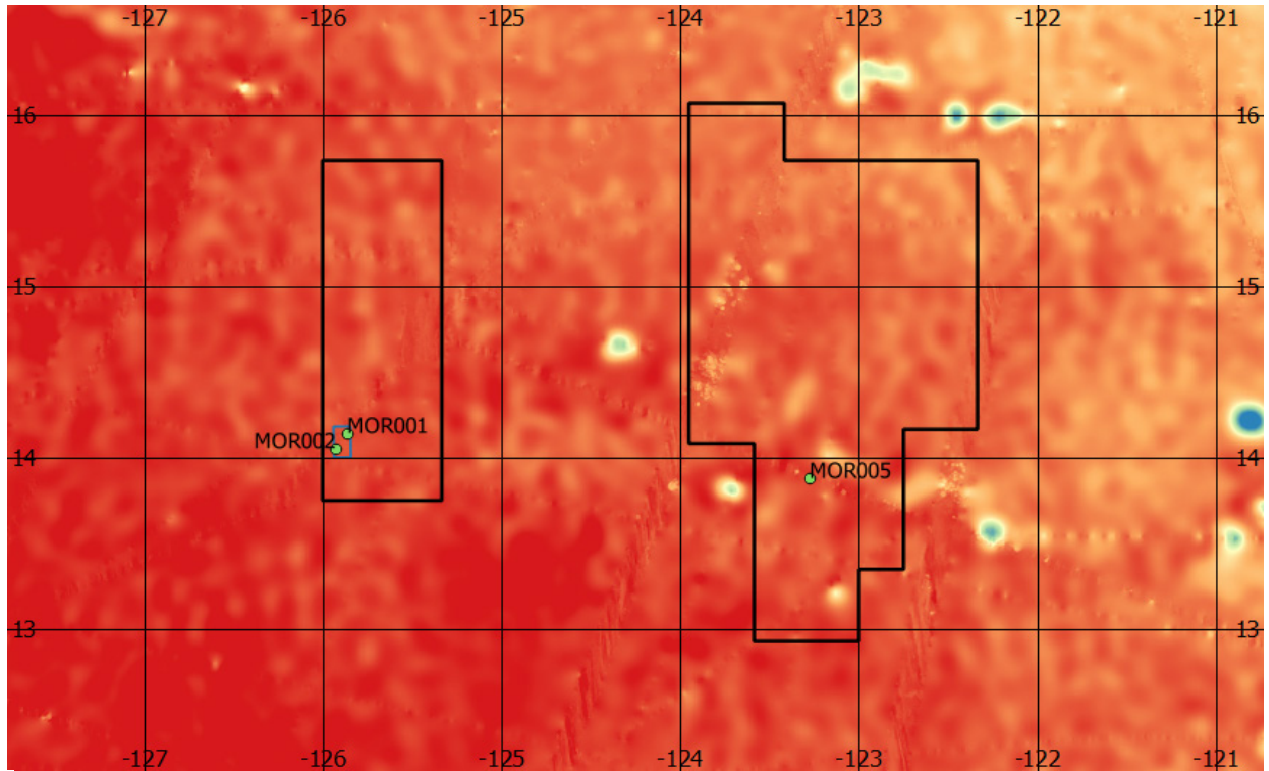


Figure 34: Location of three moorings for short-term model validation. The GEBCO bathymetry is used as background, and the boundaries of B4, B6 and B4S03 are superimposed

Table 16: Overview of short term mooring locations and terms (Metadata). UTC stands for Coordinated Universal

Mooring number	Install date (UTC time)	Recovery date (UTC time)	Duration (days)	X (UTM 10 N)	Y (UTM 10 N)
MOR001	May 26, 2017 20:20:00	June 03, 2017 21:00:00	8.03	1,565,026	190,805
MOR002	May 28, 2017 17:00:00	June 06, 2017 13:40:00	8.86	1,555,235	183,749
MOR005	June 07, 2017 19:40:00	June 24, 2017 22:00:00	16.85	1,534,210	189,174

Time series of velocity magnitude at 35 m above the seafloor from the 3 mooring measurements is displayed in Figure 35. MOR001 shows a clear diurnal signal. MOR005 and especially MOR002 display less clear signal and a higher noise level. This may be caused by a lack of sufficient scattering particles in the water column which leads to an elevated noise level in the ADCP measurements.

Mooring data was compared to model simulations from March, April and May 2009 (nested in HYCOM hindcast expt_19.1, as already explained). No model simulations were performed for the mooring deployment period (May-June 2017) since at the time of model validation no global HYCOM hindcast data were available for this period. Since the measurement and model time series do not cover the same time period, only a comparison of model statistics such as mean current velocity, standard deviation and mean direction was performed. Unfortunately, due to later availability of forcing data for the year 2017, an a posteriori verification simulation has been performed of the period May 1st 2017 until June 30th 2017 (see Appendix 12.4.5).

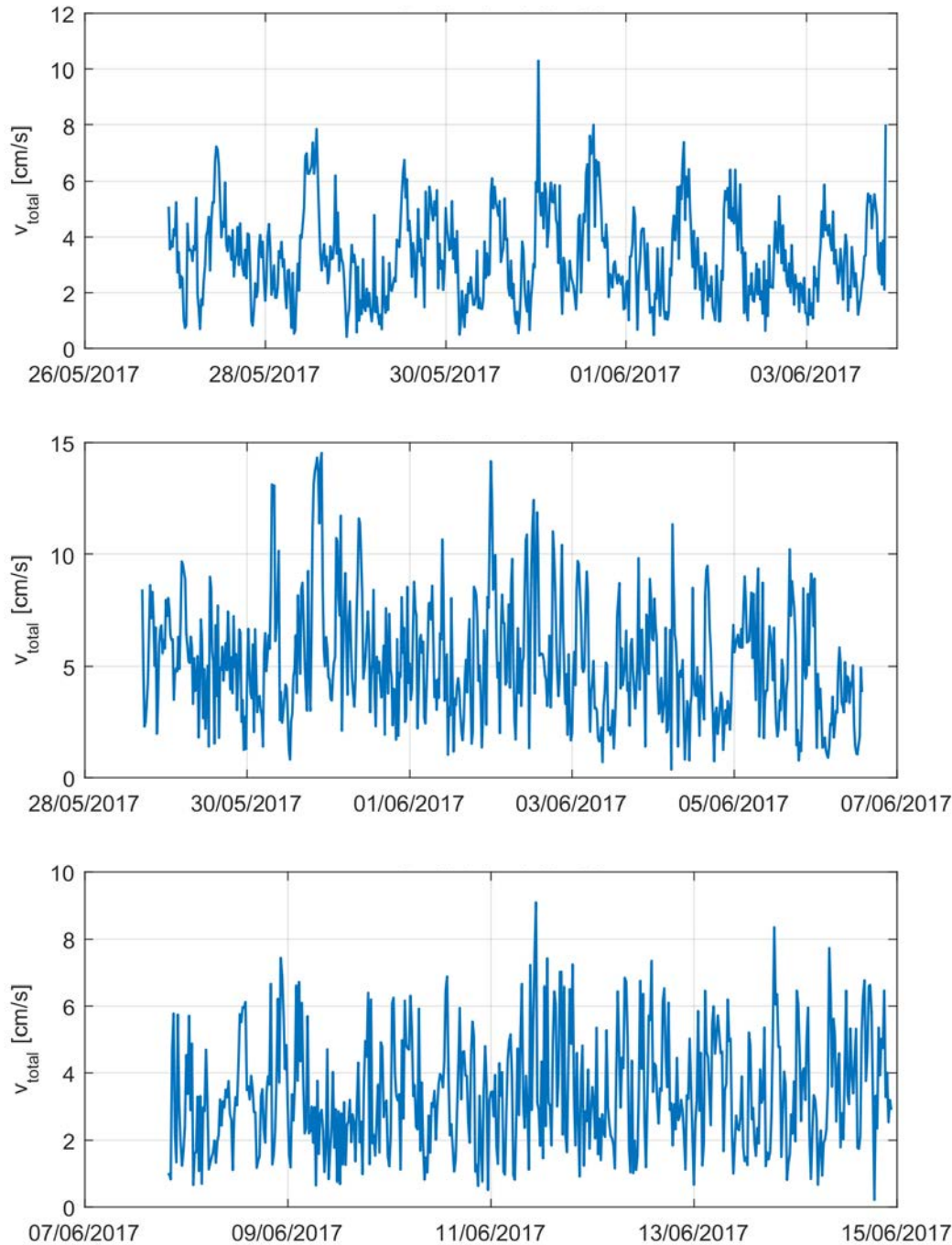


Figure 35: Measured time series 35 m above bottom of total velocity magnitude at locations MOR001 (top), MOR002 (middle) and MOR005 (bottom).

Figure 36 displays vertical profiles of the mean and maximum velocity magnitude as well as the standard deviation. Similar characteristics are observed at all three locations. The model predicts reduced velocities in the lowest ~10 m above the sea floor (bottom boundary layer). Measurements in the lower 10 m are only available at MOR002; and also display reduced current velocities, in agreement with the model. The maximum current magnitude in the bottom boundary layer is underestimated by the model at the MOR002 location, compared to the in-situ data. This may be due to a high-current velocity event in the mooring time series that was more intense than the model time series or due to ADCP noise caused by a lack of scattering particles.

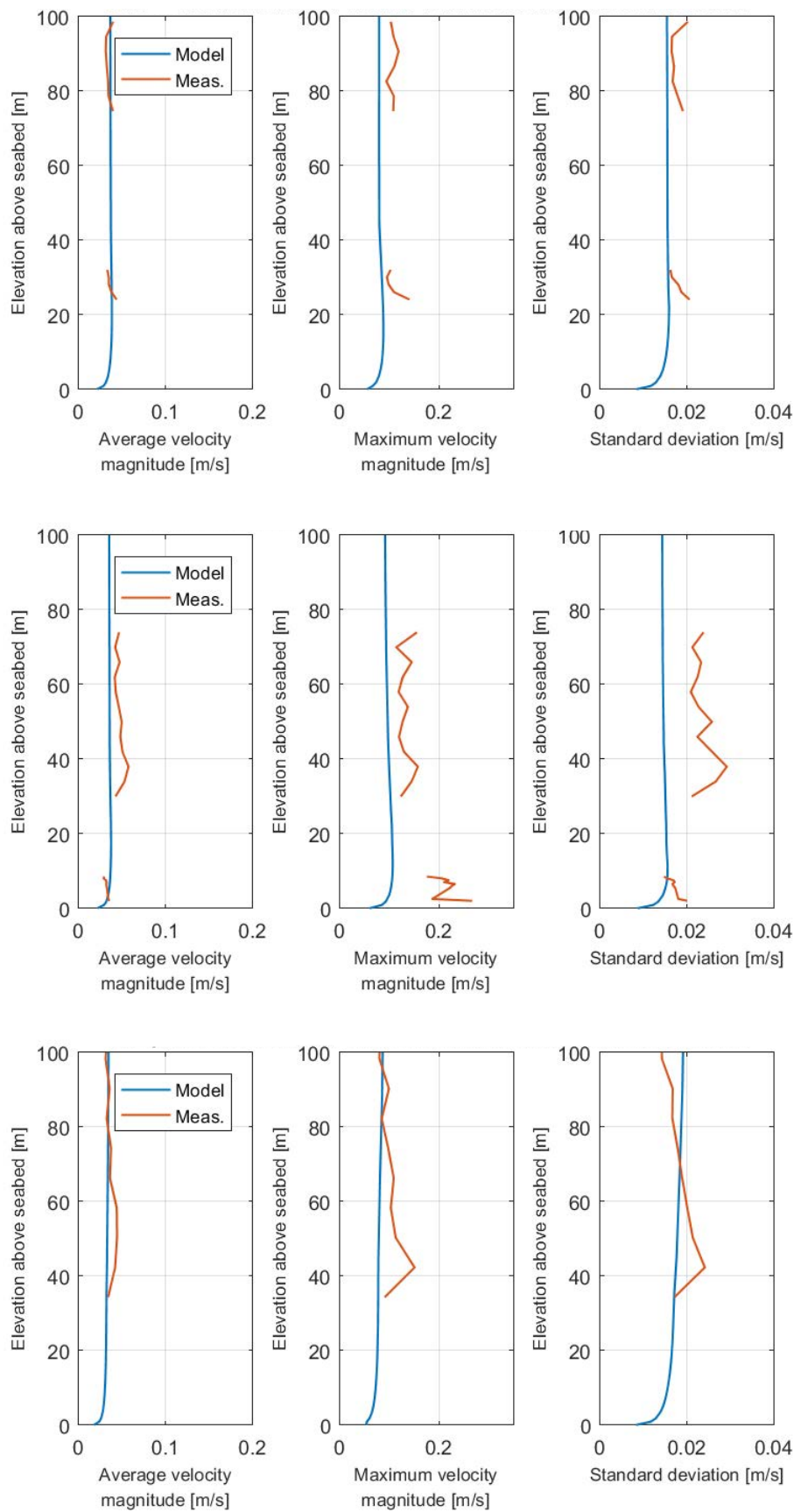


Figure 36: Vertical velocity profiles at the MOR001(top), MOR002 (middle) and MOR005 locations (model and measurements)

Figure 37, Figure 38 and Figure 39 display current direction time series for both the measurements and the model at 35 m above the seafloor. From the measurement and model time series (3 times 21 days in March, April and May), it is clear that the current direction is quite variable. Therefore, current direction observations from the 8-17 days mooring deployments are not long enough to determine the long-term directional current climate.

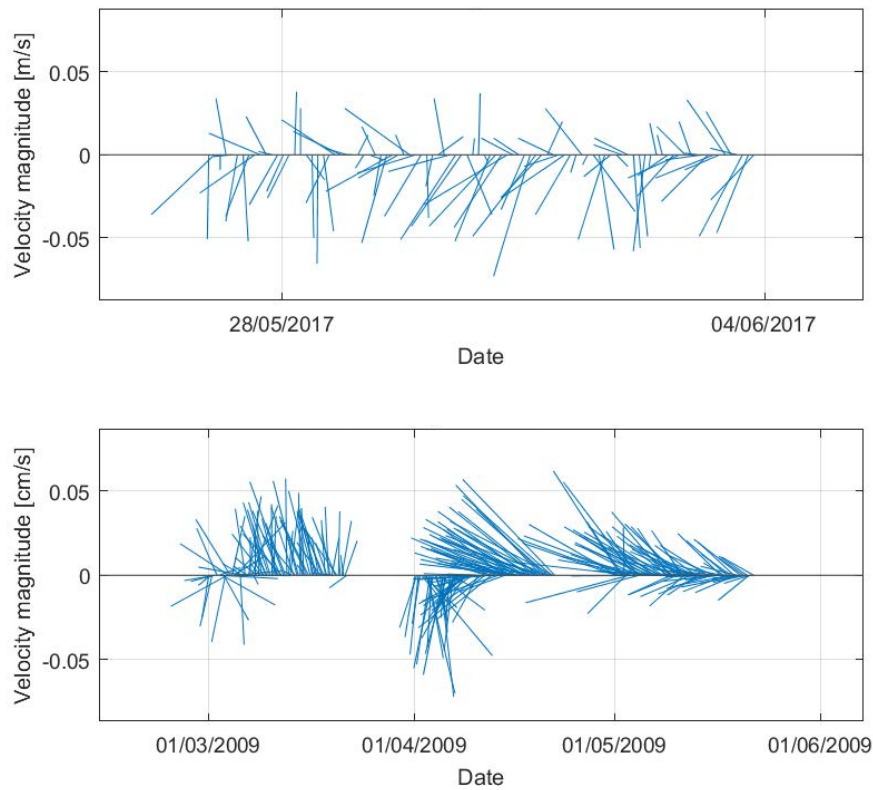


Figure 37: Current direction time series 35 m above bottom at MOR001 location of measurements (top for the deployment period between 26 May 2017 and 3 June 2017) and model (bottom for the 3 time series of 21 days in March, April and May 2009)

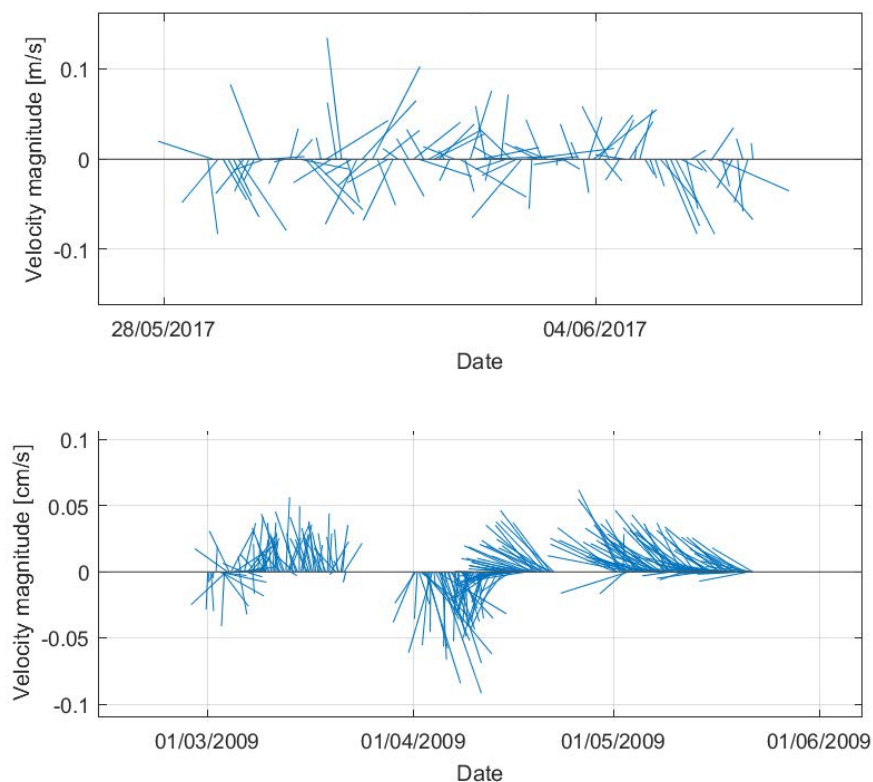


Figure 38: Current direction time series 35 m above bottom at MOR002 location of measurements (top for the deployed period between 28 May 2017 and 6 June 2017) and model (bottom for the 3 time series of 21 days in March, April and May 2009).

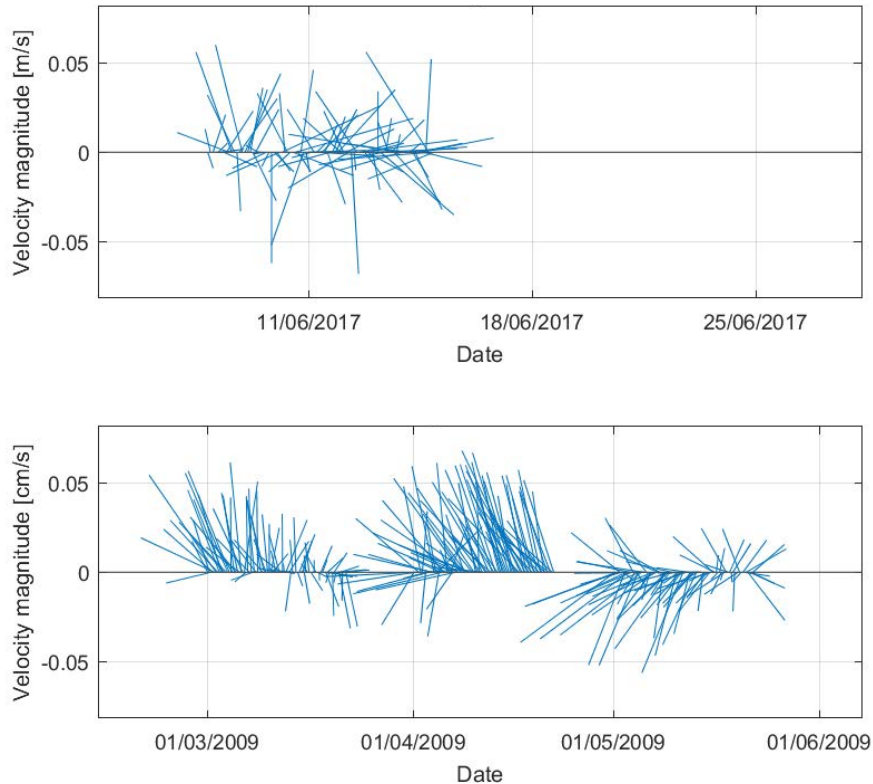


Figure 39: Current direction time series 35 m above bottom at MOR005 location of measurements (top for the deployed period between 7 June 2017 and 24 June 2017) and model (bottom for the 3 time series of 21 days in March, April and May 2009).

Current roses indicate that measured currents were predominantly WSW-directed at MOR001 (Figure 40), and ESE-directed at MOR005 (Figure 42). At MOR002 (Figure 41), no dominant current direction is visible in the current rose. In the model time series, currents at MOR001 and MOR002 are mostly northward in March 2009, southward in early April 2009 and then veer to west- and northwestwardly directions in late April and May. In other words, the model time series includes periods that are consistent with the short-term current measurements (e.g. early April 2009, which also had predominantly southward currents at MOR001).

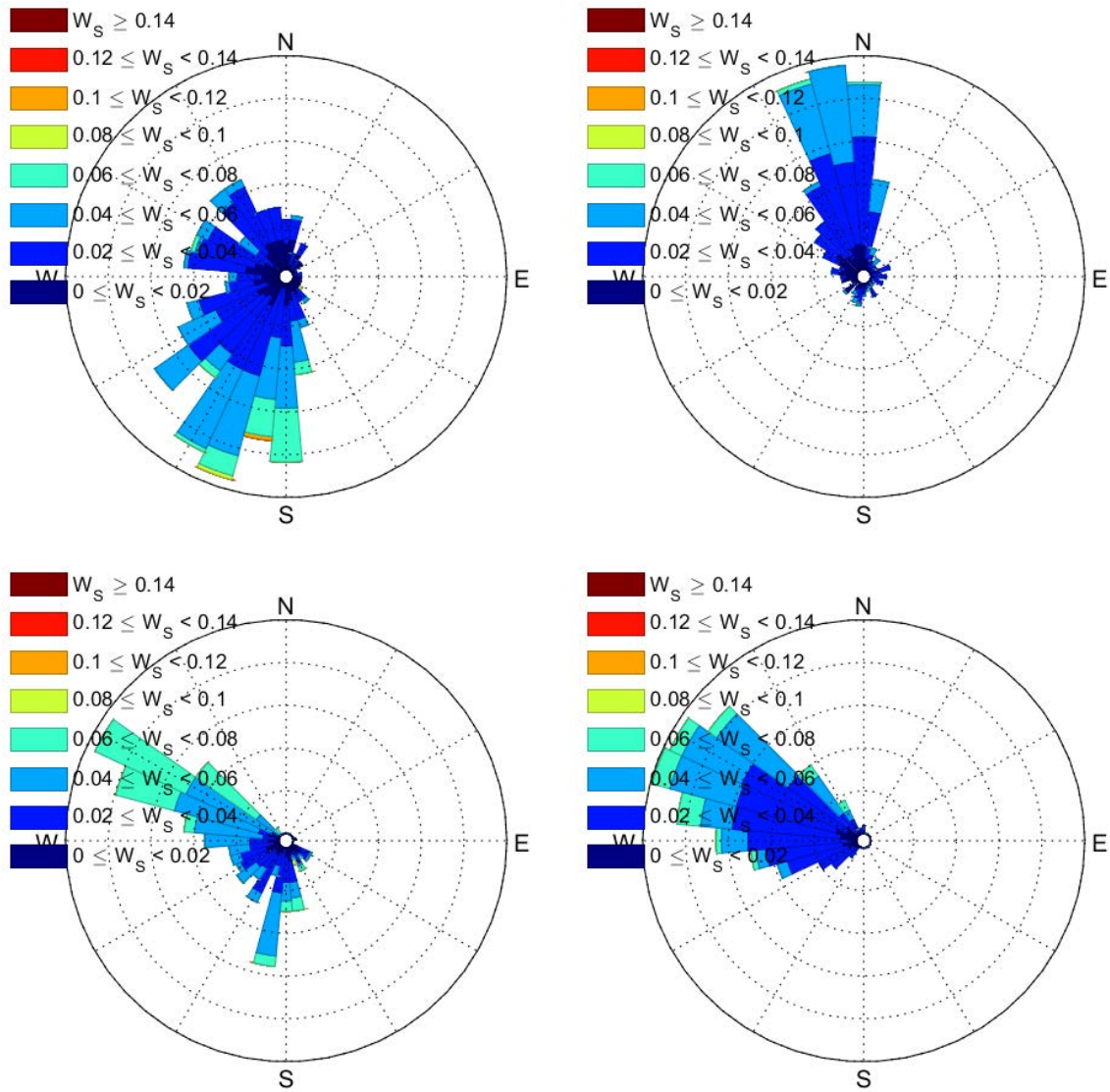


Figure 40: Current velocity [m/s] rose 35 m above bottom for MOR001 location. Top left: Average measurements over the deployed period (26 May 2017 to 3 June 2017). Top right: 21-day average model results (March 2009). Bottom left: 21-day average model results (April 2009). Bottom right: 21-day average model results (May 2009).

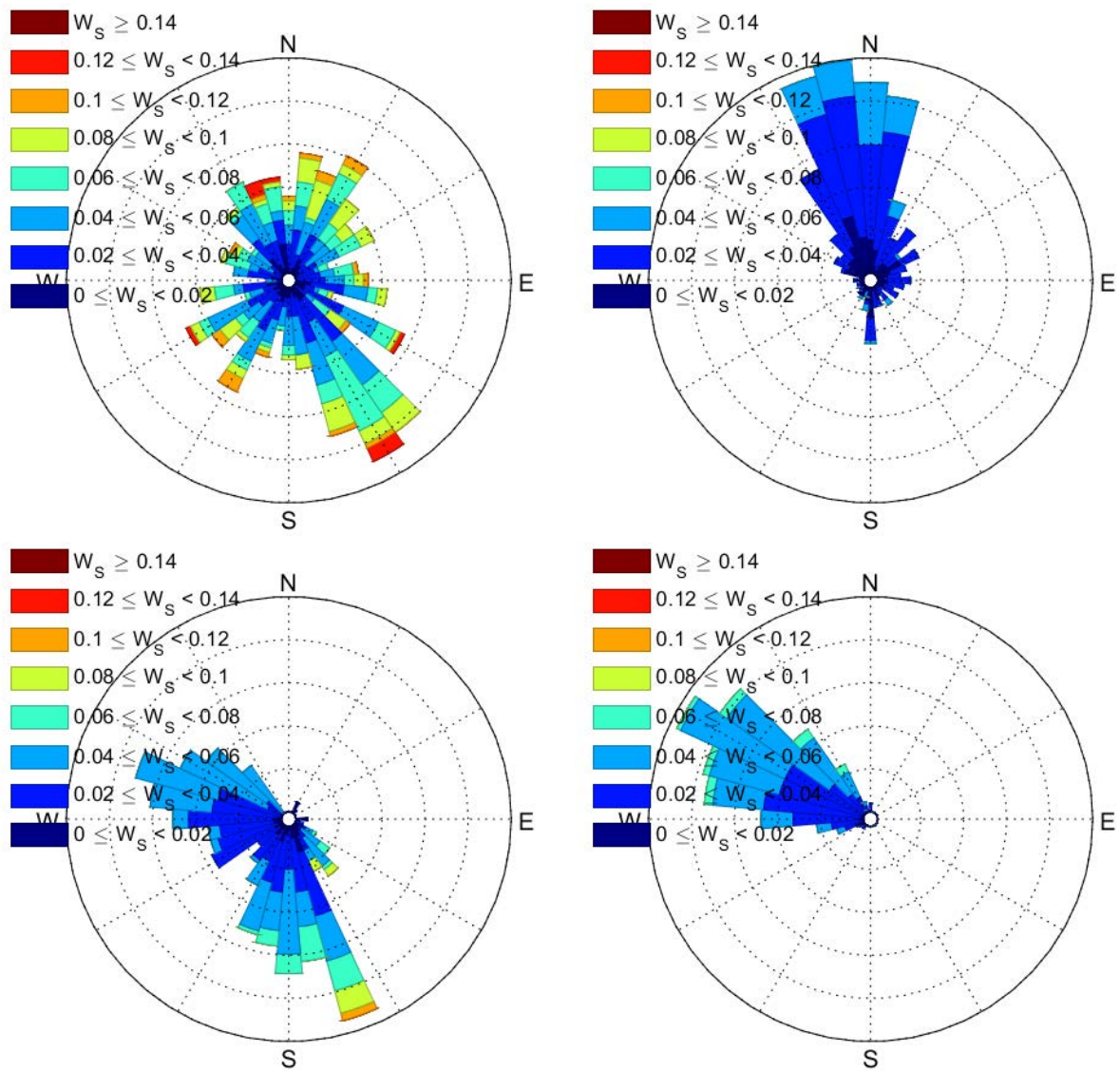


Figure 41: Current velocity [m/s] rose 35 m above bottom for MOR002 location. Top left: Averaged measurements over the deployed period (28 May 2017 to 6 June 2017). Top right: 21-day average model results (March 2009). Bottom left: 21-day average model results (April 2009). Bottom right: 21-day average model results (May 2009)

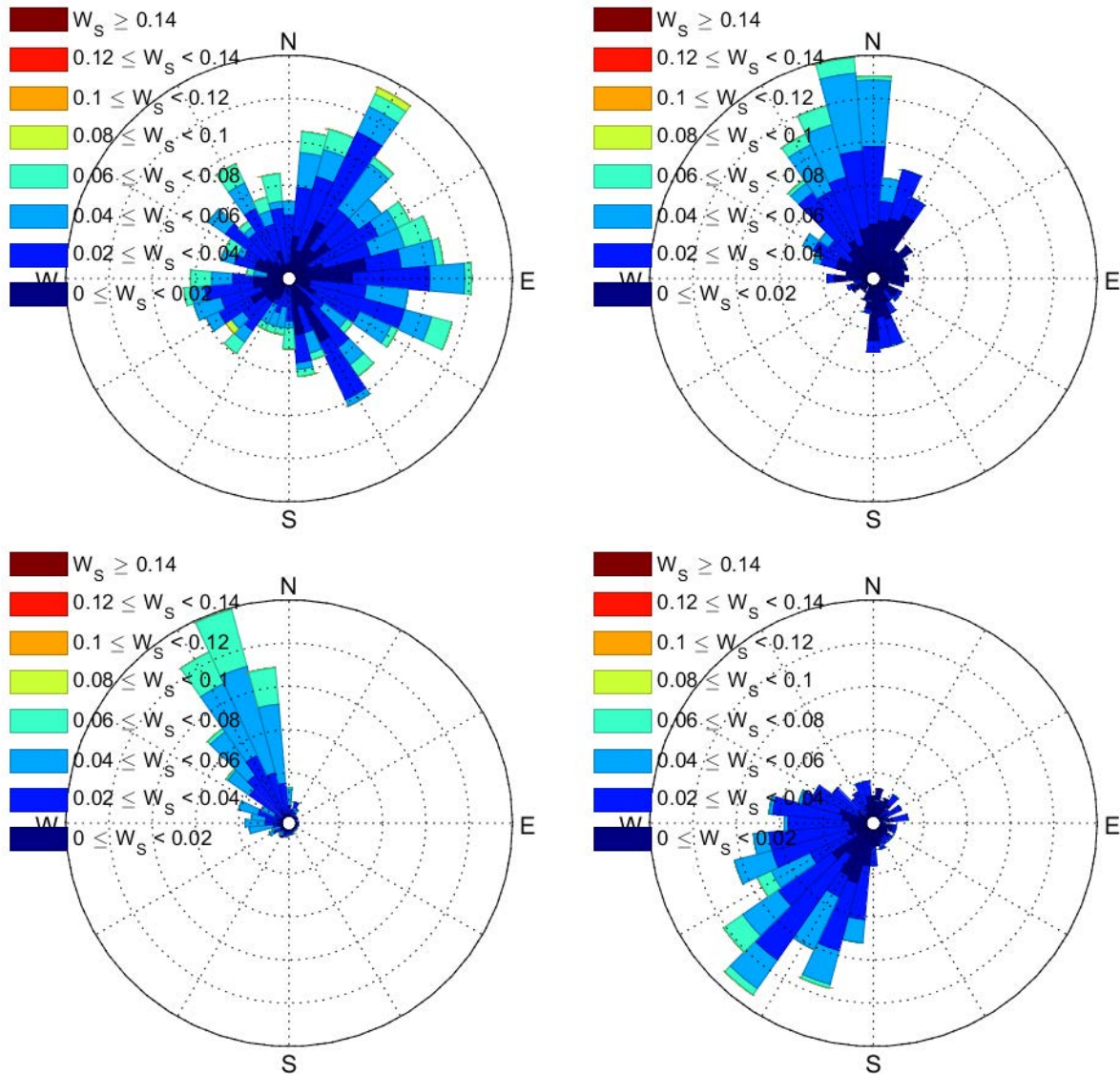


Figure 42: Current velocity [m/s] rose 35 m above bottom for MOR005 location. Top left: Averaged measurements over the deployed period between 7 June 2017 and 24 June 2017. Top right: 21-day average model results (March 2009). Bottom left: 21-day average model results (April 2009). Bottom right: 21-days averaged model results (May 2009).

In conclusion, a limited comparison between model simulations and mooring measurements shows that statistical properties such as mean current velocities and standard deviations are well-reproduced by the model. A comparison of current directions provides only limited results due to the short measurement period. The model validation will be extended further once the results from long-term mooring measurements are available.

4.1.3.4 Water turbidity and sedimentation rate

The water column in the central north Pacific Ocean is recognized as an oligotrophic environment, with a low primary productivity and a consequently poor food network. Therefore, these waters are often highly transparent, with little suspended material.

During the GSRNOD17 expedition to the CCFZ, several moorings were deployed in order to obtain temporal visualization of the hydrodynamic pattern occurring in the Contract Area. Turbidity sensors were installed on each mooring, close to the seabed, in order to collect

baseline data of the background turbidity. Three moorings, one long mooring covering the full water column and two short moorings covering the bottom water layer were deployed in B4S03. The short moorings were recovered after few days for an equipment check-up and provided a first insight of the physical oceanography information. Results in the B4S03 area indicated a very low level of light scattering; few particles are in suspension (e.g., detritus, "marine snow", plankton). The turbidity at the surface is in the range of 0.1-0.2 FTU, it fluctuates at the level of the thermocline, and then drops all along the water column, with a minimum at the seabed (about 0.02 FTU). Figure 43 here below display the collected data regarding turbidity. Background turbidity at MOR001, where the MiningImpact 2 Program will take place, varies between 0.5 and 0.84 FTU with a mean around 0.67 FTU at 3.5 m above seabed and between 0.46 and 0.72 FTU with a mean around 0.57 FTU at 12.5 m above seabed. At MOR002, located close to the designed Reference Area, turbidity fluctuates between 0.15 and 0.84 FTU with a mean around 0.3 FTU at 3.4 m above seabed and between 0.42 and 3.7 FTU with a mean around 0.54 FTU at 9.6 m above seabed.

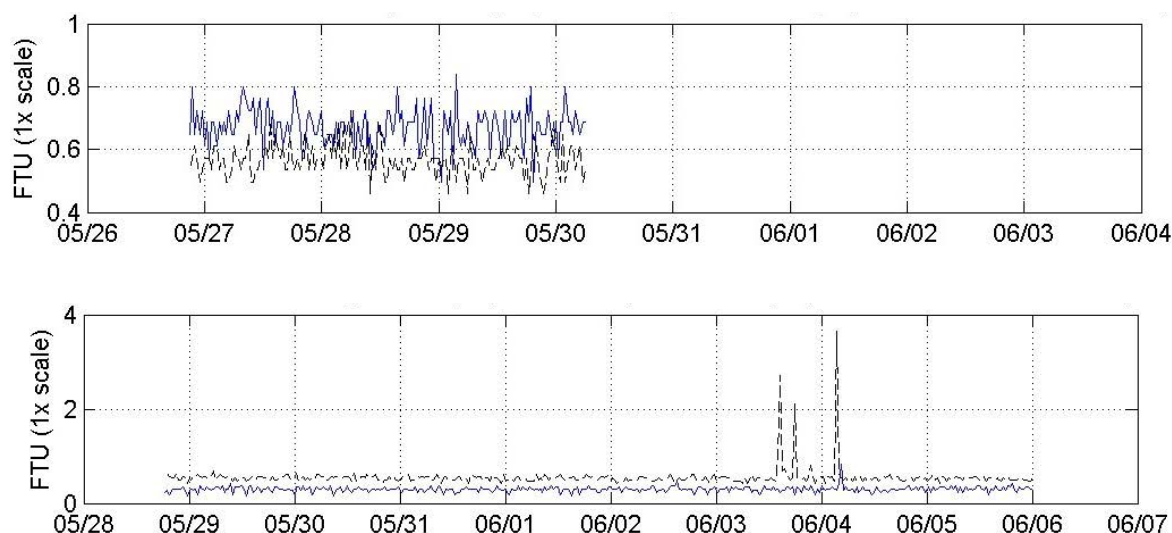


Figure 43: Time series of the background turbidity measured by the turbidity sensors located at 3.5 (blue) and 12.5 m (black, dashed) above seabed on MOR001 (top panel) and located at 3.4 (blue) and 9.6 m (black, dashed) above seabed on MOR002 (bottom panel) during the GSRNOD17 campaign. Unfortunately, due to a failure of the CTD sensor, only 3 days of data were recorded for MOR001. It must be noted that x-axis are not aligned, and that the turbidity event of June 06th 2017 for MOR002 could not be explained.

The prevailing natural sedimentation rate is thought to be only few millimeters per 1000 years in the abyssal habitat (Field et al., 1998).

4.1.4 Chemical oceanographic setting

The water column in the Eastern Pacific Ocean is reported in the literature as presenting a strong oxygen minimum zone (Lavín et al., 2006). Sampling at sub-zone B4S03 confirms this observation for this sub-zone. Dissolved oxygen level is 5 ml/l in the mixed layer, but drops to near zero just below the thermocline and remains there down to 600 m depth. Below that level, oxygen rises steadily until the seabed (~3.5 ml/l).

The area is considered to be oligotrophic due to a lack of nutrients to sustain primary productivity. The baseline data obtained during the GSRNOD2015A and GSRNOD2017 cruises confirm this observation. Nitrite and ammonia data fell below the level of detection (1 µg/l ≈ 0.07

μmol/l) at sub-zone B4S03. Maximum nitrate, phosphate and silicate levels were detected at 1000 m below the surface, at concentrations around 5.2, 25 and 50 μmol/l (data provided to ISA by GSR in its 2015, 2016 and 2017 AR, file numbers ISA-GSR_AR2014, ISA-GDR2016 and ISA-GSR_AR2016, respectively). The North Equatorial Current (see above), flowing westward through the GSR contract area, is characterized by the lowest surface nitrate concentrations of the Eastern Tropical Pacific Ocean (Pennington et al., 2006).

Regarding the temporal comparison, differences were noticed between expeditions GSRNOD15A and GSRNOD17 in terms of the shape of the vertical profile and/or the concentration depending on the nutrients analyzed. The shape of the vertical profiles of nitrate + nitrite, and phosphate (*i.e.*, showing maximal values at 1000 m water depth) were similar between the two GSR expeditions. Nitrate + nitrite concentrations were slightly lower in the GSRNOD15A (0.72 - 5.29 μmol L⁻¹) than in the GSRNOD17 water samples (6.62 - 8.84 μmol L⁻¹). In contrast, the GSRNOD15A water samples (19.41 - 23.96 μmol L⁻¹) were characterized by much higher phosphate levels than those gathered during GSRNOD17 (4.38 - 5.32 μmol L⁻¹). For silicate, both profile shape and the value of the maximal concentrations differed between the two GSR expeditions. Unlike GSRNOD15A, for which maximal values were observed at 1000 m depth, GSRNOD17 silicate concentrations were highest in the deep water samples taken at 200 m above the seabed. Silicate levels were higher in GSRNOD17 (maximal concentration: 217.67 - 263.88 μmol L⁻¹) than in GSRNOD15A samples (48.73 - 52.33 μmol L⁻¹). The GSRNOD17 silicate values also exceeded concentrations reported in other CCFZ studies (Haeckel and Arbizu (2015): 81.07 - 104.25 μmol L⁻¹, Son et al. (2014): around 150 μmol L⁻¹).

The observed differences in water column nutrients between the two GSR expeditions may be the result of inter-annual and/or seasonal variability. However, seasonal variability in the region is said to be weak (Amos and Roels, 1977; Pennington et al., 2006). Furthermore, GSRNOD15A was undertaken during an El Niño phase (SOI ranging between -1.6 and -1.7), and GSRNOD17 took place during a weak La Niña – El Niño phase (Southern Oscillation Index (SOI) for May 2017: +0.3, June 2017: -0.4). An El Niño phase is generally associated with reduced nutrient levels (Pennington et al., 2006), which may explain the reduced nitrate concentrations measured in the GSRNOD15A samples. Also the Pacific Decadal Oscillation, a source of multi-decadal variability, was shown to affect nutrient concentrations in the Pacific Ocean (Yasunaka et al., 2016).

Table 17: Nutrient concentrations of the water samples collected during GSRNOD17 in the B4S03 sub-zone. Except for the deepest water samples collected at 200 m above the seabed, for which exact depths are given, water depths provided are approximated to allow for comparisons between CTD-carousel water sampler casts

	Water depth [m]	Ammonium (μmol L ⁻¹)	Nitrite + Nitrate (μmol L ⁻¹)	Silicate (μmol L ⁻¹)	Phosphate (μmol L ⁻¹)
CTD011	4	<0.07	0.19	6.15	<0.03
	64	<0.07	5.59	264.68	3.66
	84	<0.07	0.55	3.39	<0.03
	490	<0.07	0.55	5.32	<0.03
	1000	<0.07	7.20	149.60	4.65
	4356	<0.07	0.30	5.78	<0.03
CTD012	4	<0.07	0.46	3.85	<0.03
	64	<0.07	0.21	3.55	<0.03
	84	<0.07	0.56	4.76	<0.03
	490	0.32	5.89	92.59	4.00
	1000	0.51	7.05	170.79	4.65
	4246	<0.07	5.22	240.21	3.33

	Water depth [m]	Ammonium ($\mu\text{mol l}^{-1}$)	Nitrite + Nitrate ($\mu\text{mol l}^{-1}$)	Silicate ($\mu\text{mol l}^{-1}$)	Phosphate ($\mu\text{mol l}^{-1}$)
CTD013	4	0.18	0.86	3.85	<0.03
	64	<0.07	0.60	3.91	<0.03
	84	0.14	0.67	4.37	<0.03
	490	<0.07	6.14	92.98	4.38
	1000	<0.07	7.17	154.70	4.86
	4242	<0.07	5.87	217.67	3.39

Finally, along the water column, particulate nitrogen and particulate carbon, used as proxies for pelagic biomass, measured in the area of interest, declined with an increasing depth (data provided to ISA by GSR in its 2015, 2016 and 2017 AR, file numbers ISA-GSR_AR2014, ISA-GDR2016 and ISA-GSR_AR2016 respectively). Lower PN values were measured for the GSRNOD17 than for the GSRNOD15A samples collected at B4S03. Nonetheless, PN concentrations measured during GSRNOD17 were more similar to the values reported by Chavez et al. (1996) and Eppley et al. (1992) for the Equatorial Pacific. PC values were roughly comparable between the two GSR expeditions (average over all 4 m (z) samples, GSRNOD15A: $0.12 \pm 0.11 \text{ mg L}^{-1}$, GSRNOD17: $0.07 \pm 0.02 \text{ mg L}^{-1}$).

Table 18: Particulate nitrogen (PN) and carbon (PC) data of water column samples taken during GSRNOD17 in B4S03. Except for the deepest water samples collected at 200 m above the seabed, for which exact depths are given, water depths provided are approximated to allow for comparisons between CTD casts. Because of a shortage of pre-weighed and muffled GF/F filters, no data are available for the 3-4 shallowest depths (i.e. 4, 64 and 84 m) sampled by CTD013.

	Water depth (m)	PC (mg L ⁻¹)	PN (mg L ⁻¹)
CTD011	4	0.086	0.009
	64	0.027	0.004
	84	0.310	0.012
	490	0.068	0.007
	1000	0.043	0.005
	4356	0.068	0.007
CTD012	4	0.057	0.008
	64	0.043	0.006
	84	0.086	0.016
	490	0.039	0.004
	1000	0.026	0.003
CTD013	490	0.024	0.003
	1000	0.024	0.002
	4242	0.028	0.003

4.1.5 Seabed substrate characteristics

4.1.5.1 Sedimentary facies and upper sediment layer subdivision

The results obtained from the 2015 and 2017 sub-samples, extracted from the box-cores, are summarized below. The core description was carried out following the protocol already

established for the classification of the sediments present in the GSR Contract Area, which is based on colour, texture and water content in a similar way to other contract areas within the CCFZ (Kim et al., 2012).

The core descriptions highlighted an intense burrowing in the sediment and the presence of significant boundaries within the sediment cores. The presence of two main colours of sediment (10YR4/3, 10YR5/4) and certain layers with different colours (i.e., 10YR4/1) enabled determination of the presence of many boundaries in the sediment cores. These boundaries can be sharp, gradational or burrowed, and a few examples of inclined and undulated boundaries were also found.

CT scanning has identified that in most cores a quite abrupt boundary is present at the first 2-10 centimetres of sediment, characterized by changes in radio-density and/or burrowing intensity. This boundary either can be related to changing oceanographic conditions (e.g., erosive), or it can be of diagenetic origin. CT scanning also enabled observation of the internal structure of the sediment cores, such as layers with a high concentration of burrowing, the presence of nodules and micronodules, and the dominant vertical or horizontal components of the burrows in each core. Indeed, the dynamic range of materials, each with distinct densities, can be displayed as a radio-density histogram (relative to the CT greyscale intensity). By applying a bandpass filter, cutting lower or higher densities, specific structures or features (characterized by a specific density) may be visualised. For example, burrows piercing the sediment are most frequently filled with sediments of lower density values, and can be visualised filtering out higher densities (Figure 44).

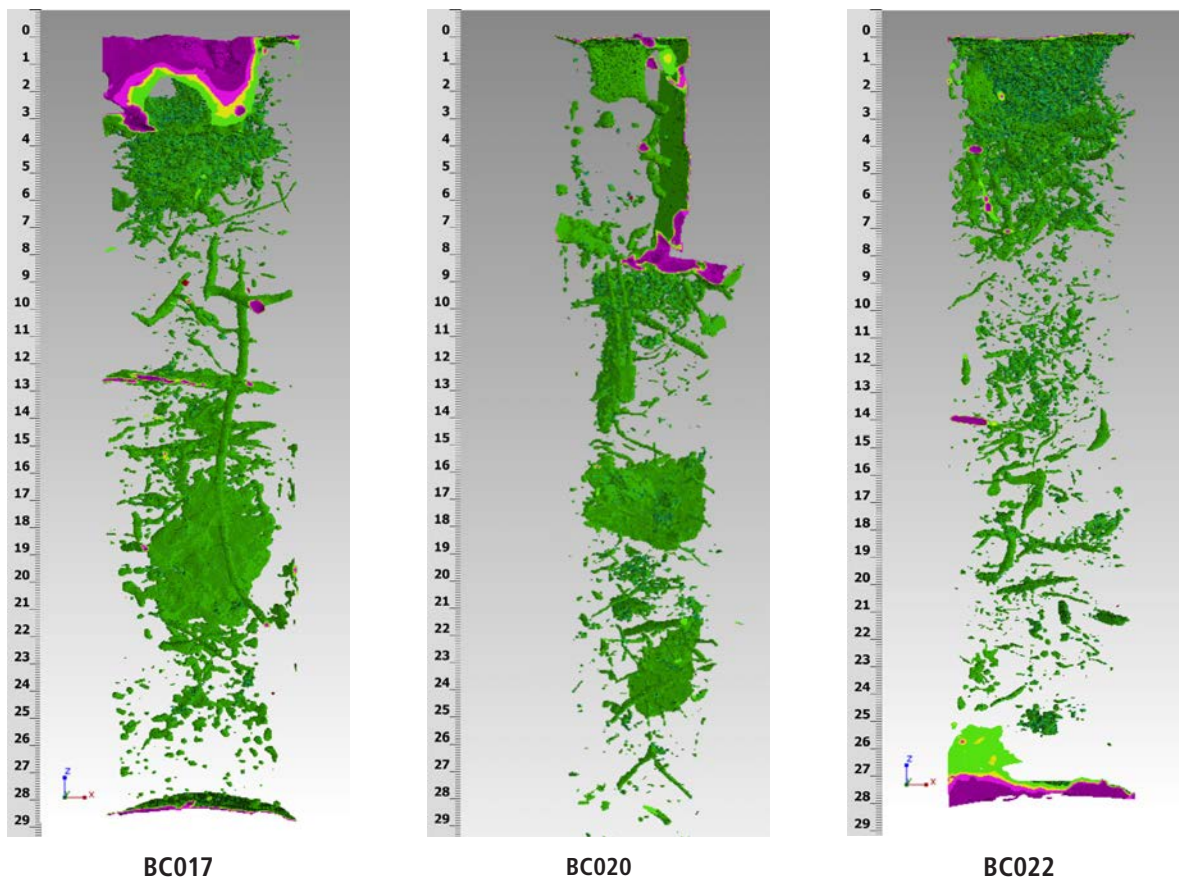


Figure 44: Burrows piercing the geological cores BC017 (left), BC020 (middle) and BC022 (right) in Area B4S03. The crack planes in BC017 and BC020 are visible (horizontal and vertical). Only few micronodules are present (red).

The analysis of the Multi-Sensor Core Logger (MSCL) data showed that most of the cores were characterized by low magnetic susceptibility and wet bulk density values at the top of the core, both quickly increasing until reaching a maximum typically at 3-5 cm deep. This common pattern suggests the presence of a regional hiatus in the GSR area. A subsurface hiatus could partly explain the unearthing of older nodules in the sediment that broke apart and acted as nuclei for new nodules. Besides this uppermost layer, variations in magnetic susceptibility and wet bulk density also enabled confirmation of the presence of boundaries already detected with other techniques (such as CT scan). Last, luminosity shows an excellent correlation with colour variations along the core.

The sediments recovered in the GSR Contract Area have been assigned in previous reports to three major sediment facies (A, B, and C, which were tentatively correlated to those defined by Kim et al. (2012).

Facies A typically corresponds to the uppermost layer of sediment (Figure 46, Figure 47 and Figure 48), characterized by brown to dark yellowish brown (10YR4/3 and 10YR4/4) sandy mud with occasional light (10YR5/3 to 10YR5/4, as well as 10YR6/3 to 10YR6/6) burrows becoming more frequent downwards. Facies B was divided into B1 and B2. The reason to distinguish them despite their similarities is the sharp transition between them in some cores and that burrows are less frequent in B2 facies. Facies B1 typically consists of yellowish brown (10YR5/4) to light yellowish brown (10YR6/4) mud that can appear either as homogeneous mud or as sandy mud dotted with burrows of various sizes mostly infilled with sediment from facies A (mostly 10YR4/3 and 10YR4/4) becoming more frequent downwards (Figure 45, Figure 46, Figure 47). Facies B2 shows intermediate colours between facies A and B1 (greyish brown to brown, 10YR5/2 to 10YR5/4) (Figure 45, Figure 46, Figure 47). Last, facies C is rarely seen in the cores, and consists of dark grey to brown sediment (10YR4/1 to 10YR4/3) below a well-defined boundary, occasionally undulated and bioturbated (Figure 45, Figure 46, Figure 47).

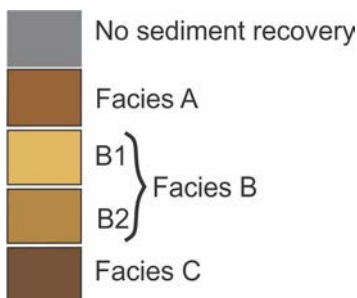


Figure 45: Diagram of the different facies characterizing the sediment cores recovered in the GSR Contract Area, based on colour and burrowing

These three major sediment facies corresponded to four basic vertical sediment patterns (simplified by considering only facies B instead of facies B1 and B2): A, A-B, A-B-C, and A-B-A. The broadening of the sediment core database with the inclusion of Y4 cores shows that these vertical sediment patterns are still correct. With the purpose of analyzing the distribution of the sediment in area B4S03 and its vicinity, a new map showing the distribution of the vertical sediment patterns have been assembled (Figure 48).

The most abundant sediment pattern in area B4S03 and its vicinity is A-B, which appears to show many combinations. The pattern A-B1-B2 mostly appears within valleys or depressions; the same applies to the pattern A-B1, which could be followed by a B2 facies if the box core had

penetrated further into the seafloor. The pattern A-B2 is always found over flat plateaus, mostly east of B4S03. Last, the pattern A-B1-B2-B1 only appears in two cores located east of area B4S03, both recovered in depressions. By contrast, the pattern A-B-C is scarce, and can appear as A-B1-B2-C (observed both in ridges and valleys), A-B1-C (observed in a flat and wide depression) and A-B2-C (observed on a ridge). Summarizing, the facies A is always present; facies B1 can be absent in elevated areas but always appears in valleys or depressions; facies B2 can appear in any environment (valleys, plateaus, ridges, depressions) and facies C has been observed mostly in a plateau environment, with the only exception of BC053.

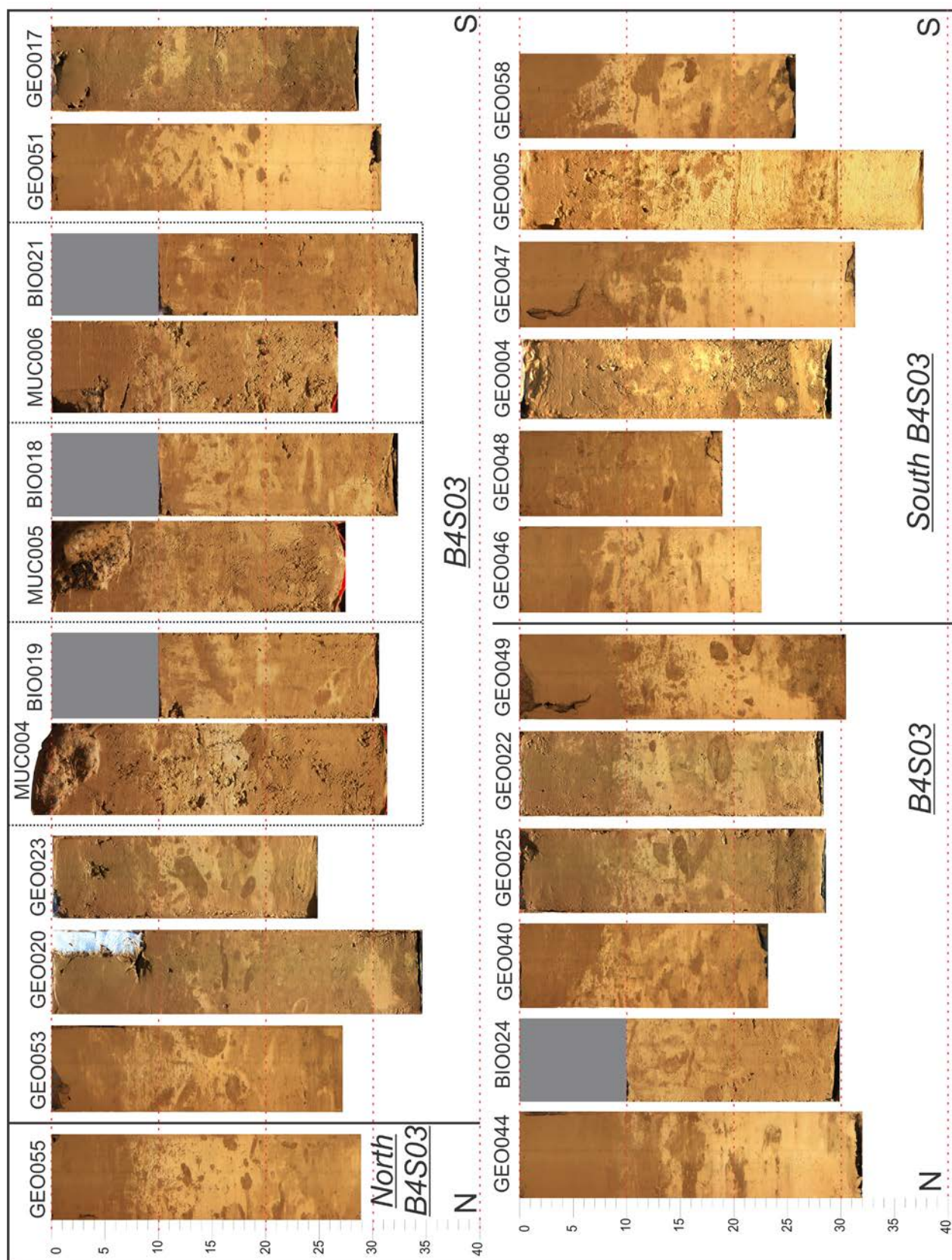


Figure 46: Box-core and multicore sediment samples recovered in area B4S03 and its vicinity during Y1, Y2 and Y4 (see Figure 48 for location). The samples recovered from the same sub-zone have been grouped within a box with dashed borders. The red dashed lines indicate the depth every 10 cm

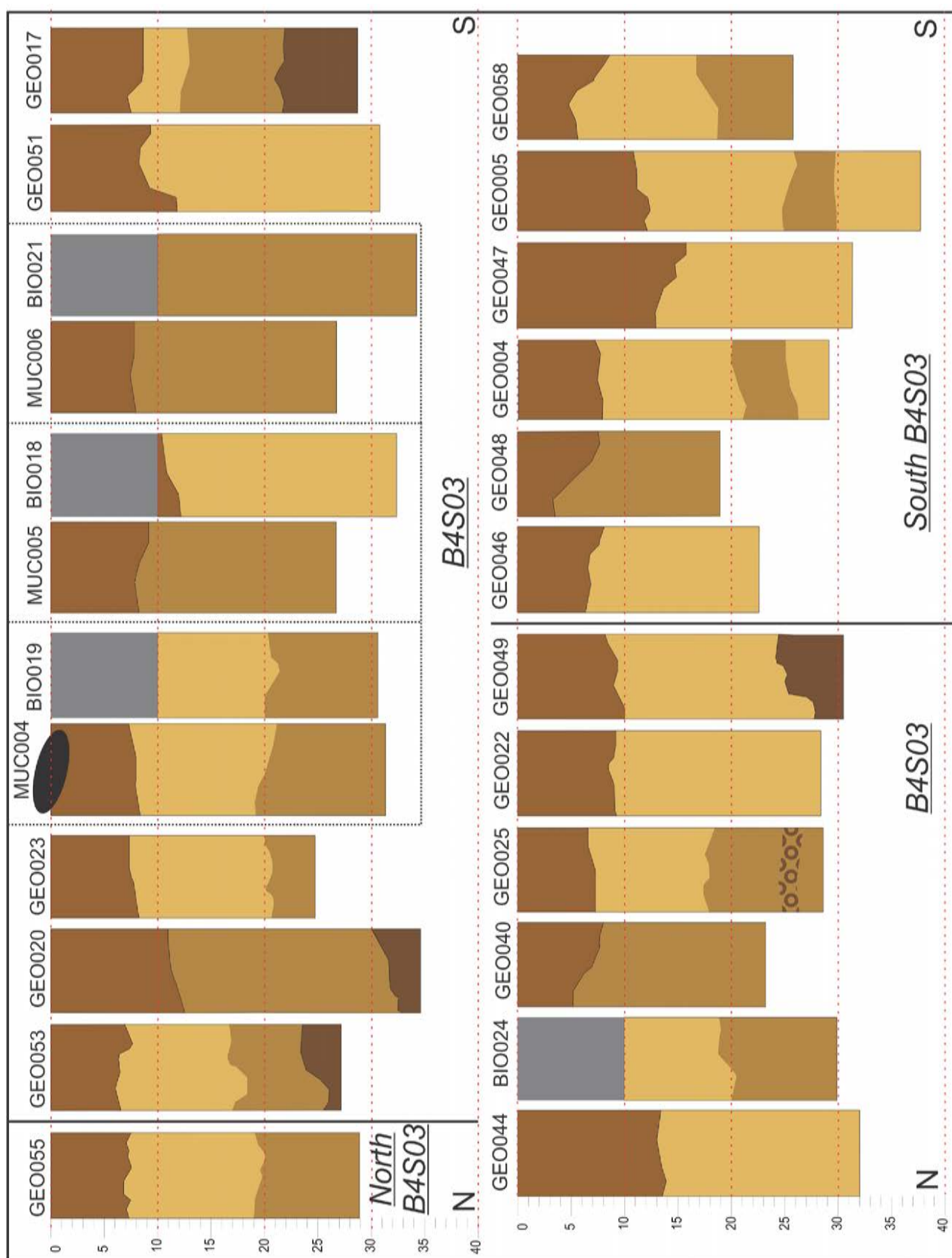


Figure 47: Diagram interpreting the box-core and multicore sediment samples recovered in area B4S03 and its vicinity during Y1, Y2 and Y4 (see Figure 48 for location)

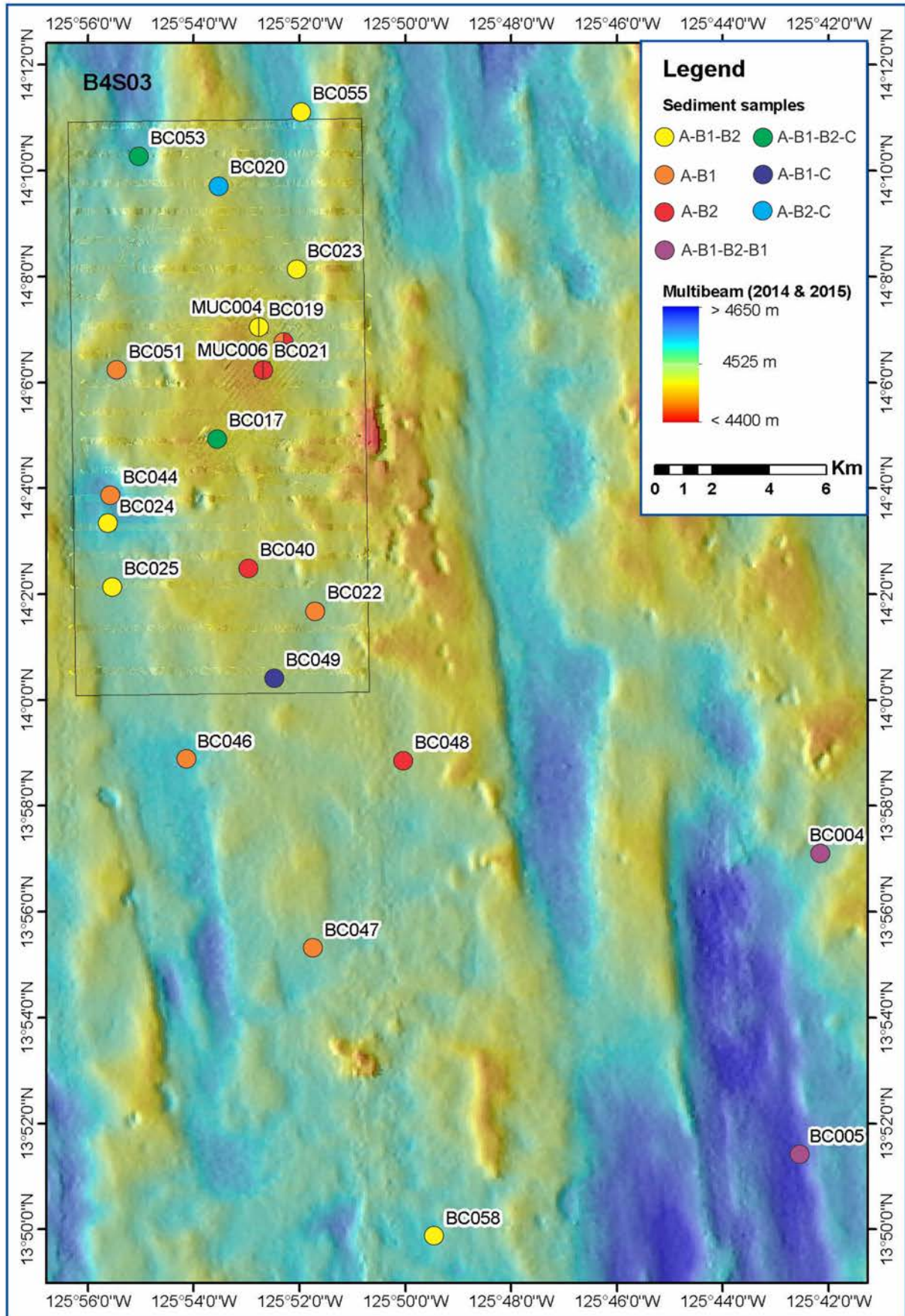


Figure 48: Distribution of the various vertical sediment patterns in area B4S03 and its vicinity

4.1.5.2 Sediment composition

The **smear slide analysis** confirms that most of the sediment consists of a biogenic siliceous clayey mud, but the visually estimated proportion of biogenic silica (~40%) was lower than that of the ICP analyses (~50%). Traces of silicoflagellates, fish debris and volcanic glass were observed, and although micronodules and other Fe minerals were estimated to be roughly 5%, locally they were estimated to make up 10% of the sediment (6-7.5% in ICP analyses). Clumps of marine organic matter (pellets) are frequent in the upper sediment, and the increase in Fe oxyhydroxides with depth may point to diagenesis. Calcareous microfossils only accounts for ~0.04 % of the sediment, and is hardly visible on the pie chart here below (Figure 49).

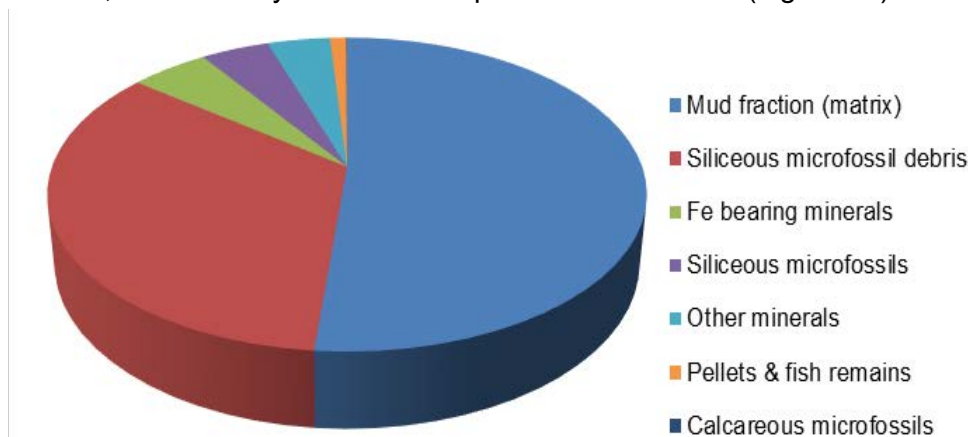


Figure 49: Average composition of the sediment recovered in campaigns GSRNOD14A and GSRNOD15A in the GSR Contract Area, according to estimations using smear slides

The **bulk grain size** demonstrated that although the sediment is generally considered as muddy, there is a significant silty component that corresponds to the biogenic portion of the sediment (later confirmed by the smear slide analyses). The variability in the grain-size distribution in areas B4S03 seems to be low. The surface sediments of all studied areas seemed to have many similarities, showing a good spatial correlation. The downcore variability can perhaps be attributed to, e.g., bottom current variations in the past (the CT scan data showed sharp boundaries), bioturbation and/or early diagenesis. These hypotheses must be verified by higher-resolution analysis, or by implementing new techniques, such as vertical thin sections.

In general terms, the sediment samples are bimodal, trimodal or polymodal, but those samples with a bimodal profile are dominant. The sorting of the samples is typically poor, and further diminishes at any depth within cores associated with narrow passages (BC051) and depressions (BC053, BC055), and within cores associated to plateaus (BC049, BC058, BC040). The sediment distribution is typically skewed towards the finer fraction of the sediment, but also presents frequent symmetrical distribution and occasional skewness towards the coarser fraction of the sediment. The major elements and trace metals were measured at the top (2 cm depth) of all the sedimentological samples recovered in GSRNOD17A cruises (Table 19 and Table 20)

Table 19: Percentage of the major elements analysed with ICP-AES (LOI = Loss on ignition)

Sample (2 cm)	Major elements (%)										LOI
	Al ₂ O ₃	CaO	Fe ₂ O ₃	K ₂ O	MgO	MnO	Na ₂ O	P ₂ O ₅	SiO ₂	TiO ₂	
BC040	13.47	1.06	6.43	3.01	3.1	0.55	4.14	0.5	50.73	1.27	14.81
BC044	13.26	1.1	6.29	2.95	3.11	0.36	4.51	0.53	51.19	1.24	15.07
BC046	13.18	1.08	6.26	2.96	3.08	0.37	4.26	0.53	51.67	1.24	14.83

Sample (2 cm)	Major elements (%)										
	Al ₂ O ₃	CaO	Fe ₂ O ₃	K ₂ O	MgO	MnO	Na ₂ O	P ₂ O ₅	SiO ₂	TiO ₂	LOI
BC047	13.64	1.07	6.16	2.9	3.11	0.37	4.53	0.51	50.41	1.22	15.44
BC048	13.56	1.09	6.48	2.96	3.07	0.62	4.17	0.55	52.17	1.25	13.86
BC049	13.59	1.1	6.49	2.95	3.13	0.73	4.33	0.53	51.9	1.26	13.96
BC051	13.72	1.11	6.52	3.02	3.18	0.41	4.38	0.55	52.36	1.28	13.42
BC053	13.57	1.15	6.52	3.01	3.16	0.78	4.29	0.6	51.84	1.27	14.01
BC055	13.27	1.14	6.4	2.97	3.14	0.78	4.42	0.57	50.85	1.26	14.61
BC058	13.26	1.06	6.3	2.93	3.08	0.72	4.44	0.49	52.15	1.23	14.33

Table 20: Content of trace elements (in ppm) analysed with ICP-AES

Sample (2 cm)	Trace elements (ppm)												
	Ba	Be	Bi	Cd	Co	Cr	Cu	Ni	Pb	S	Sr	Zn	Zr
BC040	4919	<5	<5	<10	78	71	278	183	<10	2895	237	112	176
BC044	4812	<5	<5	<10	69	69	234	179	<10	3508	235	91	168
BC046	4957	<5	<5	<10	66	71	255	132	<10	3231	237	100	169
BC047	4888	<5	<5	<10	67	68	235	127	<10	3863	234	93	168
BC048	5108	<5	<5	<10	82	69	303	293	<10	3140	242	115	171
BC049	5056	<5	<5	<10	85	69	331	241	<10	3459	243	120	169
BC051	5025	<5	<5	<10	72	70	255	146	<10	3545	242	83	174
BC053	4981	<5	<5	<10	88	70	319	237	<10	3296	245	103	172
BC055	4925	<5	<5	<10	93	69	303	277	<10	3743	245	91	169
BC058	5087	<5	<5	<10	84	69	309	273	<10	3874	242	96	167

In area B4S03, the percentages of Al₂O₃ and Fe₂O₃ are higher in the NW and over the elevated areas, and lower in depressions located within the elevated areas (such as in the case of BC022) and locally higher within shallow valleys (i.e., BC025). The content of SiO₂ is higher to the west and lower to the east. Last, despite the historical data not providing information on the MnO percentage, the density of the samples analyzed during the course of the GSR exploration allow the creation of a map detailing the distribution of MnO in area B4S03. The percentage of MnO in the sediment is higher to the north (BC053 and BC055) and over the central ridge and annex plateau (BC017, BC020, BC022 and BC049). The minimum values are always measured within valleys or depressions (BC005, BC044, BC046, BC047 and BC052).

The **XRF analysis** shows the presence of enriched layers of certain elements (i.e., Ca) in the cores. The Ca/Si, Si/Al and Mn/Fe ratios show the most relevant variations, frequently associated with changes in sediment colour and in certain cases shedding light on sharp variations in the sediment that had not been clearly identified before.

According to ICP analyses, SiO₂ makes up to 50% of the sediment. The ratio between the components containing MnO and Fe₂O₃ is always higher in the top of the sediment cores, frequently double the values of the sediment analyzed down core.

The **clay minerals**, which comprise the mineral groups of smectite, illite, kaolinite, and chlorite, are present in (not is) every BC in relatively similar concentration, suggesting that the origin is probably essentially continental.

The Clay XRD analyses were carried out in Y4 on the sediments near the top of all the GEO box-cores, at 2 cm depth to avoid disturbances caused during the recovery with the box-core (Table 21). These data were combined with those of previous years to create maps in which the spatial distribution of the main groups of clay minerals can be observed (Figure 50).

Table 21: Estimated clay content at the top of the sediment cores (2 cm deep) based on the analysis of the oriented and glycolysed diffractograms for samples recovered in GSRNOD17A cruise. hSm/hI – Height of smectite divided by height of illite peaks. Colors used in the table correspond to the colours of Figure 50.

	Illite (% clays)	Smectite (% clays)	Chlorite (% clays)	Kaolinite (% clays)	hSm/hI
BC040	48.9	36.4	9.9	4.7	0.8
BC044	49.9	35.9	9.5	4.7	0.6
BC046	50.2	34	10.3	5.6	0.5
BC047	45.4	31.8	15.5	7.3	0.8
BC048	47.9	37.6	9.7	4.8	0.7
BC049	50.1	36.4	9.3	4.2	0.7
BC051	50.3	36.8	8.7	4.1	0.7
BC053	46.5	38	10.4	5.1	0.7
BC055	48.4	37.8	9.6	4.2	0.7
BC058	45.7	39.4	10.4	4.5	0.9

The samples analyzed in area B4S03 and its vicinity show a fairly uniform distribution of the main clay mineral groups (Figure 50). Those samples located south of the study area tend to show lower illite and higher chlorite and kaolinite content.

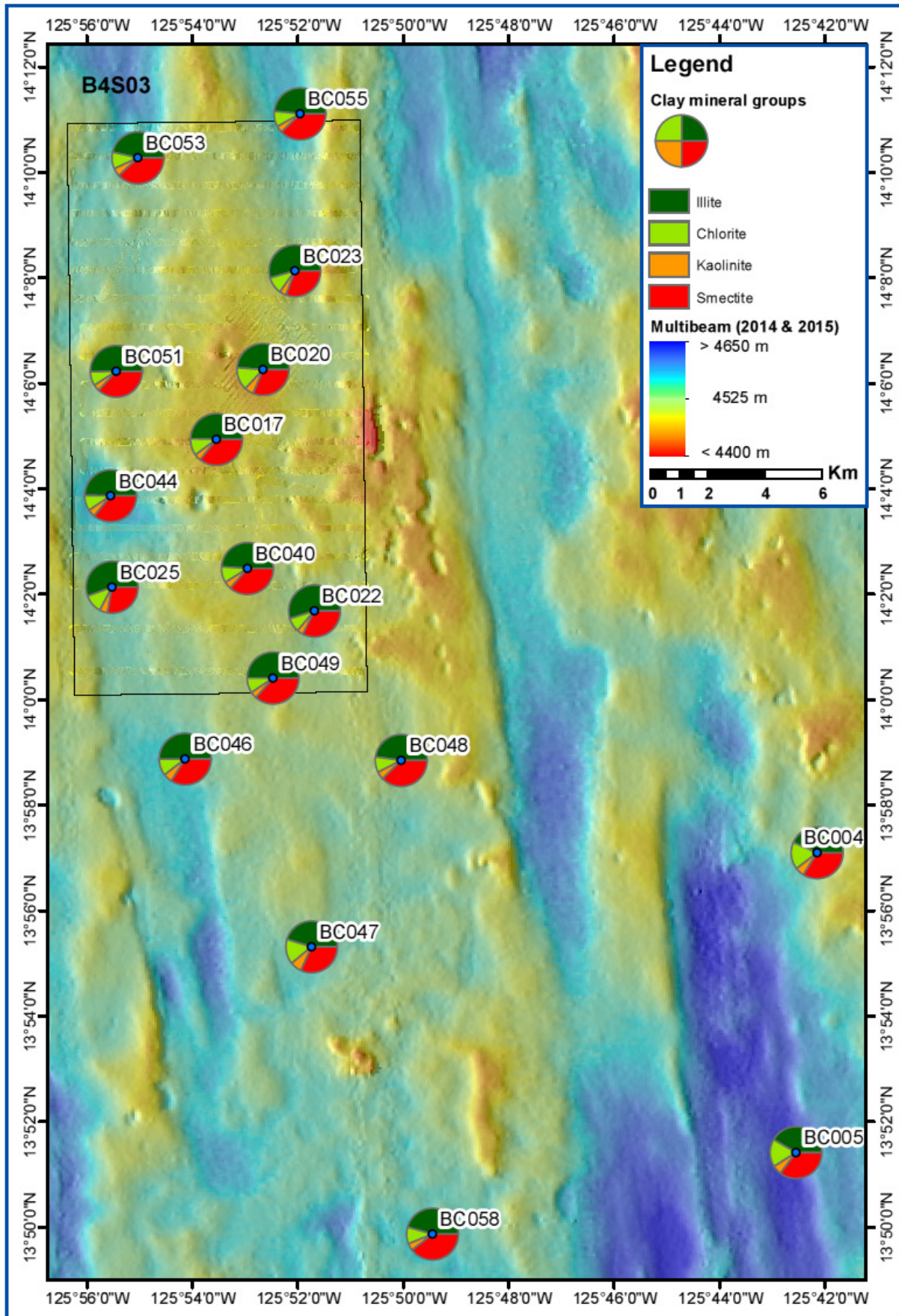


Figure 50 : Clay mineralogy distribution in area B4S03

4.1.5.3 Water content and Pore water analysis

The **water content** evaluated from the samples of the GSRNOD15A campaign was very high, between 55.63 and 72.28% in weight of water content (125.37 to 260.76% if referring to moisture content). Nevertheless, the majority of the measurements was in the range 175% - 275% (12 % of the samples around 200% (Figure 51). The high values at > 400% were ignored and are related to measuring errors.

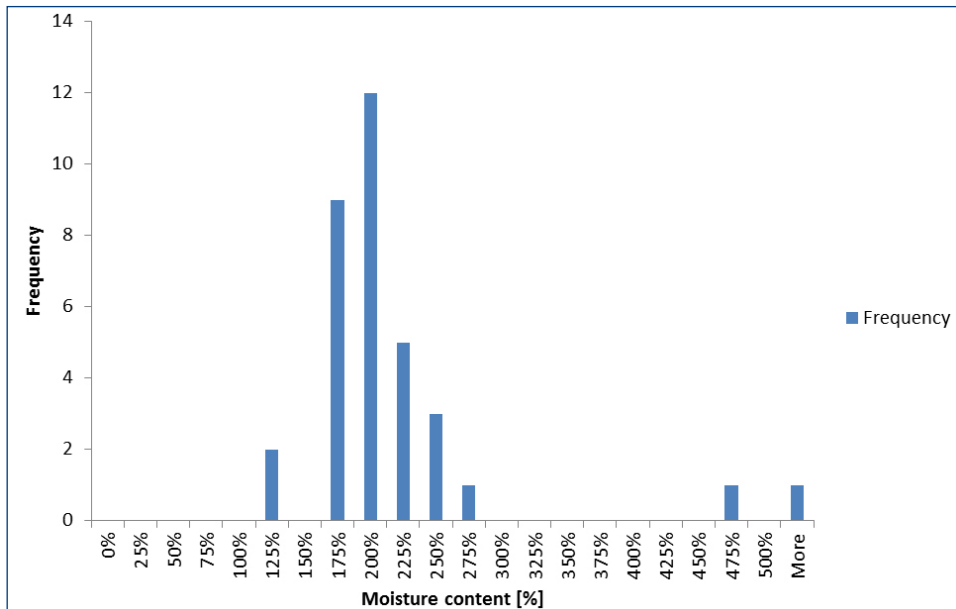


Figure 51: Summary of the moisture content determination during GSRNOD15A Campaign

Two years later, in 2017, the information regarding the **water content** (or moisture content) of the sediment samples from the GSRNOD17 expedition was obtained as a side-product of the laboratory procedures to analyze ICP-AES, Clay XRD and grain size. The smaller number of analyses carried out in Y4 (reduced from three to one for ICP-AES and Clay XRD) resulted in a decrease of the reliability of some water content data due to the impossibility of calculating an average value using various measurements. For this reason, the water content is reliable and varies within a small range of values (63.8 to 69.9 % water content in weight) within the upper centimetres of the sediment where more than one procedure provided an estimation of the water content. By contrast, the water content shows a higher scattering downcore where only one procedure provided an estimation of the water content, with outlier values such as in BC044 at 16 cm depth (76.7% water content in weight). The values of the water content in these uppermost layers of sediment are about 3% lower than those measured in previous years, possibly related to the protocol for the extraction of pore water in the sediment cores.

The **pore water analyses** proved to be a complicated procedure onboard and did not provide the expected results for $\delta^2\text{H}$ and $\delta^{18}\text{O}$, with too many samples showing values below the standard deviation. Also, only Ca, K, Mg, Na (cations, Table 22), Cl and SO_4 (anions, Table 23) could be measured to provide significant values, due to the need of using a rather high dilution (4000 times) in order to fit within the detection range of the equipment (ICP-AES).

Table 22: Pore water analysis (cations) from the BC during the GSRNOD2017 campaign. For dilution factor of 1, units are in ppm, and for dilution factors of 5, 50 or 100, units are in ppb. Al content has been tested with a dilution factor of 5 ⁽¹⁾ and 50 ⁽²⁾ while Co content has been tested with a dilution factor of 100 ⁽³⁾ and 5 ⁽⁴⁾.

Dilution		1				5					50	100		5
	Depth (cm)	Ca	K	Mg	Na	Mn	Ni	Cu	Zn	Al ₁	Al ₂	Fe	Co ₃	Co ₄
BC040	3.9	387	439	1095	8319	1	1	6	22	38		793	0	0.16
	13.9	383	434	1088	8205	2	1	4	17	33		786	0	0.14
BC044	7.2	388	426	1117	8346	4	1	3	16	18		830	0	0.24
						4	1	2	16	18		830	0	0.25
	17.2	390	413	1117	8340	1	1	3	28	12		812	0	0.18
BC046	27	388	422	1113	8362	2	2	6	19	86		798	0	0.19
	7.6	392	413	1128	8423	1	1	4	16	16		792	0	0.18
	17.6	385	413	1106	8280	2	2	3	19	16		824	0	0.22
BC047	6.3	382	413	1104	8236	0	1	3	15	7		805	0	0.19
	16.3	388	410	1118	8364	1	1	2	14	5		823	0	0.17
	26.3	391	410	1129	8426	3	1	3	15	9		811	0	0.21
BC048	13.8	82	97	238	1803	1	1	2	14	7		817	0	0.17
		83	98	239	1819									
BC049	15.4	379	487	1092	8391	2	1	3	19	36		798	0	0.19
	25.4	377	478	1086	8346	3	1	2	13	8		864	0	0.2
BC051	5.6	382	429	1112	8373	2	3	4	14	22		829	0	0.21
	15.6	380	422	1105	8310	1	2	3	28	11		787	0	0.24
						1	2	3	27	11		839	0	0.25
	25.6	384	426	1116	8382	2	1	6	22	85	139	848	0	0.19
BC053	7	376	484	1087	8396	1	1	6	18	7		1315	4	0.18
	17	370	474	1070	8245	1	1	8	20	11		789	0	0.53
BC055	8.7	377	421	1099	8273	5	2	7	51	124		904	0	0.23
	18.7	385	420	1117	8356	2	1	6	19	73	54	901	0	0.2
BC058	6	385	419	1123	8430	1	1	2	24	8		834	0	0.2
	16	382	418	1107	8302	1	1	2	16	7		846	0	0.19
BC059	7	381	421	1111	8360	1	1	3	16	6		839	0	0.19
	17	383	411	1116	8400	46	2	7	22	242	276	866	0	0.44
	27	383	429	1111	8406	145	5	9	16	679	653 603	1576	2	2.18
BC061	4	379	433	1102	8321	1	1	5	35	14		846	0	0.21
	14	374	433	1087	8257	32	6	11	171	816	710	1121	1	0.57

Table 23: Pore water analysis (anions) from the BC during the GSRNOD2017 campaign. Depth are expressed from the surface of the sediment

Box Core	Depth (cm)	Cl ⁻ (ppm)	SO ₄ ⁻² (ppm)
BC040	3.9	18957	2596
	13.9	18767	2573
BC044	7.2	19032	2528
	17.2	19113	2594
	27	18908	2475
BC046	7.6	18893	2543
	17.6	18775	2527
BC047	6.3	19383	2581
	16.3	19051	2581
	26.3	19081	2601
BC048	13.8	18619	2507
BC049	15.4	18589	2554
	25.4	19020	2590

Box Core	Depth (cm)	Cl ⁻ (ppm)	SO ₄ ⁻² (ppm)
BC051	5.6	19163	2630
	25.6	19121	2551
BC053	7	18986	2586
	17	18787	2532
BC055	8.7	19025	2558
	18.7	19335	3422
BC058	6	19064	2560
	16	19151	2628

4.1.5.3.1 Biology-related sediment characteristics

- Granulometry

Vertical profiles of the granulometric variables measured in nodule-free and nodule-rich B4S03 sediments are showed below, namely median grain size (MGS), sediment porosity, the sediment-sorting coefficient (SC) and sedimentary content of sand, silt, and clay, without differentiating between slope and flat areas. No large dissimilarities could be discerned between the nodule-rich and nodule-free area in terms of sand content, porosity or any of the other granulometric parameters assessed. Nonetheless, the top 0-6 cm of the sediment column in the nodule-rich area seemed to be somewhat less well sorted (higher SC) compared to the nodule-free area. Moreover, the nodule-rich sediments displayed higher variability (larger standard deviations) in granulometric properties relative to the nodule-free sediments. Most of the granulometric variables showed no clear trend with sediment depth, except for sediment porosity, which decreased deeper into the sediment.

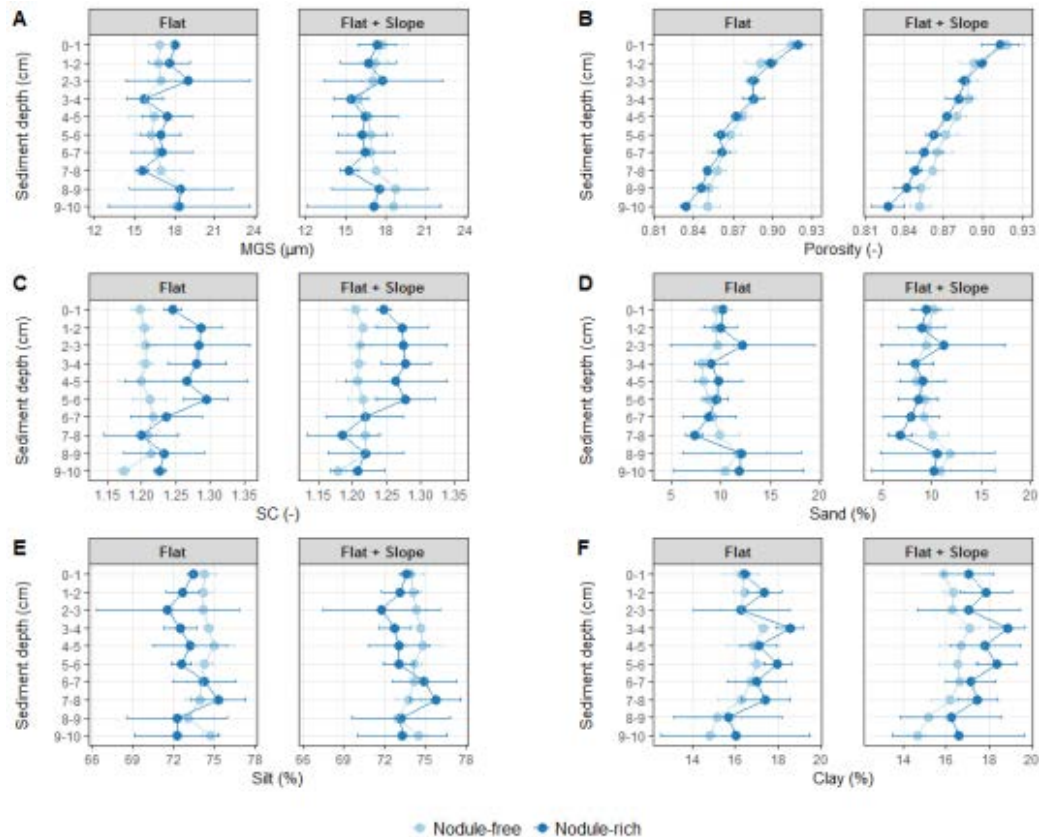


Figure 52: Average values of granulometric variables in function of sediment depth in the nodule-free and nodule-rich sediments sampled at site B4S03 in the GSR contract area. The left-hand panels show only samples collected in flat areas ($n=3$ for both nodule-free and nodule-rich sediments), and the right-hand panels include the samples collected on the slope areas ($n=4$ for both nodule-free and nodule-rich sediments). Error bars denote standard deviations. MGS: median grain size, SC: sediment-sorting coefficient.

- Total organic matter (TOM)

After sampling in the site B4S03 during the GSRNOD17 campaign, the evaluated sediment depth-averaged TOM (0-10 cm; flat and slope samples pooled) was slightly lower in the nodule-free (6.23 ± 0.43 %, mean \pm SD) than in the nodule-rich (6.49 ± 0.44 %) area. This difference was apparent for each sediment layer. The lower TOM content of nodule-free sediments may be caused by the lower infaunal biomass. TOM declined with sediment depth in both the nodule-rich and nodule-free areas, without much difference when slope samples are included (Figure 53).

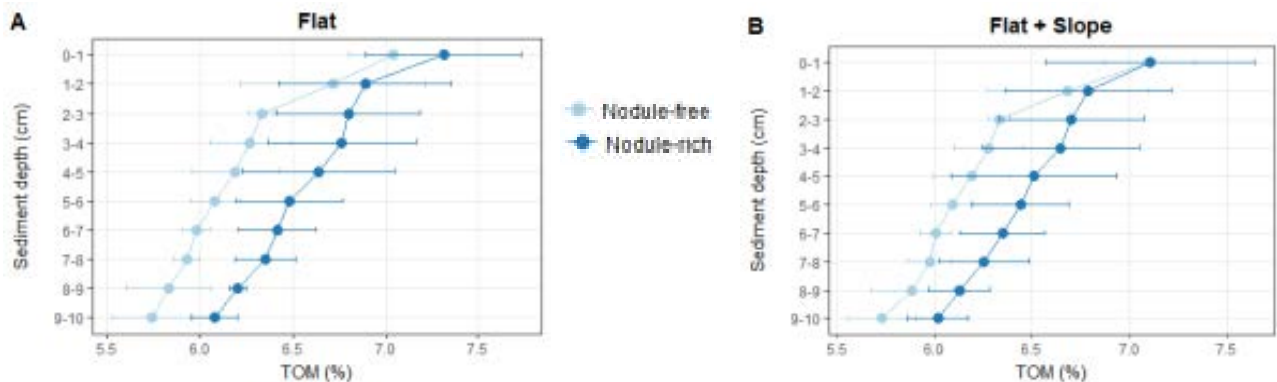


Figure 53: Average sedimentary total organic matter (TOM) content in function of sediment depth in the nodule-rich and nodule-free sediments sampled at site B4S03 in the GSR contract area. Plot A shows only samples collected in flat areas ($n=3$ for both nodule-free and nodule-rich sediments), and plot B also includes the samples collected in the slope areas ($n=4$ for both nodule-free and nodule-rich sediments). Error bars denote standard deviations.

This difference was apparent for each sediment layer. The lower TOM content of nodule-free sediments may be caused by the lower infaunal biomass. TOM declined with sediment depth in both the nodule-rich and nodule-free areas, without much difference when slope samples are included (Figure 53).

- Total organic carbon (TOC) and nitrogen content (TN)

Sediment depth-averaged values of TOC, TN and TOC/TN were highly similar between the nodule-free and nodule-rich sediments sampled at the B4S03 sub-zone. The vertical profiles of these variables, illustrated in Figure 54, did not differ substantially between the nodule-rich and nodule-free areas; little difference was observed between samples only collected in flat areas and samples collected in flat and in slope areas.

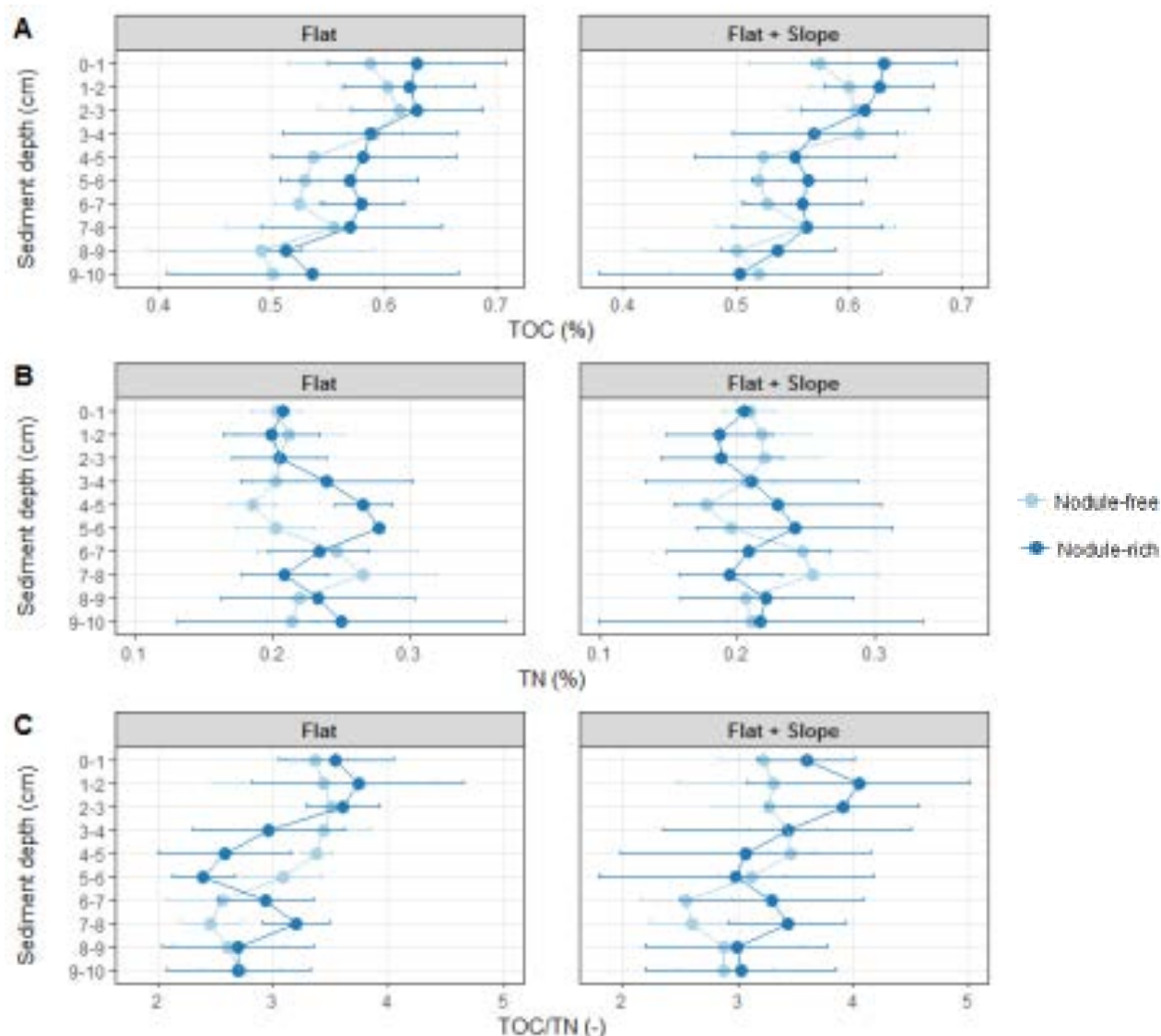


Figure 54: Average values of (A) TOC (total organic carbon content), (B) TN (total nitrogen content) and (C) TOC/TN (molar sediment total organic carbon-to-total nitrogen ratio) in function of sediment depth in the nodule-free and nodule-rich sediments sampled at site B4S03 in the GSR contract area. The left-hand panels show only samples collected in flat areas (n=3 for both nodule-free and nodule-rich sediments), and the right-hand panels include the samples collected on the slope areas (n=4 for both nodule-free and nodule-rich sediments). Error bars denote standard deviations

- Pore water nutrients

During campaigns in the B4S03 sub-zone, no large dissimilarities in bottom or pore-water nutrient concentrations, or in the vertical profiles thereof, between nodule-rich and nodule-free sediments were detected. For the GSRNOD17 expedition, plots showing only samples collected in flat areas and those that display samples from flat and slope areas were practically identical (compare left and right-hand panels in Figure 55).

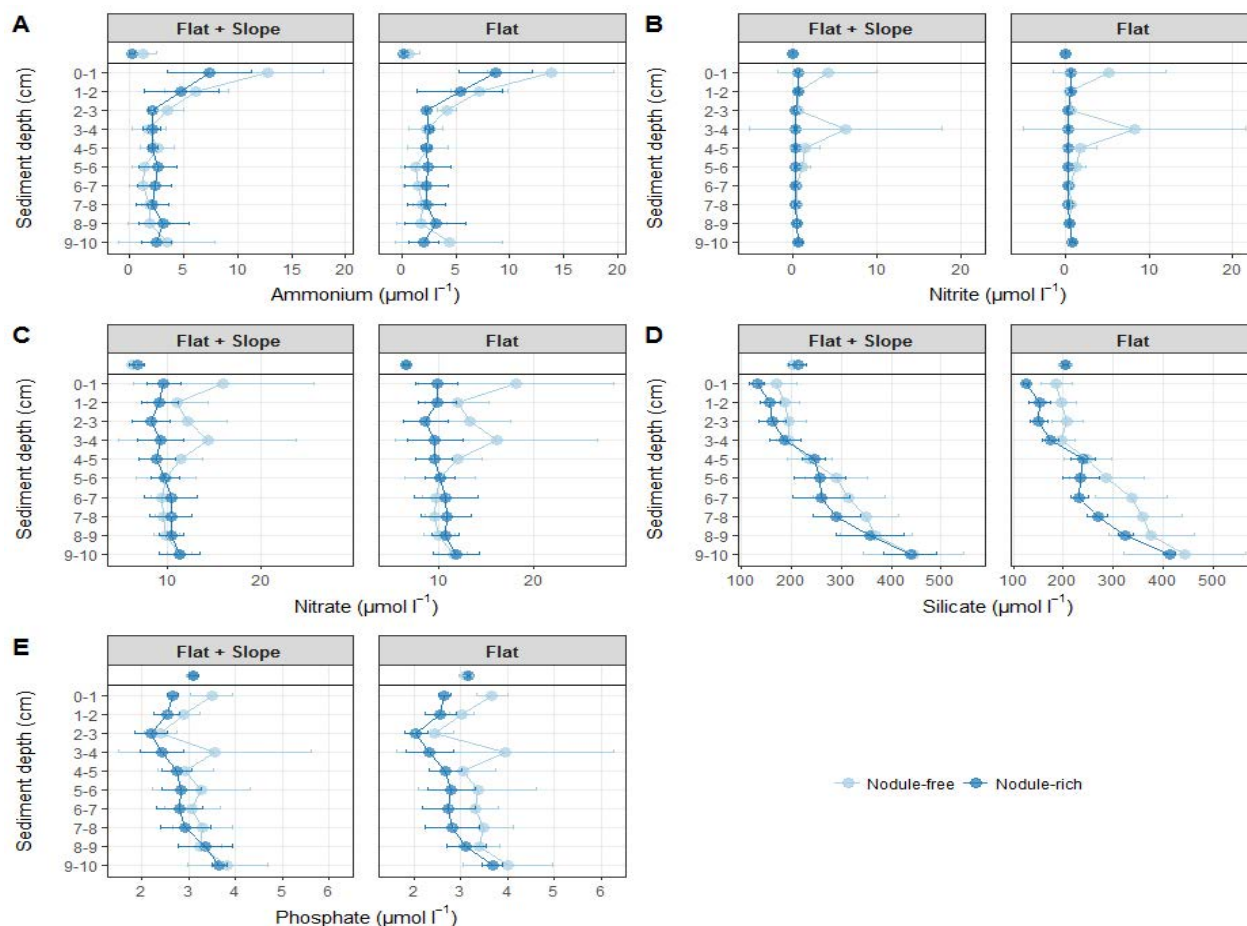


Figure 55: Bottom-water and pore-water concentration of (A) ammonium, (B) nitrite, (C) nitrate, (D) silicate, and (E) phosphate in function of sediment depth in the nodule-free and nodule-rich sediments sampled at site B4S03 in the GSR contract area. The sediment-water interface is demarcated by the black horizontal line. Values plotted above this line represent bottom-water concentrations

The concentration ranges of most nutrients analyzed differed between GSRNOD15A and GSRNOD17 expeditions in the sub-zone B4S03. Exceptions were ammonium concentrations which were similar for both expeditions (Figure 56). Nitrate and phosphate concentrations were higher and lower, respectively, for GSRNOD17 than for GSRNOD15A. The observed differences in pore-water nutrient profiles between the two GSR expeditions may be ascribed to seasonal and/or interannual variability in seafloor POC flux (Soetaert et al., 1996). The differences in NPP between expeditions did not seem to be that great (see 4.2.2.1, Surface, pp. 115). but note that NPP in the surface waters does not always accurately reflect the amount of organic material deposited at the seabed (Pape et al., 2013).

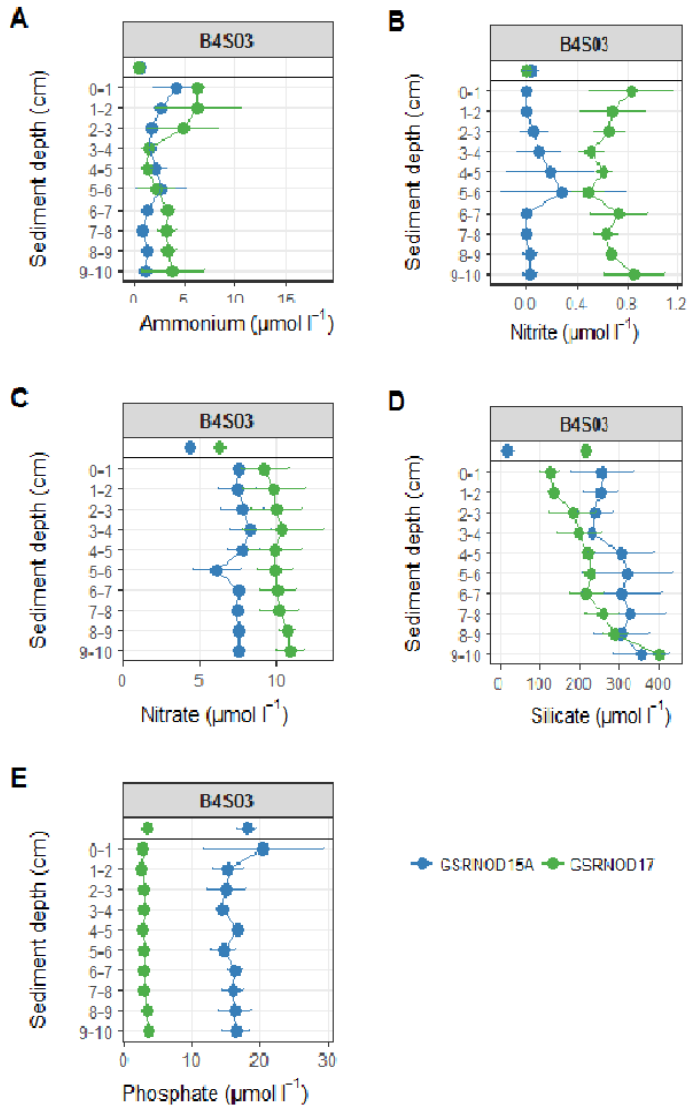


Figure 56: Average concentration of (A) ammonium (TON), (B) nitrite, (C) nitrate, (D) silicate and (E) phosphate in function of sediment depth as measured during GSRNOD15A (September-October 2015) and GSRNOD17 (May-June 2017) at site B4S03 sub-zone. Error bars denote standard deviations. The sediment-water interface is demarcated by the black horizontal line. Values plotted above this line represent bottom-water concentrations

4.1.5.4 Geotechnical Sediment Characteristics

The field geotechnical measurements consist of:

- Bulk unit weight;
- Field vane test;
- Pocket shear vane test & Pocket Penetrometer;
- Graviprobe measurement of the upper 4m.

For the **bulk density**, a summary of the results is presented in Figure 57. The majority of the samples have a bulk density in the range between 1.25 ton/m³ and 1.45 ton/m³; the majority of the samples have a bulk density of 1.35 ton/m³.

The high values at > 1.45 ton/m³ and the low values at < 1.25 ton/m³ can be ignored and are related to measuring errors.

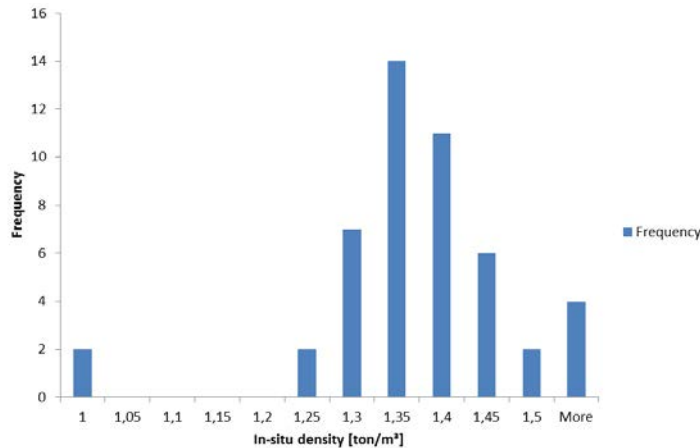


Figure 57: Summary of the bulk density determination during GSRNOD15A campaign

The determined **undrained shear strength**, field vane test results and pocket shear vane test results were conducted on BC samples. For each box core the results of the field vane test measurements (FVT) and pocket vane measurements (TV) are summarized in a single graph. In each graph, the values for unit weight and water content are also given to compare them with the strength parameters obtained (example in Figure 58). Further details can be found in annual reports 2016 (file number : ISA-GDR2016).

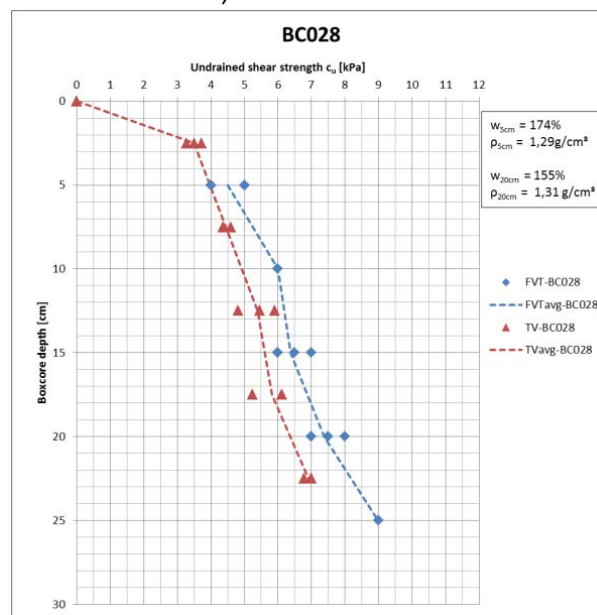


Figure 58: Undrained shear strength measurements in box core BC028 during GSRNOD15A

The general trend of the undrained shear strength is an increase with depth, going from 0 kPa at the surface up to a maximum value of 9.5 kPa in the lower part of the box-core sample (20 – 25 cm deep).

To obtain more results on the *in-situ* shear strength, a GraviProbe was also deployed in area B4S03. The geotechnical results are summarized in Table 24 below. All values on the next page are consistent with historical data and field results measured on board the vessel.

Table 24: Summarized table of the geotechnical laboratory tests performed in BC samples of the area B4 during the various GSRNOD expeditions

Sample	Specimen ID	CLASSIFICATION - Density					CLASSIFICATION - Plasticity					
		ρ_{nat} [ton/m ³]	ρ_d [ton/m ³]	$\rho_{s,n-cr}$ [ton/m ³]	$\rho_{s,cr}$ [ton/m ³]	w_{sample} [%]	w_l [%]	w_p [%]	PI [%]	I_c [-]	LI [-]	Activity [-]
BC006	15/0001	1.45	0.55	2.58	2.57	162.29	145.90	52.70	93.20	-0.18	1.18	1.76
BC007	15/0002	1.32	0.50	2.58	2.60	165.29	115.60	48.80	66.80	-0.74	1.74	1.20
BC008	15/0003	1.29	0.45	2.58	2.56	185.44	135.80	61.70	74.10	-0.67	1.67	1.22
BC009	15/0004	1.30	0.45	2.60	2.53	186.89	137.60	60.50	77.10	-0.64	1.64	1.29
BC010	15/0005	1.25	0.38	2.52	2.48	232.97	145.20	67.30	77.90	-1.13	2.13	

Sample	Specimen ID	CLASSIFICATION - PSD - Fraction [%]					Laboratory Vane Test			
		I [%]	II [%]	III [%]	IV [%]	[OC] [%]	w_{sample} [%]	$C_{u,peak}$ [kPa]	$C_{u,rem}$ [kPa]	S_t [-]
BC006	15/0001	52.90	44.90	1.50	0.70	5.40	154.01	3.70	0.40	9.30
BC007	15/0002	55.60	41.30	3.00	0.20	5.20	204.38	1.80	0.50	3.60
BC008	15/0003	60.60	38.60	0.70	0.10	5.90	195.42	5.00	0.60	8.30
BC009	15/0004	60.00	39.60	0.30	0.10	5.20	252.98	2.00	0.30	6.70
BC010	15/0005			0.70	0.20	5.40	271.17	2.10	0.30	7.00

Sample	Specimen ID	TX-UU						TX-CU							
		ρ_{nat} [ton/m ³]	ρ_d [ton/m ³]	w_{sample} [%]	σ_3 [kPa]	ϵ [%]	C_u [kPa]	ρ_{nat} [ton/m ³]	ρ_d [ton/m ³]	w_{sample} [%]	σ'_{consol} [kPa]	C_u [kPa]	ϵ [%]	v_s [m/s]	G_o [Mpa]
BC006	15/001							1.32	0.47	180.31	22.50	10.90	22.50	38.95	2.00
BC007	15/002							1.31	0.49	165.27	8.60	2.60	4.10	28.56	1.07
BC008	15/003	1.30	0.46	183.00	100.00	14.10	5.00								
BC009	15/004							1.34	0.44	205.90	45.00	13.60	5.90	59.25	4.72
BC010	15/005	1.24	0.38	226.40	100.00	1.80	9.30								

An area was also selected for more detailed investigation during GSRNOD15A (Figure 4 and Figure 59). The high-resolution survey box, the planned GraviProbe trajectory and the box-core sample locations are inside area B4S03.

There was no indication for obstacles along this trajectory and a flat area with soft sediments was expected. The trajectory enables comparison of GraviProbe measurements with box core samples from GSRNOD15A (BC017, BC021 and BC018).

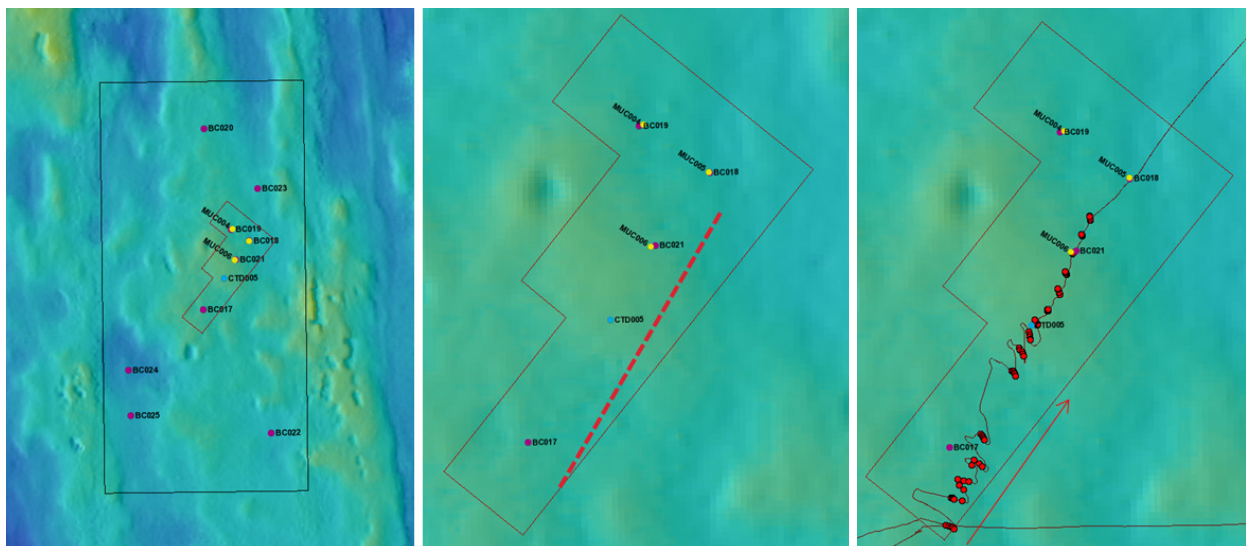


Figure 59: Sub-zone B4S03 (left) and high resolution box within B4S03; proposed GraviProbe-trajectory for testing (middle) and in-situ penetration points within area B4S03 (right)

In area B4S03, 15 stations were sampled (GP013 to GP027). For each location, five penetrations (pokes) took place. In total, 75 penetrations were done in Area B4S03 Figure 59.

For each penetration, 4 different graphics are presented: (1) acceleration vs depth, (2) speed vs depth, (3) dynamic cone resistance vs depth and also (4) the water pressure at the sea-bottom is registered. An example is given in Figure 60 and Figure 61, corresponding to GP022-03 (unprocessed and processed data).

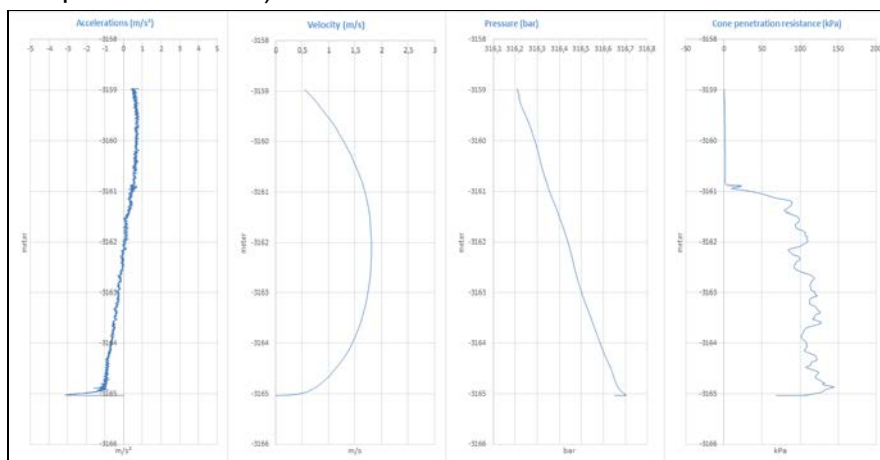


Figure 60: Unprocessed GraviProbe data at location GP022_03

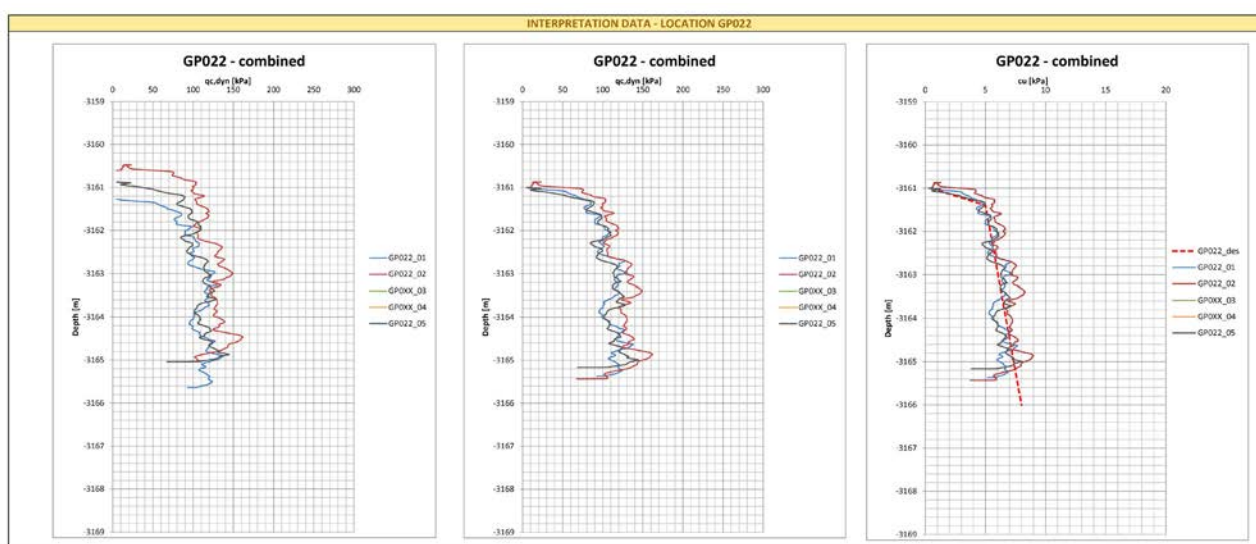


Figure 61: Processed GraviProbe profiles at location GP022

The superimposition of the 5 penetrations (or pokes) is consistent and follows the same evolution from the top to 4.1 m below the seabed level. However, the increase with depth is less obvious than the previous example (GP005), from 4 kPa at the upper layer to 8-9 kPa at 4.1 m deep. As in the previous example, we also observe a scale effect for the first 20-30 cm that we can readjust by using the torvane measurements taken from the nearest box-core sample (BC021 – Figure 62). The shear-strength measurements performed at different depths inside the sample BC021 show a general trend to increase, even if the consolidation is not linear. The Cu values fluctuate between 4 and 8 kPa, with an average around 6 kPa.

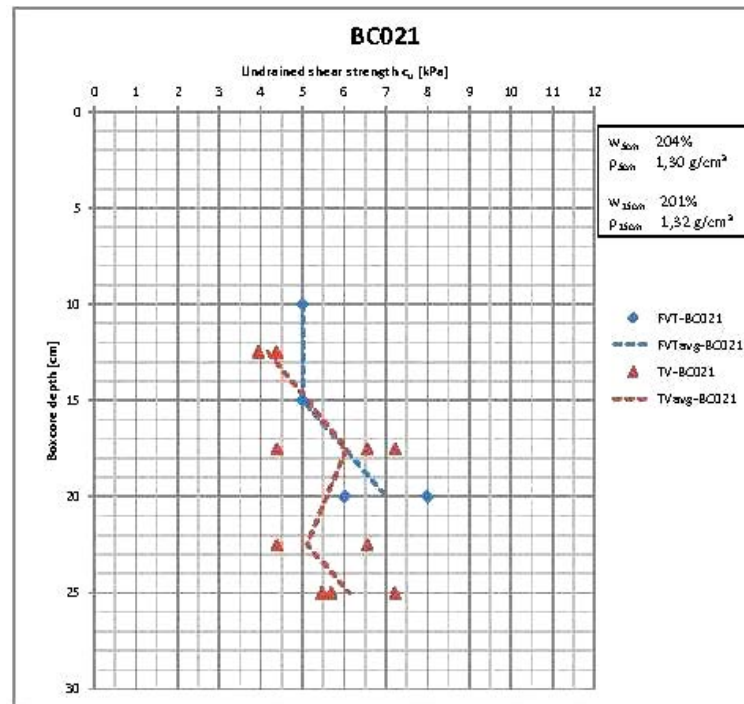


Figure 62: Undrained shear strength (kPa) vs depth below seabed (Source: Torvane and penetrometer measurements collected in box-core BC021)

4.1.6 Natural hazards

Weather conditions are generally favourable for exploration work in the months between March and May. Meteorological hazards are only to be expected from tropical storms or hurricanes; these could potentially endanger the two vessels. However, for the time period between March and May, the occurrence of such storm events is highly unlikely as the storm season only starts in mid-May. Moreover, continuous observation of the weather forecast by the ship's command would enable leaving the storm area early enough to sail to a safe place. As with previous campaigns carried out by GSR in the CCFZ, weather forecasts, issued every twelve hours by BMTARGOSS Operational Client Weather and Ocean Information support Centre (information on BMT ARGOSS BV, 2018, consulted on March 21, 2018), are available for the area of interest. Further natural hazards that could affect the environment and also the effectivity of the Patania II test include volcanism, seismic activity and the occurrence of benthic storms on the seafloor. Volcanic activity is highly unlikely during the lifetime of the project. As there is no information on recent seismic activity in the area, potential impacts are impossible to predict.

There is also little information on the potential impact of natural benthic storms on the seafloor, which are known from other oceanic regions to cause major erosion/depositional events on the seafloor. Even during times of mesoscale eddy passage (observed in the German Contract Area but not in the Belgian Contract Area), which induce a two to three-fold increase of bottom current speeds up to maximally 20 cm/s, turbidity measurements have not given evidence for the resuspension of bottom sediments and ADCP backscatter data also have shown no change in Suspended Particulate Matter (SPM) concentration in the water column. The term "benthic storm" in the CCFZ has been used confusingly in the past. The concept of "benthic storms" allegedly resuspending sediment in the CCFZ was initiated by Kontar and Sokov (1994), who used the term "benthic storm" to describe moderate enhancement of currents (to 13 cm/s) at 6 m

above the seafloor, apparently also by mesoscale eddies passing by. They did not measure any sediment resuspension, nor would this be expected based on other studies (e.g., Gardner et al., 1984) showing that flows of 13 cm/s do not cause sediment erosion in the CCFZ. Detailed photographic analyses of vast seafloor areas of the CCFZ indicate extremely clear bottom waters and no sediment deposition on the nodules, which would be expected if natural resuspension events were common. Current speeds of maximally 20 cm/s could lie around or above anticipated thresholds for natural resuspension of deep-sea muds according to McCave and Hall (2006) – but there is no evidence for it.

4.1.7 Noise and light

4.1.7.1 Light background

The work scheduled is located below 4000 m below the surface, in the middle of the Pacific Ocean. It is well established that there is very little natural (i.e., sun) light below 1000 m water depth (NOAA, 1984). Therefore, many deep sea organisms have developed bioluminescent capabilities for counter-illumination camouflage, mate attraction, defense, warning, communication and/or mimicry (Haddock et al., 2009). Most deep sea organisms have developed “super-eyes” to detect the dim light of bioluminescence. No background records of light are available for this specific area of interest. Nevertheless, during the lowering from the vessel of the TSTD Patania in 2017 through the water column, three distinct organism behaviors could be observed: (1) Attracted towards the artificial light source (in this case the Patania); (2) causing the nekton to flee; (3) complete indifference. From the literature review, the behavioural response appears to be species-dependent (Ortega (ed), 2014 and references therein).

4.1.7.2 Noise background

Sound is carried in water much faster than in air. It is used by sea-mammals, fish and some invertebrates for communication. Artificial sound can disturb animals and inhibit their communication. However, for most animals (and especially for deep-sea animals) the direct effect of increased sound is unknown (Ortega (ed), 2014). The principal sources of ambient ocean noise are:

1. Environmental parameters: Ambient background noise is dominated by (1) ocean turbulence and microseisms at the lowest frequencies (0.1 to 10 Hz) (Webb, 1992); (2) wind-related surface noise (between 1 and 30 kHz) (Naumann, 2008); (3) thermal noise of water molecules (100 kHz and more) (Dahl et al., 2007).
2. Naturally occurring and biogenic background noise: created by whales, dolphins, fishes and invertebrates for communication, navigation, echolocation and feeding purposes. The range of frequencies used by living organisms expands from less than 10 Hz to more than 200 Hz;
3. Noise from shipping activities ((Dahl et al., 2007): The frequency range is broad (50-150 Hz up to 10 kHz), because it is largely related to distance from the source (i.e., the vessel) or the type of noise emission, for instance. Drilling and dredging noise are proven to affect biological activity (Richardson et al., 1990), commercial shipping produces low-frequency ship noise, such as propeller noise, hydrodynamic hull flow, cavitation, engines and other machinery (McKenna et al., 2012). However, shipping traffic through the CCFZ is infrequent as shown by Figure 63.

Furthermore, as noise and light levels are not among the recommended baseline data elements described in the recommendation ISBA/19/LTC/8, background data in the contract area on these elements have not been gathered by GSR. Nevertheless, as explained later on, background and artificial noise at the seabed will be monitored during the GSRNOD19 expedition

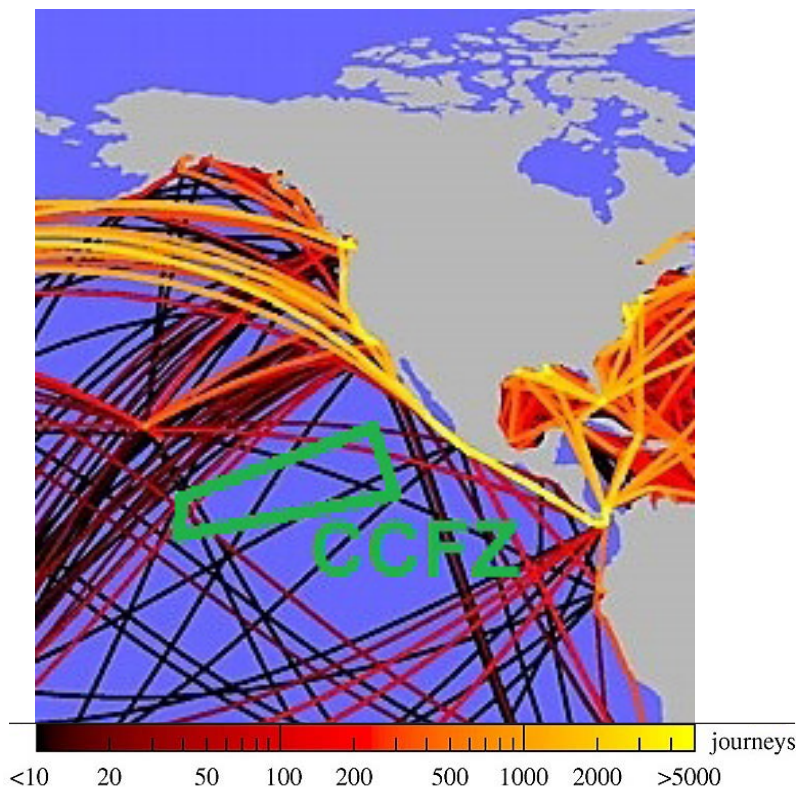


Figure 63: Shipping routes across the Pacific Ocean.

4.2 The biological environment

The following section is mainly based on the research carried by the MarBiol group from the University of Ghent, coordinated by Ellen Pape, under the supervision of Ann Vanreusel. This research is described in GSR's annual reports to the ISA from 2014, 2015, 2016 and 2017 (2014, 1015, 2016 and 2017 AR, file numbers ISA-GSR_AR2014, ISA-GDR2016, ISA-GSR_AR2016, ISA-GSR_AR2018).

To determine the biological baseline, information is needed on spatial (determined mainly by habitat heterogeneity) and temporal variability (both inter- and intra-annual) in biological communities and environmental parameters. The sampling was conducted during the GSRNOD14, GSRNOD15 and GSRNOD17 expeditions. Three stations were sampled in B4S03: two nodule-rich stations and a nodule-free station. The main objectives for the biological and environmental sampling were:

- (1) To assess inter-annual variability in benthic communities and environmental parameters,
- (2) To evaluate the influence of habitat heterogeneity, governed by the presence or absence of nodules, and/or by topography, on benthic communities,
- (3) To continue vouchers and barcoding of selected benthic taxa to complete reference databases;

(4) To collect data to set up a benthic food web model for the GSR contract area.

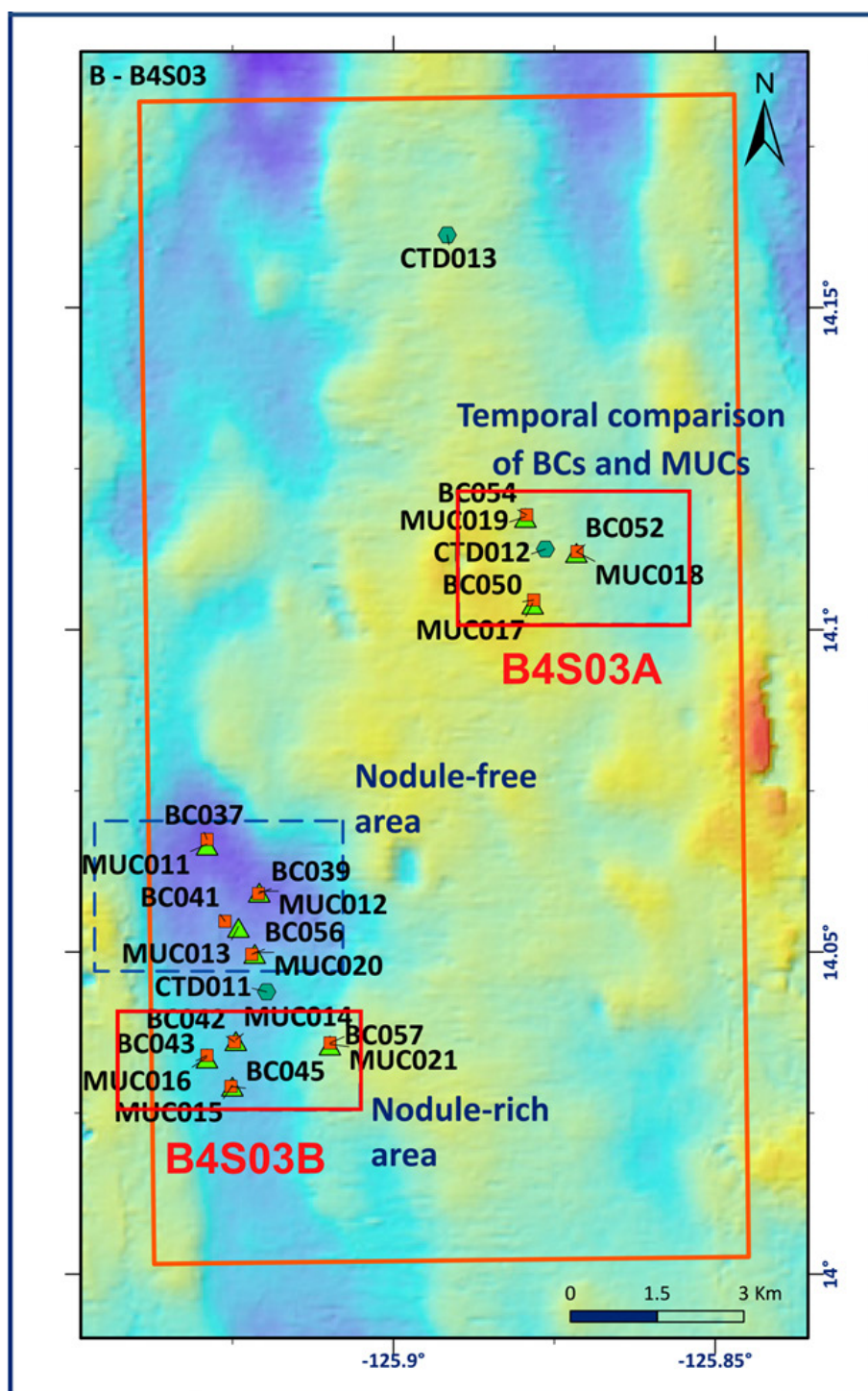


Figure 64 : Detailed map of the deployments done at site B4S03 with an indication of the nodule-free and nodule-rich areas sampled, and the area sampled for temporal comparison (GSRNOD17 vs. GSRNOD15A).

4.2.1 Key messages

- Nematode communities are similar between surface and subsurface sediments, and between nodules and surrounding sediments in the GSR contract area. In addition, both nematode (*Halalaimus* species) and polychaete data (COI barcodes) point towards a high

degree of connectivity of certain species between license areas that are separated by 100s of kilometers in the eastern CCFZ.

- The nodule-free and nodule-bearing sites sampled at site B4S03 (Figure 64) were characterized by similar sedimentary characteristics, and similar meio- and macrofauna communities. The only statistically significant difference was observed in terms of meiofaunal standing stock, which was elevated in nodule-free sediments. A potential explanation for this divergence is the possibly higher sedimentation rate at the nodule-free site (as observed in the BGR license area, Mewes et al. (2014)) and/or the expected higher epifaunal densities in nodule bearing sites competing for food, or predating on endobenthic organisms.
- The temporal comparison for sites B4S03 revealed only a difference in pore-water nutrient concentrations between GSRNOD15A and GSRNOD17. The other sedimentary characteristics, and also meio- and macrofauna communities, did not change significantly between different sampling occasions. This may be explained by the rather limited changes in productivity between sampling occasions.
- As noted already in the previous annual report (Pape et al., 2017b), there are still rather few scientific publications on the CCFZ (or other nodule-bearing abyssal regions). Most, if not all, recently (in 2017) published studies, presenting recently collected data, stem from eastern CCFZ license areas (De Smet et al., 2017; Goineau and Gooday, 2017; Gooday et al., 2017; Lim et al., 2017; Pape et al., 2017a; Wiklund et al., 2017). This hinders a region-wide comparison of environmental and biological data.
- To be able to make rigorous statements about differences in environmental and faunal parameters between different habitats or periods, replication of samples is paramount.

4.2.2 Biological communities

4.2.2.1 Surface

During GSRNOD14A, GSRNOD15A, GSRNOD17, and also during the JPI Oceans campaigns in the GSR contract area, for birds mainly boobies (masked, brown and red-footed) were identified. This was expected, because the Eastern Tropical Pacific is known to be an important booby colony area (Ballance et al. 2006). Terns and petrels were also observed. With regard to pelagic fauna, common dolphinfish, pacific blue marlin, loggerhead turtle and yellowfin tuna live in the area, as well as oceanic whitetip sharks and Minke whales, depending on the season. It must be noted that these observations were carried during transit, but none of these species was spotted in the GSR Contract Area.

Using a Vertically Generalized Production Model based on Moderate Resolution Imaging Spectroradiometer (MODIS) images, the net primary productivity calculated between October 2014 and June 2017 in the B4S03 (violet on Figure 65 below) station remains low (between 175 and 360 mg C m⁻²d⁻¹, decreasing during the warmer period, and increasing during the cooler period) and is an indicator of an oligotrophic environment. (data provided to ISA in its 2017 AR, file numbers ISA-GSR_AR2018).

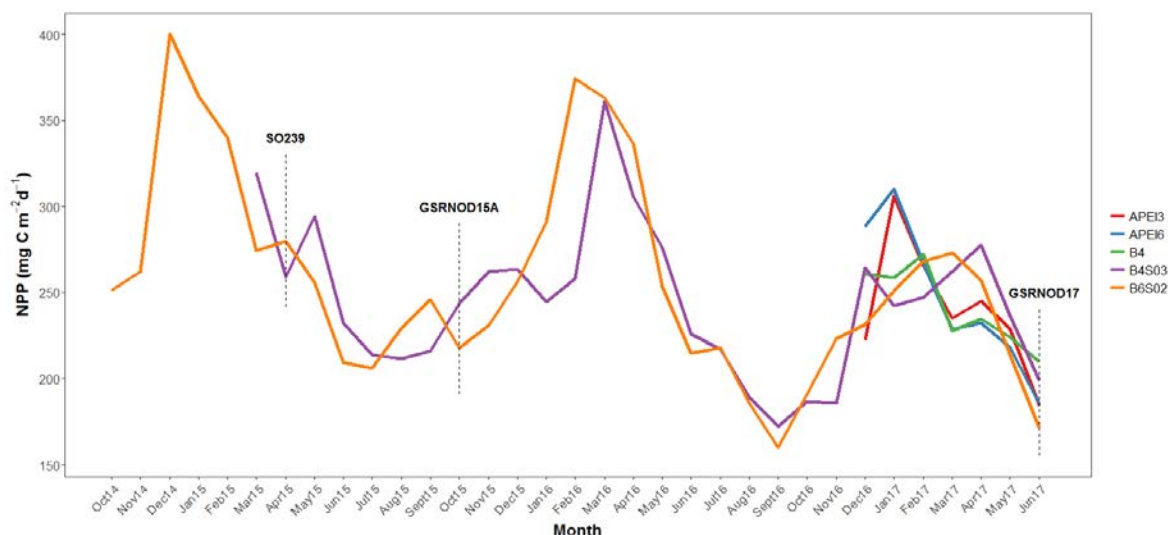


Figure 65: Monthly-averaged Net Primary Productivity (NPP) at all sites sampled during GSRNOD17 in the GSR contract area for the period October 2014 - June 2017. The dashed vertical lines denote the timing of the previous expeditions during which these sites were sampled. Only B4S03 and B6S02 were sampled during GSRNOD15A, and only B6S02 was sampled during SO239 (JPI-O 1 campaign). For each site, NPP data were obtained 7 months prior to the first sampling expedition undertaken at that particular site

4.2.2.2 Midwater

In the B4S03 sub-zone, Chlorophyll a, used as a proxy for phytoplankton biomass, shows a subsurface maximum between 75 and 100 m, reaching concentrations of 0.5-0.6 $\mu\text{g/l}$. Other pigments are also detected in the upper water layer from the GSR contract area: chlorophyll b, chlorophyll c2, β -carotene, lutein, 19'-hexanoyloxyfucoxanthin and 19'-butanoyloxyfucoxanthin. The GSR contract area is a low-nitrate zone, where phytoplankton communities are dominated by picoplankton (0.2 – 2 μm). From data collected mostly in equatorial zones ($< 10^\circ\text{N}$), the phytoplankton community close by the GSR contract area are composed of cyanobacteria, such as *Prochlorococcus* and *Synechococcus*, prochlorophytes, haptophytes and dinoflagellates (Chavez et al., 1996; Landry and Kirchman, 2002; Zhang et al., 2008).

Data obtained during the GSRNOD15A campaign suggest a comparable phytoplankton and pelagic biomass between various sub-zones in the GSR contract area (data provided to ISA by GSR in its 2015, 2016 and 2017 AR, file numbers ISA-GSR_AR2014, ISA-GDR2016 and ISA-GSR_AR2016).

The strong pycnocline existing in the Eastern Pacific Ocean impedes and usually prevents potential vertical mixing. Pigment concentrations measured along the water column indicate that chlorophyll a is the only pigment still detected below 500 m, although its concentration decreases with increasing depth from the subsurface maximum. Those differences in pigment concentrations suggest a possible vertical differentiation of phytoplankton community composition.

4.2.2.3 Seafloor

The seafloor and its superjacent near-bottom environment remain a complex and highly variable environment. Because the surface layer has been established as oligotrophic, the bulk of the organic matter that supplied the benthos with energy (food) sinking from the surface waters is restricted. The relatively low productivity at the surface is probably translated to low particulate

organic carbon flux and low productivity at the seafloor (data provided to ISA by GSR in its 2017 AR, file numbers ISA-GSR_AR2018).

In the CCFZ, there is increasing evidence that at the local scale, nodules influence the structure and composition of both infaunal (Miljutina et al., 2010) and epifaunal communities (Vanreusel et al., 2016).

4.2.2.3.1 Benthic bacterial biomass

The B4S03 sub-zone presents an average benthic bacterial biomass of $\sim 140.05 \pm 32.23 \text{ mg C m}^{-2}$, without statistically significant differences with the B4N01 or the B6S02 sub-zones, which is in line with the reported order of magnitude in previous work on the Eastern Pacific (Smith et al. 1997).

The vertical profiles of sediment bacterial biomass, approximated by the total concentration of the bacteria-specific PLFAs a15:0, i15:0 and i16:0, show a decline in bacterial biomass with sediment depth at all sites (Figure 66). A similar depth profile was observed for bacterial abundances in the Japanese claim area, in the western CCFZ (Kaneko et al., 1997), and in other nodule-free deep-sea regions (*e.g.* Boetius et al., 2000; Deming and Carpenter, 2008). Sheelu et al. (1999) did not find statistically significant differences in bacterial abundance between sediment depth layers in an area in the Central Indian Ocean Basin for the exploration of polymetallic nodules. However, these authors did not report the actual abundances, which might as well show a decline, albeit not statistically significant, with sediment depth. Note that for the CCFZ only one published study dealing with vertical profiles of bacterial standing stock was found (Kaneko et al., 1997), and it deals with bacterial abundances, not biomass. Hence, it is possible to compare general sediment depth-trends in bacterial standing stock between this study and that of Kaneko et al. (1997), as done here, but the difference in parameters measured (*i.e.* this study: bacterial biomass based on the concentrations of bacteria-specific PLFAs, Kaneko et al. 1997: counts of bacterial cells), hampers a quantitative comparison between studies.

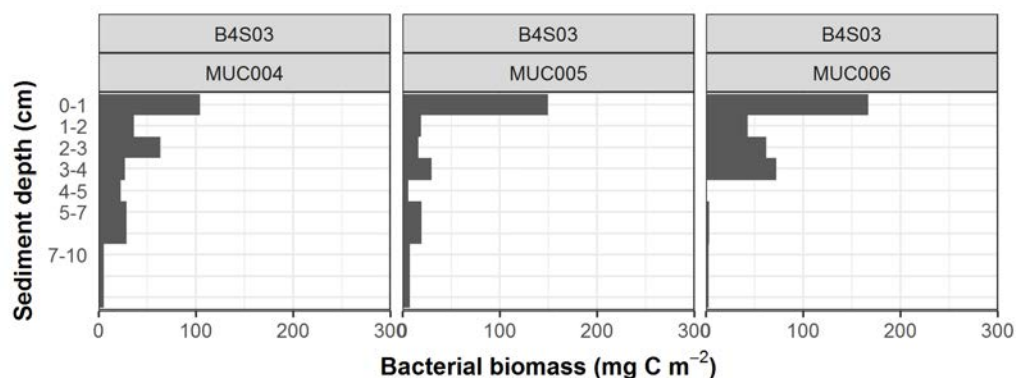


Figure 66: Bacterial biomass in function of sediment depth for all MUC samples in B4S03 during the GSRNOD15A. Note that the 5-6 and 6-7 cm samples were pooled to get a value for 5-7 cm sediment depth, and the 7-8, 8-9 and 9-10 cm samples were pooled to obtain a measurement for 7-10 cm sediment depth.

4.2.2.3.2 Benthic meiofauna

With regard to the meiofauna, total average meiofaunal abundance ranged between 55 and 194 ind.10 cm⁻², mainly living in the upper 5 cm of the sediment, without significant differences between the B4S03 and other analysed samples from the contract area. The community is

dominated by the phylum Nematoda (> 80 % of the meiofauna present), followed by the Copepoda and crustacean nauplius larvae groups. These results are in line with previous meiofaunal records in the CCFZ (data provided to ISA by GSR in its 2015, 2016 and 2017 AR, file numbers ISA-GSR_AR2014, ISA-GDR2016 and ISA-GSR_AR2016 respectively, for further information). Bivalvia, Gastropoda, Gastrotricha, Hydrozoa, Isopoda, Kinorhyncha, Ostracoda, Polychaeta, Tanaidacea, Tantulocarida and Tardigrada were also detected in sediment samples; each taxon represents less than 1% of the meiofaunal abundance. Also nematode genera composition did not differ between sites. Furthermore, the same genera dominate the surface (0-5 cm below seafloor) and subsurface (5-10 cm below seafloor) sediments in the GSR contract area, even if the relative abundances vary slightly and densities were much lower. Through molecular analysis, it is known that species of one of the more abundant nematode genera (*Halalaimus*) sampled in the GSR contract area are also detected in other deep sea areas. In terms of total meiofaunal abundance, no significant differences were found for the temporal comparison between expeditions (Figure 67, left). However, the observed average values tend to decrease with the subsequent expeditions. Within site B4S03, a higher average total meiofaunal abundance was found during GSRNOD15A (106.64 ± 29.28 ind. 10 cm^{-2}) compared to GSRNOD17 (87.1 ± 20.81 ind. 10 cm^{-2}). This trend was also reported for some of the diversity indices. At the sub-zone B4S03, Shannon-Wiener diversity H' and Pielou's evenness J' were significantly affected by the factor "Expedition" with higher values in GSRNOD15A (Figure 67, center) compared to GSRNOD17. Overall, communities within both sites were mainly composed of Nematoda (90.97 %), Copepoda (5.25 %) and nauplii (2.82 %) (Figure 67, right). The declining trend between expeditions may be (partially) driven by the decrease in surface net primary productivity (NPP) between GSRNOD15A and GSRNOD17 as already presented earlier in this section. A (strong) association between meiofaunal communities and NPP, or the resultant seabed particulate organic carbon (POC) flux, was demonstrated for the CCFZ (Miljutin et al., 2015; Radziejewska, 2002). The lack of statistically significant changes in abundance with time may be related to the relatively small changes in NPP. Moreover, except for pore-water nutrient concentrations, the sedimentary characteristics did not change between sampling expeditions (see 4.2.2.1, Surface, pp. 115).

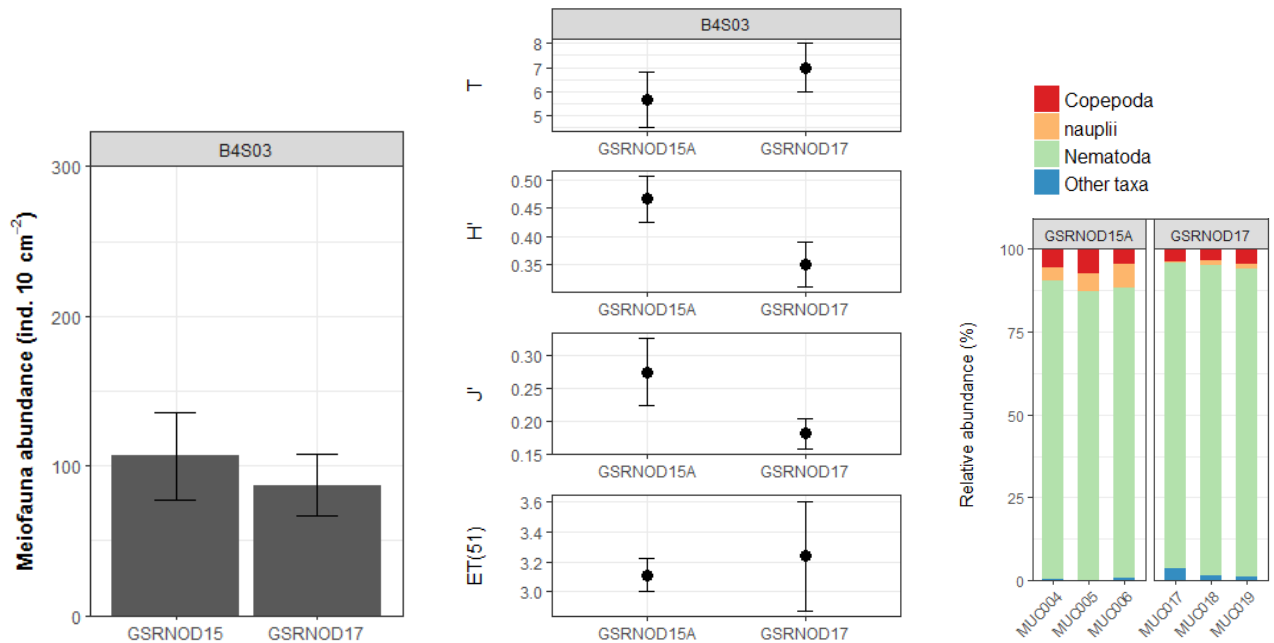


Figure 67: Temporal comparison between the different expeditions (GSRNOD15A: September-October 2015, GSRNOD17: May-June 2017) within sites B4S03, From left to right : Average values of total meiofaunal abundances. Error bars denote standard deviations (right); Average values for calculated diversity: taxon richness (T), Shannon-Wiener diversity (H'), Pielou's evenness (J) and the expected taxon richness for a sample of 51 individuals (ET(51)). Error bars denote standard deviations (centre). Relative abundances of higher meiofaunal taxa per MUC sample (right) "Other taxa" are higher meiofauna taxa that comprised < 1 % of total meiofauna abundance

4.2.2.3.3 Benthic macrofauna

The macrofauna abundance assessed in the B4S03 sub-zone reveals an average of 200 ± 42 ind. m⁻² (excluding the Nematoda, Copepoda and Ostracoda considered as meiofauna) in the ten top centimetres of the sediment, without a statistically significant difference with the other sampled stations of the GSR contract area. If the meiofauna taxa are included, this abundance rises to 514 ± 110 ind. m⁻², again without any significant difference with other sampling stations. This abundance is considered as being in the lower to middle range when compared to other sampling sites in nodule areas (CCFZ and elsewhere). The macrofaunal taxon composition is dominated by Nematoda (32-60 % of total abundance), and Copepoda (8-23 %), although these are not considered as macrofaunal taxa by most macrofaunal studies in the Pacific nodule area. Polychaetes are reported in the literature to be the most abundant taxon of macrofauna, and accounted for 8-20 % in sampled stations of the GSR contract area in 2015. Tanaidacea were also spotted (5-20 %), along with Amphipoda, Bivalvia, Isopoda, Ophiuroidea and Ostracoda (20 % all together) and Acari, Brachiopoda, Decapoda, Chaetognatha, Cumacea, Gastropoda, Mysida, Nemertea, Oligochaeta, Other Crustacea, Pycnogonida, Scaphopoda and Sipuncula (4.45 ± 1.95 % all together). If the meiofaunal taxa are not included, Polychaeta (23-45 %) and Tanaidacea (13-54 %) dominate the upper 0-10 cm of sediment. The molecular analysis suggests that several of the Polychaeta species found in the GSR stations are also found in IFREMER and BGR contract areas. Within the station B4S03, average total macrofaunal abundances were higher in the GSRNOD15A samples when compared to the GSRNOD17 samples.

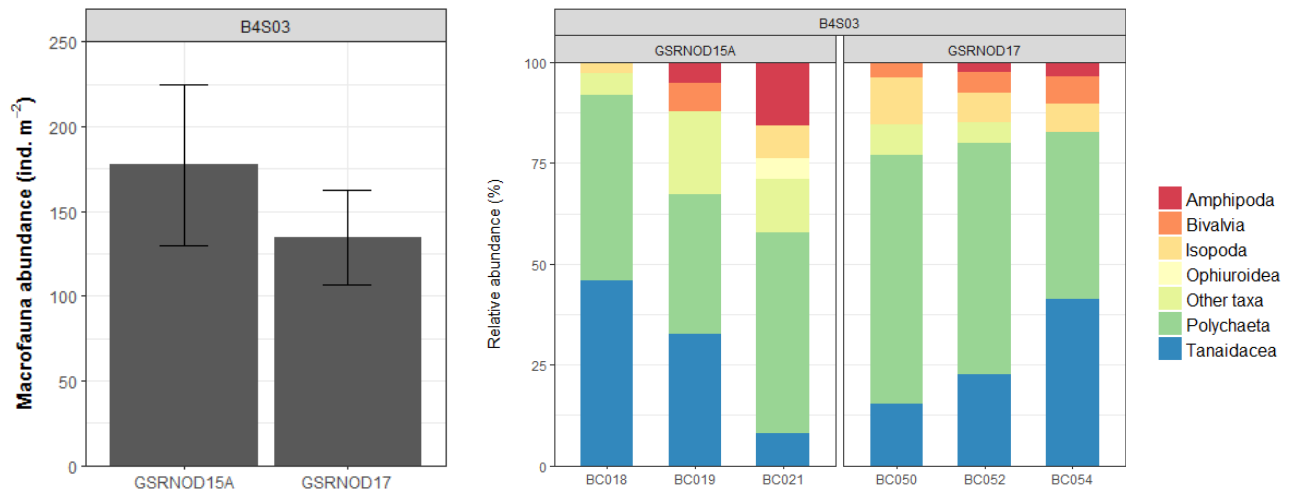


Figure 68: Average values of total macrofaunal abundances for the different expeditions (GSRNOD15A: September-October 2015, GSRNOD17: May-June 2017) within sites B4S03. Error bars denote standard deviations (left) and Relative abundances of higher macrofaunal taxa excluding typical meiofaunal groups per boxcore sample for the different expeditions (GSRNOD15A: September-October 2015, GSRNOD17: May-June 2017) within site B4S03. "Other taxa" include Acari, Brachiopoda, Chaetognatha, Gastropoda, Oligochaeta, Scaphopoda and unknown individuals (right)

4.2.2.3.4 Benthic megafauna

In the sub-zone B4S03, the megafaunal abundance was also estimated, 5.628 ± 424 ind. ha⁻¹ in 2015, including organisms from six phyla: Protozoa, Echinodermata, Cnidaria, Annelida, Porifera, Arthropoda and Chordata. Those phyla, among others, were also described in previous studies on the CCFZ. The cited megafauna density is higher than comparable works in the area. This might be due to the presence of Xenophyophores (giant protist) in the analysis of the GSR area. Megafauna at sub-zone B4S03 is characterized by a dominance of Echinodermata (921 ind. ha⁻¹; 58 %, mainly consisting of Ophiuroidea (460 ind. ha⁻¹) and Echinoidea (402 ind. ha⁻¹)) over Cnidaria (282 ind. ha⁻¹; 18 %, the latter mostly represented by Actiniaria (245 ind. ha⁻¹)), Polychaeta (157 ind. ha⁻¹) and Porifera (99 ind. ha⁻¹). Bioturbation is mainly by megafauna, through movement tracks of echinoids and holothurians, and faecal casts of holothurians and burrowing holes of polychaetes, for instance. The number of lebensspuren in B4S03 sub-zone approaches $4,441 \pm 576$ ind. ha⁻¹.

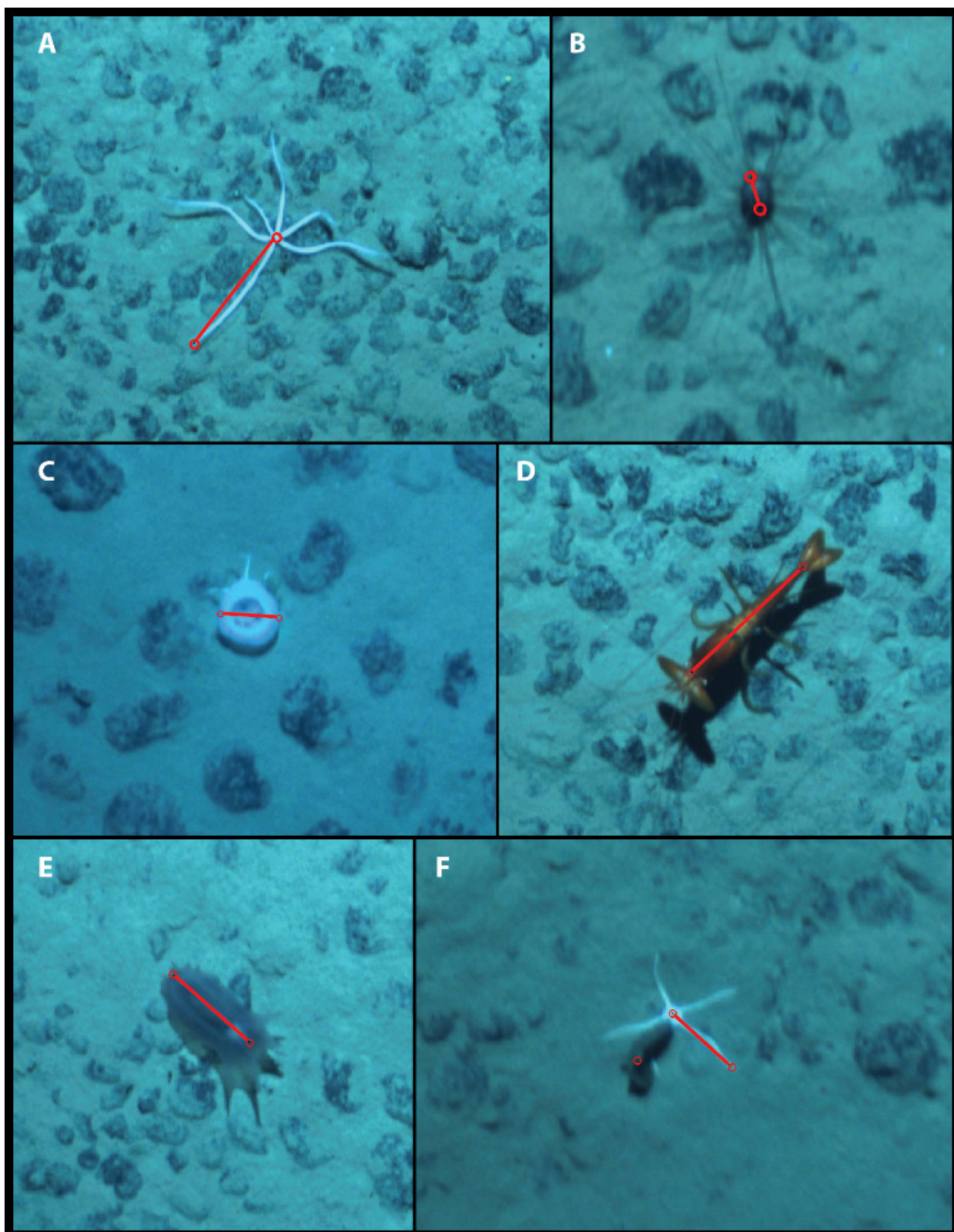


Figure 69: Examples of identified and measured megafauna taxa. **A**, radius from body centre to end of arm of Echinodermata, Asteroidea - *Brsingida* morphotype. **B**, body length (without spines) of Echinodermata, Echinoidea – *Aspidodiadematidae* morphotype. **C**, diameter of the central chamber of Porifera, Hexactinellida - *Hyalonematidae* morphotype. **D**, length of Arthropoda, Decapoda – *Aristeidae* morphotype. **E**, body length (excluding velum) of Echinodermata, Holothuroidea - *Elpidiidae* (*Peniagone* “tulip” morphotype?). **F**, radius from body centre to end of arm of Echinodermata, Ophiuroidea.

4.2.2.3.5 Nodule-associated fauna

Encrusted on the hard substrate, i.e., on polymetallic nodules, protists, mainly Foraminifera, dominate. Preliminary investigations suggest that most epifauna associated with nodules from the GSR contract area are probably also of protist origin.

Regarding nodule-associated meiofauna, Figure 70 shows the nematode family and genus composition identified from the nodule surface and crevices sampled during the GSRNOD15A expedition in the sub-zone B4S03. The nematode families *Monhysteridae* (27.9 %), *Camacolaimidae* (13.9 %) and *Chromadoridae* (10.3 %) were the most numerous over all samples. Seven families were only observed in the crevice samples, i.e. *Linhomoeidae*, *Enchelidiidae*, *Phanodermatidae*, *Siphonolaimidae*, *Selachinematidae*, *Axonolaimidae* and *Ethmolaimidae*. The genus *Monhystrella* was the most abundant genus overall (26.7 %) and dominated both nodule surface (23.9 %) and nodule crevice samples (29.4 %). *Deontolaimus* was the second and third most abundant genus in crevice (17.5 %) and surface (7.1 %) samples, respectively.

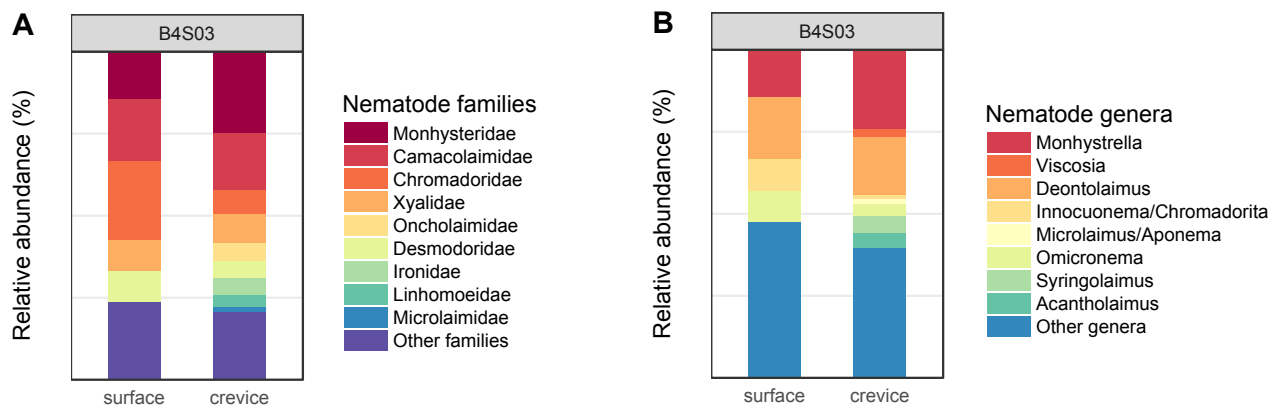


Figure 70: Relative abundance of nematode (left) families and (right) genera in nodule surface and crevice samples (all nodules combined) in B4S03 during GSRNOD15A expedition. Other families and genera comprise those that accounted for <5 % of total (over all nodule samples of all stations) nematode abundance

Vertically, in the sediments, most of the nematode families found in the top 0-5 cm of the sediment column in the GSR contract area (see Pape et al. (2017b, 2017a)) were also observed in the 5-10 cm sediment layer. Five families, i.e. *Draconematidae*, *Enchelidiidae*, *Leptosomatidae*, *Neotonchidae* and *Meyliidae*, only occurred in the 0-5 cm samples. *Monhysterids* prevailed not only in the surface sediment layer in the GSR contract area (26.9 ± 6.4 %); this family also dominated the subsurface nematofauna (36.6 ± 11.8 %). The second and third most abundant family were the *Desmoscolecidae* (11.3 ± 7.2 %) and the *Xyalidae* (11.3 ± 5.6 %), respectively. Moreover, 28 nematode genera (including *Erebus*) that were identified from the 0-5 cm samples were not found in the 5-10 cm samples collected in the GSR contract area. Nonetheless, all these genera were rare in the surface samples as well. Similar to the 0-5 cm samples, *Monhystrella/Thalassomonhystera* (38.4 ± 11.3 %) and *Acantholaimus* (5.8 ± 4.6 %) were the predominant genera in the 5-10 cm sediment layer. Again, relative to the surface sediment layer, there were changes in the relative abundance of these dominant genera with *Monhystrella/Thalassomonhystera* (0-5 cm: 27.0 ± 6.4 %) attaining higher and *Acantholaimus* (0-5 cm: 15.9 ± 4.0 %) attaining lower relative abundances deeper in the sediment. Genus diversity

showed the same trends as family diversity, with genus richness G and Shannon-Wiener diversity decreasing significantly with sediment depth (Figure 71).

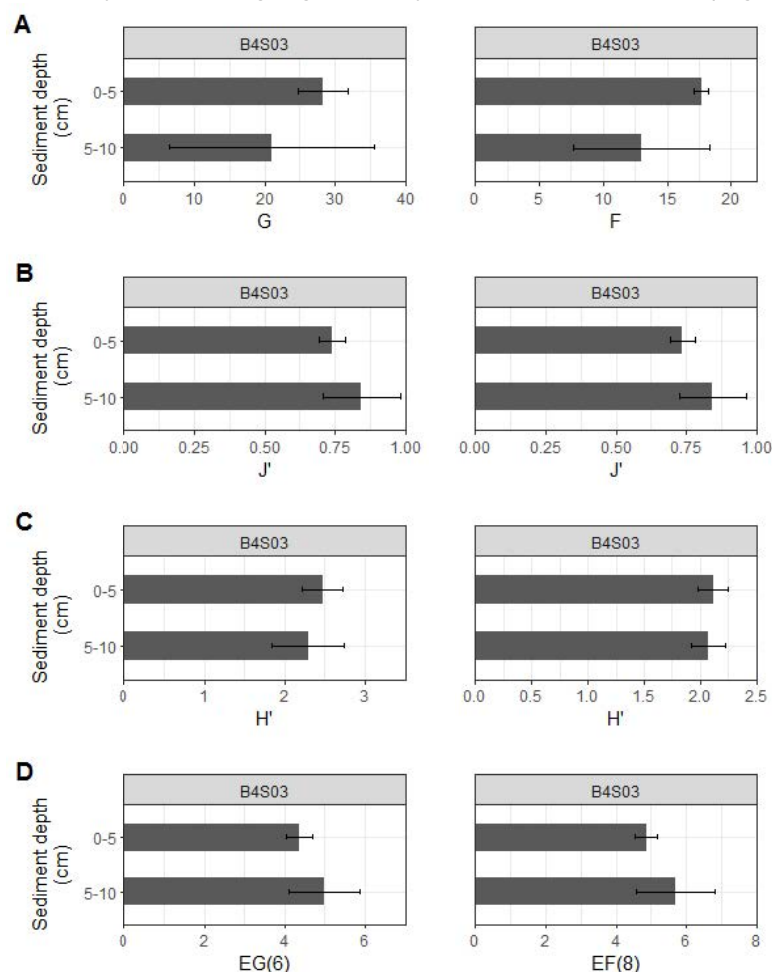


Figure 71: Vertical profiles of nematode families (left) and genus (right) diversity in B4S03 station during GSRNOD15A. Bars denote average (SD). From top to bottom, (A) values of families richness F and genus richness G ; (B) Pielou's evenness J' ; (C) Shannon-Wiener Diversity H' ; (D) expected Families richness for 8 individuals $EF(8)$ and expected genus richness for 6 individuals $EG(6)$.

4.2.2.4 Ecosystem / Community level description

4.2.2.4.1 Ecosystem functioning

The analysis of stable isotopes of carbon and nitrogen is a method which can be used to investigate food-web structure and dynamics as an alternative to traditional gut content analyses (Peterson and Fry, 1987). It has been shown that prey-consumer relationships are related to a stepwise enrichment in stable isotope ratios of carbon and nitrogen (Hobson and Welch, 1992). This enables us to determine food web relationships between different organisms in the abyssal ecosystem. During GSRNOD17 samples of macrofauna, meiofauna, bacteria and sediment were collected for stable isotope analysis. Until now, only organisms belonging to the macrofauna have been analyzed while meiofauna, bulk sediments and bacteria (the latter through stable isotope analysis of bacteria-specific PLFAs) are still awaiting analysis of carbon and nitrogen stable isotopes.

A first visual screening of all samples revealed a structure in the analyzed samples according to taxon with more enriched carbon and nitrogen ratios of Polychaeta compared to Amphipoda (Figure 72). $\delta^{13}\text{C}$ and $\delta^{15}\text{N}$ values from our macrofauna samples covered a range from -23.38 to -17.54 and 8.57 to 21.98, respectively. The measured $\delta^{13}\text{C}$ ratios are comparable to the isotopic signature measured in macrofauna from station M in the the NE Pacific (Sweetman and Witte, 2008) and in macro- and megafauna from the Porcupine Abyssal Plain (PAP) in the NE Atlantic (Iken et al., 2001). The $\delta^{15}\text{N}$ values in our study covered a broad range, exceeding values reported by Iken et al. (2001) in meio-, macro-, and megafauna from the PAP. This large range in $\delta^{15}\text{N}$ ratios may be attributed to the high degree of competition for food and overlapping food sources within and between taxonomic groups. When samples were separated according to nodule coverage, no marked differences in food-web structure were visible, which may be attributed to the small data-set (data provided to ISA by GSR in its 2017 AR, file numbers ISA-GSR_AR2018)

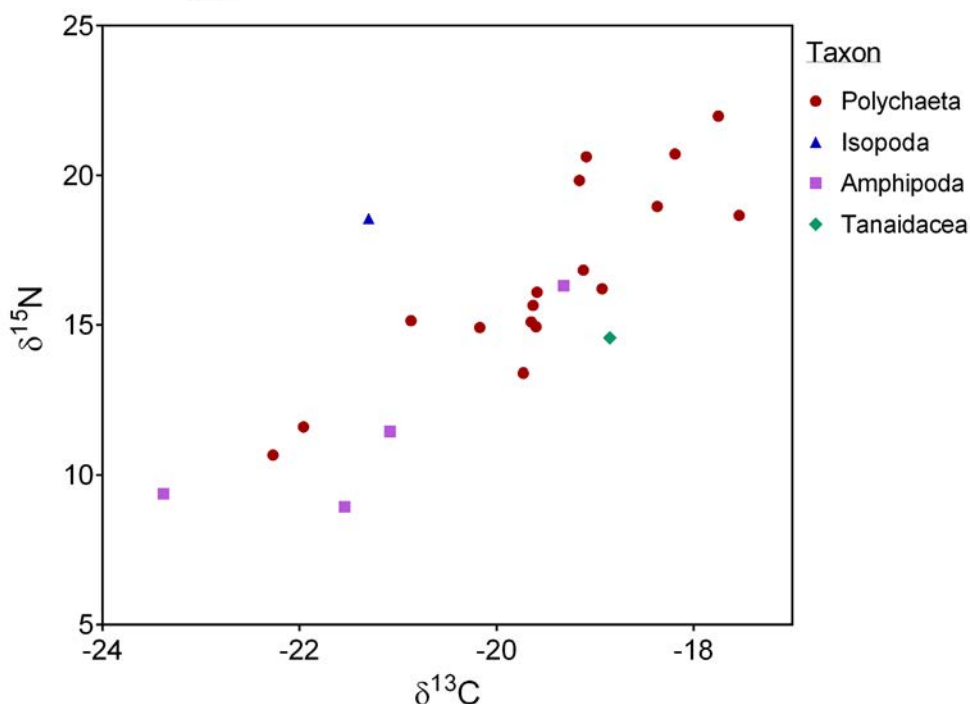


Figure 72: Visualization of isotopic carbon and nitrogen ratios of different macrofaunal taxa from GSRNOD17 samples. Carbon and nitrogen stable isotope ratios are noted in the delta notation (data provided to ISA by GSR in its 2017 AR, file numbers ISA-GSR_AR2018)

4.2.2.4.2 Macrohabitats in B4S03

Across the GSR contract area, water column characteristics are roughly comparable with regard to pigment concentration, nutrient concentration profiles, particulate carbon and particulate nitrogen, dissolved oxygen, turbidity, temperature and salinity. Water column community composition appears to be indistinguishable between stations, is bathymetry-related, and dominated by picoplankton.

At the seabed, from the sedimentary environmental perspective, the PCA analysis comparing the nodule-free and nodule-rich areas in the sub-zone B4S03 illustrates the absence of marked differences in sedimentary characteristics between macrohabitats. Indeed, the samples of the two macrohabitats did not form separate clusters in the PCA plot.

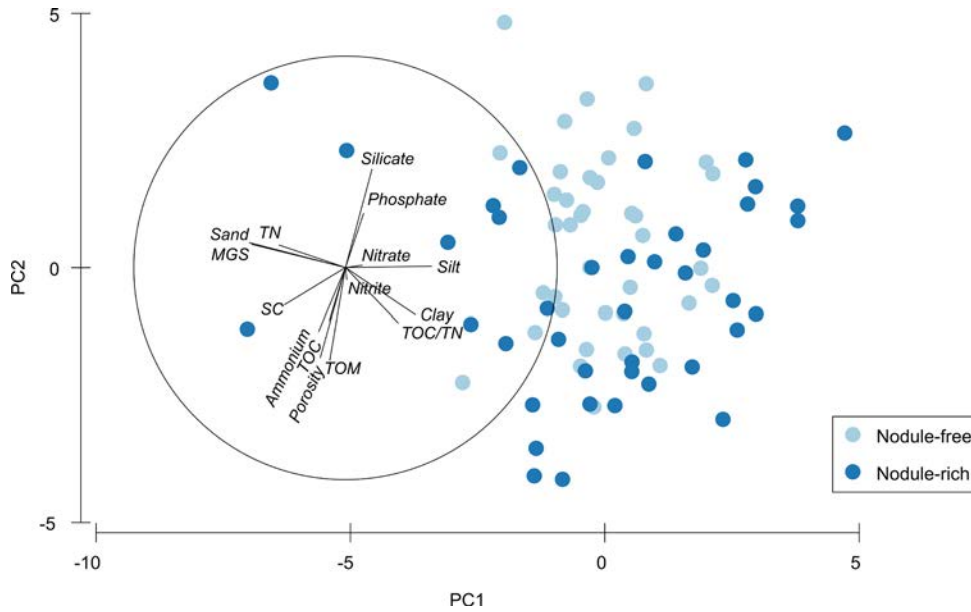


Figure 73: Principal component analysis (PCA) of sedimentary environmental variables comparing the different macrohabitats, i.e. the nodule-free (light blue) and nodule-rich (dark blue) areas, at site B4S03 in the GSR contract area. MGS = median grain size, TOC = total organic carbon content, TN = total nitrogen content, TOC/TN = molar sediment total organic carbon-to-total nitrogen ratio, TOM = total organic matter content, SC = sediment-sorting coefficient. Eigenvectors (black lines) are superimposed

Regarding communities associated with the variable habitats, macrofauna and meiofauna were analyzed. Within site B4S03, 856 macrobenthic organisms were found in the 0-5cm sediment layer. The average total macrofaunal abundances were 137 ± 36.07 ind. m^{-2} in the nodule free areas and 111 ± 57.45 ind. m^{-2} in the nodule-rich area when flat and slope samples were combined. No noticeable difference could be noted between slope areas and slope+flat areas. Although at site B4S03 in the GSR contract area average macrofaunal abundance was higher in nodule-free than in nodule-bearing sediments, this difference was not statistically significant.

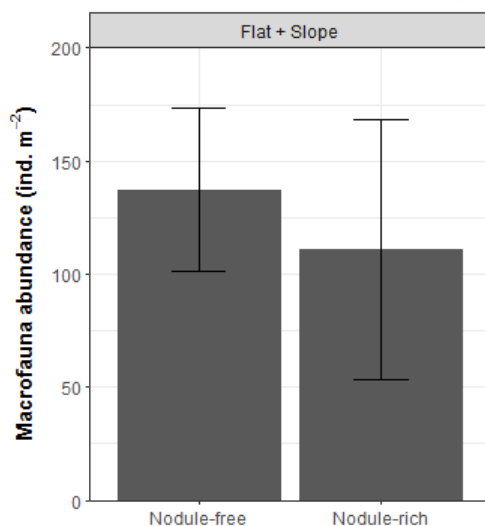


Figure 74: Average values of total macrofaunal abundances in the nodule-free and nodule-rich area (flat+slope) within site B4S03 in the GSR contract area sampled during GSRNOD17. Error bars denote standard deviations

Similarly, “Nodule presence” had no significant effect on macrofaunal community composition within site B4S03 which was dominated by Polychaeta (48.59 %), Tanaidaceae (21.49 %) and Isopoda (15.42 %) while remaining taxa made up 14.49 % of total macrofaunal abundances (see

Figure 75). Diversity and higher taxon composition did not differ between the nodule-free and nodule-bearing site. This similarity in macrofaunal communities between nodule-free and nodule-bearing sediments may be related to the highly similar sedimentary environment.

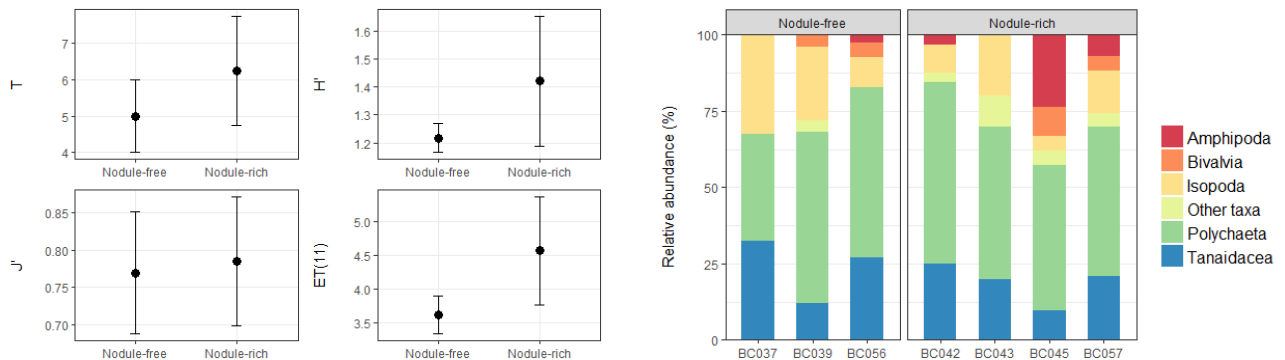


Figure 75: Left : Average values for calculated macrofaunal diversity indices in the nodule-free and nodule-rich area (flat+slope) within site B4S03 in the GSR contract area sampled during GSRNOD17: taxon richness (T), Shannon-Wiener diversity (H'), Pielou's evenness (J') and the expected taxon richness for a sample of 11 individuals (ET(11)). Error bars denote standard deviations. Right : Relative abundances of higher macrofaunal taxa excluding typical meiofaunal groups (namely Ostracoda, Nematoda and Copepoda) per boxcore in the nodule-free and nodule-rich area (flat+slope) within site B4S03 in the GSR contract area. "Other taxa" include Acari, Brachiopoda, Chaetognatha, Gastropoda, Oligochaeta, Scaphopoda and unknown individuals.

Within site B4S03, meiofaunal total abundances (average \pm SD) differed significantly between macrohabitats where higher average total meiofaunal abundances were found in nodule-free areas (flat: 112.39 ± 3.27 ind. 10 cm^{-2} , all: 126.85 ± 29.02 ind. 10 cm^{-2}) compared to nodule-rich areas (flat: 40.59 ± 36.75 ind. 10 cm^{-2} , all: 45.38 ± 31.49 ind. 10 cm^{-2}).

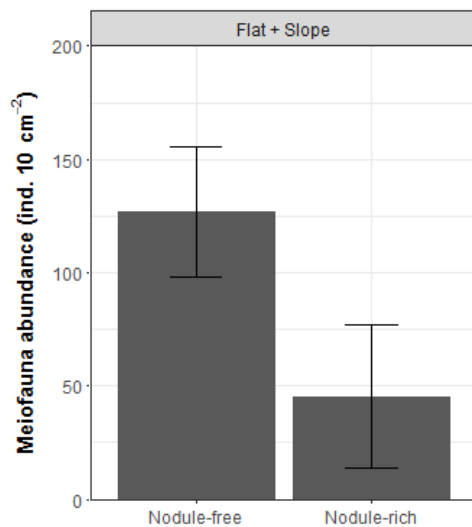


Figure 76: Average values of total meiofaunal abundances in nodule-free and nodule-rich areas (flat+slope) within site B4S03 in the GSR contract area during the GSRNOD2017 campaign. Error bars denote standard deviations

Despite the similar trend of higher average values in nodule-free areas, none of the meiofaunal taxon diversity indices showed significant differences between macrohabitats and a similar result was found for meiofaunal community composition.

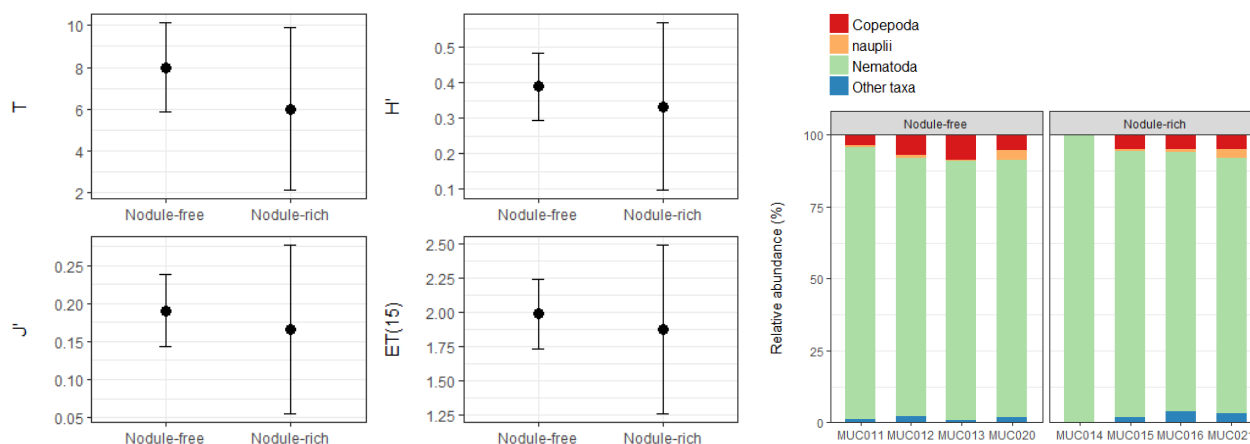


Figure 77: Average values for the calculated diversity indices in the nodule-free and nodule-rich area (flat+slope): taxon richness (T), Shannon-Wiener diversity (H'), Pielou's evenness (J') and the expected taxon richness for a sample of 15 individuals ($ET(15)$) (left) and Relative abundances of higher meiofaunal taxa per MUC sample in the nodule-free and nodule-rich area (flat+slope) (right) within site B4S03 in the GSR contract area sampled during GSRNOD17. "Other taxa" are higher meiofaunal taxa that comprised < 1 % of total meiofaunal abundance. Error bars denote standard deviations.

Relative abundances of higher meiofaunal taxa per MUC (0-5 cm) are shown in Figure 77, right-hand panel, where it can be seen that meiofaunal communities in both macrohabitat types were dominated by Nematoda (90.69 %), Copepoda (5.84 %) and nauplii (1.53 %). A possible explanation for the elevated meiofaunal standing stock in nodule-free vs. nodule-bearing sediments is the higher sedimentation rate (and thus higher food availability for meiofauna) in the former habitat, as observed by Mewes et al. (2014) for the BGR (Bundesanstalt für Geowissenschaften und Rohstoffe) contract area. Alternatively, predation pressure may be reduced in nodule-free sediments as megafauna show higher standing stock in nodule-bearing than in nodule-free sites (Radziejewska and Stoyanova, 2000; Vanreusel et al., 2016).

Meiofaunal abundance is much higher than the macrofaunal abundance. However, standing stocks of bacteria, meiofauna and macrofauna measured in B4S03 are not correlated with one another. This suggests that their distribution might be governed by other factors. For instance, analyses describe a relation between bacterial biomass and particulate organic carbon flux measured in the sediment. Meiofaunal abundance is not related to the nodule abundance of the area; the contrary is observed with macrofauna. Moreover, macro- and meiofaunal taxon richness estimation seems to be correlated; this may either mean that they are driven by common biotic/abiotic factors or that they are influencing each other's diversities (GSRNOD14A data, but not observed again during GSRNOD15A). Moreover, molecular analysis suggests a certain level of connectivity between sub-zones of the GSR contract area in the CCFZ.

Through comparison between sampling zones of the GSR contract area, it was proven that distant, equally deep nodule-bearing sediments within the GSR contract area were inhabited by similar meiofaunal communities, and that the dominant taxa also occur in remote nodule-bearing and nodule-free deep-sea locations (Pape et al., 2017a). During the GSRNOD2015A campaign, three polymetallic nodule-bearing sites, about 60–270 km apart, located at similar depths (ca. 4,500 m) were sampled, of which one site was sampled in April 2015. Despite the relatively large geographical distances and the statistically significant, but small, differences in sedimentary characteristics between sites, meiofaunal and nematode communities were largely similar in

terms of abundance, composition and diversity. Between-site differences in community composition were mainly driven by a set of rare and less abundant taxa. Moreover, although surface primary productivity in April 2015 exceeded that in October 2015, no significant changes were observed in sedimentary characteristics or in meiofaunal and nematode communities between both months. At all sites and in both periods, Nematoda were the prevailing meiofaunal phylum, which was in turn dominated by *Monhysterid* genera and *Acantholaimus*. The findings of Pape et al. support the earlier possible notion of a low degree of endemism for nematode genera and meiofauna taxa in the deep sea, and hint at the possibility of large distribution ranges for at least some *Halalaimus* species (2017).

At a larger scale, based on polychaete Cytochrome c oxidase subunit I (COI) sequence analysis, it was shown that several of the polychaete specimens sequenced from the GSR contract area were closely related to specimens from other CCFZ contract areas (as they clustered together regularly on short branches). This finding points to at least some degree of connectivity between contract areas that are separated by 100s of kilometers.

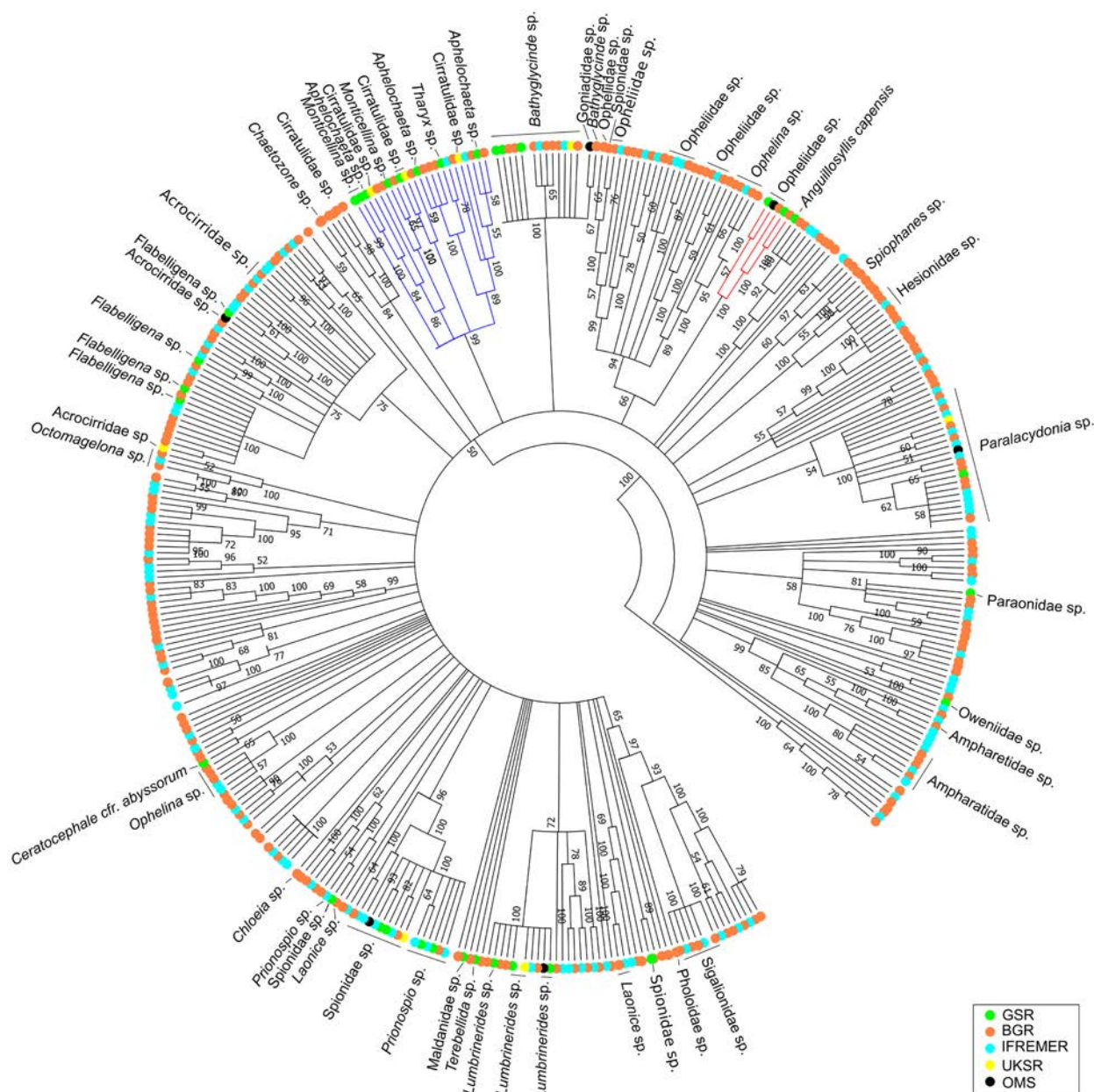


Figure 78: Condensed neighbour-joining phylogenetic tree using the *p*-distance method of polychaete COI sequences for different contract areas in the CCFZ (indicated by the different colours). Bootstrap values ($n = 500$; values lower than 50 % are not displayed) are shown on the branches of the trees. Subtrees were made of the clades indicated in red ("Subtree 1") and blue ("Subtree 2"). The analysis involved 604 nucleotide sequences. All ambiguous positions were removed for each sequence pair. All sequences without taxon name were identified as "Polychaeta sp". GSR = Global Sea Mineral Resources n.v., BGR = Bundesanstalt für Geowissenschaften und Rohstoffe, IFREMER = Institut Français de Recherche pour l'Exploitation de la MER, UKSR = UK Seabed Resources, OMS = Ocean Minerals Singapore

5 Assessment of impacts and proposed mitigation

This section offers a description of the potential impacts of the nodule collection process on the marine environment, including the physico-chemical environment and the biological environment. A complete Table of the Risk Register, including potential risks and mitigation, can be found in

Annex 12.5. The impacts expected based on modelling work prior to execution of this trial need to be validated through monitoring and a relationship needs to be established between impact and effect on the environment. GSR set up a collaboration with the JPI-O MiningImpact 2 Consortium where GSR will deliver a realistic small-scale PPV collector disturbance to enable research on the potential impact of nodule collection from the seafloor. To remain as transparent as possible, and to ensure independent scientific data results, this research will be performed by the independent JPI-O MiningImpact 2 Consortium. The following section has been mainly developed with the input of the JPI-O MiningImpact 2 Consortium partners, especially BGR, and is tailored to the Belgian Contract Area. The assessment of impact and effect is the main research topic of the JPI-O MiningImpact 2 Project.

The aim of the MiningImpact 2 project is to assess the immediate, short-term and intermediate-term (2 years) physico-chemical and biological impacts of the Patania II trial on the seafloor and its overlying waters, as well as the response of benthic organisms to the impact, which in turn will inform assessment of the recovery of benthic standing stocks, local changes in biodiversity and the maintenance of associated ecosystem functions. We thus refrain from providing detailed assessments or prognoses on the extent of impacts here, but rather refer to section 7, Environmental management, monitoring and reporting, pp. 164 for a detailed description of the scientific monitoring programme that will accompany the collector trial. Detailed analyses and input of data into models, also in terms of future risk assessment, will facilitate a much more comprehensive future assessment of the nature and extent of similar impacts and their effect on the environment. It will enable GSR to better understand the impacts of the operation and subsequent management of these impacts to reduce potential effects on the environment.

5.1 On the physico-chemical environment

5.1.1 Description of potential impact categories

The major types of physico-chemical environmental effects of nodule removal from the seafloor, that potentially might occur during the GSR technical trials, are (1) habitat/nodule removal, (2) sediment disturbance and plume formation, (3) biogeochemical alteration of the sediment (i.e., change of habitat integrity), (4) potential release of potentially toxic sediments and/or substances into the lower water column, (5) emissions to air, and (6) potential additional impacts from natural hazards such as hurricanes or benthic storms. Most of these impact categories will also affect the biological environment, as might noise and light pollution.

5.1.2 Emissions to air

The vessels used in this project strictly follow the IMO obligations and standards regarding environmental practices at sea, including the International Convention for the Prevention of Pollution from Ships, 1973, as modified by the Protocol of 1978 relating thereto (MARPOL) and the Protocol of 1997 to MARPOL concerning the prevention of air pollution from ships. In this way, the IMO regulates emissions to air and establishes required anti-pollution measures that aim at minimising all effects of air and water pollution at sea.

5.1.3 Geological setting

5.1.3.1 Nodule removal

Picking up the nodules and removing the associated fine-grained muds fundamentally disturbs the benthic habitat in the mining area, leading to significant alteration of seabed habitat, and entails the generation of sediment plumes near the seafloor. From a physical impact perspective, removing nodules (and sediments) from the seafloor will also change the micro-topography or roughness of the mined area (e.g., less friction due to nodule removal; production of small furrows and ridges), which in turn could affect the very local hydrodynamic current regime close to the seabed, as well as processes of sedimentation/re-sedimentation. Bedload (sediment) transport is more pronounced in areas of lower nodule abundance, suggesting that bedload transport will increase when nodules are removed.

In the case of the PPV trial planned here, the directly affected area where nodules are removed will have a maximum size between 0.022 and 0.1 km² and lies in an area of limited topographic constraints in the direct vicinity. We thus assume that, on a more regional scale, the removal of nodules in the trial area will have an insignificant effect on the physico-chemical regime of the area.

5.1.3.2 Sediment disturbance and plume creation

Potential environmental concerns associated with the sediment discharge (the “sediment plume”) in the course of deep-sea mining include (a) artificial rapid redeposition of sediments from the resettling plume and bottom blanketing in the vicinity of the mine site (“near field”), burying benthic organisms and clogging the respiratory surfaces of filter feeders, (b) oxygen depletion in the blanketed seabed and the water body inside the plume through reactive constituents (e.g. labile organic matter or reduced metals), and (c) the release and deposition of potentially toxic (which will depend on their bioavailability) metals, which can lead to bioaccumulation of contaminants. These processes will affect deep-sea ecosystem structure and functioning to a certain but currently unknown extent. To date only very few studies have focussed on analysing and modelling the scale of this impact at various environmentally relevant temporal and spatial scales, which is dependent on multiple local and regional factors, such as the physical and chemical properties of the bottom sediments, the nature of the hydrodynamic regime (near-field and far-field), bottom topography, the type of mining equipment being used, and mining rate, amongst others. At the moment, the amount of sediment deposition from a mining-induced plume that could either be tolerable or lethal for any of the faunal groups of the deep sea is unknown.

5.1.3.2.1 Historical review of in-situ experiments

To date, only few publications have dealt with the possible behaviour of the sediment plume in abyssal manganese nodule exploration areas; these are mainly restricted to the results of mining tests carried out in the 1970s by Ocean Mining Inc. (OMI) and Ocean Mining Associates (OMA) (e.g. Lavelle et al., 1981) and to the results of benthic impact experiments and modelling activities carried out in the 1990s by Germany (DISCOL/ATESEPP; Peru Basin), Japan (JET; Japanese CCFZ claim area) and Russia/USA (NOAA-BIE; former American CCFZ claim area). These focused primarily on determining the impact of the resettled sediment plume on benthic fauna (for a detailed description of these experiments, see Jones et al., 2017). In these experiments, the extent of redeposited sediment in the surroundings of the affected sites was inferred from seabed imagery (Yamazaki et al., 1997) and from numerical simulations forced by

time-series measurements of ocean bottom currents and imposed static particle sizes and settling velocities (e.g., Nakata et al., 1997, Jankowski and Zielke, 2001, Rolinski et al., 2001). Deep-sea observational technology at the time of those experiments did not allow comprehensive monitoring of the actual sediment plumes as they were spreading laterally and vertically away from the source site, nor could differential particle aggregation processes which critically determine the redeposition of sediments from the plume be assessed.

In the JET experiment, a Deep Sea Sediment Resuspension System (DSSRS) was towed 19 times along two parallel 2000-m-long tow zones throughout a time period of ca. 1 month, ejecting 352 tonnes of sediment slurry with at a rate of ca. 30 g/l and 60 l/s at a height approximately 5 m above the seafloor (Fukushima, 1995). Sediment trap analyses and modelling exercises showed that resedimentation or blanketing reached a maximum thickness of 2.6 mm close to the source (Barnett and Suzuki, 1997). Furthermore, empirical and modelling data of the JET and the technically very similar NOAA-BIE experiments showed that 90% of the suspended particles created by artificial disturbance of the sea floor had settled within a radius of 2 km from the impact area (Fukushima, 1995; Nakata et al., 1997). The residence time of a plume created by a single collector with an assumed trial-scale production of 10 kg/s (about 5 times the output of the DSSRS) in a relatively small area (ca. 1500 m path length) was estimated by Jankowski et al. (1996) to be 1.5 to 6 days.

In all cases, adequate validation of the models used was hampered by incomplete and sparse current measurement data (these were derived from a handful of point current sensors at fixed water depths only - in contrast to present-day ADCPs that continuously measure over a whole range of water depths), and poor bathymetric data. Furthermore, the experiments and modelling exercises carried out focussed more strongly on blanketing, bottom destruction and faunal recovery than they did on plume dispersion in the water column, and they represent relatively small-scale single-dose discharges, which probably cannot be extrapolated to a (sub-) industrial scale, continuous production situation.

During the MiningImpact 1 project, several small-scale sediment dispersal experiments using an epibenthic sled (EBS) and a ROV were conducted to suspend surface sediment. An attempt was made to track the plume using upward and downward-looking ADCPs mounted on benthic landers, light-backscatter sensors and HD cameras. Although both experiments were not set up for quantitative analyses, some qualitative statements could be made: the sediment plumes did not rise more than 10 m above the seafloor, and the lateral spread varied largely in conformity with changing current velocity and direction during the experiment as well as with seafloor topography.

Particulate elemental concentration was measured in a small-scale experimental plume that was produced by the ROV Kiel 6000 in the Peru Basin (cruise SO-242/2). DOC concentration was initially very high (immediately after production of the plume by the ROV), i.e. 57.28 mg/L after 1 minute, but strongly decreased to 0.63 mg/L after 4 minutes, and subsequently fluctuated only slightly between 0.79 and 0.57 mg/L within the 50 minutes of measurement. Background bottom water DOC values were in the range of 1.5-4 mg/L.

5.1.3.2.2 Sediment transport modelling

An operational model has been (and will be further) developed, capable to calculate the sediment plume dispersion due to JPI-O MiningImpact 2 activities in the GSR Contract Area in the CCFZ. The model consists of a hydrodynamic model using the open-source TELEMAC-3D software, coupled with the General Ocean Turbulence Model (GOTM). Plume dispersion is modelled using the sediment transport module of TELEMAC-3D. The planned Patania II trials are simulated in order to (1) provide an initial prediction of the plume dispersion impact size and concentration, (2) provide guidance for the placement of monitoring equipment during the trials, (3) perform validation of the model after the trial period.

Due to time restriction, the numerical model used in the presented simulations has had a limited calibration for hydrodynamics and is not yet calibrated for sediment transport. Therefore, the findings presented in this report are preliminary results.

The sediment motion is modelled using an advection-diffusion equation, including the effect of horizontal and vertical turbulence as well as settling of sediment due to gravity. Only sediment released as a result of the Patania II trial is taken into account in the model. Naturally occurring background suspended sediment is not considered in the model. Because of the low velocities that occur in the area of interest, erosion (resuspension) of sediment is not taken into account.

All sediment released is released from the Patania II, which moves along some predefined transects in the model. The release occurs in the nearest horizontal node of the model. A uniform sediment concentration is used in the lowest 6 m of the model, thus parametrizing the initial mixing of the released sediment.

An analysis of 50 sediment samples taken from the top 0.50 m of the seafloor shows an average median grain diameter d_{50} of 0.0120 mm (Figure 79), leading to a settling velocity of the primary particles of 0.1 mm/s.

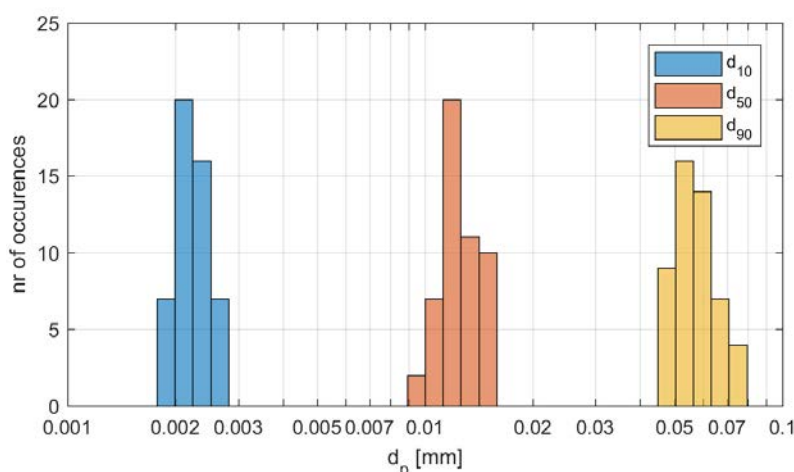


Figure 79: Distribution of d_{10} , d_{50} and d_{90} from 50 sediment samples taken from the top 0.50 m of the seafloor

In the plume dispersion model, three sediment fractions are used based on an assumed distribution between primary particles, microflocs and macroflocs.

Table 25 :Multiple sediment fractions in the sediment plume emission

Fraction number	% of total solids discharge	Settling velocity [mm/s]
1 (primary particles)	10	0.1
2 (microflocs)	40	0.5
3 (macroflocs)	50	1

- Near-field dispersion

In order to simulate the far-field plume dispersion using the model described above, knowledge of the near-field dispersion is of paramount importance. Since the large-scale far-field model is not capable of resolving the small-scale dynamics of the turbulent dispersion in the vicinity of Patania II at work (length scale in the order of 0.1 m), a separate model is set up to resolve the dispersion of the released sediments in the vicinity of the vehicle, called the near field. The near field ranges from Patania II to about 100 to 200 m downstream, depending on the dynamics.

The mixture of water, fine sediments and nodules flows into rectangular ducts and arrives at a separator at which the nodules are gravitationally separated from the water-sediment mixture. The nodules – along with a minor residue of fine sediments and an additional discharge of clear water – are pumped to the bucket where the nodules remain and the water with minor sediment load is released. The main flow of sediment-loaded water is guided towards two diffusors, located on top of the bucket. The diffusors slow down the flow, which is eventually led through a grid of panels guiding the flow to the outlet at a given angle towards the sea bed.

In order to simulate the turbulent flow responsible for the dispersion of sediments in the direct vicinity of Patania II, a Computational Fluid Dynamics (CFD) model is selected. The Reynolds-Averaged Navier-Stokes equations for the water-sediment mixture are solved in a steady state mode. Additional features are added to the formulation to take into account the multi-phase effects, by means of a mixture model including a drift flux term.

The 3D-geometry of the Patania II has been simplified and placed in a volume of ocean water of horizontal dimensions of 250 m streamwise by 100 m spanwise and a height reaching from the ocean floor up to 50 m. The volume in which the flows of water and sediment will be simulated are discretised to solve the equations numerically. The discretisation at the surface of the simplified geometry of Patania II is shown in Figure 80.

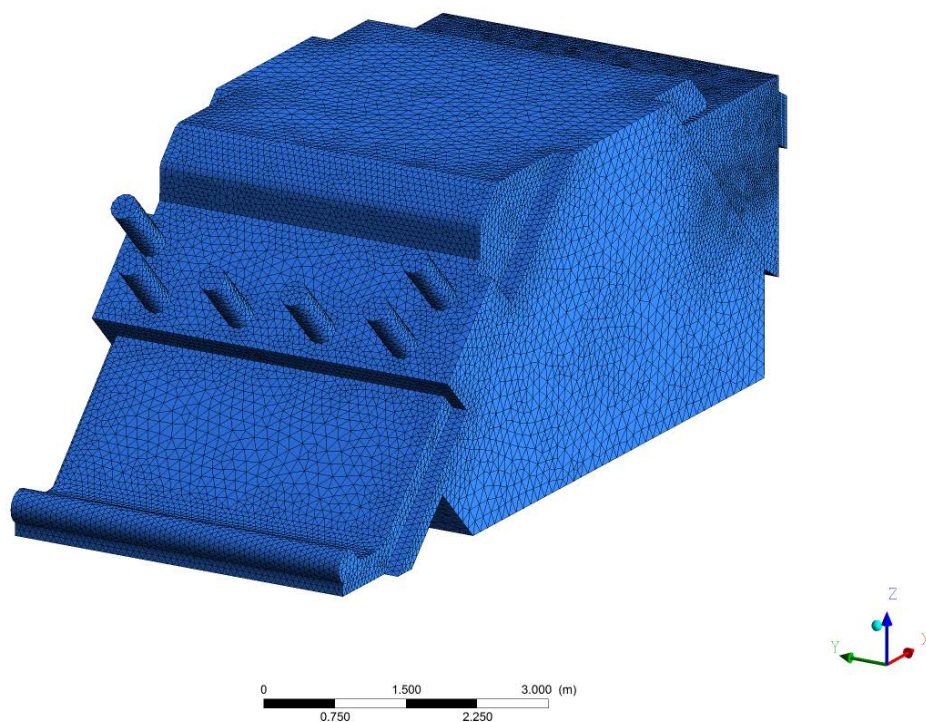


Figure 80: surface mesh at the walls of the collector, front

For the purpose of this EIA, the discussion is limited to the obtained vertical profiles of sediment concentration at a distance of 150 m behind the Patania II at work. These vertical profiles of sediment concentration - or more precisely, vertical profiles of sediment flux – are transferred to the source terms of the far-field plume dispersion model described higher in this report.

The scenarios as listed in Table 26 have been simulated using the CFD model. The scenarios include realistic sediment outflow conditions, and a number of worst-case combinations of vehicle speed and sediment outflow rates. Scenario 4A repeats scenario 2C, but without the flow guiding panels, to demonstrate their efficiency.

The resulting plumes simulated in the vicinity of the Patania II demonstrate that a so-called density current is formed. A density current is characterised by a high sediment concentration within, and a very sharp vertical gradient of sediment concentration (and mass density) at its upper edge. This strong vertical density gradient dampens turbulence, due to which very limited vertical mixing is possible.

Table 26: List of scenarios executed for CFD modelling of the near-field dispersion

Scenario	Outflow sediment concentration SSC (g/l)	Collector speed U_c (m/s)	Ambient flow velocity U_a (m/s)	Total Sediment influx F (kg/s)
1A	50	0.5	0.05	65.9
1B	50	0.5	-0.05	65.9
2A	170	1	0.05	212.3
2B	85	0.5	0.05	108.4
2C	34	0.2	0.05	46.1
3A	10	1	0.05	17.3
3B	34	1	0.05	46.1
3C	170	0.5	0.05	212.3
4A	34	0.2	0.05	46.1

An impression of the density current found for scenario 2B is shown in Figure 81.

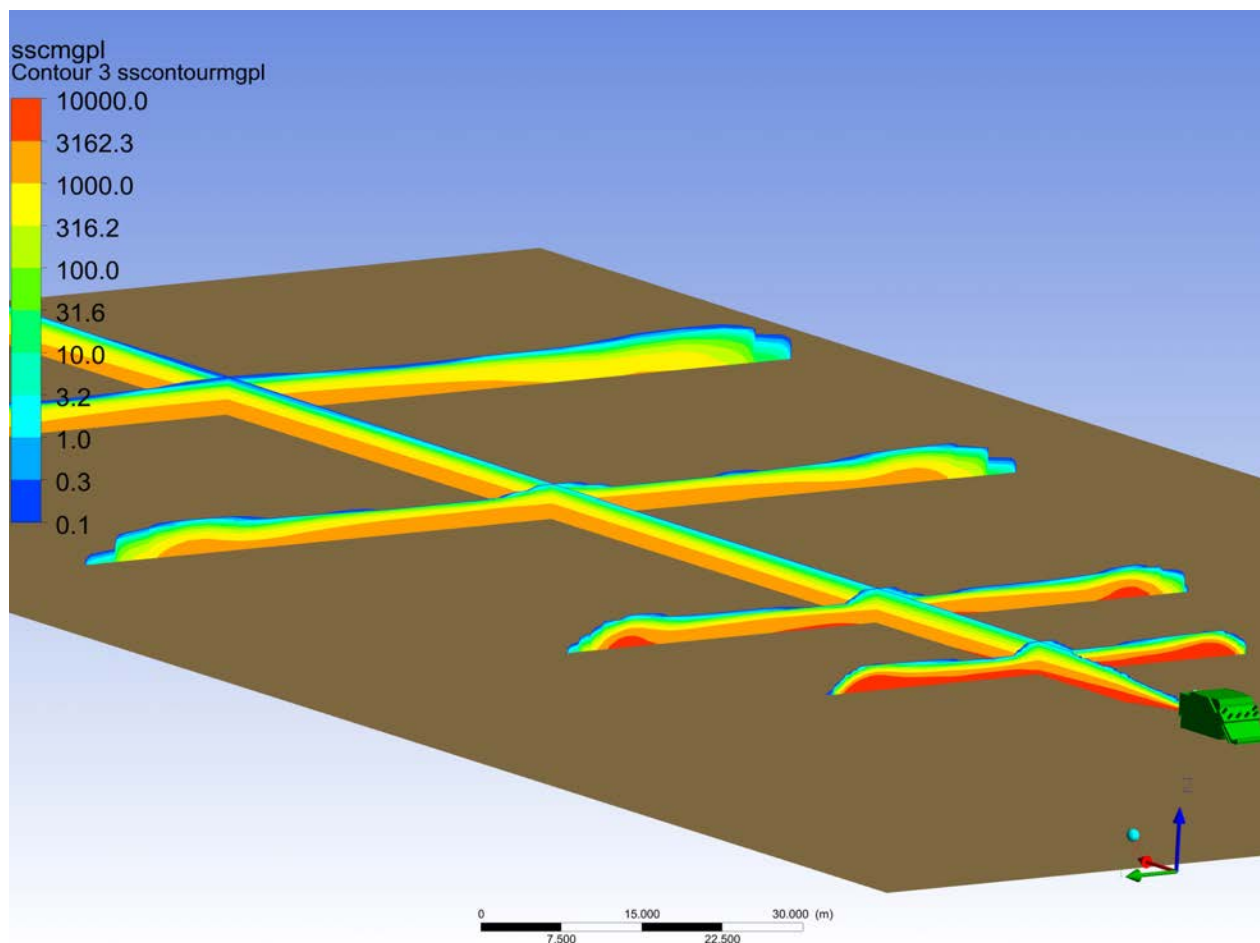


Figure 81: Contours of sediment concentration (mg/l) along the central symmetry plane ($Y=0$ m), and along lateral planes ($X=25, 50, 100$ and 150 m)

The CFD is thus carried out to determine the near-field behaviour of the sediment plumes, in order to impose realistic sediment concentration profiles to the much coarser far-field models (simulating the plumes over km scale). In the latter models, the vertical resolution above the sea bed is typically of the order of 1 m, but the horizontal resolution is of the order of 100 m. In general, it is therefore required to specify a sediment influx distribution in one horizontal model cell, but with a distribution over the vertical.

Therefore, the results of all CFD scenarios have been processed in the following way:

- At 150 m from the collector, the flux of sediment over the $X=150$ m-slice is computed as $F' = SSC * U$, with unit $[kg / m^2 s]$;
- The flux F' is integrated over the Y -direction, obtaining a vertical profile of sediment flux $F''(z)$, with units $[kg / m s]$;
- The flux $F''(z)$ is normalised by the total sediment influx by the collector (in kg/s).
Normalised flux F is a function of z and has units $[1/m]$;

When the vertical profile for all cases is plotted in one graph, Figure 82 is obtained. It can be seen that the height of the horizontally integrated plume is 3 to 5 m, with the majority of sediment flux occurring within the 2 m above seabed.

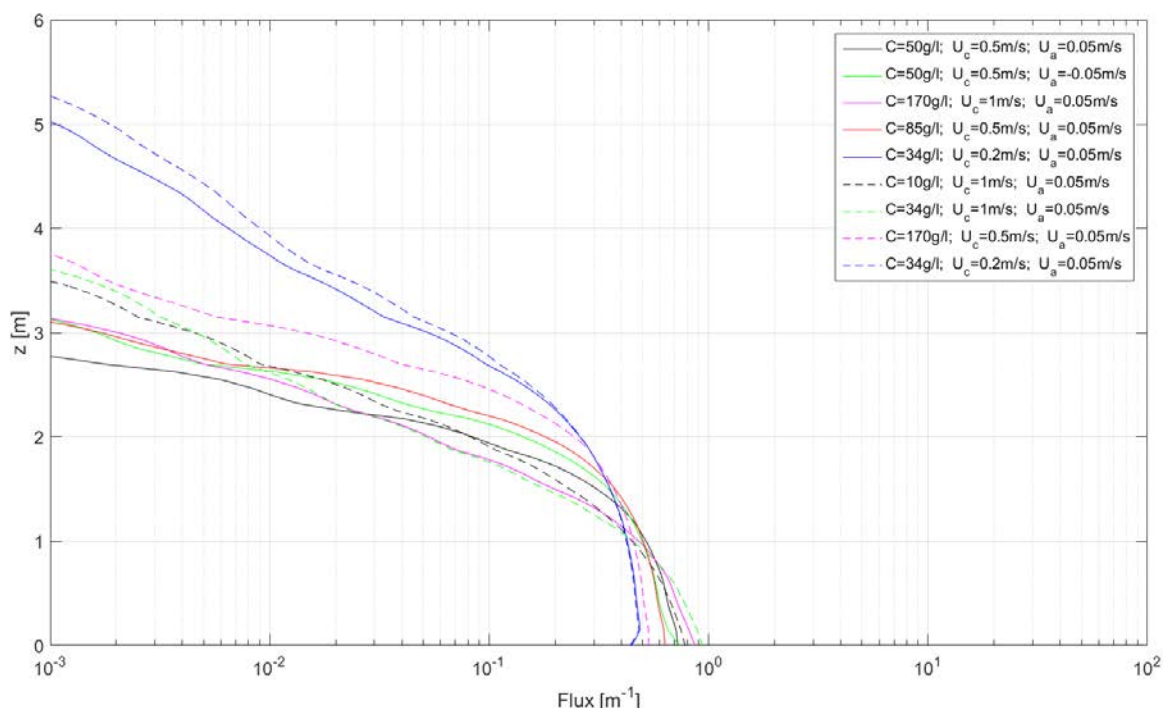


Figure 82: Integrated and normalised sediment flux, as function of vertical height above the bed. Blue dashed line is same as full blue line but without flow guidance

It must be noted that, when a density current propagates further, the sediment concentration reduces with distance propagated. As the sediment concentration reaches a critical value below which the turbulence damping effect is no longer important, the density current might be resuspended by the ambient flows. It is assumed that this event lies at the boundary between near-field model and far-field model.

The sediment profiles obtained in the CFD model have been imposed to the far-field model. The far-field models do not have sufficient resolution and not all appropriate physics implemented to account for the turbulence damping effect. Also, the sediment flux will have to be distributed over larger horizontal surface area. Therefore, the sediment layers imposed in the far-field model will be available for vertical turbulent mixing, as they will be in reality after sufficient dilution.

Further, as a conservative approach, a near-field sediment plume height of 6 m is used for the far-field plume simulations.

- Overview of the simulated scenarios

For all scenarios, the simulation period is 21 days (Table 27) and consists of a 2-day spin-up period to allow the bottom boundary layer to be fully adjusted to the local bathymetry, a 4 day Patania II trial, and a 15-day period after the Patania II trial to track the evolution of the sediment plume.

Table 27: Overview of the 21-days model simulation period

1	2	3	4	5	6	7	8	9	10	11	12	13	14	15	16	17	18	19	20	21
Mode spin-up		Patania II trial				Post-trial plume tracking														

In order to account for the temporal variability of the deep-ocean currents and since the Patania II trials will occur during boreal spring (March-May), each Patania II trial scenario was simulated three times, with hydrodynamic forcing of March, April and May 2009 respectively. The forcing

modelling period 2009 was based on the available HYCOM hindcast forcing data. Before the actual trial this exercise will be repeated with more recent HYCOM hindcast data and/or HYCOM forecasted data to inform the experiment.

All simulations start on the first day of the month. As an example, the March 2009 simulation starts on 2009-03-01, with the Patania II trial starting on 2009-03-03 (after a 2-day warmup period) and ends on 2009-03-21. The timing for the April 2009 and May 2009 simulations is analogous.

Four different scenarios were considered for the Patania II trials, each with a different trajectory, sediment flux and activity cycle of the Patania II. In each scenario, the Patania II moves through the program area in zone B4S03, shown in Figure 83. The Patania II trajectory, speed and activity sequence for each scenario are described in the following paragraphs; key numbers are summarized in Table 28.

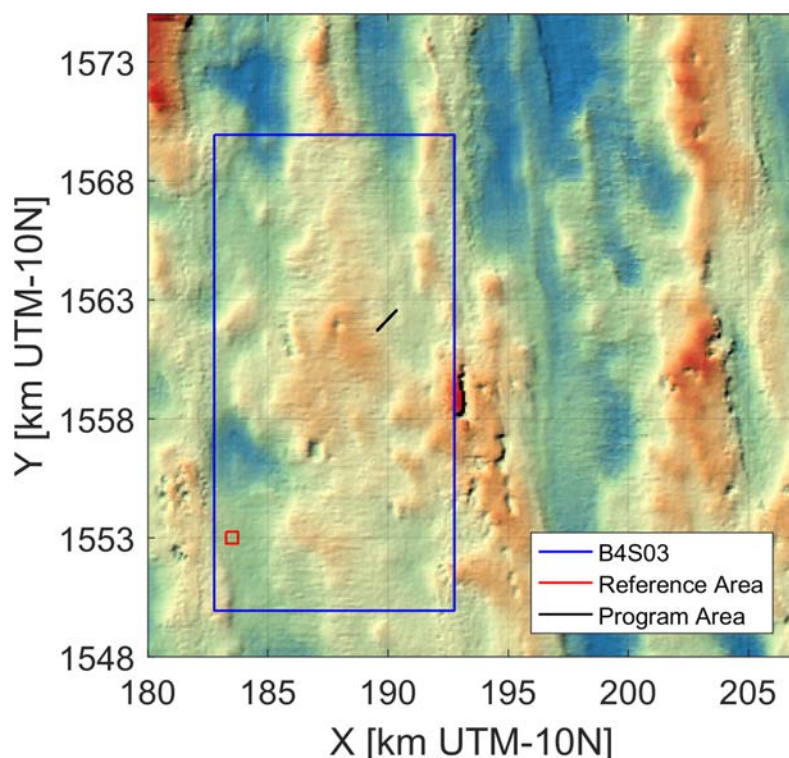


Figure 83: Program area location within B4S03

Scenario 1

In Scenario 1, the Patania II drives back and forth along the length of the MiningImpact 2 program zone (1200 m, to ensure a conservative modelling approach regarding the area impacted) at a speed of 0.3 m/s. An activity cycle is defined in which the Patania II drives and collects nodules during 2 minutes, and then remains idle for 10.5 minutes, the time hypothetically required for emptying the Patania II bin, and turn of 180°. During the idle time, the Patania II does not emit a sediment plume. During the 2 minutes of the active phase of the cycle, the Patania II emits a sediment plume at a rate of 225 tons (dry sediment mass) per hour.

Scenario 2

Scenario 2 is similar to scenario 1, in that the Patania II also drives back and forth along the length of the MiningImpact 2 program zone. However, the Patania II speed is 0.5 m/s, the

sediment flux is 374 ton per hour and the activity cycle is 2 minutes ON, 5 minutes OFF. The progress efficiency of the collector trial in this scenario is more than double the estimated efficiency, resulting in the highest sediment flux. Scenario 2 is therefore considered a worst-case scenario, but unlikely to happen.

One of the objectives of the disturbance experiment is to clear a continuous area from nodules. And since we are limited on pick-up capacity by the size of the bucket on the Patania II, the below scenarios 3 and 4 are reflecting the preferred execution plan.

Scenario 3

In scenario 3, the Patania II travels back and forth along the width of the program area in a zigzagging or 'lawn mowing' fashion (Figure 84). First, there is the two-minute active phase of the Patania II cycle in which the Patania II travels along the width of the program area, covering a stretch of 37.5 m along the width of the program zone (travel speed 0.3 m/s). Then, there is an inactive period of 8 minutes in which the Patania II U-turns to travel back along the width of the program area, with its track shifted by 4 m (the width of the Patania II) along the length of the program area. A full cycle therefore lasts 10 minutes, and 576 cycles can be performed during the 4 day trial period, so that the Patania II can cover 2304 m along the length of the program area. During the 2 minutes of the active phase of the cycle, the Patania II has a sediment emission flux of 225 ton per hour (the same as in scenario 1). No sediment emission occurs during the inactive U-turning phase of the cycle.

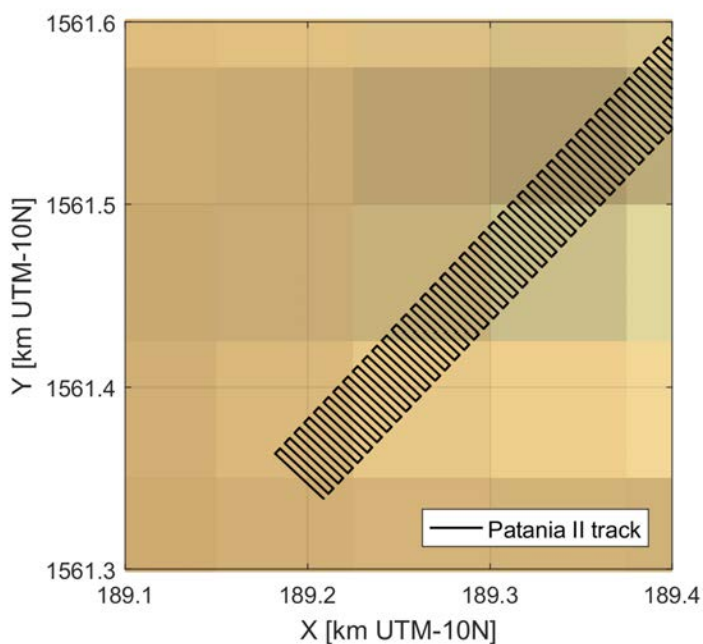


Figure 84: Map detail of Patania II track during scenario 3 and 4

Scenario 4

Scenario 4 is a variant that has the same Patania II trajectory and phasing as scenario 3. However, the sediment emission occurs continuously at a rate of 60 ton per hour during both the active and the inactive phases of Patania II cycle. This last scenario was aligned to the modelling performed by BGR to allow comparison later on.

Table 28: Overview of model scenarios

	Patania II activity cycle	Patania II speed [m/s]	Sediment flux [mT/h]	Patania II trajectory	Total displaced sediment [mT]
Scenario 1	2 minutes ON 10.5 minutes OFF	0.3	225	Back & forth along the length of the program area	3456
Scenario 2	2 minutes ON 5 minutes OFF	0.5	374	Back & forth along the length of the program area	10258
Scenario 3	2 minutes ON 8 minutes OFF	0.3	225	Zig-zag along the width of the program area	4320
Scenario 4	Collector travel: 2 minutes ON 8 minutes OFF Sediment flux: Continuous ON	0.3	60	Zig-zag along the width of the program area	5760

- Modelled sediment transport results

Near-bed current velocities at 5 m above the seafloor at the location of the program area are displayed in Figure 85. Current directions are fairly similar to the model output at MOR001, since the mooring location is relatively close to the Patania II trial location. Currents are variable: northward during early March 2009; southward during early April 2009, and westward during early May 2009.

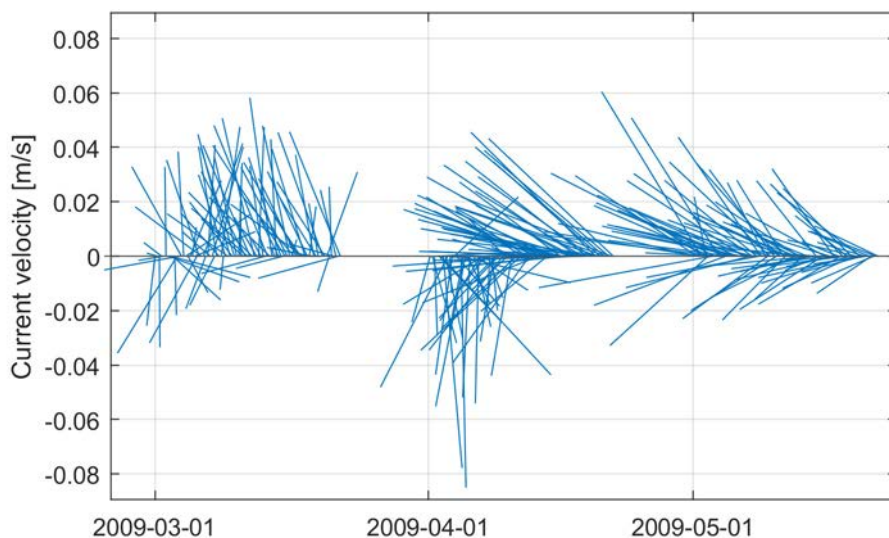


Figure 85: Simulated time series of the near-bed current velocity at the MiningImpact 2 program area

The appendices (see 12.4, Sediment plume results, pp. 236) contain results for scenario's 1 to 4, respectively. Results are based on (1) sediment deposition maps; (2) horizontal contours of suspended sediment concentration at the end of the Patania II trial (4 days after the start of the Patania II trial) and 5 days after the end of the Patania II trial (9 days after the start of the Patania II trial); (3) frequency of occurrence contours for 0.1 mg/l and 1.0 mg/l for the period from the start of the Patania II trial until 5 days after the end of the Patania II trial (9 days after the start of the Patania II trial); (4) instantaneous vertical sediment concentration contours along a transect shown in Figure 86.

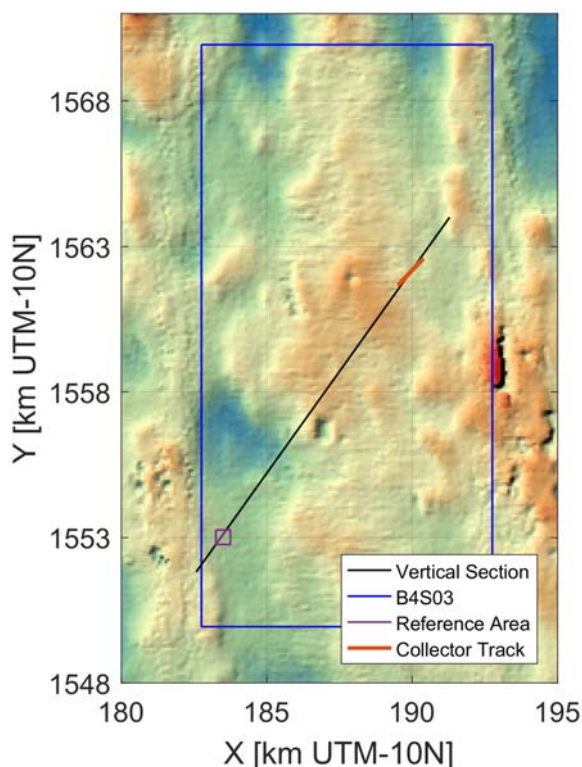


Figure 86: Location of cross section for vertical sediment contour figures

Sediment deposition

Sediment deposition figures for Scenario 1 to 4 are shown in Appendices 12.4.1.1, 12.4.2.1, 12.4.3.1 and 12.4.4.1. In addition, Table 29 shows the area of the 0.1 mm and 1 mm deposition zone. The 1 mm deposition zone has an area of roughly 1-1.3 km² for scenario 1, 2-2.5 km² for scenario 2 (worst-case scenario), 1.5-1.8 km² for scenarios 3 and 1.8-2.1 km² for scenario 4. The 0.1 mm deposition zone has an area of roughly 4.2-5.5 km² for scenario 1, 7.8-9.1 km² for scenario 2 (worst-case scenario), 6.0-8.1 km² for scenarios 3 and 7.2-9.1 km² for scenario 4.

The region of > 1 mm sediment deposition for scenario 1 (Appendix 12.4.1.1) mostly follows the shape of the Patania II track (SW-NE) and extends less than 1 km from the Patania II zone in the cross-track direction. The extent of the 0.1 mm sediment deposition zone is approximately 2-3 km and is shaped in part according to the Patania II track, and in part according to the prevailing current during the time of the Patania II trial: the deposition zone extends slightly toward the north in the March 2009 simulation, toward the south in the April 2009 simulation and toward the west in the May 2009 simulation due to the relatively strong westward current (Appendix 12.4.1.1).

Sediment deposition maps for scenario 2, considered as the worst case scenario, (12.4.2.1) are similar in shape as scenario 1, but slightly larger in extent due to the larger sediment flux during this scenario: the zone with sedimentation larger than 1 mm extends slightly more than 1 km beyond the Patania II track (but is still strongly determined by the shape of the Patania II track). The sedimentation zone of 0.1 mm extends up to 6 km from the MiningImpact 2 program area in the May 2009 simulation.

The zone of sedimentation larger than 1 mm or scenario 3 and 4 is generally confined to the vicinity of the Patania II track (~ 500-750 m around the track; Figure 87 and in appendices 12.4.3.1 and 12.4.4.1). This is likely due to the fact that the Patania II drives in a zig-zag pattern

over the width of the program area, and therefore advances only slowly along the length of the area. The maximum extent of the 0.1 mm sedimentation zone is approximately 4 km for scenario 3 and 5 km for scenario 4. The slightly larger sedimentation zone for scenario 4 is likely due the slightly higher sediment flux of the Patania II (60 ton / hour continuous for scenario 4 vs. 225 ton / hour at 25% activity rate for scenario 3).

The sediment deposition maps in the appendices also display the location of the Reference Area, located approximately 11 km to the southwest of the Patania II trial zone. No sediment deposition is observed in the reference area during any of the scenarios.

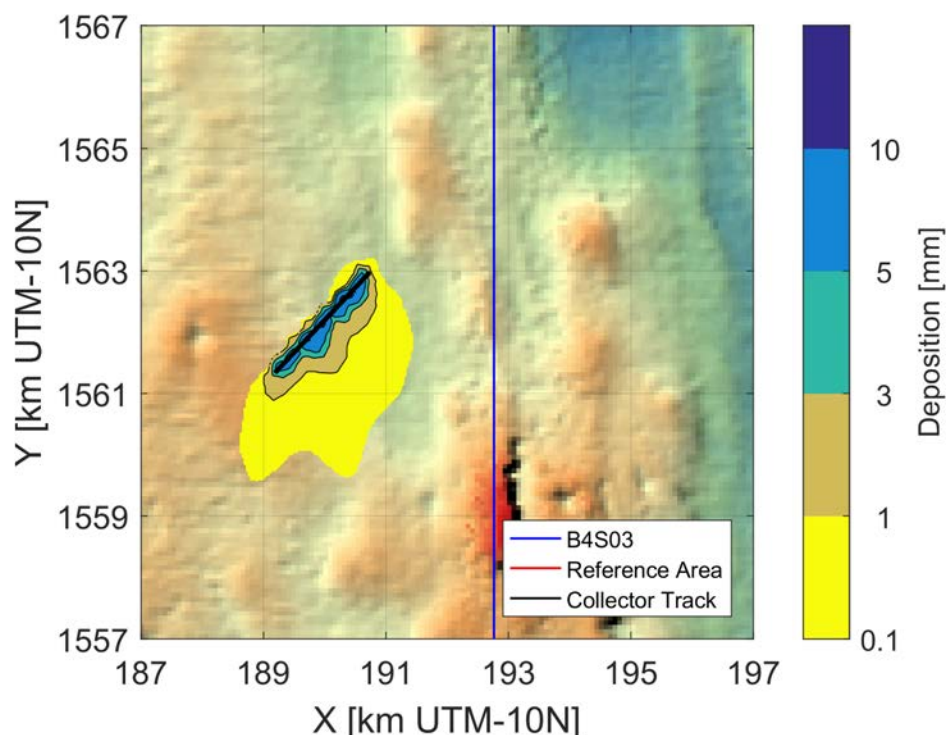


Figure 87: Zoom of sediment deposition [mm] map for Scenario 3 – April 2009 (see appendices for full figure and location reference area) 18 days after the initiation of MiningImpact 2

Table 29: Area of sediment deposition zone

	Simulation period	Area of 1 mm deposition zone [km ²]	Area of 0.1 mm deposition zone [km ²]
Scenario 1	March 2009	0.96	4.29
	April 2009	1.05	4.20
	May 2009	1.26	5.50
Scenario 2	March 2009	2.02	9.10
	April 2009	2.07	8.74
	May 2009	2.53	7.80
Scenario 3	March 2009	1.52	6.00
	April 2009	1.66	6.41
	May 2009	1.77	8.10
Scenario 4	March 2009	1.79	7.24
	April 2009	1.95	7.59
	May 2009	2.14	9.12

Suspended Sediment plume – Horizontal extent

The horizontal extent of the suspended sediment plume is visualized using instantaneous contours and using frequency of occurrence contours. Immediately at the end of the Patania II trial, the 0.1 mg/l contour has an extent of 5 km in the scenario 1 - March 2009 simulation (Figure 88), around 7 km in the April 2009 simulation and up to 10 km in the May 2009 simulation (Appendix 12.4.1.2). The plume has an elongated shape and a larger length in the May 2009 period due to the stronger and more persistent current during this simulation period (Figure 85). In contrast, the plume shape is more concentric for the March 2009 simulation due to the variable current direction during this period. Five days after the end of the Patania II trial, the plume has largely disappeared from the water column due to settling and dilution and only the 0.01 mg/l contour (near or beyond the limit of detectability for present-day measurement devices) is visible (see Appendix 12.4.1.2). Occurrence frequency contours have largely the same shape as the instantaneous concentration contours and are largely determined by the prevailing current direction during the Patania II trial (12.4.1.3).

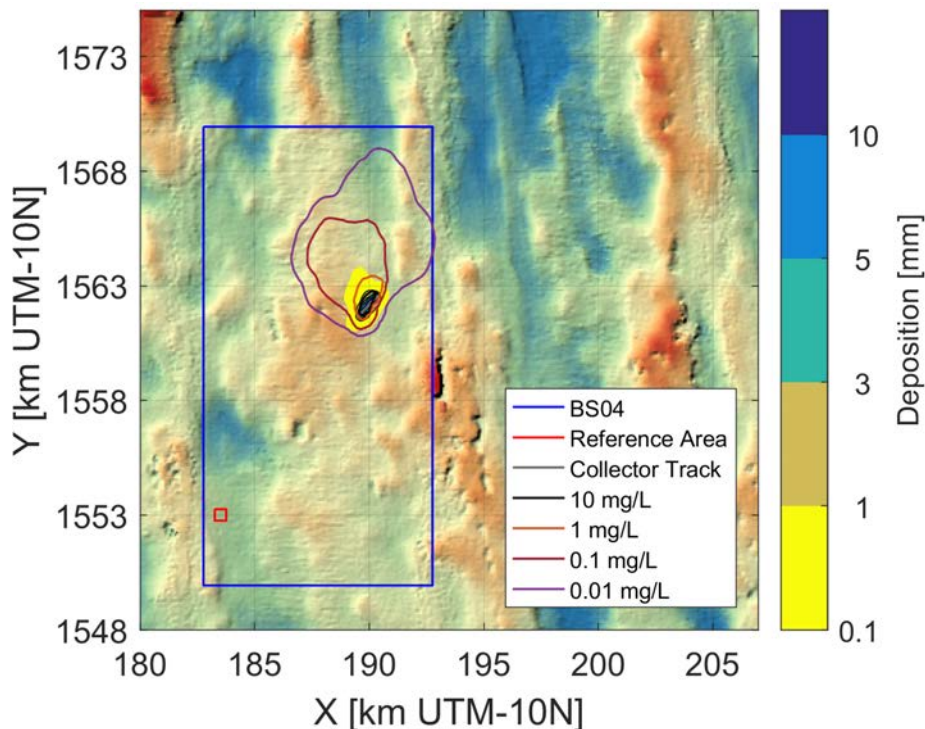


Figure 88: Suspended sediment concentration contours at 1 m above seabed at the end the 4 days of activity of the Patania II for scenario 1 - March 2009

Suspended sediment concentration contours for scenario 2 are similar in shape to scenario 1 since they are predominantly determined by the prevailing currents. The size of the contours is larger in scenario 2 than in scenario 1 due to the larger sediment flux in scenario 2: the 0.1 mg/l contour has a size of approximately 8 km to 11 km (12.4.2.2).

For scenario 3, the sediment concentration contours at the moment when the Patania II trial ends are focused on the north-eastern end of the Patania II track, especially for the highest concentration values (1-10 mg/l), since that is where the Patania II was active near the end of the MiningImpact 2 Program (Appendix 12.4.3.2). The size of the 1 mg/l contour ranges from 5 km for March 2009 to 12 km for May 2009 (12.4.3.2). Contours for scenario 4 (12.4.4.2) are similar in

shape to scenario 3 but slightly larger in size, due to the slightly larger sediment flux of the Patania II (similar to the sediment deposition area).

Suspended Sediment plume – Vertical extent

Finally, vertical suspended sediment contours along a horizontal transect (location shown in Figure 86) are shown in Appendix 12.4.1.4 for scenario 1. The sediment plume is generally largest for the March 2009 and smallest for the May 2009 simulation, given the westward current in the May 2009 simulation carries the sediment away from the transect. Suspended sediment concentrations of 0.1 mg/l reach approximately 20 m above the seafloor in scenario 1, and concentrations of 0.01 mg/l reach up to 120 m above the seafloor. The plume reaches slightly higher elevations in scenario 2 (up to 25 m for 0.1 mg/l, up to 140 m for 0.01 mg/l, Appendix 12.4.1.4).

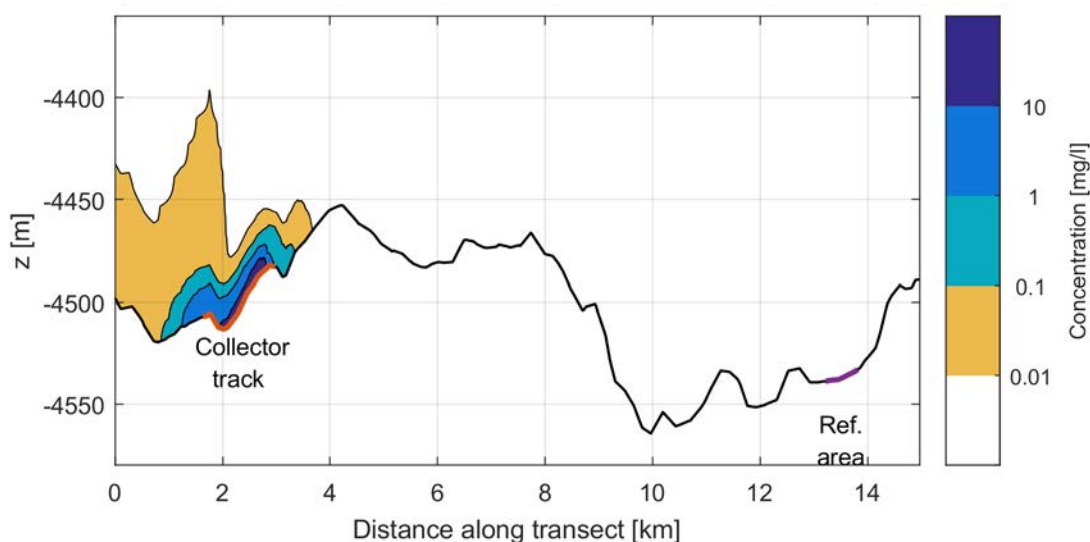


Figure 89: Vertical cross-sectional sediment concentration contours at the end of 4 days of activity of the Patania II for scenario 1 - March 2009. Location of cross-section line is shown in Figure 86

For scenario 3 (Appendix 12.4.3.4) and scenario 4 (Appendix 12.4.4.4), the zigzag progression of the Patania II along the length of the program area is visible in the fact that the zones of highest concentrations (> 10 mg/l) also progress slowly along the length of the program area. The maximal vertical extent of the sediment plume is similar to scenarios 1 and 2.

The time sequence of vertical section figures also sheds light on the settling process of the sediment plume after the end of the MiningImpact 2 Program: nearly all sediment has settled within 48 hours after the end of the Patania II trial (6 days after the start of the trial).

- **Conclusion of the preliminary modelling exercise**

Plume dispersion simulations were performed for the Patania II trials foreseen during the MiningImpact 2 program. The simulations were performed using a Telemac-3D model for hydrodynamics and sediment transport, coupled with the GOTM model for vertical turbulence.

The modelling simulation exercise is based on the Patania II operating during 4 days. In this period the collector travels across the MiningImpact 2 Program area and emits a suspended sediment plume in the bottom 6 m above the seafloor. Four different scenarios were considered with different collector trajectories, activity cycles and sediment fluxes. In order to investigate the

effect of temporal variability in the near-bed currents during the boreal spring season (March-May, the period when the trial MiningImpact 2 Programs are foreseen), each scenario was simulated three times, with the trial taking place in March, April or May respectively.

The area of sediment deposition is mostly determined by the shape of the Patania II track, with the area with more than 1 mm deposition situated approximately 500-750 m from the MiningImpact 2 Program area for realistic scenarios (scenarios 3 and 4) and 1 km for the worst-case scenario (scenario 2). The area with more than 0.1 mm deposition extends roughly 5 km from the program area under realistic scenarios and up to 6 km under the worst-case scenario.

The suspended sediment plume is mostly shaped by the prevailing current direction during the plume trial (variable/northward during the March simulations, southward during the April simulations, strongly westward during the May simulations). For realistic scenarios, the 0.1 mg/l contour reaches a horizontal extent of 5 - 12 km at the end of the Patania II trial (depending on current strength and variability). Vertical sections show that concentrations of 0.1 mg/l are reached at elevations of up to 25 m, and 0.01 mg/l at up to 140 m above the seafloor. Sediment concentration contours of 10 mg/l and 1 mg/l reach a horizontal extent of 1 km and 3 km, respectively.

The selected Reference Area is located roughly 11 km southwest of the MiningImpact 2 Program area. Sediment deposition (≥ 0.1 mm) is not expected to occur at the reference area under any flow direction condition, given that the maximum size of the deposition zone was 6 km for the performed simulations.

5.1.3.3 Impact on biogeochemical setting

5.1.3.3.1 Assessment of impacts due to normal operations

Biogeochemical processes in deep-sea sediments are nowadays recognised as key functions of abyssal ecosystems, playing a significant role in large-scale element fluxes and cycling with consequences for, e.g., the productivity of the seas (via nutrient regeneration) and for the global carbon dioxide budget (via organic matter remineralisation and burial) (e.g. Sweetman et al., 2017). The sediment biogeochemistry of undisturbed ecosystems is shaped by complex interactions of chemical and microbially controlled processes and benthic food webs. This in turn makes organic matter fluxes from the overlying water available to benthic communities, sustaining their biomass and their high biodiversity.

Most Benthic Impact Experiments addressing environmental impacts of deep-sea mining were carried out several decades ago and did not study on the effects on biogeochemical processes. First field investigations on biogeochemical alterations did not start before the late 1990s, i.e. several years after the disturbances were created (e.g., Haeckel et al., 2001a). Modern instrumentation (e.g., ROV-targeted sampling and *in situ* sensors) needed for precise characterisation of the nature and intensity of impacts and fully controlled investigations and sampling to address their biogeochemical consequences were not available at that time. Other recent methodological advances, e.g. molecular tools for the characterisation of microbial communities (e.g., DeLong, 2005), pulse-chase experiments to quantify transfer of energy and matter in benthic food webs (e.g., Witte et al., 2003), and advanced technologies for *in situ* measurements of benthic fluxes (e.g., Boetius and Wenzhöfer, 2009) have added further important tools for studying deep-sea biogeochemistry.

Investigations carried out in the DISCOL Experimental Area in the Peru Basin, successfully addressed disturbance effects on benthic biogeochemistry with a comprehensive suite of state-

of-the-art technologies (Boetius, 2015; Martínez-Arbizu and Haeckel, 2015). For the first time, these investigations could provide direct evidence for impacts on seafloor biogeochemical processes several decades after the disturbances were created (Vonnahme et al., in prep). Investigations have shown that even a few decades after disturbance, the geochemical composition and redox-layering of surface sediments in disturbed areas is still strongly altered, whereas pore waters seem to equilibrate much faster. Pore water profiles do not show major differences in concentrations of the major and trace elements between undisturbed and disturbed sites from 26 years ago. At the same time, many geochemical and biogeochemical parameters showed an unexpectedly high degree of spatial variability, suggesting the need for thorough characterisation of baseline conditions in order to identify mining-related effects and to assess their significance in relation to naturally occurring temporal and spatial variations in the benthic boundary layer (BBL) (Mewes et al., 2014, Mogollón et al., 2016). This also includes the distribution of trace metals between different physical and chemical species and the role of colloids and nanoparticles in transporting trace metals in the water column. In this respect, detailed geochemical baseline investigations of the Patania II trial area and the reference areas around it are planned for the preparatory cruise of the MiningImpact 2 project in April 2019. Investigations have also documented that biogeochemical impacts are specific to the particular nature and intensity of the physical impact, with strongest effects observed in regions where the surface reactive layer of sediment with labile organic matter was lost and deeper sediment layers were exposed at the surface. Such a situation could be comparable to the impact that the Patania II might have in removing the topmost 10-12 cm of sediment - as a conservative estimation - and 3-5 cm - as the least conservative one - depending amongst others on the height of the in situ top water-saturated layer. The remaining deeper, stiffer sediment layer will be covered by a few centimetres of plume fallout sediment. Furthermore, sediment compaction caused by the collector tracks will squeeze out pore waters. In both cases, such stiffer and less porous sediments appear to be more difficult to recolonise by bioturbating organisms that mix in fresh organic matter, and thus are unfavourable for re-establishing stable biogeochemical conditions and processes. There is a strong focus on the analysis of biogeochemical impacts of the trials in the MiningImpact 2 project.

5.1.3.3.2 Potential toxicity due to exceptional events: hydraulic oil discharge, chemical contamination

Accidental events (6.2 Potential accidental events, pp 160) could potentially lead to the release of hydraulic oil into the water column. In the unlikely event that system failure leads to oil leakage, a non-toxic, readily biodegradable oil (according to OECD criteria) is being used, of type Panolin Atlantis 5, 15 or 22 (manufactured by Panolin AG, Madetswil, Switzerland). Material Safety Data Sheets (MSDS) can be obtained from the manufacturer at info@panolin.com (Swiss Oil Technology, 2018. Consulted on March 21, 2018).

Fluorescent particle tracers (EcoTrace Fluorescent Tracer) will be added to the sediment plume generated by the PPV. These environmentally-inert tracers are expected to disperse with the sediment plume and can be detected using particle tracer cameras. The EcoTrace Fluorescent Tracer is manufactured by c/o Environmental Tracing, Helensburgh, Argyll, UK (Environmental Tracing, 2017, consulted on March 21, 2018) and is a solid, non-soluble solution of fluorescent dye in a natural mineral and thermoplastic polymer base. It does not contain any substances presenting a health hazard within the meaning of Article 27 of the Dangerous Substance Directive 67/548/EEC as amended by the Seventh Amendment 92/32/EEC. The MSDS can be

obtained from the manufacturer at jon.marsh@environmentaltracing.com. Tests were conducted on low specific gravity ETS EcoTrace particles with a particle size of ca. 5 microns in conjunction with a UK Government Research Laboratory (Centre for Environment, Fisheries and Aquaculture Science) to assess any impact on Pacific shellfish areas including oyster beds. The oysters were exposed to extremely high concentrations of EcoTrace particles and the rate of uptake and concentration held within the oyster, as well as rate of elimination, was measured over time. Results show that particles were not preferentially selected or rejected by the oysters during any of the tests as a result of tracer particle uptake. The full report is available upon request.

5.1.4 Natural hazards

Little or no impact is expected in the case of natural hazards. Indeed, through forecast, if any unsuitable weather conditions are to be expected, Patania II trials would be suspended. Safety remains one of the main concerns of DEME, and any dangerous situation will be avoided as much as possible.

5.2 On the biological environment

5.2.1 Description of potential impact categories

The major types of impacts that will or potentially might affect biological communities during the GSR collection trial are (1) habitat/nodule removal, (2) sediment disturbance and plume deposition, (3) increased concentrations of plume particles in the water column directly above the seafloor, (4) biogeochemical alterations of the sediment (i.e. change of habitat integrity), (5) potential release of toxic sediments and/or substances into the lower water column, and (6) noise and light pollution. These potential impact categories are described in more detail later on.

5.2.2 Surface

Potential biological impacts at the surface could be due to (1) accidental discharges (hydrocarbon contamination, hydraulic oil) or waste discharges from the surface vessels, (2) noise caused by the vessels themselves or by ship-based, hull-mounted acoustic systems, and (3) light from the vessel itself. As no nodules will be brought up to the surface, there will be no discharge of excess sediments or nodule abrasion at the sea surface.

The vessels that will be in use in this project strictly follow the IMO obligations and standards regarding safety and environmental practice at sea, including the International Convention for the Prevention of Pollution from Ships, 1973, as modified by the Protocol of 1978 relating thereto (MARPOL). In this way, the IMO regulates **anti-pollution measures**, regardless of whether the introduction of polluting substances into the sea is the result of an accident involving a ship or from the operational discharges from vessels. Such regulations aim at minimising all effects of air and water pollution at sea. We do not expect any discharges from normal operations except standard permitted vessel discharges. The vessel's operational deck areas will have directly accessible oil spill detainment kits in order to prevent accidental discharge of fluids into the sea. Emergency response procedures will be on board the vessel to assist in minimising the impact of any accidents that may lead to spills with potential to affect the marine environment. In addition, a shipboard marine pollution Emergency Response Plan will be implemented to combat any accidental spills or non-routine discharges of pollutants.

The **noise** caused by the vessels themselves do not exceed standard levels acceptable for shipping. The exact impacts of acoustic systems on the behaviour of larger animals are largely unknown. Depending on the distance of the animal from the source, impacts range from detection, the masking of communication calls, behavioural response (e.g. disorientation) to injury and hearing loss in close proximity to the source. However, no whales or larger sea mammals have been sighted in the Belgian Contract Area during any of the exploration cruises. Deployment of the AUV (autonomous deep multibeam system) a few tens of meters to a few meters above the seafloor has the advantage that it has no potential impacts on mammals, as these are not found at the abyssal depths of the contract area.

Light pollution refers to the introduction of light to an environment where there are no natural (i.e., sun) light sources or any occurring light is much weaker and/or irregular. Light pollution can have an impact at the surface, due to light emanating from the support vessel that attracts insects, birds, fish, sharks, cephalopods and other invertebrates, and marine mammals (DNV.GL, 2016). This impact will only be temporary for the time period that the vessels are in the trial area. Attention will be paid to ensure that there is no or limited direct light shining into the water column. During night work, deck light will be avoided as much as possible, whilst still maintaining safe operations.

5.2.3 Midwater

Because no instrumentation or technology is deployed in midwater, no biological impacts greater than those described for the surface waters above are expected for the entire water column up to a height of ca. 140 m above the seafloor, which is the maximal height of modelled operational plume dispersion with a plume concentration of 0,01mg/l., whereas the plume with a concentration of 0,1 mg/l will reach a maximum height of 25 m in the worst-case scenario modelled (scenario 2, as explained in 5.1.3.2.2, Sediment transport modelling, pp. 133). The potential impact is described under the section on seafloor impact below.

5.2.4 Seafloor

The magnitude of impacts on benthic deep-sea fauna varies widely with the scale and intensity of disturbances (Jones et al., 2017; Gollner et al., 2017). The species' potential to recover after major disturbances depends on substrate availability (its loss or alteration of its composition); substantial shifts in community structure do occur, with a wide variation in recovery rates among taxa, and in the size and mobility of fauna. Although densities and diversities of some taxa can recover to or even exceed pre-disturbance levels, community composition remains affected after decades (Miljutin et al., 2011; Vanreusel et al., 2016; Jones et al., 2017). The various types of seafloor impact are described here below.

5.2.4.1 Nodule removal and effects on the epifauna

Picking up nodules and removing the associated fine-grained muds fundamentally disturbs the benthic habitat in the mining area, leading to degradation of seabed habitat. In the framework of the JPI-O MiningImpact 1 project, several year-old to decade-old disturbance tracks in ISA contract areas in the CCFZ were re-visited in 2015. These disturbance tracks typically consisted of a single or a few multiple tracks, a couple of meters wide and up to ~2 nm long, created by a benthic disturber, epi-benthic sleds or dredges. Visual and hydroacoustic inspection of the

disturbances by AUV, ROV and OFOBS identified prominent marks on the seafloor that are clearly visible even several decades after the tracks were created (e.g., 20 years for the IOM-BIE, 37 years for the OMCO track), irrespective of their size. For the purpose of the PPV trial that is planned here, the area and duration of impact is quite comparable to that of the benthic impact experiments (BIEs) in the 1990s.

Results of biological and geochemical investigations at the disturbance sites are in line with previous studies that covered shorter time scales of only 5-7 years after the impact (e.g. in the DISCOL area in the Peru Basin: Thiel and Schriever, 1990, Thiel et al., 2001). In general, epifaunal abundances, sessile fauna attached to the nodules (e.g., sponges, hydrozoa, certain foraminifera) and also mobile fauna associated to the nodule hard substrate (e.g., ophiuroids, isopods), are reduced in the CCFZ tracks even decades after the impact was created (Vanreusel et al., 2016). In the area of impact of the PPV trial described here, which will have an approximate size between 0.022 and 0.1 km² and will be left mostly barren of nodules, we assume that a similar process of shifting in epifaunal/megafaunal community structure will occur. This is, however, unlikely to influence gene flow or connectivity of species due to the small size of the disturbed area. Moreover it remains to be seen that the pickup technology of the Patania II, which is based on hydraulic transport without touching the seafloor, is comparable to dragging an epi-benthic sled over the seafloor which is more comparable related to bottom trawling for fish than the envisaged mining technology.

5.2.4.2 Faunal abundance changes related to sediment disturbance and plume deposition (blanketing)

The PPV will potentially suck in large amounts of bottom sediment along with the nodules, and with that, many of the organisms that live in and on the topmost sediments – leading to the crushing of larger animals and mortality that depend on the original densities and size distributions of the organisms inhabiting the trial area (to be determined in baseline studies prior to the trial).

The removal of topmost sediments in the direct trial area and the re-deposition of these sediments after discharge and dispersion to more remote areas might furthermore lead to the smothering of organisms, the clogging of respiratory or filter-feeding organs of particular organisms and/or the release of potentially toxic or oxygen-consuming substances. Processes of nutrient cycling and organic matter remineralisation might also be affected. In the CCFZ, abundance and biomass of all faunal size classes (meio, macro- and megafauna) typically decrease along the productivity gradient from relatively eutrophic (eastern) to oligotrophic (western) environments (Martínez-Arbizu and Haeckel, 2015). This underlines the importance of nutrient supply and benthic-pelagic coupling for the determination of ecosystem structure and the potential negative effect on the benthos when (1) the topmost 10 to 12 cm of bottom sediment are removed, suspended in a particulate plume and consequently redeposited with very low average organic carbon content and in altered grain-size distributions, in turn leading to a change in organic matter remineralisation processes, and (2) naturally occurring phytoplankton and detritus arriving at the seafloor during times of plume dispersion aggregate and alter the nutrient dispersal pattern (Pabortsava et al., 2011; Purser and Thomsen, 2012). These processes can affect all faunal classes from microorganisms to the megafauna. Other modifications to the habitat disturbance will be caused by significant sediment compaction and pore water expulsion due to the weight of the PPV (but only in its tracks), which alter the biogeochemistry of the remaining sediment and are assumed to hinder processes of bioturbation and recolonization.

Based on the model results of the proposed impact experiment, a sediment deposition of more than 1mm is not expected beyond 1 km of the footprint of the trial area. Seafloor coverage by a 3-mm-thick layer of drill cuttings can significantly affect infaunal communities (Schaaning et al., 2008). However, significant quantitative impacts on meiofaunal abundance and community composition have also been observed beyond the extent of observable drill cuttings deposition (Netto et al., 2009). But drill cuttings are different from relocated natural sediments.

Resistance of species to enhanced particle loads and sedimentation generated by mineral extraction processes is likely to be low as natural sedimentation rates are in the order of only 1-6 mm/1000 years, but this will vary based on the ecology of individual species, for example depending on whether taxa are epifaunal or infaunal, mobile or sessile, suspension feeders, filter feeders, deposit feeders, or necrophages (Cordes et al., 2016 and references cited therein). Unfortunately, we know little about the specific effects of ecological drivers in deep-sea ecosystems, especially in these areas with extremely low sedimentation rates.

Since 1970, 11 small-scale disturbance experiments have been conducted in different parts of the world oceans (CCFZ, Peru Basin, Central Indian Ocean Basin) to study the potential effects of nodule mining on the benthos (reviewed by Jones et al., 2017). Although these studies are designed to infer mining-related impacts, it is important to highlight that these experiments differ from the methodology proposed for this experiment, which reflects a more realistic mining scenario. One example is that no compaction is expected beyond the footprint of the tracks of the PPV rather than the complete track of an epi-benthic sledge or dredge. Nevertheless, effects comparable to those from previous disturbance experiments, could be expected.

The results of meta-analyses performed on population density and diversity recovery after these disturbances have been published in Jones et al. (2017) and Gollner et al. (2017). Despite the fact that different methodologies were used and that these are not comparable to the methodology of the Patania II, putting limitations on the quality and comparability of the data (for details see Jones et al., 2017), several general conclusions could be drawn. At seven sites in the Pacific, multiple surveys assessed recovery in fauna over periods of up to 26 years. Impacts are often severe immediately after mining, with major negative changes occurring in density and diversity of most groups. Of all the faunal groups studied, 64% of the faunal classes, in addition to bulk meiofauna and megafauna, showed negative impacts in faunal density relative to the controls <1 year after disturbance. Reductions in density were also observed for polychaetes (INDEX, DISCOL), crustaceans (JET) and total macrofauna (INDEX, DISCOL). The greatest standardised reduction in density following initial disturbance from mining simulations was for polychaete macrofauna at the JET site (CCFZ). However, there are also some exceptions to the general pattern of reductions in density after simulated mining disturbance. At the BIE II site (NOAA BIE), two macrofaunal groups show an increase in density: polychaetes and isopods, which lead to associated increases in the total crustaceans.

When the time series of biological effects of disturbance experiments are considered, there is evidence of minor recovery of density in some groups in some experiments. In some cases, the mobile fauna and very small-sized fauna experienced fewer negative impacts over the longer term, i.e. almost all studies show some recovery in faunal density and diversity for meiofauna and mobile megafauna, often within one year. On the other hand, some faunal groups showed no evidence of recovery (Figure 90).

The only study of sessile fauna specifically was DISCOL, and sessile megafauna did not show any evidence of recovery. Also, very few faunal groups return to baseline or control conditions

after two decades. The data presented in Jones et al. (2017) suggest that some signs of recovery were observed, i.e. there is a general reversion, mainly in density, towards control levels over time, most obviously for meiofauna. However, although species richness and biomass of, for example, harpacticoid copepods recover after 26 years (DISCOL site), differences in community composition remain obvious. This could be validated for the German, French, Belgian and IOM contract areas even after 37 years. Thus, it can be concluded that a total recovery process of meiofauna after anthropogenic impact would take at least several decades.

Species diversity is often more sensitive to change than species density and appears to be more significantly affected (Jones et al., 2017). Recolonisation of benthic communities has long been thought to be slow in the deep sea, although recolonisation of deep-sea soft sediment by macrofauna and meiofauna can take place relatively rapidly (months to years). As the experiments removed nodules, this could lead to slower recolonisation rates, although almost all of the experiments (with the exception of megafaunal evaluations) focussed on the soft-sediment fauna and not on the fauna associated with nodules. Although knowledge of the epifauna in the ecosystem and their function, as well as their total biomass compared to other benthic fauna is limited, nodule epifaunal communities would be unlikely to recover for millennia owing to lack of nodule habitat to recolonise, as the growth rate of new nodules is only a few millimetres per million years.

The first study to address mining-related impacts on microbial communities, conducted in the Peru Basin during the MiningImpact 1 project, indicated that, surprisingly, even the microbial communities do not seem to be capable of adapting to the seafloor disturbances within several decades, which is expressed, for example, in reduced metabolic activity and reduced oxygen consumption in the surface sediments (Vonnahme, 2016). Although the removal of the active surface layer of sediment and/or the nature of the remnant compacted sediment may affect these communities, the effects of small-scale disturbances in plough tracks are not easy to distinguish from natural variability (Janssen et al., 2017). This calls for an extension of the suite of molecular tools and for studies in more realistic mining scenarios, as is planned in the context of the MiningImpact 2 project.

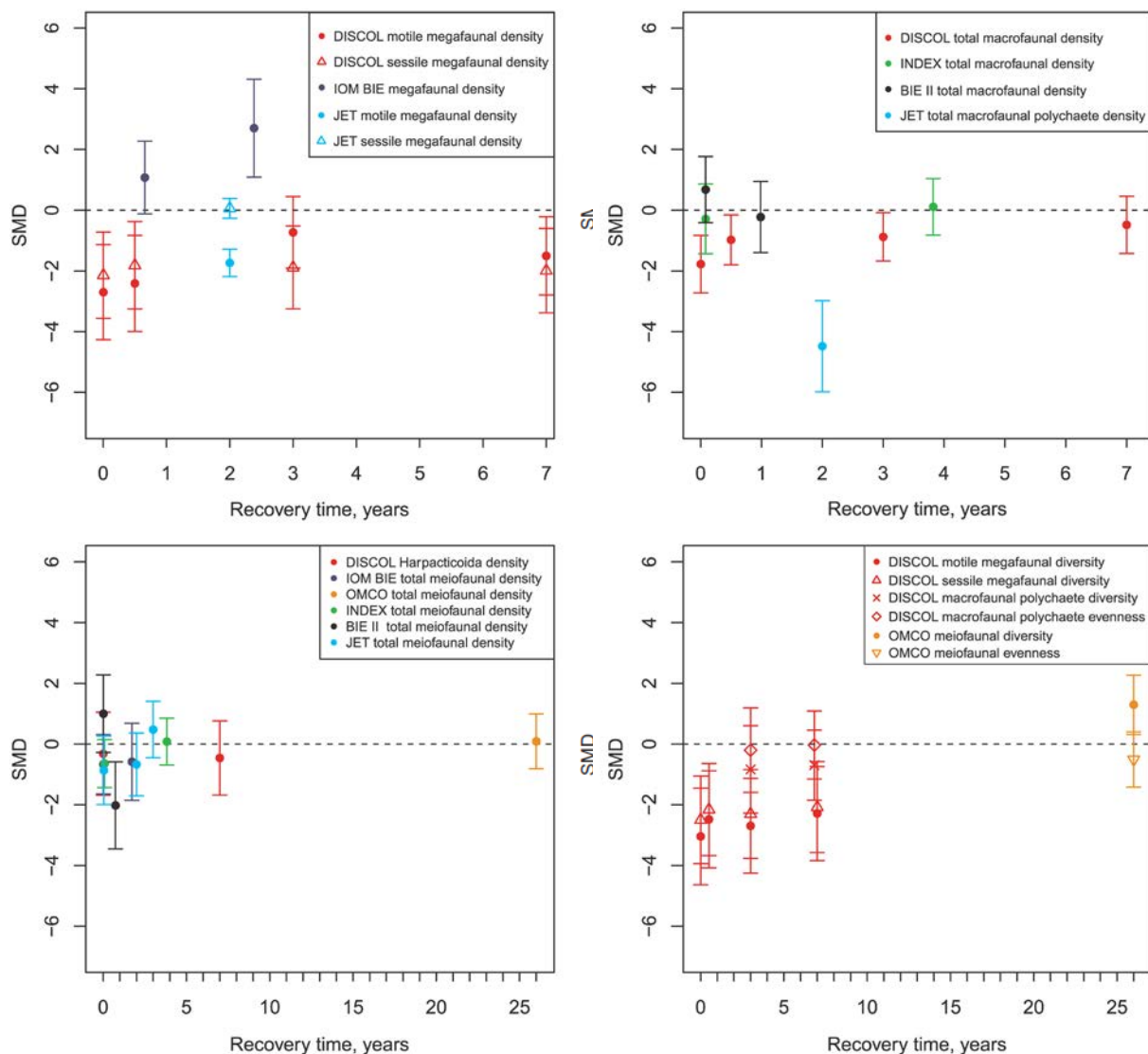


Figure 90: Changes in effects of mining activities over time on faunal density and diversity (from Jones et al., 2017). Changes shown for megafaunal density (top left), macrofaunal density (top right) and meiofaunal density (bottom left) and diversity (including evenness) of megafauna and meiofauna (bottom right). If totals were not available, the value for the most abundant taxon was plotted and indicated in the legend. Values represent standardised mean differences (SMD) between faunal densities or diversities at impact sites and control sites and 95% confidence intervals. Diversity was reported as Shannon-Wiener diversity and evenness was Pielou evenness index in the studies used.

All in all, insufficient information is currently available to generalise the observed biological effects to the scale of GSR's Patania II trial that is being planned in the framework of the MiningImpact 2 project, but not yet on longer terms, larger scales, and greater disturbance intensities expected to result from full-scale mining activities. In the case of the PPV trial proposed here, it appears to be essential to accurately and precisely quantify baseline conditions of the abyssal ecosystem that is going to be affected, particularly with regard to ecosystem processes and functions. The systematic monitoring of the nature and extent of impacts at high resolution over relevant temporal and spatial scales will be an essential element to increase the knowledge of potential mining impacts beyond what has been analysed before.

5.2.4.3 Effects of plumes on epifauna, demersal scavengers and fish

Although the impact of blanketing on the benthic ecosystem by resettling sediment particles has been addressed in some of the BIEs (e.g., Radziejewska et al., 2001a,b; Radziejewska, 2002) and by natural analogue studies (e.g., volcanic ash fallouts: Hess and Kuhnt, 1996; Haeckel et al., 2001b), we lack information on whether and to what extent resuspended high particle concentrations and prolonged life-times of the plumes harm the deep-sea fauna by e.g., smothering of organisms, clogging respiratory and filter-feeding organs, or releasing potentially toxic or oxygen-consuming substances. Our current understanding of the impact of mining plumes on the deep-sea environment is thus not based on direct observation, but inferred from ecological status assessments before and after impact experiments, *ex situ* sediment exposure and ecotoxicological experiments conducted with model species from shallow water depths, and observations made in shallow-water settings.

In the framework of the MIDAS (Managing Impacts of Deep-sea resource exploitation - was a multidisciplinary research programme investigating the environmental impacts of extracting mineral and energy resources from the deep-sea environment) and MiningImpact 1 projects, different responses of deep-water corals and sponges exposed to various types of particulate matter were tested and observed: (1) high survival and minor sub-lethal effects in the scleractinian coral *Lophelia pertusa* (Larsson et al., 2013); (2) reduction in metabolic rates, deteriorating tissue condition, tissue necrosis and death in the octocoral *Dentomuricea meteor*; and (3) high tolerance to sedimentation with reduced metabolic activity in the sponge *Geodia baretii* (Kutti et al., 2015). Similar tests and experiments will be carried out to test the effects of the plume (particulates and enhanced dissolved metal concentrations) on sessile and mobile epifaunal organisms (e.g. Anthozoans, Holothurians).

For the short temporal and low spatial scale of the Patania II activity, we assume that larger mobile epifaunal organisms and demersal scavengers and fish will readily move out of the area of impact under the influence of light, noise, vibration and enhanced particle concentrations in the lowermost water layers, if these are experienced as disturbing. During the trial of the TSTD in 2017 we observed that resuspension of sediment by the tracks attracted fish as a potentially increased food source was made available. A similar effect has been observed during dredging works.

5.2.4.4 Biogeochemical alterations, benthic ecosystem processes and microbial activities

Biogeochemical impacts are specific to the particular nature and intensity of the physical impact, with strongest effects observed in regions where the surface reactive layer of sediment with labile organic matter is lost and deeper sediment layers are exposed at the surface. Such stiffer and less porous sediments may be more difficult to recolonise by bioturbating organisms that mix in fresh organic matter and created favourable conditions for re-establishing stable geochemical conditions and biogeochemical processes. Potential impacts of nodule mining activities on biogeochemical processes from a physico-chemical perspective were described above.

Analyses of benthic processes and fluxes measured *in situ* as a function of disturbance intensity and nodule coverage in the DISCOL area (Peru Basin) confirm that oxygen uptake rates are reduced in all disturbed habitats as compared to rates observed in the reference areas (Vonnahme, 2016). Reductions are particularly prominent in the fresh disturbance tracks created with an EBS tow approx. 5 weeks before.

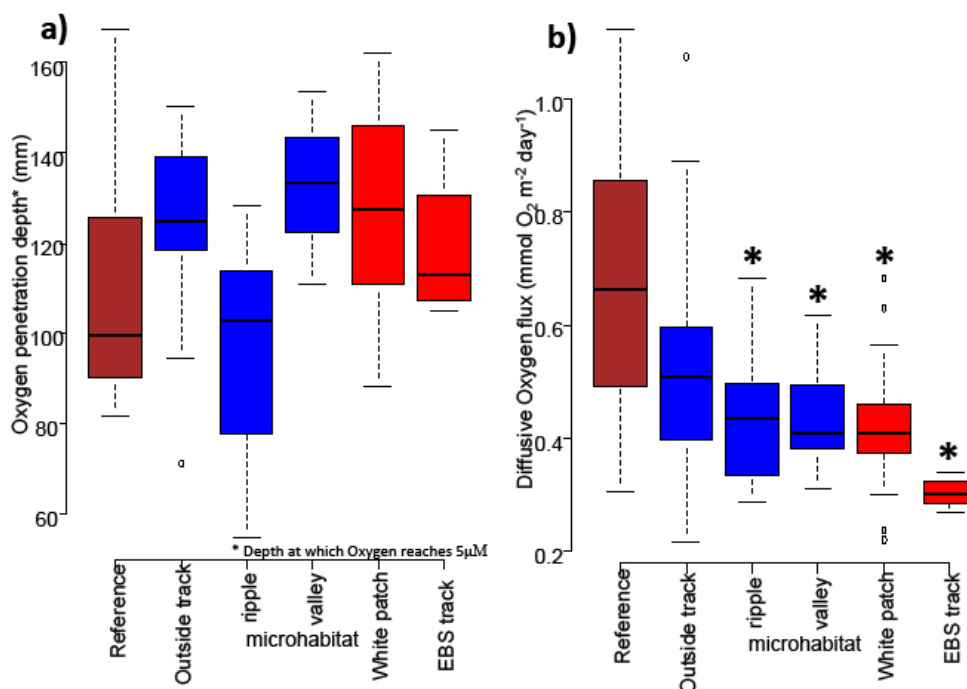


Figure 91: Oxygen penetration depth and diffusive oxygen flux in sediments from the DISCOL experimental area (Peru Basin) 26 years after the disturbance and in a 5-week-old EBS track. a) Depth at which oxygen reaches concentrations below 5 μM for the different microhabitats of the disturbance, b) Diffusive oxygen flux from the bottom water into the surface sediment (Figure from Vonnahme, 2016).

Reduced rates of microbial activity based on radiotracer incubations were also observed at the disturbed sites, particularly where surface sediments were lost or covered upon disturbance, i.e., in the EBS track and within the historical ploughmarks. In addition, DIC and leucine uptake rates were also reduced in ripples where sediments have been piled up by ploughing 26 years ago. The disturbance of the sediments clearly reduced microbial community metabolic rates even after 26 years, with largest effects observed for DIC uptake and for potential activities of glucosidase, esterase, and chitinase.

Activities of organic-matter-degrading enzymes, oxygen consumption rates, organic matter quality, porosity, and radio-isotopes constraining bioturbation activity are very effective monitoring variables for assessing the overall status of benthic biogeochemical functions (Vonnahme et al., in prep). However, in order to conduct comprehensive numerical simulations of effects on biogeochemical functions and food webs, including prognostic modelling of their expected recovery, an even more comprehensive suite of biogeochemical variables is required. This will be a strong aim of the monitoring work that is planned in the framework of the MiningImpact 2 project.

5.2.4.5 Effects of toxic discharges on faunal organisms

In the EU MIDAS project, considerable research capacity was invested in assessing the lethal and sub-lethal sensitivity of different megafaunal (shallow water) species to single metal toxicants, such as copper, and to combinations of different metals and potential by-products of mining as a function of temperature and pressure. Interactions were found to be extremely complex and species-dependent (e.g. MIDAS, 2016).

In the CCFZ, if there is any release of metals from the sediments and potentially crushed nodules, there will be a low-level metal exposure through the dispersal of the sediment plume created by the Patania II at the seafloor. This is, however, minimised as no crushing technique is

used on the Patania II and is not directly envisaged for a later prototype. We currently lack detailed information on how re-suspended, high (nano) particle concentrations harm the deep-sea fauna by e.g. releasing potentially toxic or oxygen-consuming substances.

During the MiningImpact 1 cruise to the DISCOL experimental area in the Peru Basin in 2015, *in situ* effects of metal exposure on bioaccumulation and gene transcription in megafauna and meiofauna community structure were analysed by the University of Southampton (UK), University of Gent (Belgium) and the Institute of Marine Research (IMAR, Portugal).

Enclosure corals (40 cm height, 40*40 cm top and 30*30 cm bottom dimensions) were used to isolate meiofauna and assigned the following treatments: Control without sediment addition, Control with uncontaminated sediment and four treatments with copper-spiked sediment of 4 concentrations (1, 5, 10 and 20 ppm Cu²⁺, C1-4). After ca. 96 h bottom incubation time, three push cores were taken from each corral and analysed. Total meiofaunal densities ranged between 101 ind. 10 cm⁻² in the highest copper treatment (C4) and 334 ind. 10 cm⁻² in the control without added substrate. Although a decreasing trend with copper concentration could be observed, total meiofaunal densities did not significantly differ between the different treatments and the controls (Figure 92A). Interestingly, a large proportion of the meiofauna migrated into the added substrate. Although about 35.1 ± 3.2 % of nematodes migrated into the artificial sediment, this proportion was significantly higher (ANOVA, *p* < 0.001) for copepods and nauplii (61.67 ± 2.65 % and 66.42 ± 2.91 %, respectively)(Figure 92B).

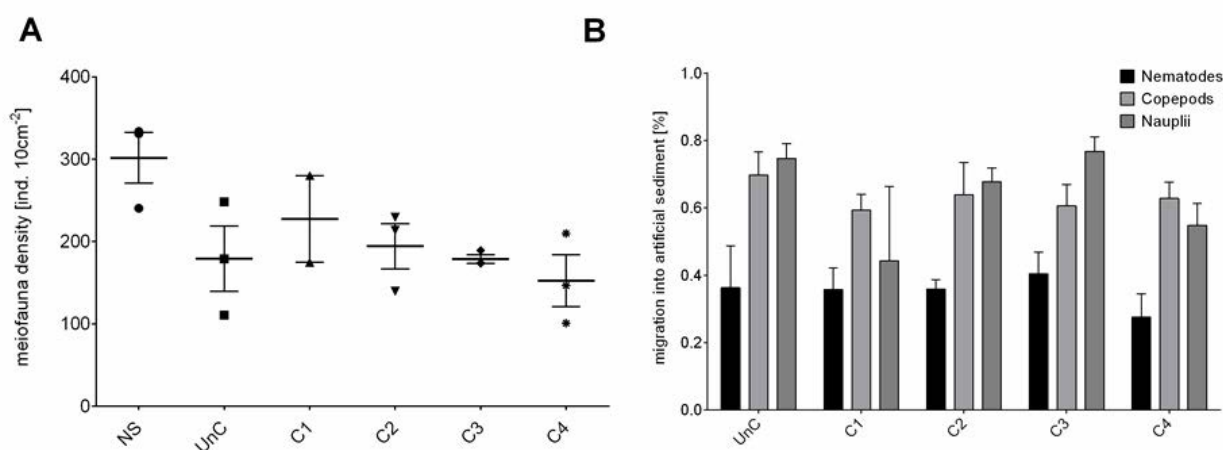


Figure 92: **A)** Meiofaunal densities per core expressed in ind. 10 cm⁻². The line and error bars indicate mean and standard error, all data points are shown. **B)** Proportion of nematodes, copepods and nauplii that migrated into the added substrate. NS = no sediment addition, UnC = addition of uncontaminated sediment, C1-C4 = addition of sediment spiked with 1, 5, 10 and 20 ppm Cu.

Burial with sediment apparently alters vertical meiofaunal community structure, but copper toxicity did not affect total meiofaunal densities. However, further analyses on the tissue copper concentrations of nematodes in different treatments, by means of X-ray imaging, will provide more information on their mortality and the actual impact of copper-contaminated sediment. A similar migratory response, especially by copepods and nauplii, was found during *in situ* experiments in which bottom sediments were covered by 2 cm of (1) crushed nodule material, and (2) bottom sediment, for a few days.

The behavioural and physiological (antioxidant enzyme activity) response of a deep-sea holothurian (*Amperima* sp.) and a shallow-water proxy holothurian (*Holothuria forskali*) to copper-spiked artificial sediments were analysed *in situ* in the Peru Basin and in the laboratory,

respectively. Interestingly, these studies demonstrated that holothurians are sensitive to contaminated sediments and exhibit consistent avoidance responses, which appear to reduce the oxidative stress imposed on this biological group. No antioxidant response was observed in either species, which was interpreted to be the consequence of avoiding copper exposure (Brown et al., 2017). It must however be noted that copper toxicity occurs only with reduced copper, to assess if collection trials will reduce this copper to any significant toxic levels.

To better assess the potential impacts of mining activity with respect to the release of toxic metals, several *in situ* and *ex situ* experiments are planned within the framework of the MiningImpact 2 project (see the monitoring program in the next section). In addition to investigating the possible physical damage inflicted by suspended sediment particles on fauna living on or close to the seafloor (sediment clogging, thus impairing filter-feeding and suspension-feeding megabenthos such as corals and sponges), the MiningImpact 2 project also aims at investigating ecotoxicological effects due to metal-containing particles and dissolved metals.

5.2.4.6 Light and noise pollution

The response of species to light and sound/vibration/electromagnetic radiation produced by mining operations is poorly understood. Shallow-water marine mammals, fish, and invertebrates are physiologically sensitive to acoustic disturbance (Aguilar de Soto and Kight, 2016), with potential for ecological effects such as alteration in natural behaviour, reduction in communication ranges, reduction in foraging ability, prevention of predator avoidance, complete habitat avoidance, and death (Stanley and Jeffs, 2016; Burritt and Lamare, 2016). However, causal effects of these potential stressors on deep-sea fauna are poorly constrained and data on sound/vibration and/or electromagnetic radiation impact at nodule fields are few and uninformative in a deep-sea mining context.

From a technical perspective, light and noise pollution are unavoidable around the PPV. Nevertheless, care is taken to reduce it as much as possible. Cameras, associated with the **lighting**, will be aiming at the vehicle itself, to monitor the vehicle, the tracks, the hoses, potential hydraulic leakage, hydraulic and electric connectors. Light will not be aimed directly at the surrounding environment, with the exception of an HD camera with light to observe the faunal behaviour in front of the PPV, visibility permitting. Eight lamps are also installed on the current design of the vehicle. The lamps are all independently dimmable from 0 up to 100%, with a max of 3200 lumens per lamp.

The main components of the collector responsible for generating **noise** are the HPU hydro-power-unit, pumps and nodule transport itself. The HPU and pumps used in the PPV are designed for noise reduction. Hydraulic pump design features having to do with noise emission, like hydrostatic bearing, commutation, canalling interfaces and housing shape have been optimized with regard to pulsation and noise transmission. A general assumption is that activities at the seabed and in the water column will create general background noise of up to 50 dBA (DNVGL, 2016).

Unfortunately, limited information is available currently regarding the *in situ* noise pollution of the future PPV. To alleviate this lack of information, a hydrophone will be placed on the PPV to record the evolution of the noise. It will then be compared with the dive logbook, to link recorded noise and the activity of the PPV and/or any other artificial noises present.

Most deep-sea organisms have developed “super-eyes” to detect the dim light of bioluminescence. Therefore, the artificial white light of the collector, as also of the ROV/AUV,

could potentially induce temporary or long-term blindness, or obscure or even completely block the function of bioluminescence. From the literature review, it appears to be species-dependent (Ortega (Ed.), 2014 and references therein).

5.2.5 Cumulative impacts

Cumulative impacts of multiple operations are not expected as the trial consists of a single component that will only mimic a single activity. Cumulative impacts from different pressures of one activity can be expected, but at this stage limited information is (publicly) available on causal activity-pressure-effect relations of the targeted ecosystem and its components (i.e. species populations and communities, habitats and ecosystem functions), and the cumulative pressures that mining activities will likely exert on ecosystems and their components (Tamis et al., 2017). In particular in the CCFZ, more data are needed to quantify the impact of mining activities and to identify specific pressures and their cumulative effects on the vulnerability and recovery potential of the ecosystem. Figure 93 illustrates potential relations between activities and pressures on different ecosystem components.

Although a few studies have documented the individual effects of different mining pressures on species and ecosystems (Auguste et al., 2016; Mevenkamp et al., 2017), research on cumulative and interactive impacts of multiple stressors from nodule mining in the abyss is still completely lacking. One major aim of the monitoring study proposed here is to use the results of the different individual impact studies around the Patania II trial to collectively and statistically analyse possible scales and ranges of cumulative impacts.

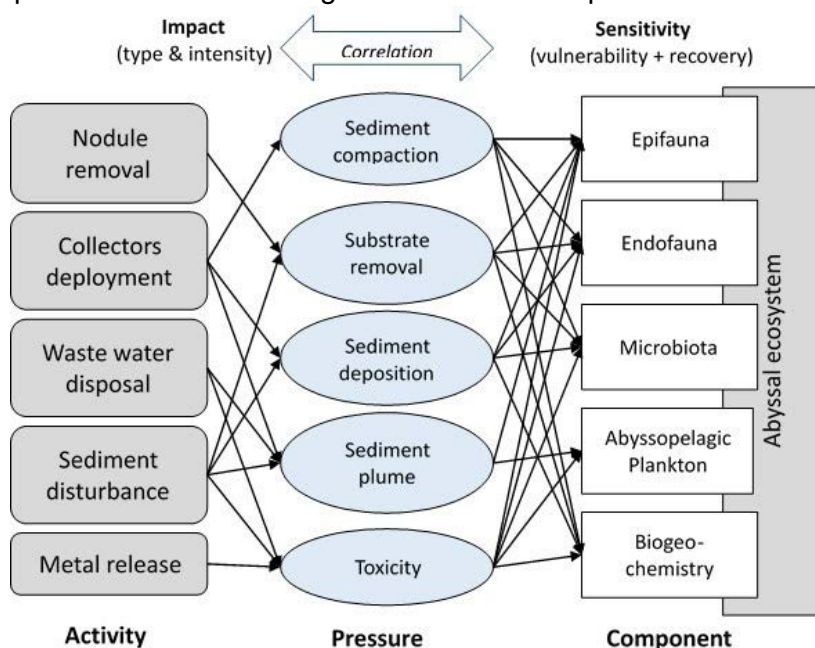


Figure 93: Generic outline for cumulative effect assessment of potential future mining-related activities that may generate pressures on different ecosystem components. The conceptual scheme visualizes potential relationships between impact intensity and sensitivity that need to be assessed (modified after Tamis et al., 2017).

6 Accidental events and natural hazards

6.1 Extreme weather and natural hazards

6.1.1.1 Tropical cyclones

Tropical cyclones (storms and hurricanes) are difficult to integrate into a climate/hydrodynamic model, due to their erratic nature (extreme intensity, small time scale, local effect). Most hurricanes are predictable in that they follow a similar cycle of development, called the hurricane life cycle. These life cycles may run their course in as little as a day or last as long as a month. Past and present data about tropical storms and hurricanes can be found at the National Hurricane Center, developed by NOAA (NOAA, Coastal Zone Management. 2017. Consulted on March 21, 2018).

Since 1998, NOAA keeps track of all storms and hurricanes, per ocean (Atlantic and Pacific) and per region (Central and Northeast Pacific). From January 2002 to December 2012 (10 years), 164 tropical cyclones (storms + hurricanes) have been identified in the Eastern Pacific Basin, i.e., an average of 16 storms or hurricanes per year. From 1966 to 1996 (30 years), the same yearly number of tropical cyclones has been calculated. 56 % were classified as hurricanes, 25 % were classified as tropical storm category 3 or more (Figure 94). Tropical cyclones are usually concentrated between July and December. In recent years cyclones were found to appear in August and September.

The 2019 offshore expedition in the CCFZ is planned between late February and early May 2019. Focusing on this timeframe for the hurricanes, during the period from 1951 to 2015 a total of 42 storms were recorded over the North Eastern Pacific Ocean (Figure 95), all of them occurring in May (see Table 30). Of all those storms, only four crossed the Southern boundaries of the GSR Contract Area. Subsequently, the chance of having this type of natural hazard is minor, moreover that most offshore work will take place in March – April 2019. Nevertheless, as already explained (see 4.1.6 Natural hazards, pp 111) the weather forecasts, by BMTARGOSS Operational Client Weather and Ocean Information support Centre (information on BMT ARGOS BV, 2018, consulted on March 21, 2018), will be carefully analysed every 12 h.

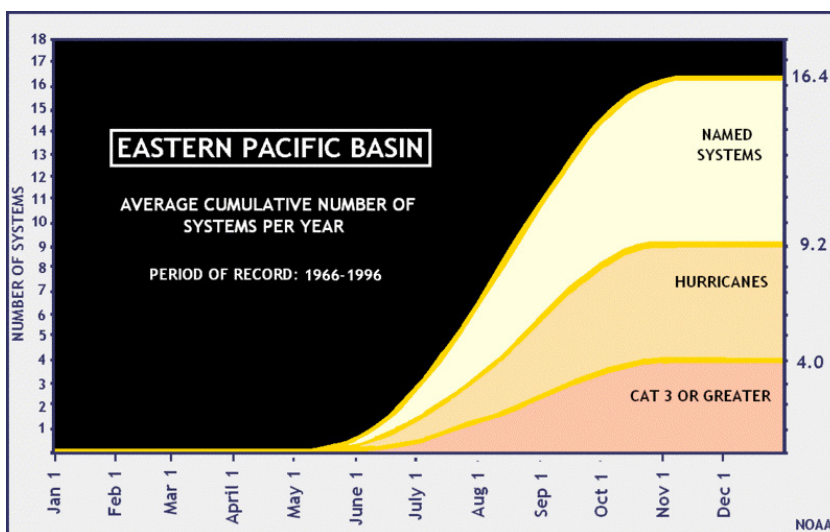


Figure 94: Simplified Graph showing the average cyclone repartition between 1966 and 1996 and their intensity.

The spatial distribution and individual tracks of the tropical cyclones (hurricanes) in the NE Pacific Ocean from 1951 to 2015 are shown in Figure 95. There is a prevailing East-West trajectory, with a higher concentration of cyclones along the Central American coasts.

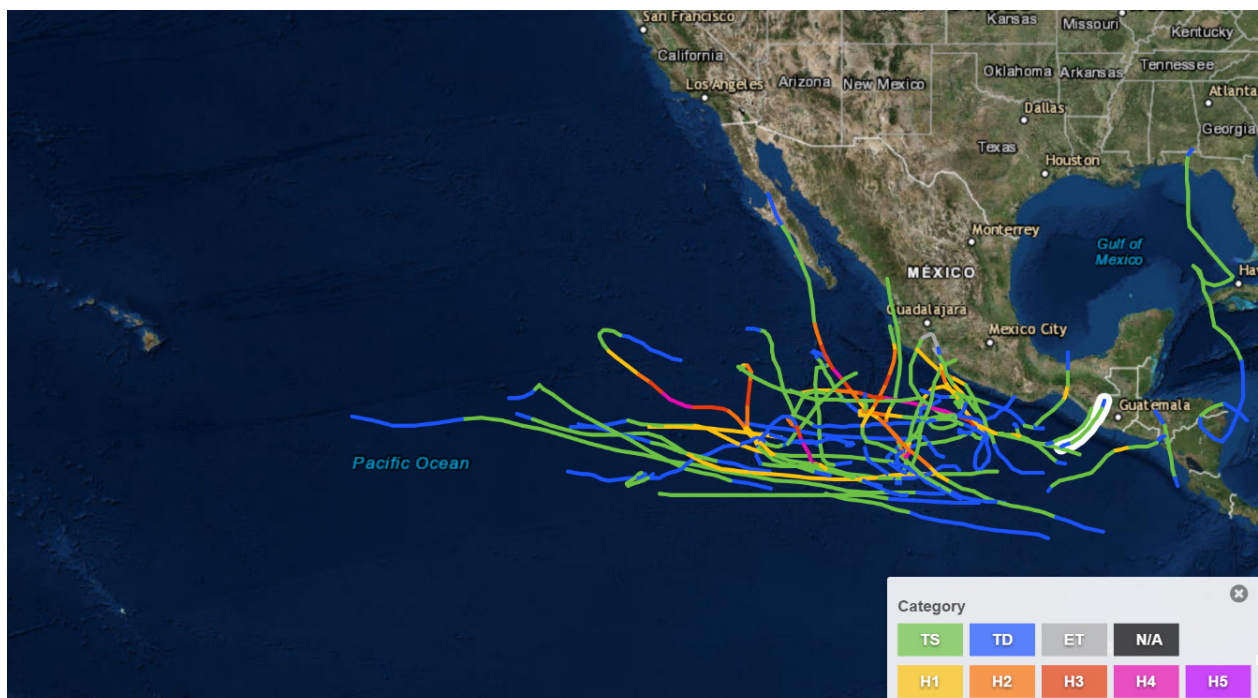


Figure 95: Storms recorded by the NOAA Hurricane center between 1951 and 2015 for the months February, March, April and May. The red square represents GSR Contract Area. Hurricane wind categories are as follows: H5 (> 135 knots), H4 (114–135 knots), H3 (96–113 knots), H2 (83–95 knots), H1 (64–82 knots), TS (tropical or subtropical storm; 34–63 knots), TD (tropical depression; < 34 knots), and ET (extra-tropical storm, varies). Source : NOAA, Coastal Zone Management. 2017, Consulted on March 21, 2018).

Table 30: Storms recorded by the NOAA Hurricane center in the North Eastern Pacific Ocean in February, March, April and May between 1951 and 2015. Chronological order is applied.

Storm Name	Period	Storm Name	Period
UNNAMED 1951	May 17, 1951 to May 21, 1951	UNNAMED 1995	May 21, 1995 to May 23, 1995
UNNAMED 1952	May 29, 1952 to May 31, 1952	UNNAMED 1996	May 13, 1996 to May 16, 1996
ALICE 1953	May 25, 1953 to Jun 07, 1953	UNNAMED 1996	May 15, 1996 to May 19, 1996
UNNAMED 1956	May 18, 1956 to May 19, 1956	ALETTA 2000	May 22, 2000 to May 28, 2000
UNNAMED 1956	May 30, 1956 to Jun 03, 1956	ADOLPH 2001	May 25, 2001 to Jun 01, 2001
ADELE 1970	May 30, 1970 to Jun 07, 1970	ALMA 2002	May 24, 2002 to Jun 01, 2002
AGATHA 1971	May 21, 1971 to May 25, 1971	ANDRES 2003	May 19, 2003 to May 26, 2003
ALETTA 1974	May 28, 1974 to May 30, 1974	AGATHA 2004	May 22, 2004 to May 26, 2004
AVA 1977	May 26, 1977 to May 30, 1977	ADRIAN 2005	May 17, 2005 to May 21, 2005
ALETTA 1978	May 30, 1978 to Jun 01, 1978	ALETTA 2006	May 27, 2006 to May 31, 2006
ANDRES 1979	May 31, 1979 to Jun 04, 1979	ALVIN 2007	May 27, 2007 to Jun 06, 2007
ADRIAN 1981	May 30, 1981 to Jun 04, 1981	BARBARA 2007	May 29, 2007 to Jun 02, 2007
ALETTA 1982	May 20, 1982 to May 29, 1982	AGATHA 2010	May 28, 2010 to May 30, 2010
ADOLPH 1983	May 21, 1983 to May 28, 1983	ALETTA 2012	May 13, 2012 to May 20, 2012
ALMA 1984	May 17, 1984 to May 21, 1984	BUD 2012	May 20, 2012 to May 26, 2012
BORIS 1984	May 28, 1984 to Jun 18, 1984	ALVIN 2013	May 13, 2013 to May 17, 2013
AGATHA 1986	May 22, 1986 to May 29, 1986	AMANDA 2014	May 22, 2014 to May 29, 2014
ADOLPH 1989	May 31, 1989 to Jun 05, 1989	ANDRES 2015	May 28, 2015 to Jun 07, 2015
ALMA 1990	May 12, 1990 to May 18, 1990	BLANCA 2015	May 31, 2015 to Jun 09, 2015
ANDRES 1991	May 16, 1991 to May 20, 1991		

6.2 Potential accidental events

The company GSR, as subsidiary of the group DEME, has a long experience of working in the marine environment. Safety and environment are two of the core values, through its Quality, Health and Safety, Environmental, Sustainability and Security (QHSE-S) charters. Therefore, GSR works according to a management system complying with various standards:

- OHSAS 18001 "Occupational Health & Safety Management System - Requirements";
- SCC** "Safety, Health & Environment Checklist Contractors" (VCA** two stars);
- ISO 9001 "Quality Management Systems - Requirements";
- ISO 14001 "Environmental Management Systems - Requirements";
- ISO 14064 "Greenhouse gasses - Part 1: Specification with guidance at the organization level for quantification and reporting of greenhouse gas emissions and removals";
- ISM "International Safety Management Code";
- ISPS "International Ship & Port Facility Security Code"

Furthermore, everything is done to avoid any adverse and irremediable consequences, and the best available practices are promoted. Nevertheless, working in sometimes remote and hostile environments often presents specific challenges and risks. It is important to anticipate all the potential accidental events, knowing that the study area is located at five steaming days from port in case of emergency.

6.2.1 Vessel failures

6.2.1.1 Toxic discharges

GSR does not expect any discharges from normal operations except standard vessel discharges such as macerated food waste and discharge from the on-board sewage treatment plant. During unforeseen circumstances, waste, ballast water, or other fluids may be discharged unplanned from the vessel into the surrounding marine environment. The vessel's operational deck areas will also have directly accessible oil spill detainment kits in order to prevent accidental discharge of fluids into the seawater. Emergency response procedures will be on board the vessel to assist in minimizing the impact of any accidents that may lead to spills with potential to affect the marine environment.

In addition, a shipboard marine pollution Emergency Response Plan will be implemented to combat any accidental spills or non-routine discharges of pollutants.

6.2.2 Patania II – System failures

During the operational deployment of Patania I it took some effort to reach the seabed. Component equipment failures were encountered; however, these never led to an accidental event, such as equipment loss or unwanted releases into the marine environment. The previous campaign enabled the technical team to gain experience to mitigate equipment failure and resolve unexpected breakdowns. Furthermore, a buffer period of 21 days is incorporated in the planning if equipment failure occurs and a return to San Diego is unavoidable.

The Patania II system is electrically powered. The electrical power provided by the ship's generators and delivered to the Patania II is transferred to hydraulic power by a subsea HPU. HPUs take care of driving the hydraulic pump motors, hydraulic track drives and activating the cylinders. Accidental discharge of biodegradable oil (~0.9 m³) could happen only in the case of mechanical or hydraulic failure on the vehicle.

6.2.2.1 Hydraulic failures: mitigation of discharges

The hydraulic system and gearboxes are filled with hydraulic oil. The complete system will be pressure-tested and checked on any leaks before entering the water.

Pre-dive checklists as part of the operational management program are executed prior to launching (an example can be found in the appendix 12.2, pp. 234).

The large oil volumes on the vehicle are constantly monitored in the control cabin during descent/ascent/operation on the seafloor. If a leak occurs, the system will detect this and the vehicle can be recovered on board for repair. Furthermore, on the vehicle, hydraulic hoses are used which can withstand a nominal system pressure of 320 bar. The vehicle is limited to 250 bar system pressure, so some safety margins are included. The burst pressure of the hydraulic hoses is far beyond the 320 bar. Finally, in case oil leaks occur, a biodegradable oil will be used, type Panolin Atlantis 5, 15 or 22. The corresponding Safety Data Sheet can be found in the appendix 12.3, pp. 235.

6.2.3 Patania II – Emergency Recovery

6.2.3.1 Patania II Hydraulic / Electrical Failure : Dead Sub Recovery

In the event of a total failure of the Patania II while in operation on the seabed, the procedure for recovery is as follows:

- 1) Position vessel over Patania II using the navigation equipment on the Patania II and the vessel to give a vertical lift from seabed,
- 2) Simultaneously with the above, pull in on the umbilical winch to maintain correct catenary and protect the umbilical cable,
- 3) When the vessel is over the Patania II, confirmed by the navigation equipment, lift Patania II to 10m clear off the seabed and hold until system seems stabilized,
- 4) Commence recovery of the Patania II,
- 5) Lift the Patania II, using the umbilical winch to a depth of 20 meters under the docking head using the vessel to achieve this position,
- 6) Recover as per standard launch and recovery procedures.

6.2.3.2 A-Frame Failure

The wide-angle A-Frame comprises a fabricated steel portal frame pivoted at the bottom of the two legs. The gantry is moved back and forth by the action of two hydraulic cylinders which are mounted on two base sections, positioned one on each side of the gantry.

A lift beam or cursor system that is docked onto the top part of the vehicle is used for deployment and recovery throughout the splash zone to a clear distance (approx. 20 m) from the keel of the vessel. The cursor system provides added mass, unloads the umbilical during in air lifting and correctly orients the vehicle during recovery. Two separate lifting winches mounted on the A-

Frame top beam will lower and hoist the cursor system – vehicle assembly through the splash zone.

A docking cone on the cursor system provides a lead in for the vehicle bullet and a smooth-running surface for the umbilical. The 360° latches on the cursor are completely failsafe, meaning that even in the event of a failure in the lift beam controls or hydraulics, the vehicle can always be latched. Indicators are provided to confirm when the vehicle is latched.

In the event of a failure of the A-Frame whilst in the inboard position, the first action would be to replace the failed part. If this is impossible, then the hoses are removed and the A-Frame is manually jacked out. A vessel's winch and / or crane is used as a hold back to control the speed of deployment of the A-frame.

If the A-Frame fails in the outboard position, recovery will use the vessel's winch and / or crane. A sequence of the following actions are undertaken:

- 1) Release all hoses,
- 2) Open valves to release ram pressures,
- 3) Attach the vessel's winch and / or crane to the A-Frame and slowly pull A-Frame to inboard position.

6.2.3.3 Cursor System Failure

If the cursor system fails, then the first course of action is to repair the broken parts. If this is impossible, then the option to recover the vehicle using the umbilical could be implemented, but this in turn may compromise the umbilical and could possibly lead to internal conductor failure. As the Patania II will not be securely locked in to the cursor, then this option would require good umbilical management during the operation of in-boarding the A Frame.

Depending on availability, a possible option to temporarily rig a recovery wire and with the use of the ship's crane, in tandem with a work class ROV, connect the wire to Patania II could be implemented. This option depends on the vessel, vessel crane and available deck space in which to safely land the Patania II and requires risk assessment prior to any recovery taking place.

6.2.3.4 Lift Wire Winch Failure

If the Lift wire winch fails then the first course of action is to repair the broken parts. Failure of a drive motor can be overcome by disconnecting the hydraulic lines to the faulty motor, so it is free to rotate, and operate the lift winches with the one remaining motor. The hydraulic lines would require capping.

Up to moderate depths only, if it is impossible to repair the winch(es) before recovering the Patania II, it will be necessary to use temporary rigging to choke and pull on-board the lift wires in stages, until the cursor can be recovered and secured to the docking head. Recovery of Patania II could then be carried out as for 6.2.3.3 Cursor System Failure.

6.2.3.5 Umbilical Winch Failure

The primary purpose of the umbilical winch is to store the umbilical and enable launching and recovery of Patania II to depth along with communication and control of the vehicle via the slipring.

If the umbilical winch fails then the first course of action is to repair the broken parts.

The winch assembly consists of a single drum supported by a drive end (DE) and non-drive end NDE0 pedestal. The winch is driven several (assumed 3 to 4) hydraulic motor/gearbox units with an option for redundancy included for one motor; i.e., if failure of one drive unit occurs then the winch is still capable of functioning on the remaining two operational drives. Failure of a drive motor can be overcome by disconnecting the hydraulic lines to the faulty motor, so it is free to rotate and operate the winch with the other (assumed 2 to 3) motors. The hydraulic lines would require capping.

Up to moderate depth only, in the unlikely event that it is impossible to repair the winch before recovering the Patania II it will be necessary to use temporary rigging to choke and pull on-board the umbilical in stages, until such time as the Patania II is 20 meters below surface / under the A frame to allow the cursor to be deployed and recovery of Patania II to be completed.

6.2.3.6 Umbilical Cable Internal Failure

In the event of umbilical cable internal failure the Patania II will be recovered in the same manner as used in 6.2.3.1 Patania II Hydraulic / Electrical Failure : Dead Sub Recovery.

6.2.3.7 Severing of the Umbilical

The umbilical monitoring remains complex, because no to limited visuals are available along the water column once the Patania II is driving on the seafloor. A safety margin of three regarding the minimum breaking strength of the umbilical was taken into account: submerged vehicle weight, including the lift umbilical at 5000 m of water depth, is estimated at 250 kN; the umbilical is designed to attain a minimum breaking load of 700 kN.

If the umbilical breaks or is cut when the Patania II is on the seabed, then unlike most ROVs, there is no possibility that Patania II will, due to its inherent buoyancy, float to the surface where it can be tracked using the fitted radio beacon. The Patania II should remain stationary on the sea bed at the location where the umbilical parted.

In the unlikely case of a Patania II loss on the seafloor, the PPV is equipped with a battery-driven beacon. Subsequently, the vessel's USBL system should be able to locate the vehicle.

Once tracking and visual sighting with a 3rd-party ROV has been confirmed, then an on-board decision between the Patania II superintendent, GSR management and the vessel's representative can be made to proceed with the safe recovery of Patania II. On top of the vehicle a mechanical lifting point is installed, by means of a work-class ROV, and a lifting wire or a plasma line can be hooked up to recover the Patania II. It can be recovered up to the splash zone, from where it will be connected to the cursor frame to pull it inboard.

This option depends on the vessel being used, the vessel crane, and available deck space in which to safely land the Patania II and the operation being risk-assessed prior to any attempted recovery taking place.

6.2.3.8 Surface Equipment Hydraulic Power Unit (HPU) Failure

The HPU is used when launching and recovering the Patania II; it has no direct contact with the Patania II and therefore failure should cause no immediate danger to the Patania II. If failure does occur, then the vessel and Patania II will hold station until repairs are implemented / completed.

If repairs prove to be impossible, then the A-frame and Umbilical winch can be operated and the Patania II recovered in same manner as for 6.2.3.2 A-Frame Failure and 6.2.3.5 Umbilical Winch Failure.

7 Environmental management, monitoring and reporting

7.1 Organisational structure and responsibilities

7.1.1 Organisation on board on board of GSR vessel

The Party Chief (TDI Brooks, 2010) is head of the professional science/technical staff. Since the science/technical staff may not be certificated mariners they will have a unique relationship with the vessel crew. The scientific/technical staff includes the Party Chief, navigators, scientists, laboratory staff, equipment staff, and deck staff. Deck personnel may be composed of both ship's crew and technical party staff, depending upon the nature of the work and expertise required.

The Party Chief is a Company senior management representative on the vessels. As such each needs to conduct himself or herself in a highly professional manner in interactions with the vessel crew, science/technical staff, contractors, and client representatives. The Party Chief is responsible for the daily operations of the technical staff and interactions with the Master to meet the project objectives. Additional responsibilities are listed:

- The Party Chief shall be responsible to the Master for the safe conduct of scientific work aboard the vessel and for the conduct of scientific/technical party while on board.
- The Master has the overall responsibility and authority for the safety of the ship and all personnel aboard as well as pollution prevention.
- The Master is responsible for implementing the scientific program in accordance with the Party Chief's requirements while operating the vessel in accordance with all applicable codes and regulations.
- The Party Chief will undergo safety training and familiarization of the vessel.
- The Party Chief may serve as the company representative in matters of contracts and negotiations with clients, port authorities, and other entities that have vessel business.
- The Party Chief executes the project execution plan.
- The Party Chief generates the daily progress report (DPR) for the duration of the project-related field campaign

The Party Chief is responsible to promote environmental awareness by providing sufficient and adequate resources for proper implementation and to ensure that all project activities comply and are in line with the conditions as described in the EMMP.

The organization chart allocates the position of the QHSE officer as a specialised staff function that reports immediately to the Party Chief. The QHSE officer has also direct communication lines with the Team leaders to ensure a continuous follow up of the eventual environmental impacts of the works executed at a certain moment at a certain place.

To this end they carry out the following tasks:

- Overview the safety aspects of GSR operations on board.
- Determine cause(s) of any environmental or safety accident(s)/incident(s) and recommend means of preventing recurrence

- Determine cause of any non-conformances/incidents and recommend means of preventing recurrence
- Consult with the client on environmental issues
- Keep all relevant safety, environmental records up to date

All project supervisory personnel (Team, Operations and Science leaders) are responsible for the operational and environmental aspects of the work performed under their supervision. They shall provide guidance and direction in their day-to-day supervisory roles and lead by example. To this end, they carry out the following tasks:

- Ensure that all persons under their control have received adequate information, training and briefing in their task or function and are aware of all applicable environmental aspects and their subsequent conditions and necessary precautions and restrictions that have to be observed.
- Organise, attend and regularly hold toolbox meetings
- Investigate environmental accidents and incidents on the workplace and propose measures to prevent similar accidents and incidents
- Timely seek the advice of the corporate HSE Officer
- Check if the distribution of the tasks and responsibilities occur in a way that the tasks are carried out by employees who have the required competences and skills and have received the required instructions and training

All other personnel, employees have the following responsibilities and obligations:

- To comply with the instructions and recommendations given for safety and environmental issues on the vessel
- Not to wilfully and in a harmful way impact the surrounding work environment
- To immediately inform their supervisor of all work situations which they presume entails an immediate danger and/or could have a negative and harmful impact on the environment
- Attend and positively participate in all safety and environmental trainings (i.e. inductions, toolbox meetings, external training, drills, ...)

The Environmental Team will further develop the baseline information in the GSR contract area outside the MiningImpact 2 area, a compliance scope in accordance with the ISA exploration contract. The Environmental Manager will ensure environmental legislative compliance and have a coordinated role to assist aligning the GSR disturbance experiment and MiningImpact 2 monitoring activities during the trials.

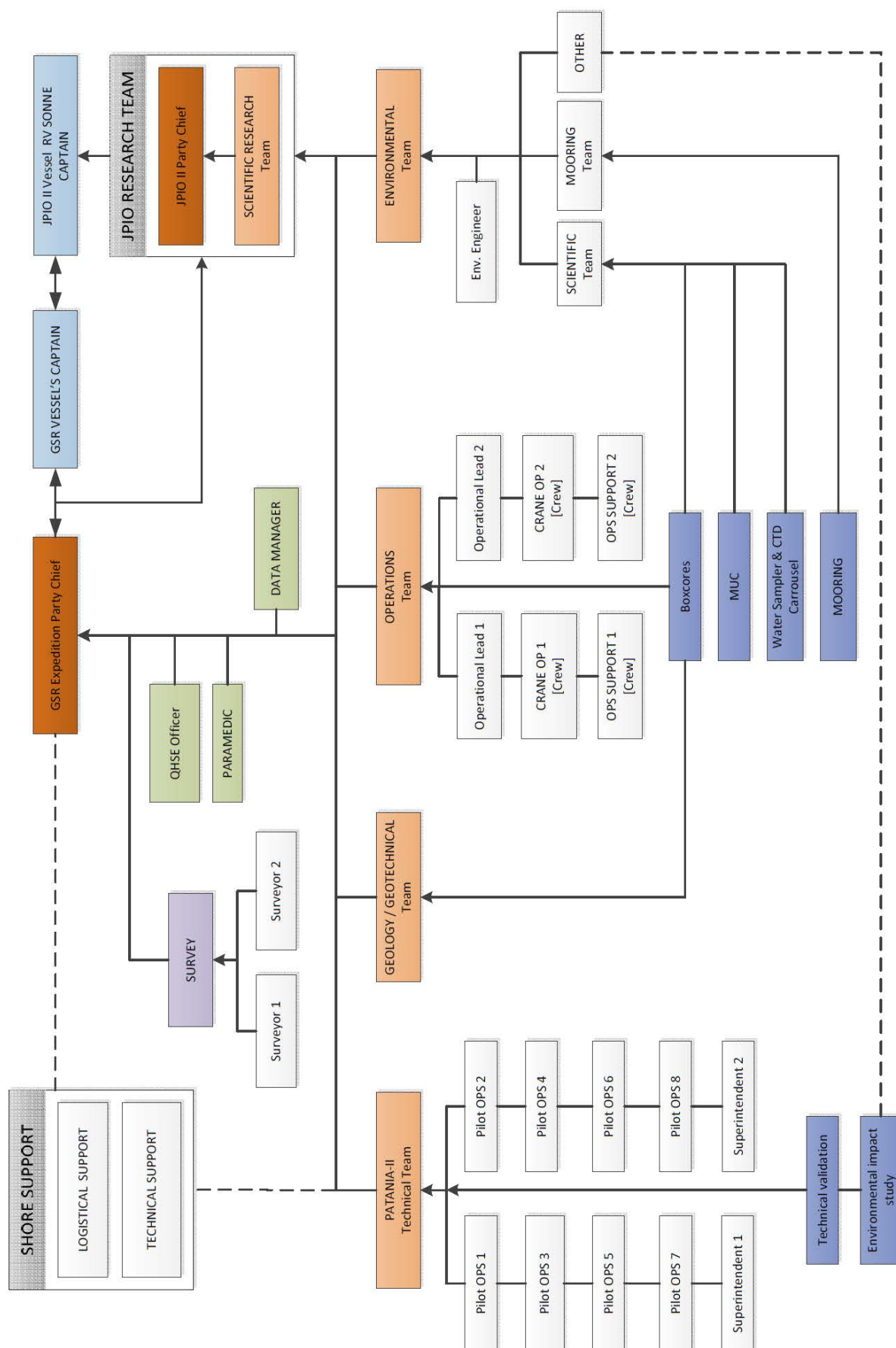


Figure 96: Organigram of the GSRNOD19 campaign in the CCFZ

7.1.2 Organisation within JPI-O MiningImpact 2 consortium

The organisational structure of the JPI-O MiningImpact 2 project consists of 5 different work packages (WP) and 3 cross-cutting themes (CCT). A high degree of coordination between the WPs and CCTs is required in order to achieve a good overall baseline sampling strategy, an efficient monitoring of the Patania II trial that simultaneously facilitates implementation of all monitoring objectives, the setting up of a coordinated monitoring programme, and an efficient data management, reporting and dissemination programme. These highly interconnected tasks necessitate a comprehensive project governance structure that enables collaborative decision-making and consultation within the JPI Oceans framework.

Responsibilities in terms of project dissemination, data and sample management as well as outreach and reporting are elaborated.

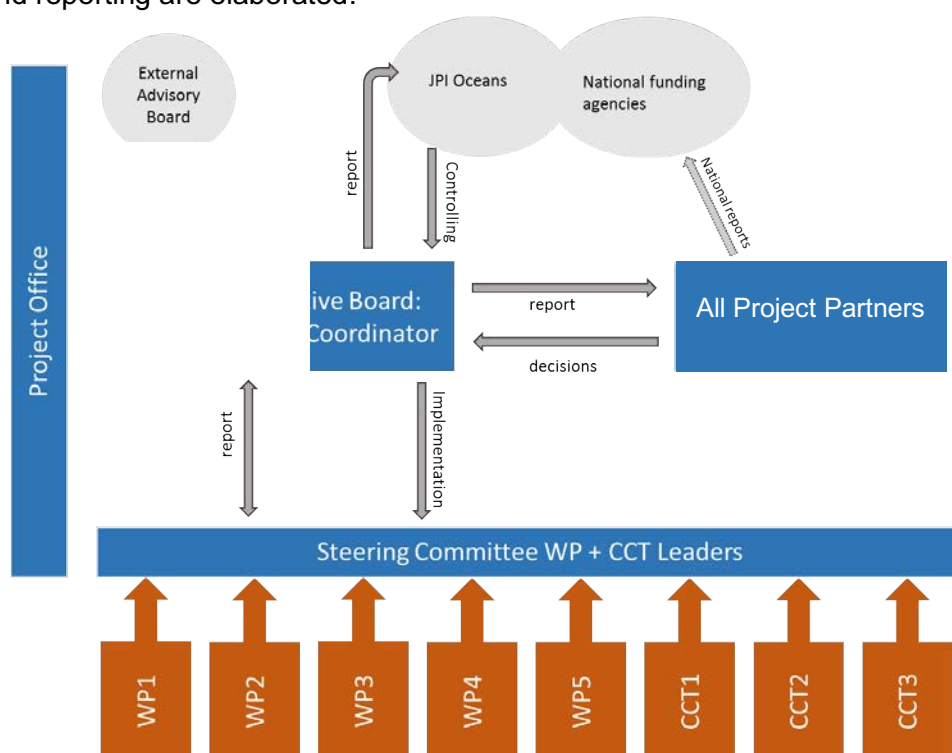


Figure 97: Outline of the JPI-O MiningImpact 2 project structure.

7.1.3 Coordination between GSR and JPI-O MiningImpact 2 consortium

The operational coordination between GSR and the scientific consortium partners will be addressed in a Simultaneous Operations (SIMOPS) plan before the scheduled activity to avoid any misunderstanding between parties and align the operations.

7.2 Environmental Management and Monitoring Plan (EMMP)

The objective of the Environmental Management and Monitoring Plan (EMMP) is to manage environmental hazards and risks associated with GSR activities in order to assure that no additional unwanted impacts are produced other than the impacts from the intended disturbance experiment. The focus of the EMMP at this stage of exploration is on the monitoring aspect.

The early stage of the EMMP lies in the design of the PPV itself, in order to minimize and mitigate as much as possible the impact on the seafloor. Further adaptations were taken into account (and more will be considered, as the design is not yet finalized) to reduce environmental

consequences. Moreover, it must be recalled that the vehicle to be deployed is a pre-prototype. It will be the basis for the elaboration of the prototype of a future mining vehicle and the integrated system. Therefore, the environmental monitoring designed and set out hereafter is of major importance for the later stages, especially regarding the plume created and the depth of penetration into the seabed.

The Environmental Monitoring Plan (EMP) will focus on the immediate, short- and intermediate-term (2 years) physical and chemical impacts of the PPV trial on the seafloor and its overlying waters, as well as on the response of benthic organisms. These data are crucial for assessing the potential for recovery of benthic standing stocks and biodiversity and for the maintenance of associated ecosystem functions.

The EMP JPI-O II MiningImpact is rolling out involves the following activities, which can also be seen as project objectives:

1. planning of the EMP layout around the PPV trial;
2. cruise station time planning;
3. onsite pre-impact physical, chemical and biological assessment;
4. *in situ* and *ex situ* plume experimentation before the Patania II trial takes place;
5. near real-time modelling to predict plume fallout areas directly before the PPV trial;
6. comprehensive *in situ* monitoring survey of the PPV trial itself;
7. validation of plume modelling;
8. onsite post-impact physical, chemical and biological assessment;
9. evaluation of the effectiveness of the EMP workflow and monitoring technologies used;
10. recolonization/restoration experiments (to assist ecosystem recovery);
11. evaluation of mining-related pressures and effects on ecosystem components;
12. development of tools for integrated (cumulative) environmental impact assessment.

A schematic presentation of the spatial and temporal coverage of pre- and post-impact assessment and the recolonization/restoration experiments is given in Figure 98. The trial plan and monitoring programme includes, to the maximum extent currently possible, a detailed description of the aims and designs of the surveys, but will be adapted and/or refined prior to testing and at other appropriate times, if refinement is necessary (e.g. due to the collection of new baseline data shortly before the test takes place).

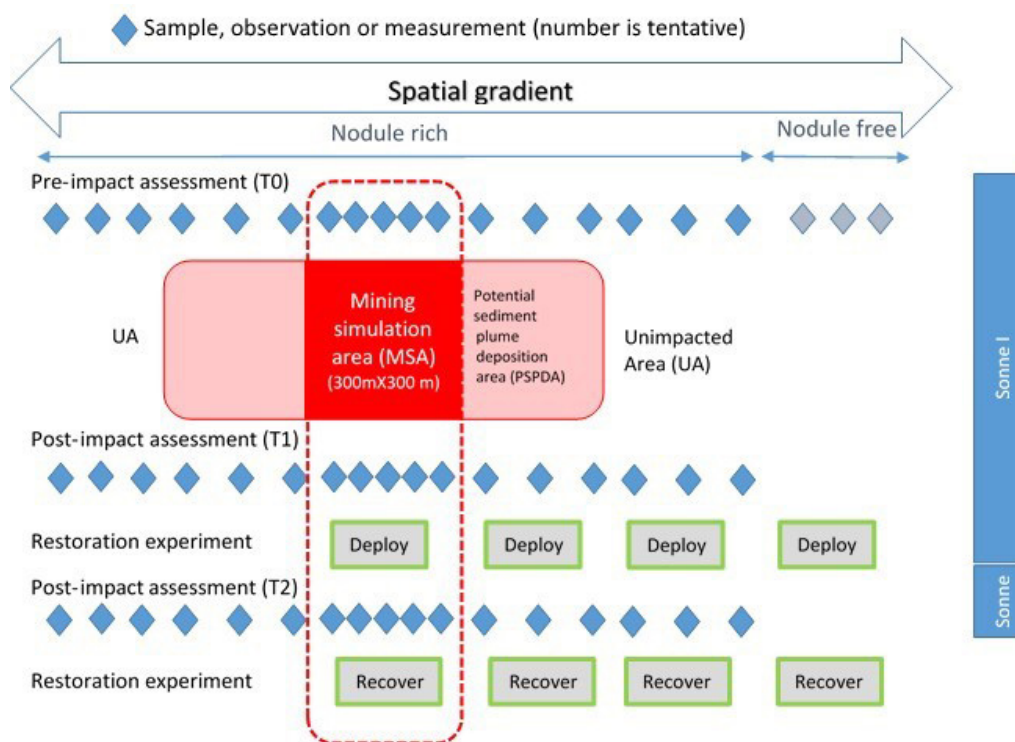


Figure 98: Schematic presentation of the spatial and temporal coverage of pre- and post-impact assessment, and the restoration/recovery experiment

The geographical scale / sampling scale of the monitoring survey depends on the predicted size of the impact; this is determined by the modelled dispersion distance of the sediment plume, the results of seafloor classification and habitat mapping efforts using ship- and AUV-based bathymetric and optical information, and by geological and biological sediment sampling data (baseline data). Spatial design involves defining the Impact Zone and the gradients of impact within that zone, as well as defining one or more control reference sites (potentially reflecting different habitats as appropriate) against which any changes in the biodiversity of the trial area can be assessed. Depending on the bottom current dynamics at the time of testing, the distance that the suspended plume in the water column is likely to have spread after 4 days of testing is predicted to vary between 1 and 3 km (cut-off concentration value respectively 10 mg/L and 1 mg/L) and 5-12 km (cut-off value 0.1 mg/L), depending on current conditions at the seafloor. For the intended disturbance experiment the sediment deposition from the plume is expected to reach approximately 500-750 m (cut-off value of 1 mm deposition) and roughly 5 km (cut-off value of 0.1 mm deposition) from the source (as presented in 5.1.3.2.2 Sediment transport modelling, pp. 133).

One or more control reference sites will be established around the trial IRZ. One already fixed reference site will be the area in which analyses have been carried out in 2017, which lies approximately 11 km to the SW of the trial IRZ and hence will not be affected by the trials, including effects from the discharge plume. Such reference sites should ideally have a species composition comparable to that of the trial area. Therefore, a preliminary biological comparison of the abiotic and biotic variables was carried out between the IRZ and the reference site (section 7.2.2, Choice of impact reference zone and reference zone, pp. 171). A Plume Impact Reference Zone is envisaged to be an area in which time-series analyses have been carried out throughout

the last few years (2015, 2017), which lies approximately 1.5 to 2 km to the west of the trial IRZ and is expected to be affected by the Plume but outside the footprint of the program area. Monitoring of the plume towards and in this area will determine whether this area is impacted and will have ultimately a role as PIRZ or as Control Reference Area (PRZ).

7.2.1 Technical mitigation

From a technical point of view, the following environmental measures were implemented in the design of Patania II:

7.2.1.1 Patania II design

First, the initial choice of caterpillar tracks. Compared to other available technology (Archimedes screws and sledge device), this active system was preferred for its predictability, which is essential for adaptive management. Furthermore, caterpillar tracks appear to be more energy-efficient than Archimedes screws.

Another mitigation option was related to the type of collector. The current hydraulic collection system could minimize sediment resuspension as compared to a mechanical collection system as the collector head will hover over the seafloor to pick-up the nodules therefor expected only taking up the loose water saturated sediment layer. However we note that for modelling purpose of plumes we assumed that an initial conservative 12 cm of sediment layer will be removed.

Additionally, after CFD modelling of the PPV and the sediment produced, preliminary results showed a density flow mainly concentrated in the few first meters above the seabed. Nearfield assessment showed a slightly lower up-whirling of the plume with a downwards directed diffusor, although the difference was limited. .

7.2.1.2 Instruments

It is crucial to know the flow along the collection duct. Density and flow measurements in the dredging industry are commonly done by gamma radiation directed across the dredge pipeline. As an alternative to the gamma radiation measurement, a densitometer and a flowmeter based on conductivity are being developed for the in-situ trials with Patania II.

All electronic components are enclosed in an oil-filled box. The potential for oil leaks exists and hence a seawater-biodegradable, non-toxic oil will be used (see also above).

Noise/vibration concerns are addressed by choosing pumps (ARBO Pompen en Filters, 1016. Consulted on March 21, 2018) known for their low noise and vibration level, as well as for their use of solid machined plastic and non-toxic materials.

7.2.1.3 Operations

During operation on the seafloor, a complete check-up of the Patania II will be carried out every 500 m driven, following a strict procedure (see Appendix 12.2, pp 234 for the procedure concerning the Patania in 2017. This procedure will be adapted for Patania II in 2019) in order to prevent any leaks or malfunctions. If any major issue is observed, the Patania II would be immediately retrieved.

Noise and light pollution concerns (see above) will also be addressed by using the pumps as much as technically possible in maximum noise-reduction mode as recommended by the manufacturer. As the response to noise and light is species-dependent, light and sound (mainly from HPU units) emission will be switched ON and OFF step by step, to give nearby mobile

organisms (with the appropriate ability) the opportunity to flee, as suggested by Ortega (Ed.) et al. (2014).

Finally, all the equipment will remain well maintained during the entire expedition: this is best practice and facilitates anticipation and prevention of a potential break down and its consequences.

7.2.2 Choice of impact reference zone and reference zone

For the implementation of these first equipment and collection trials, impact and reference sites must be carefully chosen. Ideally, impact and reference sites should be characterized Impact and Control Reference Zone.

We described above that the samples collected during GSRNOD17 were evaluated to investigate 1) temporal changes in biological and environmental parameters and 2) the influence of macrohabitat types (nodule-free (bare) vs. nodule-bearing (D/I) and slope vs. flat). Within site B4S03, each of both comparisons was based on samples from a different area. Samples from the southwestern part of the site were used to study the effect on macrohabitats, whereas samples from the more northeastern part served as a temporal comparison (combined with samples from previous expeditions). In this section, we set out the differences between those two sites in order to evaluate their use as possible impact and reference zones.

The environmental and biotic variables reported above (section 4, Description of the existing environment, pp. 52) were re-analyzed to compare conditions between stations located in the same site (B4S03). For this purpose, sampling stations in B4S03 were renamed in B4S03A (the northeastern station) and B4S03B (the southwestern station, Figure 99). The use of B4S03B is proposed as a reference site for the possible impact site B4S03A.

To evaluate differences between sites, sedimentary environmental variables were compared visually using depth profiles and bar graphs. Statistical analyses were performed to characterize the abiotic environment in its entirety with the sampled variables. A PCA was performed on all measured environmental variables after normalization and across all depth layers (0-10 cm) in Primer v6 (Clarke and Gorley, 2006).

Additionally, environmental variables and community compositions of meiofauna and macrofauna (based on relative abundances) were statistically compared with a permutational analysis of variance (Permanova). Permanova was performed on a resemblance matrix based on Euclidean distances (environmental data) and Bray-Curtis similarities (biological data) with 9999 permutations and an unrestricted permutation of raw data method as described in Anderson et al. (2008) on a one-factor design (factor “sites”). When the number of possible permutations was lower than 100, Monte Carlo (MC) tests were applied. A PermDisp test was executed to ensure homogeneity of data dispersion. In the case of a significant Permanova, a similarity of percentages (SIMPER) test was performed to identify the contributions of each variable to the observed differences.

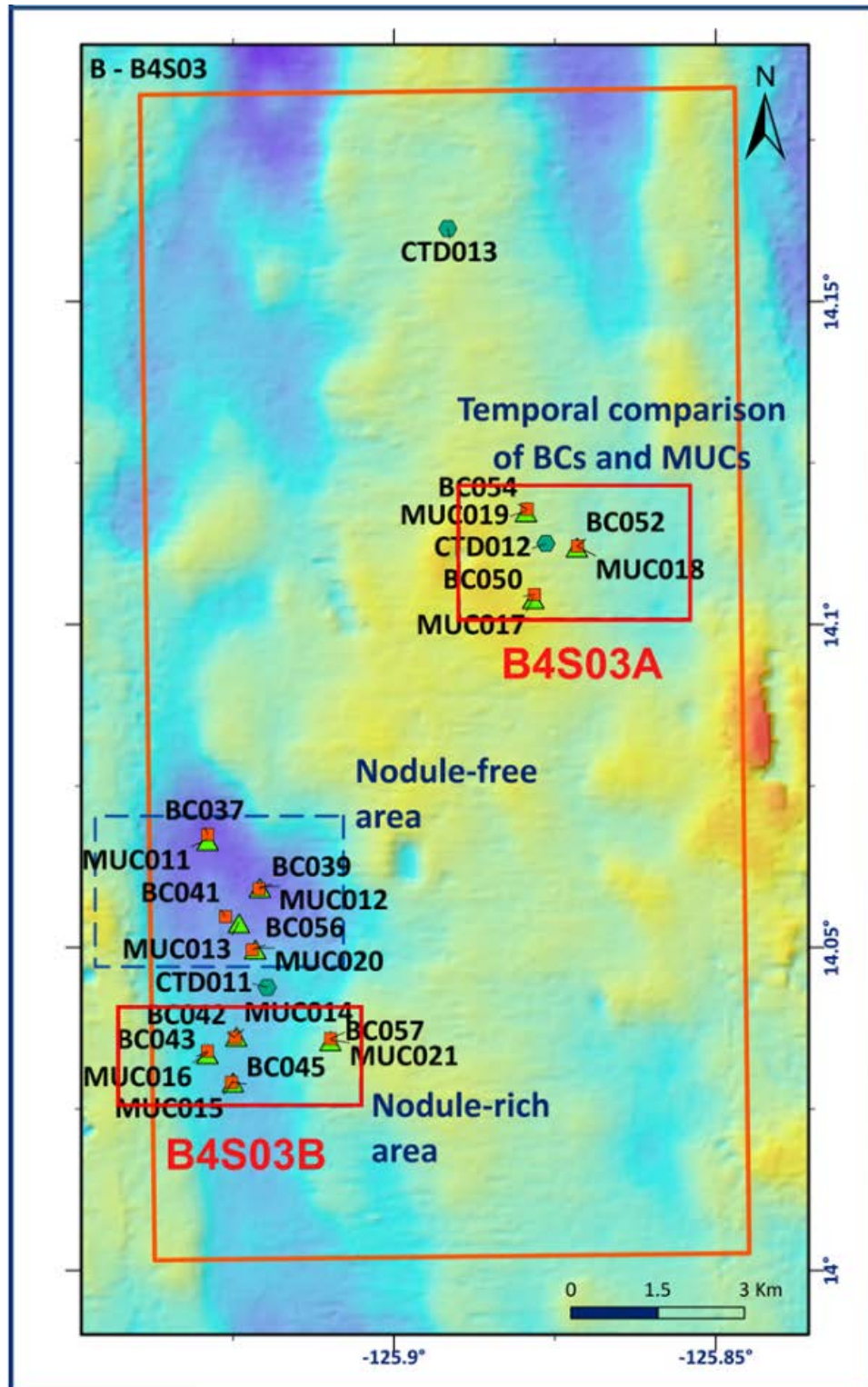


Figure 99: Map of site B4S03 showing the biological deployments, i.e. box corer (BC), multicorer (MUC) and CTD-carousel water sampler (CTD) collected during expedition GSRNOD17. Red boxes indicate the renamed stations B4S03A and B4S03B that are referred to in this section.

7.2.2.1 Environmental variables

Both sites are located on a flat, nodule-rich area at approximately the same depth of 4502 ± 16 m (mean \pm standard deviation (SD)) and 4551 ± 4 m for B4S03A and B4S03B, respectively.

Visual inspection of variables associated with granulometric properties revealed no difference between both sites for all depth layers (Figure 100). Similarly, total organic carbon and nitrogen values were comparable across all depth layers (Figure 101). Total organic matter content revealed slight differences between sites only in the deeper sediment layers (>5 cm, Figure 101). Finally, most nutrient concentrations measured in the pore water were similar between sites with the exception of slightly lower nitrite concentrations in B4S03B compared to B4S03A (Figure 102).

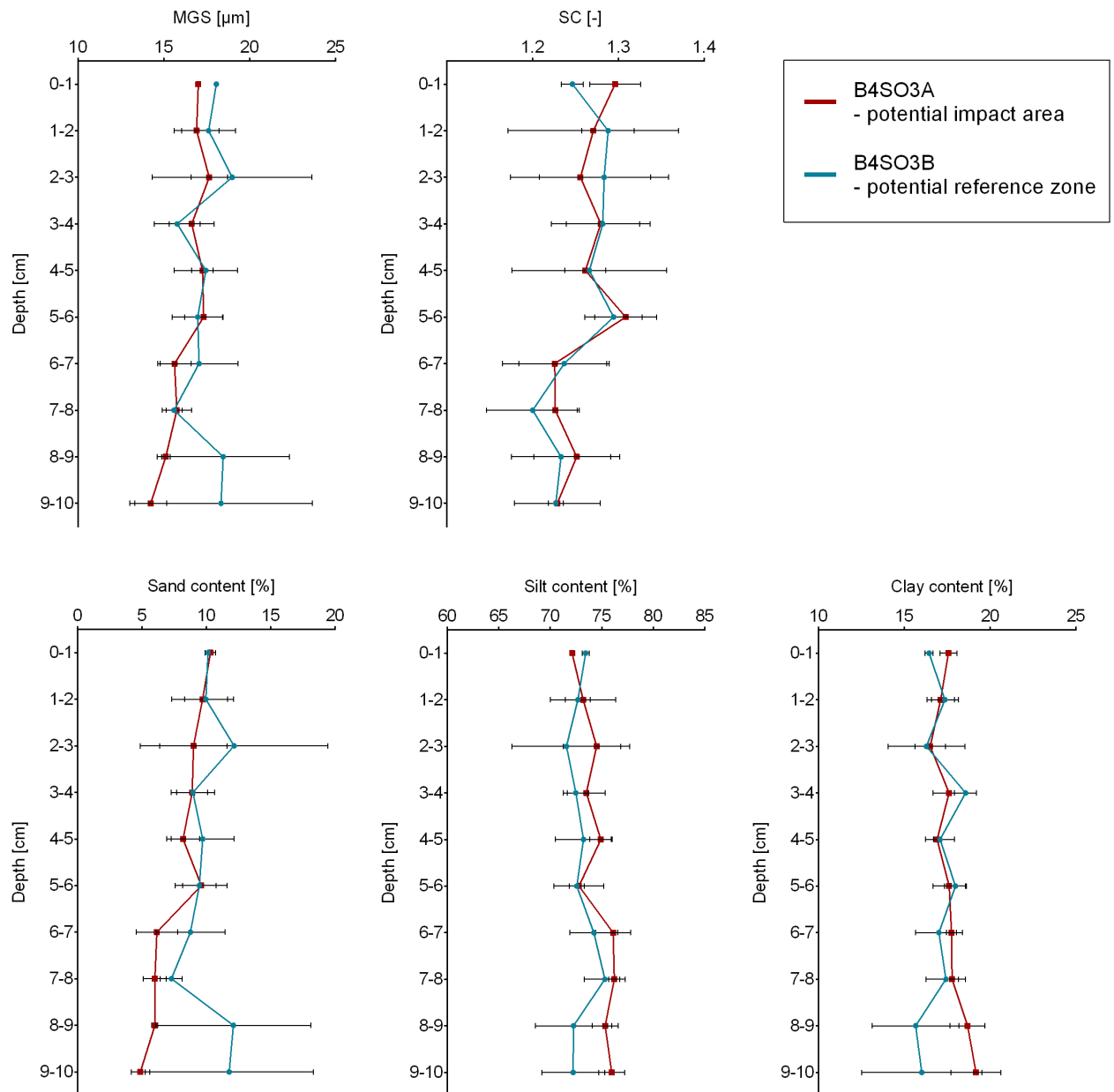


Figure 100: Average values of variables associated with the sediment granulometry in function of sediment depth in samples collected during the GSRNOD17 expedition at sampling stations B4S03A and B4S03B. Error bars denote standard deviations.

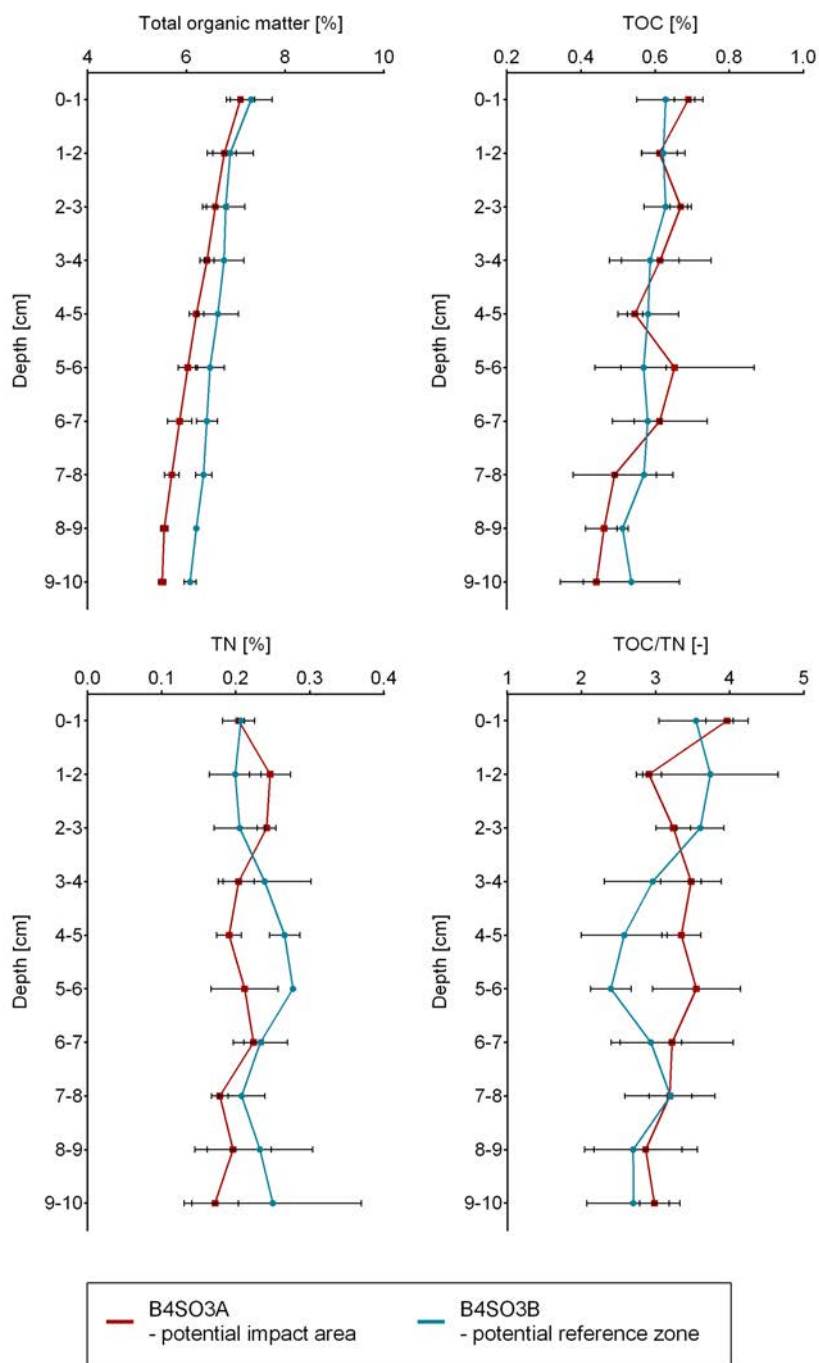


Figure 101: Average values of total organic matter (TOM), total organic carbon (TOC), total nitrogen (TN) and the molar sediment total organic carbon- to- nitrogen ratio (TOC/TN) in function of sediment depth in samples collected during the GSRNOD17 expedition at sampling stations B4S03A and B4S03B. Error bars denote standard deviations.

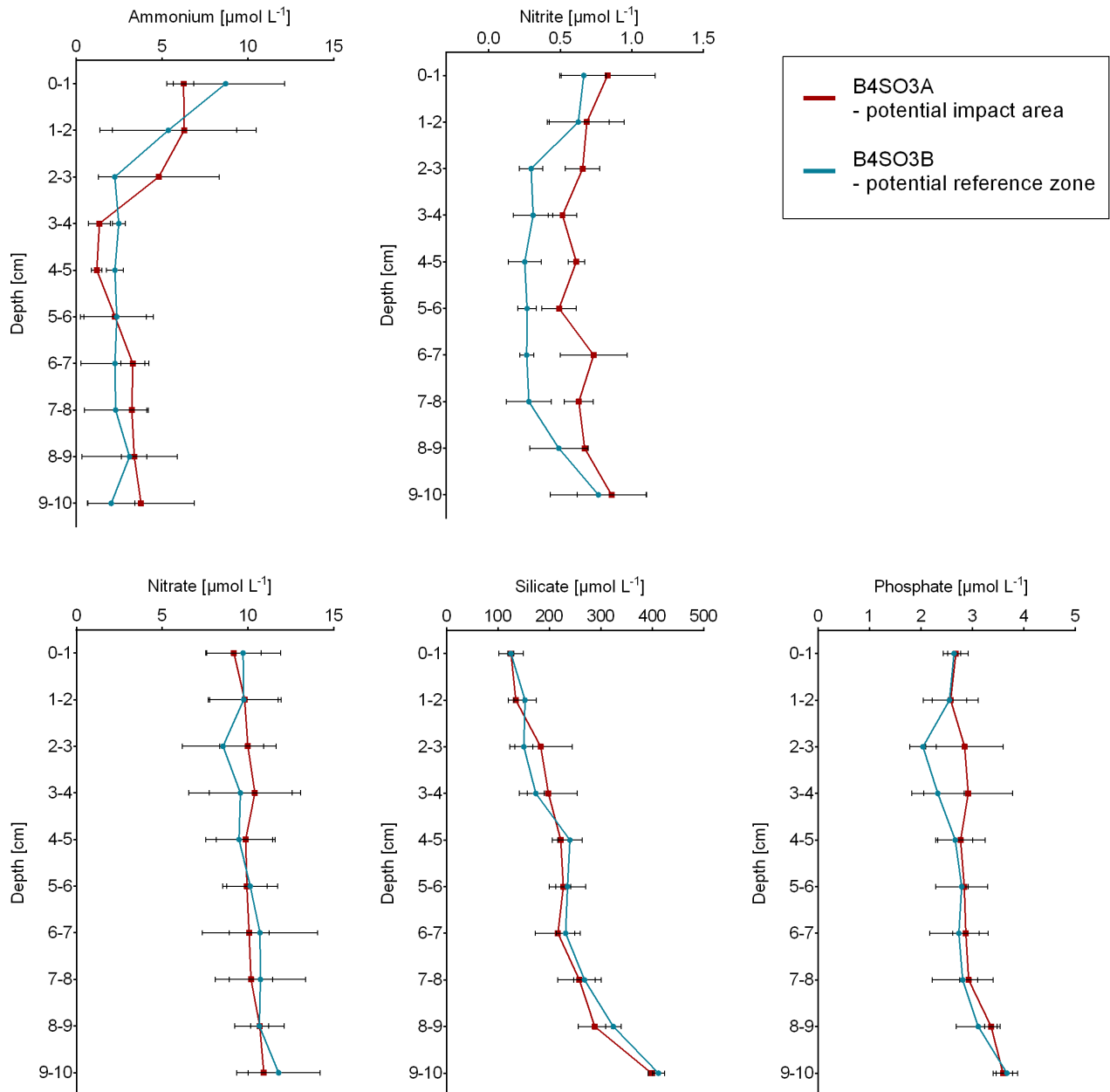


Figure 102: Average values of pore water nutrient concentrations (Ammonium, Nitrite, Nitrate, Silicate, Phosphate) in function of sediment depth in samples collected during the GSRNOD17 expedition at sampling stations B4S03A and B4S03B. Error bars denote standard deviations.

The PCA analysis of all variables together did not reveal any apparent clustering of samples from both locations (Figure 103). Nevertheless, Permanova revealed significant differences between both sites (Pseudo-F=4.0384, $p_{\text{Perm}}=0.0017$), but the PermDisp test was non-significant. Based on the SIMPER analysis, differences were largely caused by nitrite concentrations (7.84 % contribution) and total organic matter content (7.23%). However, contributions of all other variables also ranged between 6 and 7%.

Despite the significant Permanova test, we conclude that environmental conditions in the sediment of site B4S03B closely resemble those of site B4S03A and that differences in TOM and nitrite are negligible.

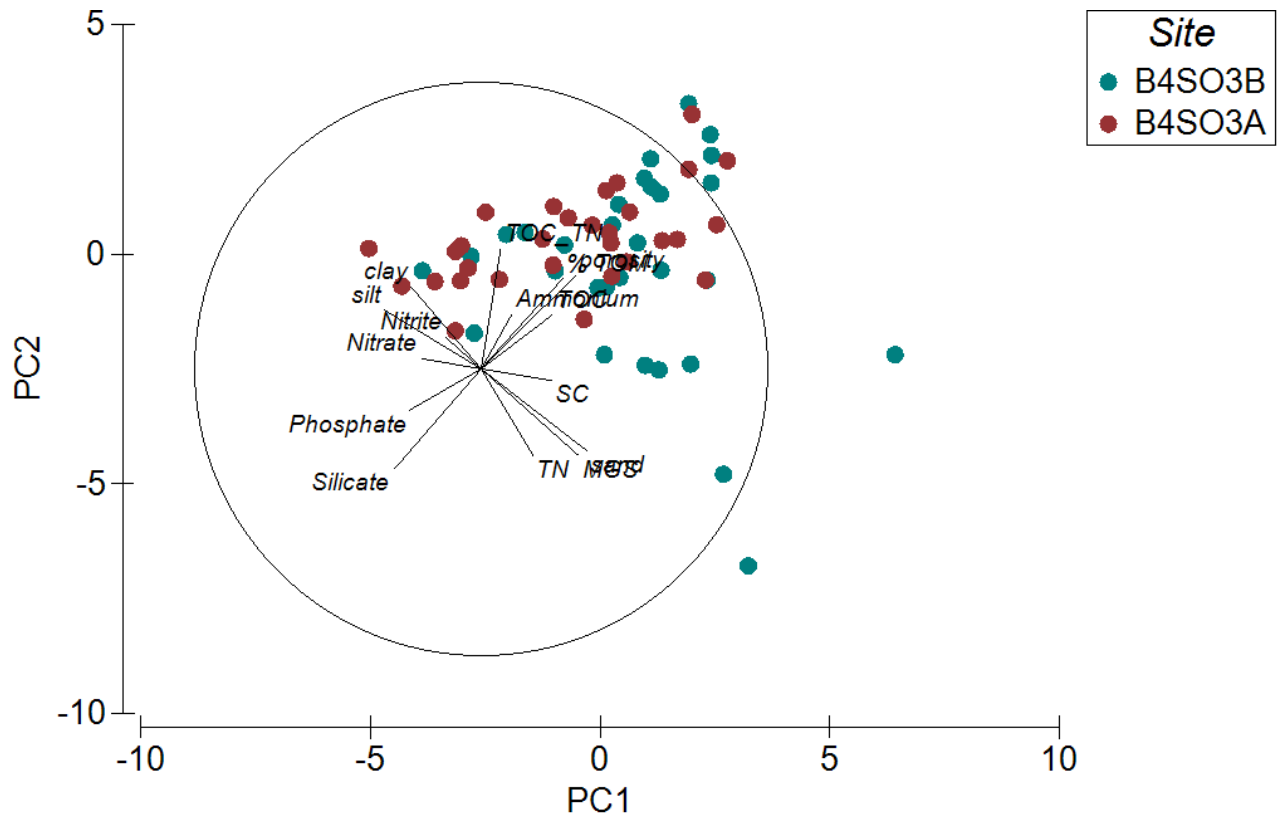


Figure 103: Principal component analysis (PCA) of samples from stations B4S03A (red) and B4S03B (blue) collected during expedition GSRNOD17 according to their sedimentary environmental variables across all depth layers (0-10 cm).

7.2.2.2 Biological (meiofauna and macrofauna) variables

Total meiofaunal densities were lower in B4S03B compared to B4S03A, but did not differ significantly (Figure 104). Similarly, Permanova did not indicate significant differences in higher taxon meiofaunal community composition (Pseudo-F= 0.26217, $p_{MC}=0.7433$, Figure 104).

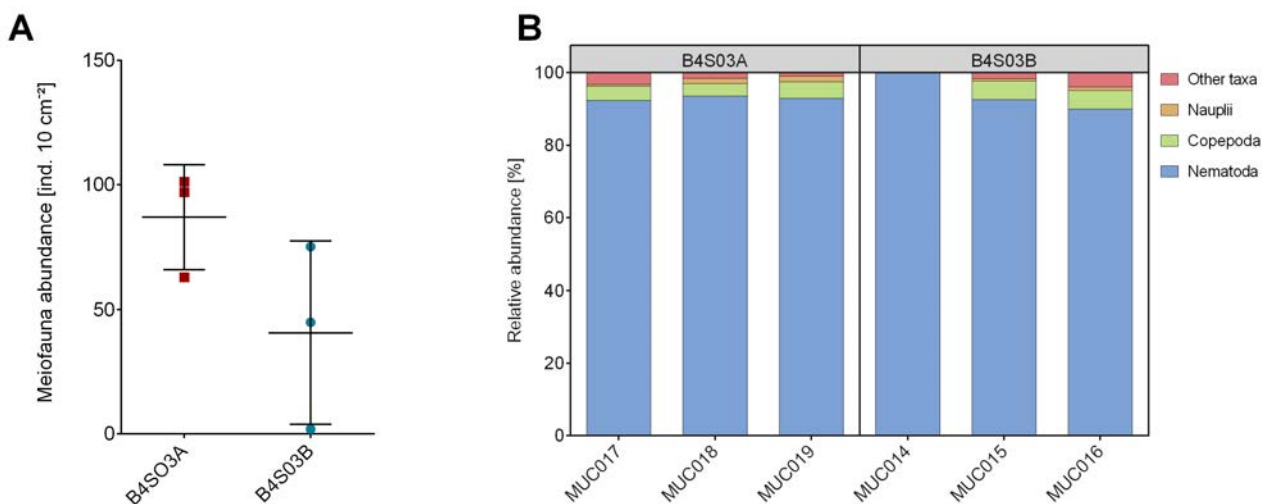


Figure 104: A) Total meiofaunal abundance and B) relative abundances of meiofaunal taxa in samples collected during GSRNOD17 at site B4S03A and B4S03. In A): Lines indicate mean values and error bars denote standard deviations.

The same was true for macrofaunal densities and higher taxon macrofaunal community composition, where no significant differences were detected between B4S03A and B4S03B (Figure 105).

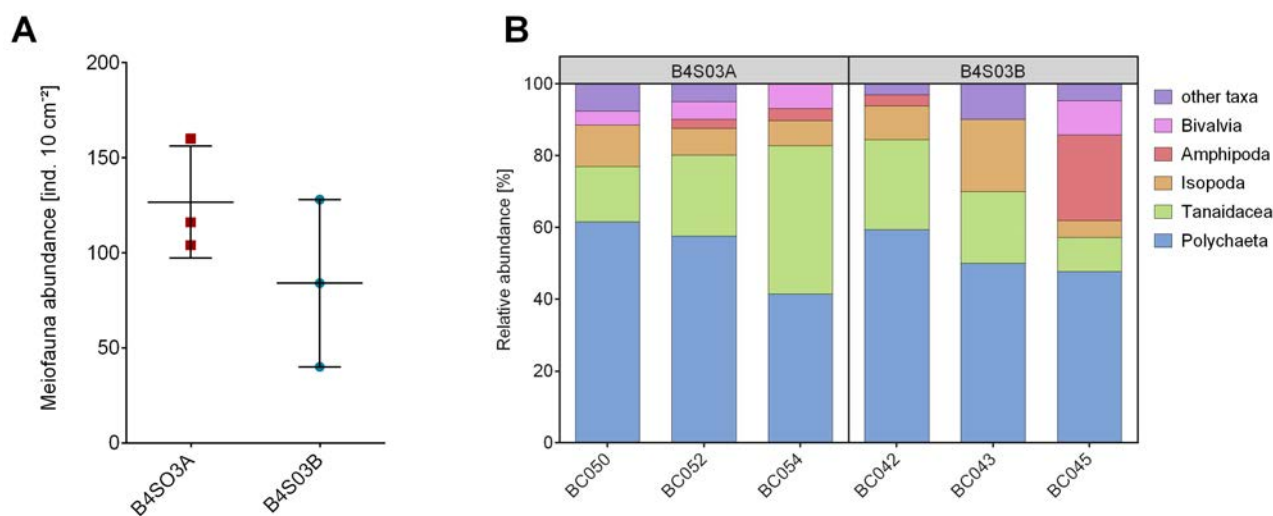


Figure 105: A) Total macrofaunal abundance and B) relative abundances of macrofaunal taxa in samples collected during GSRNOD17 at site B4S03A and B4S03. In A): Lines indicate mean values and error bars denote standard deviations.

In conclusion, the minor differences in abiotic variables are not reflected in the biological communities. Therefore, both sites offer similar biotic and abiotic conditions and may be used as Impact and Control Reference Zone. furthermore, biotic and abiotic baseline data of both sites were presented and the selected areas were approved by the scientific community of the JPI-O consortium.

7.2.3 Environmental monitoring plan

7.2.3.1 Monitoring approach

7.2.3.1.1 Biodiversity, connectivity, resilience (WP1)

WP1 will focus on taxonomic and functional biodiversity, connectivity and resilience of benthic communities and will address both natural variability and the effects of impacts connected to the PPV trial. Studies on benthic assemblages (microbiome, meiofauna, macrofauna and megafauna) will follow a Before-After Control Impact (BACI) design with replication conducted during both the baseline study and the impact study at stations located in the areas defined in the general environmental impact monitoring plan (EMP). The exact location of impact sites for faunal sampling (using e.g. boxcorer, multicorer, EBS, ROV, faunal traps), combined optical and hydroacoustic surveys (with e.g. ROV, AUV, OFOBS), and time-lapse camera deployments will be identified based on plume impact monitoring carried out during and immediately after the PPV trial (WP2, CCT1). Both image-based and acoustic surveys to assess habitat structure and megafauna community structure have been conducted in polymetallic nodule areas previously, but have seldom been used to monitor a disturbance event (Bluhm, 2001; Greinert, 2015; Boetius, 2015; Purser et al., 2016; Vanreusel et al., 2016). In this project a range of innovative acoustic and imaging static, towed and autonomous free swimming devices will be used to map at high resolution habitat features and faunal distributions across the surveyed region prior,

during and after disturbance. Data collected will be processed using workflows developed during MiningImpact 1 (Marcon and Purser, 2017; Dreutter, 2017; Purser et al., in press).

Results obtained on changes in presence, activity and functions of specific groups of faunal and microbial communities and any impact indicator taxa that can be identified will contribute to the analysis of disturbance effects (CCT2). Particular emphasis will be on the analysis of similarities in the response of different faunal components (meio-, macro- and megafauna) and microbial communities to specific impact types and intensities and to effects on biogeochemical processes. This knowledge will help assess the suitability of biodiversity and community structure analyses of the different faunal compartments and microbial assemblages for future impact monitoring and contribute to risk assessment and recommendations (CCT3).

WP1 focusses on four main tasks:

- Megafaunal communities and their connection to physical habitat characteristics addressing natural variabilities, disturbance effects, and their temporal evolution

At each station, detailed seafloor imaging and acoustic data will be collected using AUV, ROV and the towed camera platform OFOBS to characterise habitat features and the megafauna communities present at the time of the survey. Each station will be visited prior to and after the PPV trial to enable any changes in megafauna community structure to be identified. Where possible, time-lapse camera units will be deployed on the seafloor prior to the PPV trial to observe any visual responses of epifauna to the disturbance.

ROV transects will be conducted at each station before and after the PPV trial to collect image data to help assess the plume impact on detritivores, suspension feeders and filter feeders. Once the plume has settled (expected to occur within maximum 5 days after the end of the patania II trials), one transect will be carried out along the direction of the created plume. Two more transects will be carried out at different angles from the same starting point, to analyse different degrees of disturbance and to evaluate possible fleeing movements of mobile fauna. These transects will be repeated several times following the PPV trial, allowing both temporal and spatial responses to be gauged. From the ROV image data, a selection of three key representative megafaunal taxa (a suspension feeder, a detritivore and a filter feeder) will be chosen for direct physical sampling. The ROV will collect representatives of the three taxa to assess their ecophysiology.

- Meio- and macrofaunal assemblages and their connection to physical habitat characteristics addressing natural variabilities, disturbance effects, and their temporal evolution

This task aims to decipher the spatio-temporal dynamics of the meiofauna and macrofauna from quantitative samples obtained according to the plan described above. On-board sampling of faunal specimens for taxonomic work (morphological and molecular) will follow methodology set out in Glover et al. (2015). A combined morphological and molecular approach will be used whenever possible, to facilitate accurate taxonomic identifications, detection of cryptic diversity, and description of new faunal species. Invertebrate markers, such as cytochrome oxidase I mitochondrial gene (COI), 16S mitochondrial ribosomal RNA coding genes and 18S or 28S nuclear genes, will be targeted. This work will contribute to and improve existing datasets and will be crucial for further assessments of biodiversity and connectivity.

Taxonomic and trophic diversity and community structure (e.g. alpha and beta-diversity) will be analysed in each faunal compartment and compared between faunal compartments. Functional and trophic relationships within meiofaunal and macrofaunal assemblages will be explored (e.g. by stable isotope analysis). A metagenomic approach will be used for biodiversity assessments and comparative analyses of selected taxa (e.g. nematode, polychaete and amphipod assemblages). Spatial and temporal patterns of faunal assemblages will be analysed (e.g. using multivariate analyses) in relation to comparable data obtained during MiningImpact 1 and to available abiotic and biotic environmental parameters, and will enable establishing criteria for the definition of “good environmental status”. Species sensitive versus resistant to mining plumes will be identified and listed.

The sponge *Plenaster craigi* is one of the common filter feeders located on nodules and is likely to be susceptible to increased turbidity and nodule removal (Lim et al., 2017); hence it was chosen as a potential indicator species for monitoring the impact of a mining plume. Mapping of *Plenaster craigi* abundance will be carried out using data from box cores and high-resolution *in situ* photography, and the impact from exposure to experimental sediment plumes will be subsequently assessed.

Short-term impacts of the Patania II trial on connectivity will be investigated by assessing the dispersal of larvae and resuspended benthos by the sediment plume (e.g. via resuspended sediment, passive larval dispersal via currents).

Newly obtained molecular data will be used to complement previous and/or ongoing analyses of data from MiningImpact 1 and other projects (Glover et al., 2016b; Dahlgren et al., 2016; Wiklund et al., in press) and detect shared species at a regional scale within the CCFZ. Novel Next-Generation RAD-seq techniques (Burford-Reiskind et al., 2016) will be applied to investigate the population genomics of amphipod species and provide data on population histories and connectivity at high resolution and high statistical confidence. Genetic connectivity of mobile and sessile species will be analysed and related to their recovery potential in the disturbed area and on restoration substrates (CCT2). Population genomics can enable the detection of Single Nucleotide Polymorphisms (SNP) under selection, which can be used to unravel species-specific adaptations to deep-sea environments and obtain new data on their resilience.

- Effects of sediment disturbance on microbial and micro-eukaryote communities

Molecular approaches will be applied to sediment samples collected with ROV push-cores prior to and after the PPV test to characterise the microbial and micro-eukaryote communities within undisturbed, directly mined and plume-exposed seafloor areas.

Microbial community composition and diversity (via 16S rRNA gene Tag sequencing), functional diversity (via metagenomes), and dominant active microbial taxa (via 16S rRNA/cDNA Tag sequencing and metatranscriptomes) will be identified. Analyses will address microbial biodiversity at taxonomic levels ranging from phyla to individual ‘species’ (i.e. operational taxonomic units), as well as links of key ecosystem functions to specific groups. Investigations of sediments from undisturbed sites will assess regional variability of microbial biodiversity and spatial connectivity, and samples obtained after the test will focus on mining-related effects on communities and ecosystem functions. Manganese nodule material will be analysed to investigate the contribution of communities on the outer nodule layer to the overall taxonomic diversity found in the area.

Following the same sampling strategy used for microbial assemblages, changes in benthic micro-eukaryote biodiversity (i.e. protists and fungi) will be investigated through a metagenomic approach applied to extracellular DNA. The extracellular DNA will be selectively extracted from the sediments using a combination of physical and chemical procedures (Corinaldesi et al., 2005; Danovaro, 2010), which excludes the contamination by the DNA of any biological component, including viruses. Once extracted, the extracellular DNA will be amplified by using primer sets targeting 18S rRNA genes and ITS (internal transcribed spacer) of eukaryotes and the amplicons analysed by high-throughput sequencing platforms (e.g. Illumina MiSeq).

- Development of molecular methods and protocols for rapid biodiversity assessments and environmental monitoring

Methodological improvements provide evidence that the majority of DNA pools in benthic ecosystems is not associated directly with living biomass, but rather with extracellular DNA (eDNA) (Dell'Anno and Danovaro, 2005) containing amplifiable prokaryotic and eukaryotic gene sequences suitable for assessing biodiversity at different spatial and temporal scales (Corinaldesi et al., 2008, 2011). Other molecular methods increasingly used in biodiversity assessments are the metabarcoding and the Maldi-TOF proteome approach (Bik et al., 2012; Laakmann et al., 2013). These three molecular methods will be tested and compared to determine their suitability and/or complementarity as tools for rapid assessments of biodiversity and monitoring of the impact of mining activities on deep-sea microbial and faunal assemblages. The reference databases built up during MiningImpact 1 enable a wide application of metabarcoding and eDNA techniques, revolutionising our ability to undertake biodiversity and connectivity analyses. The new droplet digital PCR (ddPCR) technology (Doi et al., 2015) will be used to develop molecular identification assays for a set of REM taxa, and evaluate their presence and abundance across the CCFZ. A set of ddPCR assays will be developed to target REM (Rare, nodule-Endemic and Megafauna) indicator species based on the existing reference dataset (Glover et al., 2016b; Dahlgren et al., 2016; Wiklund et al., in press). eDNA samples of mud and bottom water will be collected at different stations and extracted on board (Lekang et al., 2015). Initial assay feasibility tests will be carried out on CCFZ samples that are readily available and optimal standardised method protocols for use of eDNA and ddPCR in environmental monitoring will be developed.

Sediments will be sampled and fixed for molecular studies prior and after disturbance in the areas influenced by plume deposition, as well as non-affected reference areas, and three different molecular methods for rapid biodiversity assessment will be applied. Ground-truthing will be performed by comparing with results generated in WP2. Changes in the pristine abyssal eDNA signature will be investigated following the PPV trial and subsequently changes through time. For the metabarcoding approach, organisms will be extracted from the sediment first and the DNA will be extracted from the whole community without further sorting. Different gene fragments (COI-mini, 18s V1-V2, V4 and V9 regions) will be amplified and sequenced in parallel using Illumina NGS technology and compared to a genetic library for the assignment of taxonomic entities. The suitability of the different gene regions to capture abyssal meiofauna diversity and structure will be examined. For the proteome approach, the whole proteome from single specimens will be measured using Maldi-ToF (matrix-assisted laser-desorption/ionization time-of-flight) mass spectrometry that generates a species-specific fingerprint of the proteins' mass. The aim of this study is to test the efficiency and sensitivity of the three different molecular

approaches to detect and monitor changes produced by mining impacts and recovery through time of the standing stocks and community structure in micro-, meio- and macrofaunal communities.

7.2.3.1.2 Fate and potential toxicity of the sediment plume (WP2)

WP2 focuses on assessing the fate and impact of the sediment plume generated by the PPV trials. The work will involve monitoring of the dispersal of suspended sediment and sediment redeposition in space and time, assessment of the evolution of physical (e.g., particle concentration, size, and aggregation) and chemical (e.g., trace metals) characteristics of the plume as it drifts away from the site of its origin, and assessment of the impact of the sediment plume on seafloor sediments and biota.

Field observations and experimental work will generally follow the EMP-based strategy developed in CCT1. Baseline data on bottom water, surface sediments, nodules, and biota will be collected before the test occurs from sites where the major plume impact is expected to occur (PIRZ), as well as from unaffected reference sites. A 3D array of optical and acoustic turbidity sensors and particle cameras on static and mobile platforms will be deployed along the anticipated main direction of plume dispersal prior to the onset of the PPV trial to monitor the dispersal of the sediment plume in space and time. Plume modelling efforts will be supported by *in situ* observation and *ex situ* experiments addressing turbulence-induced particle aggregation in the bottom boundary layer, as well as scavenging of particles by seasonal phytodetritus falls. Plume monitoring data and experimental results will be used for calibration and validation of near-field and far-field sediment transport models which are an important tool for predicting the areal extent of sediment dispersal resulting from later full-scale mining operations.

Results from *in situ* and *ex situ* geochemical and biological experiments will be integrated with diagenetic and food web modelling carried out in WP3 to improve predictions of mining impacts on the deep-sea ecosystem. Potential mobilization of trace metals in sediment plumes and redeposited sediments will be addressed by geochemical analysis of bottom water and surface sediment samples, shipboard and laboratory experiments, and numerical modelling of trace metal reactions. The different impacts that mining plumes may have on deep-sea biota will also be investigated, such as translocation of benthic microbial communities and small meiobenthos from the mined area where the plume is generated to the area of redeposition of plume material, physical damage inflicted by suspended sediment particles on meroplankton and zooplankton living in the near-bottom water, impaired feeding and respiration in filter-feeding and suspension-feeding megabenthos, like corals and sponges, due to sediment clogging, and ecotoxicological effects due to metal-containing particles and dissolved metals. Much of this work will be conducted for the first time, not only for this part of the Pacific Ocean, but also for this water depth in general and will be complemented by *in situ* and *ex situ* sediment exposure studies.

The potential environmental hazard presented by the plume will be evaluated by means of the quantitative weight of evidence (WOE) model, in which impact on biota and ecosystem functioning is assessed with information from the chemistry (in the different environmental matrices) and from the ecotoxicological impact. Knowledge obtained on the suitability of instruments and methods for monitoring and evaluating mining impact will contribute to the development of policy recommendations.

The work of WP2 is organised in three interconnected tasks:

- Plume dispersal and sediment deposition

This task addresses the dispersal of suspended material in the sediment plume in space and time and the spatial extent and amount of sediment redeposition from the plume. Following the experimental design of the EMP, a 3D sensor array of moorings and landers will be geared up and deployed across the area designated for the PPV field trial. Apart from standard oceanographic sensors, the array will include acoustic and optical turbidity sensors with different sensitivity and measuring ranges, as well as particle cameras, to monitor the lateral and vertical dispersal of the plume and evolution of its physical characteristics as it drifts away from its site of origin. A focus will be on the determination of long-term (seasonal) variability of currents and rates of sediment deposition. During the PPV trial, the traps will be redeployed close to the seafloor at a proximal and a more distal position downstream of the PPV trial site, in concert with traps deployed on landers in order to record particle fluxes settling from the plume within certain proximities to the trial site. Another focus is on particle aggregation in the bottom boundary layer, assessed *in situ* by particle cameras, in relation to suspended particulate matter concentration determined by different types of turbidity sensors and turbulence determined from high-frequency ADV current measurements.

In addition to the static sensor array, AUV and ROV will be deployed for dynamic monitoring of the plume. Next to optical turbidity sensors, multibeam WCI technology and ADCP-backscatter on the ROV will track the sediment plume in real time, enabling adaptive monitoring (real-time data access via the ROV). The AUV will record turbidity along predefined vertical and lateral transects through the plume, using standard optical turbidity sensors and haze analysis of photos taken with HD camera along the transects. Data processing will be conducted directly on board to adapt the monitoring scheme if necessary and to support targeted sampling for sedimentological, geochemical and biological studies. To assess net deposition of sediment from the plume (blanketing), automated image analysis of photomosaics collected by AUV prior, during and after the disturbance experiment will be carried out, as well as advanced AUV-based multibeam backscatter analysis to quantify the extent and thickness of sediment blanketing. Resettled sediment thickness will also be constrained by placing checker boards with ruler sticks in the expected impact area to be photographed by ROV and AUV. These image-based analyses will be compared with results from physical and radionuclide analyses of sediment cores.

Fluorescent tracer material will be added to the sediment plume generated by the PPV by means of a diffusor. These environmentally-inert tracers are expected to disperse with the sediment plume and care will be taken to fabricate tracer particles that closely mimic the plume particle properties with respect to sinking speed and hydrodynamics. These experiments will be conducted prior to the PPV trial. The tracer itself can be detected up to several years after deployment and thus also enables tracing of secondary sediment suspension and redeposition. A rapid evaluation can already be carried out on board using fluorescence microscopy.

Modifying numerical models developed for shallow-water dredging plumes, and using turbidity sensor data from the direct vicinity of the collector trial area for validation and calibration, model simulations of the initial stages of the plume in the near-field of the PPV will be performed. Results from the comprehensive plume monitoring program and from experiments addressing sediment particle properties and ensuing evolution of sediment concentration and sediment deposition will enable project partners to calibrate and test the new flocculation module integrated in the numerical regional ocean circulation-sediment transport model developed during

the MiningImpact1 phase. The complete set of *in situ* / *ex situ* experiments will enable adaptation of the flocculation model of Winterwerp (1998) to the deep-sea environment and provide a suitable flocculation parameterisation applicable to other deep-ocean environments.

- Evolution of physical and chemical characteristics of the plume

This task addresses the physical and chemical characteristics of the plume, as well as its temporal and spatial evolution.

Laboratory experiments focusing on aggregation and hydrodynamic behaviour of particles in the plume will be carried out, if possible on board. Experiments will be conducted under *in situ* temperature and salinity conditions with sediments from the test site, using shear tanks, roller tanks and benthic resuspension chambers. Using different particle concentrations and turbulence regimes, optimal conditions for aggregate formation and thereby enhanced redeposition of plume particles will be determined. This should provide guidance for engineering solutions and operational practices to help reduce plumes formed in the wake of mining operations. In addition, the effect of seasonal phytodetritus falls on the removal and redeposition of fine-grained suspended sediment from the plume will be determined using isolated microalgae from the trial area cultivated on board, and with particle concentrations of 175-2000 mg L⁻¹ (as also used for discharge models of drill cuttings in the oil & gas industry by Norwegian authorities).

Potential mobilisation of trace metals in the plume and their bioavailability will be addressed. Plume samples (particles and surrounding water) will be collected using CTD/Niskin bottles and ROV in spatial and temporal gradients during and after the PPV trial. The samples will be analysed for major and trace element composition, as well as natural radionuclide concentrations. Laboratory experiments will study the sorption-desorption and dissolution-precipitation equilibria between plume particles and bottom water under defined conditions, e.g. redox, particle density, type and size of suspended particles. Of particular interest is the role of microbial interactions with plume particles on trace metal reactions, e.g. the role of heavy-metal-resistant bacteria, the role of particle aggregation in the plume on trace metal distributions, and the distribution of trace metals between different physical and chemical species and the role of colloids in transporting trace metals in the water column. A numerical model of trace metal reaction kinetics will be developed, using published data on reaction kinetics and integrating empirical results from the particle aggregation experiments described above. On the basis of the model, potentially toxic metal fluxes induced by mining activities might be predicted.

- Ecological impact of the plume

This task assesses the impact of the sediment plume and sediment deposition on biota, and integrates all impact data into a weight-of-evidence (WOE) model to classify potential environmental hazards.

Toxicity bioassays will focus on different endpoints (e.g. survival, reproduction, larval development) with different organisms (Bebianno et al., 2015; Simpson et al., 2016) such as *V. fischeri* bacteria, amphipods and/or bivalves. Results will be compared with those previously obtained from sediments and nodules from PA1, thus providing an overview of natural trace metal and other potentially toxic substances levels of the region. Collected specimens of representative faunal groups will be analysed for metal contents and for baseline biomarker levels indicative of oxidative stress, metal exposure, biotransformation, oxidative damage, and neurotoxicity (Mestre et al., 2017). In addition, the bioconcentration factor of "legacy" (referred to

as such on the unlikely assumption that these contaminants are no longer being added to the marine environment by other actors) contaminants (PCBs, PBDEs, organochlorine pesticides; extendable to PAHs and non-targeted screening) in the sediment plume and in amphipods (Lysianassidae), using techniques outlined in Jamieson et al. (2017), will be analysed. Metal contents, changes in molecular signaling pathways, epigenetic regulation and gene expression will be evaluated before and during plume generation.

Collected Anthozoans from areas exposed to the plume will be analysed to assess the response of the coral host to sedimentation. Anatomy and changes in the gonadal tissue within the mesoglea will be investigated by optical and electron microscopy (Waller and Baco, 2007; Hall-Spencer et al., 2007). In addition, the microbiome response to increased sedimentation will be assessed, using high-throughput 16S rRNA gene next-generation sequencing and transcriptomics (Hall-Spencer et al., 2007; Lawler et al., 2016) in order to describe (a) taxonomically or functionally conserved bacterial associates of the selected species, and (b) shifts in anthozoan microbiome composition and function in response to increased sediment load. Collected corals will also be subjected to condition index analyses, energy budget analysis (proteins, lipids, carbohydrates), and biomass measurements. *Ex situ* controlled aquarium experiments will test the impact of different concentrations of CCFZ sediments with and without POC using cold-water corals from the Azores region. Eco-physiological responses in aquaria will be compared with *in situ* octocoral responses to better understand the interaction between sediments and POC and determine the effect of sediment concentration thresholds on the physiology of these organisms.

A WHOI SyPRID plankton sampler (Billings et al., 2017) adapted to the ROV will be deployed to collect meroplankton (e.g. larvae) and zooplankton (e.g. copepods) inside and outside of the plume. SyPRID is a novel sampling device to obtain paired, large-volume plankton samples of well-preserved specimens at specified depths. Optical and electron microscopic analyses will assess physical damage to body parts, entanglement of particles with swimming structures, inclusion of particles in stomach contents, damage to feeding structures (e.g., mouth parts) and organs. These results, combined with those obtained in WP1, will represent the first data on larvae of CCFZ communities. If enough material is collected, the metal accumulation and biomarker levels will also be assessed. The SyPRID samples will also be used to assess the presence of resuspended benthic meiofauna in the plume. Changes in microbial community composition, functions and metabolic activities that occur when sediments are translocated within the plume will also be studied. The primary interest of these investigations is to follow the fate of resuspended organisms and the functions that they provide from source to sink, but data may also enable addressing effects of the resuspended matter and contaminants on the native microbial communities in bottom waters.

Short-term effects of exposure to sediment plumes will be investigated in deposit-feeding megafauna (e.g., holothurians), using benthic corrals (Brown et al., 2017) that will be deployed *in situ* by ROV over targeted specimens. Filter/deposit-feeder organisms and other components of the benthic community (prokaryotes, meio- and macrofauna) will be sampled close to the corral deployment locations before disturbance and within corrals after disturbance for analysis of bioaccumulation, biomarkers and guided *de novo* transcriptomes. In another *in situ* experiment, physiological responses of filter feeders exposed to sediment plumes will be investigated within CUBE benthic incubation chambers (slightly modified from Stratmann et al., in prep). The CUBEs will be placed by ROV over specimens of common filter-feeding species before and after the trial,

followed by respiration measurements and water sampled at pre-set time steps to detect changes in nutrient fluxes – from which changes in uptake or excretion by the organism can be assessed.

The environmental hazard at each sample location, including sites exposed to the plume, will be analysed using a quantitative weight-of-evidence (WOE) model (e.g. Bebianno et al., 2015; Mestre et al., 2017) that integrates data from different levels of evidence (LOE), such as sediment/plume chemistry, bioaccumulation/bioavailability, sub-lethal effects/biomarkers, bio-assay results. The WOE model will be applied to different sampling times, i.e. before impact, shortly after impact, and if additional ship-time is available, also 1-2 years after the impact, to provide insight into the temporal evolution of plume impact hazards.

7.2.3.1.3 Biogeochemistry and ecosystem functioning (WP3)

WP3 aims at assessing mining impacts on seafloor ecosystems with a focus on sediment physical characteristics (e.g., shear strength, porosity, diffusivity) and their effects on sediment biogeochemical characteristics, processes and fluxes (e.g., oxygen, nutrients, organic matter, metals) as well as ecosystem functions (e.g., organic matter remineralisation, element and energy transfer in food webs). Natural heterogeneity and as effects of direct (e.g., compaction, sediment and nodule removal) and indirect disturbance (sediment blanketing) will be addressed. Baseline investigations, particularly to fill the gaps in the existing data on the trial area, will be carried out prior to the trial. Effects of the impacts created by the PPV will be studied directly after the disturbance to assess severity and spatial extent of immediate effects and to establish a starting point for investigations of longer-term changes (secondary effects and recovery) during future post-impact expeditions. *Ex situ* analyses, shipboard incubations and land-based experiments using sediment samples obtained from ROV pushcores and deployments of the video-guided multicorer, gravity corer and boxcorer will be combined with *in situ* measurements and dedicated experiments performed directly at the seafloor.

Studies on the natural heterogeneity and on the effects of different impact types and intensities on biogeochemical processes and overall benthic ecosystem functions will be captured and harmonised with investigations carried out in WP1 and 2. In order to conduct comprehensive numerical simulations of the effects of the physical impact on biogeochemical functions / process rates and food webs, including prognostic modelling of their expected recovery, a comprehensive suite of biogeochemical variables is required, e.g., *in situ* studies of sediment geomechanical properties and benthic fluxes, radionuclide and stable isotope studies, food web experiments directly at the seafloor, and investigations of microbial and viral productivity and functions. As investigations will address freshly created impacts by a heavy PPV that probably involves significant sediment compaction and pore water expulsion, investigation will enable addressing effects that occur on shorter temporal scales and better represent realistic scenarios compared to studies in decade-old disturbances created with relatively small and light-weight gear. Furthermore, the PPV trial will, for the first time, enable representative investigations of secondary disturbance effects (i.e., sediment blanketing by resettling plume material) and preclude apparent recovery of biogeochemical conditions by lateral processes (e.g., diffusion and recolonisation) from areas in the direct vicinity of the disturbance tracks.

Knowledge obtained on the applicability of state-of-the-art instruments and methods and the relevance of the obtained data for assessing mining effects on seafloor ecosystems will contribute to a set of recommendations for monitoring and assessment (CCT3).

The work of WP3 is organised into five interconnected tasks:

- **Compaction effects on sediment physical properties and pore water expulsion**

This task assesses the physical impact associated with the PPV trial and its effect on key sediment properties, such as shear strength, compaction/porosity and diffusivity.

To investigate the mechanical response of the sediment to a vehicle with caterpillar propulsion in terms of compaction and pore water expulsion, geomechanical properties of the surface sediments will be determined before and after the PPV trial using a 'GraviProbe', an innovative geotechnical device provided by GSR for *in situ* analyses of the top 4 m of sediment. Using a combination of accelerometer with pressure sensor, natural variability and changes in static bearing strength of the sediments will be determined and compared to shear strength measurements performed in GEOMAR's high-pressure experiment lab (Deusner et al., 2016). Furthermore, effects on porosity and the effect of the reduced pore space on diffusion and sorption/desorption properties will be determined. Investigations will focus on trace metal behaviour and will include measurements of porosity and trace metal distribution in multicores and push cores, as well as experiments on trace metal diffusion in sediment slides of different porosity. Natural radium, thorium and actinium radioisotopes will be measured in samples obtained with bottom water samplers and *in situ* pumps to quantify the loss of pore water from the sediments during the PPV trial.

- **Assessment of sedimentation and bioturbation dynamics**

This task addresses sedimentation rates and bioturbation characteristics (depth, rate) as key factors of natural sediment deposition and reworking and key input parameters for diagenetic modelling (Task 3). Natural variabilities and impact effects will be addressed to quantify changes and to serve as a starting point for subsequent assessments of recovery.

Vertical distributions of natural and anthropogenic radionuclides in sediments will be analysed using multicores and push cores to assess rates of sediment accumulation and bioturbation, as well as the depth of the bioturbated layer. In cores taken directly from the trial site, this will enable quantifying the layers of sediment lost by disturbance or deposited from settling plumes. Studies focusing on different radionuclides in sediment solids and pore waters with different chemical properties and half-lives (^{226}Ra , ^{210}Pb , ^{137}Cs , ratios of $^{230}\text{Th}/^{231}\text{Pa}$, $^{234}\text{U}/^{238}\text{U}$) will be combined to address processes associated with different sediment compounds and different time scales. The studies will be complemented by high-resolution 3D X-ray imaging (Computed Tomography, CT) of intact cores sampled nearby. This will enable visualising and quantifying structures indicative of disturbance effects (e.g., exposed dense subsurface sediments, blanketing with unconsolidated plume sediments, cracks, buried nodule debris) and biogenic activity (e.g., macrofaunal burrows). CT analyses will be compared to geochemical and radionuclide data and validated with radionuclide analyses performed on samples from specific structures in selected cores.

- **Effects on sediment biogeochemistry (redox zonation, diagenetic fluxes, biogeochemical processes)**

This task quantifies the degree of change in sediment biogeochemical characteristics and diagenetic processes and fluxes and their footprints in comparison to natural variability observed at undisturbed sites. Investigations will be based on a comprehensive dataset of biogeochemical

process variables comprised of dissolved pore water and solid phase constituents and key isotopic signatures measured in sediment core samples collected by means of multicores, push cores, and gravity cores and will be complemented by *in situ* respiration measurements.

Extensive geochemical analyses of pore waters and solids including nutrients, the carbonate system, dissolved metals, major cations, sulphate and total sulphur, and isotopic ratios (e.g., of C, H, O, Sr and Li) will be carried out. One focus will be on the effects of sediment and nodule removal on pore water distributions of oxygen and nutrients, and on different Fe and Mn mineral phases. Fe and Mn reactivity will be addressed by sequential extraction and analyses of stable Fe isotopes. Analyses of the effects of sediment compaction on redox zonation and the distribution of elements, with special emphasis on trace metals and their dynamic biogeochemical reactions, will be investigated. This also includes investigation of N-isotopes and organic compounds (DOC, amino acids) indicative of organic matter degradation processes. Spectrophotometric/fluorometric methods will be applied to quantify organic compounds (e.g., phytopigments, proteins, carbohydrates, lipids, extracellular DNA concentrations), assess their bioavailability and contribution to Phosphorus cycling, as well as changes in response to the PPV impact. HPLC-based characterisation of phytopigments and fluorometric quantification of Chlorophyll α and phaeopigments will also be carried out on selected cores. Data on sediment biogeochemistry changes will inform experiments and contribute to biogeochemical model simulations.

Sample-based investigations will be complemented by *in situ* quantifications of diffusive and total benthic solute fluxes (primarily oxygen) to assess respiration rates as a proxy for microbial activity and organic matter remineralisation, using automated micro-profilers and benthic chambers deployed with autonomous lander platforms or as self-contained modules manipulated by ROV.

State-of-the-art numerical diagenetic modelling will help quantify processes and fluxes to identify key effects on biogeochemical ecosystem function and to predict the time scales required for the environment to return to its previous state. The geochemical data collected at discrete sites and corresponding model-derived rates and fluxes will be correlated with spatial information obtained from habitat and plume mapping procedures to estimate the overall impact of the PPV trial.

- **Effects on microbial ecology and functions**

This task assesses ecosystem functions of microbial communities as key components of benthic ecosystems in terms of biomass and their contribution to biogeochemical processes. Using a combination of molecular and microscopic methods with shipboard tracer incubations, key functions of microbial communities and viruses can be identified and quantified, and compared to the data obtained on biogeochemical processes (Task 3 above).

Microbial activity and biomass production will be determined using ^3H -labelled leucine and ^{14}C bicarbonate in both undisturbed and disturbed sediments. Additional measurements in ground nodule material will address the activity of nodule-specific microbial communities. Microbial activities will further be quantified (in terms of radiotracer incorporation and extracellular enzymatic activity) in samples taken from the sediment plume to investigate the effects on functions of microorganisms relocated from pristine surface sediments and of natural bathypelagic microbial communities. Rate measurements in sediments will be accompanied by microscopic quantifications of microbial abundance and biomass. In addition, molecular techniques for the quantification of microorganisms will be combined with measurements of

radiotracer uptake into microbial cells to assess the contribution of specific functional groups to overall microbial biomass production. Furthermore, shipboard incubations with fluorescent analogues of organic substrates will be carried out to determine potential activities of the main extracellular enzymes as a proxy for the degradation potential of organic matter by prokaryotes. Effects on virus productivity and virus-induced prokaryotic mortality (using epifluorescence and transmission electron microscopy) will also be assessed.

- Effects on ecosystem functioning

This task assesses the scale of the impact on benthic ecosystem functioning at the abyssal seafloor through *in situ* experiments and food web modelling with a focus on effects of the settling and re-suspension of plume material on organic matter processing. Experimental work will be carried out directly at the seafloor using open 'corrals' and sealed benthic enclosures ('CUBES') that are deployed by ROV. All experiments follow the pulse-chase approach, during which labelled particulate organic material (^{13}C and ^{15}N algae 'POM') or dissolved organic material (^{13}C labelled and ^{15}N 'DOM') is added to the enclosures. In this way, the transfer of matter and energy in benthic food webs can be assessed in taxa of all size classes with special emphasis on surface deposit and filter-feeding megafauna that are expected to be particularly affected by sediment blanketing and suspended matter loads. The analysis of the samples also involves ecotoxicological / transcriptome studies. Natural C and N stable isotope signatures of all the benthic assemblages will be quantified by isotope ratio mass spectrometry in undisturbed samples taken close to the impact site. In addition, the freshness of sedimentary organic matter will be determined at the experimental sites.

Corrals will be deployed before the PPV trial along the predicted gradient of settling plume material to investigate immediate effects of PPV-induced sedimentation on organic matter utilisation in benthic food webs, with a focus on holothurians as key deposit-feeding megafaunal organisms. The uptake of ^{13}C and ^{15}N -labelled POM added to the corrals will be quantified in holothurians and all other benthic organisms collected from the corrals. After the PPV trial, CUBEs will be deployed over sessile encrusting and stalked sponges and in control areas without sponges that have been exposed to different amounts of resettled plume material. ^{13}C and ^{15}N -labelled DOM will be added to address the effects on the uptake of DOM and the metabolic activity of sponges and other members of the benthic community. In addition to quantifications of uptake of labelled DOM by the microbial, meio-, macro- and megafaunal assemblages, total oxygen uptake will be determined by continuous oxygen monitoring in the overlying water and discrete samples for the determination of nutrient fluxes will be taken throughout the deployment. Additional deployments of CUBEs over sponges and sponge-free control areas that were subjected to thick plume sediment blanketing will be used to assess the effect of resuspended plume material on the physiology of sponges. Clouds of suspended sediment will be artificially created in the CUBEs by intense stirring or sediment injection. Changes in oxygen and nutrient fluxes will be determined throughout the incubation. Remineralisation of added labelled DOM and the alteration of its composition will be determined by ^{13}C -DIC measurements and fluorometric FDOM-scanning in water samples. Additionally, the uptake of labelled DOM will be quantified in sponges and all other benthic organisms collected from the CUBEs.

Results from the experiments described above will be combined with benthic biomass estimates (input from WP1) and assessments of organic matter freshness and biogeochemical process

rates (Task 3) in order to carry out model-based food web analyses. Linear inverse food web models that proved successful to assess disturbance effects in the DISCOL disturbance area during the first project phase (Stratmann et al., in prep) will be utilised with a focus on the effects of difference in nodule coverage and organic matter availability.

7.2.3.1.4 Plume monitoring and habitat/disturbance characterisation (CCT1)

Operational monitoring of deep-sea mining activities and of environmental impacts requires an integrated approach. The overall aim is to avoid (or at least minimise) the negative effects on the abyssal ecosystem, particularly to sensitive or rare fauna, outside the mined area. Real-time sensor-based monitoring which can be tied closely to monitoring operations is mainly performed with landers, ROVs, and increasingly with AUVs. MiningImpact 2 will apply these technologies as part of its environmental monitoring program around the PPV trial to provide more realistic information on the environmental footprints and consequences. This is a critical step forward, because upscaling of the “small-scale” experiments undertaken in the past, such as the Benthic Impact Experiment II (Brockett and Richards, 1994; Tsurusaki, 1997), the Japan Deep-Sea Impact Experiment (Barnett and Suzuki, 1997), and the IOM-BIE (Kotlinski and Stoyanova, 1998; Radziejewska, 2002), is very difficult, if not impossible.

The methodologies used so far in impact studies are often based on traditional sampling strategies, where data is collected with various sampling platforms (moorings, landers) and sensors, resulting in substantial temporal and spatial gaps. Little emphasis has been placed on integration of information between time periods of investigation, thus limiting the possibility to separate the impacts from overall natural variation in an area. Thus, a primary goal of CCT1 is to provide a guidance document on how monitoring of the seabed around mining operations should be performed. However, lack of standardisation of monitoring techniques in accordance with present knowledge and latest advances in technologies precludes comparison of the situation before mining, during mining, and after mining, creating challenges comparable to those pertaining to deep-water drilling (Purser and Thomsen, 2012). This further demonstrates the need for systematic and scientifically acceptable approaches, the utilisation of adequate sampling and observation technologies and the design of appropriate monitoring strategies. In addition to using cost-efficient technologies for real-time monitoring of plume dispersion and sediment resettling, the main bathymetric and oceanographic features of the MiningImpact 2. The proposed disturbance activity must be implemented in a predictive dispersion model to enable evaluating the likely transport pathways of sediments, thereby facilitating a much better positioning of monitoring gear. Particle aggregation processes, not taken into account in previous modelling exercises of mining-induced plumes, should be implemented in updated regional and near-field ocean circulation and sediment transport models. This will be supported by *in situ* observation and *ex situ* experiments addressing turbulence-induced particle aggregation in the bottom boundary layer, as well as scavenging of particles by seasonal phytodetritus falls (Thomsen and McCave, 2000; Pabortsava et al., 2011).

The JPI-O MiningImpact 2 project will investigate the dispersal of the test-related plume in great detail, complemented by *in situ* and *ex situ* sediment exposure studies. All field data from both *in situ* sensors and *ex situ* experiments will be transferred onshore to the physical oceanography partners to be fed into a near-field plume model which will be used for both ground-truthing of model results and to predict the plume dispersal under varying hydrodynamic conditions, which is a requirement for adaptive monitoring.

7.2.3.1.5 Disturbance effects in time and space (CCT2)

Polymetallic nodule mining will increase the pressure on abyssal ecosystems, which may lead to the loss of genetic and species diversity, the fragmentation of natural habitats and the degradation of ecosystem functions (Jones et al., 2017; Gollner et al., 2017). To inform (i) a clear and effective policy (e.g. by the ISA) to minimise impacts of future mining, and (ii) a sound environmental management plan for regions of interest in the Area, more insight is needed on the targeted ecosystem and its components (i.e. species populations and communities, habitats and ecosystem functions) to the effects of cumulative pressures that mining activities will exert on ecosystems and their components (Tamis et al., 2017). In particular in the CCFZ, more data are needed to quantify the impact of mining activities and to identify specific pressures and their cumulative effects on the vulnerability and recovery potential of the ecosystem.

The proposed monitoring of the PPV trial will enable description of the cumulative impact of different pressures resulting from mining activities on various ecosystem characteristics and identification of the sensitivity of different ecosystem components. A range of variables to identify the intensity of the impact will be assessed (pre- and post-disturbance) and correlated to different variables for ecosystem structure and function. For these purposes, a detailed analysis and integration of spatial and temporal variability in (bio)geochemistry, element fluxes, bioturbation, and sediment and pore water characteristics will be carried out, and the intensity of the observed changes after disturbance will be related to specific (combinations of) pressures compared to the observed variability in baseline environmental conditions. Similarly, a detailed analysis and integration of spatial and temporal variability in benthic communities (microorganisms, meio-, macro-, and megafauna) with respect to biodiversity, faunal abundances and biomass will be carried out, and the intensity of the observed changes after disturbance will be related to specific (combinations of) pressures compared to the observed variability in baseline benthic faunal conditions. Last but not least, the spatial and temporal variability in benthic ecosystem functions (e.g., organic matter processing, microbial growth, element and energy transfer in food webs) will be analysed in the same way. The integration of results obtained from the different work packages (WP1, 2 and 3) and CCT1 will be organised in different steps starting from a qualitative and semi-quantitative presentation and scoring of pressures on and responses by all ecosystem components. This initial step is a first broad-scale, low-detail assessment based on the available information and/or expert judgement and classification schemes (Tamis et al., 2017). The criteria for this assessment form an important part of this process and will be adapted from existing procedures from other marine ecosystems (Halpern et al., 2007; Knight et al., 2015). In a second step, a quantitative assessment of intensities of pressures on and responses by ecosystem components will be undertaken. This step is required for a focused, high-detail assessment based on functional relationships. This approach will generate measures of sensitivity based on both empirical data (evidence-based) and expert judgement (Stelzenmüller et al., 2015).

An environmental management plan for the CCFZ requires that pressures caused by mining activities on the marine ecosystem are kept within acceptable minimum levels. To identify these pressure levels many environmental assessment (EA) approaches are possible, but given the size of the area and the different stakeholders (contract holders), a harmonised and integrated EA approach is needed: one that considers cumulative impacts and at the same time is sufficiently evidence-based. Given the interactions of multiple stressors and pressures, an integrated assessment is required by combining multiple Lines of Evidence (LOE) that reflect

different biological, chemical and physical data (Bebianno et al., 2015; Caeiro et al., 2017; Mestre et al., 2017). The integration of LOE through Weight of Evidence (WOE) approaches is one of the tools developed for informed decision-making. Overall, a WOE approach is the process of considering strengths and weaknesses of different types of information and evidence to take a decision among competing alternatives.

It is important to assess the scale of analysis (sampling units, surface covered, distance of transects, etc.) and replication necessary to reveal ecologically significant patterns. Assessments of deep-sea diversity and community composition are observed to change with the scale analysed. At the temporal scale, ecotoxicological parameters can also identify sub-lethal effects in deep-sea fauna from hours of exposure to months or years (e.g. Mestre et al., 2017). Hence, a multiple-scale analysis is proposed in which the importance of the observation scale (both spatial and temporal) is put forward. The possibility of making predictions and extrapolations based on small observation windows for similar ecosystems and distances from the impact will be tested. Identification of thresholds and indicators is important for effective environmental management and monitoring of deep-water mining projects. Both ensure that consistent and representative environmental measurements are being obtained in monitoring programmes. There is little consensus on the appropriate indicators for deep-sea mining. Thus, the outcomes of experimental assessment here will be used to identify suitable indicators and to assess how they change in response to the impact.

7.2.3.2 Environmental monitoring program

7.2.3.2.1 Planning of the EMP layout around the collector trial (outlined in CCT1)

Based on the information from numerical oceanographic and sediment plume modelling exercises as outlined in section 5.1.3.2.2, Sediment transport modelling, pp. 133, the layout of the sampling and monitoring array in and around the Patania II trial area can be planned in advance. However, it will be susceptible to adaptation and change (through improvement and adaptation of the numerical plume models over time until the start of the project). In general the array will consist of 2 stationary landers (DOS and BoBo: equipped with CTDs, cameras, ADCPs, sediment traps) and short moorings with ADCP and CTDs, as well as bottom stations consisting of, e.g., sediment traps, upward-looking ADCPs, CTDs with optical sensors, particle cameras and ruler-boards (i.e., chess-boards with an upward-directed stick with millimetre marks, see WP2). Depending on availability of equipment, 13 to 16 monitoring stations will be prepared and distributed over a ~2 to 5 km² large monitoring array. Based on the results of pre-impact studies and the bottom current conditions at the time of the PPV trial, the EMP layout will be adjusted during the cruise, if necessary.

7.2.3.2.2 Cruise station time planning (outlined in CCT1)

The different partners of the JPI-O-Consortium will work in close collaboration with GSR and based on the results and recommendations that emerge from point (1) above, develop a detailed cruise plan that accounts for AUV and ROV survey times, biological, geological and biogeochemical field work, as well as deployment times for moorings. Technical pre-conditions for the PPV and safety issues for the two-vessel operation, as well as real-time communication will be prepared in dialogue with the JPI-O-Consortium. Monitoring technologies as outlined in the previous section will be prepared and large quantities of monitoring equipment and moored sensors must be precisely deployed and inter-calibrated at suitable facilities of partner institutions prior to the trial. The monitoring activities below will be subject to an optimized cruise station planning taking into account a repeat of the disturbance experiment in the BGR contract area.

7.2.3.2.3 On-site pre-impact assessment (outlined in WP1, 2, 3)

A coordinated approach of the pre-impact assessment within the designated zones is required. This will include sediment sampling to determine baseline sedimentological, geochemical and biological conditions, as well as improved habitat characterisation using statistical methods to make biological/optical sampling more effective with regard to habitat distribution.

Pre-impact assessment especially involves taking multicores for biological and geochemical analyses, video-surveying the seafloor, epibenthic sled and multicore deployment in the vicinity of the trial area and the deployment of 2 ADCP/RCM moorings and a sediment trap that will measure background current conditions close to the seafloor directly in the vicinity of the trial area and background particle fluxes in the water column to better contribute to predictive models for the dispersion of the sediment plume.

7.2.3.2.4 Small-scale *in situ* experiments related to plume behaviour (outlined in WP2 and 3)

A coordinated approach of *in situ* experiments and observations of the behaviour of small plumes produced by the ROV on the seafloor will help to determine changes in aggregation behaviour, including the effects of the injection of phytodetritus (local species cultivated on board), and dispersion of plumes of different sediment densities. This information will also be important to ground-truth particle data collected by camera.

7.2.3.2.5 Modelling to predict fallout areas (outlined in WP2)

In advance and during the disturbance experiment plume dispersion modelling will be performed based on the most recent HYCOM forecast forcing data to facilitate an adaptive monitoring effort. During execution, model results can be verified by newly obtained field data and observations.

7.2.3.2.6 *In situ* monitoring of the plume produced by the PPV trial (outlined in WP1, 2, 3)

A coordinated monitoring design for the quantification of plume concentration and dispersion will be developed that involves all previously mentioned technologies. Modelled plume behaviour will be ground-truthed and validated using stationary and mobile observations with ADCPs, Ocean Bottom Seismometer (OBS), cameras, particle cameras, tracer particle cameras. Important will be the use of a water column-imaging multibeam echo-sounder and parallel downward-looking ADCP on the ROV to actively map the distribution of the plume.

7.2.3.2.7 On-site post-impact assessment (outlined in WP1, 2, 3)

After the PPV trial, all monitoring activities of the pre-impact assessment will be repeated to determine the extent of the plume fallout area and the thickness of sediment blanketing, as well as the impact on fauna, microbial activity and biogeochemical conditions/processes. This will include the determination of blanketing effect/layer thickness by AUV-based imagery, possible changes in multi-beam backscatter intensity, measurement by ROV, and the observation of ruler-boards deployed before the experiment. In addition the resuspension and aggregation behaviour of freshly deposited plume particles, including introduced fluorescent particle tracers, will be investigated.

7.2.3.2.8 Evaluation of the effectiveness of the EMP workflow and monitoring technologies used (outlined in CCT1)

An evaluation of the workflow outlined above for the planning and execution of a plume/impact monitoring campaign will be carried out to assess its effectiveness in covering all important aspects and processes. The performance of the deployed sensors and platforms will be analysed with respect to, e.g., detection ranges of particle concentrations and determining the footprint and thickness of the deposited sediment blanket. A best practice guidance document on monitoring technology, layout scheme and workflow will be produced by the consortium in order to inform monitoring activities accompanying future mining trials.

7.2.3.2.9 Colonisation experiment (outlined in CCT2)

The feasibility of artificial hard substrates for restoration through time and space will be tested in the BGR area only. GSR supports the recolonization through the existing left in place natural resources. This can be monitored in the GSR area. A further holistic assessment is required on including artificial substrates into the natural environment.

7.2.3.2.10 Evaluation of mining-related pressures and effects on ecosystem components (outlined in CCT2)

A detailed analysis and integration of spatial and temporal variability in (i) (bio)geochemistry, element fluxes, bioturbation, and sediment and pore water characteristics, (ii) benthic communities, biodiversity, abundance and biomass, and (iii) benthic ecosystem functions, such as organic matter processing, microbial growth and food web structure, can be carried out, and the intensity of the observed changes after disturbance will be related to specific (combinations of) pressures compared to the observed variability in baseline environmental conditions. A quantitative assessment of intensities of pressures and responses of ecosystem components will be done. The aim is to carry out a focused, high-detail assessment of ecosystem components based on functional relationships, which will generate measures of sensitivity based on both empirical data (evidence-based) and expert judgement.

7.2.3.2.11 Development of tools for integrated (cumulative) environmental impact assessment (outlined in CCT2)

Robust approaches for ecological impact/risk assessment will be identified (e.g. Weight of Evidence approach [WOE]; Environmental Hazard and Impact Identification [ENVID]). A multiple-scale analysis to test the importance of the scale of sampling and observation (both spatial and temporal) for impact assessment will be performed. The types of impacts (compaction, nodule and/or surface sediment removal, blanketing, particle concentration and shape in the water column, toxicity, etc.) that have the largest effects on benthic communities and functions and determine the relevant 'intensity thresholds' (thickness of surface sediment mixed or lost, thickness of blanketing layer, etc.), will be identified. 'Indicator species' / 'indicator groups' / 'indicator functions' as a proxy for effects on specific parts of the benthic ecosystem (e.g., distinct taxonomic or functional groups, size classes), and distinct functions (e.g., organic matter remineralisation, bioturbation, element and energy transfer in food webs) and on the ecosystem in general (i.e. 'seafloor integrity') will be sought. All tools developed will contribute to new proposed methodologies for mining-related risk assessment and to develop concepts for monitoring impacts on the environment (i.e., environmental management tools).

7.3 Reporting

7.3.1 Monitoring

Reporting on the monitoring results is part of the objectives of the JPI-O MiningImpact 2 Project. The project is committed to organising, facilitating and effectively managing the archival of generated data and samples in databases with established structures and capabilities, such as PANGAEA and European museum collections, based on established protocols and best practices for research expeditions, the specific code of conduct for marine sciences, and the EU principles of data and knowledge sharing. Work package workshops and annual meetings will ensure the exchange of knowledge between project partners. Consortium members of the JPI-O MiningImpact 2 project make a commitment to publish their results in peer-reviewed scientific publications, and data and outcomes will be made publicly available in an appropriate time frame.

7.3.1.1 Data management

The project will generate huge volumes of data across all work packages and scientific disciplines. These comprise a large variety of different data types, such as acoustic data from e.g. multibeam and side-scan sonars and ADCPs, photo and video images from AUV, ROV and towed camera surveys, comprehensive datasets of a multitude of chemical compound concentrations in the water column and the sediment, faunal diversity and abundances, genetic information and microbial parameters.

The entire life cycle of data management from recording, processing, standardisation, consistency and technical quality assessment, to archiving of data needs to be covered. Tools, working plans, deployments and the ship's handling will be checked and controlled for potential environmental imprint on a regular daily basis; protocols of every deployment comprise notes on bottom time, sampling, biodiversity, geological setting, and oceanographic measurements and will be summarised in the cruise reports. Directly after the SONNE cruises, the ship's station list and all metadata from sampling and observations as well as raw and processed hydroacoustic data will be stored in the MaNIDA database, which is also accessible via the EMODnet data portals. GEOMAR will facilitate the long-term storage of the project data in the information system PANGAEA at the World Data Center for Marine Environmental Sciences (WDC-MARE) through its Ocean Science Information System (OSIS-Kiel). OSIS-Kiel will also be used for the sharing of datasets among project partners. PANGAEA is operated on a long-term basis by AWI and MARUM. All data will be geo- and time-referenced and deposited with a Digital Object Identifier (DOI) to make them citable and retrievable by library catalogues or Google Scholar. Data published within PANGAEA are provided through harvesting techniques for global distribution. These techniques include standard metadata exchange formats such as ISO19115, Dublin-Core and OAI-PMH. Two further features of PANGAEA are geo-referencing of data and establishing best-practice guidelines to allow efficient browsing in spatially and temporally organised data.

A project data policy will be generated to specify time schedules from data creation to internal project availability and final publication (time periods will be adjusted according to the scientific disciplines) in PANGAEA as well as general data use agreements. These data sharing modalities will achieve a stable research support environment for all project and collaborative partners and will guarantee the availability of the project data to the deep sea mining and scientific community beyond the project's life time.

All molecular data concerning fauna will be deposited in GenBank (overseen by Sol Genomics Network (SGN)). All sequencing data with the appropriate sets of metadata will be uploaded via GFBio to the European Nucleotide Archive (ENA) and PANGAEA. MPI will further upload all image and hydroacoustic OFOBS survey data to PANGAEA. Video data collected with OFOBS as well as other video-footage provided by project partners will be uploaded to the video annotation platform vidlib (vidlib.marum.de) for joint analysis by project members. This may be extended to other video-footage provided by project partners if needed, e.g. for comparison with the video annotation functionality added to BIIGLE 2.0.

7.3.1.2 Sample management

The distribution of samples taken for faunal analyses and the standardisation of sampling and processing techniques will be coordinated by the German Center for Marine Biodiversity Research (DZMB at SGN). After the life time of the project, participants will be asked to return

any non-needed samples and biological material to SGN for long-term storage. Holotypes of new species will be deposited in an appropriate collection of a European natural history museum (e.g. Natural History Museum in London, Muséum National D'Histoire Naturelle in Paris, Senckenberg in Frankfurt) and information on the fate of samples and specimens will be made available to SGN. Storage of microbial samples will take place at MPI. Sediment and pore water samples from collected cores will be stored in the GEOMAR core repository.

7.3.1.3 Data image analysis and archiving

A main objective of the project is to further develop the functionalities of the BIIGLE 2.0 image annotation software (Benthic Image Indexing, Graphical Labelling and Exploration) of the University of Bielefeld in order to cater for the increasing demand for sharing of knowledge and image data between partners (e.g., morphotype catalogues, annotation of videos, and integration of geospatial information or maps with annotation results such as species abundances).

The field of computational marine image analysis is rather novel. The ultimate aim of developing a fully generalizable, automated marine image annotation system appear unrealistic at this stage due to the strong variation in imaging conditions, large species' diversity and low per-species density. To make manual annotation through visual inspection by experts more efficient, different tools have been proposed in the last years, such as SQUIDLE, CATAMI, PAPARAZZI, ECOTAXA and BIIGLE. Although these systems provide valuable support for the annotation process, the integration of all the data (annotation, taxonomic catalogues, etc) across many institutes has not been adequately addressed so far.

Only very few annotation systems have been proposed for video annotation (e.g. VIDLIB, Adelie), even though the analysis of video data collected with ROV is one standard procedure in marine biology, environmental sciences or underwater infrastructure inspection. One special problem seems to be the lack of a clear general problem specification, like a definition of a labelling protocol and how to avoid a time consuming labelling of objects in multiple consecutive frames. This task could benefit from an integration of algorithmic solutions like machine learning to make video annotation more efficient.

In the first phase of the MiningImpact project, the focus was put on the development of DIAS, a first alpha-version of a mobile software for the annotation of marine image collections recorded with different platforms such as AUV, ROV or OFOBS during the expeditions with RV SONNE in 2015. After the cruises the DIAS system was merged with the already existing BIIGLE database to form a new online annotation database system BIIGLE 2.0 (Langenkämper et al., 2017) and used for annotation in the acquired image data.

In the proposed project MiningImpact 2, the aim is to address image analysis issues in a practical mining monitoring context and to develop methods to deal with problems related to temporal mining impact monitoring and posterior observation. The algorithmic basics and software structures for an advanced marine image analysis toolbox BIIGLE 2.0 will be developed by the University of Bielefeld. In all phases of mining we can expect that images with a variety of platforms such as OFOBS, AUV and ROV will be collected, but in the context of this project video data will play a role of greater significance as well as the evaluation of (time lapse) image sequences from camera-equipped underwater observatories (FUO) or landers. These large amounts of accumulating image and video data (with some images covering a visual footprint of approx. 400 m² per image) need to be evaluated and assessed, e.g. sediment plume patterns, habitat information (nodule abundance; associated fauna). The University of Bielefeld will

develop new video annotation capabilities for the BIIGLE 2.0 tool (Langenkämper et al., 2017), which is currently limited to still images only. To develop the video annotation tool, a number of studies with experienced users from marine biology will be carried out to carefully render the specifications for the tool. This includes data specification (e.g. volumes, codecs, etc.) as well as usability issues. In addition to the software development itself, general guidelines for video annotation will be set up, similar to those outlined for still images in the first project phase. A large part of this image and video evaluation is still done by human observers who shall jointly annotate regions of interest with pre-defined semantic categories, morphologies or taxonomies and integrate the annotation results with geospatial information.

In addition to the BIIGLE 2.0 system that is installed at partner institutes GEOMAR, SGN and the University of Bielefeld, the *mobile* BIIGLE 2.0 system will be used during cruises at sea. To support a flexible use not only of the image data but also of derived data, such as label trees and morphotype catalogues, all of these data need to be hosted by a global data server together with user ID and user information. It should be noted that such a server is not intended to become a new data repository itself (as these already exist, e.g. PANGAEA). The aim is to support collaboration and standardisation in annotation and to avoid redundancies at the local BIIGLE spots.

During mining operations the annotations and statistics of the objects and events in the images and videos must be analysed in a geospatial and temporal context. Thus, new interfaces and routines will be implemented that support a data fusion in the geospatial and/or temporal domain. These new integrated datasets enable users to browse and analyse the data from different perspectives, which is necessary to work on different scales in time (short/long-term impact) or space.

To link the annotation results to geographical information, a more sophisticated tool for geospatial visualisation, browsing and filtering will be implemented. Currently, BIIGLE 2.0 visualises the locations of the images using *OpenStreetmap*. Users can visualise images (e.g. selected according to a species abundance filter) at a geographical location or select images according to their geographical location for a detailed visualised inspection. The new module shall support users to plot this information on imported bathymetric maps or other kinds of maps. If video data is provided with geospatial information, geospatial gating or filtering through the map will also be supported.

7.3.1.4 Dissemination

In order to achieve effective dissemination of the project outcomes, an audience analysis will be performed by GRID-Arendal that will lead to an updated compilation of the existing stakeholder database. Dissemination and outreach will be carried out both in a passive (making information available) and an active (targeted events) way. Part of the outreach efforts will be devoted to disseminate to a high-level audience (e.g. decision-makers).

The ISA, as a partner in the MiningImpact 2 project, will organise targeted workshops on specific topics, such as spatial management, risk assessment, monitoring plans and technology, and environmental impacts. These are aimed at discussing and exchanging knowledge with ISA's contractors, policymakers, NGOs, the interested deep-sea mining industry, as well as countries planning offshore mining activities in their exclusive economic zones (EEZ). In addition, at least one Side Event at an ISA Annual Meeting in Jamaica is planned to present the project's results and policy recommendations to the ISA Council, LTC, contractors, mining industries, and NGOs.

International conferences, such as UMC, OMS, EGU, AGU and Goldschmidt, are good opportunities to inform the science community, but also industry and the general public about the project results. Special sessions at several conferences will be organised during the project's life time.

Outreach products are planned that explain deep-sea mining impacts on the environment to both a non-specialised and a specialised audience, such as policy stakeholders, who are interested in specific aspects of deep-sea mining. The content of these outreach products will be carefully selected so that they match the different purposes and audiences for which they will be produced. As part of this task, GRID-Arendal will develop a number of policy briefs in order to highlight the major research findings obtained through the project, explore policy options if suitable and provide recommendations on the best options. Supporting science to policy outreach and dissemination could also be served by innovative geospatial products like Story Maps. This will be determined as part of the audience analysis mentioned above.

The existing project website, consisting of public and secure internal areas, will be used for external, but also internal communication. The secure internal project website will be used as a vehicle to enhance communication between project partners including GSR and facilitate data management by providing entrance to PANGAEA and the OSIS-Kiel data portal. GRID-Arendal and GEOMAR will be responsible for updating and maintaining the website. These activities include publication of a project newsletter, press releases, and social media feeds running throughout the project's life-cycle. Updated information on project progress and developments in research, policy and industry related to deep-sea mining will be further disseminated, including social media activities. A project benchmarking system will be developed by GRID-Arendal at the onset of the project and this will be included in the internal protected area of the website to allow for internal monitoring and evaluation of progress (quality, time/cost) in the achievement of the project goals.

The project coordination at GEOMAR will organise annual meetings for all participants to present their results and discuss further joint data analyses and interpretation. As in the first project phase, interested stakeholders and policymakers will be invited to these meetings to foster knowledge exchange, but also help the project to focus on relevant issues, e.g. towards policy and regulations. Individual WP workshops will be organised by the respective WP leaders. In addition, the coordination will organise joint project reporting to JPI-Oceans and at the SONNE status seminar. Finally, a special issue publication of the main project results is envisioned in an internationally reviewed scientific journal, ideally with open-access policy, such as Biogeosciences.

Furthermore, An Advisory Board with broad stakeholder representation (final composition to be determined) will be set up to follow the Project and provide advice as necessary and assist with public outreach. The Board will be briefed at regular intervals by an independent academic rapporteur who is able to convey the progress of the Project, and ultimately its final results, in accessible language. The Rapporteur will be engaged from August 2018. An interim Report will be provided to the Advisory Board six months (i.e., in September 2019) after the first test, and the final Report 18 months (i.e., September 2020) after that first test.

7.3.2 Exploration and trials reporting

The work conducted during the coming expedition, the deep sea trials of Patania II, the exploration strategy and the results obtained will be reported as requested by the regulation 6 of

the Regulations on Prospecting and Exploration for Polymetallic Nodules in the Area (ISBA/19/C/17). As for each previous annual report submitted by GSR to the ISA, the structure of the “Recommendations for the Guidance of Contractors on the Content, Format and Structure of Annual Reports” issued by the Legal and Technical Commission (ISBA/21/LTC/15), and the technical results will be included in the *Part V: Mining tests and proposed mining technologies*. Furthermore, the environmental assessment conducted will be reported in the *Part IV: Environmental baseline studies (monitoring and assessment)*.

7.3.3 Incident reporting

Even if best practices are applied the future Patania II trials in the CCFZ, and critical accidental events have been anticipated (see paragraph 6, Accidental events and natural hazards, pp. 158), unexpected incidents are still possible when working offshore. Therefore, any incident arising from activities which have caused, are causing or pose a threat of serious harm to the marine environment will be reported by GSR to the Secretary-General in writing, using the most effective means, as required in the regulation 33, Emergency orders, paragraph 1 of the Regulations on Prospecting and Exploration for Polymetallic Nodules in the Area (ISBA/19/C/17).

8 Abbreviations

AGU	American Geophysical Union
ADCP	Acoustic Doppler Current Profiler
ADV	Acoustic Doppler Velocimeters
AES	atomic emission spectroscopy
ANOVA	Analysis Of Variance
AR	Annual Report
ATESEPP	Auswirkungen Technischer Eingriffe in Das Ökosystem Der Tiefsee Im Südpazifik Vor Peru
AUV	Autonomous Underwater Vehicle
BACI	Before-After Control Impact
BC	Boxcore
BGR	Bundesanstalt für Geowissenschaften und Rohstoffe (Federal Institute for Geosciences and Natural Resources)
BIE	Benthic Impact Experiment
BR	Burial Ratio
BS	Epibenthic sledge
BTM	Benthic Terrain Model
CAPEX	Capital Expenditure
CCT	Cross-Cutting Theme
CCZ	Clarion-Clipperton Zone
cDNA	complementary Deoxyribonucleic acid
CFD	Computational Fluid Dynamics
Chl a	Chlorophyll a
Co	Cobalt
COI	Cytochrome c oxidase subunit I
CSD	cutter suction dredge
CT scan	Computed Tomography scan
CTD	Conductivity Temperature Depth
Cu	Copper
D/I	Dense/Intermediate
ddPCR	new droplet digital PCR
DEME	Dredging, Environmental and Marine Engineering
DIC	Dissolved Inorganic Carbon

DIC	Dissolved Inorganic Carbon
DISCOL	Disturbance and recolonisation experiment
DNA	Deoxyribonucleic acid
DOM	Dissolved Organic Material
DSSRS	Deep Sea Sediment Resuspension System
DVL	Doppler Velocity Log
ECM	Earth Continuity Monitoring
ECMWF	European Centre for Medium-Range Weather Forecast Re-Analysis
eDNA	environmental Deoxyribonucleic acid
EEC	European Economic Community
EEZ	Exclusive Economic Zone
EGU	European Geosciences Union
EIA	Environmental Impact Assessment
EMMP	Environmental Management and Monitoring Plan
ENSO	El Niño-Southern Oscillation
ENVID	Environmental Hazard and Impact Identification
EU	European Union
FAT	Factory Acceptance Test
FDOM	Fluorescent Dissolved Organic Matter
Fe	Iron
FVT	Field Vane Test measurements
GEO	Geological
GP	GraviProbe
GSR	Global Sea Mineral Resources
HD	High Definition
HPU	Hydraulic Power Units
IA	Implementing Agreement
ICP	inductively coupled plasma
IFREMER	Institut Français de Recherche pour l'Exploitation de la MER (French Institute for Research and exploitation of the sea)
IMO	International Maritime Organization

Ind.	Individual
INDEEP	International Network for Scientific Investigations of Deep-Sea Ecosystems
INS	Inertial Navigation System
IOM	InterOceanMetal joint organization
IRZ	Impact Reference Zone
ISA	International Seabed Authority
ITCZ	Intertropical Convergence Zone
ITS	internal transcribed spacer
JET	Japan Deep-Sea Impact Experiment
JPI-Oceans	Joint Programming Initiative Healthy and Productive Seas and Oceans
LoC	Levels of Confidence
LOE	Levels/Lines Of Evidence
LOI	Loss of Ignition
LOSC	Law Of Sea Convention
LTC	Legal and Technical Commission
Maldi-TOF	matrix-assisted laser-desorption/ionization time-of-flight
MarBiol	Marine Biology Research Group (University of Ghent, Belgium)
MARPOL	International Convention for the Prevention of Pollution from Ships
MC	Monte Carlo
MGs	median grain size
MIDAS	Managing Impacts Of Deep Sea Resource Exploitation
Mn	Manganese
MODIS	MOderate-Resolution Imaging Spectroradiometer
MSCL	Multi-Sensor Core Logger
MSDS	Material Safety Data Sheet
MUC	Multicore
NEC	North Equatorial Current
NGO	Non-Governmental Organisation
NGS	next-generation sequencing
Ni	Nickel
NOAA	National Oceanic and Atmospheric Administration
NPP	Net Primary Productivity

NTU	Nephelometric Turbidity Unit
o.a	over all
OBS	ocean bottom seismometers
OD	Operational Days
ODT	Ocean Data Technologies
OECD	Organisation for Economic Co-operation and Development
OFOBS	Ocean Floor Observation and Bathymetry System
OMCO	Ocean Minerals Company
OMI	Ocean Management Inc.
OMS	Ocean Minerals Singapore
PAHs	Polycyclic aromatic hydrocarbons
PAT	Patania dive location
PBDEs	Polybrominated diphenyl ethers
PC	Particulate Carbon
PCA	Principal component analysis
PCBs	polychlorinated biphenyl
PIRZ	Plume Impact Reference Zone
PN	Particulate Nitrogen
POC	Particulate Organic Carbon
POM	Particulate Organic Material
PPV	Pre-Prototype Vehicle
PRZ	Preserved Reference Zone
PSU	Practical Salinity Unit
PU	Pick-Up
QHSE-S	Quality, Health and Safety, Environmental, Sustainability and Security
R&D	Research and Development
RALS	riser and lift system
RCM	Rotor Current Meters
RCMG	Renard Centre of Marine Geology (University of Ghent, Belgium)
REM	Rare, nodule-Endemic and Megafauna
RNA	Ribonucleic acid
ROV	Remotely Operated Vehicle
rRNA	Ribosomal ribonucleic acid
SC	Sediment sorting Coefficient
SD	Standard deviation

SGN	Sol Genomics Network
SIMPER	Similarity of percentage
SNP	Single Nucleotide Polymorphisms
SOG	Speed Over Ground
SOI	Southern Oscillation Index
SOV	Surface Operation Vessel
SPM	Suspended Particulate Matter
SSS	Side-scan sonar
TOC	Total Organic Carbon
TOM	Total Organic Matter
TON	Total Organic Nitrogen
TR	Transport
TSTD	Tracked Soil Testing Device
TV	Pocket Vane Test
UKSR	United Kingdom Seabed Resources

UMC	Underwater Mining Conference
UNCLOS	United Nations Convention of the Law of the Sea
USA	United States of America
USBL	Ultra-Short Baseline
WCI	water column imaging
WHOI	Woods Hole Oceanographic Institution
WOE	Weight Of Evidence
WP	Work Package
XRD	X-Ray Diffraction analysis
XRF	X-ray fluorescence
Y1	Year 1
Y2	Year 2
Y3	Year 3
Y4	Year 4

9 Study team

People	Expertise and affiliation
Tom De Wachter	GSR Environmental Manager
Kris De Bruyne	BDC Technical engineer
Harmen Stoffer	Auxilium Offshore Project Manager
François Charlet	GSR Exploration Manager
Céline Taymans	GSR Environmental Engineer
Charles Janssens	GIS Engineer
Boudewijn De Crop	Senior Consultant for IMDC

9.1 EIA specialist sub-consultants

People	Expertise and affiliation
Annemiek Vink	Bio-geologist at BGR (Germany)
Lisa Mevenkamp	Marine biology Post-Doctoral Researcher, UGent (Belgium)
Carmen Juan Valenzuela	Marine geologist Post-Doctoral Researcher, Ugent (Belgium)
Matthias Haeckel	Dr., Senior Scientist Biogeochemistry, GEOMAR Helmholtz Centre for Ocean Research Kiel (Germany)

9.2 JPI-O MiningImpact 2 Applicants

- **Matthias Haeckel**, Dr., Senior Scientist Biogeochemistry, 30.9.1969, German. Former proposals: e.g. 03F0707A, 03G0856A, 03F0734B, 03G0819A, 03G0687A, AZ31-13, MerMet15-121. GEOMAR Helmholtz Centre for Ocean Research Kiel, Wischhofstr. 1-3, 24148 Kiel. Tel: 0431-6002123, Fax: 0431-6002928, Email: mhaeckel@geomar.de
- **Jens Greinert**, Prof. Dr., Leader Deep-Sea Monitoring Group, 12.4.1966, German. Former proposals: 03F0707A. GEOMAR Helmholtz Centre for Ocean Research Kiel, Wischhofstr. 1-3, 24148 Kiel. Tel: 0431-6002590, Fax: 0431-6002928, Email: jgreinert@geomar.de

- **Sabine Kasten**, PD Dr., Senior Scientist Marine Geochemistry, 20.07.1963, German. Former proposals: 03F0707F, 03G0205C, KA 2769/3-1. Alfred-Wegener Institute Helmholtz Centre for Polar and Marine Research, Am Handelshafen 12, 27570 Bremerhaven. Tel: 0471-4831-1936, Fax: 0471-4831-1149, Email: sabine.kasten@awi.de
- **Andrea Koschinsky**, Prof. Dr., Professor of Geosciences, 05.04.1964, German. Former proposals: KO 2310/3-2/3, KO 2906/4-1/6-1, KO 2906/6-1, 03F0707G, 03G0229B, 03G0240C, 03G0253A. Jacobs University Bremen, Department of Physics and Earth Sciences, Campus Ring, D-28759 Bremen. Tel: 0421-200-3567, Fax: 0421-200-3229, Email: a.koschinsky@jacobs-university.de
- **Pedro Martínez Arbizu**, Prof. Dr., Head of German Centre of Marine Biodiversity Research. 20.05.1969, Spanish. Former proposals: MA2557/3-1, MA2557/4-1+2, MA2557/7-2, MA2557/8-1, 03F0707E, 03F0499A, Gz725-40003, 03G0205D. DZMB-Senckenberg am Meer, Südstrand 44, 26382 Wilhelmshaven. Tel: 04421-9475-100, Fax: 04421-9475-111, Email: pmartinez@senckenberg.de
- **Tim Wilhelm Nattkemper**, apl. Prof. Dr.-Ing., Akademischer Oberrat, 17.10.1968, German. Former proposals: 03F0707C, BE3280/3-1, GRK1906/1, BO1910/3-1. Technical Faculty, University of Bielefeld, Postfach 100131, 33501 Bielefeld. Tel: 0521-1066059, Fax: 0521-1066495, Email: tim.nattkemper@uni-bielefeld.de
- **Volker Steinbach**, Dr., Direktor und Professor, 16.04.1961, German. Bundesanstalt für Geowissenschaften und Rohstoffe, Stilleweg 2, 30655 Hannover. Tel: 0511-6432352, Fax: 0511-643532353, Email: volker.steinbach@bgr.de
- **Annemiek Vink**, Dr., Wiss. Rätin, 02.10.1972, Dutch. Former proposals: 03F0708A. Bundesanstalt für Geowissenschaften und Rohstoffe, Stilleweg 2, 30655 Hannover. Tel: 0511-6432392, Fax: 0511-643532353, Email: annemiek.vink@bgr.de
- **Maren Walter**, Dr., Senior Scientist Physical Oceanography, 1971, German. Former proposals: WA2556/1 WA2556/2-1+2 WA2556/4, 03S0514. MARUM Center for Marine Environmental Sciences, University Bremen, Otto-Hahn-Allee, 28359 Bremen. Tel: 0421-218-62147, Fax: 0421-218-65505, Email: maren.walter@uni-bremen.de
- **Frank Wenzhöfer**, Dr., Senior Scientist Benthic Ecology, 25.4.1969, German. Former proposals: WE-4111. HGF-MPG Group for Deep Sea Ecology and Technology, Max Planck Institute for Marine Microbiology, Celsiusstr. 1, 28359 Bremen. Tel: 0421-2028-862, Fax: 0421-2028-690, Email: frank.wenzhoefer@awi.de

10 Expert review

People	Expertise and affiliation
Philomène A. Verlaan	Oceanographer and attorney-at-law, JD PhD FIMarEST, Visiting Colleague, University of Hawai'i
Michel Hoffert	Specialized geologist in sedimentology, Teacher at the University Strasbourg 1 (France)
Ann Vanreusel	Head of the research group Marine Biology of Ghent University (Belgium)
Samantha Smith	Environmental Consultant at Blue Globe Solutions (Canada), co-author of several peer-reviewed journal articles related to the environmental management of the deep sea
Charles Morgan	Former President of IMMS, longtime worker in the area of seabed minerals, and 2015 IMMS Moore Medal Award recipient, has served as Professor Moore's successor since 1994 through 2015. From 2016 on, the technical chair of the conference is the standing president of IMMS.

11 References

11.1 Scientific literature

- Aguilar de Soto, N., Kight, C. (2016). Physiological effects of noise on aquatic animals. In: Solan, M., Whiteley, N.M. (Eds.), *Stressors in the Marine Environment*. Oxford University Press, Oxford, 135-158.
- Aleynik D., Inall M.E., Dale A. & Vink A. (2017). Impact of remotely generated eddies on plume dispersion at abyssal mining sites in the Pacific. *Sci. Rep.*, *7*(1), 16959, doi: 10.1038/s41598-017-16912-2.
- Amador, J. A., Alfaro, E. J., Lizano, O. G., & Magaña, V. O. (2006). Atmospheric forcing of the eastern tropical Pacific: A review. *Progress in Oceanography*, *69*(2), 101-142.
- Amos, A. F., and Roels, O. A. (1977). Environment aspects of manganese nodule mining. *Marine Policy* *1*, 156–163.
- Anderson, M. J., Gorley, R. N., and Clarke, K. R. (2008). PERMANOVA+ for PRIMER: guide for software and statistical methods. Plymouth: Primer-E Ltd
- Auguste, M., Mestre, N.C., Rocha, T.L., Cardoso, C., Cambon-Bonavita, M.A., Cueff-Gauchard, V., Le Bloa, S., Ravaux, J., Shillito, B., Zbinden, M., Bebianno, M.J. (2016). Development of an ecotoxicological protocol for the deep-sea fauna using the hydrothermal vent shrimp *Rimicaris exoculata*. *Aq. Tox.* *175*:277-285.
- Ballance, L.T., Pitman, R.L., Fiedler, P.C., 2006. Oceanographic influences on seabirds and cetaceans of the eastern tropical Pacific: A review. *Progress in Oceanography*, A Review of Eastern Tropical Pacific Oceanography *69*, 360–390. doi:10.1016/j.pocean.2006.03.013 *Bibcode:1998Sci...281..237F. doi:10.1126/science.281.5374.237. PMID 9657713.*
- Barnett, B., T. Suzuki (1997). The use of kringing to estimate resedimentation in the JET experiment. Proceedings, international symposium on environmental studies for deep-sea mining.
- Bebianno, M.J., Pereira, C.G., Rey, F., Cravo, A., Duarte, D., D'Errico, G., Regoli, F. (2015). Integrated approach to assess ecosystem health in harbor areas. *Sci. Total Env.* *514*, 92-107.
- Bik, H.M., Porazinska, D.L., Creer, S., Caporaso, J.G., Knight, R., Thomas, WK. (2012). Sequencing our way towards understanding global eukaryotic biodiversity. *Trends in Ecology & Evolution* *27*, 233-243.
- Billings, A., Kaiser, C., Young, C.M., et al. (2017). SyPRID sampler: A large-volume, high-resolution, autonomous, deep-ocean precision plankton sampling system. *Deep-Sea Res II* *137*, 297-306.
- Bluhm, H. (2001). Re-establishment of an abyssal megabenthic community after experimental physical disturbance of the seafloor. *Deep-Sea Research II*, *48*, 3841-3868.
- Boetius A. (ed.) (2015). RV SONNE Cruise Report SO242-2: JPI OCEANS Ecological Aspects of Deep-Sea Mining, DISCOL Revisited. GEOMAR Report 27, 552 pp.
- Boetius, A., Ferdelman, T., & Lochte, K. (2000). Bacterial activity in sediments of the deep Arabian Sea in relation to vertical flux. *Deep Sea Research Part II: Topical Studies in Oceanography*, *47*(14), 2835-2875.

- Boetius, A., Wenzhöfer, F. (2009). In Situ Technologies for Studying Deep-Sea Hotspot Ecosystems. *Oceanography* 22, 177.
- Brockett, T., Richards, C.Z. (1994). Deep-sea mining simulator for environmental impact studies. *Sea Technology* 35 (8), 77-82.
- Brown, A., Wright, R., Mevenkamp, L., Hauton, C. (2017). A comparative experimental approach to ecotoxicology in shallow-water and deep-sea holothurians suggests similar behavioural responses. *Aquatic Toxicology*. doi:10.1016/j.aquatox.2017.06.028.
- Burchard H., Bolding K. & Villarreal M.R. (1999). GOTM, a general ocean turbulence model: theory, implementation and test cases. Space Applications Institute.
- Burford-Reiskind, M. O., Coyle, K., Daniels, H. V., Labadie, P., Reiskind, M. H., Roberts, N. B., Roberts, R. B., Schaff, J., Vargo, E.L. (2016). Development of a universal double-digest RAD sequencing approach for a group of nonmodel, ecologically and economically important insect and fish taxa. *Mol. Ecol. Resour.* 16, 1303-1314.
- Burritt, D.J., Lamare, M.D. (2016). The cellular responses of marine algae and invertebrates to ultraviolet radiation, alone and in combination with other common abiotic stressors. In: Solan, M., Whiteley, N.M. (Eds.), *Stressors in the Marine Environment*. Oxford University Press, Oxford, pp. 117e134.
- Bussau, C., Schriever, G., and Thiel, H. (1995). Evaluation of abyssal metazoan meiofauna from a manganese nodule area of the Eastern South Pacific. *Vie Milieu* 45, 39–48.
- Caeiro, S., Vaz-Fernandes, P., Martinho, A.P., Costa, P.M., Silva M.J., Lavinha J., et al. (2017). Environmental risk assessment in a contaminated estuary: an integrated weight of evidence approach as a decision support tool. *Ocean & Coast. Manag.* 143, 51-62.
- Chamley, H., 1989. *Clay sedimentology*. Springer, Berlin.
- Chamley, H., 1997. Clay mineral sedimentation in the ocean, *Soils and Sediments*. Springer, pp. 269- 302.
- Chassignet E.P., Hurlburt H.E., Smedstad O.M., Halliwell G.R., Hogan P.J., Wallcraft A.J., Baraille R. & Bleck R. (2007). The HYCOM (HYbrid Coordinate Ocean Model) data assimilative system. *J. Mar. Syst.*, 65(1–4), 60–83, doi: 10.1016/j.jmarsys.2005.09.016.
- Chavez, F. P., Buck, K. R., Service, S. K., Newton, J., and Barber, R. T. (1996). Phytoplankton variability in the central and eastern tropical Pacific. *Deep Sea Research Part II: Topical Studies in Oceanography* 43, 835–870. doi:10.1016/0967-0645(96)00028-8.
- Clarke, K. R., and Gorley, R. N. (2006). User manual/tutorial. *PRIMER-E Ltd., Plymouth*.
- Contreras R.F. (2002). Long-Term Observations of Tropical Instability Waves. *J. Phys. Oceanogr.*, 32(9), 2715–2722, doi: 10.1175/1520-0485(2002)032<2715:LTOOTI>2.0.CO;2.
- Copano, C., 1984. Les Nodules Du Pacifique Central Dans Leur Environnement Géologique, Résultats des campagnes a la mer. Centre National pour l'Exploration des Océans.
- Cordes, E.E., Jones, D.O., Schlacher, T.A., Amon, D.J., Bernardino, A.F., Brooke, S., Carney,
- Corinaldesi C., Barucca M., Luna G.M., Dell'Anno A. (2011). Preservation, origin and genetic imprint of extracellular DNA in permanently anoxic deep-sea sediments. *Molecular Ecology* 20, 642-654.

- Corinaldesi C., Beolchini F., Dell'Anno A. (2008). Damage and degradation rates of extracellular DNA in marine sediments: implications for the preservation of gene sequences. *Molecular Ecology* 17, 3939-3951.
- Corinaldesi C., Danovaro R., Dell'Anno A. (2005). Simultaneous recovery of extracellular and intracellular DNA suitable for molecular studies from marine sediments. *Applied and Environmental Microbiology* 71, 46-50.
- Dahl, Peter H., et al. "Underwater ambient noise." *Acoustics Today* 3.1 (2007): 23-33.
- Dahlgren, T.G., Wiklund, H., Rabone, M., Amon, D.J., Ikebe, C., Watling, L., Smith, C.R., Glover, A.G. (2016). Abyssal fauna of the UK-1 polymetallic nodule exploration claim, Clarion-Clipperton Zone, central Pacific Ocean: Cnidaria. *Biodiversity Data Journal* 4, e9277.
- Danovaro R. (2010). *Methods for the Study of Deep-Sea Sediments, Their Functioning and Biodiversity*. CRC Press, Taylor & Francis Group.
- De Smet, B., Pape, E., Riehl, T., Bonifácio, P., Colson, L., and Vanreusel, A. (2017). The Community Structure of Deep-Sea Macrofauna Associated with Polymetallic Nodules in the Eastern Part of the Clarion-Clipperton Fracture Zone. *Front. Mar. Sci.* 4. doi:10.3389/fmars.2017.00103.
- Dee, D. P., Uppala, S. M., Simmons, A. J., Berrisford, P., Poli, P., Kobayashi, S., ... & Bechtold, P. (2011). The ERA-Interim reanalysis: Configuration and performance of the data assimilation system. *Quarterly Journal of the royal meteorological society*, 137(656), 553-597.
- Dell'Anno A., Danovaro R. (2005). Extracellular DNA plays a key role in deep-sea ecosystem functioning. *Science* 309, 2179.
- DeLong, E.F. (2005). Microbial community genomics in the ocean, *Nature Reviews Microbiology* 3 (6), 459-469.
- Deming, J. W., & Carpenter, S. D. (2008). Factors influencing benthic bacterial abundance, biomass, and activity on the northern continental margin and deep basin of the Gulf of Mexico. *Deep Sea Research Part II: Topical Studies in Oceanography*, 55(24-26), 2597-2606.
- Deusner C., Kossel E., Bigalke N., Haeckel M., Gupta S., Freise M., Anbergen H., Wille T. (2016). The role of high-pressure flow-through experiments for evaluating the mechanical behaviour of gas hydrate-bearing soils. In: Wuttke, Bauer, Sanchez (eds.) *Energy Geotechnics*. CRC Press, 437-443.
- DNV.GL (2016). Recommended Practice. Managing environmental aspects and impacts of seabed mining. DNV GL-RP-O601 Edition September 2016.
- Doi, H., Takahara, T., Minamoto, T., Matsushashi, S., Uchii, K., Yamanaka, H. (2015). Droplet digital polymerase chain reaction (PCR) outperforms real-time PCR in the detection of environmental DNA from an invasive fish species. *Environmental Science & Technology* 49 (9), 5601-5608.
- Dreutter, S. (2017). Multisensor microbathymetric habitat mapping with a deep-towed ocean floor observation and bathymetry system (OFOBS). Master Thesis, HafenCity University Hamburg.
- Du Castel, V., 1985. Etablissement d'une carte géologique au 1/20.000 d'un domaine océanique profond dans une zone riche en nodules polymétalliques du Pacifique Nord (zone Clarion-Clipperton), *Geosciences: Geodynamique, Geophysique et Geochemie des oceans*. Université de Bretagne Occidentale, Brest.

- Egbert G.D. & Erofeeva S.Y. (2002). Efficient Inverse Modeling of Barotropic Ocean Tides. *J. Atmospheric Ocean. Technol.*, **19**(2), 183–204, doi: 10.1175/1520-0426(2002)019<0183:EIMOB>2.0.CO;2.
- Eppley, R. W., Chavez, F. P., and Barber, R. T. (1992). Standing stocks of particulate carbon and nitrogen in the equatorial Pacific at 150 W. *Journal of Geophysical Research: Oceans* **97**, 655–661.
- Fagel, N., 2007. Clay Minerals, Deep Circulation and Climate, pp. 139-184.
- Fiedler, P. C., & Talley, L. D. (2006). Hydrography of the eastern tropical Pacific: a review. *Progress in Oceanography*, **69**(2-4), 143-180.
- Field, C.B.; Behrenfeld, M.J.; Randerson, J.T.; Falkowski, P. (1998). "Primary production of the Biosphere: Integrating Terrestrial and Oceanic Components". *Science*. **281**(5374): 237–240.
- Fukushima, T. (1995). Overview: Japan deep-sea impact experiment = JET. Proceedings of the first ISOPE Ocean Mining Symposium, Tsukuba, Japan, 47-53.
- Gardner, W.D., Sullivan, L.S., Thorndike, E.M. (1984). Long-term photographic, current, and nephelometer observations of manganese nodule environments in the Pacific. *Earth and Planetary Science Letters* **70** (1), 95-109.
- Glover, A., Dahlgren, T.G., Wiklund, H., Mohrbeck, I., Smith, C.R. (2015). An End-to-End DNA Taxonomy Methodology for Benthic Biodiversity Survey in the Clarion-Clipperton Zone, Central Pacific Abyss. *Journal of Marine Science and Engineering* **4** (1), 2.
- Glover, A., Wiklund, H., Rabone, M., Amon, D., Smith, C., O'Hara, T., Mah, C.L., Dahlgren, T.G. (2016b). Abyssal fauna of the UK-1 polymetallic nodule exploration claim, Clarion-Clipperton Zone, central Pacific Ocean: Echinodermata. *Biodiversity Data Journal* **4**: e7251–48.
- Goineau, A., and Gooday, A. J. (2017). Novel benthic foraminifera are abundant and diverse in an area of the abyssal equatorial Pacific licensed for polymetallic nodule exploration. *Sci Rep* **7**. doi:10.1038/srep45288.
- Gollner, S., Kaiser, S., Menzel, L., Jones, D.O.B., Brown, A., Mestre, N.C., van Oevelen, D., Menot, L., Colaco, A., Canals, M., Cuvelier, D., Durden, J.M., Gebruk, A., Egho, G.A., Haeckel, M., Marcon, Y., Mevenkamp, L., Morato, T., Pham, C.K., Purser, A., Sanchez-Vidal, A., Vanreusel, A., Vink, A., Martinez Arbizu, P. (2017). Resilience of benthic deep-sea fauna to mining activities. *Marine Environmental Research* **129**, 76-101.
- Gooday, A. J., Holzmann, M., Caille, C., Goineau, A., Kamenskaya, O., Weber, A. A.-T., et al. (2017). Giant protists (xenophyophores, Foraminifera) are exceptionally diverse in parts of the abyssal eastern Pacific licensed for polymetallic nodule exploration. *Biological Conservation* **207**, 106–116. doi:10.1016/j.biocon.2017.01.006.
- Greiner J. (ed.) (2015). RV SONNE Cruise Report SO242-1: JPI OCEANS Ecological Aspects of Deep-Sea Mining, DISCOL Revisited. GEOMAR Report 26, 290 pp.
- Haddock, S. H., Moline, M. A., & Case, J. F. (2009). Bioluminescence in the sea.
- Haeckel, M., and Arbizu, P. M. (2015). RV SONNE Fahrtbericht / Cruise Report SO239: EcoResponse Assessing the Ecology, Connectivity and Resilience of Polymetallic Nodule Field Systems, Balboa (Panama) – Manzanillo (Mexico,) 11.03.-30.04.2015. Kiel.
- Haeckel, M., van Beusekom, J., Wiesner, M., König, I. (2001b). The impact of the 1991 Mount Pinatubo tephra fallout on the geochemical environment of the deep-sea sediments in the South China Sea. *Earth and Planetary Science Letters* **193**, 153-168.

- Haeckel, M., König I., Riech V., Weber M. E., Suess E. (2001a). Pore water profiles and numerical modelling of biogeochemical processes in Peru Basin deep-sea sediments. *Deep-Sea Research II* 48 (17–18), 3713-3736.
- Halbach P, Friedrich G, von Stackelberg U (1988). The manganese nodule belt of the Pacific Ocean. Enke, Stuttgart, p 254
- Hall-Spencer, J.M., Pike, J., Munn, C.B. (2007). Diseases affect cold-water corals too: *Eunicella verrucosa* (Cnidaria: Gorgonacea) necrosis in SW England. *Diseases of aquatic organisms* 76 (2), 87-97.
- Halpern, B.S., Selkoe, K.A., Micheli, F., Kappel, C.V. (2007). Evaluating and ranking the vulnerability of global marine ecosystems to anthropogenic threats. *Conserv Biol* 21, 1301-1315.
- Heezen, B.C., Hollister, C., 1964. Deep-sea current evidence from abyssal sediments. *Marine Geology* 1, 141-174.
- Hervouet J.-M. (2007). *Hydrodynamics of Free Surface Flows*. John Wiley & Sons, Ltd, Chichester, UK.
- Hervouet J.-M., Pavan S. & Ata R. (2015). Distributive advection schemes and dry zones, new solutions. Telemac User Conference, STFC Daresbury Laboratory, UK,.
- Hess, S., & Kuhnt, W. (1996). Deep-sea benthic foraminiferal recolonization of the 1991 Mt. Pinatubo ash layer in the South China Sea. *Marine Micropaleontology*, 28(2), 171-197.
- Hobson, K. A., and Welch, H. E. (1992). Determination of trophic relationships within a high Arctic marine food web using $\delta^{13}\text{C}$ and $\delta^{15}\text{N}$ analysis. *Marine Ecology Progress Series* 84, 9–18.
- Hoffert, M., 2008. Les nodules polymétalliques dans les grands fonds océaniques: une extraordinaire aventure minière et scientifique sous-marine. Société géologique de France.
- Hollister, C.D., Elder, R.B., 1969. Contour currents in the Weddell Sea, *Deep Sea Research and Oceanographic Abstracts*. Elsevier, pp. 99-101.
- Iken, K., Brey, T., Wand, U., Voigt, J., and Junghans, P. (2001). Food web structure of the benthic community at the Porcupine Abyssal Plain (NE Atlantic): a stable isotope analysis. *Progress in Oceanography* 50, 383–405. doi:10.1016/S0079-6611(01)00062-3.
- Jackett D.R., McDougall T.J., Feistel R., Wright D.G. & Griffies S.M. (2006). Algorithms for Density, Potential Temperature, Conservative Temperature, and the Freezing Temperature of Seawater. *J. Atmospheric Ocean. Technol.*, 23(12), 1709–1728, doi: 10.1175/JTECH1946.1.
- Jamieson, A. J., Malkocs, T., Piertney, S. B., Fujii, T., Zhang, Z. (2017). Bioaccumulation of persistent organic pollutants in the deepest ocean fauna. *Nature Ecology and Evolution* 1, 1-4.
- Jankowski Kim, J., Hyeong, K., Lee, H.-B., Ko, Y.-T., 2012. Relationship between polymetallic nodule genesis and sediment distribution in the KODOS (Korea Deep Ocean Study) Area, Northeastern Pacific. *Ocean Science Journal* 47, 197-207
- Jankowski, J. A., Malcherek, A., & Zielke, W. (1996). Numerical modeling of suspended sediment due to deep-sea mining. *Journal of Geophysical Research: Oceans*, 101(C2), 3545-3560.
- Jankowski, J., Zielke, W. (2001). The mesoscale sediment transport due to technical activities in the deep sea. *Deep Sea Research Part II: Topical Studies in Oceanography* 48 (17), 3487-3521.

- Janssen, F., Vonnahme, T., Molari, M., Wenzhöfer, F., Haeckel, M., Boetius, A. (2017). Effects of experimental polymetallic nodule mining on deep-sea microbial communities and functions (DISCOL experimental area, tropical SE Pacific), Goldschmidt Conference, Paris, 14-18.8.2017.
- Jones, D.O.B., Kaiser, S., Sweetman, A.K., Smith, C.R., Menot, L., Vink, A., Trueblood, D., Greinert, J., Billett, D.S.M., Arbizu, P.M., Radziejewska, T., Singh, R., Ingole, B., Stratmann, T., Simon-Lledó, E., Durden, J.M., Clark, M.R. (2017). Biological responses to disturbance from simulated deep-sea polymetallic nodule mining. *PLoS One* 12 (2), e0171750, 10.1371/journal.pone.0171750.
- Kaneko, T., Maejima, Y., Teishima, H., 1997. The abundance and vertical distribution of abyssal benthic fauna in the Japan deep-sea impact experiment. In: Proceedings of the VII Ocean Mining Symposium, Honolulu, USA, May 25–30, pp. 475–479.
- Kessler, W. S. (2006). The circulation of the eastern tropical Pacific: A review. *Progress in Oceanography*, 69(2-4), 181-217.
- Knight, A.M., Piet, G.J., Jongbloed, R.H., Tamis, J.E., White, L., Akoglu, E., Boicenco, L., Churilova, T., Kryvenko, O., Fleming-Lehtinen, V. et al. (2015). An exposure-effect approach for evaluating ecosystem-wide risks from human activities. *ICES J. Mar. Sci.* Available from: DOI: 10.1093/icesjms/fsu245.
- Koehl, M., 1982. The interaction of moving water and sessile organisms. *Sci. Am* 247, 124-134.
- Koehl, M.A.R., 1984. How Do Benthic Organisms Withstand Moving Water? *American Zoologist* 24, 57- 70.
- Kontar, E.A., Sokov, A.V. (1994). A benthic storm in the northeastern tropical Pacific over the fields of manganese nodules. *Deep Sea Research Part I: Oceanographic Research Papers* 41 (7), 1069-1089.
- Kotlinski, R., Stoyanova, V. (1998). Physical, Chemical, and Geological Changes of Marine Environment Caused By the Benthic Impact Experiment At the 10M BIE Site. The 8th International Offshore and Polar Engineering Conference, International Society of Offshore and Polar Engineers.
- Kutti, T., Bannister, R.J., Foss, J., Krogness, C.M., Tjensvoll, I., Søvik, G. (2015). Metabolic responses of the deep-water sponge *Geodia barretti* to suspended bottom sediment, simulated mine tailings and drill cuttings. *Journal of Experimental Marine Biology and Ecology* 473, 64-72.
- Laakmann, S., Gerdts, G., Erler, R., Knebelsberger, T., Martínez-Arbizu, P., Raupach, M.J. (2013). Comparison of molecular species identification for North Sea calanoid copepods (Crustacea) using proteome fingerprints and DNA sequences. *Molecular Ecology Resources* 13, 862-876.
- Lalot E., Curie F., Wawrzyniak V., Baratelli F., Schomburgk S., Flipo N., Piegay H. & Moatar F. (2015). Quantification of the contribution of the Beauce groundwater aquifer to the discharge of the Loire River using thermal infrared satellite imaging. *Hydrol Earth Syst Sci*, 19(11), 4479–4492, doi: 10.5194/hess-19-4479-2015.
- Landry, M.R., Kirchman, D.L., 2002. Microbial community structure and variability in the tropical Pacific. *Deep Sea Research Part II: Topical Studies in Oceanography, The Equatorial Pacific JGOFS Synthesis* 49, 2669–2693. doi:10.1016/S0967-0645(02)00053-X, M. F., Fiedler, P. C.,

- Amador, J. A., Ballance, L. T., Färber-Lorda, J., & Mestas-Núñez, A. M. (2006). A review of eastern tropical Pacific oceanography: Summary. *Progress in Oceanography*, 69(2), 391-398.
- Langenkämper D., Zurowietz M., Schoening T., Nattkemper T.W. (2017). BIIGLE 2.0 - browsing and annotating large marine image collections. *Frontiers in Marine Science* 4, 83.
- Large W.G., McWilliams J.C. & Doney S.C. (1994). Oceanic vertical mixing: A review and a model with a nonlocal boundary layer parameterization. *Rev. Geophys.*, 32(4), 363–403.
- Larsson, A.I., van Oevelen, D., Purser, A., Thomsen, L. (2013). Tolerance to long-term exposure of suspended benthic sediments and drill cuttings in the cold-water coral *Lophelia pertusa*. *Marine Pollution Bulletin* 70 (1-2), 176-188.
- Lavelle, J., Ozturgut, E., Swift, S., Ericson, B. (1981). Dispersal and resedimentation of the benthic plume from deep-sea mining operations: a model with calibration. *Marine Mining* 3 (1/2), 59-93.
- Lawler, S. N., Kellogg, C. A., France, S. C., Clostio, R. W., Brooke, S. D., Ross, S. W. (2016). Coral-Associated Bacterial Diversity Is Conserved across Two Deep-Sea Anthothela Species. *Frontiers in Microbiology* 7 (14), doi:10.3389/fmicb.2016.00458.
- LEE, Sang HOON et KIM, Ki-Hyune. Side-Scan Sonar Characteristics and Manganese Nodule Abundance in the Clarion—Clipperton Fracture Zones, NE Equatorial Pacific. *Marine Georesources and Geotechnology*, 2004, vol. 22, no 1-2, p. 103-114.
- Lekang, K., Thompson, E. M., Troedsson, C. (2015). A comparison of DNA extraction methods for biodiversity studies of eukaryotes in marine sediments. *Aquatic Microbial Ecology* 75 (1), 15-25.
- Lim, S.C., Wiklund, H., Glover, A.G., Dahlgren, T.G., Tan, K.S. (2017). A new genus and species of abyssal sponge commonly encrusting polymetallic nodules in the Clarion-Clipperton Zone, East Pacific Ocean. *Systematics and Biodiversity*, 1-13.
- Marchesiello P., Capet X., Menkes C. & Kennan S.C. (2011). Submesoscale dynamics in tropical instability waves. *Ocean Model.*, 39(1–2), 31–46, doi: 10.1016/j.ocemod.2011.04.011.
- Marcon, Y., Purser, A. (2017). PAPARA(ZZ)I: An open-source software interface for annotating photo-graphs of the deep sea. *SoftwareX* 6, 69-80.
- Martínez-Arbizu P., Haeckel M. (2015). RV SONNE Cruise Report SO239: EcoResponse Assessing the Ecology, Connectivity and Resilience of Polymetallic Nodule Field Systems. GEOMAR Report 25, 204 pp.
- McCave, I.N., Hall, I.R. (2006). Size sorting in marine muds: Processes, pitfalls, and prospects for paleoflow-speed proxies. *Geochemistry, Geophysics, Geosystems*, doi: 10.1029/2006GC001284.
- McKenna, Megan F., et al. "Underwater radiated noise from modern commercial ships." *The Journal of the Acoustical Society of America* 131.1 (2012): 92-103.
- McKenney, B.A., Kiesecker, J.M. (2010). Policy Development for Biodiversity Offsets: A Review of Offset Frameworks. *Environmental Management* 45,165-176.
- Mestre, N.C., Rocha, T.L., Canals, M., Cardoso, C., Danovaro, R., Dell'Anno, A., Gambi, C., Regoli, F., Sánchez-Vidal, A., Bebianno, M.J. (2017). Environmental hazard assessment of a marine mine tailings deposit site and potential implications for deep-sea mining. *Environ. Poll.* 228,169-178.

- Mevenkamp, L., Stratmann, T., Guilini, K., Moodley, L., Van Oevelen, D., Vanreusel, A., Westerlund, S., Sweetman, A.K. (2017). Impaired short-term functioning of a benthic community from a deep Norwegian Fjord following deposition of mine tailings and sediments. *Frontiers in Marine Science*, <https://doi.org/10.3389/fmars.2017.00169>.
- Mewes, K., Mogollón, J. M., Picard, A., Rühlemann, C., Kuhn, T., Nöthen, K., et al. (2014). Impact of depositional and biogeochemical processes on small scale variations in nodule abundance in the Clarion-Clipperton Fracture Zone. *Deep Sea Research Part I: Oceanographic Research Papers* 91, 125–141. doi:10.1016/j.dsr.2014.06.001.
- Mewes, K., Mogollón, J.M., Picard, A., Rühlemann, C., Eisenhauer, A., Kuhn, T., Ziebis, W., Kasten, S. (2016). Diffusive transfer of oxygen from seamount basaltic crust into overlying sediments: An example from the Clarion-Clipperton Fracture Zone. *Earth and Planetary Science Letters* 433, 215-225.
- MIDAS Report D3.5 (2016). Validation report on the response of biological indices to toxicant exposure in macro- and megafauna from exposures to contaminant complexes collected, including field exposures, to feed into WP7 and WP8. 75 pp.
- Miljutin, D., Miljutina, M., and Messié, M. (2015). Changes in abundance and community structure of nematodes from the abyssal polymetallic nodule field, Tropical Northeast Pacific. *Deep Sea Research Part I: Oceanographic Research Papers* 106, 126–135. doi:10.1016/j.dsr.2015.10.009.
- Nakata, K., Kubota, M., Aoki, S., Taguchi, K. (1997). Dispersion of resuspended sediment by ocean mining activity – modelling study. *Proceedings of the first International Symposium on Environmental Studies for Deep-Sea Mining*, Tokyo, Japan, 169-186.
- Naumann and the ANTARES Collaboration 2008 *J. Phys.: Conf. Ser.* **136** 042064
- Netto, S.A., Gallucci, F., Fonseca, G. (2009). Deep-sea meiofauna response to synthetic-based drilling mud discharge off SE Brazil. *Deep-Sea Res. II* 56, 41e49.
- Nikuradse J. (1933). Strömungsgesetze in rauhen Rohren. *VDI-Forschungsheft* 361. Beilage zu 'Forschung auf dem Gebiete des Ingenieurwesens' Ausgabe B Band 4.
- NOAA 1984, Deep Seabed Mining: Draft environmental impact statement on issuing an exploration license to Ocean Mining Associates, Office of Ocean and Coastal Resource Management, Ocean Minerals and Energy Division, Washington
- Ortega, A. (Ed.)(2014). Towards Zero Impact of Deep Sea Offshore Projects – An assessment framework for future environmental studies of deep-sea and offshore mining projects. Report IHC Merwede.
- Pabortsava, K., Purser, A., Wagner, H., Thomsen, L. (2011). The influence of drill cuttings on the physical characteristics of phytodetritus. *Marine Pollution Bulletin* 62, 2170-2180.
- Pape, E., Bezerra, T. N., Hauquier, F., and Vanreusel, A. (2017a). Limited Spatial and Temporal Variability in Meiofauna and Nematode Communities at Distant but Environmentally Similar Sites in an Area of Interest for Deep-Sea Mining. *Front. Mar. Sci.* 4. doi:10.3389/fmars.2017.00205.
- Pape, E., De Smet, B., Bogaert, K., and Vanreusel, A. (2016). Biological and environmental report on the 2014 and 2015 expeditions in the GSR license area. Ghent, Belgium: Marine Biology Research Group, Ghent University. (Submitted to ISA, file reference : ISA-GDR2016_PartIV)

Pape, E., De Smet, B., Gheerardyn, H., Bezerra, T. N., and Vanreusel, A. (2017b). Report on the continued analyses of the biological and environmental samples collected during the 2015 expedition in the GSR exploration area. Marine Biology Research Group, Ghent University. (Submitted to ISA, file reference : ISA-GSR_AR2016_PartIV)

Pape, E., Jones, D. O. B., Manini, E., Bezerra, T. N., and Vanreusel, A. (2013). Benthic-Pelagic Coupling: Effects on Nematode Communities along Southern European Continental Margins. *PLOS ONE* 8, e59954. doi:10.1371/journal.pone.0059954.

Pavan S. (2016). Nouveaux schémas de convection pour les écoulements à surface libre. Ph.D. Thesis, Saint-Venant - Laboratoire d'Hydraulique Saint-Venant / Saint-Venant laboratory for Hydraulics.

Pennington, J. T., Mahoney, K. L., Kuwahara, V. S., Kolber, D. D., Calienes, R., and Chavez, F. P. (2006). Primary production in the eastern tropical Pacific: A review. *Progress in Oceanography* 69, 285–317. doi:10.1016/j.pocean.2006.03.012.

Peterson, B. J., and Fry, B. (1987). Stable Isotopes in Ecosystem Studies. *Annual Review of Ecology and Systematics* 18, 293–320. doi:10.1146/annurev.es.18.110187.001453.

Purser, A., Marcon, Y., Dreutter, S., Hoge, U., Sablotny, B., Hehemann, L., Lemburg, J., Dorschel, B., Biebow, H., Boetius, A (in press). OFOBS - Ocean Floor Observation and Bathymetry System: A new towed camera / sonar system for deep-sea habitat surveys. *IEEE Journal of Oceanic Engineering*.

Purser, A., Marcon, Y., Hoving, H.-J., Piatowski, U., Eason, D., Vecchione, M., Boetius, A. (2016). Recent observations of deep sea incirrate octopi from three manganese-rich locations in the Pacific Ocean. *Current Biology* 26 (24), R1268-R1269.

Purser, A., Thomsen, L. (2012). Monitoring strategies for drill cutting discharge in the vicinity of cold-water coral ecosystems. *Marine Pollution Bulletin* 64 (11), 2309-2316.

R., DeLeo, D.M., Dunlop, K.M., Escobar-Briones, E.G., Gates, A.R., Genio, L., Gobin, J., Henry, L.-A., Herrera, S., Hoyt, S., Joye, S., Kark, S., Mestre, N.C., Metaxas, A., Pfeifer, S., Sink, K., Sweetman, A.K., Witte, U.F. (2016). Environmental impacts of the deep-water oil and gas industry: a review to guide management strategies. *Front. Environ. Sci.* 4, 58.

Radziejewska, T. (2002). Responses of deep-sea meiobenthic communities to sediment disturbance simulating effects of polymetallic nodule mining. *International Reviews Hydrobiology* 87, 457-477.

Radziejewska, T., Drzycimski, I., Galtsova, V.V., Kulangieva, L.V., Stoyanova, V. (2001a). Changes in genus-level diversity of meiobenthic free-living nematodes (Nematoda) and harpacticoids (Copepoda Harpacticoida) at an abyssal site following experimental sediment disturbance. *Proceedings of the Fourth Ocean Mining Symposium, Szczecin, Poland*, 38-43.

Radziejewska, T., Rokicka-Praxmayer, J., Stoyanova, V. (2001b). IOM BIE revisited: meiobenthos at the IOM BIE site 5 years after the experimental disturbance. *Proceedings of the Fourth Ocean Mining Symposium, Szczecin, Poland*, 63-68.

Radziejewska, T., Stoyanova, V., 2000. Abyssal epibenthic megafauna of the Clarion-Clipperton area (NE Pacific): changes in time and space versus anthropogenic environmental disturbance. *Oceanological Studies* 29, 83–101.

- Richardson, W.J., Wursig, B., and Greene, C.R. Jnr. 1990. Reactions of bowhead whales (*Balaena mysticetus*) to drilling and dredging noise in the Canadian Beaufort Sea, *Marine Environmental Research*, vol 29, p. 135-160
- Rolinski, S., Segschneider, J., Sündermann, J. (2001). Long-term propagation of tailings from deep-sea mining under variable conditions by means of numerical simulations. *Deep-Sea Research II* 48, 3469–3485.
- Salençon, M.-J. & Thebault J.M. (1997). *Modélisation d'écosystème lacustre*. Masson, Paris, France.
- Schaaning, M.T., Trannum, H.C., Øxnevad, S., Carroll, J., Blake, T. (2008). Effects of drill cuttings on biogeochemical fluxes and macrobenthos of marine sediments. *J. Exp. Mar. Biol. Ecol.* 361, 49e57.
- Segschneider, J., Sündermann, J. (1998). Simulating large scale transport of suspended matter. *Journal of Marine Systems* 14, 81–97.
- Sheelu, G., Bharathi, L., Nair, S., Raghukumar, C., & Mohandass, C. (1999, January). Validation of EIA sampling methods-bacterial and biochemical analyses. In *Third ISOPE Ocean Mining Symposium*. International Society of Offshore and Polar Engineers.
- Simpson, S.L., Campana, O., Ho, K.T. (2016). Sediment toxicity testing. In: Blasco J., Campana O., Chapman P., Hampel M. (Eds.), *Marine Ecotoxicology: Current Knowledge and Future Issues*, 197-235.
- Smagorinsky J. (1963). General circulation experiments with the primitive equations: I. the basic experiment*. *Mon. Weather Rev.*, 91(3), 99–164.
- Smith, C.R., Berelson, W., Demaster, D.J., Dobbs, F.C., Hammond, D., Hoover, D.J., Pope, R.H., Stephens, M., 1997. Latitudinal variations in benthic processes in the abyssal equatorial Pacific: control by biogenic particle flux. *Deep Sea Research Part II: Topical Studies in Oceanography, A JGFOS Process Study in the Equatorial Pacific* 44, 2295–2317. doi:10.1016/S0967-0645(97)00022-2
- Soetaert, K., Herman, P. M. J., and Middelburg, J. J. (1996). Dynamic response of deep-sea sediments to seasonal variations: A model. *Limnol. Oceanogr.* 41, 1651–1668. doi:10.4319/lm.1996.41.8.1651.
- Son, J., Kim, K. H., Kim, H. J., Ju, S.-J., and Yoo, C. M. (2014). Evaluation of Similarity of Water Column Properties and Sinking Particles between Impact and Preserved Sites for Environmental Impact Assessment in the Korea Contracted Area for Manganese Nodule Development, NE Pacific. *Ocean and Polar Research* 36, 423–435. doi:10.4217/OPR.2014.36.4.423.
- Stanley, J.A., Jeffs, A.G. (2016). Ecological impacts of anthropogenic underwater noise. In: Solan, M., Whiteley, N.M. (Eds.), *Stressors in the Marine Environment*. Oxford University Press, Oxford, pp. 282e297.
- Stelzenmüller, V., Fock, H.O., Gimpel, A., Rambo, H., Diekmann, R., Probst, W.N., Callies, U., Bockelmann, F., Neumann, H., Kroncke, I. (2015). Quantitative environmental risk assessments in the context of marine spatial management: Current approaches and some perspectives. *ICES J. Mar. Sci.* 72, 1022-1042.
- Stoffers, H. (2016). *Propulsion test document*. Zwijndrecht: Global Sea Mineral Resources.

- Stratmann, T., Lins, L., Purser, A., Marcon, Y., Rodrigues, C., Ravara, A., Cunha, M.R., van Oevelen, D. (in prep.). Carbon flows in deep-sea food webs need more than twenty-six years to recover from an experimental disturbance in the Peru Basin.
- Sweetman, A. K., and Witte, U. (2008). Response of an abyssal macrofaunal community to a phytodetrital pulse. *Marine Ecology Progress Series* 355, 73–84.
- Sweetman, A.K., Thurber, A.R., Smith, C.R., Levin, L.A., Mora, C., Wei, C.-L., Gooday, A.J., Jones, D.O.B., Rex, M., Yasuhara, M., Ingels, J., Ruhl, H.A., Frieder, C.A., Danovaro, R., Würzberg, L., Baco, A.R., Grupe, B.M., Pasulka, A., Meyer, K.S., Dunlop, K.M., Henry, L.-A., Roberts, J.M., (2017). Major impacts of climate change on deep-sea benthic ecosystems. *Elementa Science of the Anthropocene* 5 (4), doi: 10.1525/elementa.203.
- Swinbank W.C. (1963). Long-wave radiation from clear skies. *Q. J. R. Meteorol. Soc.*, 89(381), 339–348, doi: 10.1002/qj.49708938105.
- Tamis, J.E., de Vries, P., Jongbloed, R., Lagerveld, S., Karman, C., Tjalling J., Van der Wal, J., Slijkerman, D.M.E., Klok, C. (2017). Toward a Harmonized Approach for Environmental Assessment of Human Activities in the Marine Environment. *Integr. Environ. Assess. Manag.* 12, 2016.
- Thiel, H., Schriever, G. (1990). Deep-Sea Mining, Environmental Impact and the DISCOL Project, *Ambio* 19 (5), 245-250.
- Thiel, H., Schriever, G., Ahnert, A., Bluhm, H., Borowski, C., Vopel, K. (2001). The large-scale environmental impact experiment DISCOL: reflection and foresight. *Deep-Sea Research II* 48, 3869-3882.
- Thiel, H., Schriever, G., Bussau, C., and Borowski, C. (1993). Manganese nodule crevice fauna. *Deep Sea Research Part I: Oceanographic Research Papers* 40, 419–423. doi:10.1016/0967-0637(93)90012-R.
- Thomsen, L., McCave, I.N. (2000). Aggregation processes in the benthic boundary layer at the Celtic Sea continental margin. *Deep-Sea Research I* 47, 1389-1404.
- Tilot, V., 2006. Biodiversity and distribution of the megafauna: The polymetallic nodule ecosystem of the Eastern Equatorial Pacific Ocean. UNESCO.
- Tsurusaki, K. (1997). Concept and Basic Design of the Plume Discharge. Proceedings, international symposium on environmental studies for deep-sea mining Tokyo, Japan.
- Vanreusel, A., Hilario, A., Ribeiro, P. A., Menot, L., and Arbizu, P. M. (2016). Threatened by mining, polymetallic nodules are required to preserve abyssal epifauna. *Scientific Reports* 6, 26808. doi:10.1038/srep26808.
- Vonnahme, T.R. (2016). Microbial diversity and function of deep-sea manganese nodule ecosystems. Master Thesis, Max-Planck Institute for Marine Microbiology, Bremen, 145 pp.
- Vonnahme, T.R., Molari, M., Janssen, F., Wenzhöfer, F., Haeckel, M., Titschack, J., Boetius, A. (in prep.). Effects of simulated deep-sea mining impacts on microbial communities and functions in the DISCOL experimental area after 26 years.
- Waller, R.G., Baco, A.R. (2007). Reproductive morphology of three species of deep-water precious corals from the Hawaiian archipelago: *Gerardia* sp., *Corallium secundum*, and *Corallium lauense*. *Bulletin of Marine Science*, 533-542.
- Weaver, C.E., 1989. Clays, muds, and shales. Elsevier, Amsterdam.

- Webb, The equilibrium oceanic microseism spectrum, *J. Acoust. Soc. Am.* **92**, 2141–2158 (1992).
- Wiklund, H., Taylor, J. D., Dahlgren, T. G., Todt, C., Ikebe, C., Rabone, M., et al. (2017). Abyssal fauna of the UK-1 polymetallic nodule exploration area, Clarion-Clipperton Zone, central Pacific Ocean: Mollusca. *ZooKeys* 707, 1–46. doi:10.3897/zookeys.707.13042.
- Wiklund, H., Taylor, J.D., Dahlgren, T.G., Todt, C., Ikebe, C., Rabone, M., Glover, A.G. (in press). Abyssal fauna of the UK-1 polymetallic nodule exploration area, Clarion-Clipperton Zone, central Pacific Ocean: Mollusca. *Zootaxa*.
- Winterwerp, J.C. (1998). A simple model for turbulence induced flocculation of cohesive sediment. *Journal of Hydraulic Research* 36 (3), 309-326
- Witte, U., Wenzhöfer, F., Sommer, S., Boetius, A., Heinz, P., Aberle, N., Sand, M., Cremer, A., Abraham, W.-R., Jørgensen, B. B., Pfannkuche, O. (2003). In situ experimental evidence of the fate of a phytodetritus pulse at the abyssal sea floor. *Nature* 424, 763-766.
- Wong, J. (2008). *Theory of ground vehicles*. John Wiley & Sons, Inc.
- Wong, j. (2013). *Terramechanics and off-road vehicle engineering*. Elsevier.
- Wong, J. (2016). *Review of the GSR Technical Development Program*. Toronto: Vehicle Systems Development Corporation (VSDC).
- Yamazaki, T., Barnett, B.G., Suzuki, T. (1997). Optical determination of the JET deep sea sediment disturbance. *Proceedings of the International Symposium on Environmental Studies for Deep-Sea Mining*, Tokyo, Japan, 153-167.
- Yasunaka, S., Ono, T., Nojiri, Y., Whitey, F. A., Wada, C., Murata, A., et al. (2016). Long-term variability of surface nutrient concentrations in the North Pacific. *Geophys. Res. Lett.* 43, 2016GL068097. doi:10.1002/2016GL068097.
- Zenk, W., 2008. Abyssal and Contour Currents, in: Rebesco, M., Camerlenghi, A. (Eds.), *Contourites, Developments in Sedimentology*. Elsevier, pp. 35-57.
- Kessler, W. S. (2006). The circulation of the eastern tropical Pacific: A review. *Progress in Oceanography*, 69(2-4), 181-217.
- Zhang, Y., Jiao, N., Hong, N., 2008. Comparative study of picoplankton biomass and community structure in different provinces from subarctic to subtropical oceans. *Deep Sea Research Part II: Topical Studies in Oceanography, Understanding the Ocean's Biological Pump: results from VERTIGO* 55, 1605–1614. doi:10.1016/j.dsr2.2008.04.014

11.2 Online resources

- “ARBO Pompen en Filters”. 2016. Online. /www.arbo-pumps.com/en/. Consulted on March 21, 2018
- BMT ARGOS BV, 2018. “Meteocean Web-Portals”. Online, <http://www.bmtargoss.com/meteocean-web-portals/www.waveclimate.com/> Consulted on March 21, 2018
- Environmental Tracing, 2017. “EcoTrace Fluorescent Tracer”. Online. <https://www.environmentaltracing.com/> Consulted on March 21, 2018
- Geomar, 2018. “ROV KIEL 6000”, Online. www.geomar.de/en/centre/central-facilities/tlz/rovkiel6000/. Consulted on March 21th 2018.

- International Seabed Authority, 2018. “*exploration areas*”, Online : www.isa.org.jm/contractors/exploration-areas. Consulted on March 21th 2018.
- Kongsberg Maritime, 2018. “*Autonomous Underwater Vehicle, REMUS 6000*”. Online www.km.kongsberg.com/ks/web/nokbg0240.nsf/AllWeb/481519DA1B0207CDC12574B0002A8451?OpenDocument Consulted on March 21, 2018
- National Oceanography Centre, University of Southampton. 2018. “*International network for scientific investigation of deep-sea ecosystems*”. Online. www.indeep-project.org Consulted on March 21, 2018
- NOAA, Coastal Zone Management. 2017 “*Historical Hurricane Tracks*”.. Online. www.coast.noaa.gov/hurricanes/. Consulted on March 21, 2018
- Quadrant, 2018. “*Ertalon ® 6 PLA*”, Online. www.quadrantplastics.com/eu-en/products/engineering-plastics/engineering-80-160-c/ertalon-R-and-nylatron-R-products/ertalon-R-6-pla.html. Consulted on March 21, 2018.
- Swiss Oil Technology. 2018. “*Products : Atlantis*”. Panolin® Online. www.panolin.com/inten/products/product.php?ID=1348, Consulted on March 21, 2018.
- TDI Brooks, 2010. “*Safety Management Manual – Party chief Responsibilities*.” Online. <http://geodatapub.com/publicweb/smm/Paper%20SMM%2014-6/Gen%20SOPs/pdfs/sop-gen-007c%20Party%20Chief%20Responsibilities%20rev6.pdf>. Consulted on March 21, 2018

12 Appendices

12.1 Technology development

12.1.1 Background : theory approach of the hydraulic collector

Several parameters have been identified as driving parameters for the design of the collector head:

- (1) **Pick-up efficiency** [$\eta_{pick-up}$; -]: the pick-up efficiency has been defined as the ratio of nodules picked-up over a certain stretch over the total amount of nodules available on the same stretch. This parameter needs to be maximized.

$$\eta_{pick-up} = \frac{M_{pick-up}}{M_{total}}$$

- (2) **Production** [P; T/year]: target production figures must be met for economic viability of deep sea polymetallic nodule mining. Production figures range between 2,000,000 and 2,500,000 tons of dry nodules per year, meaning on average 400 to 500 tons per hour.
- (3) **Water flow** [Q; m³/s]: hydraulic collector concepts require a certain water flow to pick-up the nodules (mechanical collectors also need a water flow to separate and clean the nodules from the sediment). The water flow should be minimized for 2 main reasons. First, the flow is directly related to the power required for the pumps and the corresponding costs are proportional (1). Second, a flow of water near the seabed will generate a sediment plume which, from an environmental point of view, should be minimized as much as possible (2).

$$Q_{water} \uparrow \sim P_{pump} \uparrow \sim cost \uparrow \quad (1)$$

$$Q_{water} \uparrow \sim Turbidity \uparrow \sim Environmental\ impact \uparrow \quad (2)$$

- (4) **Environmental pressures**: minimizing the environmental impact is an important factor to be considered when designing the collector head. Of these, the most important are:
- a. **Turbidity** [T; mg/l]: Turbidity is an important parameter that needs to be taken into account in designing the collector head. All different components should be developed with the aim of keeping the turbidity as low as possible. There are 3 main sources of turbidity:
 - Turbidity caused by the collection mechanism ($T_{collection}$)
 - Turbidity caused by the separation system ($T_{separation}$)
 - Turbidity caused by the driving system ($T_{driving}$)
 - b. **Seafloor disturbance**: the physical disturbance of the seafloor is a factor that should be minimized at all times.
 - c. **Noise**: noise levels should be minimized.
- (5) **Seafloor interaction**: The collector head should have minimal seafloor interaction. The soil is known to be soft and sticky (ooze clay). Nodules should be picked up with a minimal amount of soil to avoid clogging. Clogging is a situation in which fine cohesive sediments fills up the openings of the system. Soil that does get picked-up should be separated from the nodules early in the process.

- (6) **Reliability:** the collector head should have a minimal amount of active parts. This can either be a rotating drum, a conveyor belt, scoops or something else. The more active (moving) components, the higher the risks of failure and corresponding downtime.
- (7) **Lifetime:** Lifetime of the collector should be maximized. The design should incorporate components with high wear resistance.

12.1.2 Choice of pick-up system

Beside the presented hydraulic pick-up system, mechanical collectors were also explored. The latter use different pick-up techniques and are comparable to what is used in the land-based mining industry. All mechanical collection systems use a similar methodology of scraping off the upper layer of the seabed (Figure 106). The fenestrated ramp (the most widespread system) consists of a conveyor belt with or without (both systems are possible) a soil-cutting knife at the front. From there, the mixture is transported laterally to a central discharge point either by injecting water (hydraulic transport by fluidization) or mechanically (conveyor belt or similar). Every scraper system, regardless of the geometrical configuration, always uses the same principle: the top layer of the seabed is removed together with the nodules (a “slice” of soil and nodules is being cut off). The nodule pick-up efficiency, despite possible bulldozing effects and side-spills, is consequently relatively high (theoretically 100% is possible). However, by slicing off a layer of the upper seabed, a significant amount of sediment is added into the process flow.

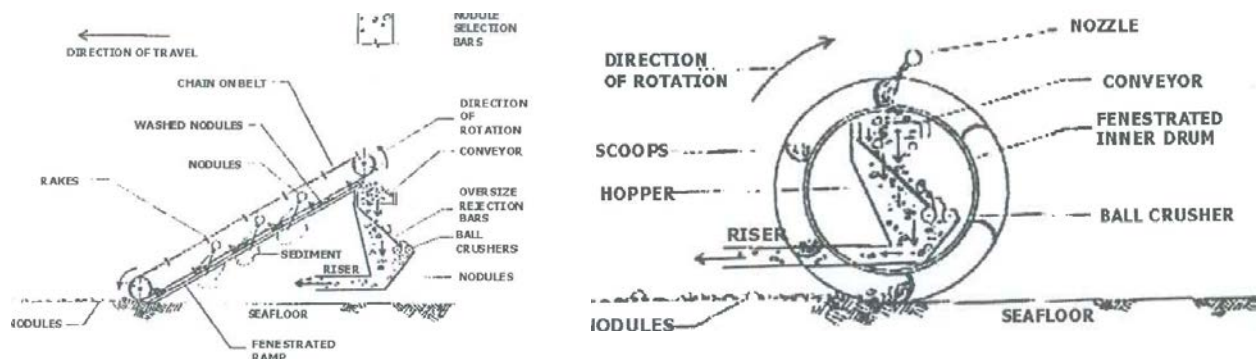


Figure 106: Examples of mechanical collectors Fenestrated ramp (cutter blade scraper) (left) and Rotating drum (right)

The main questions in choosing between a mechanical or a hydraulic pick-up system (presented earlier) are actually the following: Assuming a theoretical 100% pick-up efficiency for both systems, how does the water flow, what are the consequential power requirements (and corresponding costs), how does the generated sediment plume used for nodule pick-up with hydraulic collectors relate to the water flow (and consequential power and generated turbidity) used for separating the nodules from the sediment with mechanical collectors? The trade-off using the design drivers above are displayed in

Table 31: Collection principle trade-off

Driver	Symbol	Hydraulic lift collector	Fenestrated ramp
Pick-up efficiency	$\eta_{pick-up}$	To be determined, laboratory tests	Assumed to be relatively high if compared to land-based mining systems
Production	P	To be determined, laboratory tests	To be determined, laboratory tests
Water flow	$Q_{pick-up}$	To be determined, laboratory tests	Null
	$Q_{separation}$	Null	To be determined, laboratory tests
Environmental pressures	$T_{pick-up}$	High	Low
	$T_{separation}$	Lower	High
	$T_{driving}$	Tracks	Tracks
	Disturbance	Water flow parallel to the seabed	Slice of seabed cut off
	Noise	Water pumps	Water pumps and mechanical drive
Seafloor interaction	/	Top layer affected by the water flow: fluidization and dragging of nodules	Entire top layer is being removed and processed in-situ
Reliability	/	Minimal moving parts: only water pumps are required for the collection and separation	Water pumps are required for the nodule separation; mechanical drives are required for the nodule collection method
Lifetime	/	To be determined	To be determined

The hydraulic lift concept as explained above was put forward as the most promising hydraulic concept mainly because of its simplicity and envisaged production reliability.

GSR investigated mechanical and hydraulic concepts. After an initial exploratory concept study and small-scale laboratory tests, the hydraulic lift collector was chosen.

In the case of hydraulic systems where the sediment is fluidized, it might be possible that entire chunks of clay are being collected. This significantly increases the risk of clogging and blockage downstream of the collector head. Ted Brockett, from the OMI consortium, describes the working principle from the hydraulic collector as follows: *“The primary nozzle, or nozzles, is configured so that the nodules are lifted from the seafloor by the low pressure and scouring action of the water jets. Flow from the “jet sheet” nozzles follows the contour of the curved base plate and entrains surrounding water to assist in lifting the nodules and transporting them up the ramp. The ramp,*

which is actually an enclosed duct, confines the nodules and transports them to a height sufficient for sediment separation and lateral transport across the collector. Because of the turbulence of the water jets and flow in the duct, the nodules are generally cleaned of sediment before they reach the top of the duct. The discharge of the duct is directed at the sediment separating screen which deflects the nodules down to a trough from where they are pumped to the riser. The orientation and bar spacing of the screen allows the water stream containing the sediment to pass through and discharge out the back of the collector”.

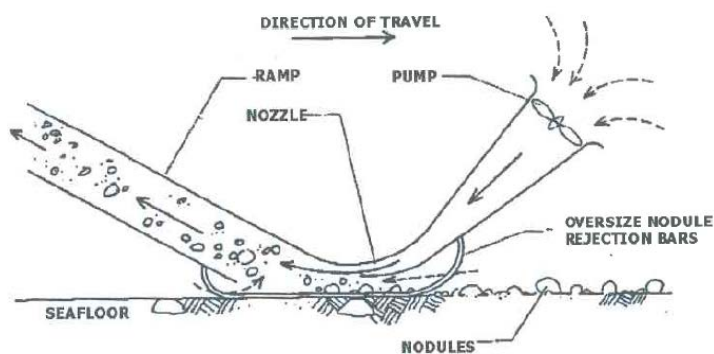


Figure 107: Hydraulic lift concept¹

12.1.3 Pre-design study : Optimized collector design

Current Computational Fluid Dynamic (CFD) software is very well capable of modelling solid particles injected in a fluid flow. However, due to model complexity and computing power restraints, the shape of these solid particles is restricted to either spheres or ellipsoids. In order to validate the hydraulic lift concept, lift and drag coefficients of nodules were determined and compared with standard values of spheres and ellipsoids.

Three nodules of different sizes (small – medium – large) were scanned in 3D to adequately evaluate the flow over these nodules:

Table 32: Characteristic nodule sizes

	Length [mm]	Width [mm]	Height [mm]
Nodule 1	40	25	15
Nodule 2	75	55	35
Nodule 3	95	80	55

Figure 108 here below shows the result of this small 3D-analysis.



1 Nodule Collector Subsystems” by Ted Brockett in “Proposed Technologies for Deep Seabed Mining of Polymetallic Nodules” – Proceedings of the ISA Workshop held in Kingston (Jamaica), August 3-6, 1999.

Figure 108: Example of 3D scan of characteristic nodules : Side view of Nodule 3 (left); side view of Nodule 2 (centre) and Top view of Nodule 3 (right)

The results of the force calculation are summarized and shown in Table 33 below. Based on these results, the following conclusions can be defined:

The lift coefficient is approximately zero for a free nodule in a free stream due to symmetry conditions;

The lift coefficient of a nodule embedded in soil is of a similar order compared to a spherical nodule;

An under pressure between -500 Pa and -800 Pa is at least required to lift the nodules.

Table 33: Drag and lift characteristics

	Free		Embedded in soil (1/2)	
	Drag C_D	Lift C_L	Drag C_D	Lift C_L
Sphere	0.25	0	0.0	0.45
Ellipsoid	0.16	0	0.09	0.66
Nodule 1	0.12	0.05	0.05	0.24
Nodule 2	0.23	0.16	0.10	0.39
Nodule 3	0.41	0.04	0.17	0.36

Figure 109 shows the flow over nodule 3 in order to determine C_D and C_L .

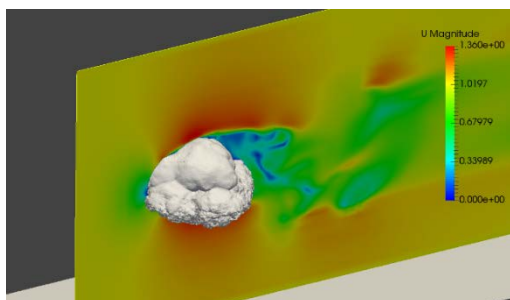


Figure 109: Flow over a nodule.

It should be noted that the lift force only plays a relevant role in lifting the nodules from the seabed. As soon as the nodules are free from the seabed and flowing with the induced flow, their motion is predominantly influenced by the drag and buoyancy forces. Any rotation of the nodule may cause some lift (magnus effect), but this is not included in the present CFD simulations.

12.1.3.1 Forces on nodule

When the nodules are transported through the water, different forces are acting on it. Figure 110 shows the different forces on a nodule when a flow of water is applied. These forces have to be taken into account during the design of the collector head.

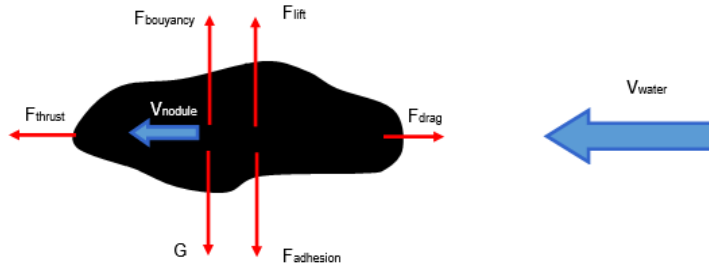


Figure 110: Forces on nodule in water flow

F_{buoyancy}: The buoyancy force is the upward force exerted by a fluid on the nodule. It is equivalent to the weight of the displaced fluid.

G: The gravitational force is the weight of the nodule.

F_{lift}: The lift force is the force generated as on the wings of an airplane and can be calculated with:

$$F_{lift} = \frac{1}{2} \rho v^2 A C_{lift}$$

F_{thrust}: The thrust is the force generated by the flow of water on the nodule. Assuming that the nodule is fully transported with the flowing water, the thrust force is completely balanced with drag force.

F_{adhesion}: The adhesion force is the force required to pick up the nodules out of the sediment. Only one reference has been found in the literature describing this force (Fundamental study for the development of a collector sub-system and its future technology needs; Katsuya Tsurusaki). Measurements were done on nodules in a box core on the deck of a research vessel and are summarized in Figure 111. This force is also referred to as the “sticky force”.

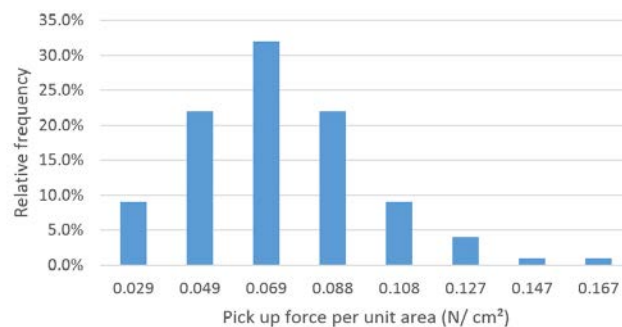


Figure 111: Pick-up force

The pick-up forces for the 3 characteristic nodules were calculated and are displayed in Table 34, assuming that half of a nodule is buried into sediments and average pick-up force to be 0.073 N/cm².

Table 34: Pick-up force for 3 characteristic nodules

	Length	Width	Height	a	b	c	A	Burial	Force
	[cm]	[cm]	[cm]	[cm]	[cm]	[cm]	[cm²]	[cm²]	[N]
Nodule 1	4	2.5	1.5	2	1.25	0.75	21.63	10.82	0.78
Nodule 2	7.5	5.5	3.5	3.75	2.75	1.75	93.57	46.78	3.40
Nodule 3	9.5	8	5.5	4.75	4	2.75	183.38	91.69	6.65

The adhesion force of the nodules in the sediment is relatively small. Moreover, it is assumed that the surrounding sediment has not been blown away by the collection mechanism, which is, in most cases, not realistic. It is therefore conservative to assume very low adhesion forces. This was qualitatively confirmed by French scientists who performed several in-situ tests using a manned submarine (Nautilus) in the French contract area (Figure 112). A suction nap ("ventouse") was used to pick up nodules.

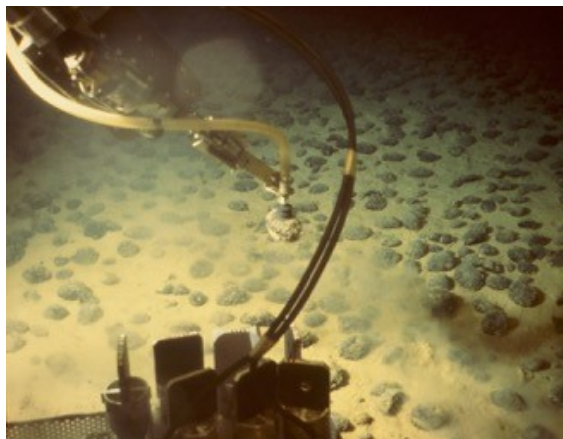


Figure 112: "Ventouse" deployed by IFREMER during Nautilus - 1998 (Michel Hoffert)

F_{drag} : The drag force is a force acting opposite to the motion of an object in the fluid and can be calculated using the formula:

$$F_{\text{drag}} = \frac{1}{2} \rho v^2 A C_{\text{drag}}$$

F_{gradient} The gradient force is generated by a difference in pressure and is always directed from the high pressure zone to the low pressure zone. The pressure difference created by the jet generates a flow of water, entraining the nodules

12.1.3.2 Initial Design variables

The main objectives of the CFD optimization analysis are (1) Assessment of the working principle of a hydraulic lift system and (2) perform a parameter sensitivity analysis.

A set of variable parameters that define the geometry and working principle of the hydraulic lift concept have been defined prior to the CFD calculations. These parameters have been changed in the CFD optimization process and are listed in the Table 35 below.

Table 35: Initial variable parameters

Parameter	Symbol	Unit	Description
Jet velocity	V_{jet}	[m/s]	The velocity of the water flow that entrains the surrounding seawater creating a flow over the nodules on the seabed. It should be able to stir up the nodules and lift them from the seabed.
Section nozzle width	B_{nozzle}	[mm]	Height of the jet nozzle or jet sheet ($\sim A$). A and define the volume of water (Q). Q should be minimized.
Jet nozzle injection direction	α	[deg]	The jetting direction is considered to be parallel to the bottom, in opposite direction to the direction of travel. Downward direction should be avoided to minimize soil disruption.
Height CL-jet above seabed (-x)	H_{jet}	[mm]	Distance should be adjusted for optimal pick-up efficiency.

Length active suction zone	L	[mm]	The length of the active suction zone is defined as the horizontal part of the collector head.
Coanda curve	R	[mm]	The radius of curvature of the coanda plate should be optimized in order to minimize turbulence in the collector head.
Jet curve	R _{jet}	[mm]	The radius of curvature of the jet plate.
Duct angle inlet	β	[deg]	Nominal 45°.
Duct entrance height above seabed	h _{duct}	[mm]	Scraping the seafloor must be avoided. On the other hand, to avoid loss of flow at the back, the opening cannot be too wide.

Duct width	β_{duct}	[mm]	Width of the duct is should be optimized with regard to flow (mass balance). A minimum width must be maintained to avoid clogging (estimated min. 250mm).
Collector forward speed	v	[m/s]	Important factor with respect to productions. Should be maximized.
Seabed flatness (bumpiness)	[-]	[-]	Variability of the terrain and the effect on the collection.
Additional nozzle in duct	[-]	[-]	An additional nozzle in the duct will generate a zone of lower pressure
Nozzle vs. jet sheet (3D)	[-]	[-]	Effect unknown.
Flow guiding trays in suction zone (3D)	[-]	[-]	Should stabilize jet flow and avoid turbulence. Effect unknown.
Nodule oversize rejection bars (3D)	[-]	[-]	Effect unknown.

The collector head has 2 major functions:

- **Pick-up function [PU]:** Pick-up the nodules at the entrance of the collector by means of the entrained water caused by the hydraulic jet system,
- **Transport function [TR]:** Transport of the nodules up the duct.

All parameters described above have an influence on either just one of these functions or on both. Subsequently, the parameters can be divided amongst these two functional categories as illustrated in the Venn diagram of Figure 114 with an overlap area. Within these two types of categories, parameters can further be categorized as either **process control parameters**, **geometrical parameters** or **environmental parameters**.

Process control parameters are the parameters with which the collection process is going to be monitored and controlled. Production rates depend highly on the collector (forward) speed, which can be modified depending on the nodule abundance (kg/m²) within a certain zone. H_{jet} was initially considered to be a geometrical parameter but as the design developed, it became apparent that the height of the collector head was of key importance to the pick-up efficiency. For that reason, H_{jet} needs to be considered as a control parameter to optimize the nodule collection. A benefit of adjustable collector head height is the ability to comply with a variable soil profile. Another advantage of being able to control the height of the jet above the seabed, is to enable

more water inside the collection system. If downstream pressures rise, this might indicate clogging and so more water needs to enter the system. The last set of process control parameters are the jet flow: v_{PU} (pick-up jet) and v_{TR} (transport jet). The pick-up jet is the main jet at the front of the collector head. The transport jet inside the duct was assumed to be required but as it implies an additional water flow (and consequential power increase, sediment plume increase) this was initially not considered in the calculations.

The geometrical parameters are optimized through design. These geometrical parameters are constrained by the general layout of the trial. At present, none of these parameters are considered to be adjustable depending on the ongoing collection process. The analogue with different type of cutter heads on cutter suction dredgers is apparent. A **cutter suction dredge (CSD)** is a **stationary** dredge plant equipped with the means to pry loose the seabed, fluidize it to a mixture that is suitable for pumping and subsequent hydraulic transport to its final deposit area. In different type of soils, different kind of cutter heads are being used. For example, cutter heads with a large opening are used in soft, loosely packed soils where cutting forces are limited to enable large production rates. On the other hand, in rocky soils, more robust and compacter cutter heads are being used, enabling higher cutting forces and size separation of boulders at the entry of the suction process.



Figure 113: Analogy with cutter heads allowing geometrical variations depending on the soil : Sand cutter head on CSD Ambiorix– open design (left) and Rock cutter head on CSD Ambiorix – robust and “closed” design (right)

These two different kind of heads can be changed depending on the soil type; this is a geometrical variation. Similar variations are possible with nodule collection principles depending for example on the type of soil or the average size of the nodule field. However, this requires a configuration change (just like the cutter heads) that cannot be done during collection operations. Therefore, within one geometrical configuration, only control parameters can be changed to steer the nodule collection process.

The seabed flatness (bumpiness) is an external environmental parameter that cannot be directly controlled, though it has a significant influence on the efficiency of the pick-up process.

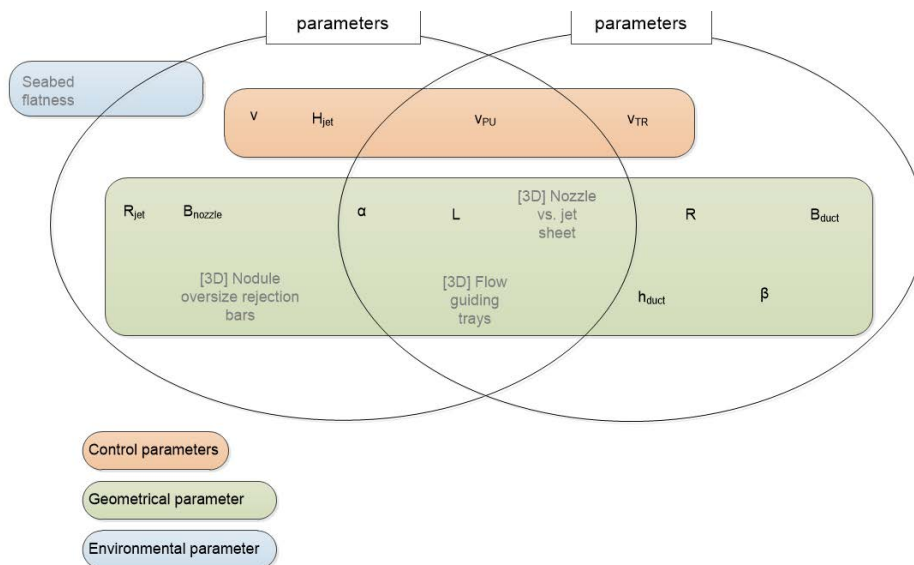


Figure 114: Different collector defining parameters (status: initial with differentiation for V_{PU} and V_{TR})

During the CFD development, other and different variables were identified and defined, whereas others included in the initial list of parameters were found to be not of significant importance to the design and disregarded.

The CFD collector analysis has been split up into two distinct parts, each with different research objectives:

The first part deals with the flow optimization at the pick-up nozzles. The objective is to optimize the collector head geometry so that the jet flow reaches a uniform velocity as quickly as possible across the entire width of the collector head. In this part, only water is being used in the model.

The second part assumes a uniform flow over the entire width of the collector (output part 1) and has the objective to optimize the design in order to maximize the nodule pick-up efficiency. A significant amount of work has been conducted in order to simulate the soil and nodules.

There is a clear interface between the two research questions: the assumption of a uniform flow at a certain velocity over the entire width of the collector head with the least amount of energy (part 2) is the only objective of the first part, meaning both programs can be done in parallel. This has the advantage that the computation time, especially for the first part, is reduced significantly as there are no nodules and sediment to be considered.

The subsequent chapters only give a short overview of the main results of the CFD study, although many more cases and variations have been analyzed within both parts.

The methodology used in the CFD analysis is rather straightforward. For every part and within every iteration step, a base case was defined. With every calculation, only one parameter at a time was varied so comparison with the defined base case was clear and evident. In this way, the influence of every parameter can be properly assessed and correct conclusion have been drawn.

12.1.3.3 Part 1: Inflow optimization

As mentioned before, the main objective was to optimize the collector head geometry so that the jet flow reaches a uniform velocity as quickly as possible across the entire width of the collector head. The main variations were the shape, size and position of the inlet nozzles, the geometry of the curved upper plate, and the configuration of the front jet water feeding pipes.

Basically 3 different nozzle geometries were analyzed: (1) circular nozzles (2) ellipsoid nozzles and (3) a jet sheet.



Figure 115: Geometrical configurations (CFD Part 1) : (1) Circular configuration (left), (2) Ellipsoid configuration (centre) and (3) Rectangular configuration (right)

The analysis enabled configuring an optimized geometry of the collector head. Several iterations were performed in the course of the study. The main findings are listed:

- Inclination of the front feeder pipe to 45° (parallel with the discharge duct) and increase of pipe diameter (decrease of water velocity) for an optimized flow in the front pressure chambers.
- The nozzles need to be attached to the top plate of the collector to optimize the Coanda effect. This resulted in semi-circular and -ellipsoid nozzles.

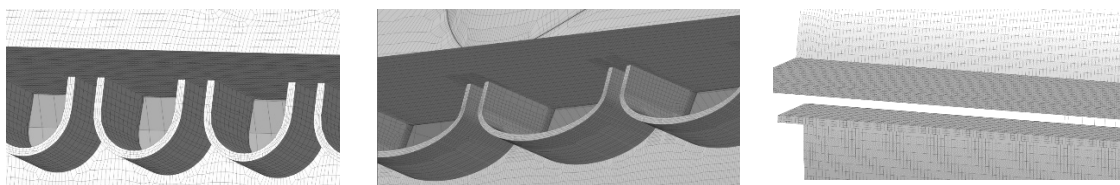
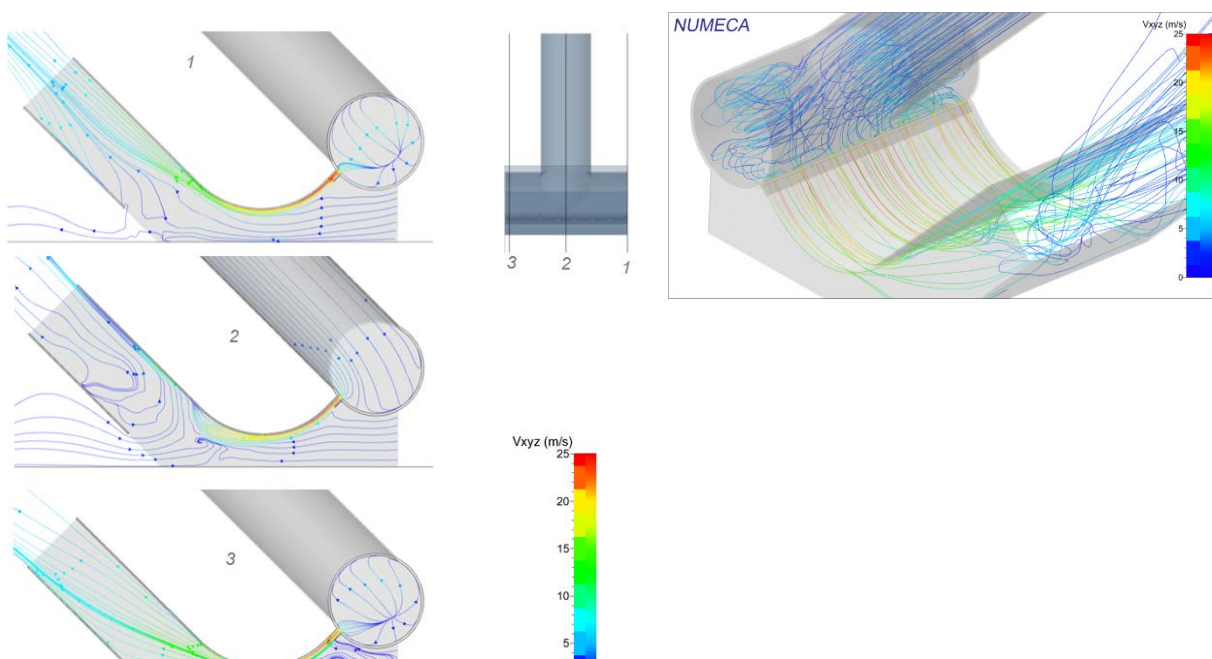


Figure 116: Optimized nozzle shape : (1) Semi-circular (left), (2) Semi-ellipsoidal (centre) or (3) Rectangular (right)

- A continuous curved shape of the upper top plate enhances the adhesion of the Coanda flow to the top plate (so no horizontal piece).

From all 3 configurations, it was decided to use the rectangular configuration (jet sheet) in the design of the lab-test collector. Some results of the CFD analysis are visualized Figure 117.



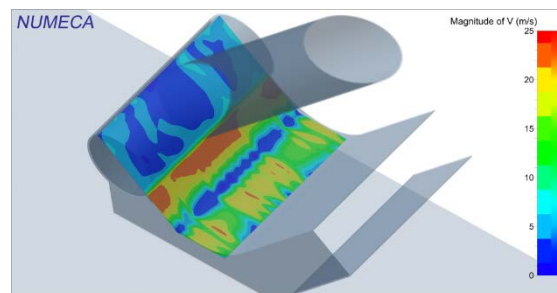


Figure 117: Overview results rectangular configuration : 2D streamlines by cross section (Rectangular) (left); 3D streamlines (Rectangular) (upper right) and Jet path - Velocity magnitude (Rectangular) (lower right)

12.1.3.4 Part 2: Collection and discharge optimization

Part two's major objective is optimizing the design of the duct entry and fine tune the control parameters of the collection process in order to maximize the nodule pick-up efficiency. A significant amount of work has been conducted in order to obtain a reliable simulation of the soil and nodules. A stepped approach has been considered:

- (1) 2D variations: an array of different geometries was analyzed using only water. No sediment or nodules have been considered during this exploratory sub-analysis. The objective was to optimize the flow pattern of the collector head. Most of the variables were geometrical: Jet nozzle injection direction, Coanda curve, duct angle inlet...
- (1) 2D variations: similar calculations as in (1) were performed using nodules, modelled as spheres.

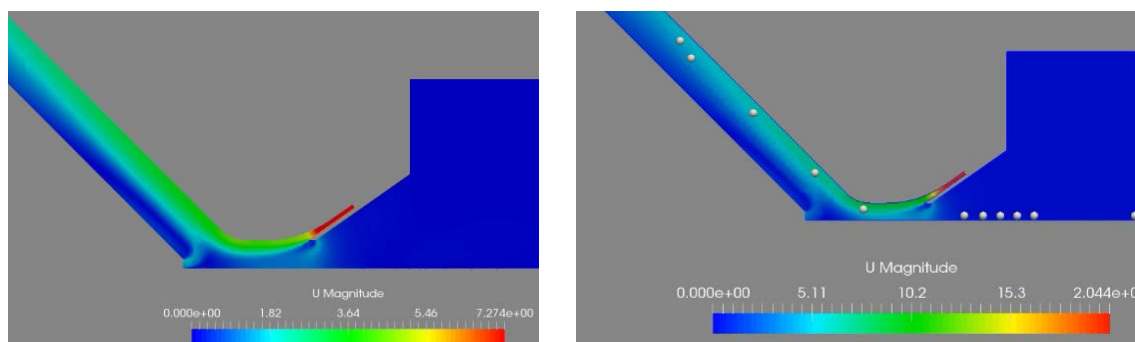


Figure 118: Example of Initial 2D variations for the design of the duct : Water only (left) and water with nodules (right)

- (2) An important factor that had to be taken into account was the characteristics of the seabed as it was expected to play an important role in the nodule collection process. A lot of effort has been put into a correct simulation of the seabed. Small-scale laboratory validation trials have been done in as well.
- (3) 2D analysis of the collection process using nodules, sediment and water. Main variables for these simulations are the flow velocities.
- (4) 3D validation analysis of the collection process using nodules, sediment and water.

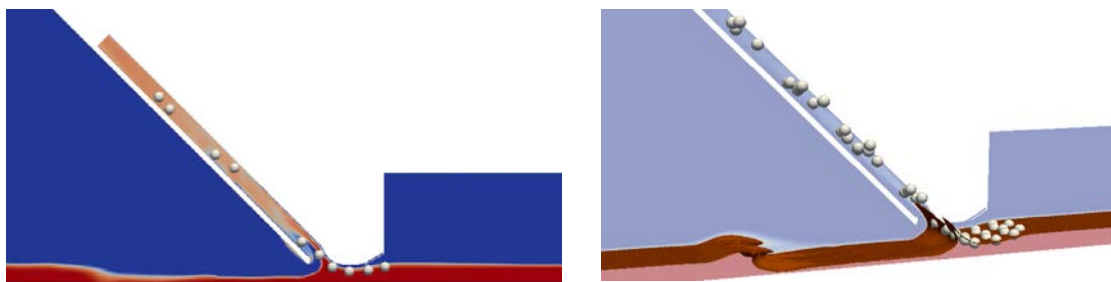


Figure 119: Example of CFD analysis using nodules, sediment and water in 2D (left) or in 3D for a validation simulation (left)

Based on the results of the extensive CFD analysis, the geometrical design of the collector head has been optimized. Additionally, the results provided valuable input for the laboratory test set-up such as necessary flows (and required pump power), traveling carriage speed set-points etc.

12.1.4 Laboratory tests with the hydraulic collector

12.1.4.1 Test set-up

The design of the collector head allowed for nine different geometrical variations. These (small) geometrical variations are necessary to validate the CFD analysis. In accordance with what was mentioned in the previous section on geometrical parameters, a conversion of the test set-up and/or collector head was required for every geometrical variation. The standard configuration, „Standard-10“, has a forward jet sheet opening of ten mm. All other geometrical variations differ from this standard with only one parameter. Hence, the influence of this single variation is clearly noticeable in the test results.

Within every geometrical configuration, test runs were performed varying the 4 process control parameters (v_{PU} , v_{TR} , $v_{Carriage}$ and H_{jet}).

The tests were done in collaboration with the Flanders Hydraulic Research Laboratory in Antwerp. The wave flume was 70m long and separated into 2 interconnected channels: a channel of 1,07m wide for the hydraulic collector and one channel of approx. 2.5m for the water pumps. The pump dimensions were based on the CFD analysis. The feeding pipes and collector itself were equipped with pressure, flow and velocity sensors. The artificial testbed inside the collector channel was approx. 250mm thick. To avoid start-up and end variances in the measurements, only a part of the entire 70m was effectively used for the nodules and testbed. Over a length of 22m, nodules were laid on top of the testbed. Nodule abundance ranged from 15kg/m² to 35kg/m² resulting in a net mass of 330kg to 700kg of nodules.



Figure 120: Laboratory test set-up.

A travelling carriage was used to move the collector forward through the channel. The water pumps, used to feed the jets, were also mounted to the travelling carriage (see Figure 120). The speed of the carriage could be varied between 0.2m/s and 1 m/s.

Tumbled lava stones were used as artificial nodules; these have similar characteristics (weight, density...) but are much harder and less brittle than actual nodules. This is important for the statistical reproducibility of the different tests. Two sizes of lava stones were defined and recognizable by different colours:

- Small: $x < 50\text{mm}$
- Large: $50\text{mm} < y < 100\text{mm}$

The stones were dropped from a laying carriage on top of the wave flume. The laying carriage was exactly 1m x 1m. The required amount of nodules (depending on the abundance) was distributed over the 1m² area. The lower plate was subsequently retracted so the nodules would fall down vertically into the water of the test flume. This procedure allowed an even distribution of the nodules with a correct nodule abundance.



Figure 121: Lava stones handling : Lava stones being separated into different sizes (left) and 1 m² of nodule traveling carriage (right)

The seabed of the CCFZ has some particular characteristics. Analysis on undisturbed samples have been done by the Ghent University and by the Hydraulic Research laboratory in Antwerp. The exact composition and the way how the different layers are built-up have been analysed prior to the laboratory tests.

Despite all these analyses, a more pragmatic approach was used for the testbed with the nodule collector. Some geological characteristics were difficult to match with the objective of the collector tests. In order to maximise the number of test runs, some engineering shortcuts had to be taken with regard to the testbed.

- (1) The top layer has been disregarded for the tests: this loose, “unconsolidated” layer present in the CCFZ has not been considered in the laboratory. The engineering assumption that the nodules lie on a more firm sublayer simplifies the laboratory test set-up significantly. The reasoning behind this assumption is that this first unconsolidated layer of thick water to loose sediment is sucked-up or blown away by the collector, so it has no real added value for the collection process. On the other hand, disregarding the first unconsolidated layer reduced settling time significantly and consequently increased the number of test runs.
- (2) Diluted loam was used to simulate the firm layer underneath the unconsolidated top one. Comparative geotechnical tests were performed on in-situ samples and on different kinds of artificial soils (loam, clay, and bentonite). Loam has similar macro-characteristics (texture, feel, stickiness etc.) that are important for the laboratory tests. Compared to bentonite, loam is ‘user friendly’ and less messy. Companies that manufacture bricks in the north-east of Belgium have supplied the loam that was subsequently further diluted at the laboratory facility to the predetermined specification.
- (3) Nodule penetration into the testbed has not been considered in the tests. According to the engineering assumption made in (1), nodules are partially embedded in the top layer (the equatorial belt of a nodule) and lie on top of the firm layer underneath. By disregarding the top unconsolidated layer, no nodule penetration into the testbed is required in the laboratory trials. Again, this simplifies the test set-up significantly.



Figure 122: Artificial sediment: Testbed (left) and Loam pit (North-East Belgium) (right)

Because of these assumptions, the laboratory tests with the collector head cannot be used to draw conclusions on the depth of penetration. At the time of writing, an assumption is made that the depth of influence of the water jets varies between $50\text{mm} < \text{depth of influence} < 150\text{mm}$. The maximum depth depends on the thickness of the unconsolidated top layer of the seabed.

12.1.4.2 Laboratory test results

An overview of the 85 runs is provided in Table 36 below.

Table 36: Results laboratory tests. *F** stands for Final and *WT** stands for nodules

Test Results Overview			Control Parameters				Efficiency
Geometrical configuration	#Test	Nodule abundance	Vcarriage	VPU	VTR	HCOL	η PU
	runs						
		[kg/m ²]	[m/s]	[m/s]	[m/s]	[mm]	[%]
Standard-10	43	20	[0.5 – 1]	[05 – 20]	[5-15]	[50 - 160]	[17 - 99]
Standard-05	4	20	[1]	[10 – 20]	[5-10]	[55 - 120]	[10 - 75]
Standard-15	3	20	[1]	[10 - 16]	[5-10]	[80 - 100]	[70 - 91]
Rubber-10	3	20	[0.5 - 1]	[13 - 15]	[0 - 10]	[85 - 100]	[83 – 98]
Finger-10	11	20	[0.5 – 1]	[10 – 16]	[0 – 10]	[85 – 120]	[01 – 98]
Circular-10	5	20	[0.75 – 1]	[14 – 16]	[6 – 8]	[100 – 120]	[75 – 97]
Standard-7.5	4	20	[0.75 – 1]	[16 – 21.5]	[5 - 8]	[80 – 100]	[84 – 99]
Standard-10F*	6	20	[0.75]	[10 – 16]	[5 – 8]	[80 – 100]	[87 – 98]
Standard-10WT**	6	20	[0.5 – 1]	[0 – 16]	[0 – 10]	[80 – 150]	[ntb]
Total	85	[-]	[-]	[-]	[-]	[-]	Max 99%

After the trials with nodules in the testbed, the sediment was removed from the test tank in order to perform some test runs in clear water. The main focus of these test runs was to visually validate the results, especially for the runs that resulted in poor efficiencies. Before these tests, only an educated guess could be made of the cause. Several cameras were mounted around the collector head. Below is a snapshot from a movie taken underneath the collector (hence poor quality). Nodules are visible at the front.



Figure 123: Test runs with clear water


12.2 Pre- and Post-Dive Check-up list

Document Title: Patania Pre-Dive Checklist

Project Document Reference: GSR PROCAT I revB

Client Document Reference: N.A.

Issue date: 25-5-2017



GSR
Global Sea Mineral Resources

Location number:	Dive number:	Date: ____/____/2017	Dive main objectives
TSTD Patania crew:		Time: ____:____	Technical / Problem solving Terra mechanical Collector simulation (Pump) Automatisation Operational Other:
General comment:			
Toolbox Talk ref #:	External Supervisor(s) – OFG / TOPAZ		

A	Visual Checks	B	Instrumentation Checks	C	Compensator Check	E	Functional Tests Dry (Deck)	F	Final launch checks
A1	Vehicle						Vehicle	F1	Disc 1 (aft) up
A2	Track chain PS / SB	B1	Start POD	C1	Start up HPU	E1	Disc 1 Up / Down	F2	Disc 2 (fwd) up
A3	Chain tensioner PS / SB	B2	POD Vacuum [bar]	C2	Main Reservoir [%]	E2	Disc 1 length measurement	F3	Drawbar up
A4	Road wheels PS / SB	B3	Pan & Tilt Front	C3	HPU Motor [%]	E3	Disc 2 Up / Down	F4	Sea fastening Removed
A5	Hoses secured / leaks	B4	Lamp Led Front	C4	Valve pack [%]	E4	Disc 2 length measurement	F5	Earth Strap Removed
A6	Hydr. connectors secured	B5	SD Camera Front	C5	Umbilical Termination [%]	E5	Drawbar Up / Down	F6	Umbilical Free (ropes)
A7	Electr. connectors secured	B6	Pan & Tilt Aft	C6	Max hydr. Pressure [bar]	E6	Drawbar length measure	F7	PHINS cover removed
A8	Mechanical fittings secured	B7	Lamp Led Aft			E7	Drawbar loadcell top	F8	ADCP cover removed
A9	POD & valve pack integrity	B8	SD Camera Aft			E8	Drawbar loadcell SB	F9	SD Front cover removed
A10	Structural inspection	B9	Center Lamp Beva			E9	Drawbar loadcell PS	F10	SD Aft cover removed
A11	Track pads inspected	B10	HD/SD Camera	D	Start-up	E10	Thruster (Cw / Ccw)	F11	HD camera cover removed
A12	Buoyancy modules	B11	HD Strobe					F12	SOLO record plug connected
A13	Lifting arrangement + floater	B12	Camera Winch	D1	Clear Com test	E17	Deck HPU & winch	F13	Patania HPU stopped
A14	Umbilical + Termination	B13	Camera Outtrigger	D2	Back up com. with bridge	E18	HPU cooling water started		
A15	SOLO camera mounting	B14	PHINS	D3	Lamp test control panel	E19	Check HPU oil level	G	Functional Tests Wet
A16	Main deck	B15	DVL	D4	Check alarm list	E20	Start-up deck HPU	G1	Instrumentation B3 - B19
A17	Umbilical floats ready (35)	B16	ADCP	D5	Dive logs available	E21	Winch length measurement	G2	Start HPU
A18	Umbilical condition	B17	CTD	D6	Video log & USB available		Winch load pressure sensor	G3	Func. Tests Dry E2 - E11
A19	All umbilical sheaves	B18	MIDAS	D7	ECM POD [Q]			G4	PS track Fwd / Aft
A20	Load path outtrigger	B19	USBL beacon	D8	ECM HPU [Q]			G5	PS & SB track simult. Fw/Aft
	Other:	B20		D9	LIM POD >10 MΩ			G6	PS track encoder
	USBL beacon ClumpW			D10	LIM POD >10MΩ			G7	SB track encoder
				D11				G8	Env. Pump functioning (la)
								G9	

Comments:	Signed	
	Name:	
	Position:	
Notes:	<div style="display: flex; justify-content: space-between;"> <div>N/A</div> <div>Box when items is not required / fitted</div> </div> <div style="display: flex; justify-content: space-between;"> <div>✓</div> <div>Box when checked and accepted</div> </div> <div style="display: flex; justify-content: space-between;"> <div>X</div> <div>Box when checked and faulty</div> </div>	

12.3 Panolin oil Safety data sheet

Safety Data Sheet

according to Regulation (EC) No. 1907/2006 (amended by Regulation (EU) No 453/2010)



Trade name :	PANOLIN ATLANTIS 15	Version (Revision) :	1.1.0 (1.0.0)
Revision date :	29.10.2015		
Print date :	25.01.2016		

SECTION 1: Identification of the substance/mixture and of the company/undertaking

1.1 Product identifier

PANOLIN ATLANTIS 15 (36060)

1.2 Relevant identified uses of the substance or mixture and uses advised against

Relevant identified uses

Hydraulic oil, Lubricant

1.3 Details of the supplier of the safety data sheet

Manufacturer/Supplier :

Panolin AG

Street/P.O.Box :

Bläsimühle

Country code/Postal code/Town/City :

8322 Madetswil

Country :

Switzerland

Telephone :

+41(0)44 956 65 65

Contact :

info@panolin.com

1.4 Emergency telephone number

Swiss Toxicological Information Centre
Phone: +41 (0)44/ 251 51 51

SECTION 2: Hazards identification

2.1 Classification of the substance or mixture

The product is not classified according to the calculation method of the General Classification guideline for preparations of the EU in the latest version.

Classification according to Regulation (EC) No. 1272/2008 [CLP]

None

2.2 Label elements

None

2.3 Other hazards

None

SECTION 3: Composition / information on ingredients

3.2 Mixtures

Mixture of synthetic esters and additives.

Hazardous ingredients

None

SECTION 4: First aid measures

4.1 Description of first aid measures

General information

Remove affected person from the danger area and lay down. Contaminated, soaked clothing and shoes change and clean. When in doubt or if symptoms are observed, get medical advice. Never give anything by mouth to an unconscious person or a person with cramps.

Following inhalation

Remove casualty to fresh air and keep warm and at rest. In case of respiratory tract irritation, consult a physician. If

12.4 Sediment plume results

12.4.1 Scenario 1 results – 2009

12.4.1.1 Sediment deposition

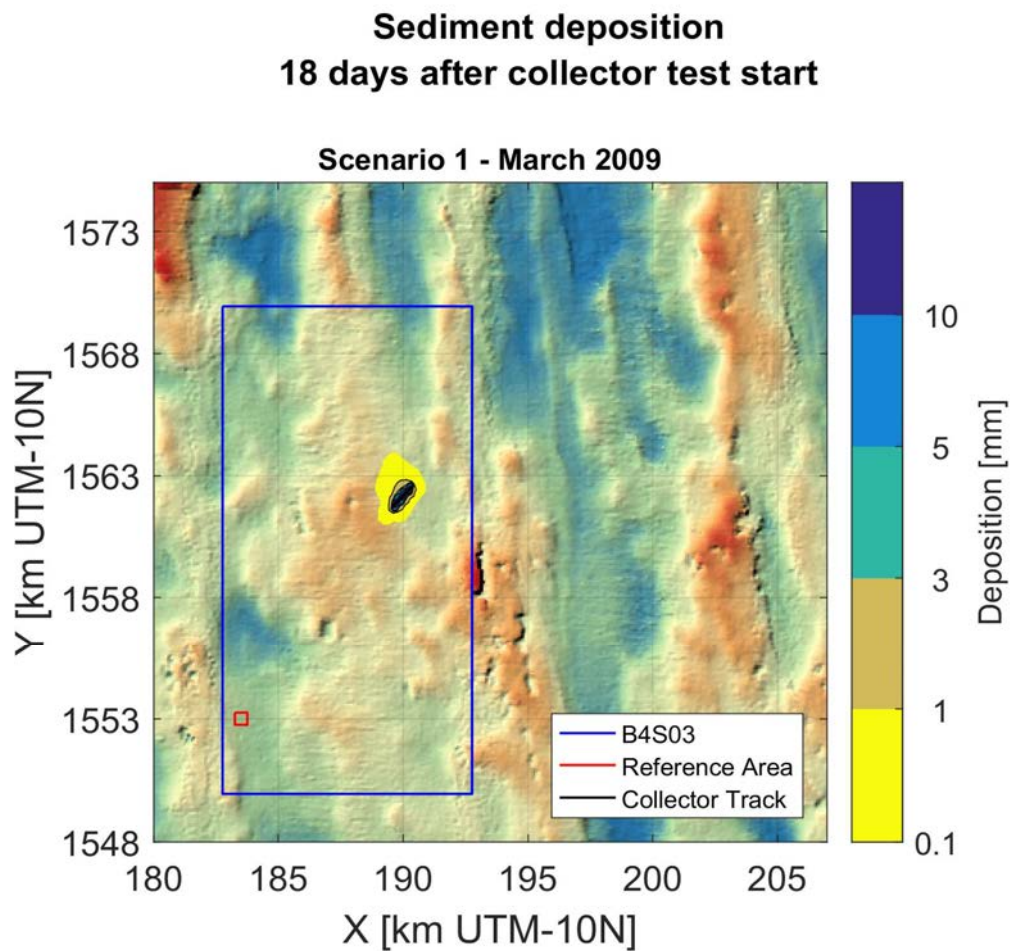


Figure i: Sediment deposition at the end of the model simulation for scenario 1 - March 2009

Sediment deposition 18 days after collector test start

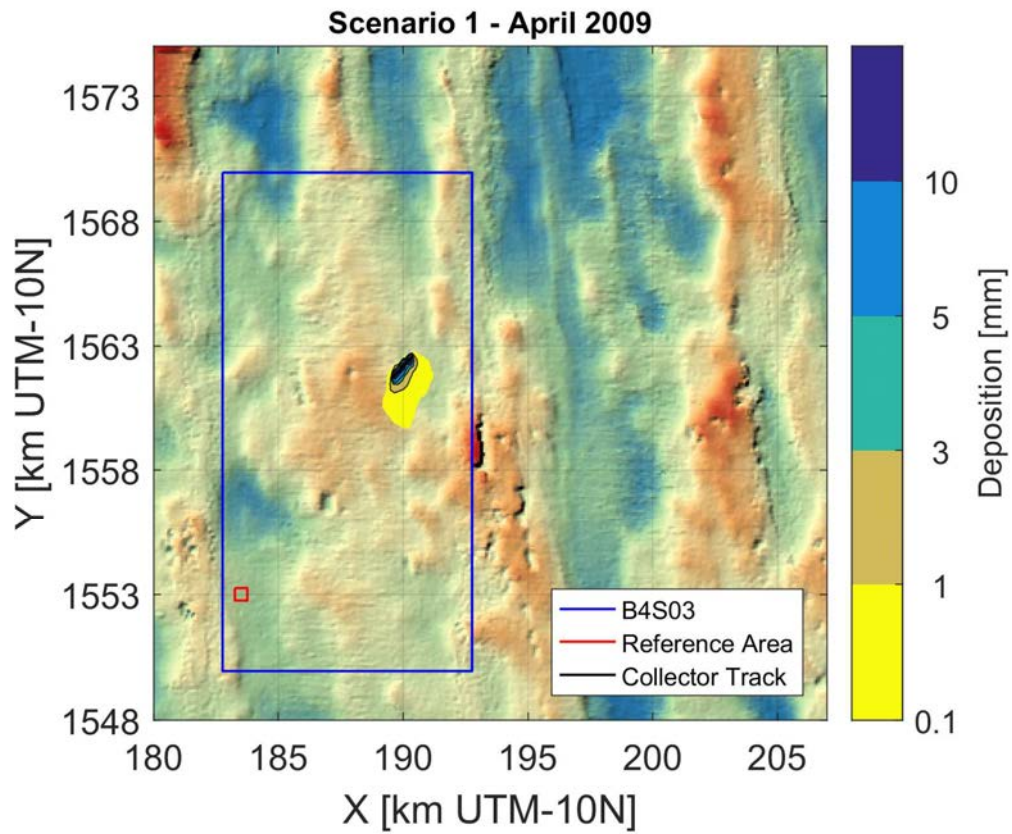


Figure ii: Sediment deposition at the end of the model simulation for scenario 1 - April 2009

Sediment deposition 18 days after collector test start

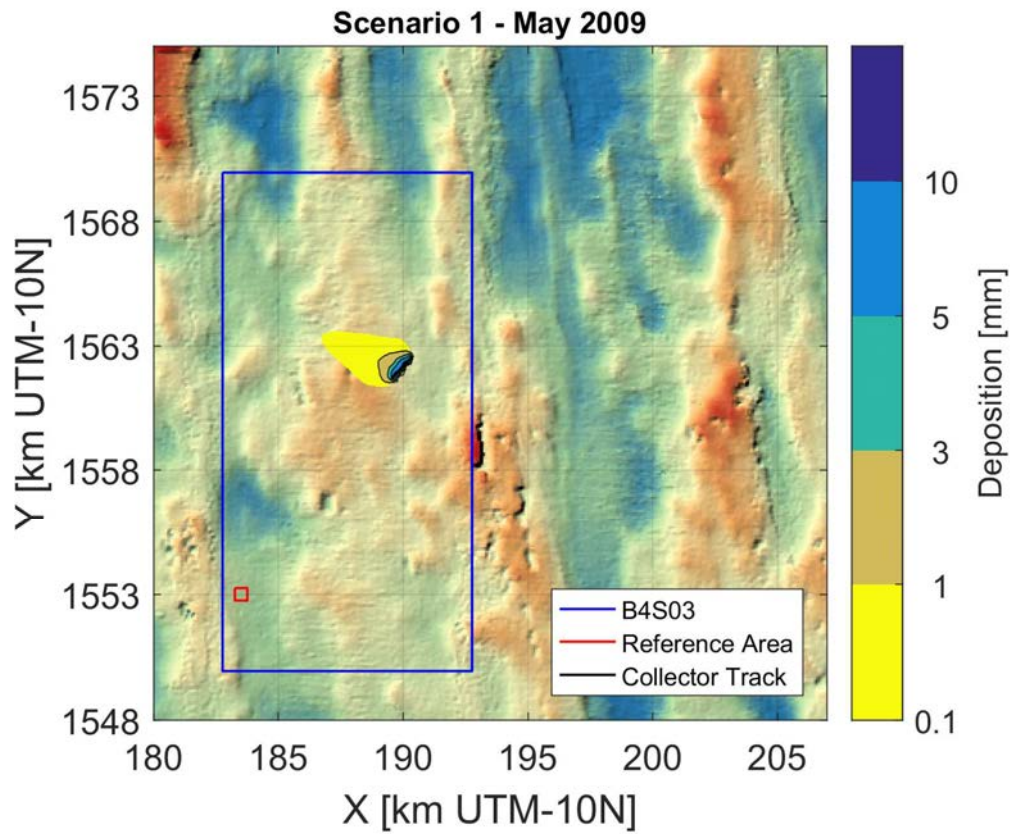


Figure iii: Sediment deposition at the end of the model simulation for scenario 1 - May 2009

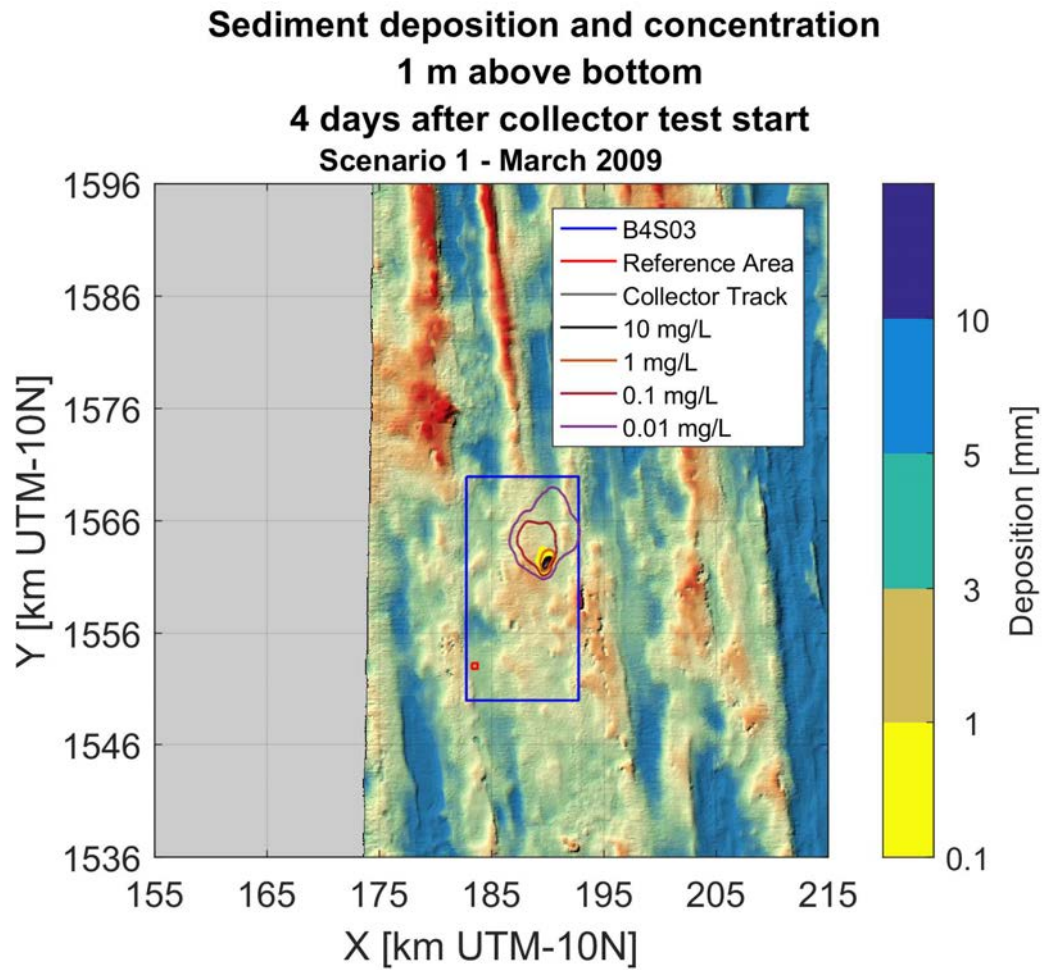


Figure iv: Sediment suspension contours at the end of the Patania II trial for scenario 1 - March 2009

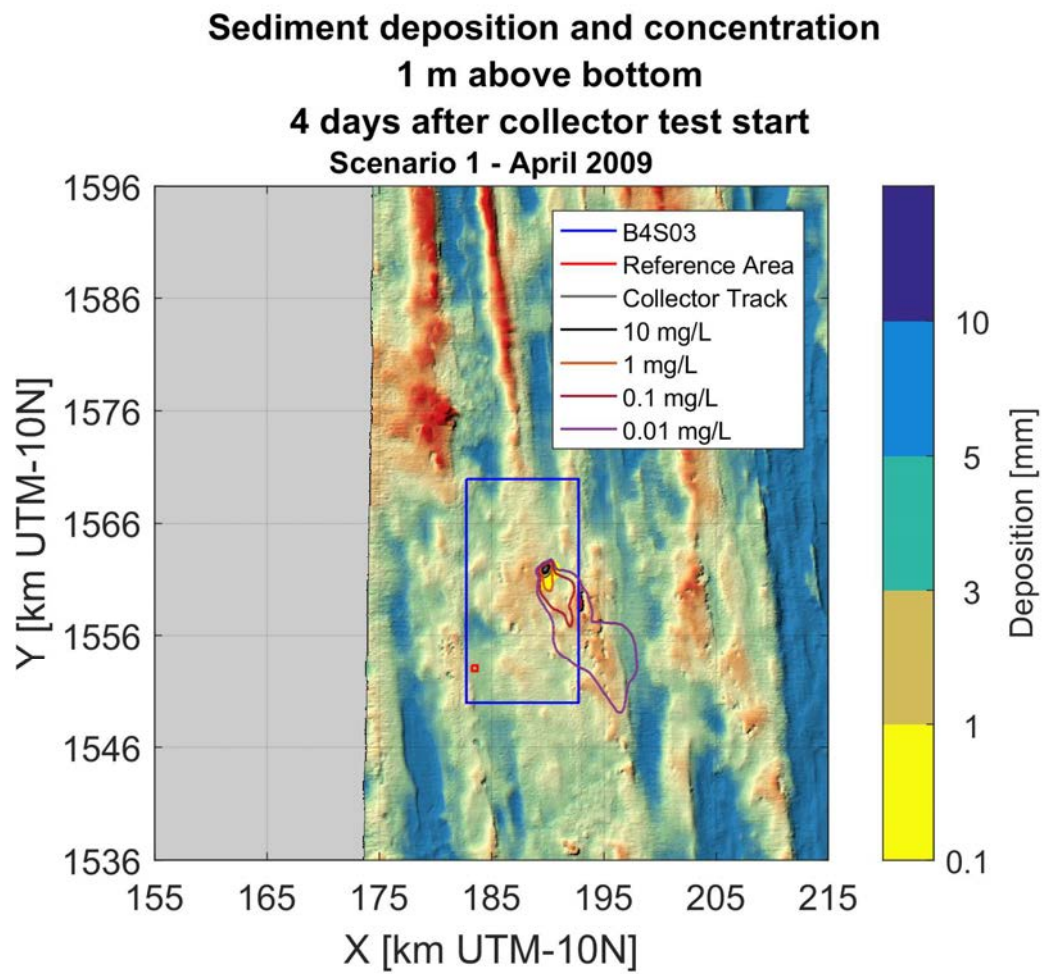


Figure v: Sediment suspension contours at the end of the Patania II trial for scenario 1 - April 2009

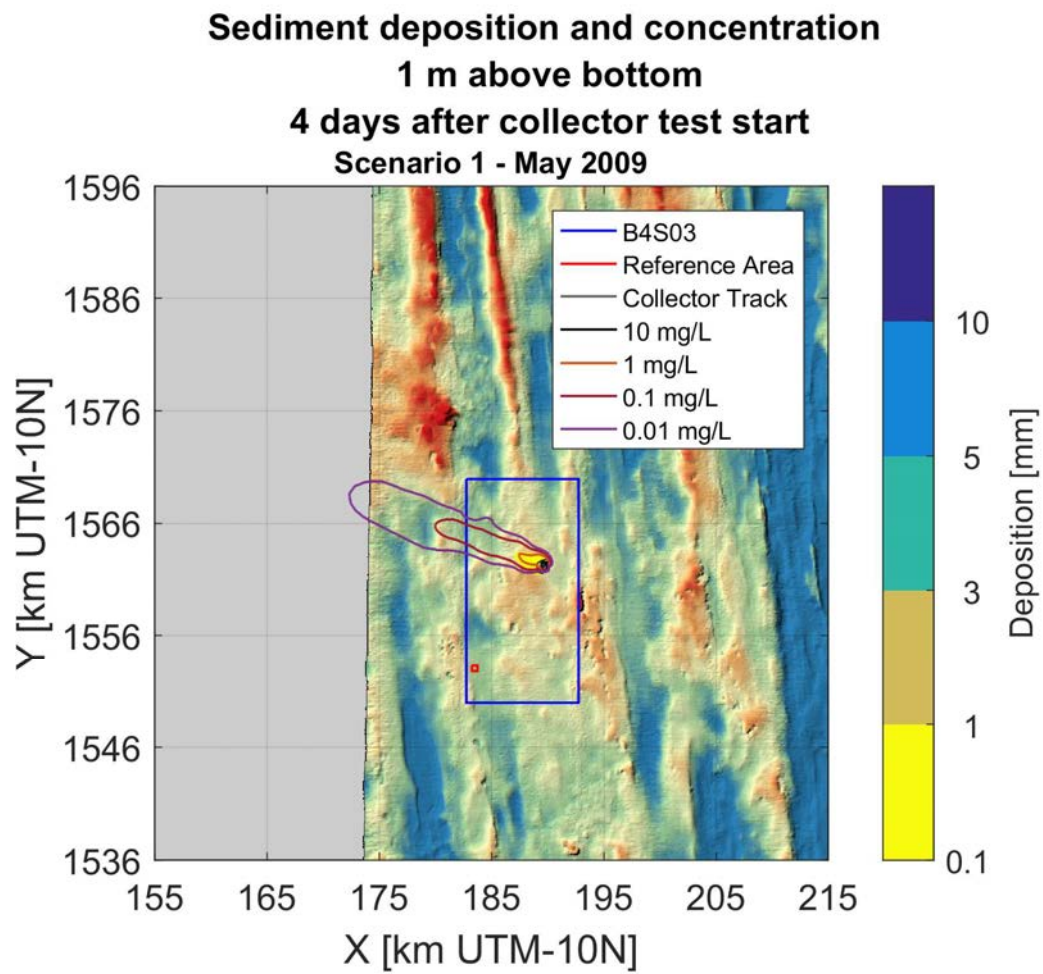


Figure vi: Sediment suspension contours at the end of the Patania II trial for scenario 1 - May 2009

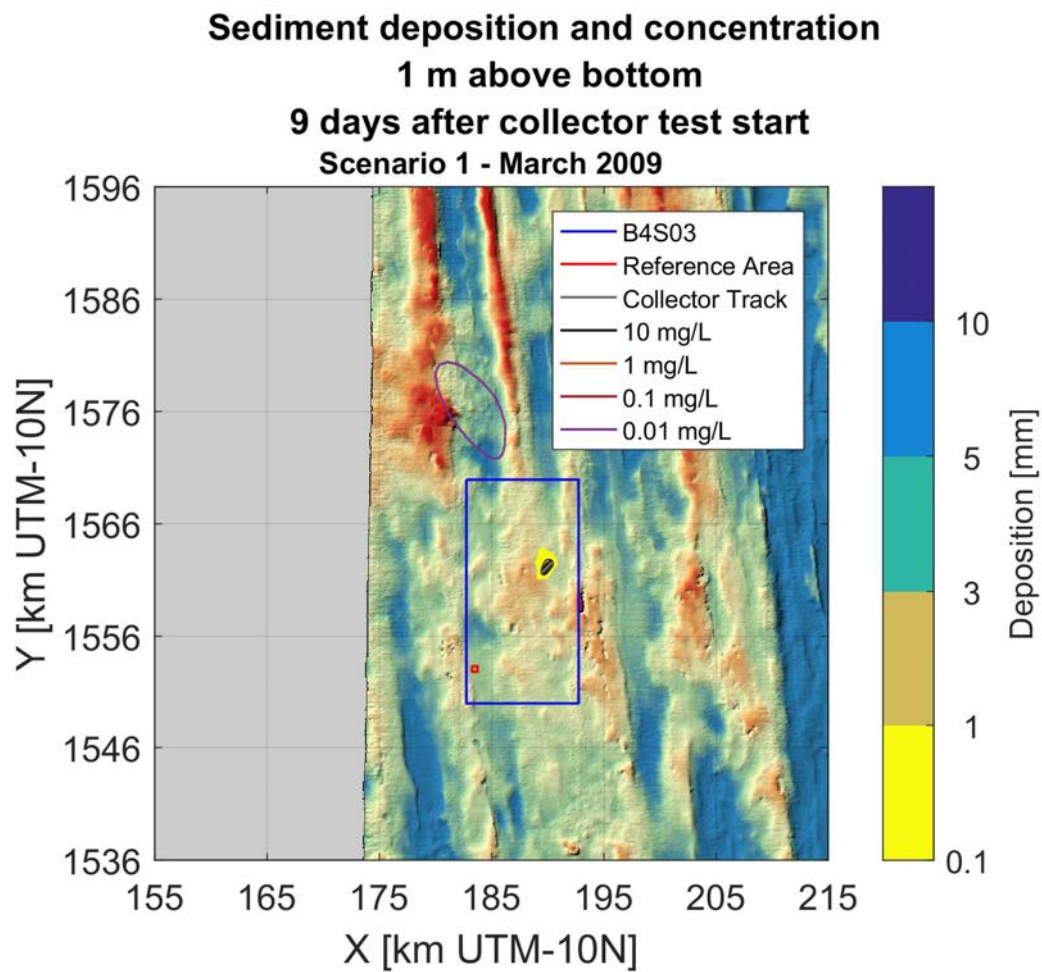


Figure vii: Sediment suspension contours 5 days after at the end of the Patania II trial for scenario 1 - March 2009

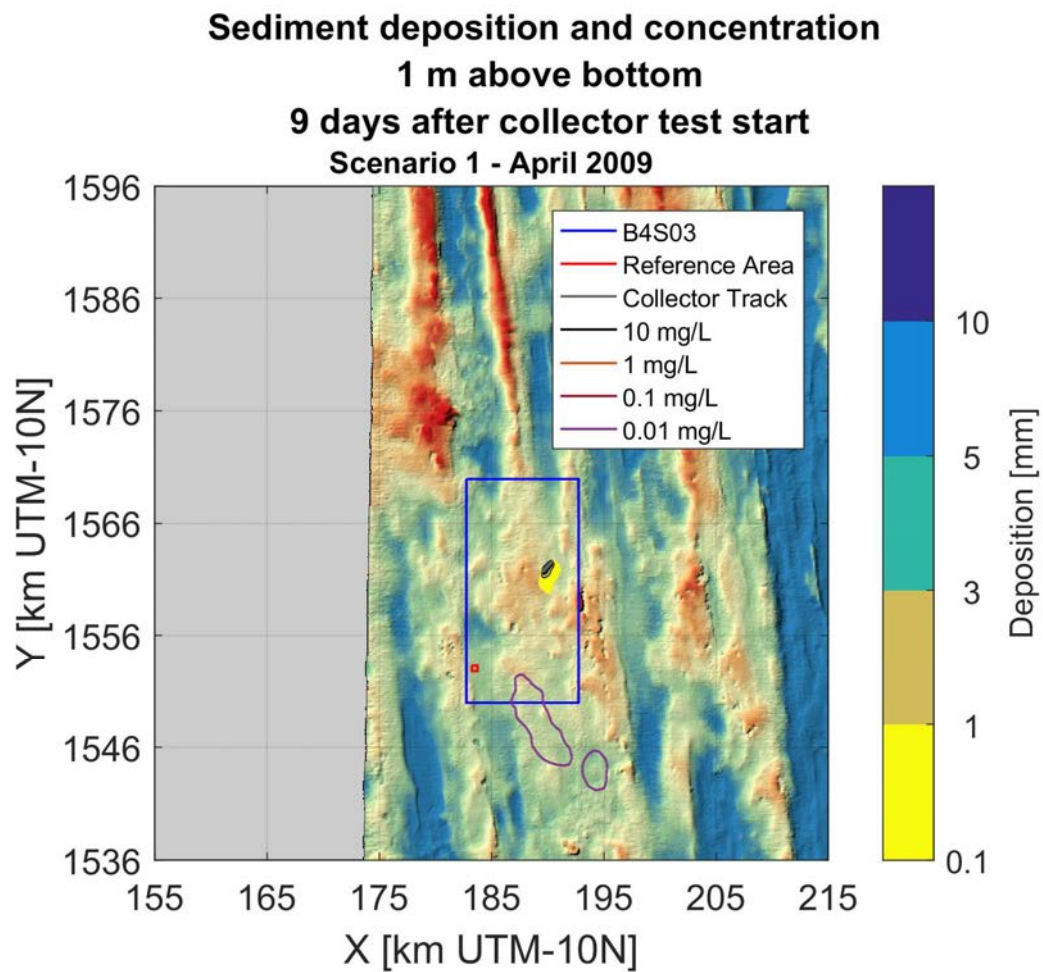


Figure viii: Sediment suspension contours 5 days after at the end of the Patania II trial for scenario 1 - April 2009

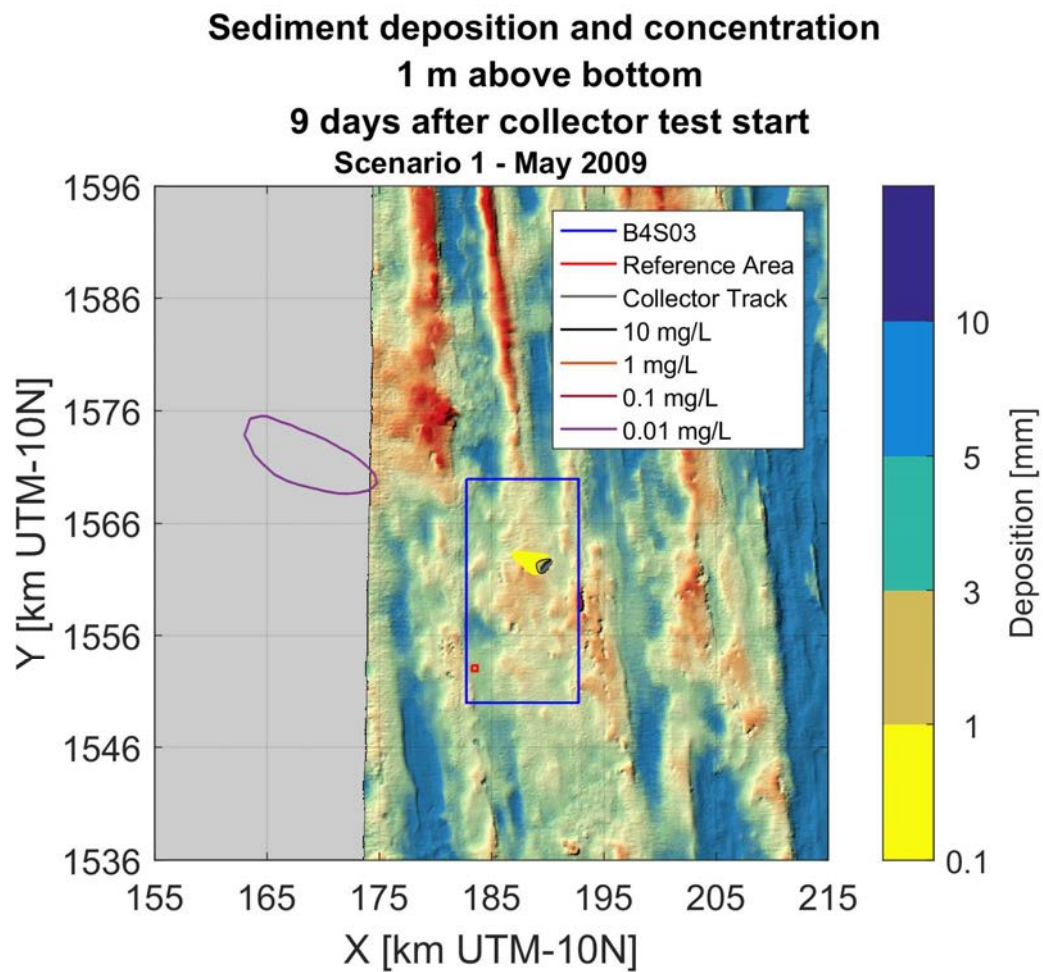


Figure ix: Sediment suspension contours 5 days after at the end of the Patania II trial for scenario 1 - May 2009

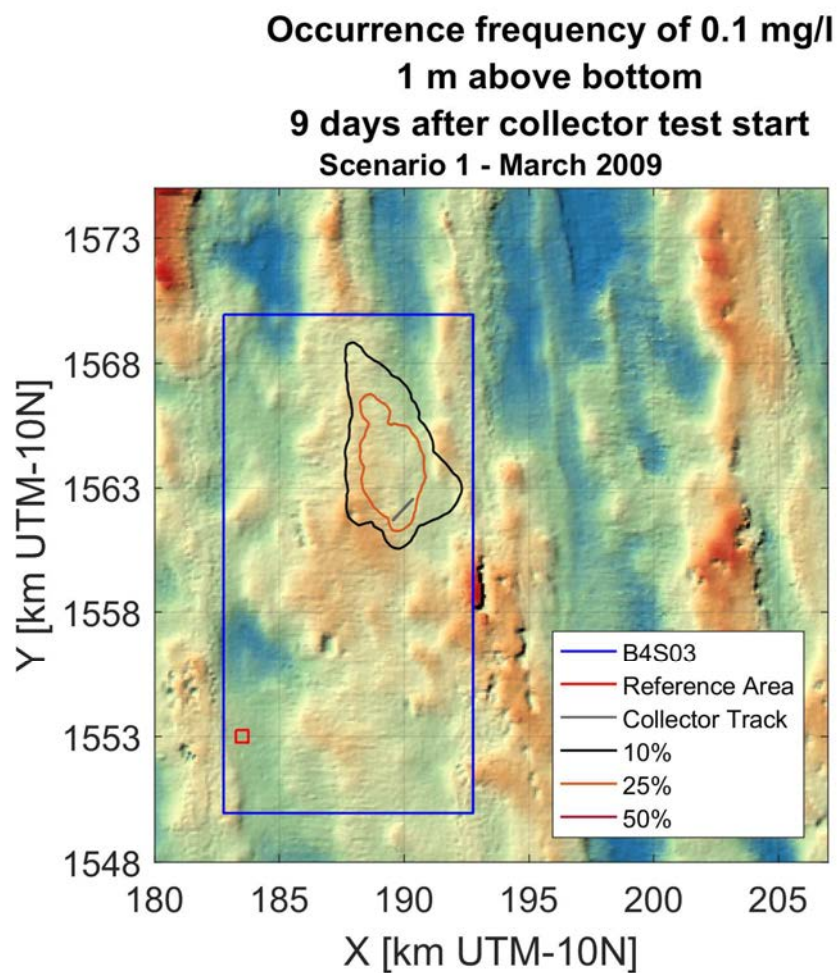


Figure x: Frequency of occurrence for 0.1 mg/l sediment concentration for scenario 1 - March 2009

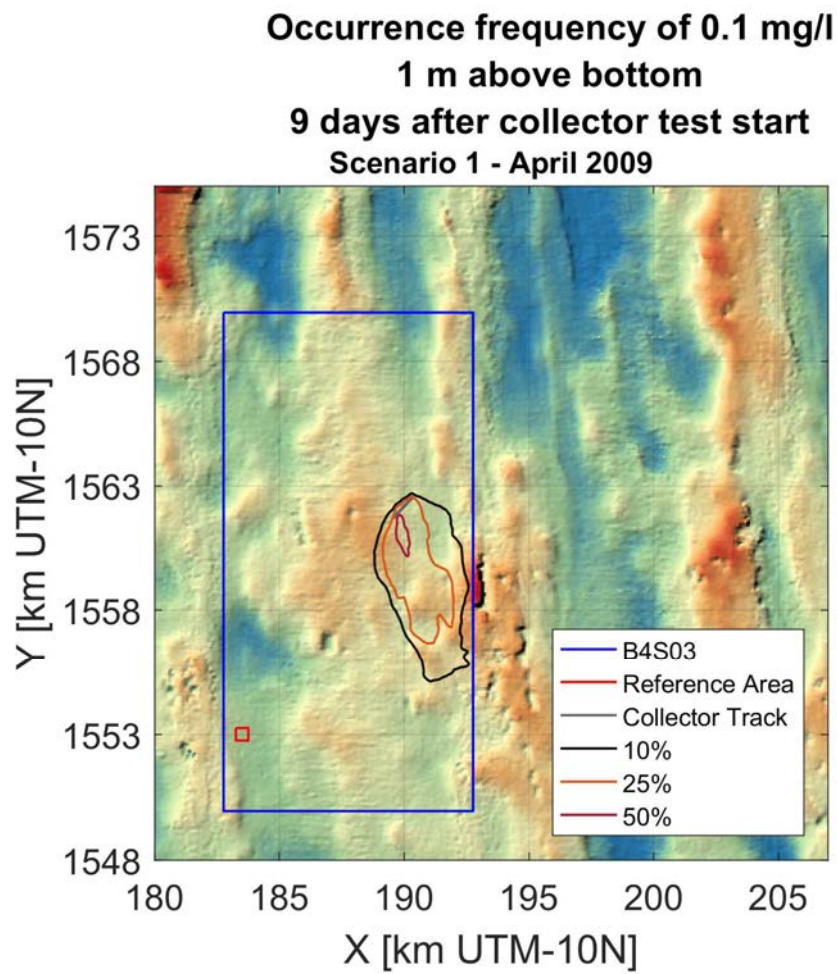


Figure xi: Frequency of occurrence for 0.1 mg/l sediment concentration for scenario 1 - April 2009

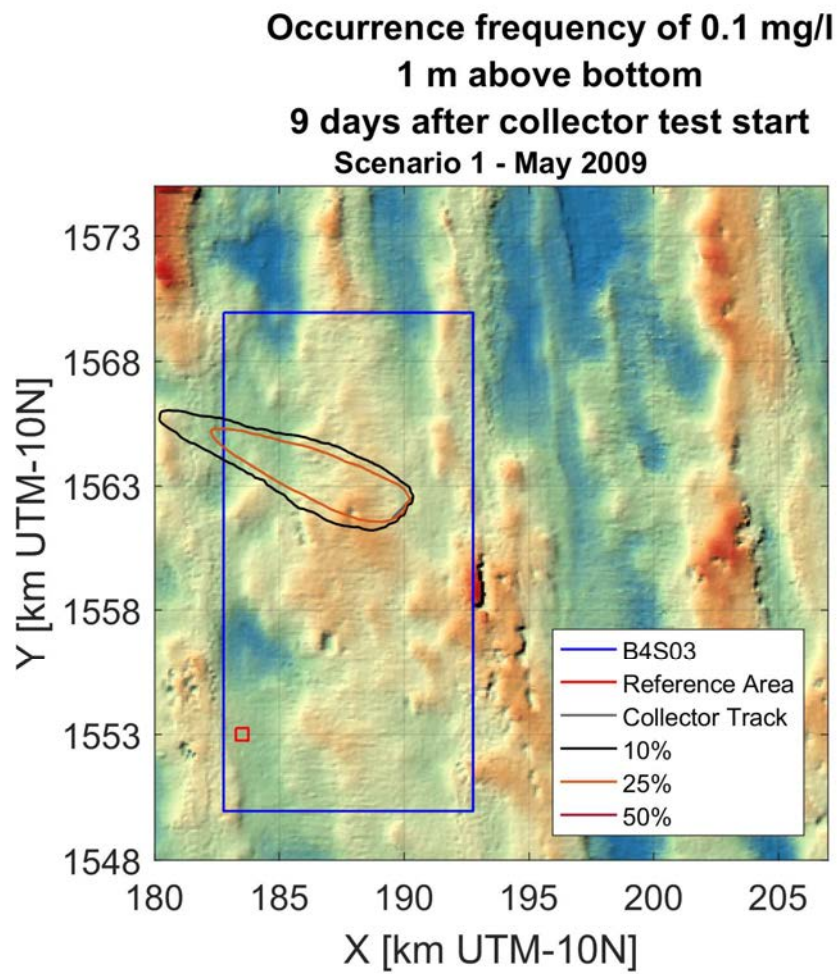


Figure xii: Frequency of occurrence for 0.1 mg/l sediment concentration for scenario 1 - May 2009

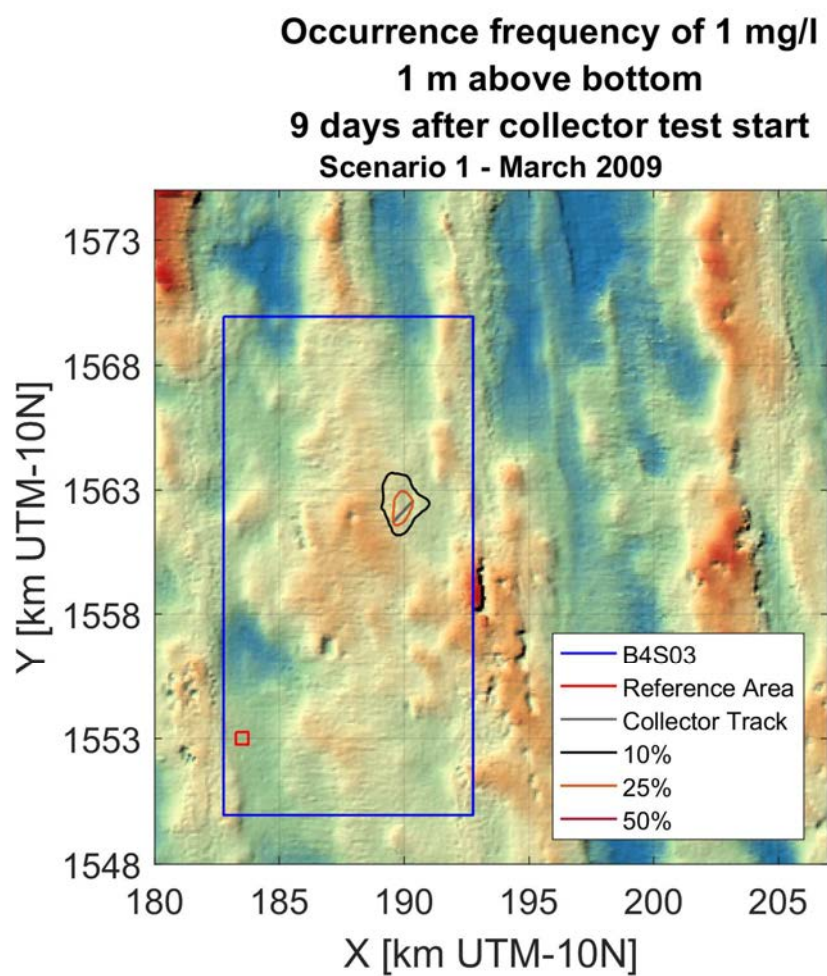


Figure xiii: Frequency of occurrence for 1 mg/l sediment concentration for scenario 1 - March 2009

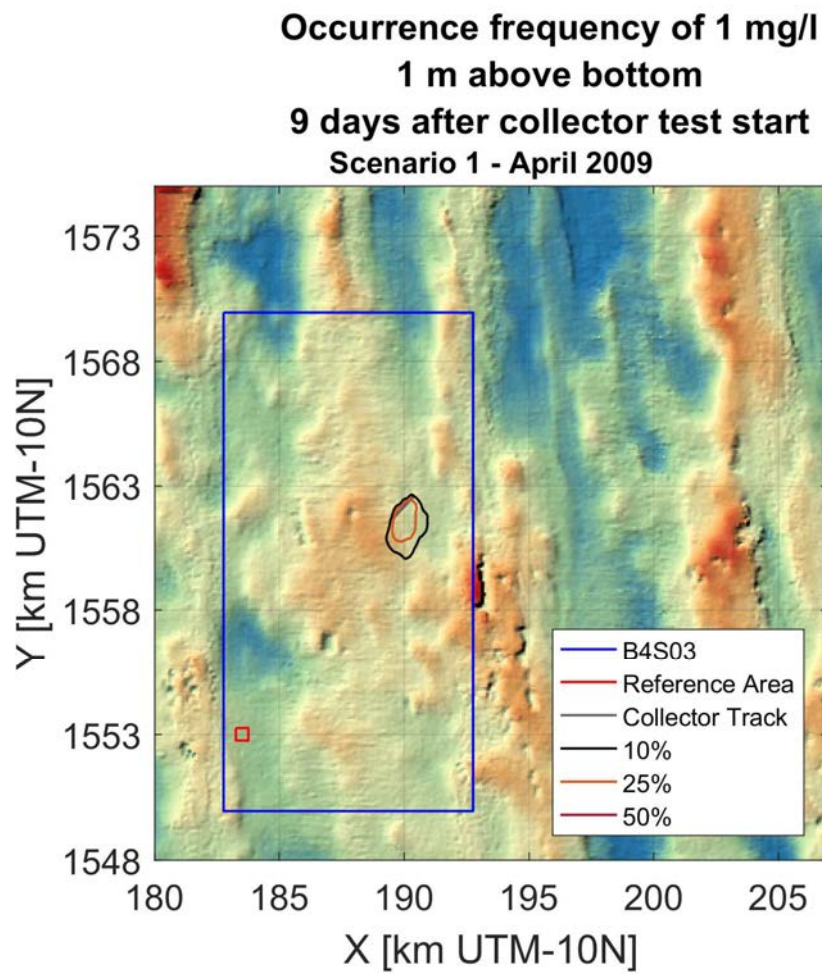


Figure xiv: Frequency of occurrence for 1 mg/l sediment concentration for scenario 1 - April 2009

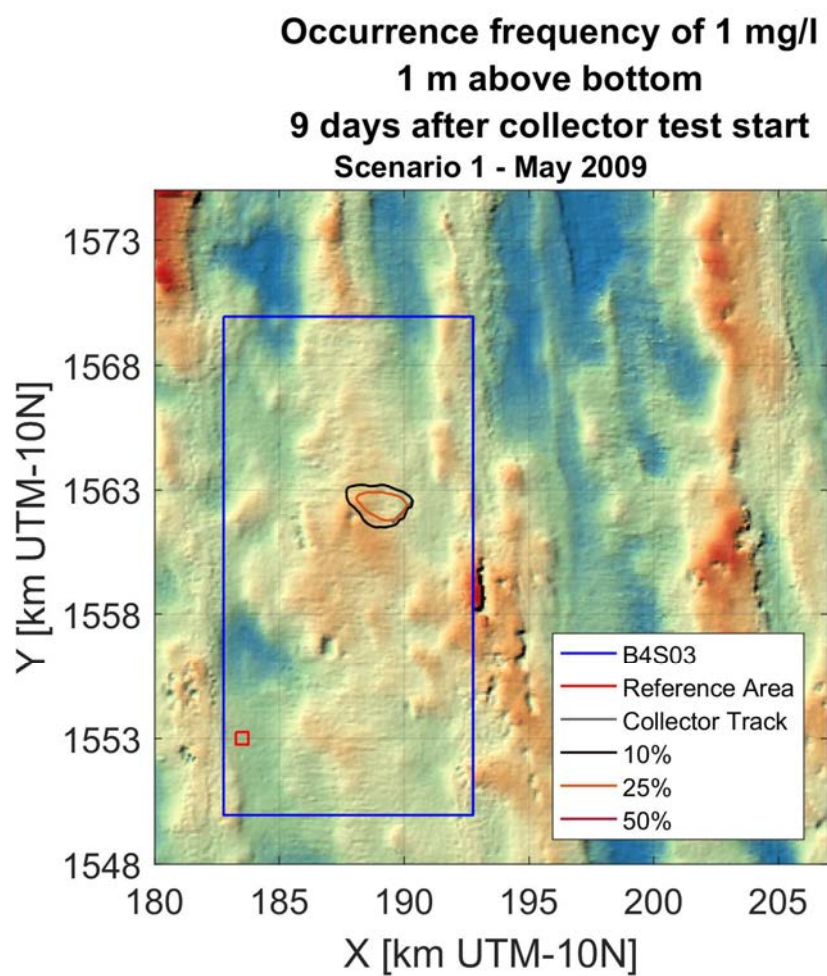


Figure xv: Frequency of occurrence for 1 mg/l sediment concentration for scenario 1 - May 2009

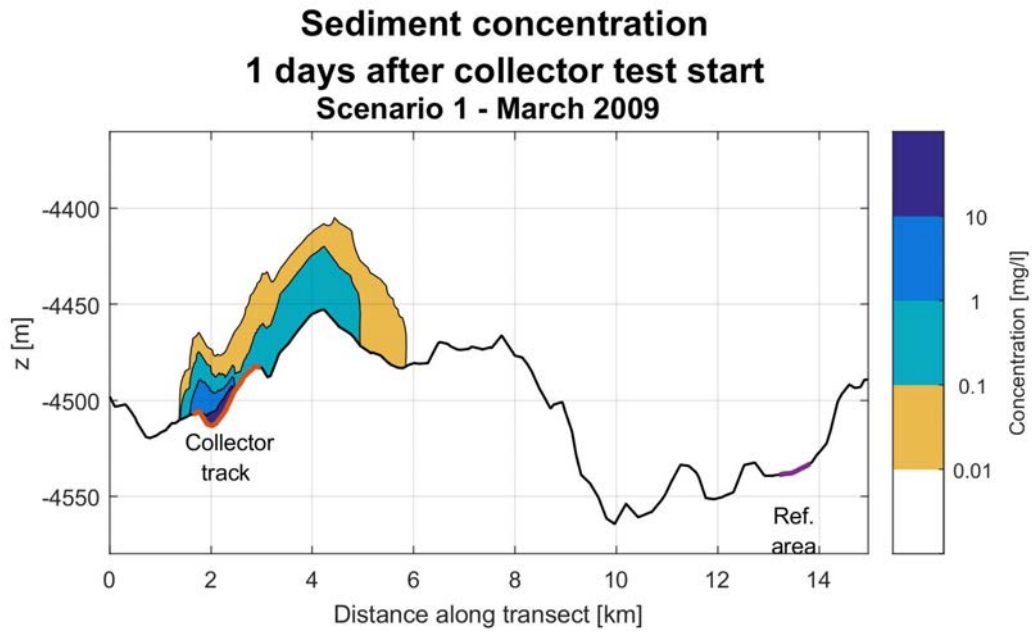


Figure xvi: Cross-sectional sediment concentration contours 1 day after the start of the Patania II trial for scenario 1 - March 2009

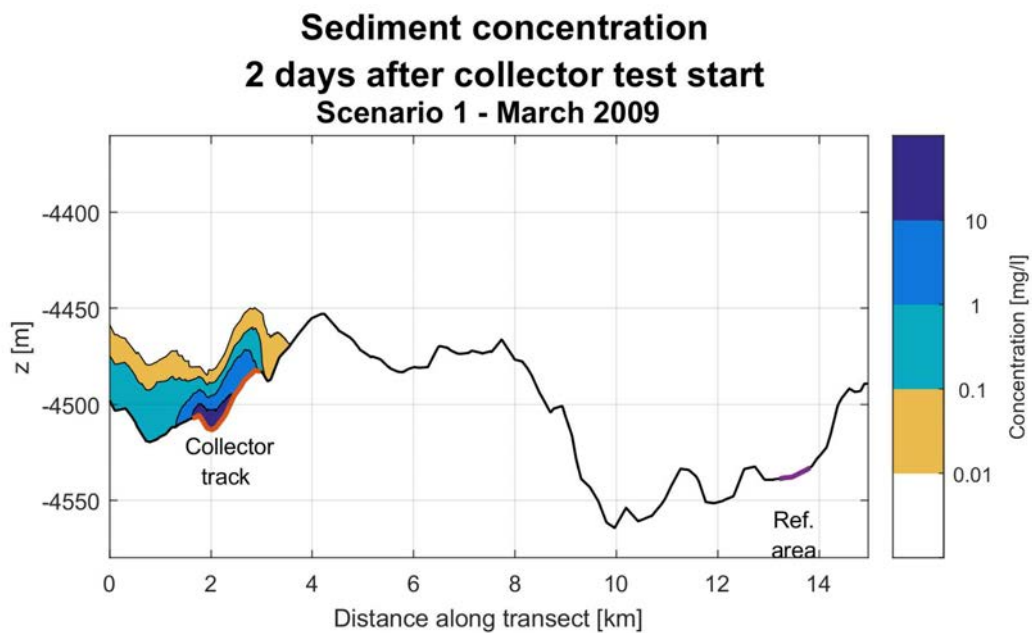


Figure xvii: Cross-sectional sediment concentration contours 2 days after the start of the Patania II trial for scenario 1 - March 2009

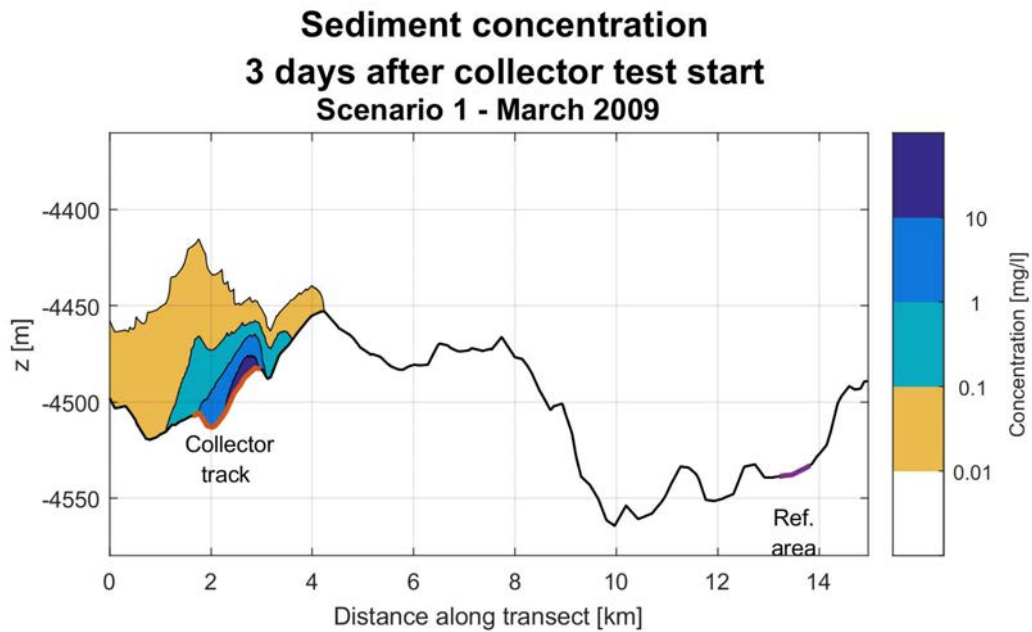


Figure xviii: Cross-sectional sediment concentration contours 3 days after the start of the Patania II trial for scenario 1 - March 2009

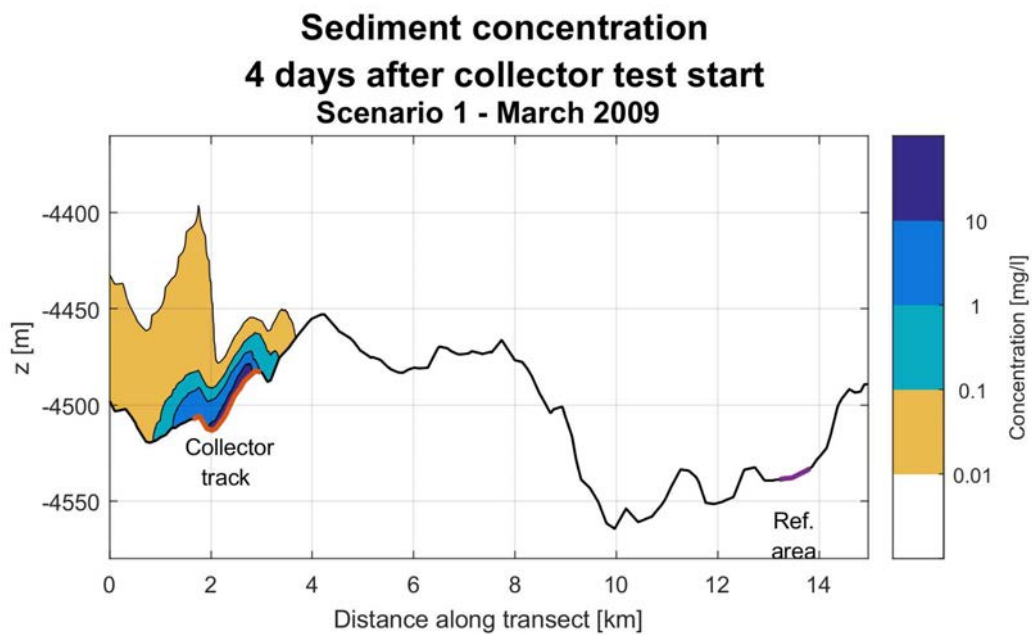


Figure xix: Cross-sectional sediment concentration contours 4 days after the start of the Patania II trial for scenario 1 - March 2009

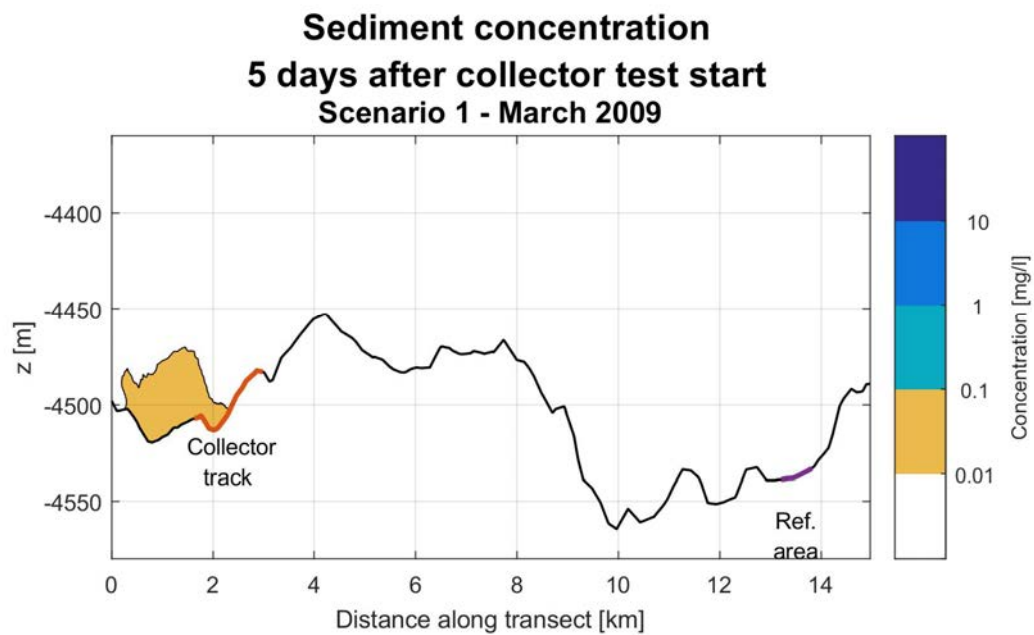


Figure xx: Cross-sectional sediment concentration contours 5 days after the start of the Patania II trial for scenario 1 - March 2009

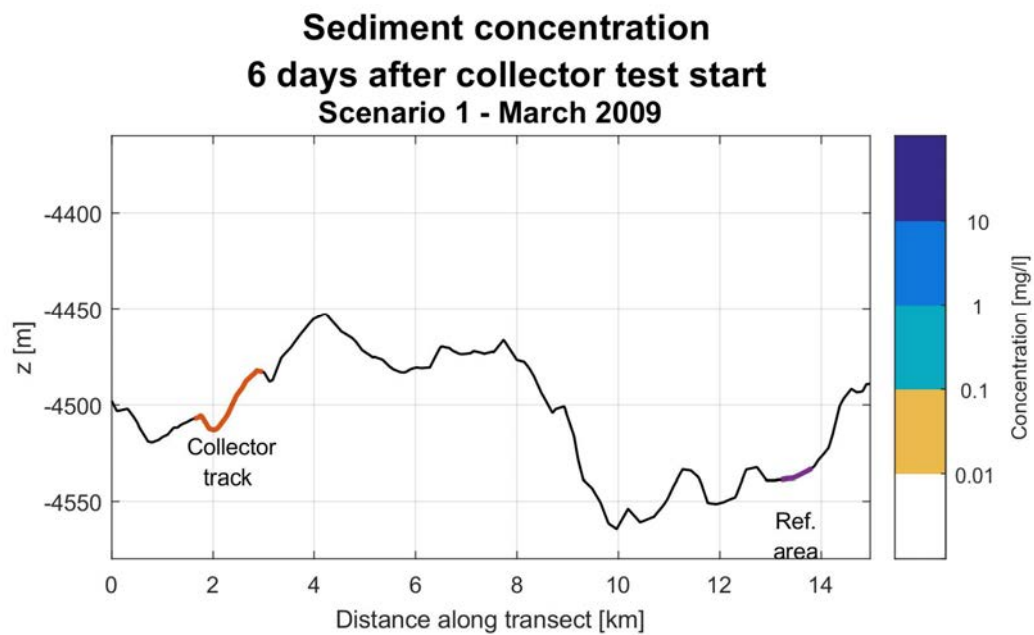


Figure xxi: Cross-sectional sediment concentration contours 6 days after the start of the Patania II trial for scenario 1 - March 2009

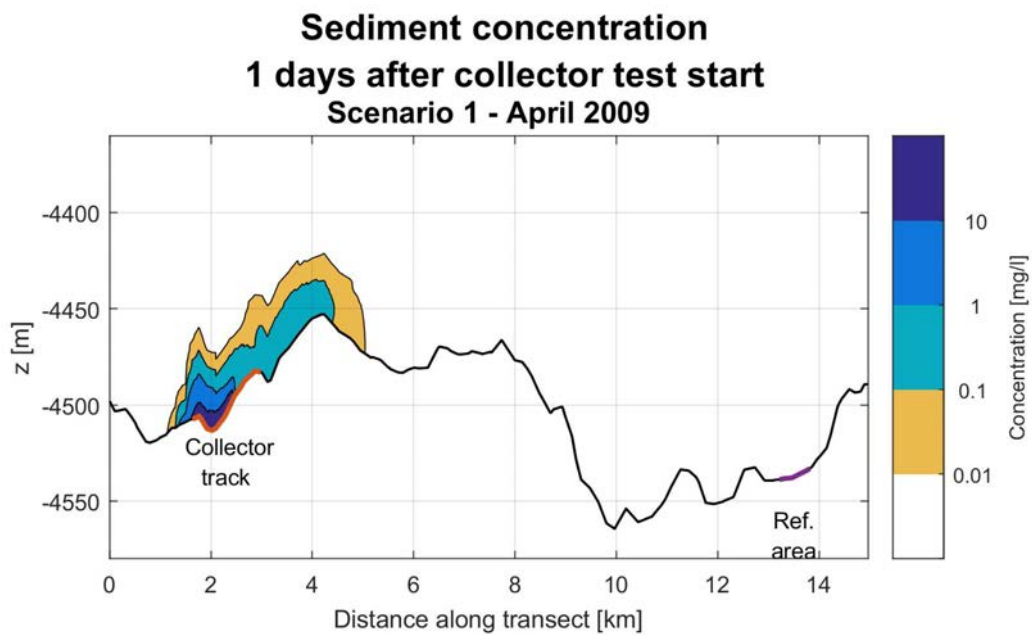


Figure xxii: Cross-sectional sediment concentration contours 1 day after the start of the Patania II trial for scenario 1 - April 2009

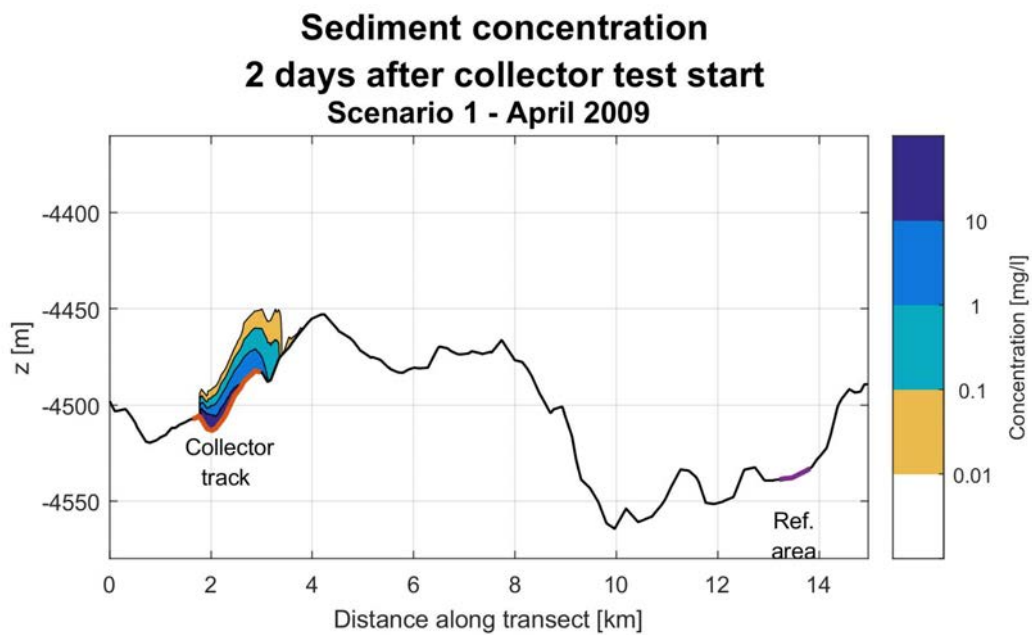


Figure xxiii: Cross-sectional sediment concentration contours 2 days after the start of the Patania II trial for scenario 1 - April 2009

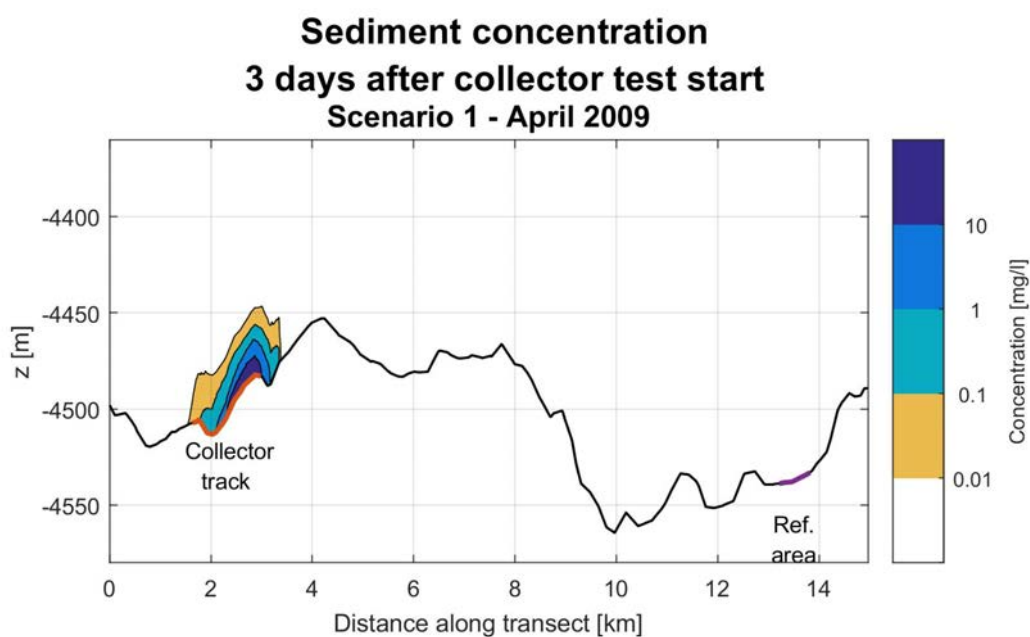


Figure xxiv: Cross-sectional sediment concentration contours 3 days after the start of the Patania II trial for scenario 1 - April 2009

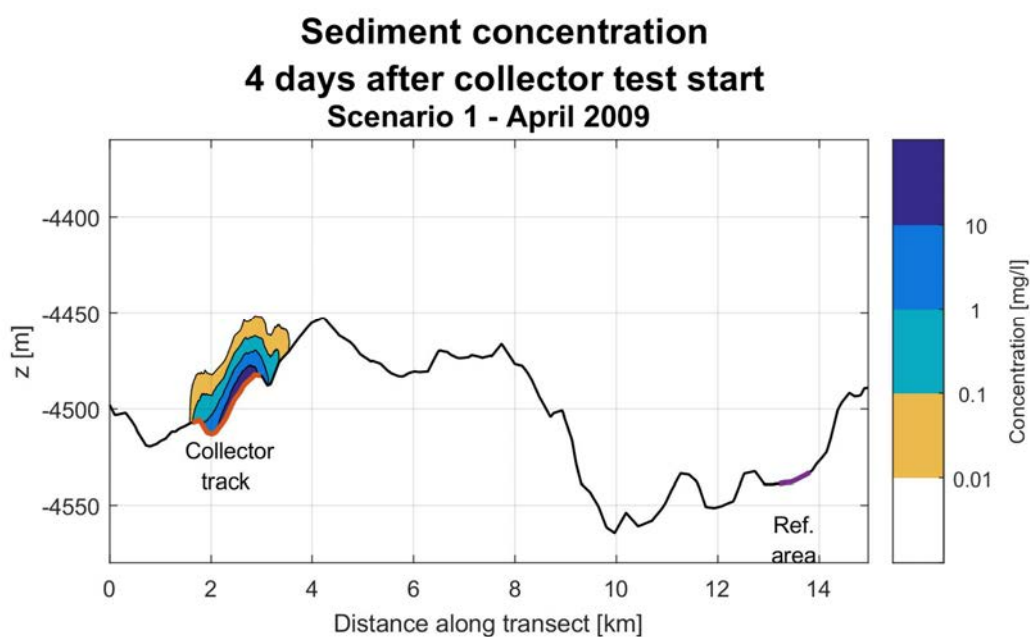


Figure xxv: Cross-sectional sediment concentration contours 4 days after the start of the Patania II trial for scenario 1 - April 2009

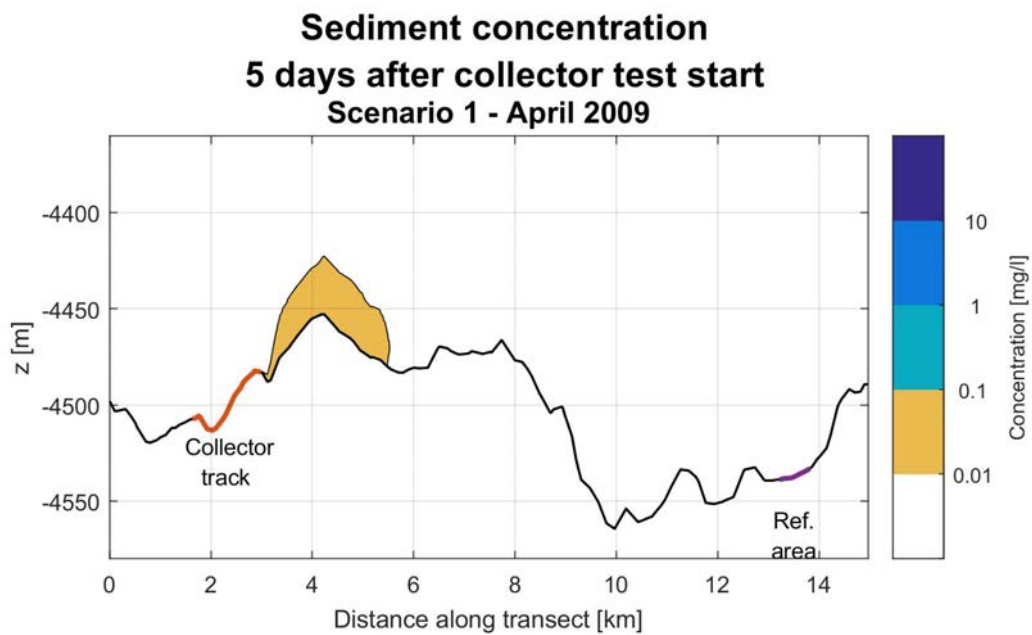


Figure xxvi: Cross-sectional sediment concentration contours 5 days after the start of the Patania II trial for scenario 1 - April 2009

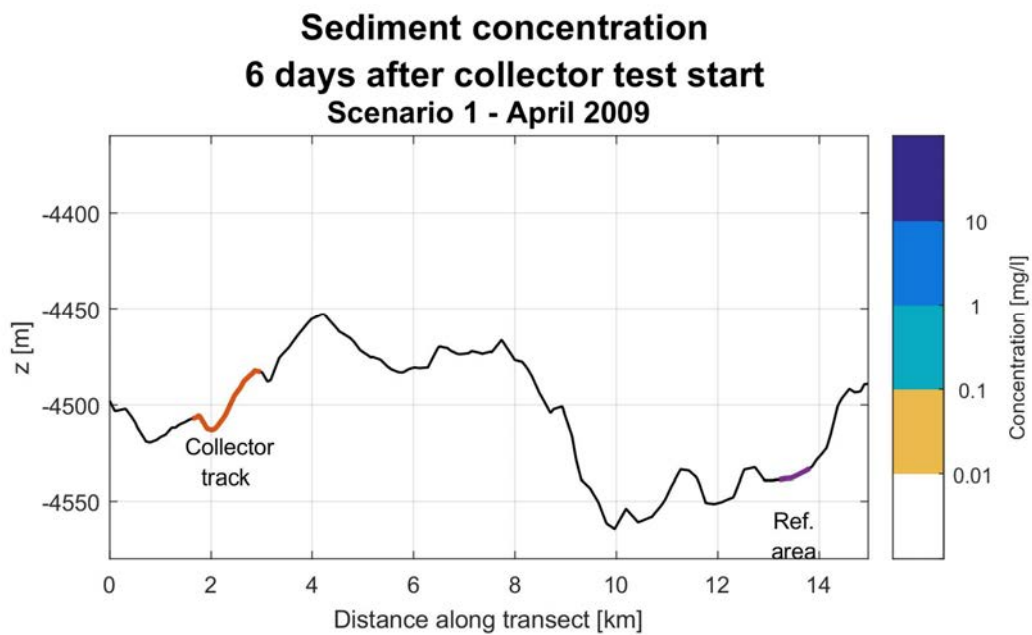


Figure xxvii: Cross-sectional sediment concentration contours 6 days after the start of the Patania II trial for scenario 1 - April 2009

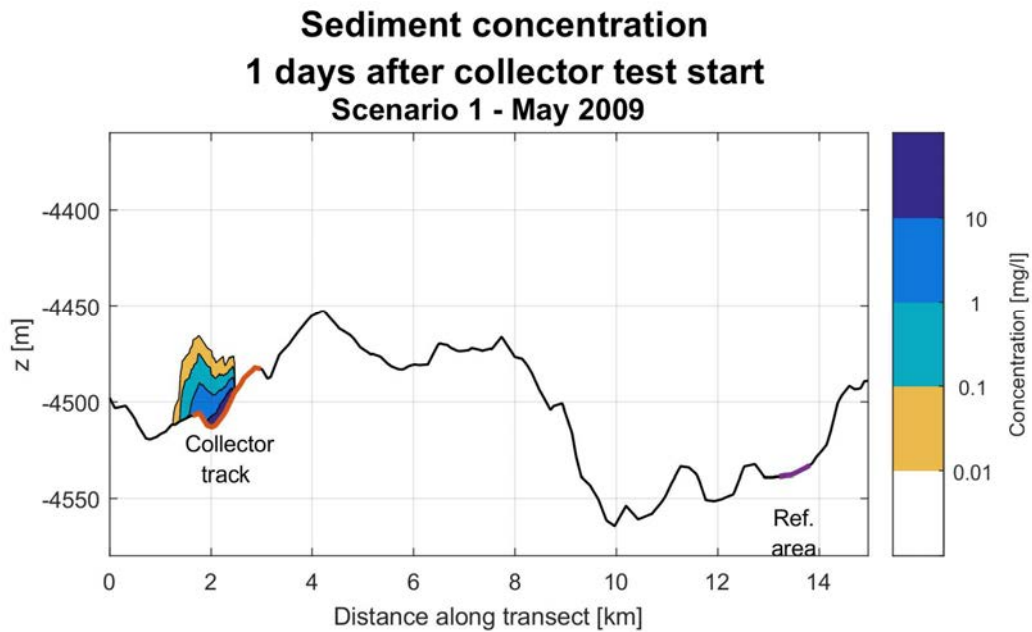


Figure xxviii: Cross-sectional sediment concentration contours 1 day after the start of the Patania II trial for scenario 1 - May 2009

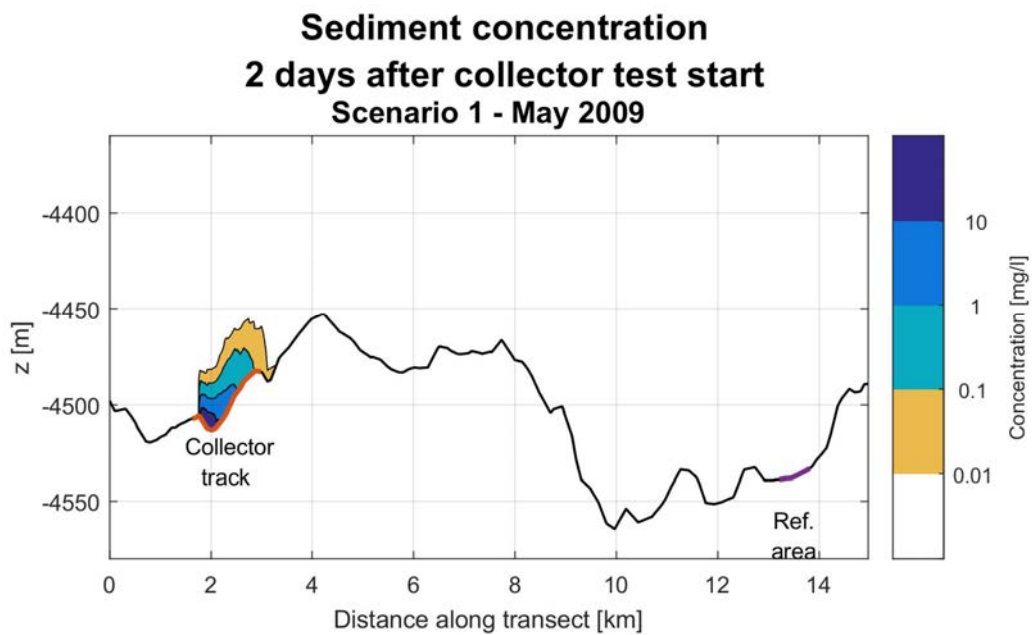
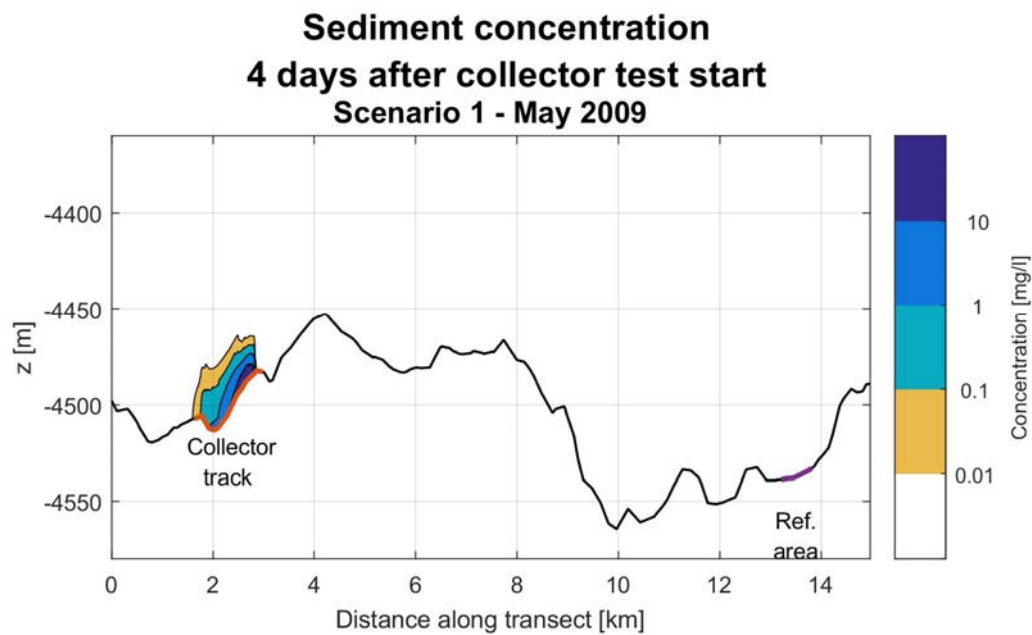
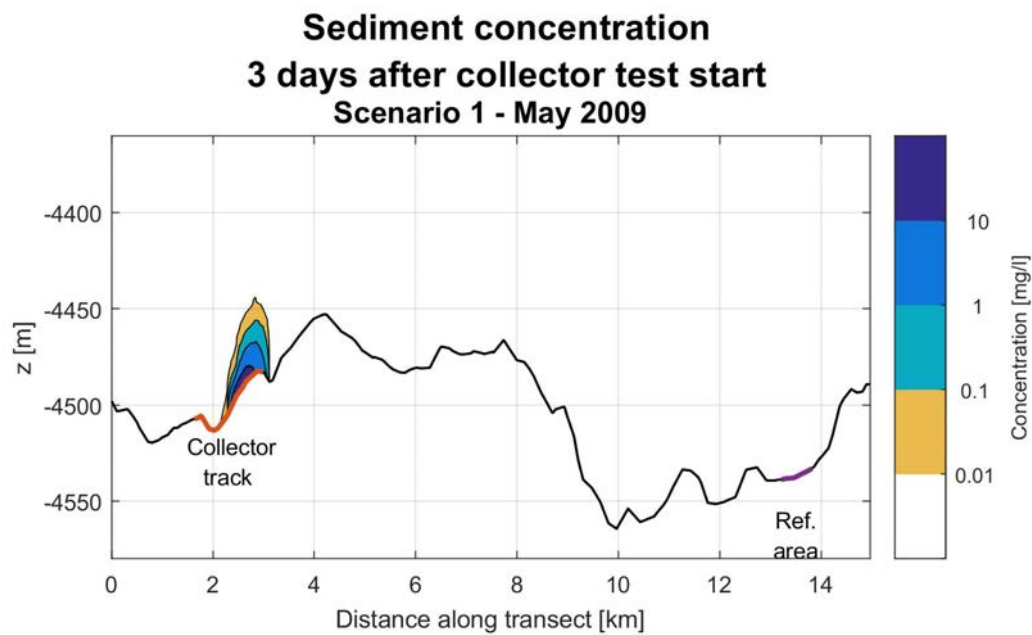


Figure xxix: Cross-sectional sediment concentration contours 2 days after the start of the Patania II trial for scenario 1 - May 2009



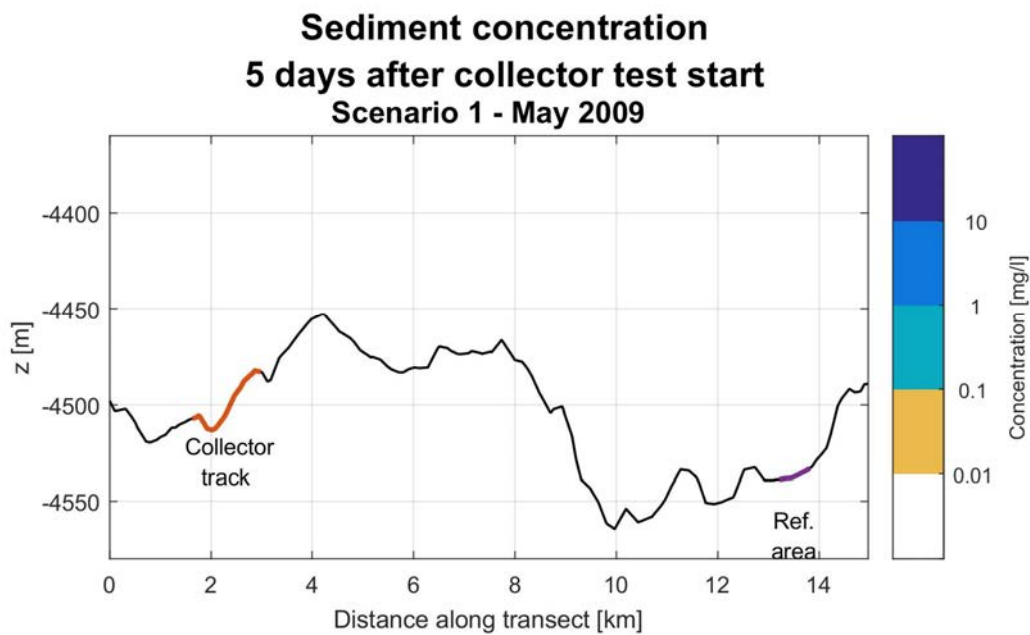


Figure xxxii: Cross-sectional sediment concentration contours 5 days after the start of the Patania II trial for scenario 1 - May 2009

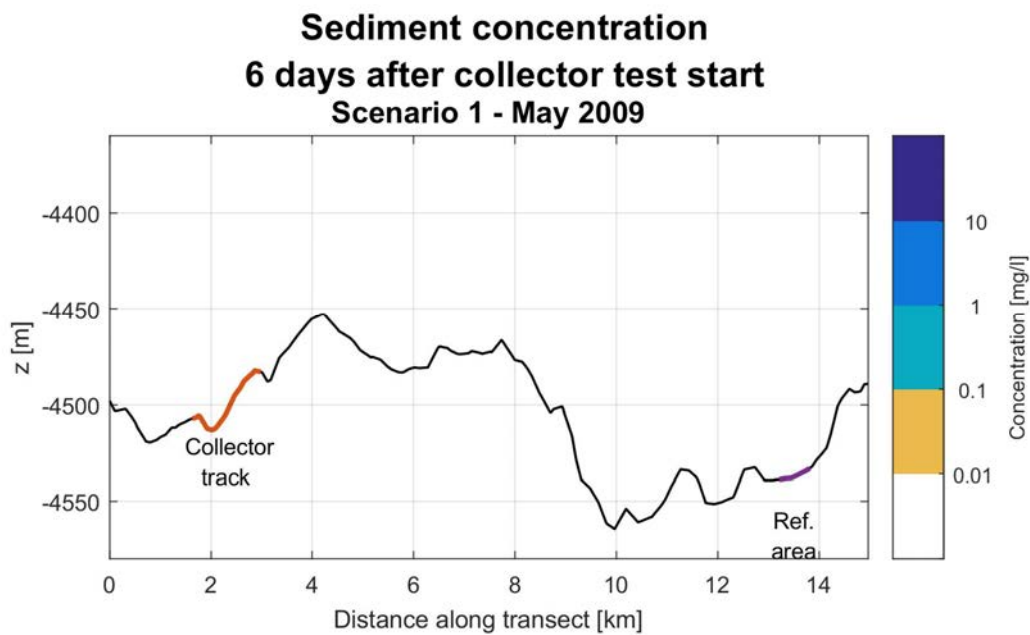


Figure xxxiii: Cross-sectional sediment concentration contours 6 days after the start of the Patania II trial for scenario 1 - May 2009

12.4.2.1 Sediment deposition

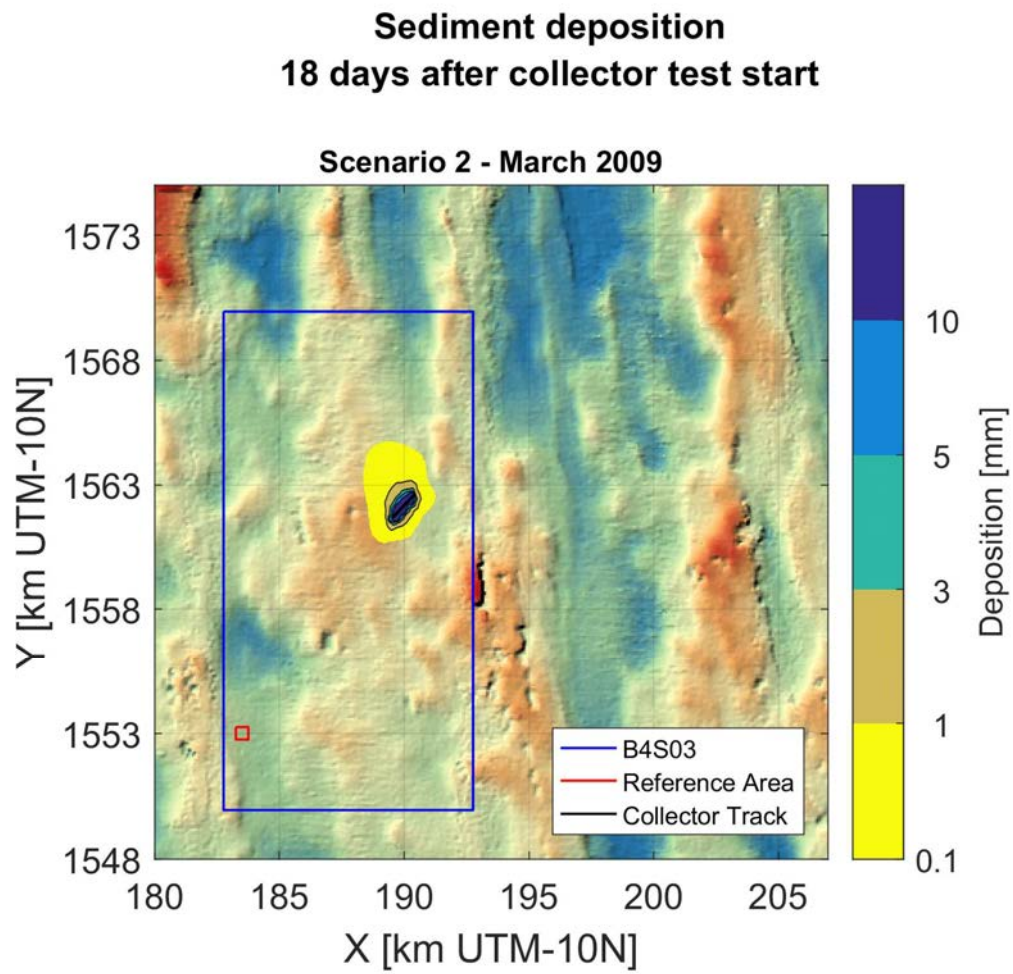


Figure xxxiv: Sediment deposition at the end of the model simulation for scenario 2 - March 2009

Sediment deposition 18 days after collector test start

Scenario 2 - April 2009

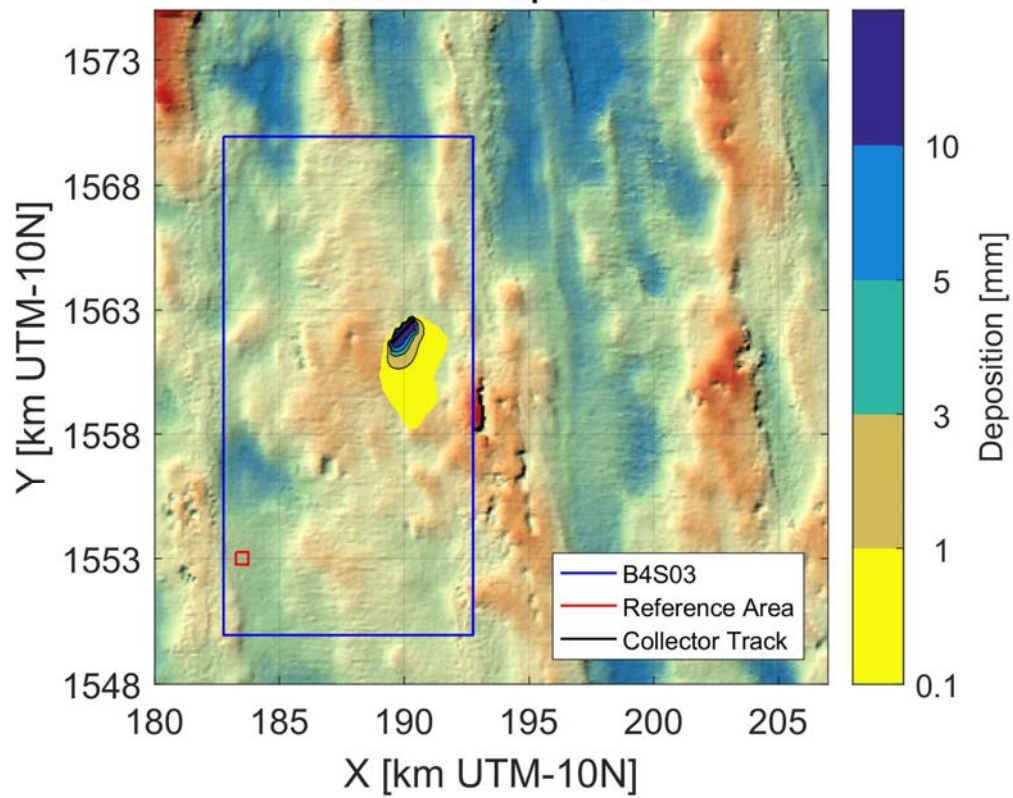


Figure xxxv: Sediment deposition at the end of the model simulation for scenario 2 - April 2009

Sediment deposition 18 days after collector test start

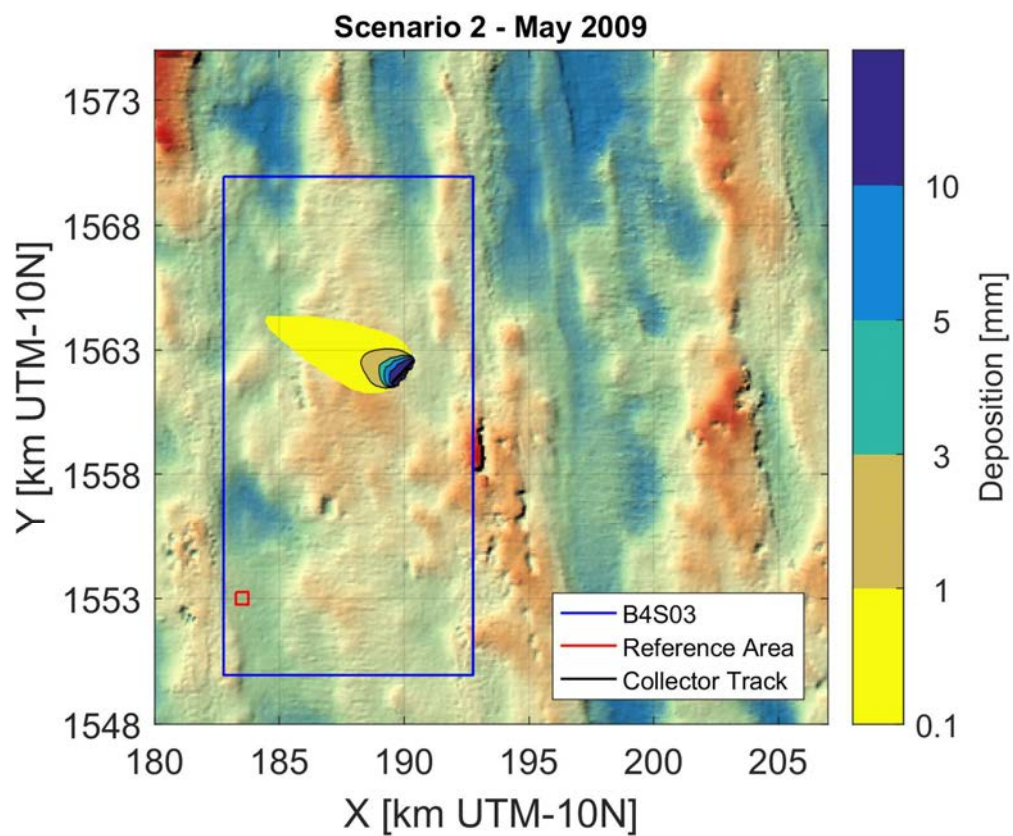


Figure xxxvi: Sediment deposition at the end of the model simulation for scenario 2 - May 2009

12.4.2.2 Suspended sediment plume – concentration contours

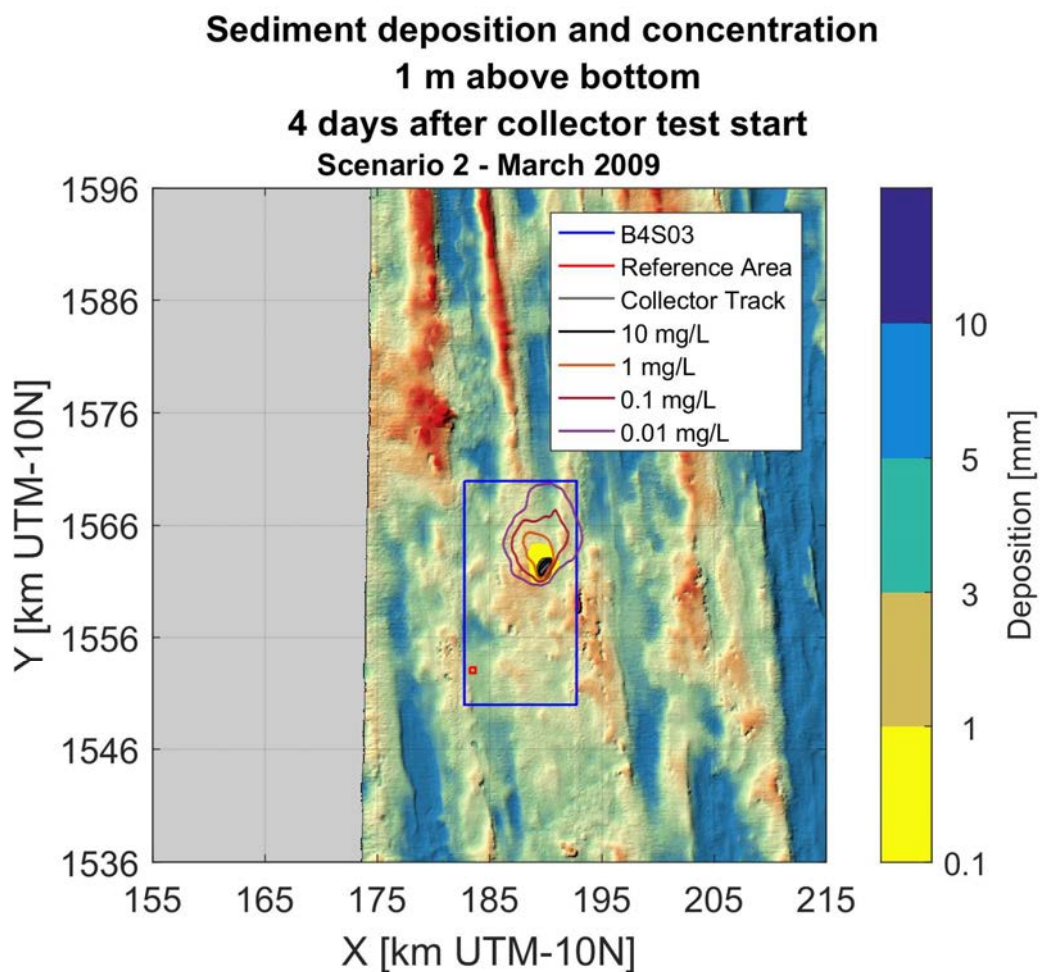


Figure xxxvii: Sediment suspension contours at the end of the Patania II trial for scenario 2 - March 2009

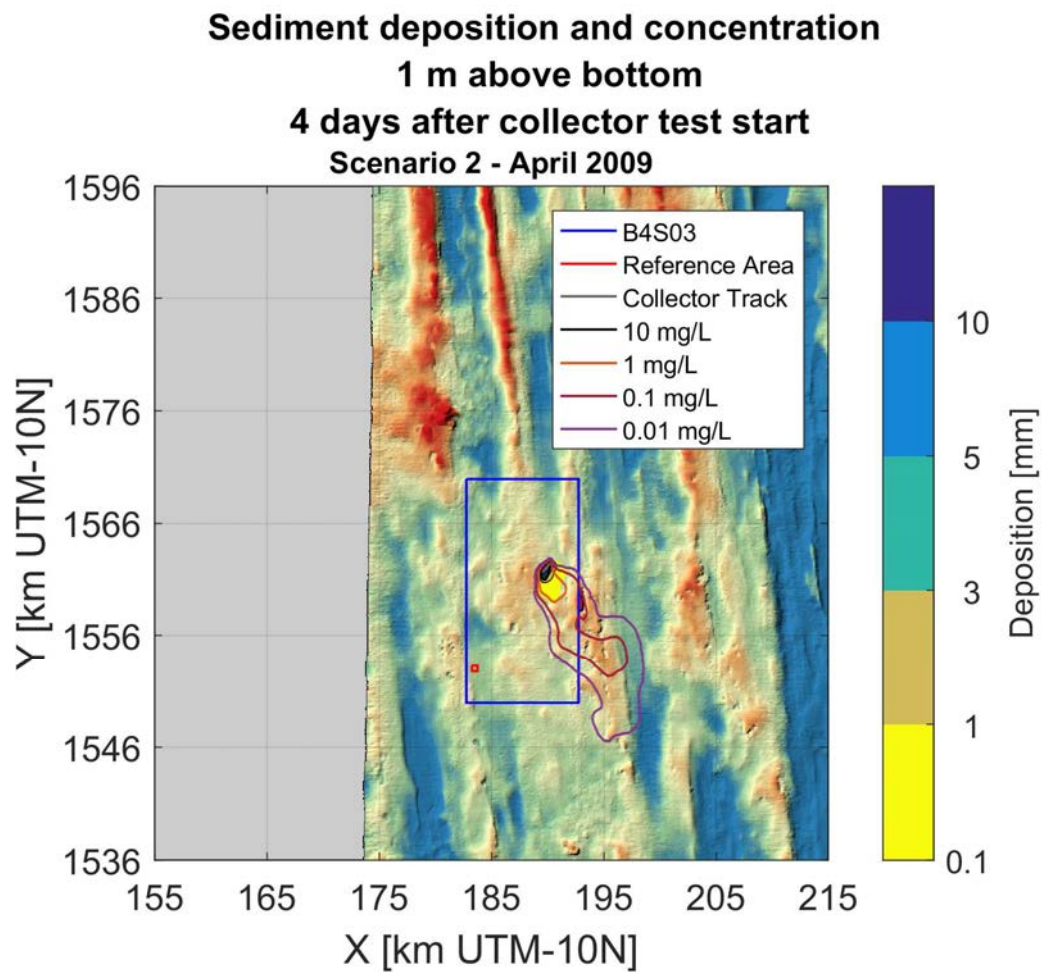


Figure xxxviii: Sediment suspension contours at the end of the Patania II trial for scenario 2 - April 2009

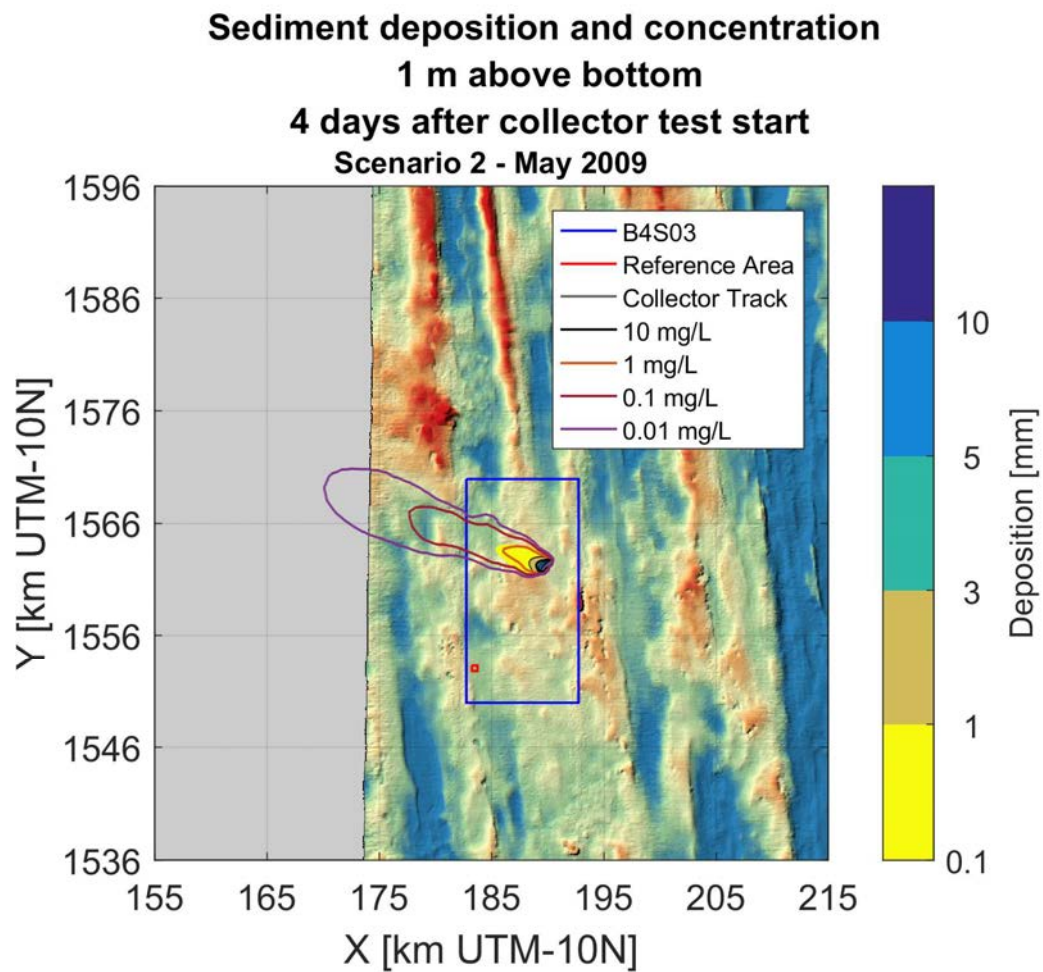


Figure xxxix: Sediment suspension contours at the end of the Patania II trial for scenario 2 - May 2009

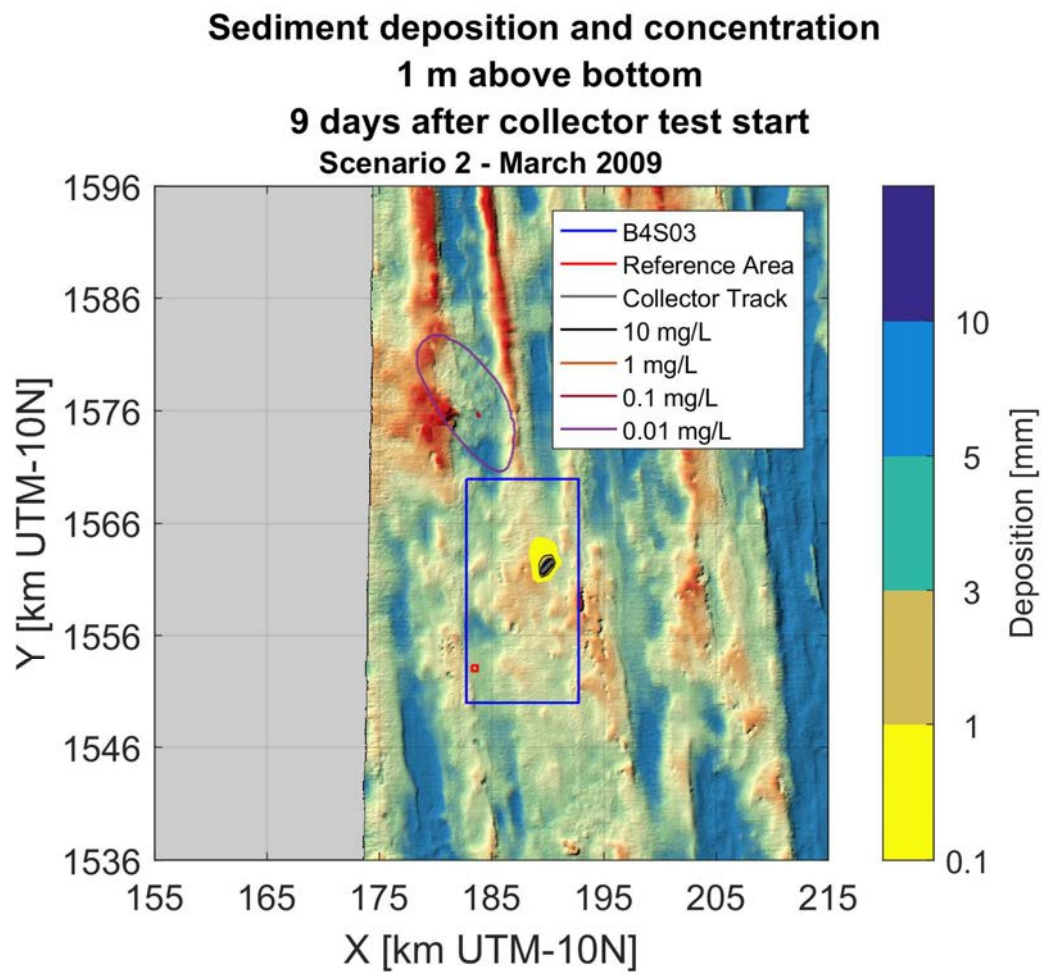


Figure xl: Sediment suspension contours 5 days after at the end of the Patania II trial for scenario 2 - March 2009

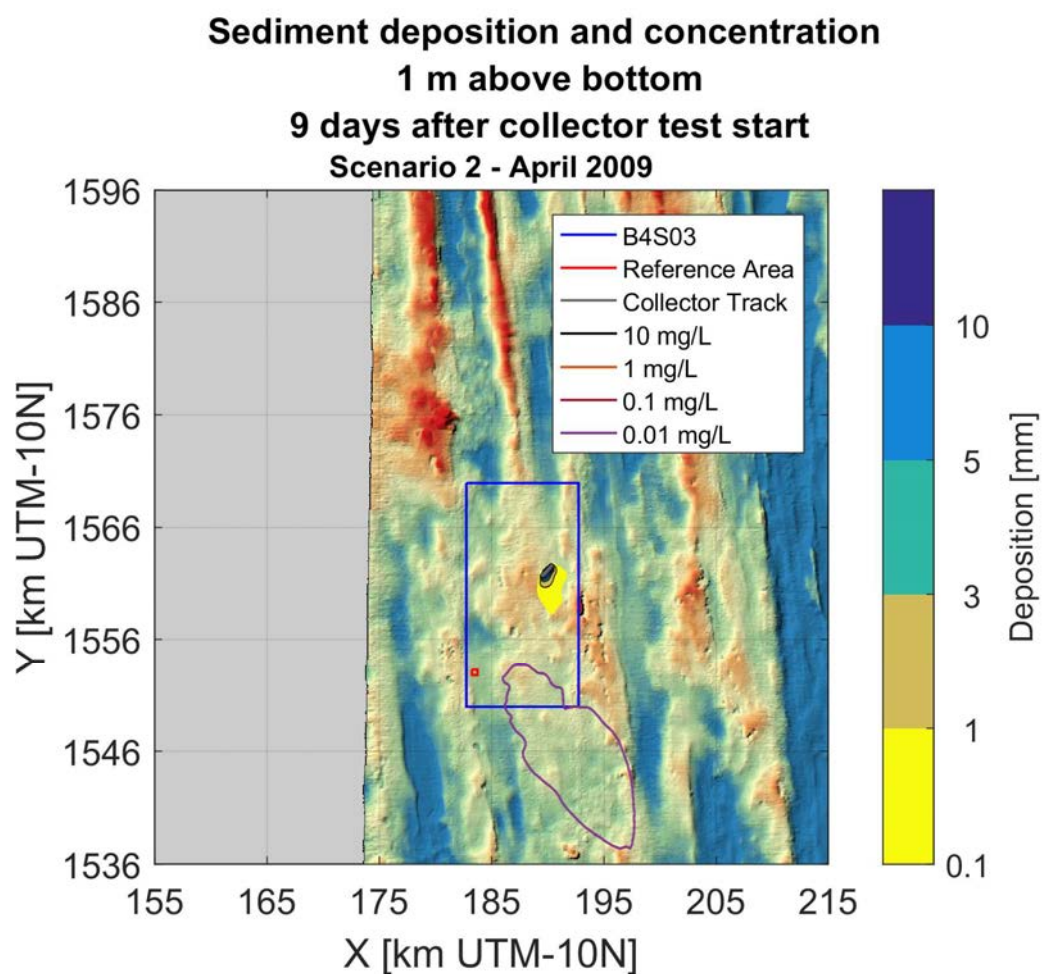


Figure xli: Sediment suspension contours 5 days after at the end of the Patania II trial for scenario 2 - April 2009

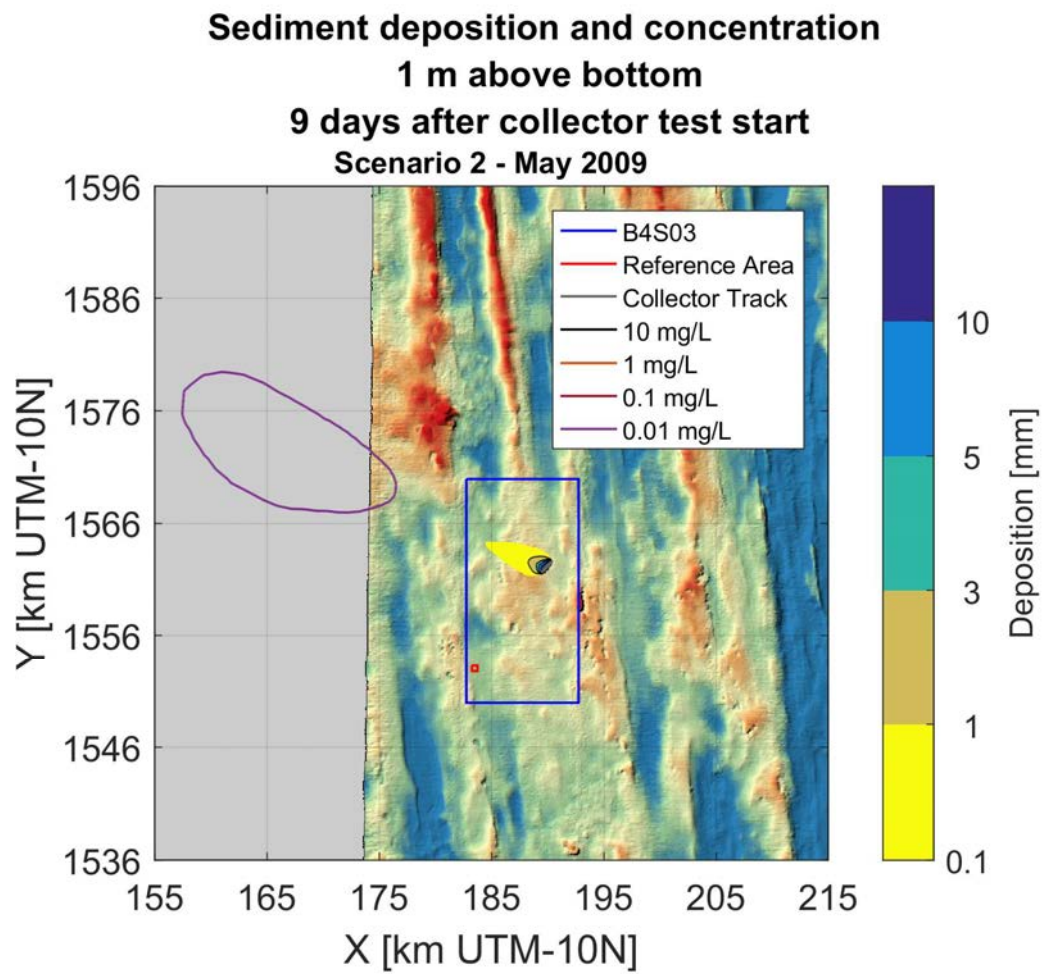


Figure xlii: Sediment suspension contours 5 days after at the end of the Patania II trial for scenario 2 - May 2009

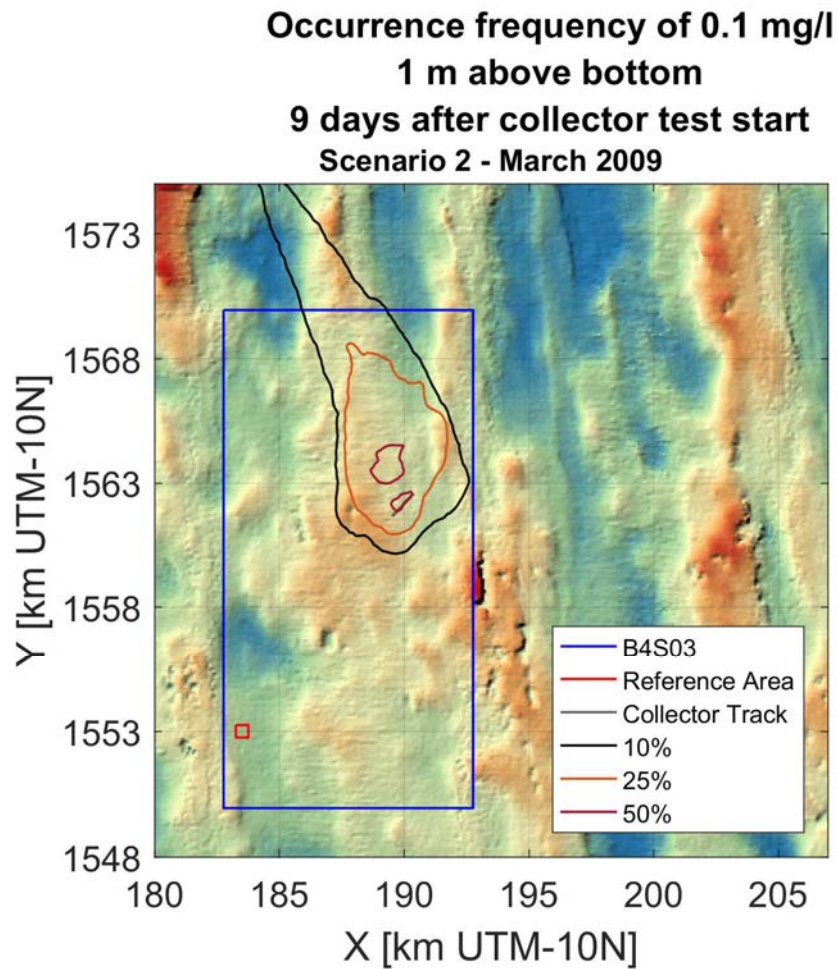


Figure xliii: Frequency of occurrence for 0.1 mg/l sediment concentration for scenario 2 - March 2009

**Occurrence frequency of 0.1 mg/l
1 m above bottom
9 days after collector test start
Scenario 2 - April 2009**

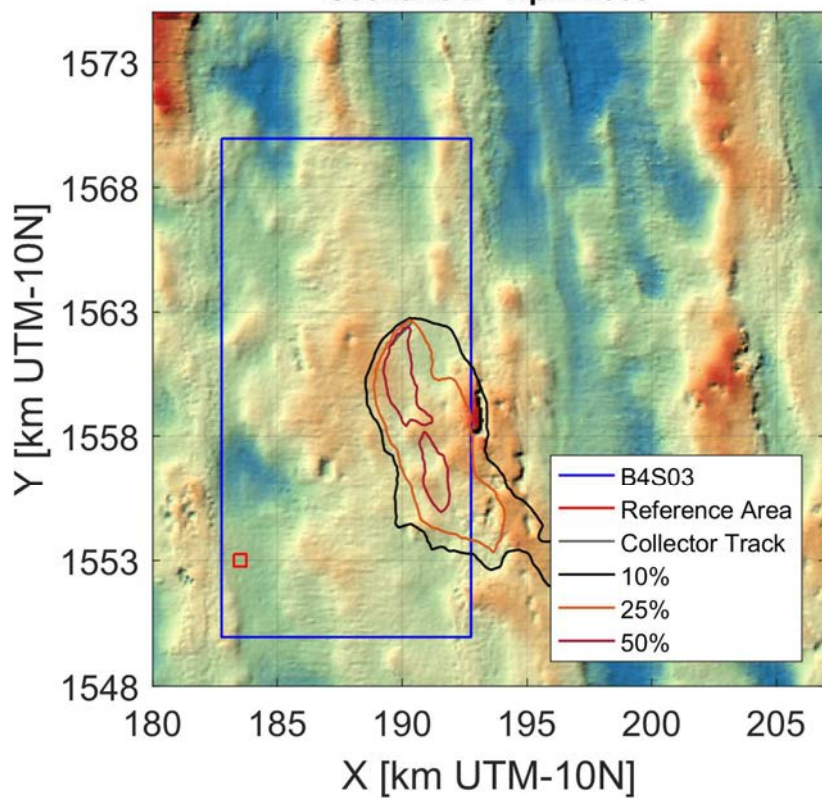


Figure xlv: Frequency of occurrence for 0.1 mg/l sediment concentration for scenario 2 - April 2009

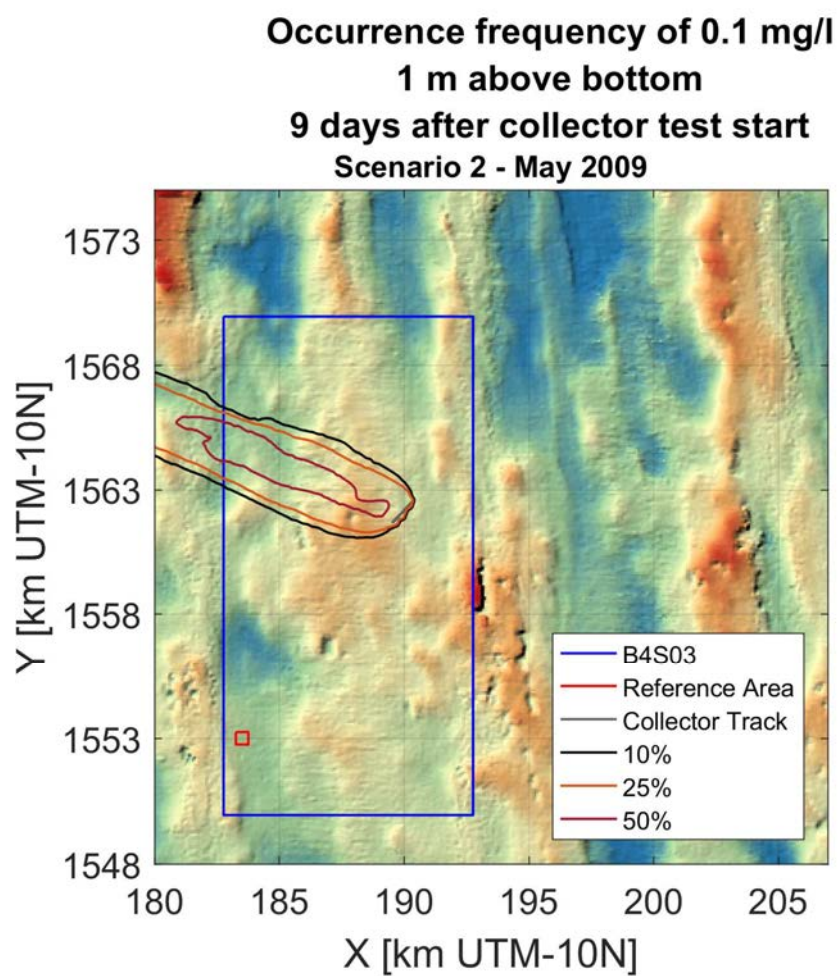


Figure xlv: Frequency of occurrence for 0.1 mg/l sediment concentration for scenario 2 - May 2009

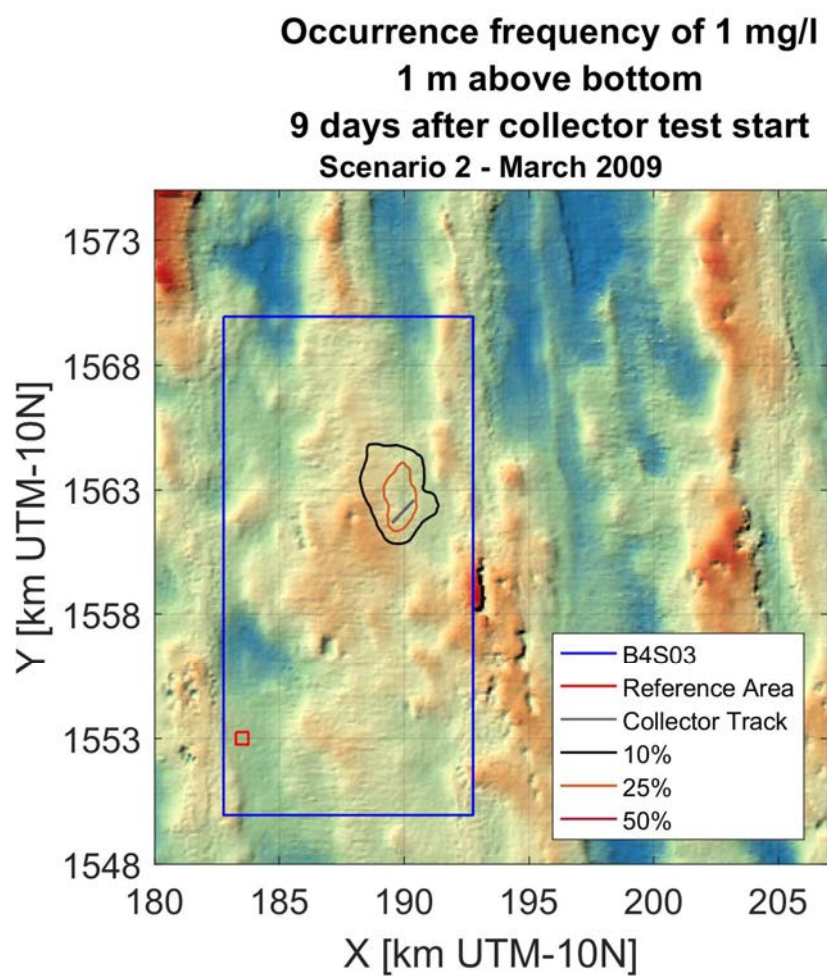


Figure xlvii: Frequency of occurrence for 1 mg/l sediment concentration for scenario 2 - March 2009

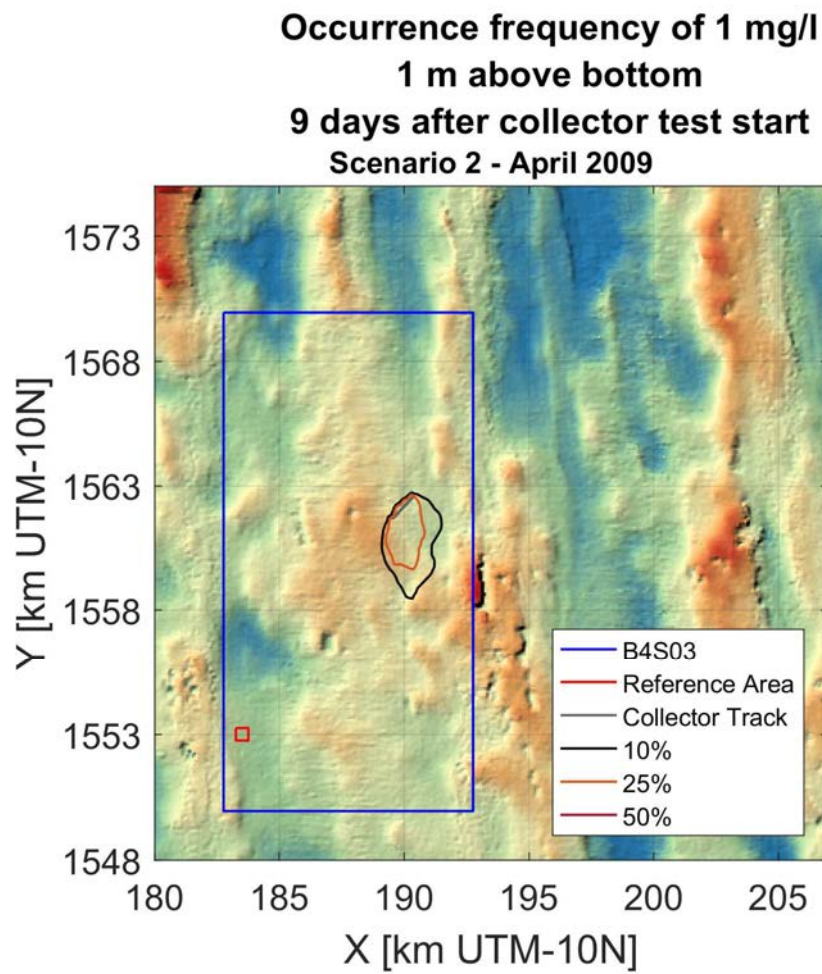


Figure xlvii: Frequency of occurrence for 1 mg/l sediment concentration for scenario 2 - April 2009

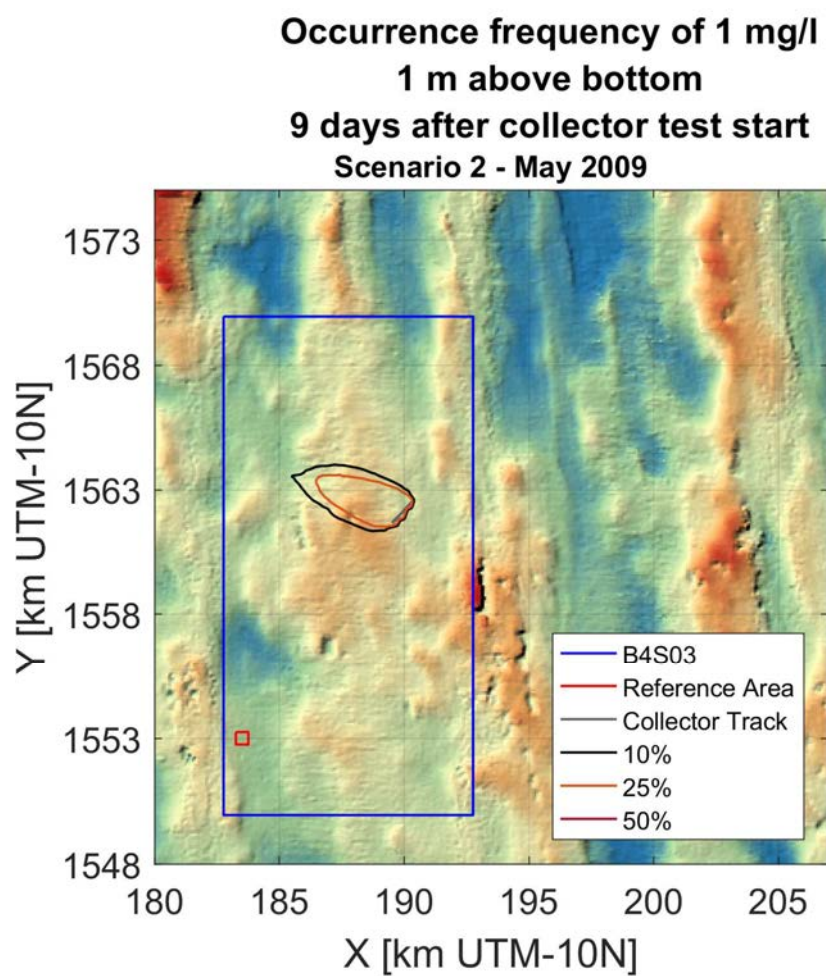


Figure xlviii: Frequency of occurrence for 1 mg/l sediment concentration for scenario 2 - May 2009

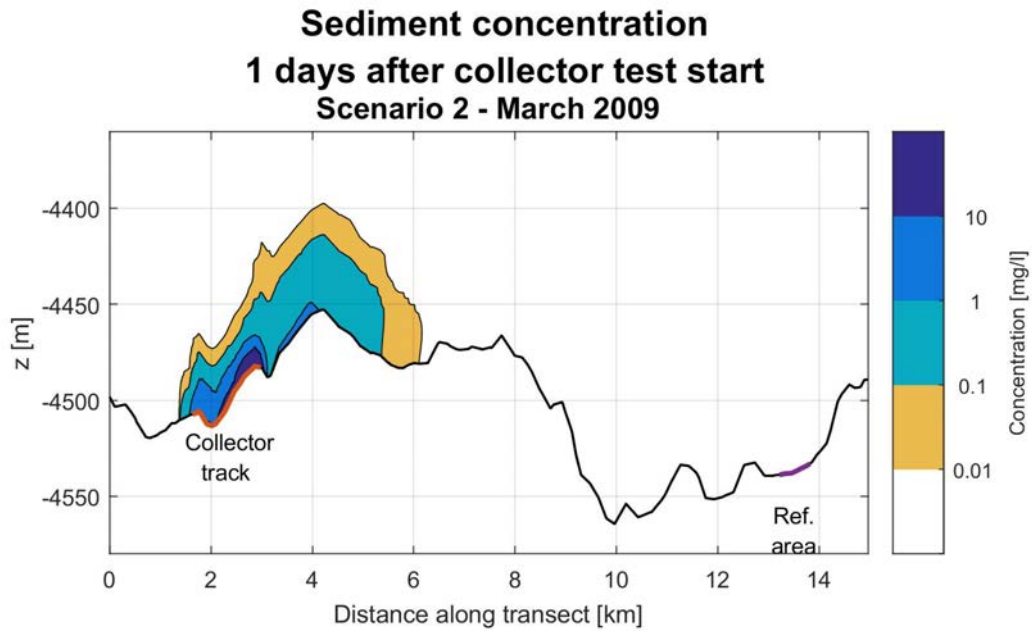


Figure xlix: Cross-sectional sediment concentration contours 1 day after the start of the Patania II trial for scenario 2 - March 2009

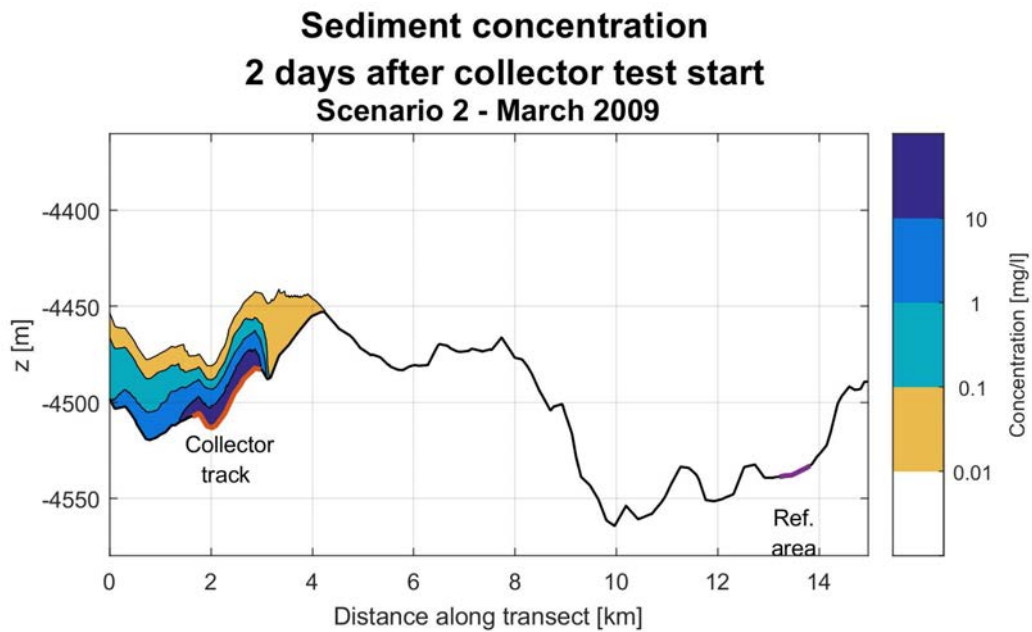


Figure l: Cross-sectional sediment concentration contours 2 days after the start of the Patania II trial for scenario 2 - March 2009

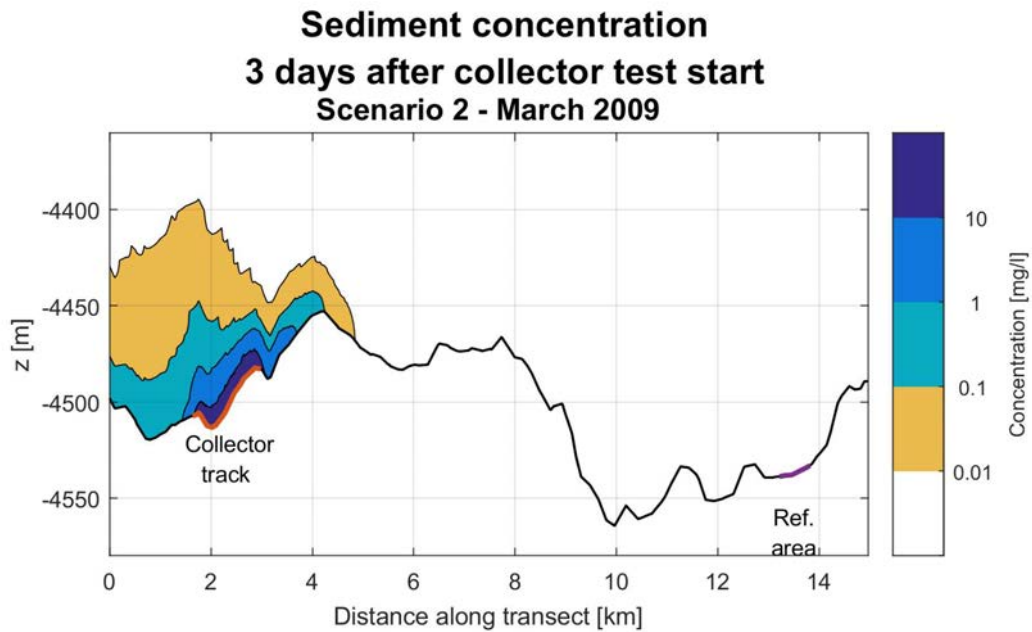


Figure li: Cross-sectional sediment concentration contours 3 days after the start of the Patania II trial for scenario 2 - March 2009

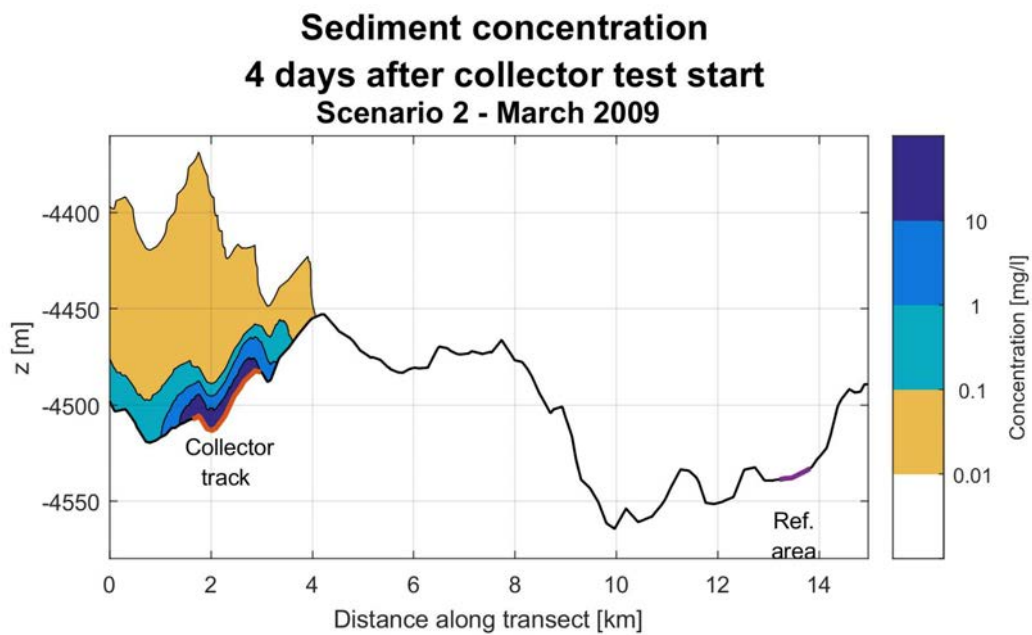


Figure lii: Cross-sectional sediment concentration contours 4 days after the start of the Patania II trial for scenario 2 - March 2009

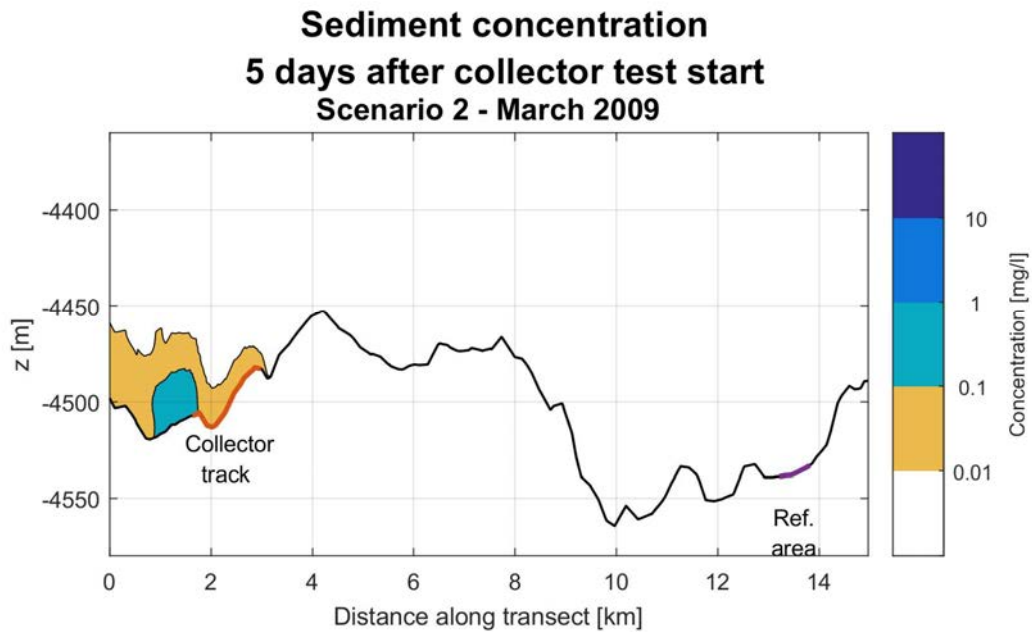


Figure liii: Cross-sectional sediment concentration contours 5 days after the start of the Patania II trial for scenario 2 - March 2009

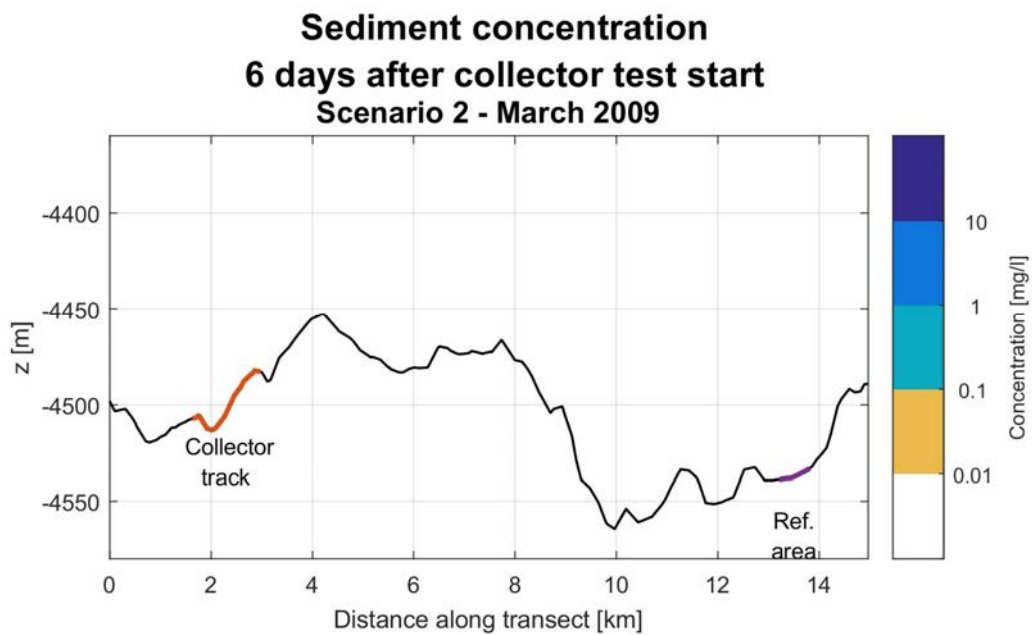


Figure liv: Cross-sectional sediment concentration contours 6 days after the start of the Patania II trial for scenario 2 - March 2009

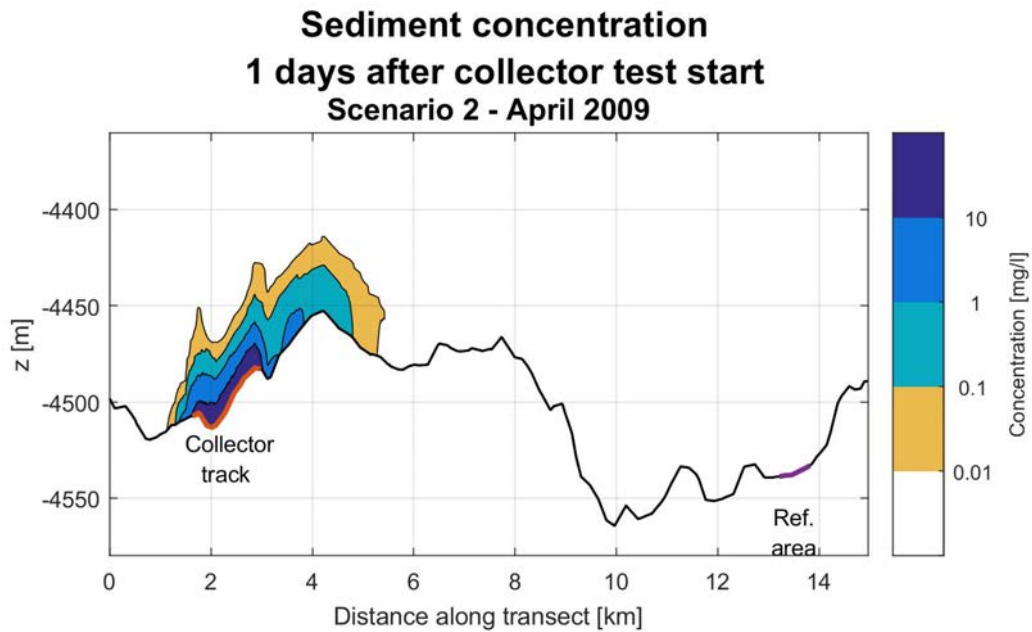


Figure Iv: Cross-sectional sediment concentration contours 1 day after the start of the Patania II trial for scenario 2 - April 2009

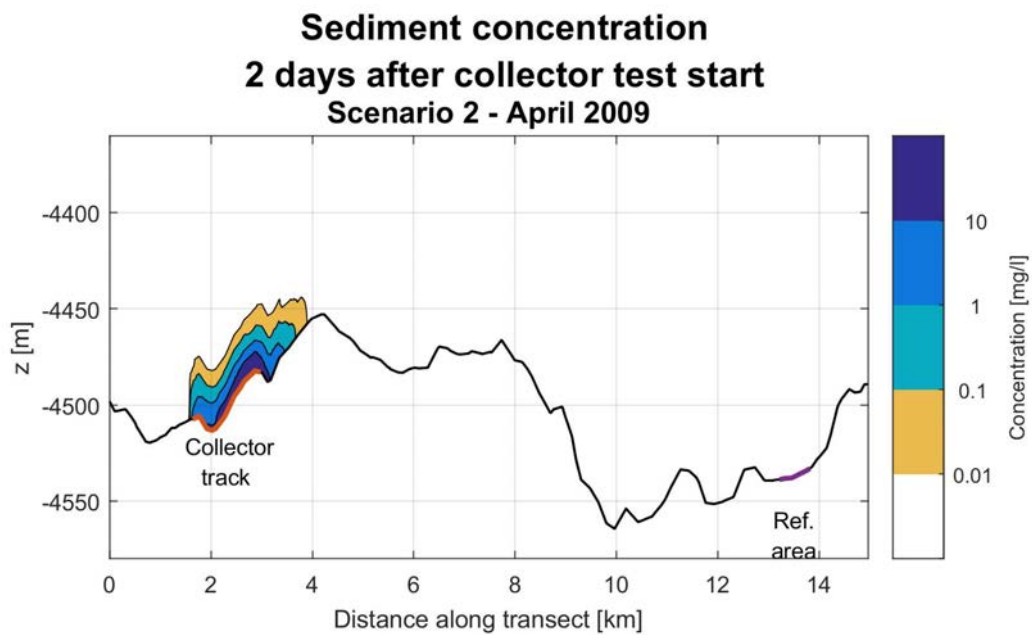


Figure Ivi: Cross-sectional sediment concentration contours 2 days after the start of the Patania II trial for scenario 2 - April 2009

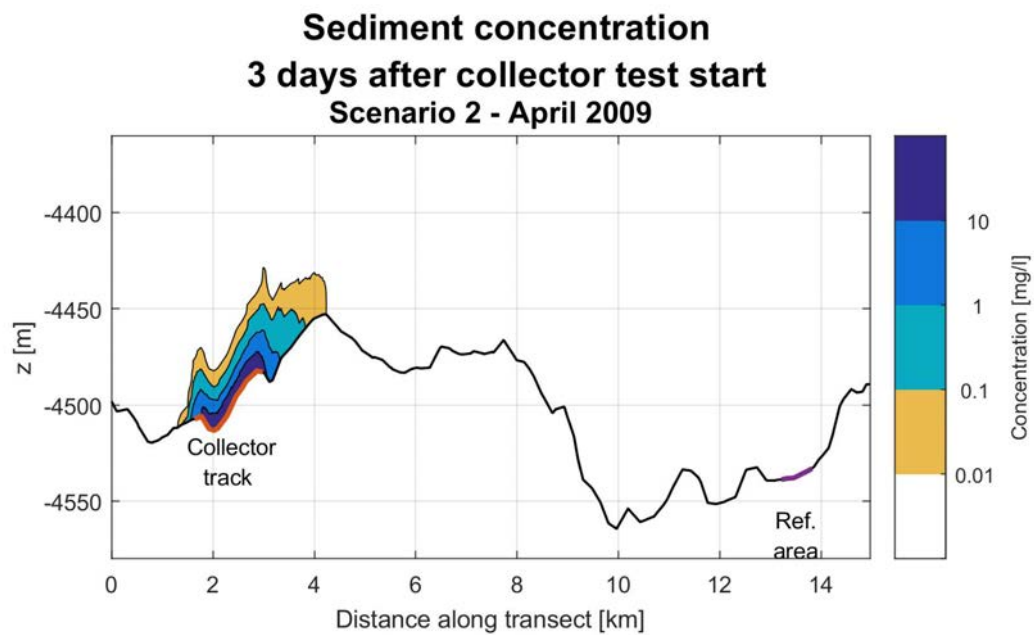


Figure Ivii: Cross-sectional sediment concentration contours 3 days after the start of the Patania II trial for scenario 2 - April 2009

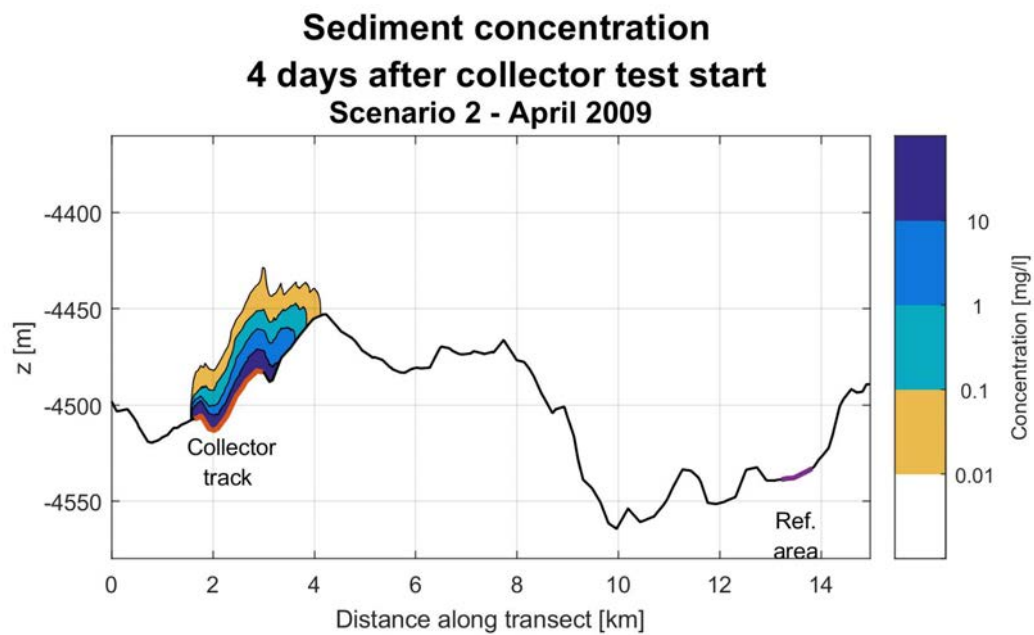


Figure Iviii: Cross-sectional sediment concentration contours 4 days after the start of the Patania II trial for scenario 2 - April 2009

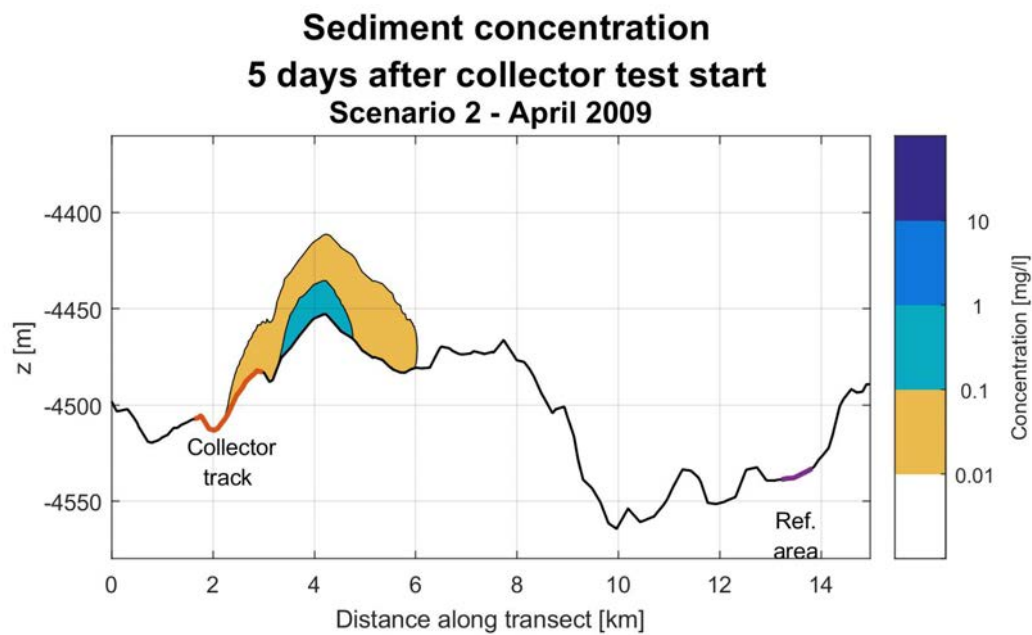


Figure Iix: Cross-sectional sediment concentration contours 5 days after the start of the Patania II trial for scenario 2 - April 2009

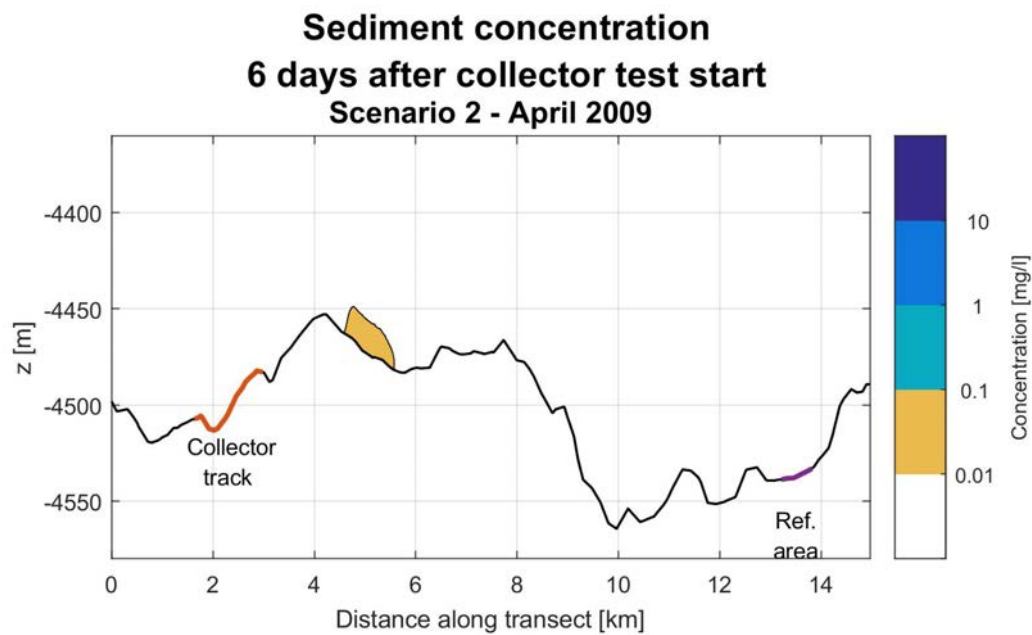


Figure Ix: Cross-sectional sediment concentration contours 6 days after the start of the Patania II trial for scenario 2 - April 2009

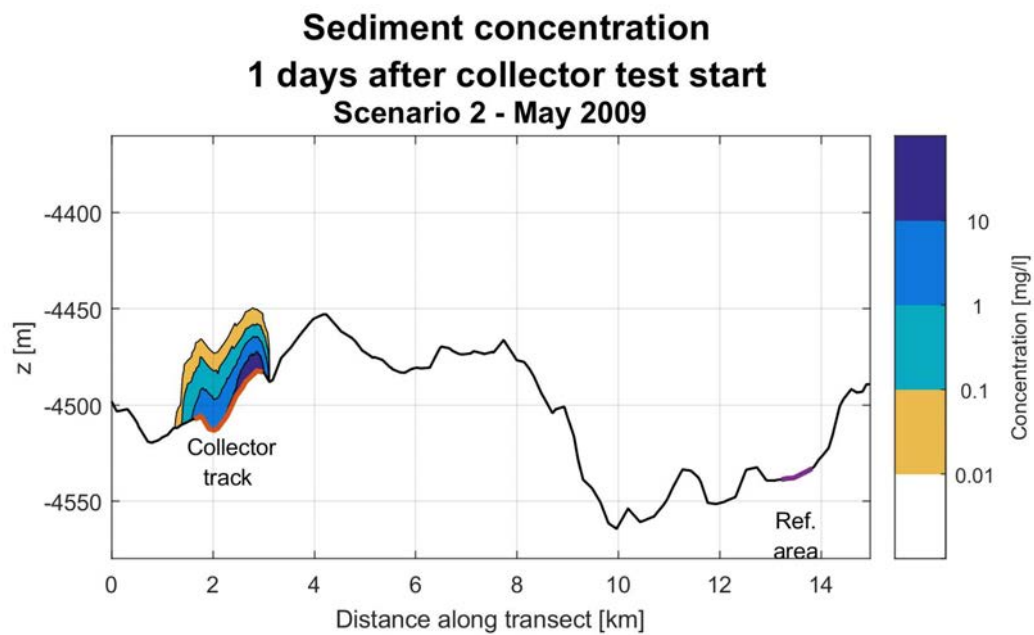


Figure 1xi: Cross-sectional sediment concentration contours 1 day after the start of the Patania II trial for scenario 2 - May 2009

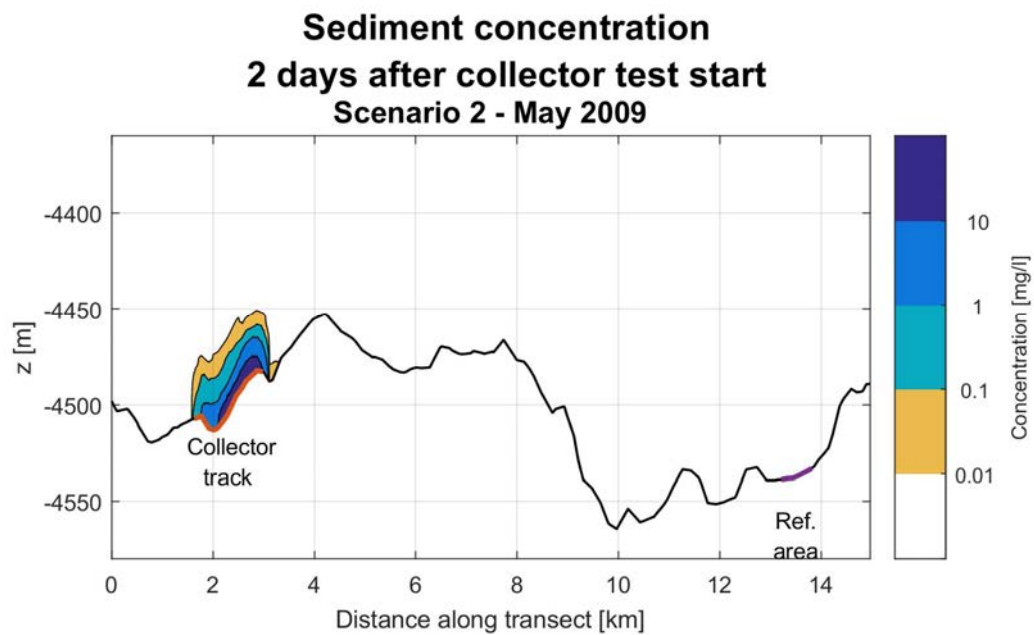


Figure 1xii: Cross-sectional sediment concentration contours 2 days after the start of the Patania II trial for scenario 2 - May 2009

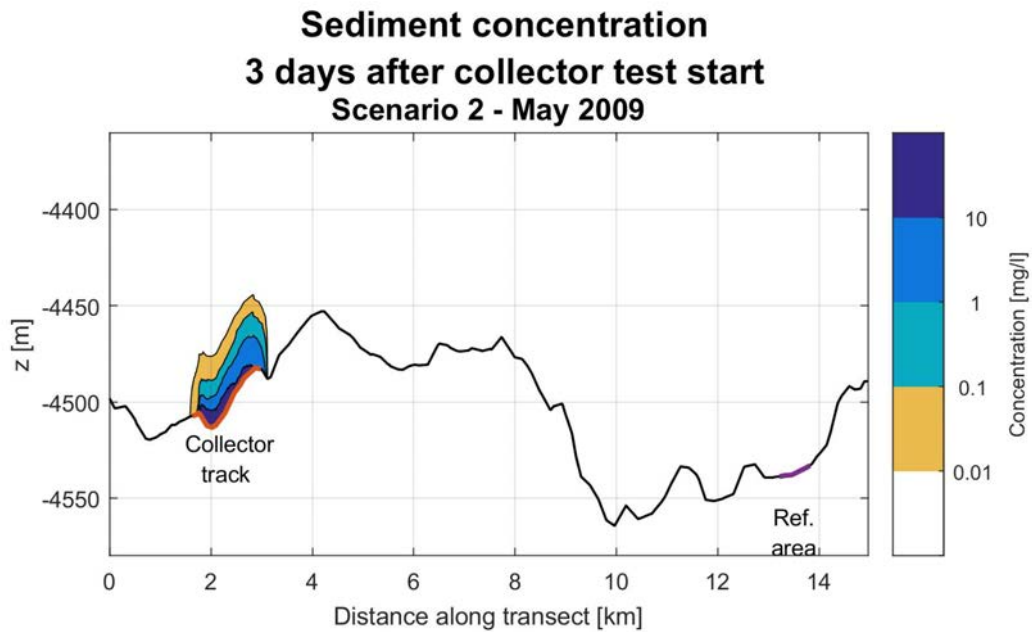


Figure 1xiii: Cross-sectional sediment concentration contours 3 days after the start of the Patania II trial for scenario 2 - May 2009

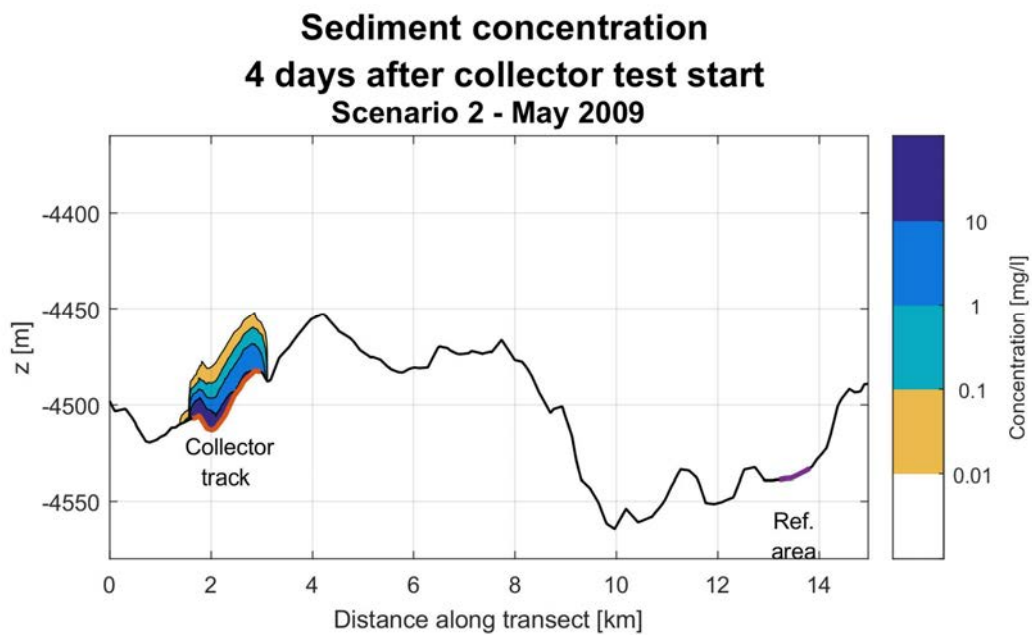


Figure 1xiv: Cross-sectional sediment concentration contours 4 days after the start of the Patania II trial for scenario 2 - May 2009

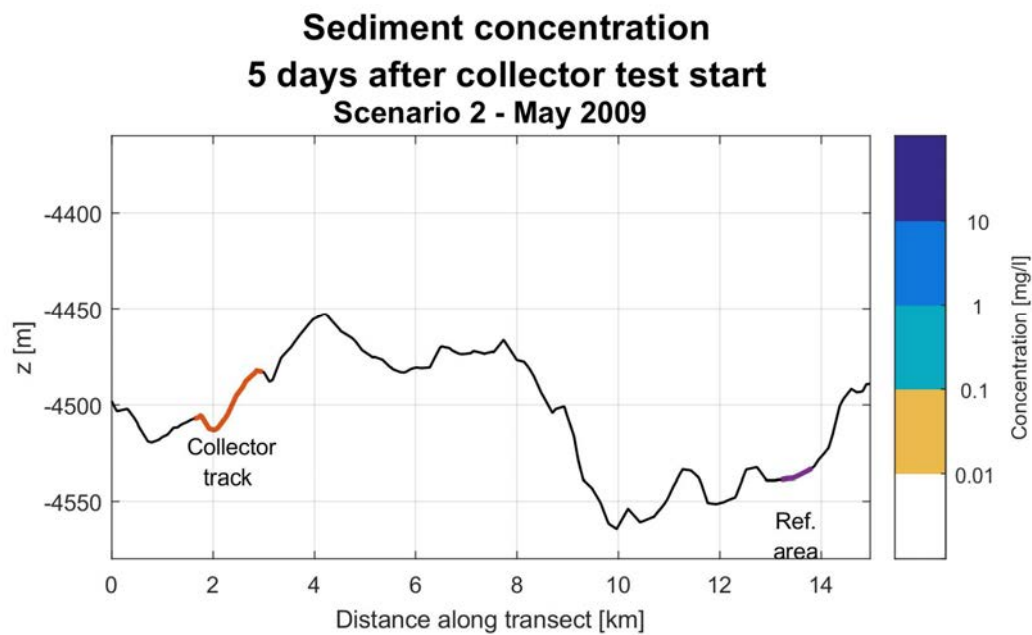


Figure Ixv: Cross-sectional sediment concentration contours 5 days after the start of the Patania II trial for scenario 2 - May 2009

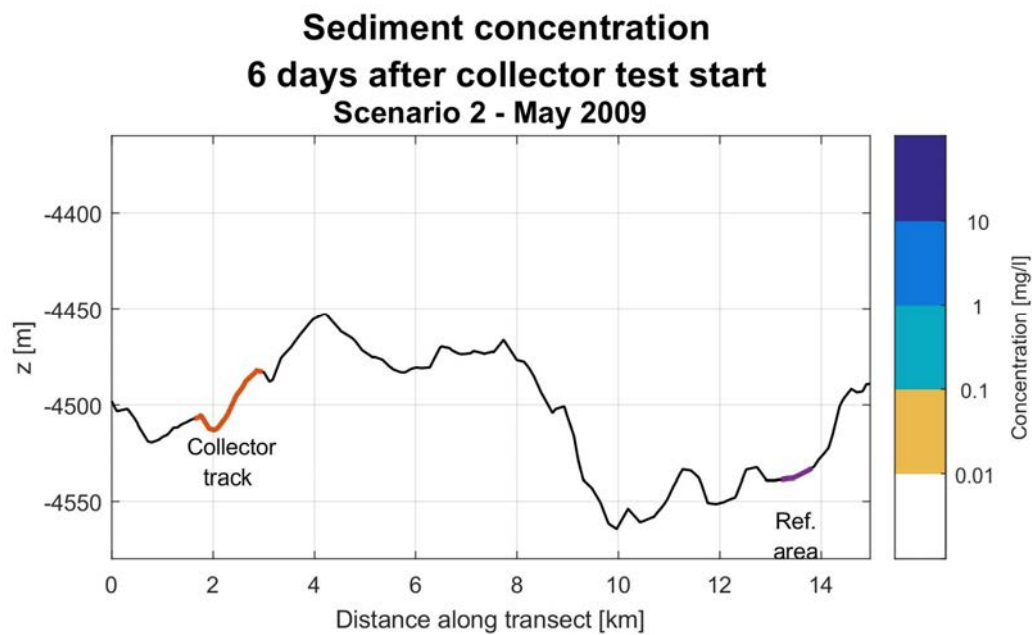


Figure Ixvi: Cross-sectional sediment concentration contours 6 days after the start of the Patania II trial for scenario 2 - May 2009

12.4.3.1 Sediment deposition

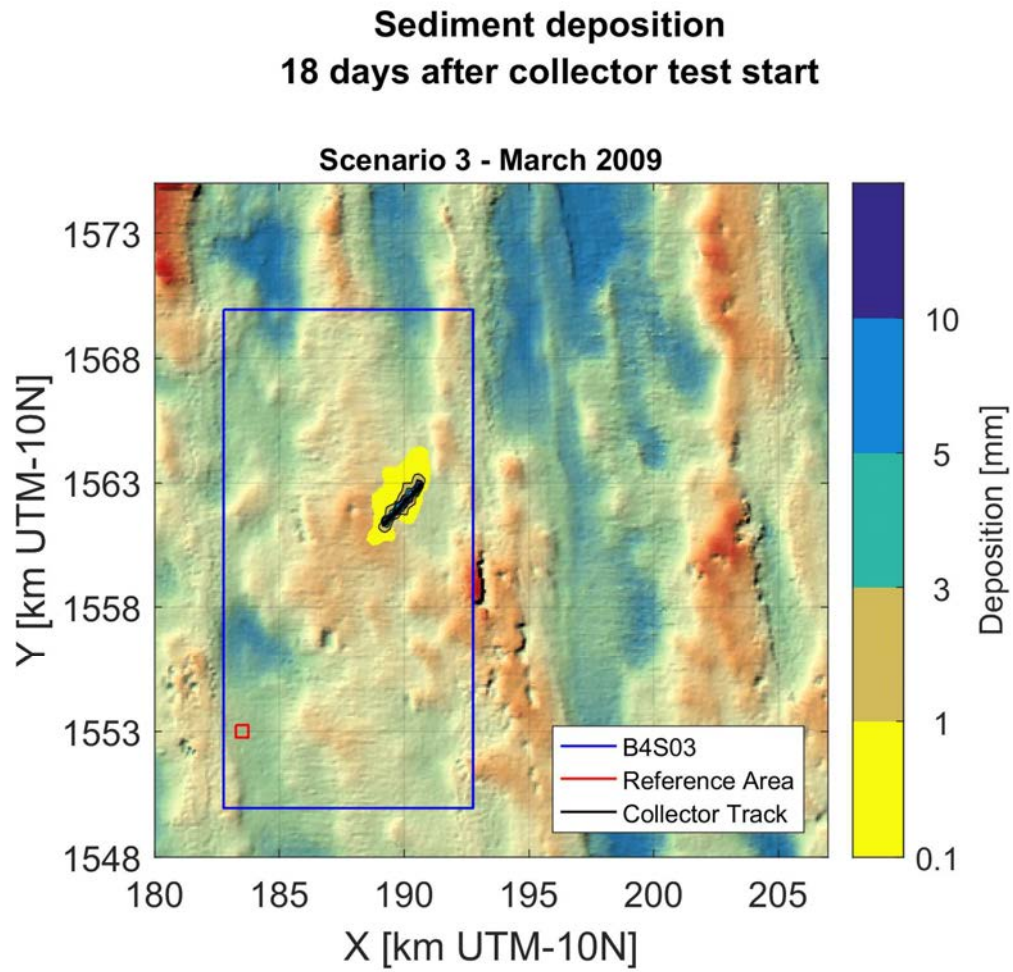


Figure Ixvii: Sediment deposition at the end of the model simulation for scenario 1 - March 2009

Sediment deposition 18 days after collector test start

Scenario 3 - April 2009

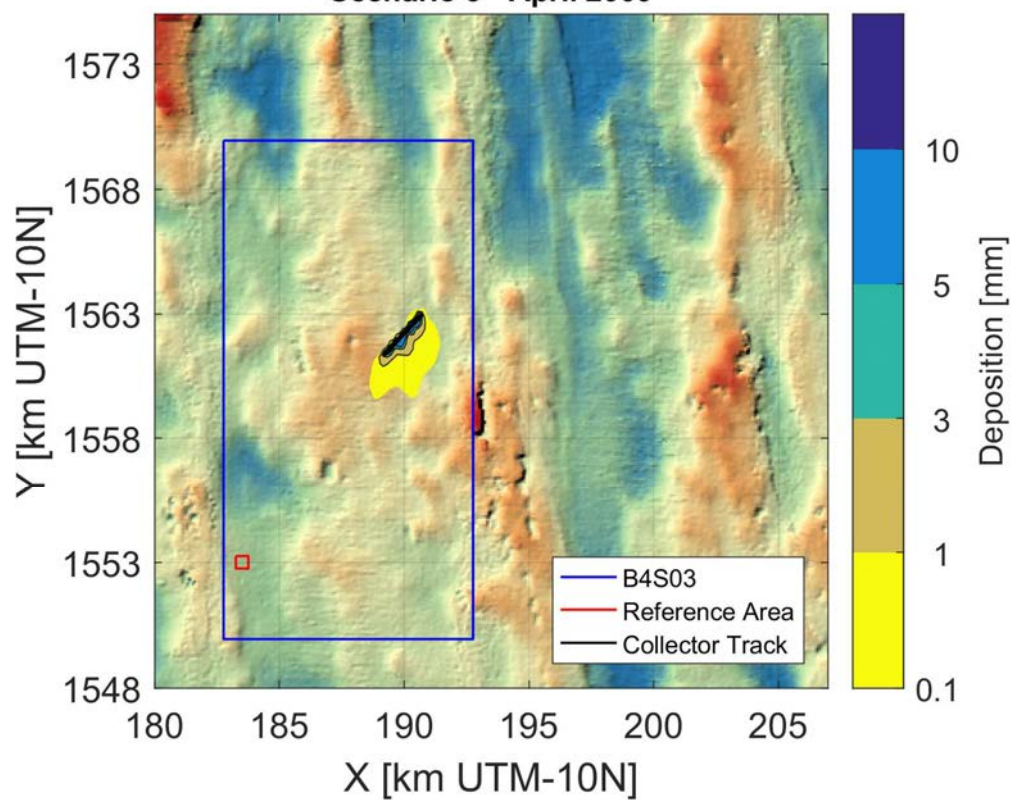


Figure lxviii: Sediment deposition at the end of the model simulation for scenario 1 - April 2009

Sediment deposition 18 days after collector test start

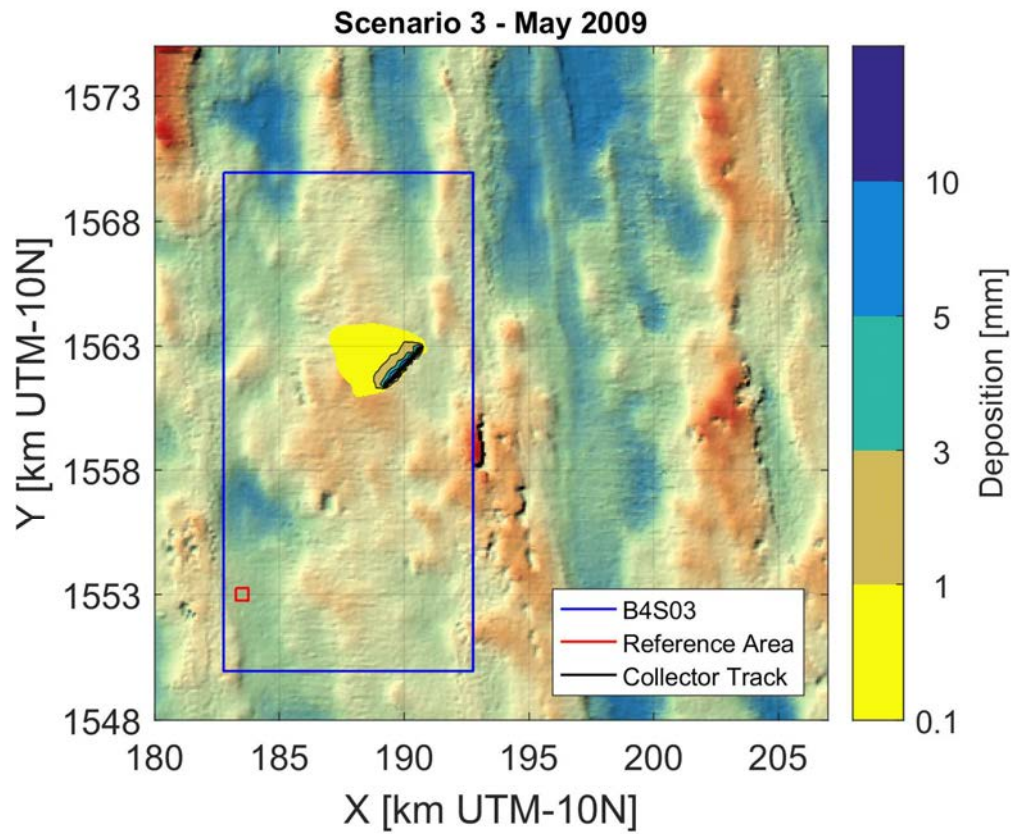


Figure Ixix: Sediment deposition at the end of the model simulation for scenario 1 - May 2009

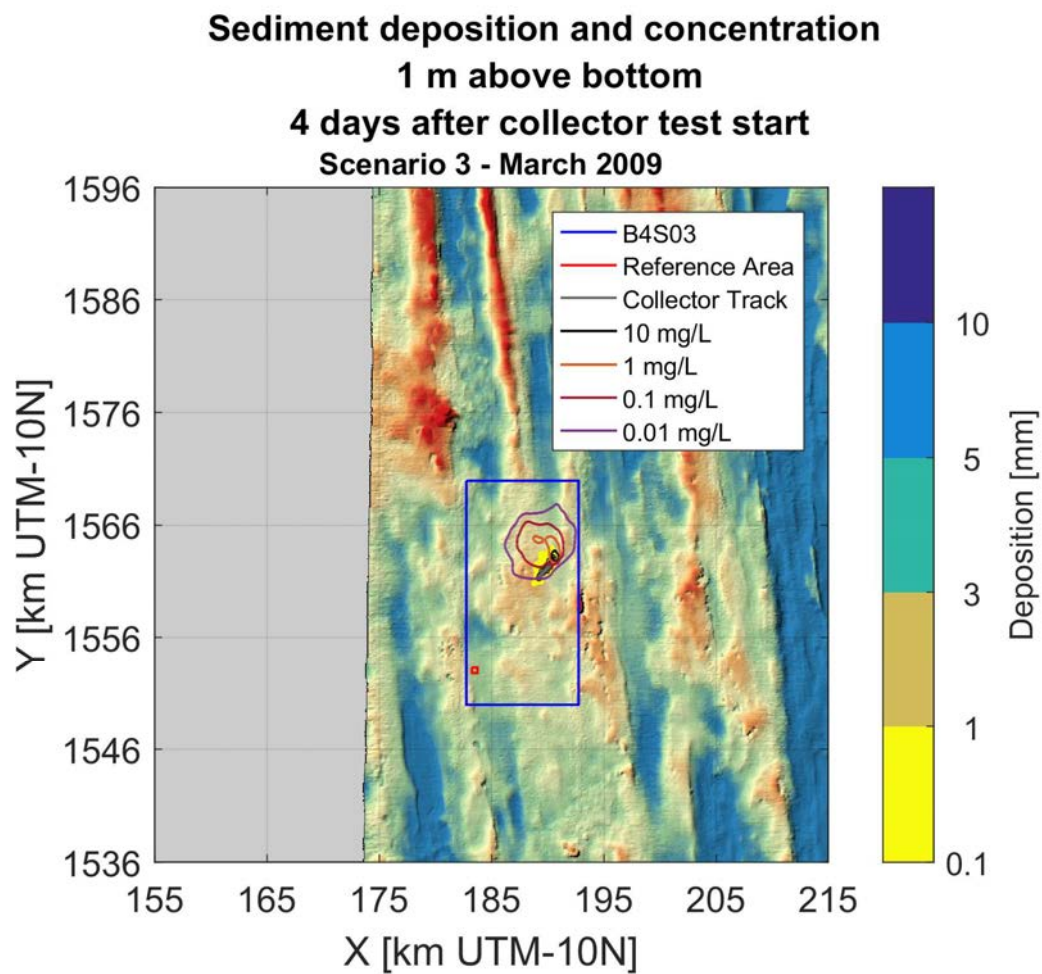


Figure lxx: Sediment suspension contours at the end of the Patania II trial for scenario 1 - March 2009

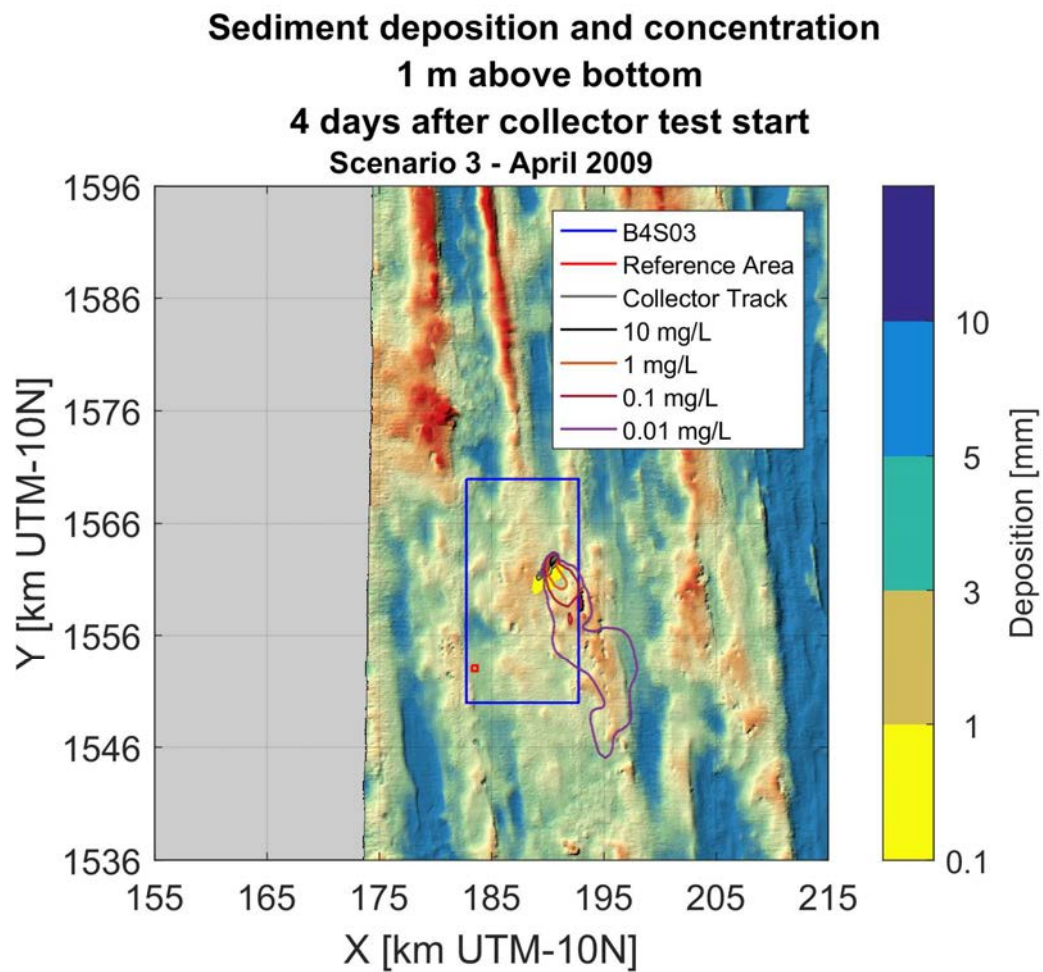


Figure lxxi: Sediment suspension contours at the end of the Patania II trial for scenario 1 - April 2009

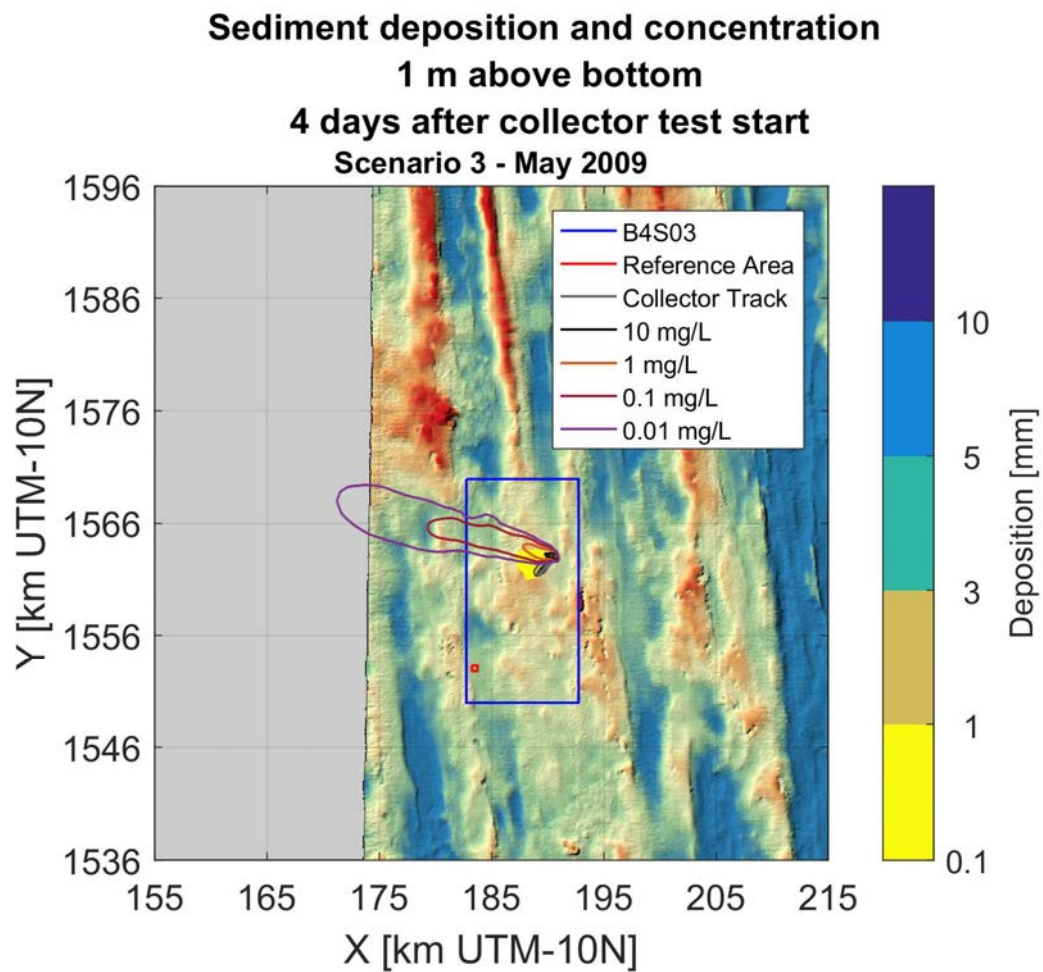


Figure lxxii: Sediment suspension contours at the end of the Patania II trial for scenario 1 - May 2009

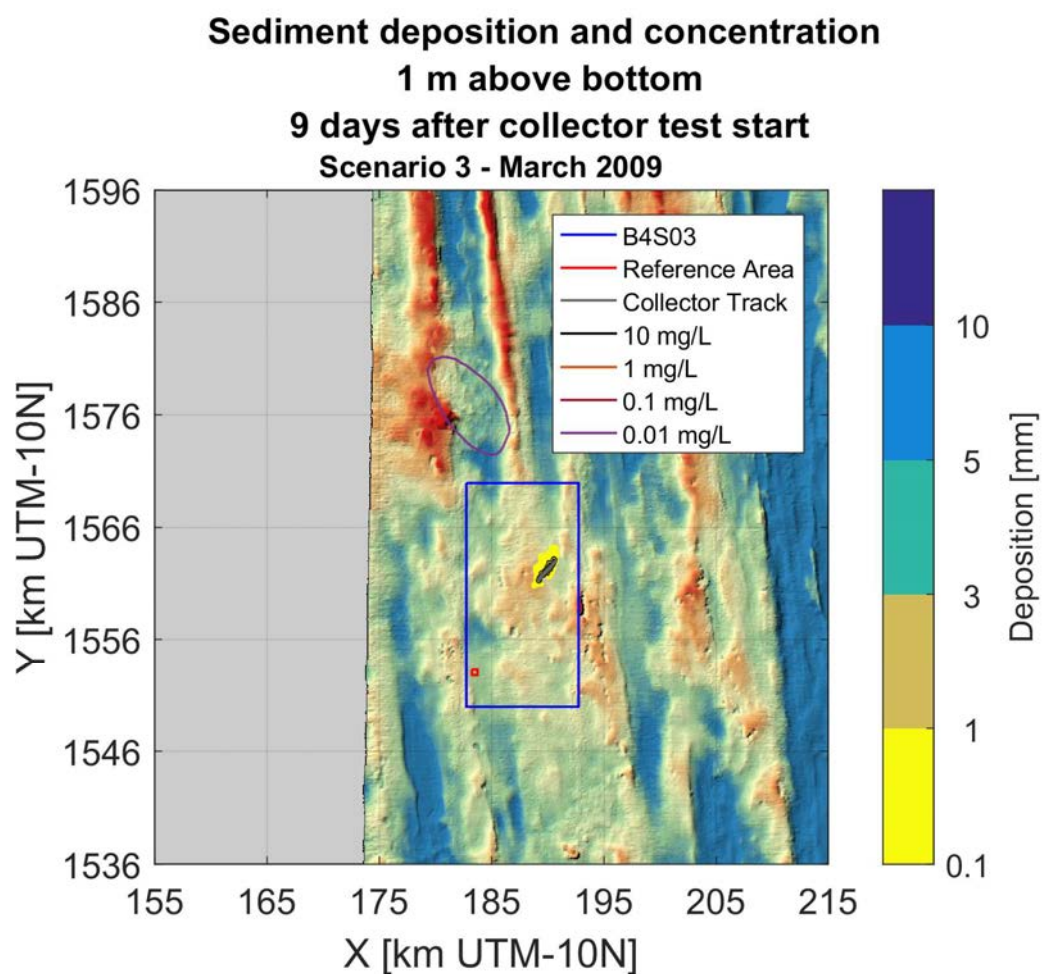


Figure lxxiii: Sediment suspension contours 5 days after at the end of the Patania II trial for scenario 1 - March 2009

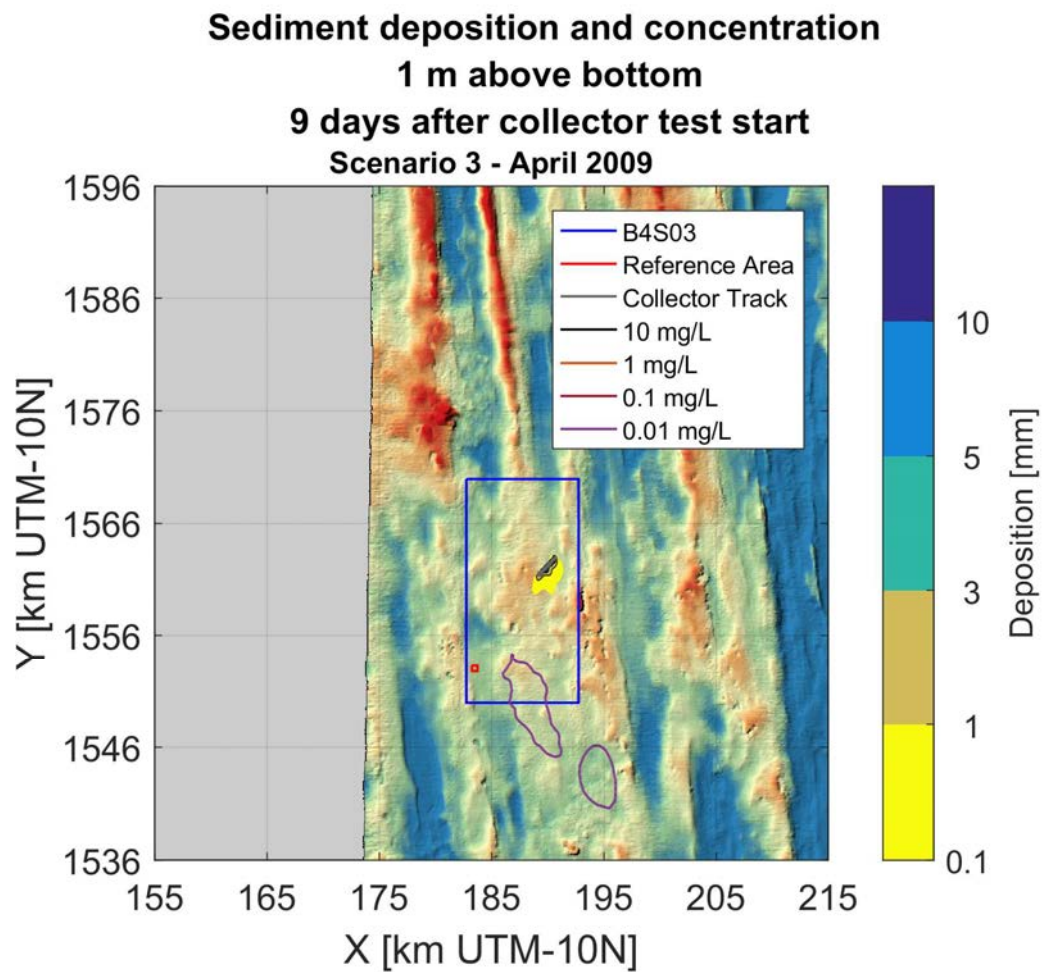


Figure lxxiv: Sediment suspension contours 5 days after at the end of the Patania II trial for scenario 1 - April 2009

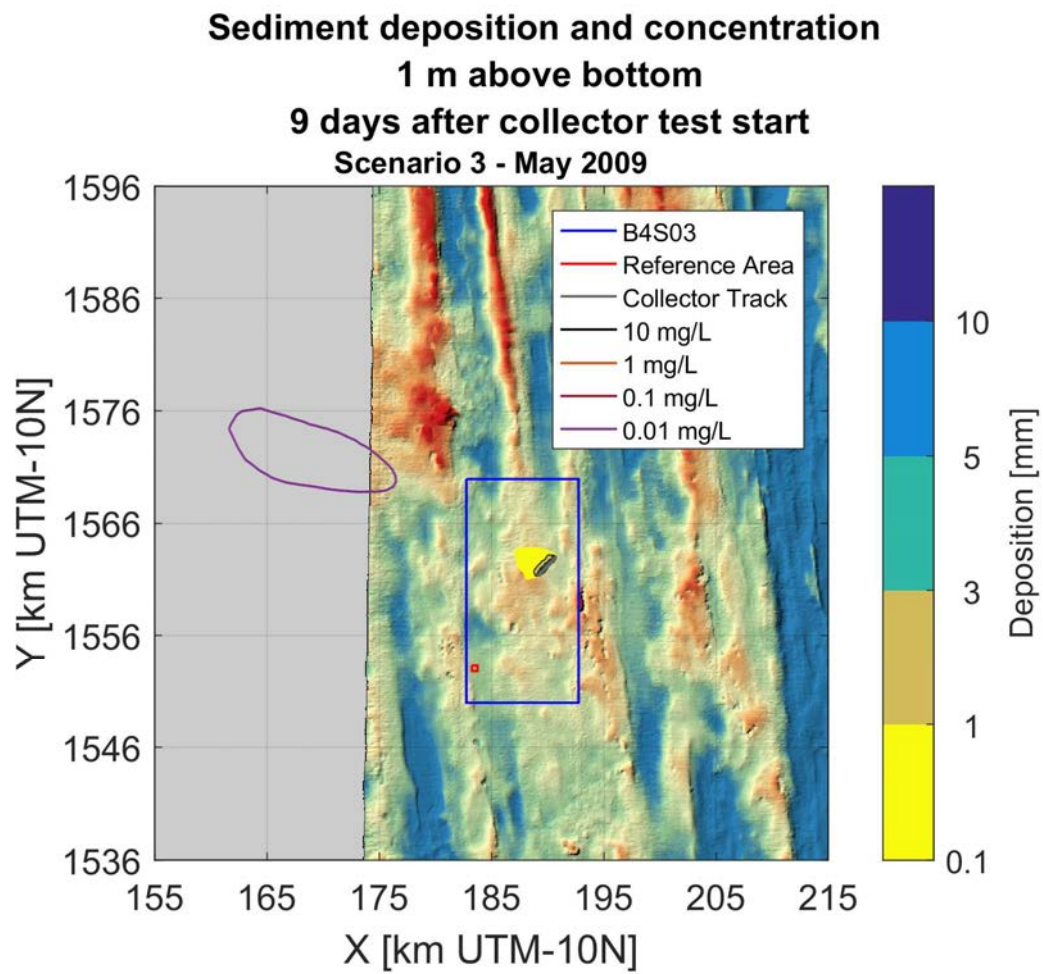


Figure lxxv: Sediment suspension contours 5 days after at the end of the Patania II trial for scenario 1 - May 2009

12.4.3.3 Suspended sediment plume – occurrence frequency contours

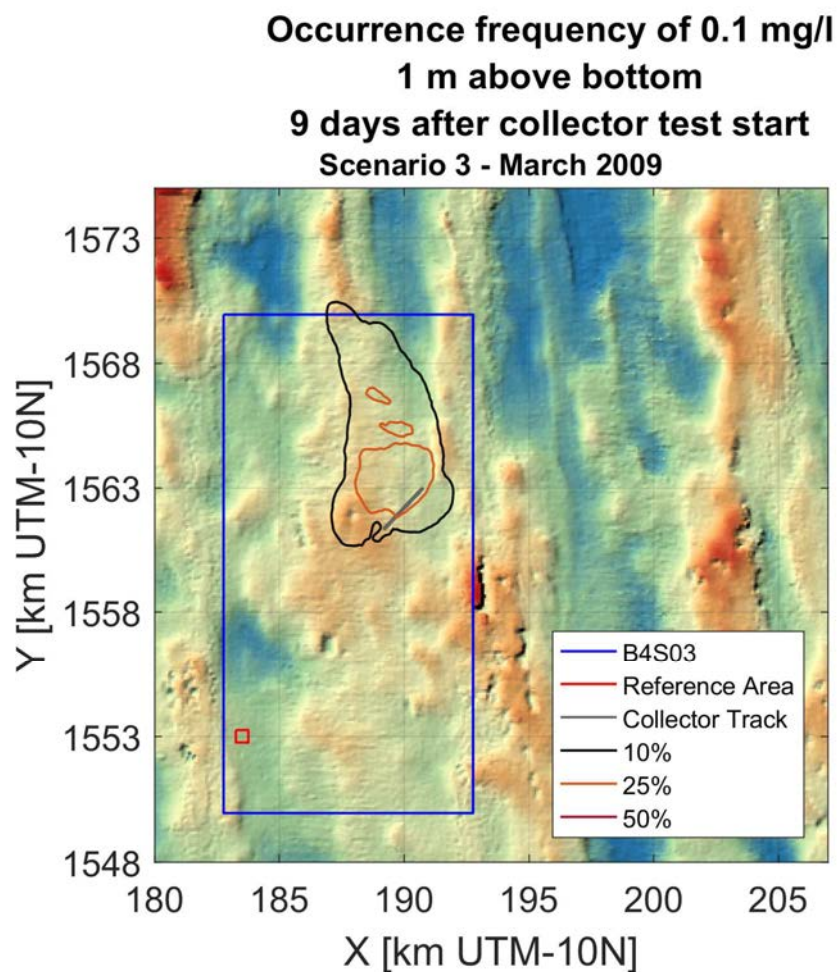


Figure lxxvi: Frequency of occurrence for 0.1 mg/l sediment concentration for scenario 1 - March 2009

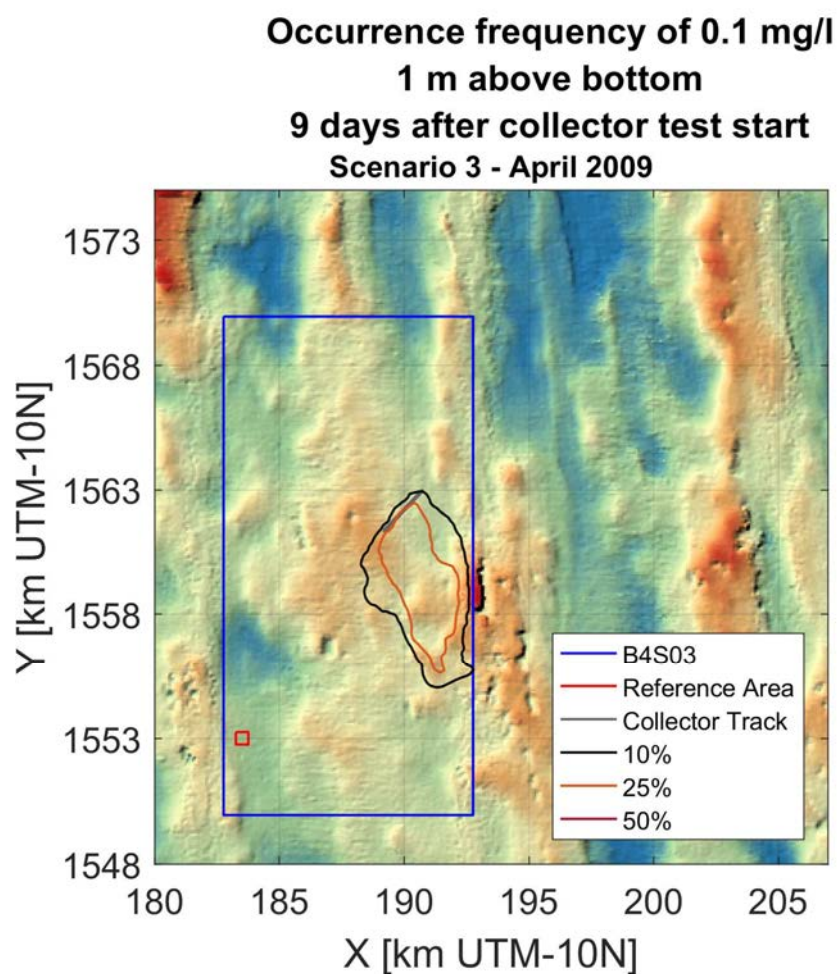


Figure lxxvii: Frequency of occurrence for 0.1 mg/l sediment concentration for scenario 1 - April 2009

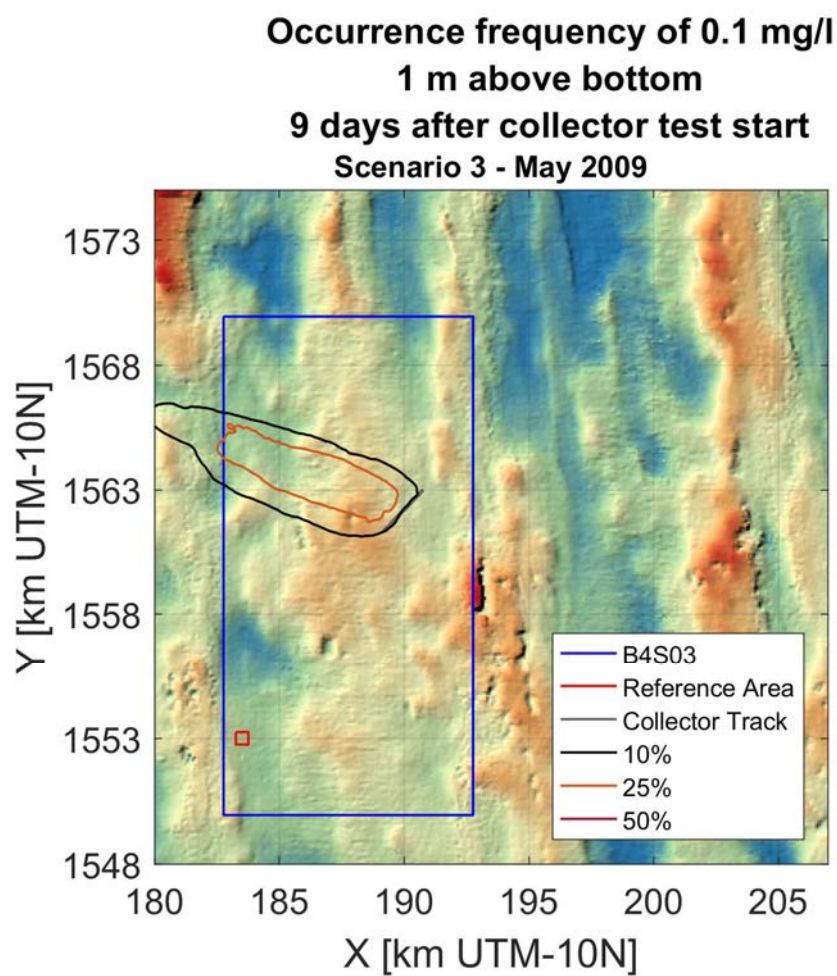


Figure lxxviii: Frequency of occurrence for 0.1 mg/l sediment concentration for scenario 1 - May 2009

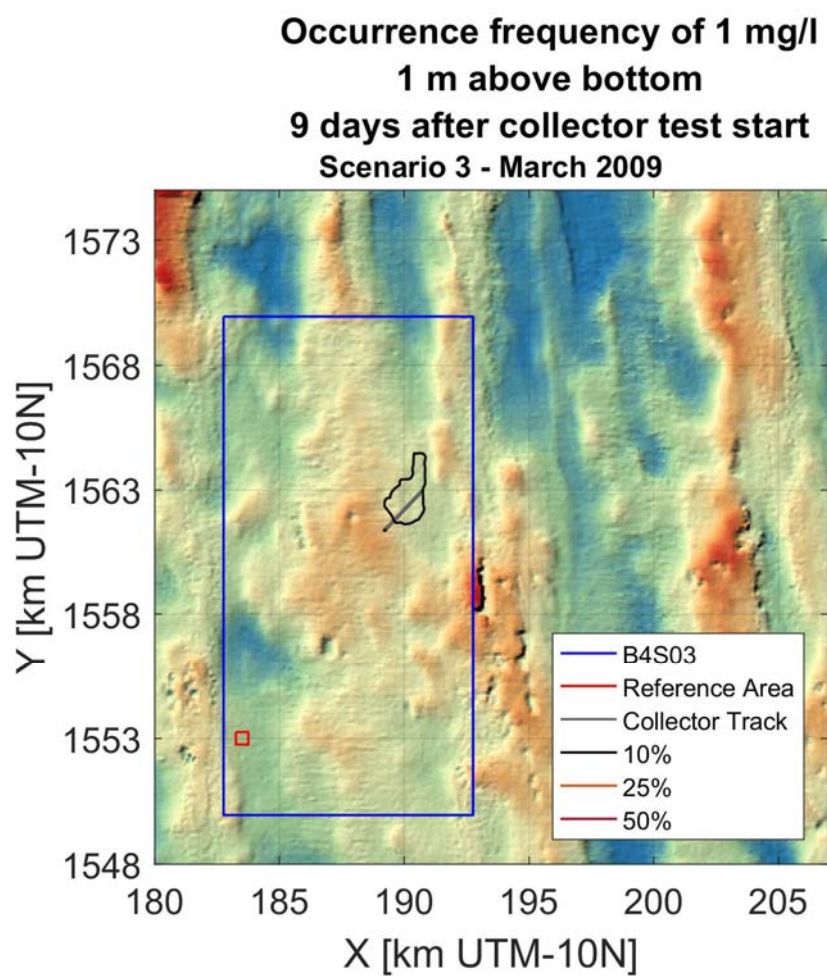


Figure lxxix: Frequency of occurrence for 1 mg/l sediment concentration for scenario 1 - March 2009

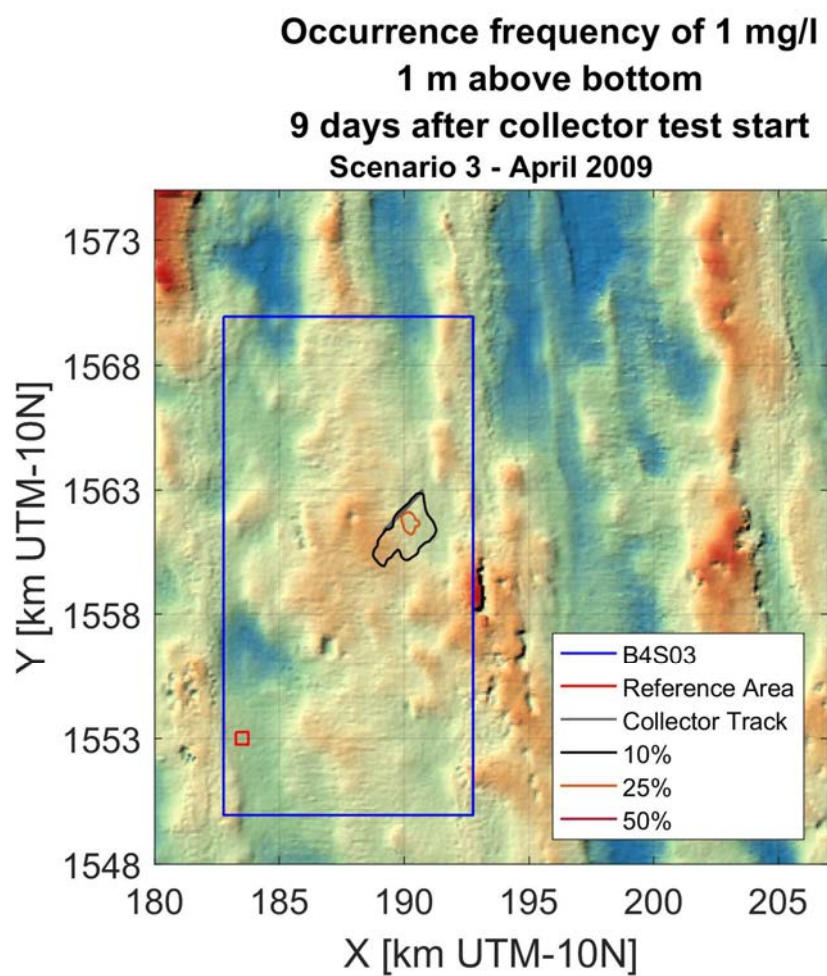


Figure lxxx: Frequency of occurrence for 1 mg/l sediment concentration for scenario 1 - April 2009

**Occurrence frequency of 1 mg/l
1 m above bottom
9 days after collector test start
Scenario 3 - May 2009**

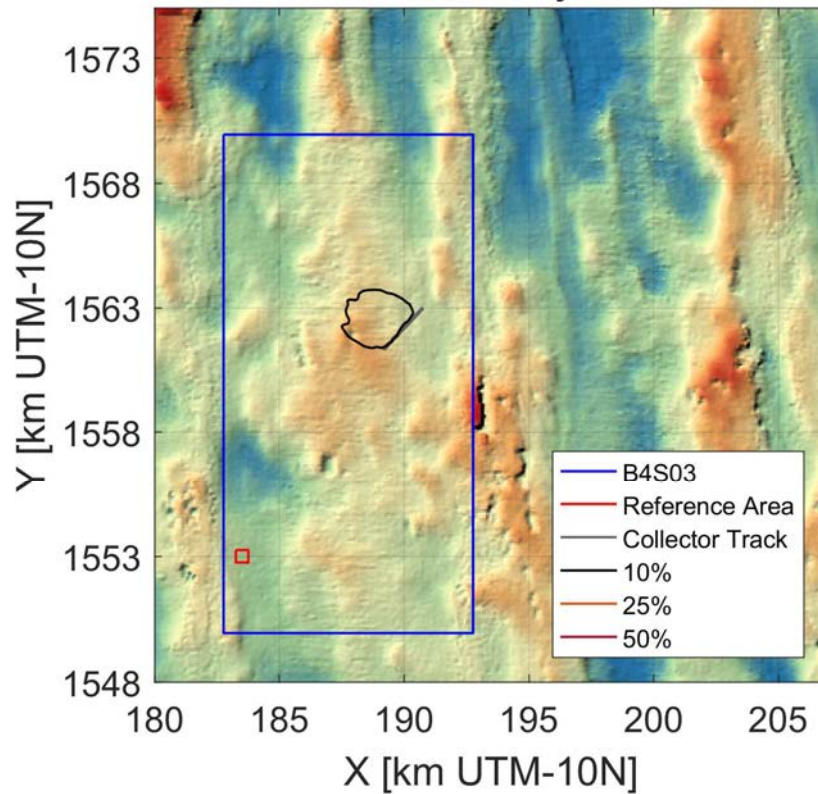


Figure lxxxi: Frequency of occurrence for 1 mg/l sediment concentration for scenario 1 - May 2009

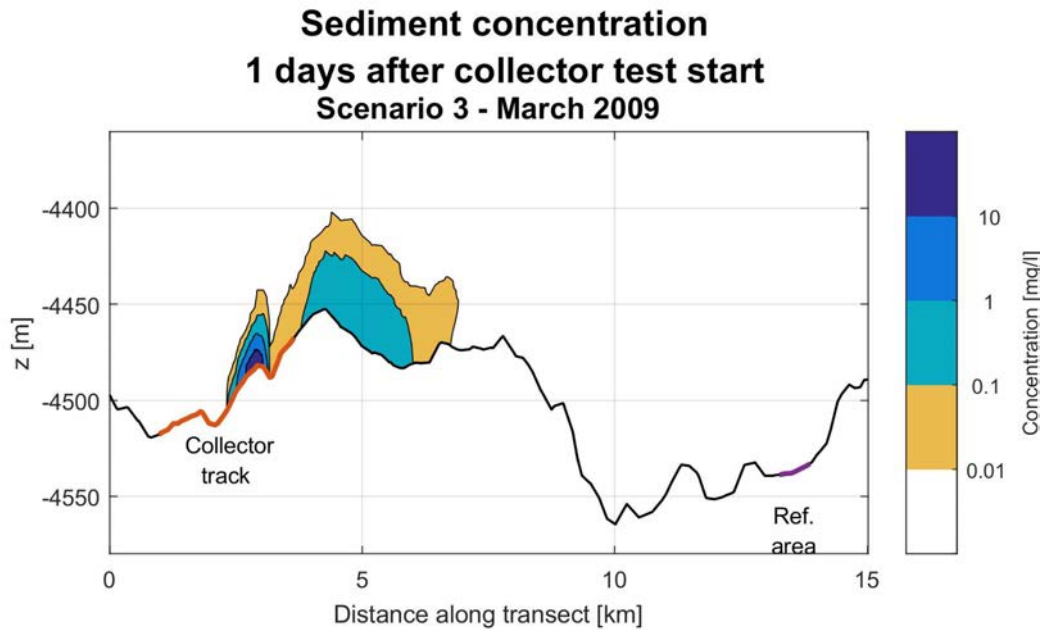


Figure lxxxii: Cross-sectional sediment concentration contours 1 day after the start of the Patania II trial for scenario 1 - March 2009

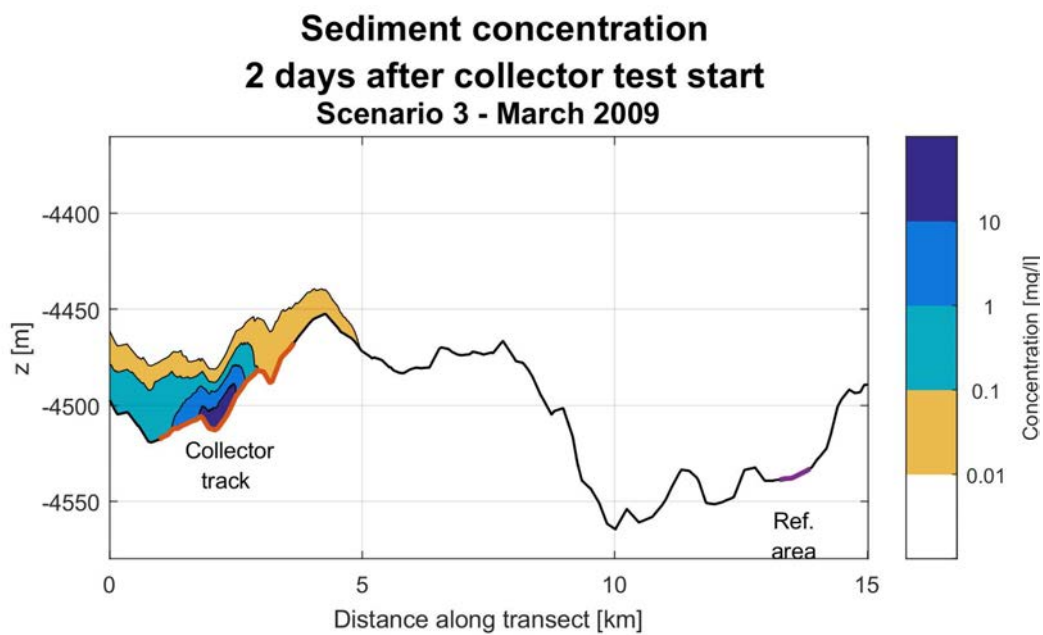


Figure lxxxiii: Cross-sectional sediment concentration contours 2 days after the start of the Patania II trial for scenario 1 - March 2009

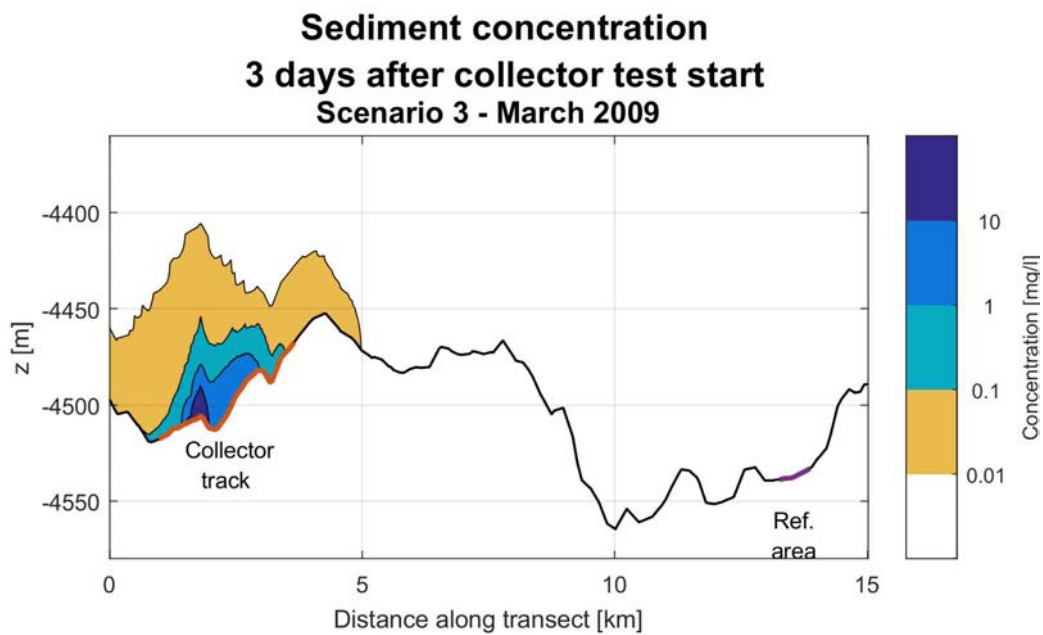


Figure lxxxiv: Cross-sectional sediment concentration contours 3 days after the start of the Patania II trial for scenario 1 - March 2009

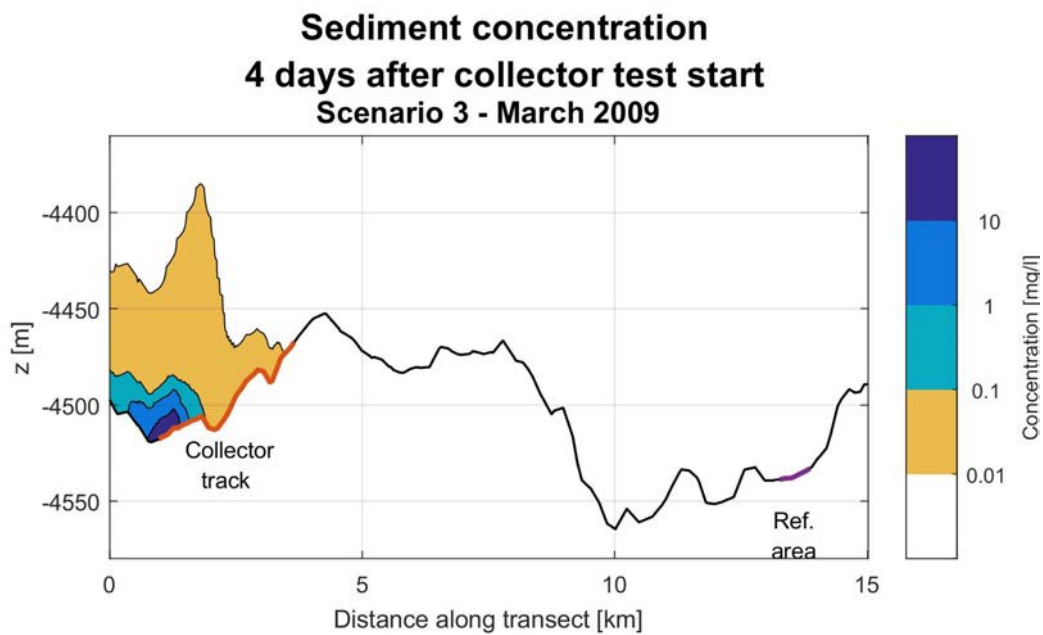


Figure lxxxv: Cross-sectional sediment concentration contours 4 days after the start of the Patania II trial for scenario 1 - March 2009

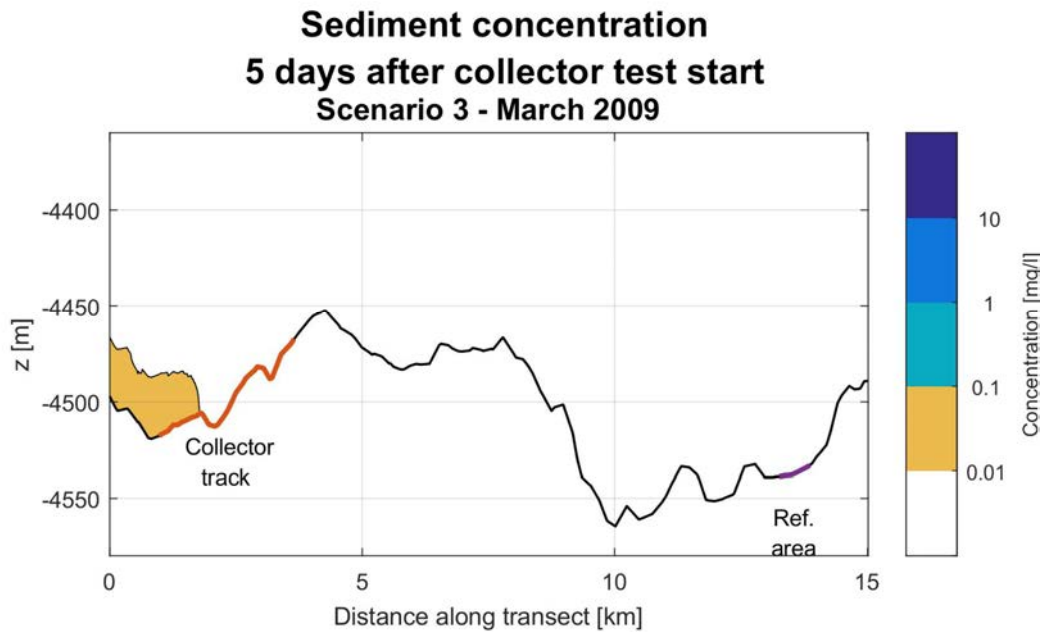


Figure lxxxvi: Cross-sectional sediment concentration contours 5 days after the start of the Patania II trial for scenario 1 - March 2009

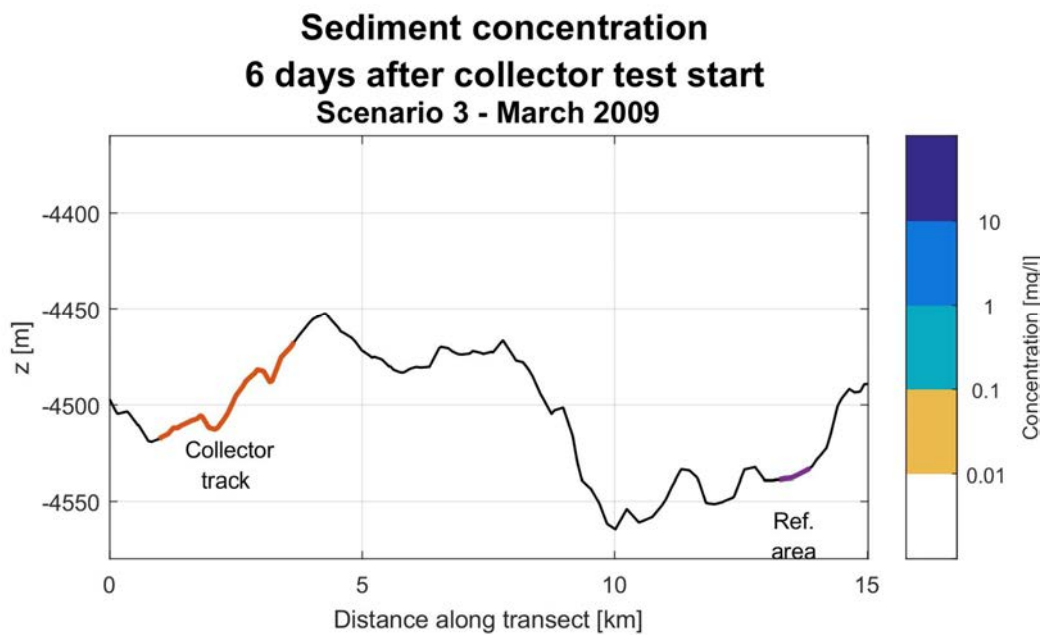


Figure lxxxvii: Cross-sectional sediment concentration contours 6 days after the start of the Patania II trial for scenario 1 - March 2009

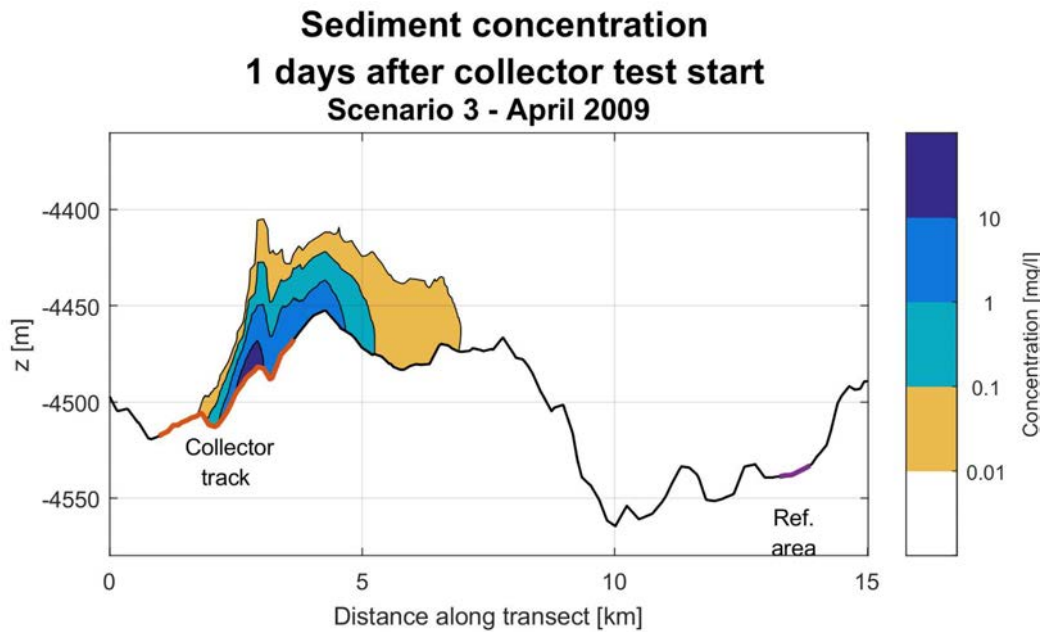


Figure lxxxviii: Cross-sectional sediment concentration contours 1 day after the start of the Patania II trial for scenario 1 - April 2009

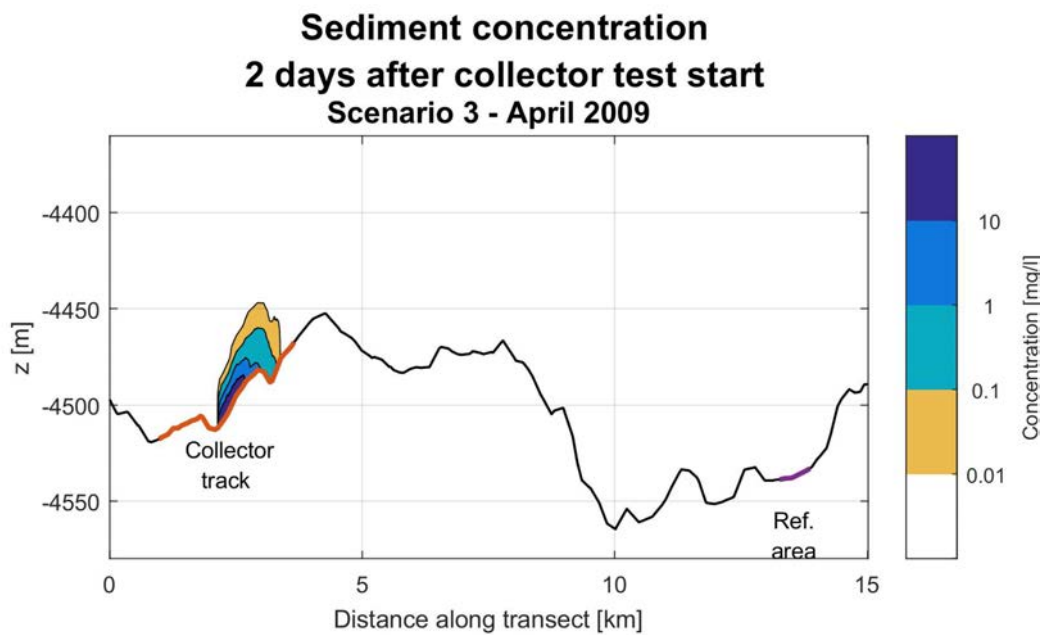


Figure lxxxix: Cross-sectional sediment concentration contours 2 days after the start of the Patania II trial for scenario 1 - April 2009

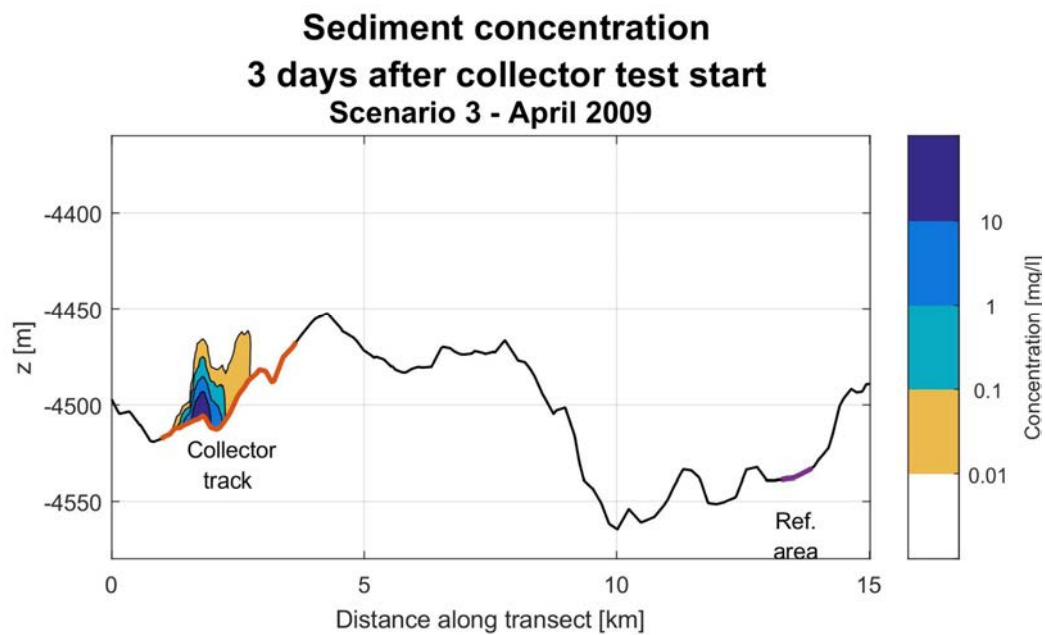


Figure xc: Cross-sectional sediment concentration contours 3 days after the start of the Patania II trial for scenario 1 - April 2009

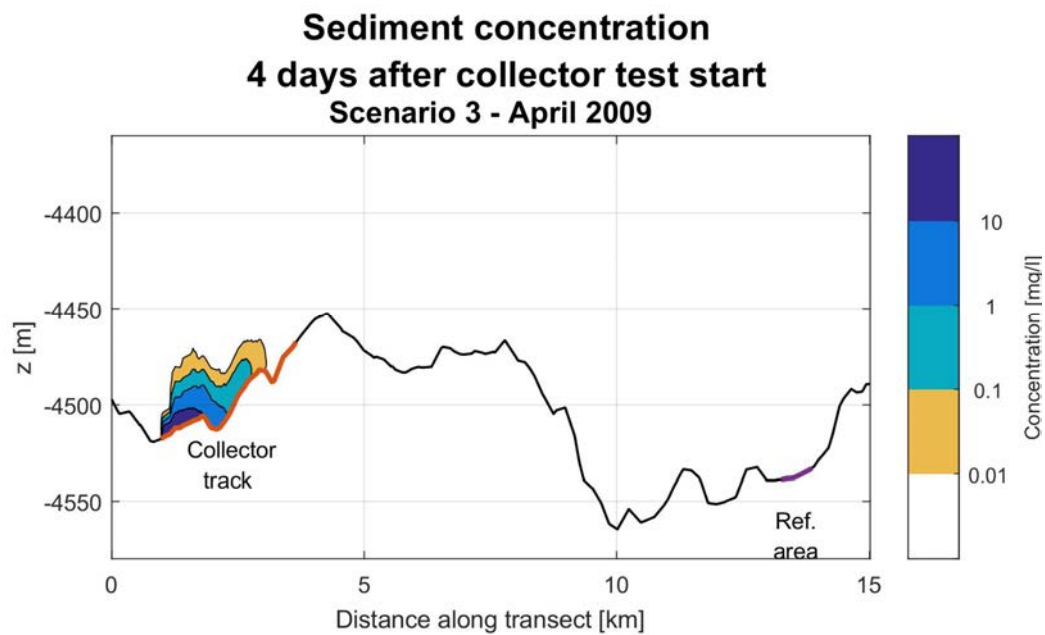


Figure xci: Cross-sectional sediment concentration contours 4 days after the start of the Patania II trial for scenario 1 - April 2009

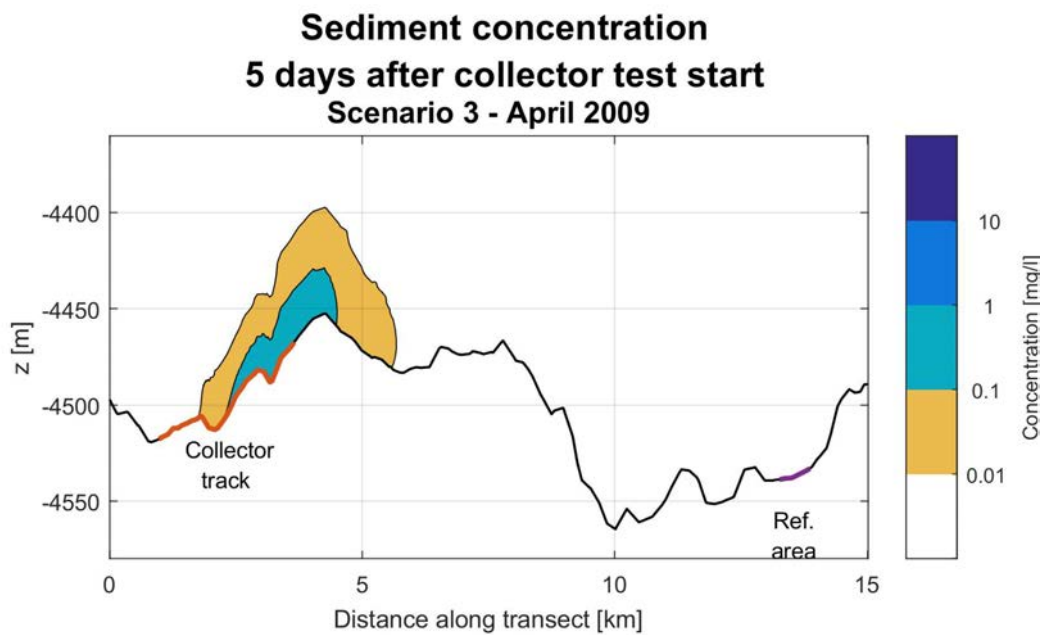


Figure xcii: Cross-sectional sediment concentration contours 5 days after the start of the Patania II trial for scenario 1 - April 2009

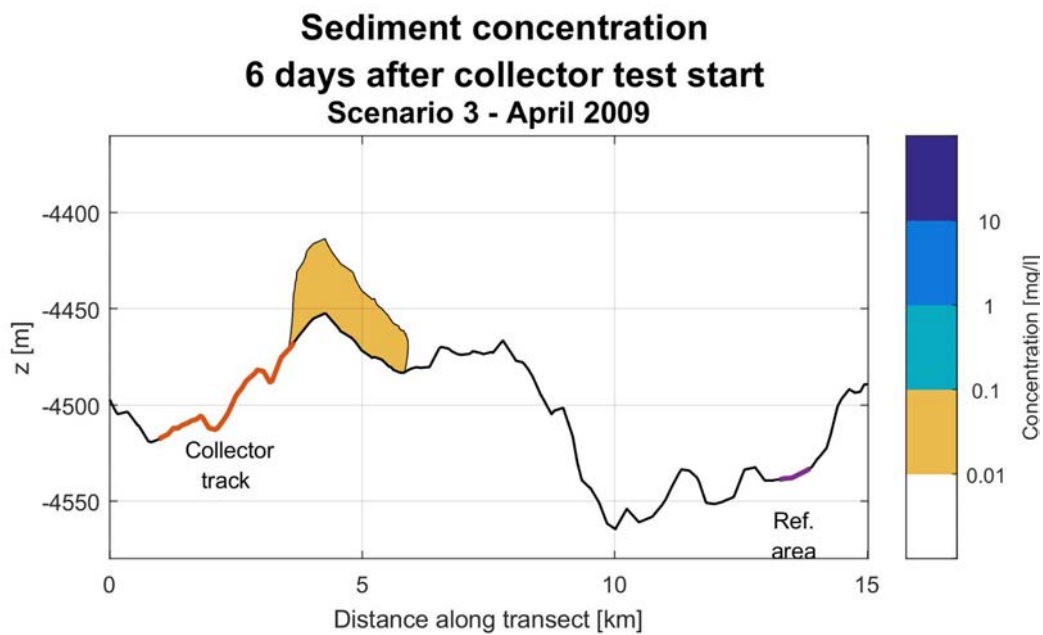


Figure xciii: Cross-sectional sediment concentration contours 6 days after the start of the Patania II trial for scenario 1 - April 2009

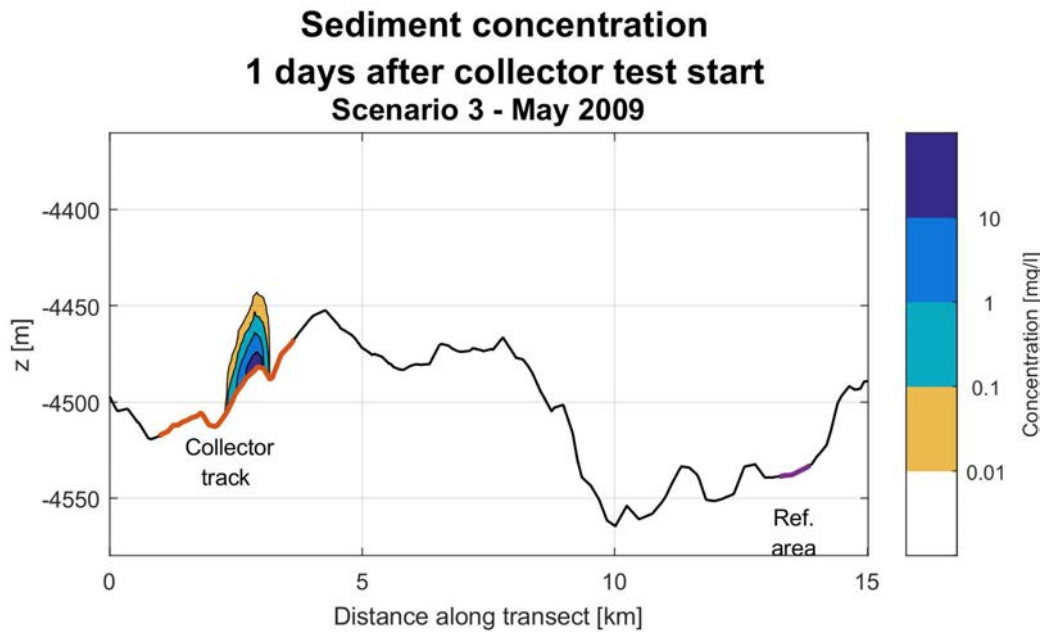


Figure xcv: Cross-sectional sediment concentration contours 1 day after the start of the Patania II trial for scenario 1 - May 2009

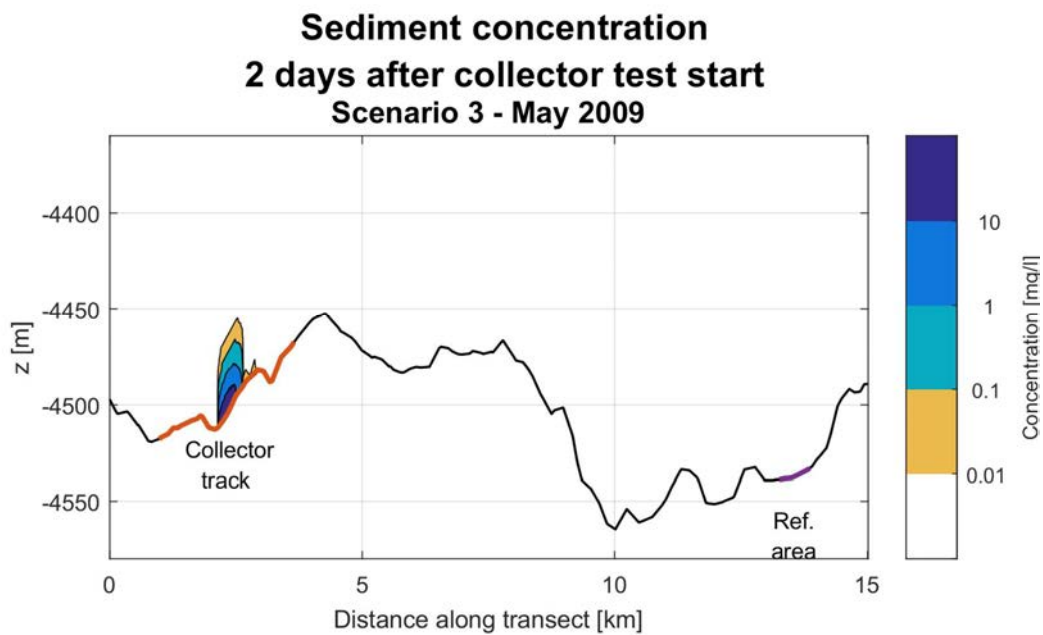


Figure xcv: Cross-sectional sediment concentration contours 2 days after the start of the Patania II trial for scenario 1 - May 2009

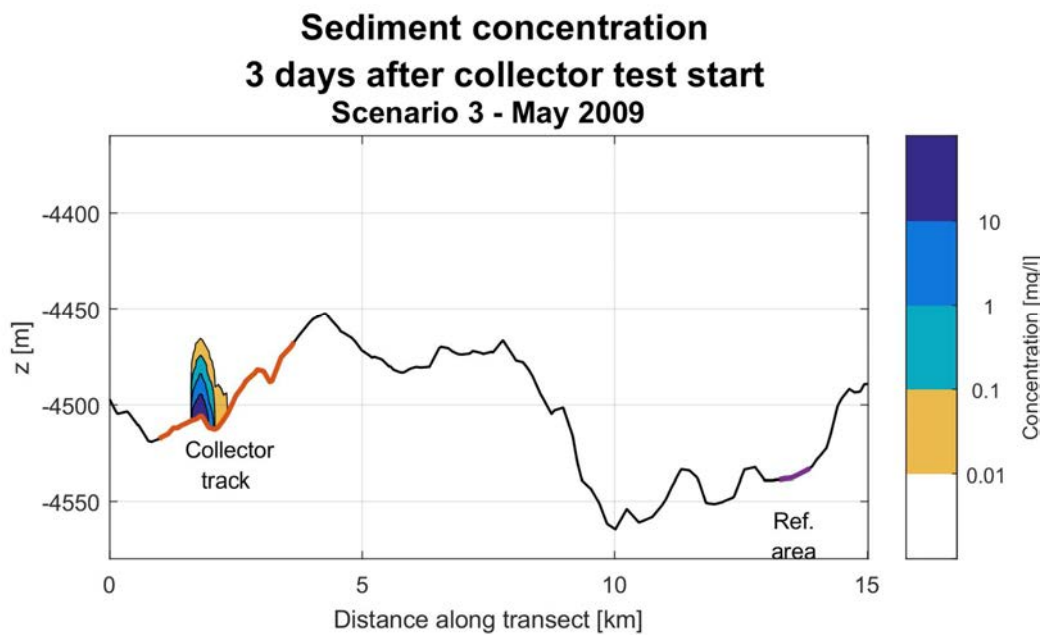


Figure xcvi: Cross-sectional sediment concentration contours 3 days after the start of the Patania II trial for scenario 1 - May 2009

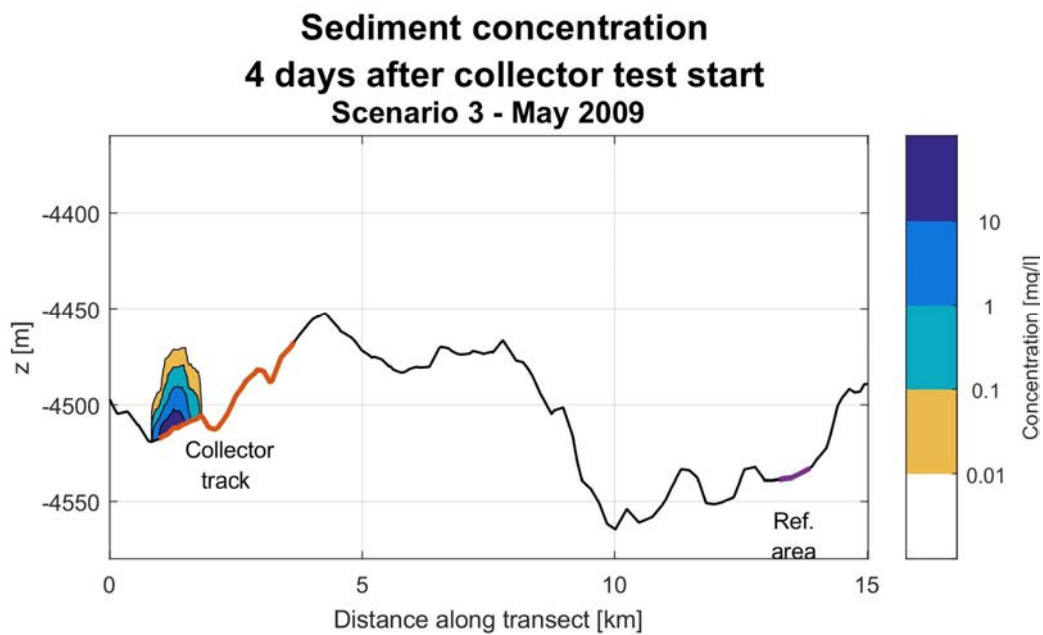


Figure xcvi: Cross-sectional sediment concentration contours 4 days after the start of the Patania II trial for scenario 1 - May 2009

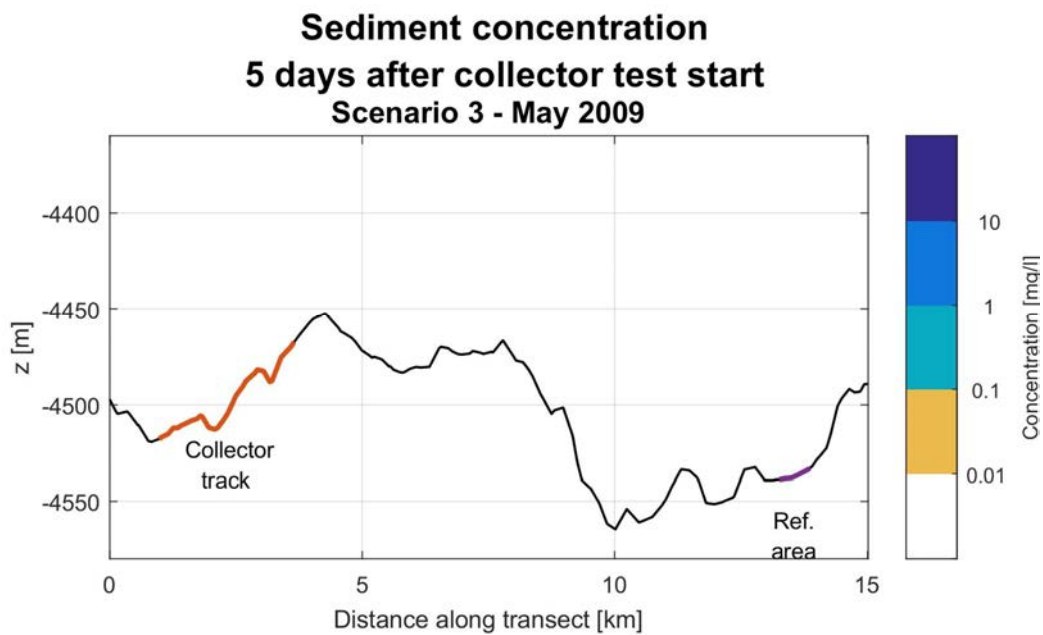


Figure xcviii: Cross-sectional sediment concentration contours 5 days after the start of the Patania II trial for scenario 1 - May 2009

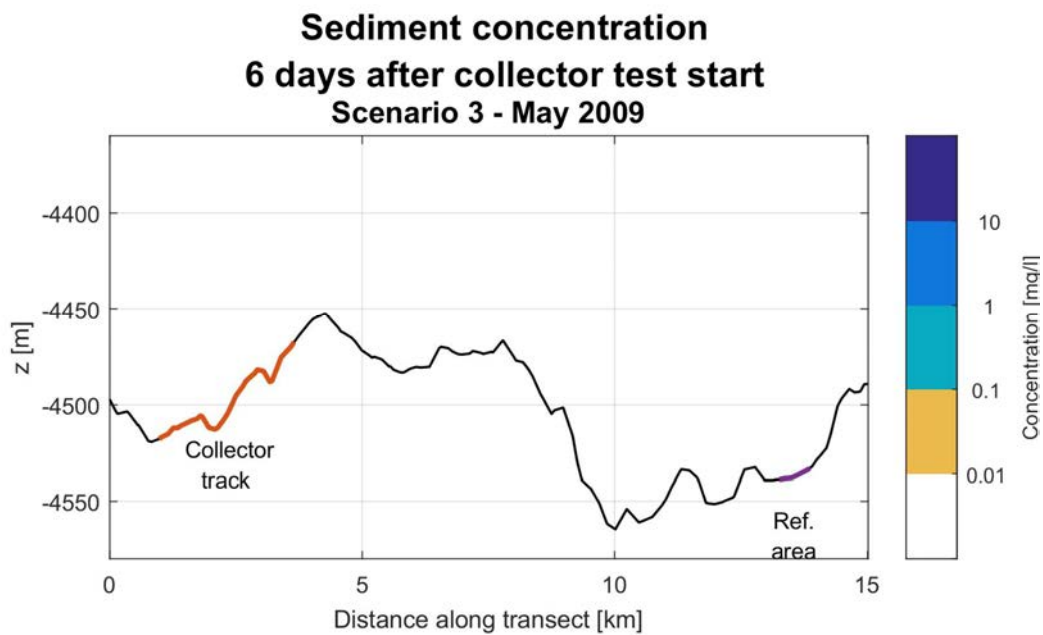


Figure xcix: Cross-sectional sediment concentration contours 6 days after the start of the Patania II trial for scenario 1 - May 2009

12.4.4.1 Sediment deposition

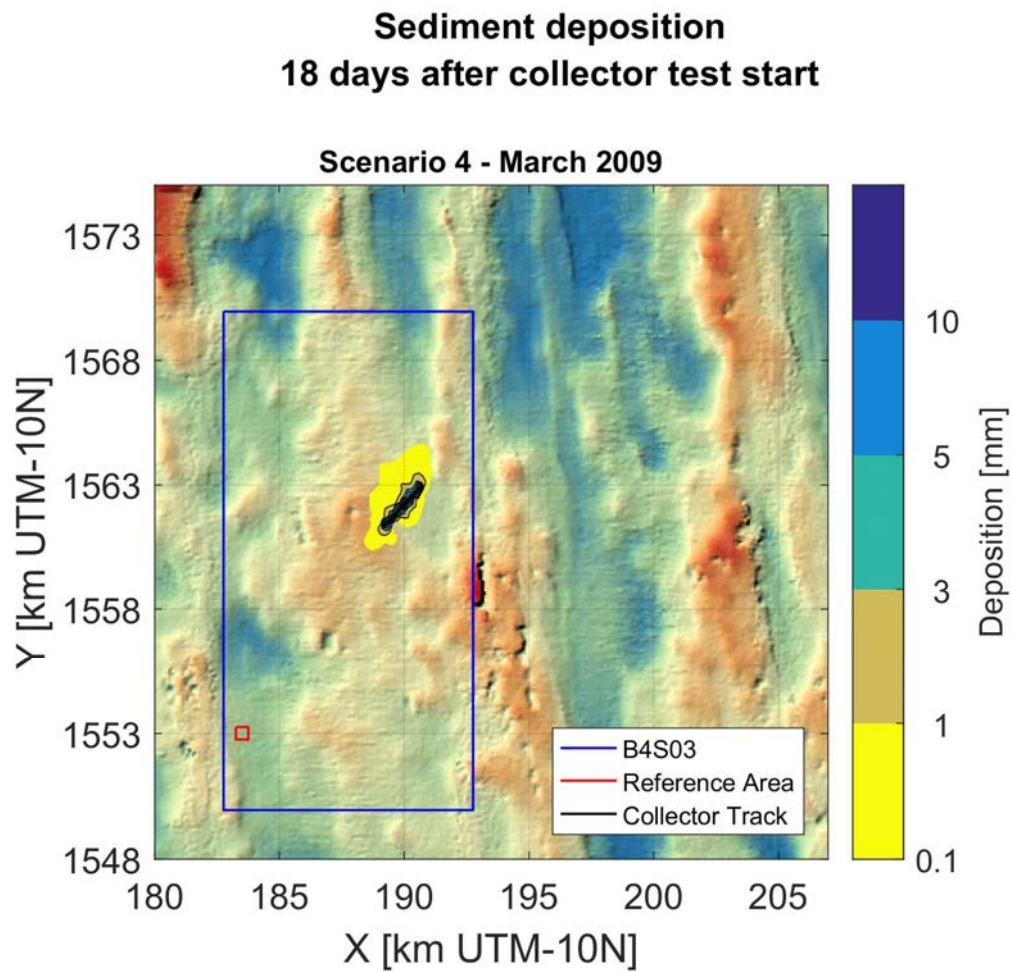


Figure c: Sediment deposition at the end of the model simulation for scenario 1 - March 2009

Sediment deposition 18 days after collector test start

Scenario 4 - April 2009

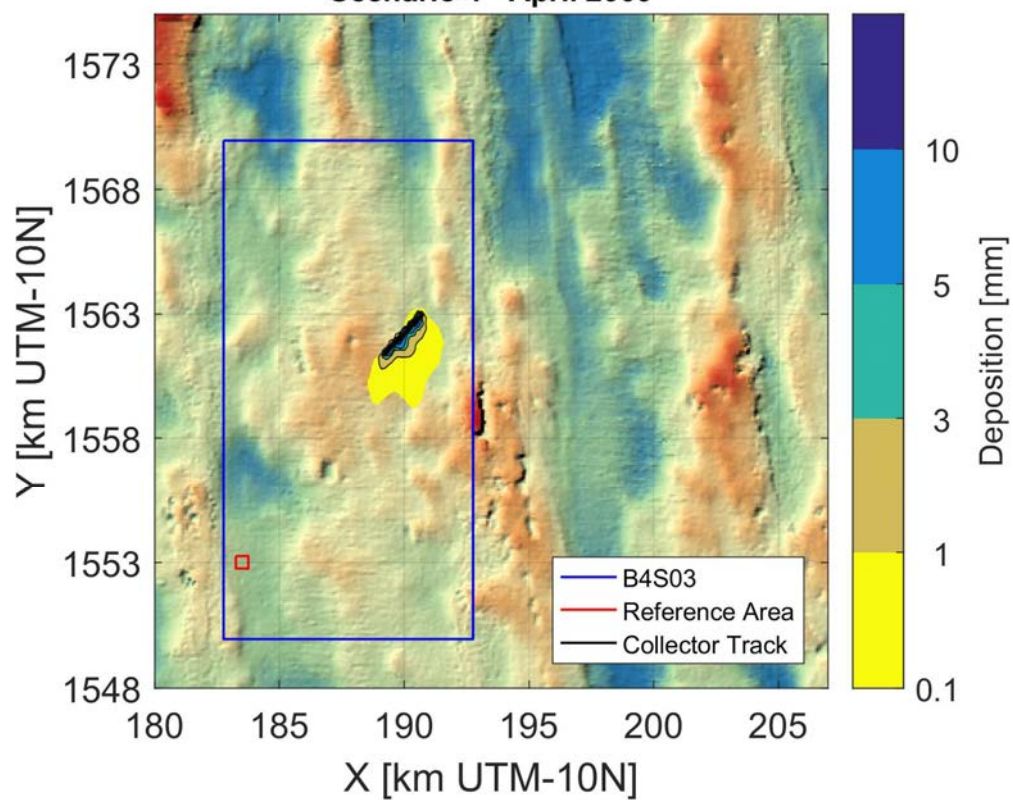


Figure ci: Sediment deposition at the end of the model simulation for scenario 1 - April 2009

Sediment deposition 18 days after collector test start

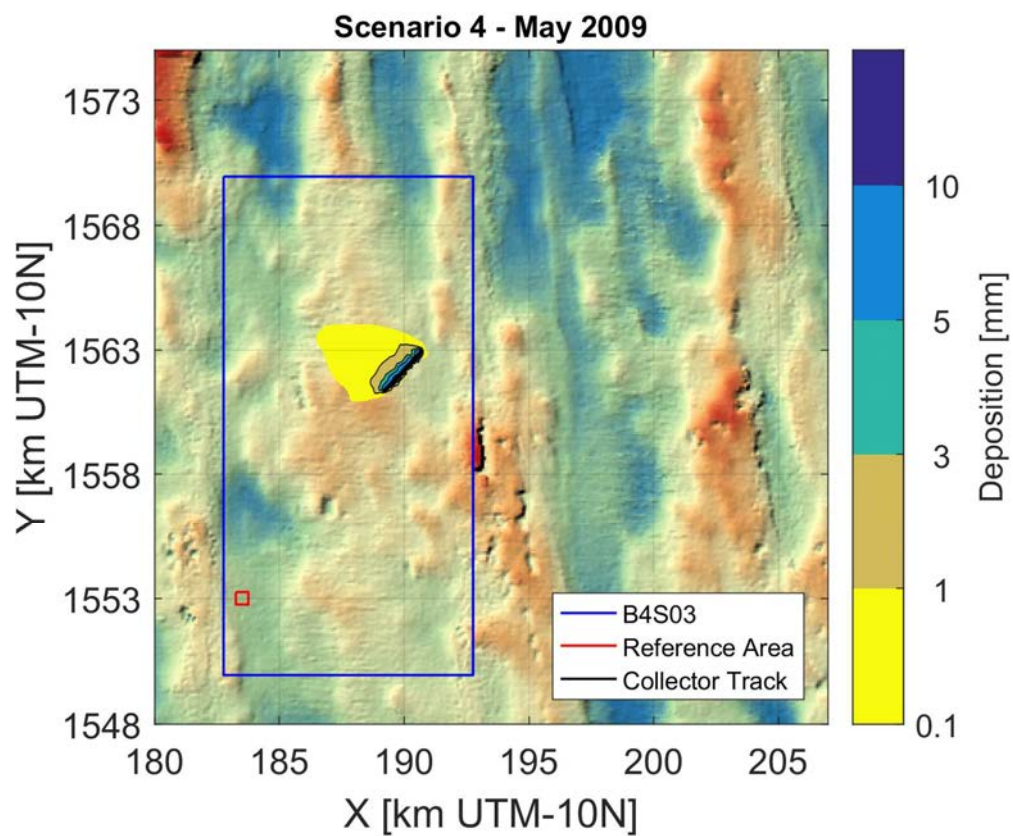


Figure cii: Sediment deposition at the end of the model simulation for scenario 1 - May 2009

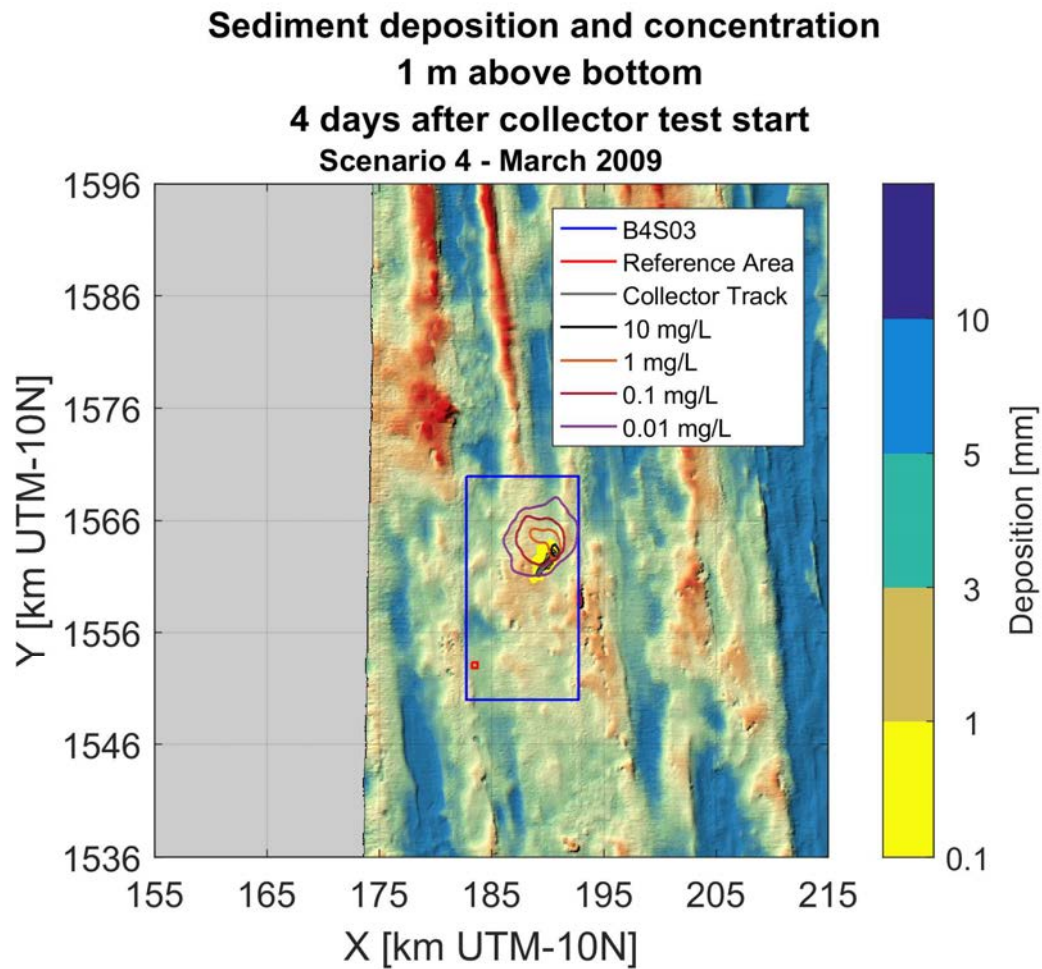


Figure ciii: Sediment suspension contours at the end of the Patania II trial for scenario 1 - March 2009

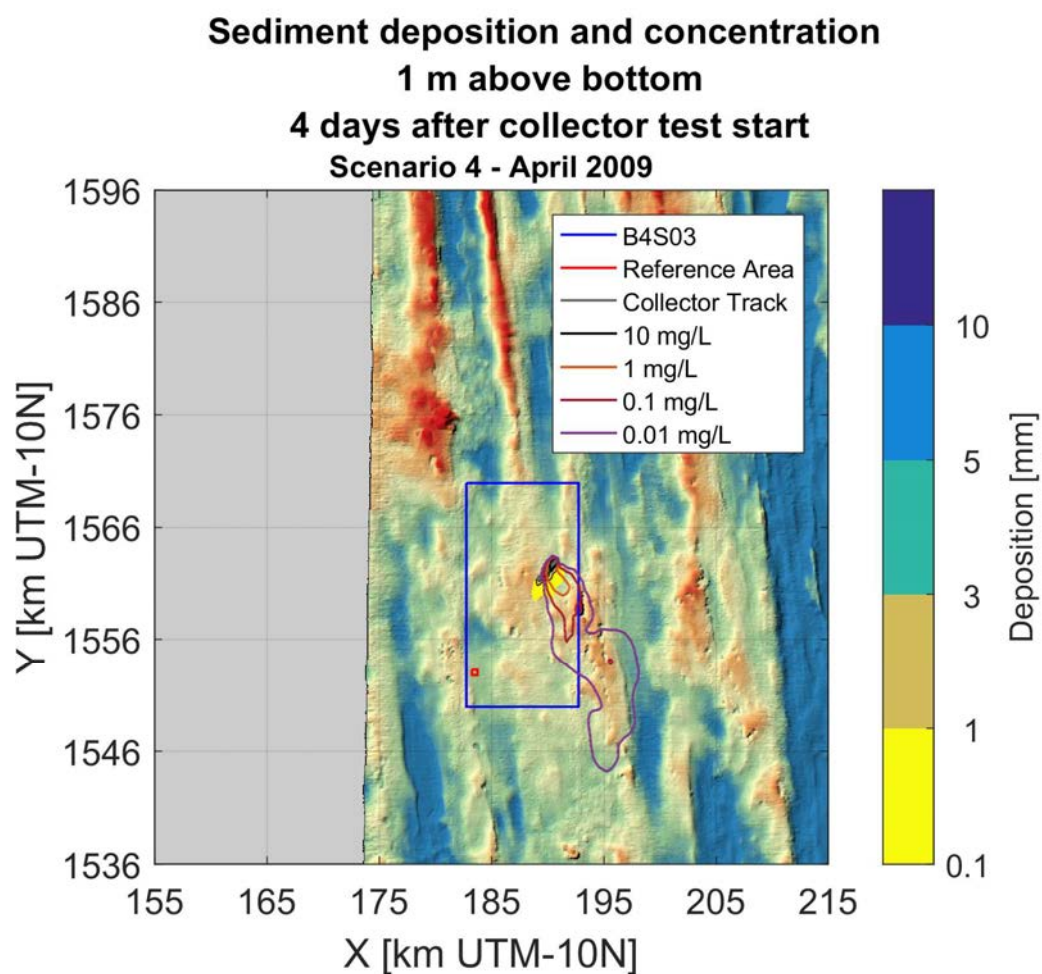


Figure civ: Sediment suspension contours at the end of the Patania II trial for scenario 1 - April 2009

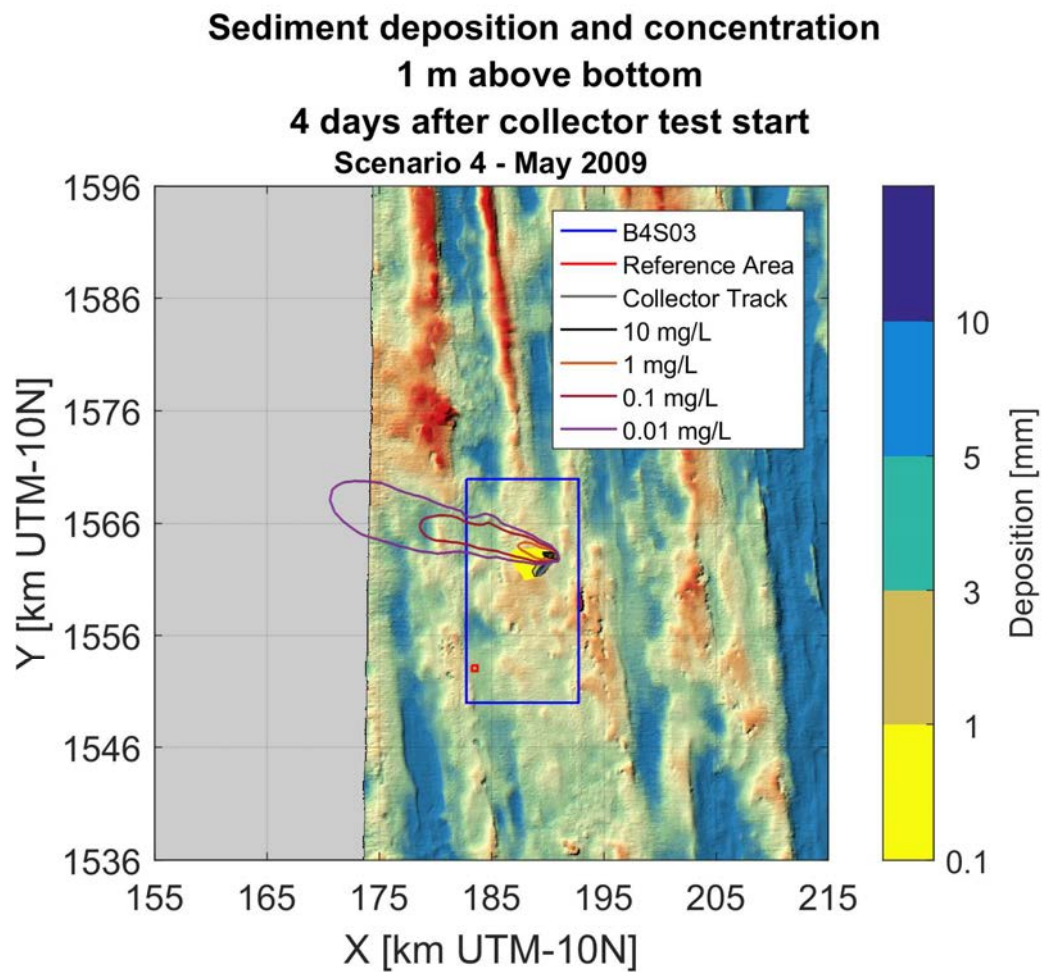


Figure cv: Sediment suspension contours at the end of the Patania II trial for scenario 1 - May 2009

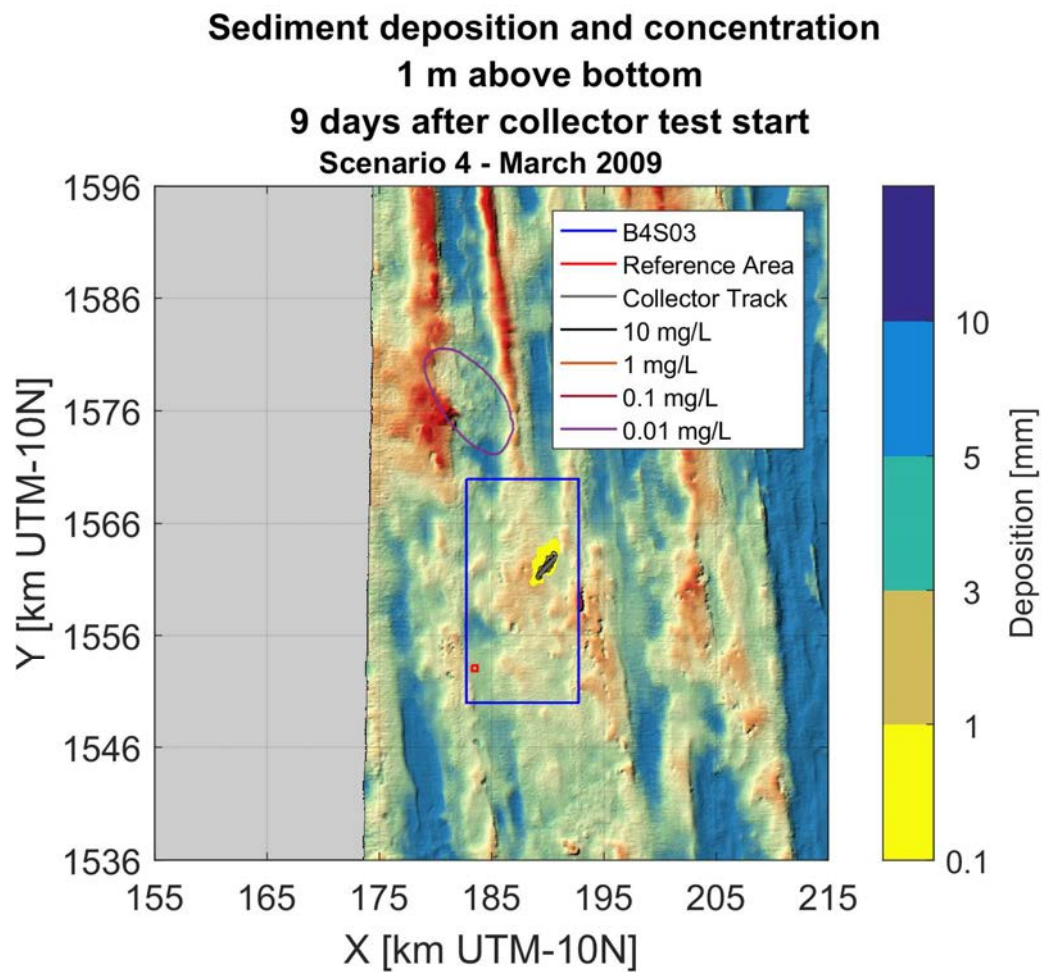


Figure cvi: Sediment suspension contours 5 days after at the end of the Patania II trial for scenario 1 - March 2009

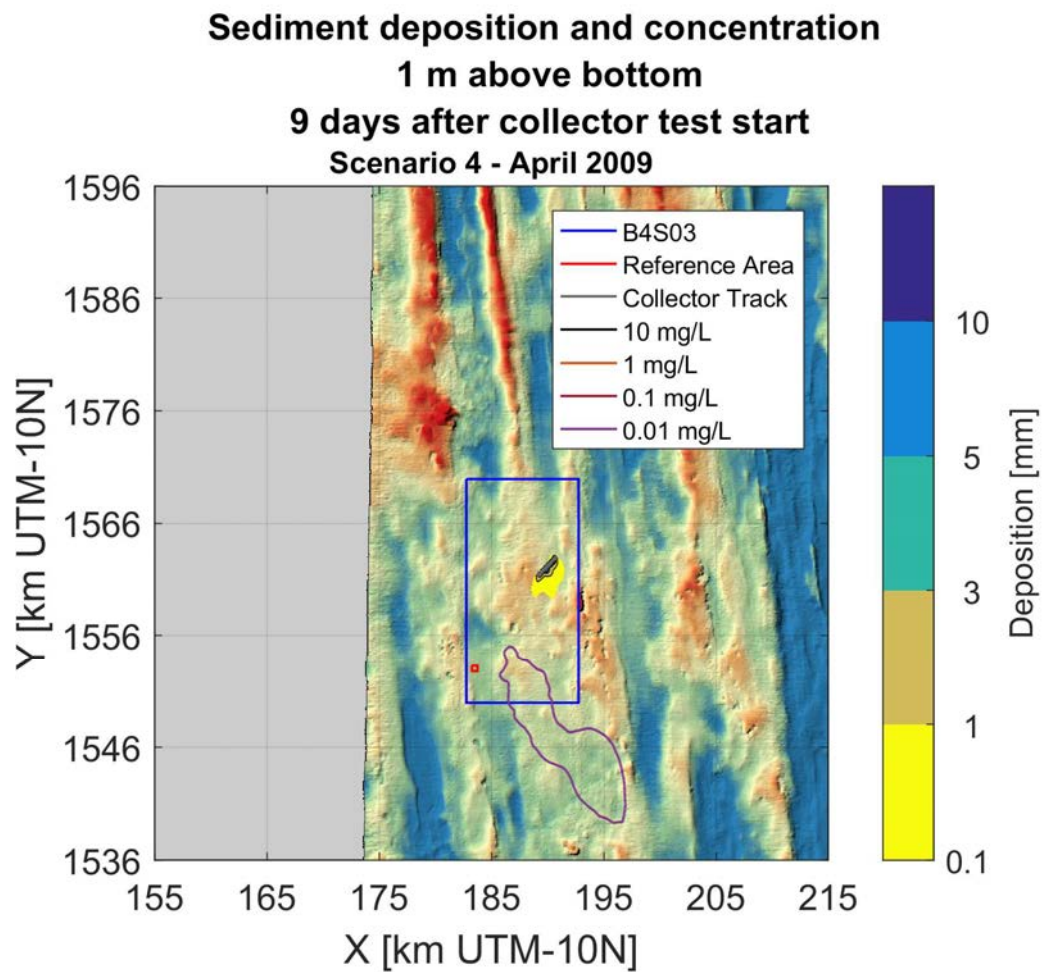


Figure cvii: Sediment suspension contours 5 days after at the end of the Patania II trial for scenario 1 - April 2009

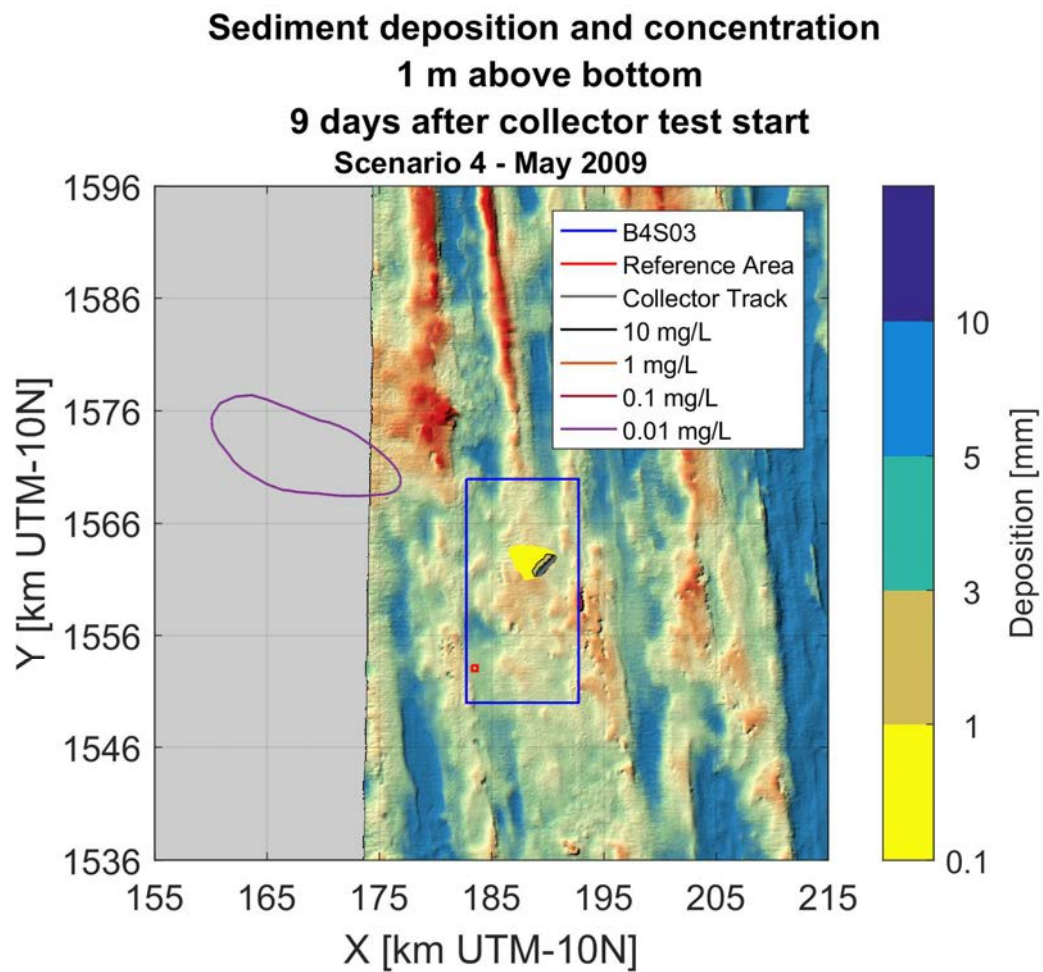


Figure cviii: Sediment suspension contours 5 days after at the end of the Patania II trial for scenario 1 - May 2009

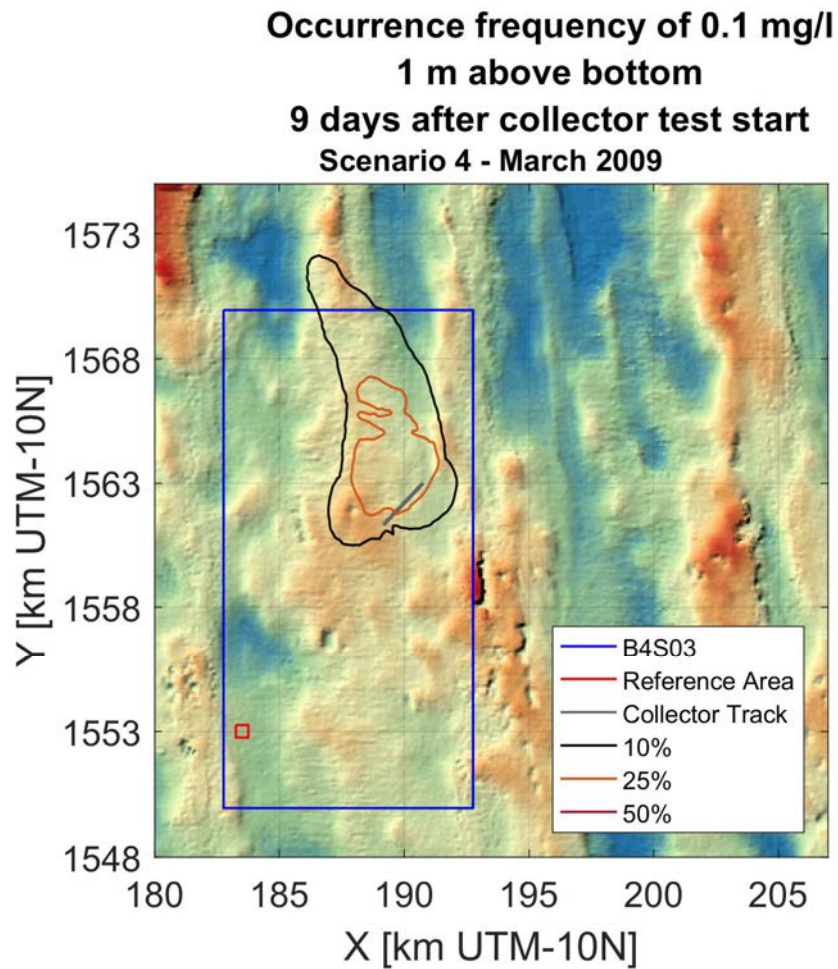


Figure cix: Frequency of occurrence for 0.1 mg/l sediment concentration for scenario 1 - March 2009

**Occurrence frequency of 0.1 mg/l
1 m above bottom
9 days after collector test start
Scenario 4 - April 2009**

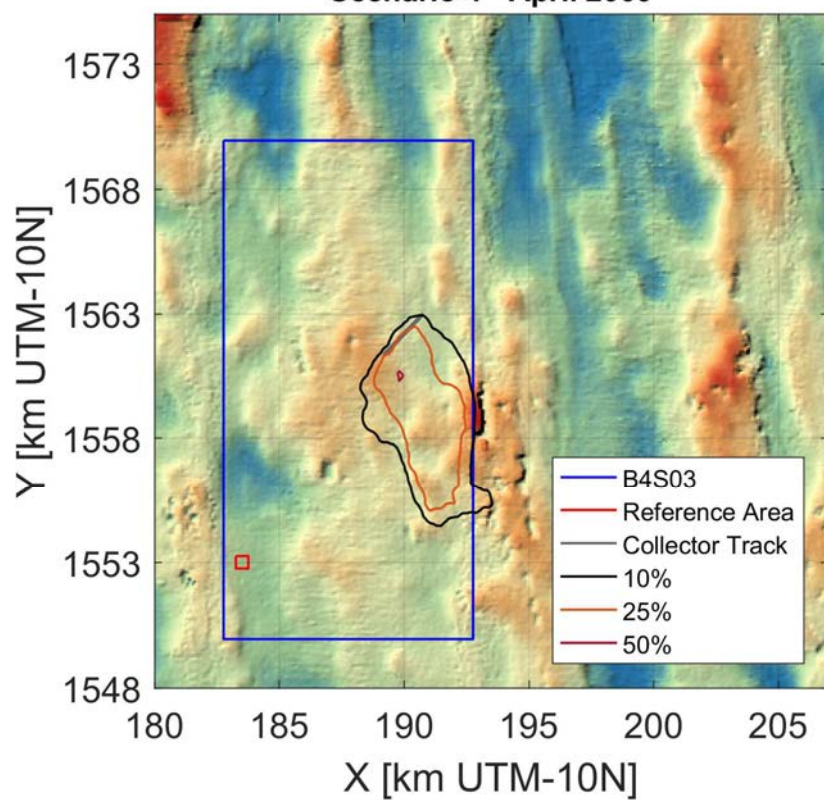


Figure cx: Frequency of occurrence for 0.1 mg/l sediment concentration for scenario 1 - April 2009

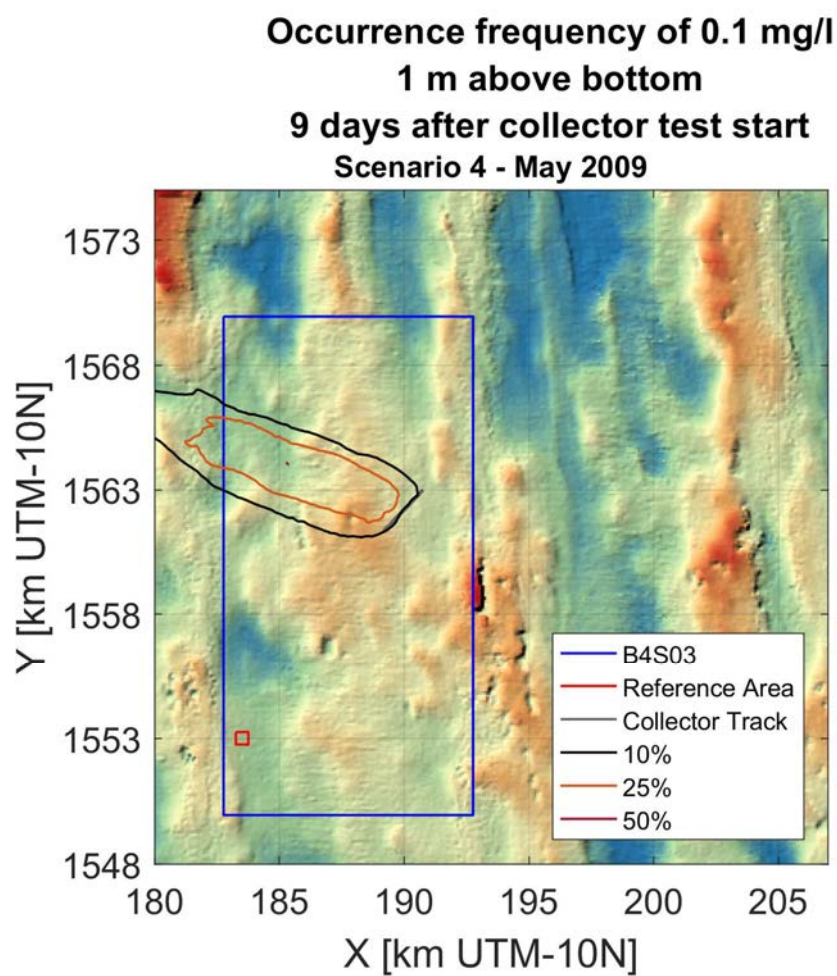


Figure cxi: Frequency of occurrence for 0.1 mg/l sediment concentration for scenario 1 - May 2009

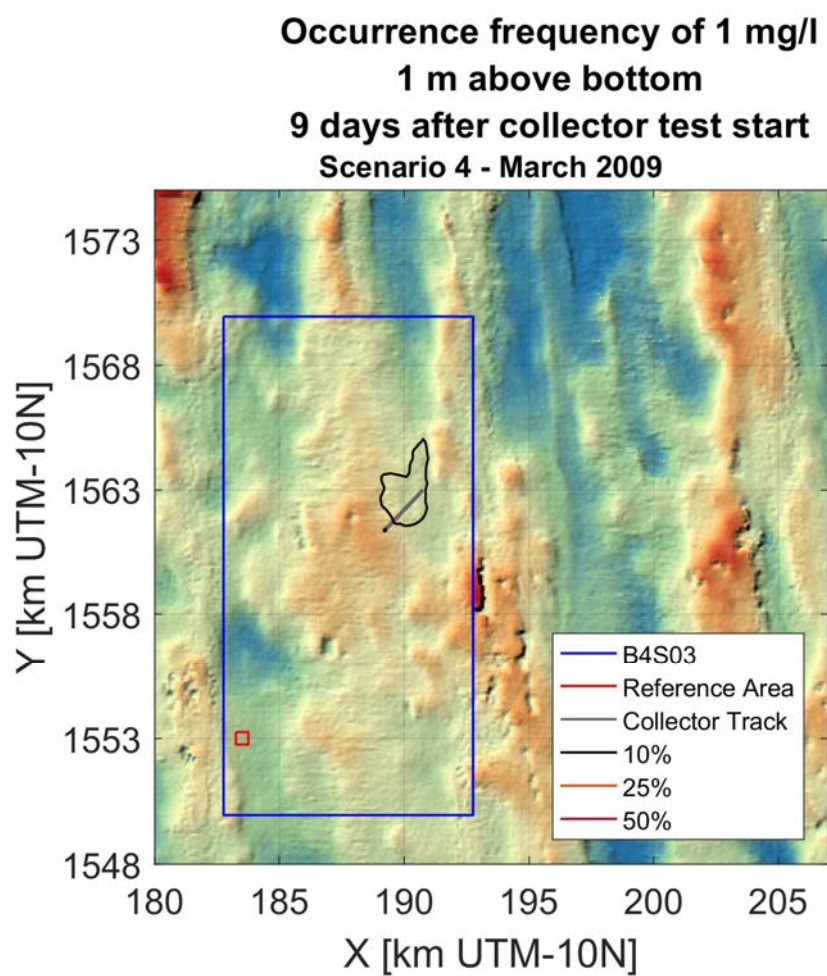


Figure cxii: Frequency of occurrence for 1 mg/l sediment concentration for scenario 1 - March 2009

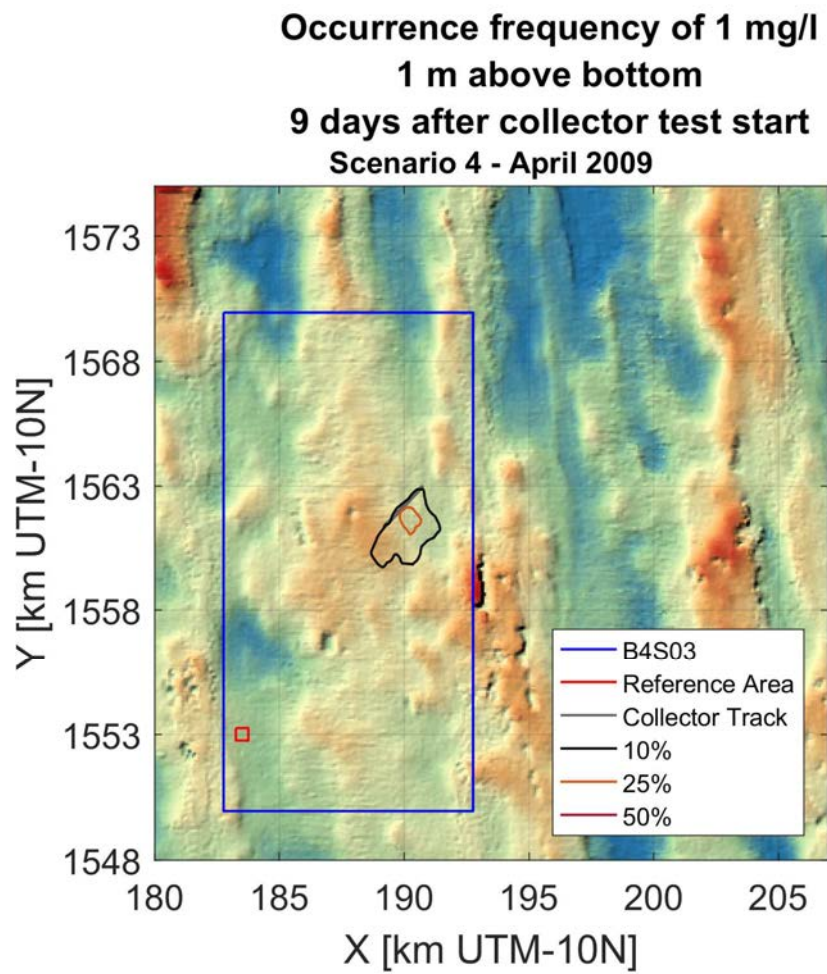


Figure cxiii: Frequency of occurrence for 1 mg/l sediment concentration for scenario 1 - April 2009

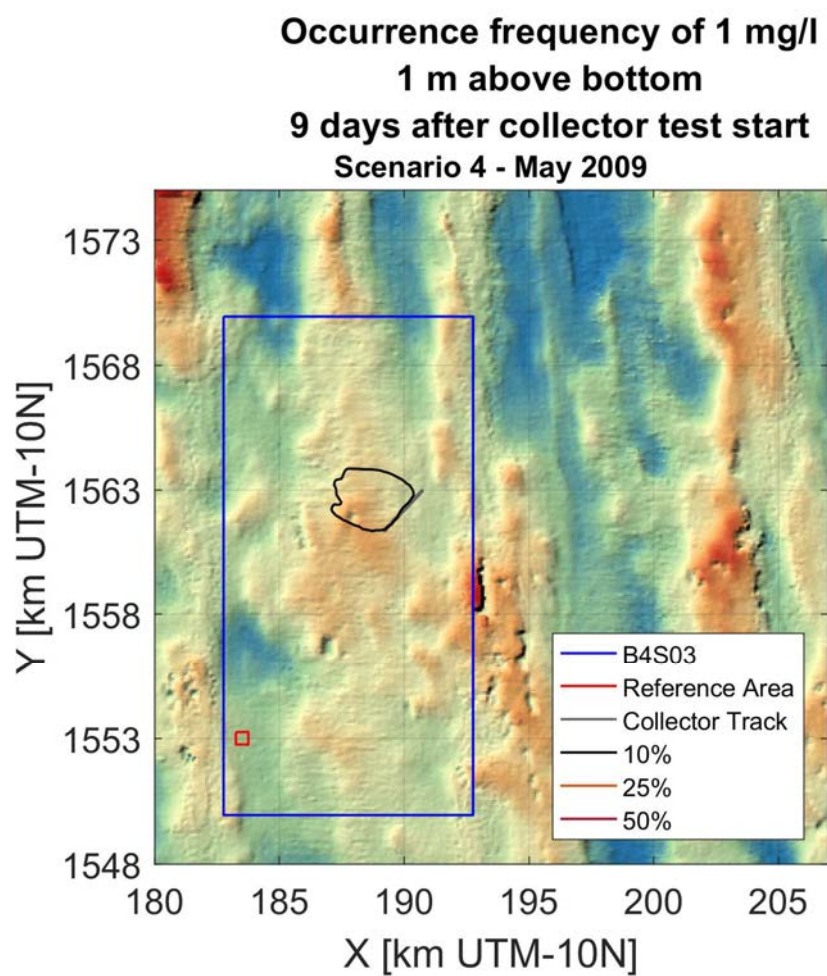


Figure cxiv: Frequency of occurrence for 1 mg/l sediment concentration for scenario 1 - May 2009

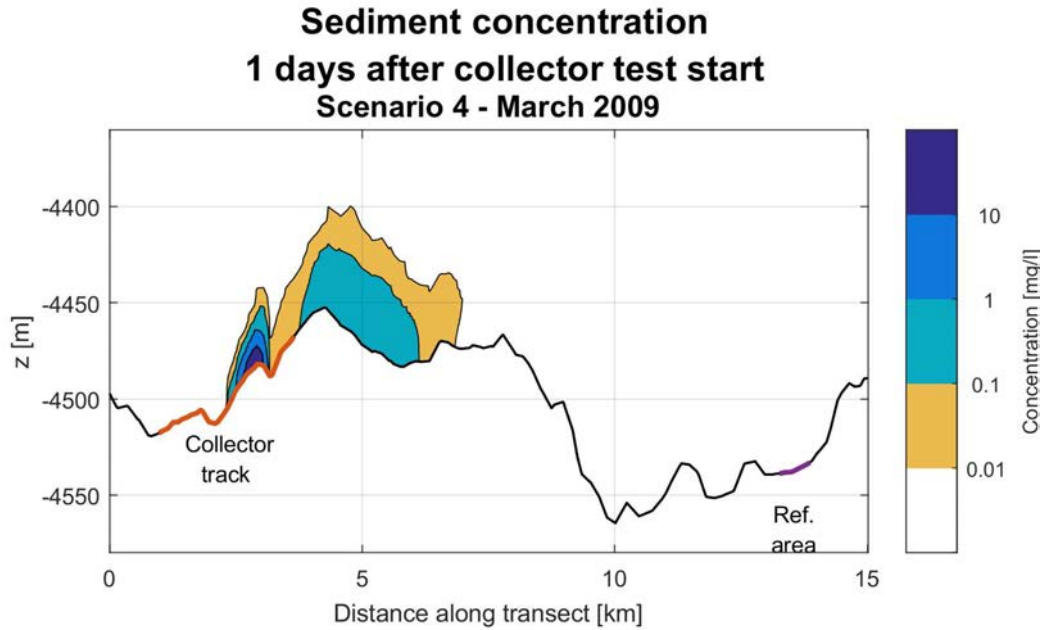


Figure cxv: Cross-sectional sediment concentration contours 1 day after the start of the Patania II trial for scenario 1 - March 2009

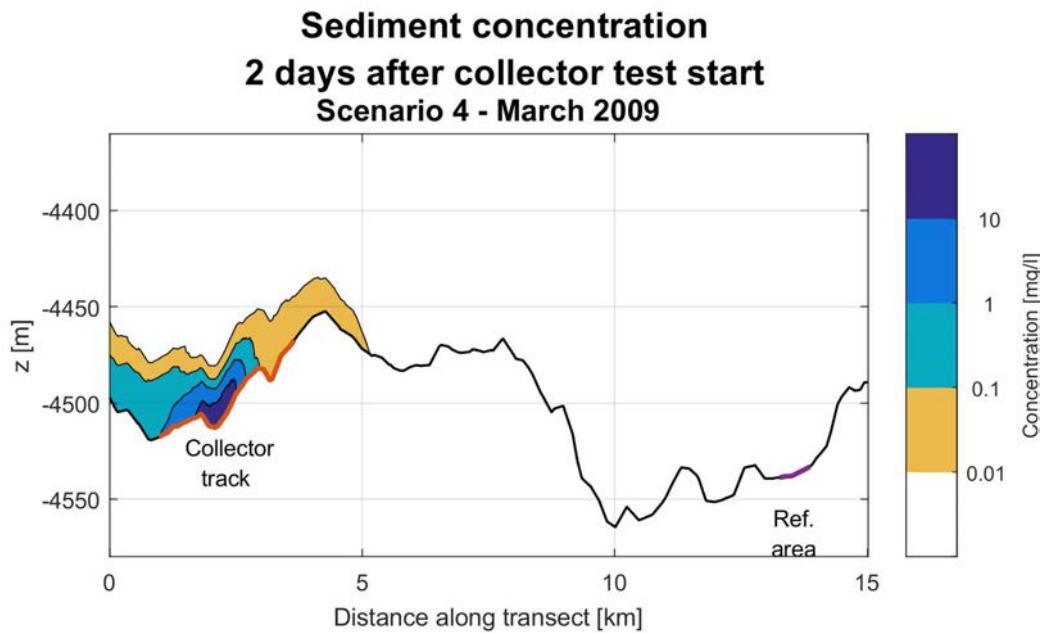


Figure cxvi: Cross-sectional sediment concentration contours 2 days after the start of the Patania II trial for scenario 1 - March 2009

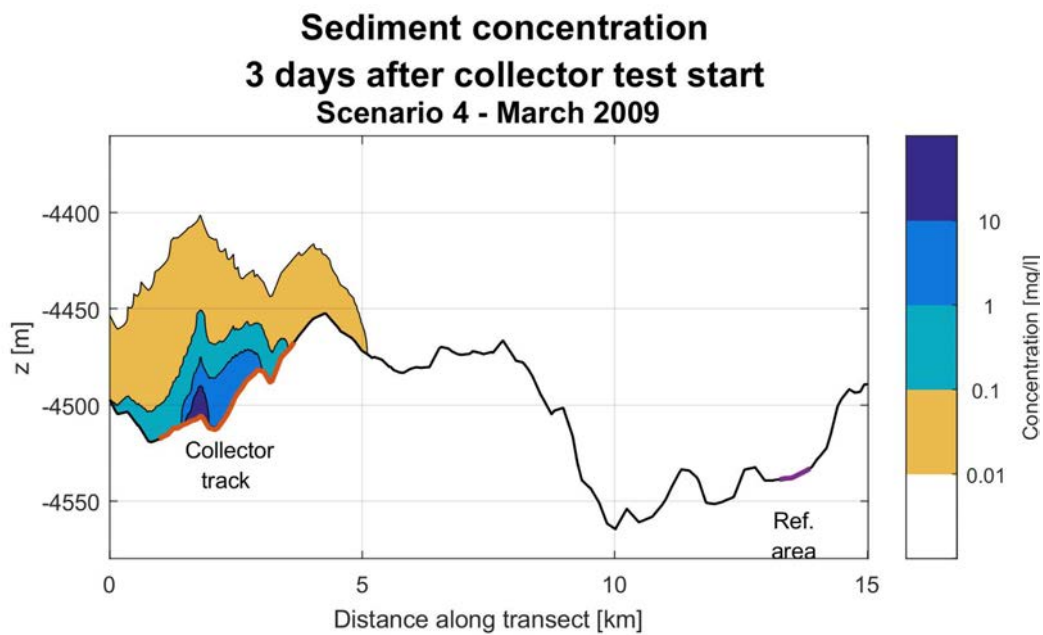


Figure cxvii: Cross-sectional sediment concentration contours 3 days after the start of the Patania II trial for scenario 1 - March 2009

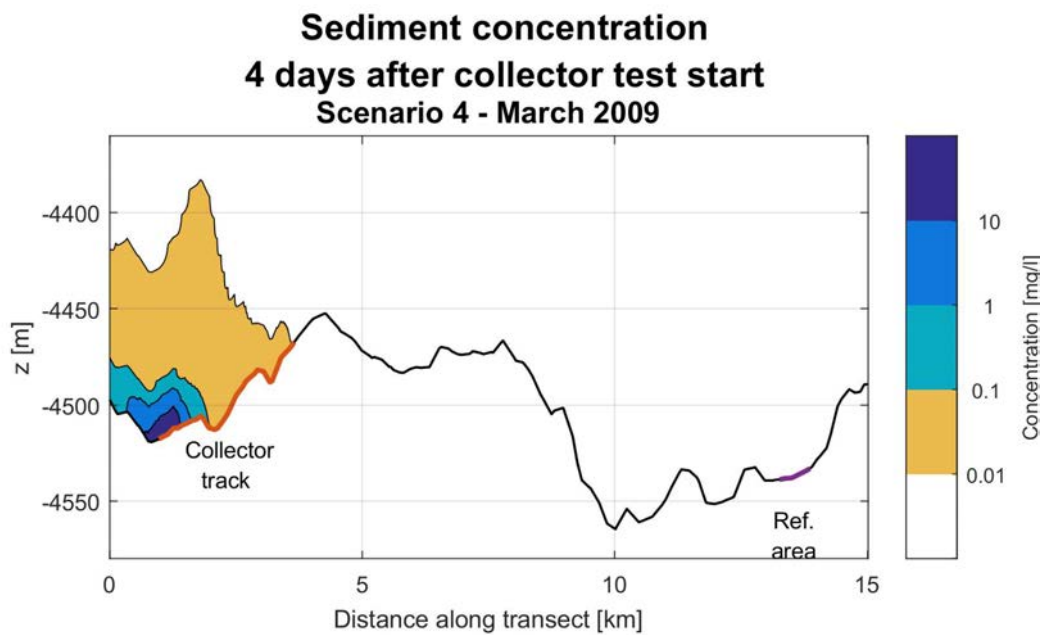


Figure cxviii: Cross-sectional sediment concentration contours 4 days after the start of the Patania II trial for scenario 1 - March 2009

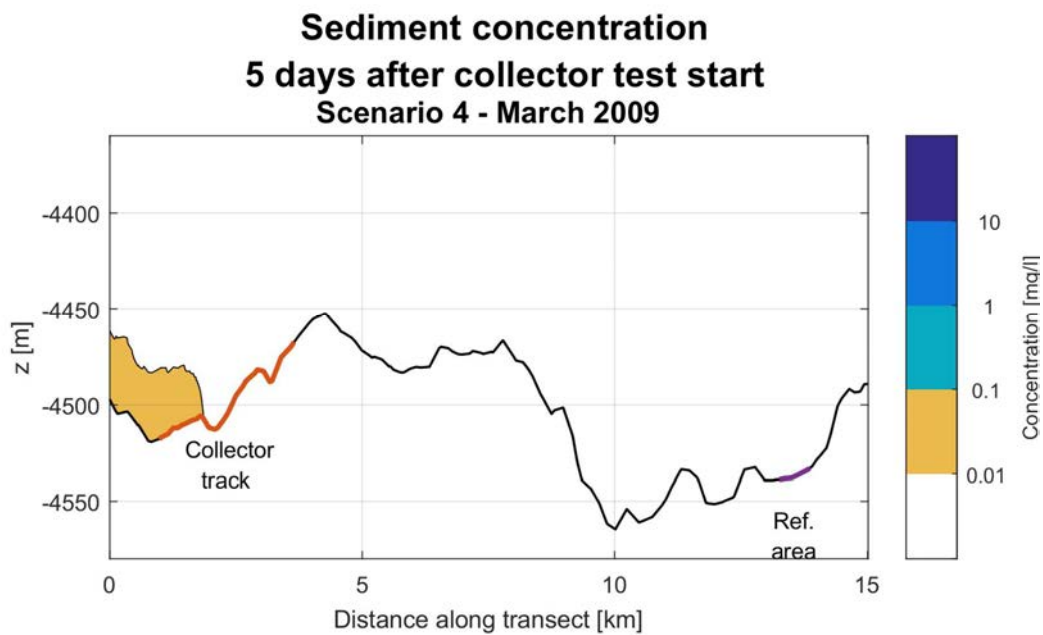


Figure cxix:: Cross-sectional sediment concentration contours 5 days after the start of the Patania II trial for scenario 1 - March 2009

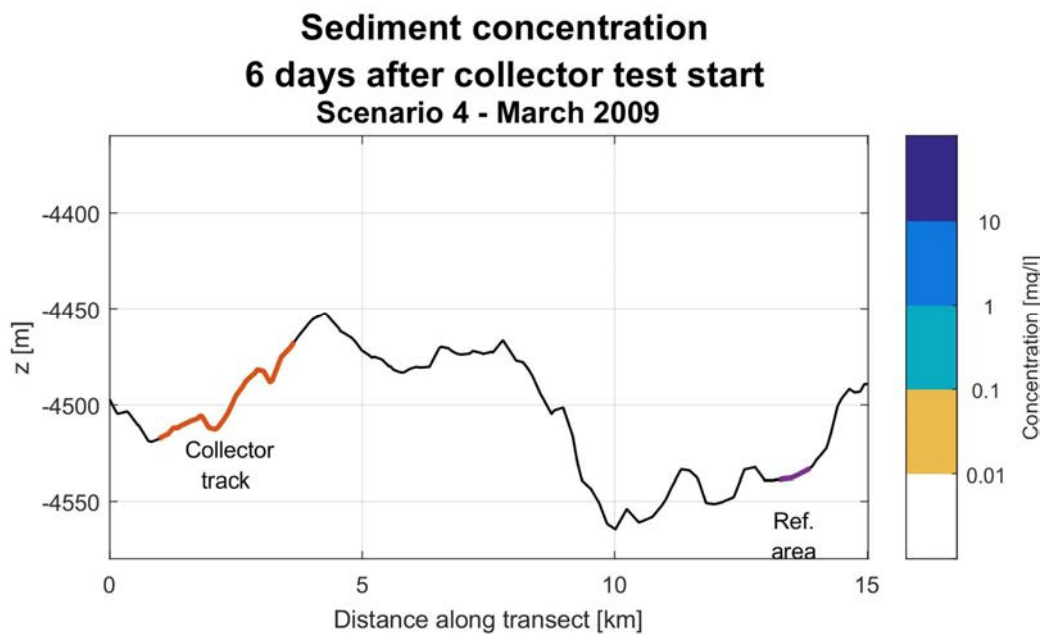


Figure cxx: Cross-sectional sediment concentration contours 6 days after the start of the Patania II trial for scenario 1 - March 2009

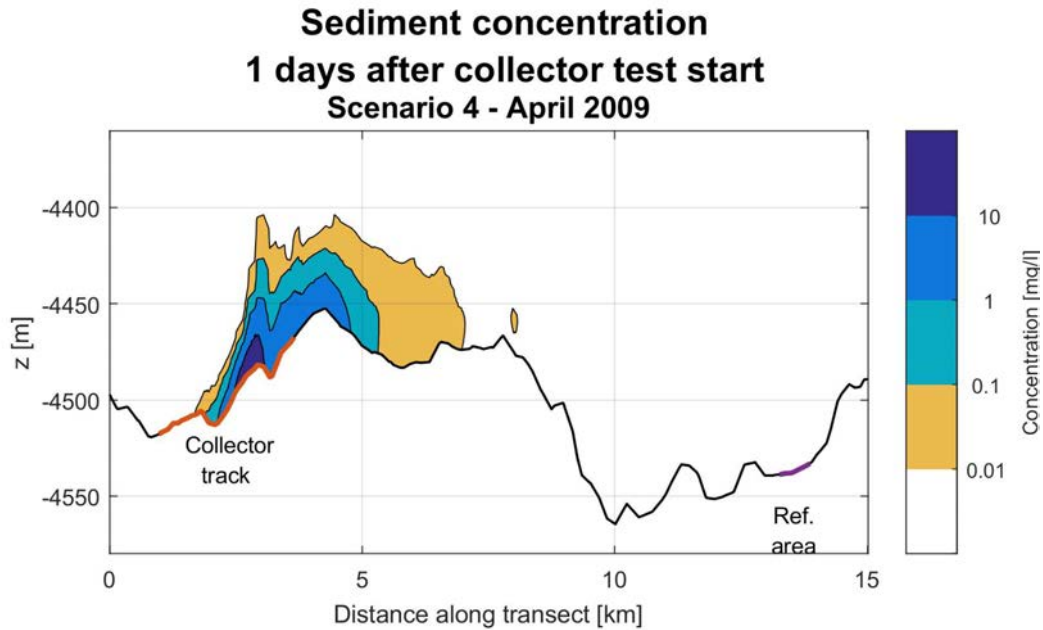


Figure cxxi: Cross-sectional sediment concentration contours 1 day after the start of the Patania II trial for scenario 1 - April 2009

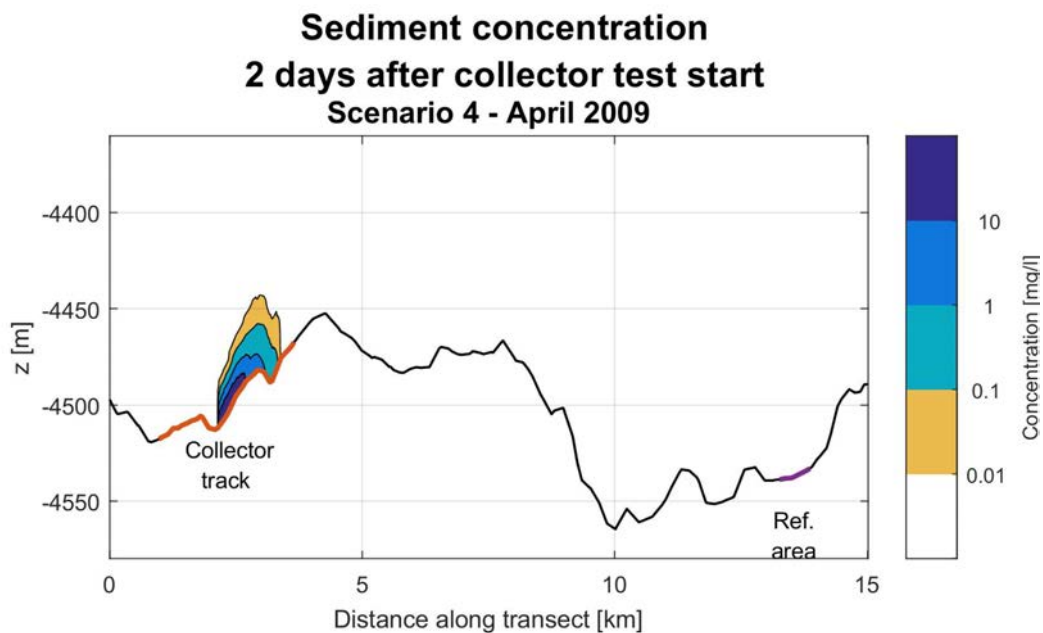


Figure cxxii: Cross-sectional sediment concentration contours 2 days after the start of the Patania II trial for scenario 1 - April 2009

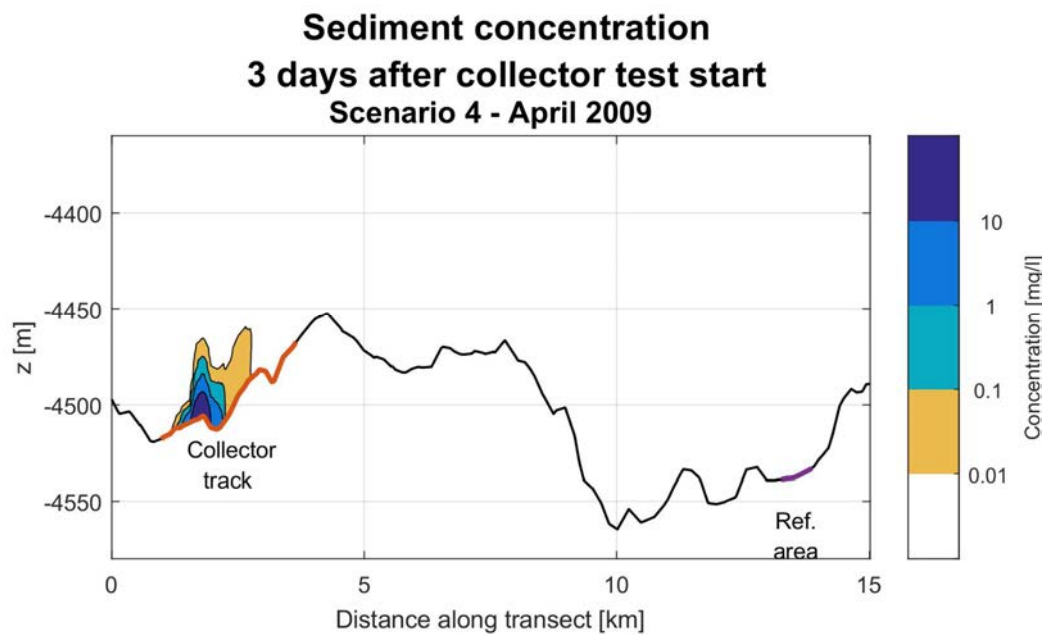


Figure cxxiii: Cross-sectional sediment concentration contours 3 days after the start of the Patania II trial for scenario 1 - April 2009

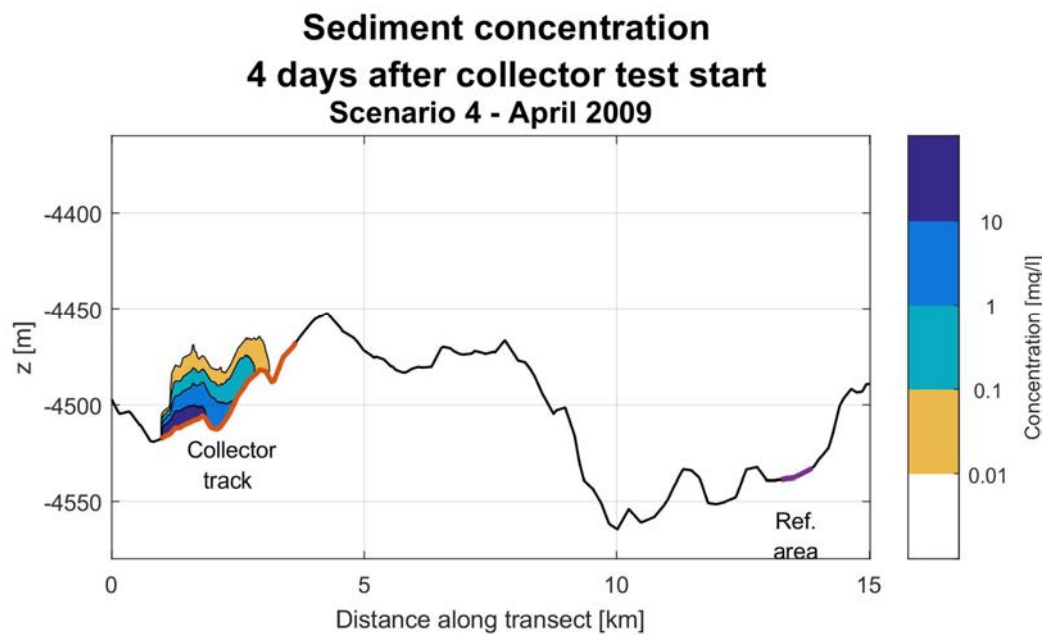


Figure cxxiv: Cross-sectional sediment concentration contours 4 days after the start of the Patania II trial for scenario 1 - April 2009

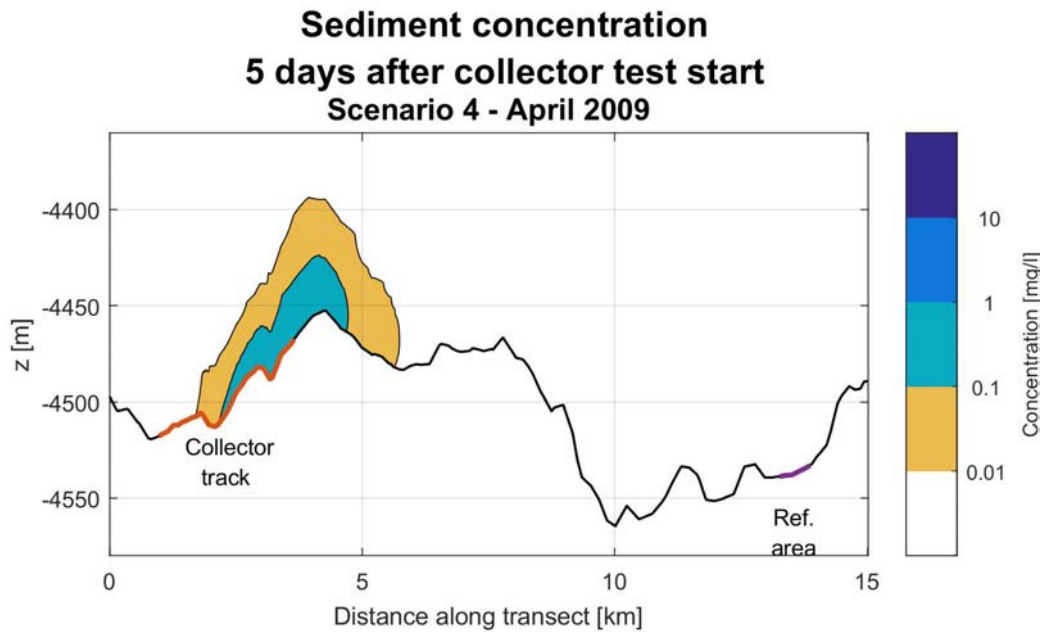


Figure cxxv: Cross-sectional sediment concentration contours 5 days after the start of the Patania II trial for scenario 1 - April 2009

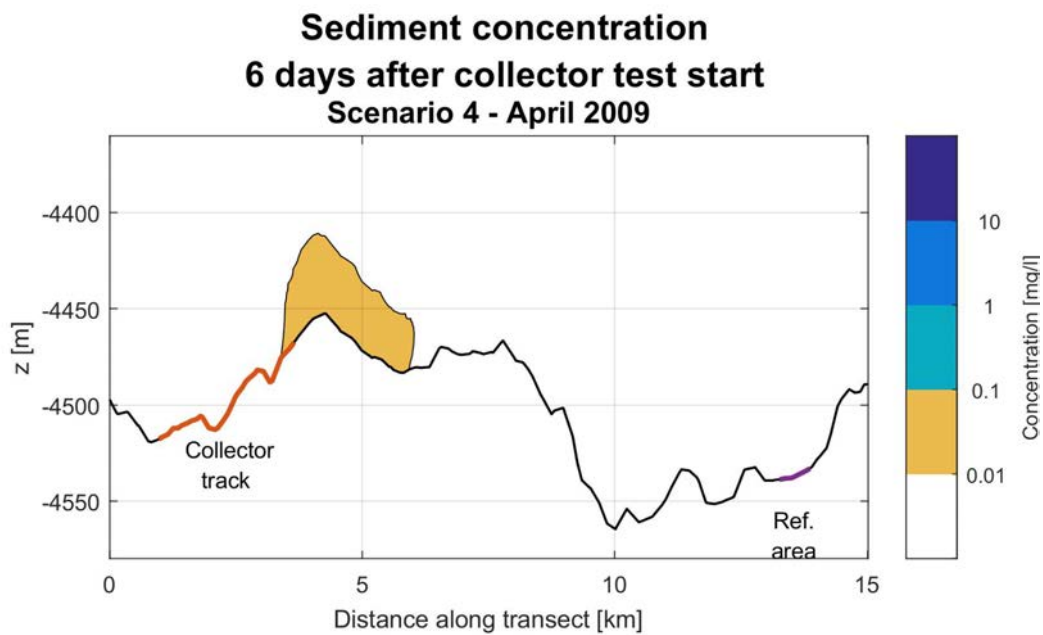


Figure cxxvi: Cross-sectional sediment concentration contours 6 days after the start of the Patania II trial for scenario 1 - April 2009

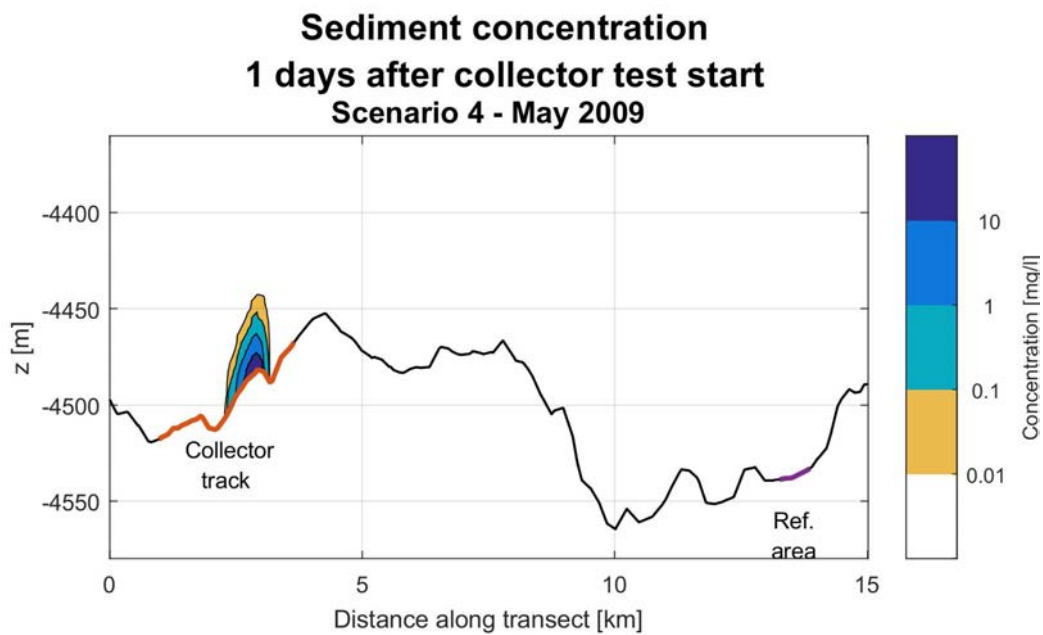


Figure cxxvii: Cross-sectional sediment concentration contours 1 day after the start of the Patania II trial for scenario 1 - May 2009

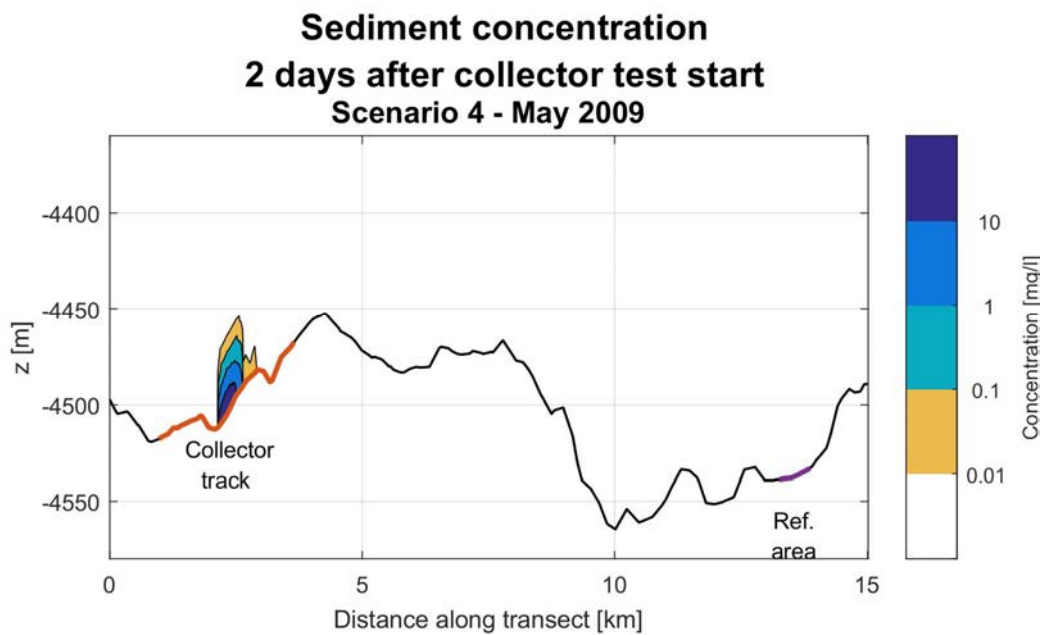


Figure cxxviii: Cross-sectional sediment concentration contours 2 days after the start of the Patania II trial for scenario 1 - May 2009

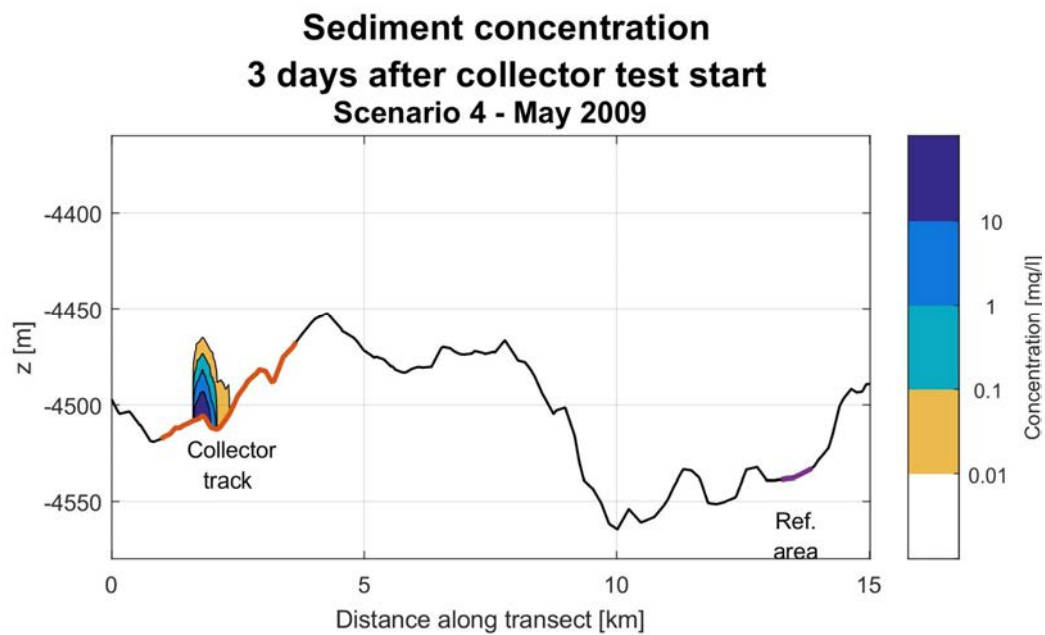


Figure cxxix: Cross-sectional sediment concentration contours 3 days after the start of the Patania II trial for scenario 1 - May 2009

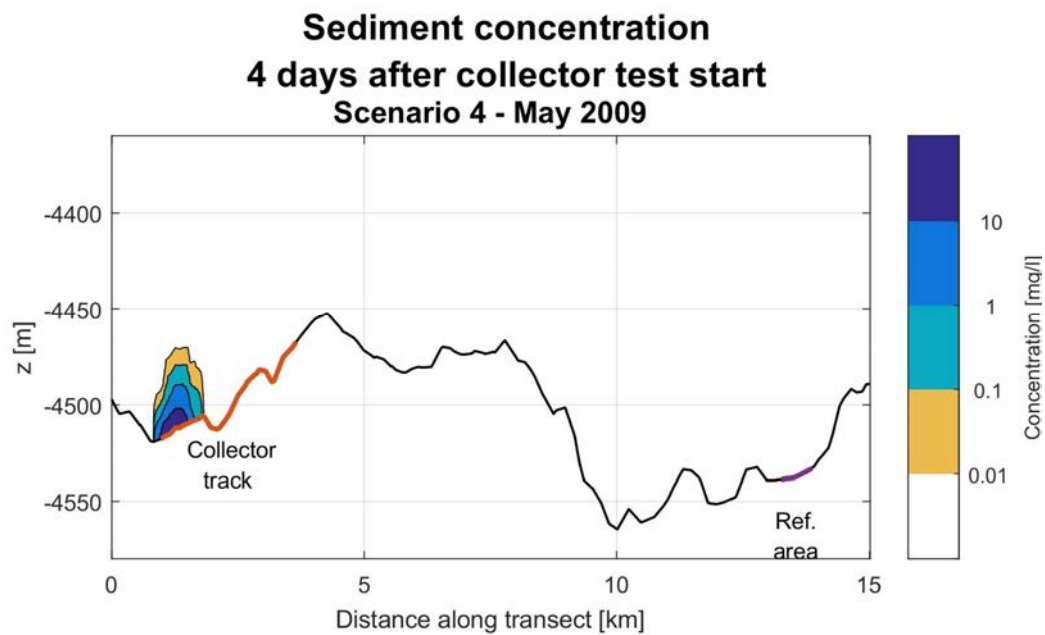


Figure cxxx: Cross-sectional sediment concentration contours 4 days after the start of the Patania II trial for scenario 1 - May 2009

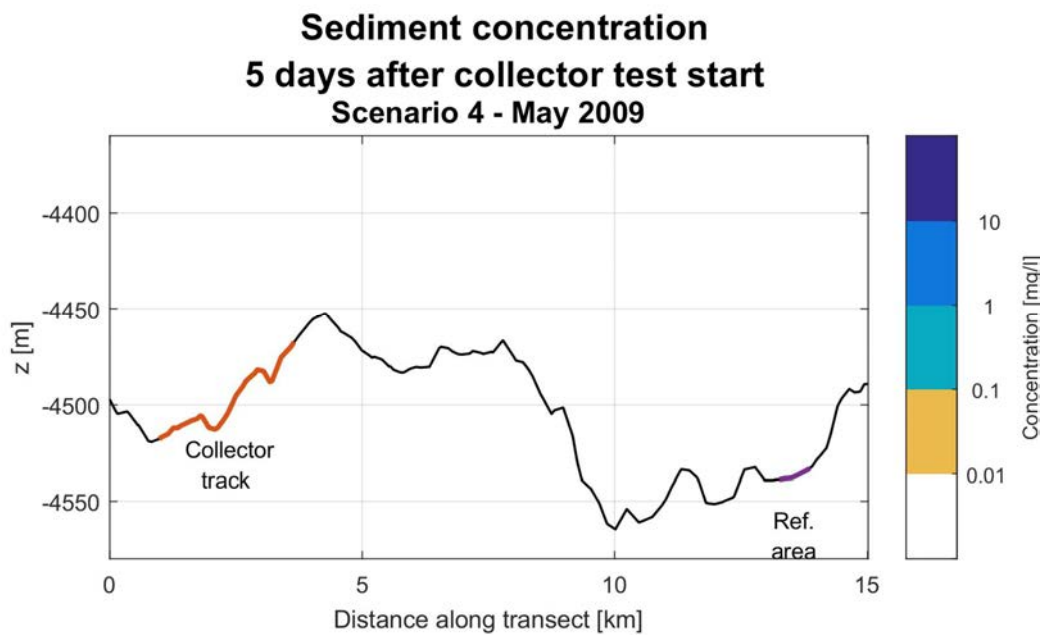


Figure cxxxii: Cross-sectional sediment concentration contours 5 days after the start of the Patania II trial for scenario 1 - May 2009

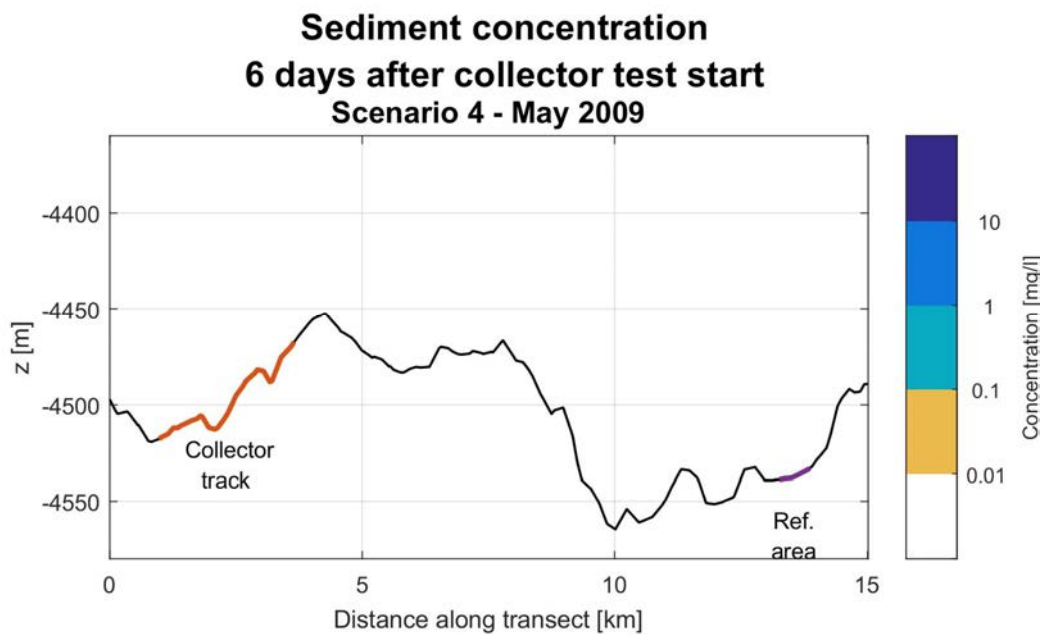


Figure cxxxii: Cross-sectional sediment concentration contours 6 days after the start of the Patania II trial for scenario 1 - May 2009

12.4..5 Comparison with hydrodynamic simulation during the year 2017

Due to later availability of forcing data for the year 2017, an a posteriori verification simulation has been performed of the period May 1st 2017 until June 30th 2017. At the time of writing, short-term data was available (8-17 days) recorded during the cruise held to deploy long-term moorings, but no long-term data was available yet. Once long-term data (> 6 months) is available, a direct comparison of the model with long-term data will be the starting point for model calibration. In the present report, the comparison of the uncalibrated model with the short-term data is shown below.

the comparison is made of TELEMAC model output (blue), short-term monitoring (orange) and HYCOM output (yellow), for Mooring 1 (Figure a). In Figure cxxxiv, the comparison at the location of Mooring 2 is shown. It must be noted that the near-bed layer of HYCOM has a height of 500m and that the HYCOM model does not contain tidal variations.

In general, the Telemac model predicts a current velocity magnitude in the same range as the observed data. Current direction averages around 270° (flowing to West), both in the model and in the data. The data shows more variability in current magnitude and direction. This can be partially explained by scatter in the data and partially by a slightly stronger tidal component in the data. In the model, the semi-diurnal component is present in the signal, but it is at times weaker than the inertial component, which has a period of around 2 days at this latitude. Currents predicted by HYCOM are on average somewhat weaker and less variable, especially due to the absence of tidal peaks, which are present both in the observed and in the Telemac model signals.

Clearly, longer data series are required to allow further analysis of the variability in the current field, both observed and modelled. This will be performed in the next stage of model development after long-term data becomes available.

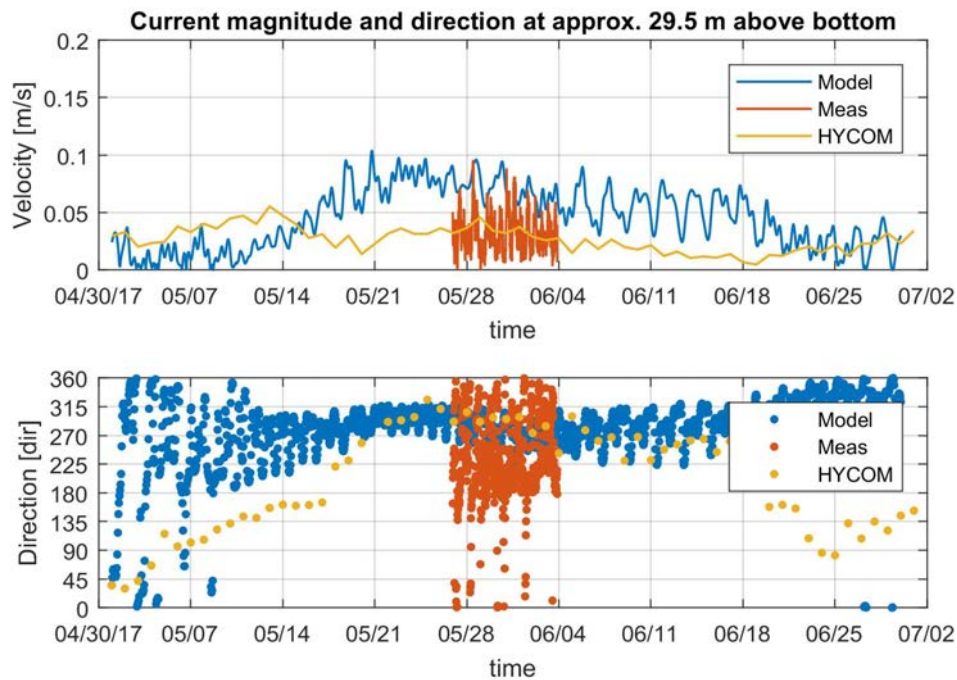


Figure cxxxiii: Comparison of TELEMAC model output (blue), short-term monitoring (orange) and HYCOM output (yellow) at MOR001 location.

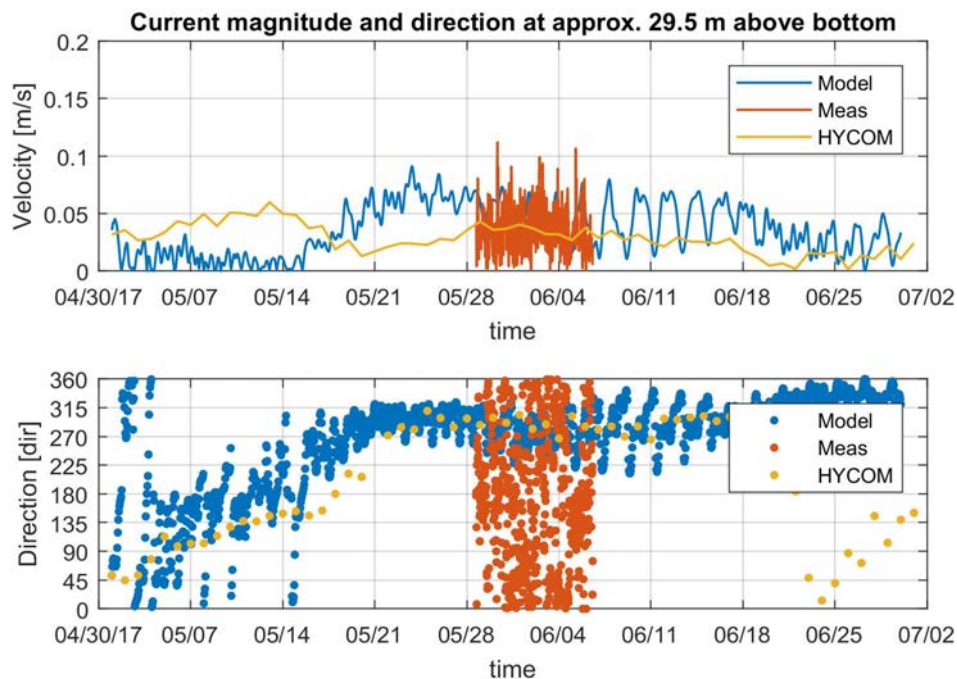


Figure cxxxiv: Comparison of TELEMAC model output (blue), short-term monitoring (orange) and HYCOM output (yellow) at MOR002

12.5 Risk Assessment Table

Attachment A – Risk Register				
Component	Activity / Hazard	Event	Potential Impact / Effect	Mitigation
Patania II	Settling on seafloor and moving	Local disturbance of habitat	Seafloor surface structure will change	Monitoring Test. Limit the impact area of track propulsion system, technology development. BAT (Best Available Techniques)
		Compaction of sediment	Death of organisms changes species diversity	Monitoring Test. Limit the track pressure of the propulsion system, technology development. BAT (Best Available Techniques)
		Removal of habitat	Seafloor surface structure will change	Monitoring Test. Nodule habitat unavoidable, other habitat limit removal of top layer, technology development. BAT (Best Available Techniques). Maximize return of collected sediment and organisms near the seafloor.
		Removal of organisms	Death of organisms, change in abundance and species diversity	Monitoring Test. Nodule epifauna unavoidable, other fauna limit removal of top layer, technology development. BAT (Best Available Techniques). Maximize return of collected sediment and organisms near the seafloor.
		Hydraulic Fluid Leaks	~0.9m ³ fluid leaks to environment (assuming total loss from a single machine)	The use of pressure tested systems and biodegradable oils. Regular maintenance
		Stops working / loss of power and/or communications	Could result in tool being left on the seafloor	Testing of equipment/ operational system prior to deployment. Design of umbilical load
	Collector Head Operation	Plume generation	Smothering of organisms	Monitoring Test. Technology development. Limit the removal of top sediment layer
			Increased food supply for benthos	Monitoring Test. Technology development. Limit the removal of top sediment layer
			Reduction of bioluminescence, leading to changes in biodiversity	Monitoring Test. Technology development. Limit the removal of top sediment layer
		Release of metals (from sediments) into water column	Trace metal uptake	Monitoring Test. Testing of availability in-situ during component test. Copper toxicity occurs only with reduced copper, to assess if collection test will reduce this copper to any significant toxic levels.
		Lighting of Patania II, fauna attraction	Some individuals attracted to the suction area may be lost	No practicable controls. Visual Monitoring.
		Noise	Local, disturbance to fauna	Monitoring Test. No practicable controls, engineering design (Vibration ALARP)
		Vibration	Local, disturbance to fauna	No practicable controls, engineering design (Vibration ALARP)
	Raising/lowering machine to/from vessel	Fauna attraction during ascent and descent	Entanglement of fauna	Monitoring during Test.
Umbilicals	Sonar	Noise	Cetacean disturbance	No practicable controls. Monitoring of Test.
		Entanglement	Loss of equipment, production impact	Umbilical management systems including response measures in place, and adequate spares and skills offshore to enable repairs
		Hazard in water column	Cetacean entanglement	Umbilical management systems including response measures in place, and adequate spares and skills offshore to enable repairs

Attachment A – Risk Register				
Component	Activity / Hazard	Event	Potential Impact / Effect	Mitigation
Support Vessel	Operating and movement according Patania II	Dynamic positioning fails / Power Loss	Patania II could be dragged along seafloor damaging habitat	Umbilical management system including response measures in place
	Operating and movement according Patania II	Sinking	Loss of life, spillage of fuels/chemicals causing pollution/individual animal mortality/bioaccumulation	Maintenance, ship designed for appropriate conditions, crew competency, maintenance of vessel class/in survey, Emergency Response Plans
	Operating and movement according Patania II	Collision with other ships	Damage, spills, sinking	Consider establishing exclusion zone around the mine site, normal maritime communication procedures
Natural Hazards	General operations Patania II	Tropical Storms/hurricanes	Late retrieval of Patania II. Damage, spills, sinking	Management of operations / use of weather and early warning forecasting system